Oxidation and Coordination Chemistry of E_n Ligand Complexes under Weakly Coordinating Conditions

DISSERTATION

ZUR ERLANGUNG DES
DOKTORGRADES DER NATURWISSENSCHAFTEN
(DR. RER. NAT.)
DER FAKULTÄT FÜR CHEMIE UND PHARMAZIE
DER UNIVERSITÄT REGENSBURG

vorgelegt von
Martin Fleischmann
aus Sulzbach-Rosenberg
im Jahr 2015

Diese Arbeit wurde angeleitet von Prof. Dr. Manfred Scheer.

Promotionsgesuch eingereicht am: 4. November 2015
Tag der mündlichen Prüfung: 4. Dezember 2015

Vorsitzender:	Prof. Dr. Arnd Vogler
Prüfungsausschuss:	Prof. Dr. Manfred Scheer
	Prof. Dr. Nikolaus Korber
	Prof. Dr. Frank-Michael Matysik

Universität Regensburg

Eidesstattliche Erklärung

Ich erkläre hiermit an Eides statt, dass ich die vorliegende Arbeit ohne unzulässige Hilfe Dritter und ohne Benutzung anderer als der angegebenen Hilfsmittel angefertigt habe; die aus anderen Quellen direkt oder indirekt übernommenen Daten und Konzepte sind unter Angabe des Literaturzitats gekennzeichnet.

_____

Martin Fleischmann

This thesis was elaborated within the period from January 2012 until November 2015 in the Institute of Inorganic Chemistry at the University of Regensburg, under the supervision of Prof. Dr. Manfred Scheer.

List of publications:

Fleischmann, M., Dielmann, F., Gregoriades, L. J., Peresypkina, E. V., Virovets, A. V., Huber, S., Timoshkin, A. Y., Balázs, G. and Scheer, M.
*"Redox and Coordination Behavior of the Hexaphosphabenzene Ligand in [(Cp*Mo)$_2$(μ,η^6:η^6-P$_6$)] Towards the "Naked" Cations Cu$^+$, Ag$^+$ and Tl$^+$"*
Angew. Chem. Int. Ed. **2015**, *54*, 13110–13115;
Angew. Chem. **2015**, *127*, 13303–13308.

Fleischmann, M., Welsch, S., Peresypkina, E. V., Virovets, A. V. and Scheer, M.
"Highly Dynamic Coordination Behavior of P$_n$ Ligand Complexes Towards "Naked" Cu$^+$ Cations"
Chem. Eur. J. **2015**, *21*, 14332–14336.

Albrecht, F., Repp, J., Fleischmann, M., Scheer, M., Ondráček, M. and Jelínek, P.
"Probing Charges on the Atomic Scale by Means of Atomic Force Microscopy"
Phys. Rev. Lett. **2015**, *115*, 076101.

Fleischmann, M., Dütsch L., Elsayed Moussa M., Schindler A., Balázs G., Lescop C. and Scheer, M.
"Organometallic Polyphosphorus and –arsenic Ligands as Linkers Between Pre-assembled Linear Cu^I Fragments"
Chem. Commun. **2015**, *51*, 2893–2895.

Fleischmann, M., Jones J. S., Gabbaï, F. P. and Scheer, M.
"A Comparative Study of the Coordination Behavior of cyclo-P$_5$ and cyclo-As$_5$ Ligands Towards the Trinuclear Lewis Acid Complex (perfluoro-ortho-phenylene)mercury"
Chem. Sci. **2015**, *6*, 132–139.

Arleth, N., Gamer, M. T., Köppe R., Pushkarevsky N. A., Konchenko S. N., Fleischmann M., Bodensteiner M., Scheer M. and Roesky P. W.
"The Approach to 4d/4f-polyphosphides"
Chem. Sci. **2015**, *6*, DOI: 10.1039/c5sc02252e.

Fleischmann, M., Welsch, S., Gregoriades, L. J., Gröger, C. and Scheer, M.
"Supramolecular Assemblies of Polyphosphorus Ligands Based on Weak Tl-P and In-P Interactions"
Z. Naturforsch. **2014**, *69b*, 1348–1356.

Fleischmann, M., Welsch, S., Krauss, H., Schmidt, M., Bodensteiner, M., Peresypkina, E. V., Sierka, M., Gröger, C. and Scheer, M.
"Complexes of Monocationic Group 13 Elements with Pentaphospha- and Pentaarsaferrocene"
Chem. Eur. J. **2014**, *20*, 3759–3768.

Fleischmann, M., Heindl, C., Seidl, M., Virovents, A. V., Peresypkina, E. V., Tsunoda, M., Gabbaï, F. P. and Scheer, M.
"Discrete and Extended Supersandwich Structures Based on Weak Interactions between Phosphorus and Mercury"
Angew. Chem. Int. Ed. **2012**, *51*, 9918–9921;
Angew. Chem. **2012**, *124*, 10056–10059.

"... the scientist finds his reward in what
Henri Poincaré calls the joy of comprehension,
and not in the possibilities of application to
which any discovery of his may lead."

Albert Einstein

To my family

Preface

Some of the presented results have already been published during the preparation of this work (*vide supra*). The relevant content is reprinted with permission of the respective scientific publisher. The corresponding citation and the respective license numbers are given at the beginning of the particular chapters.

Each chapter includes a list of authors. At the beginning of each chapter the individual contribution of each author will be described. Additionally, if some of the presented results have already been partly discussed in other theses, it is stated at the beginning of the respective chapters.

To ensure a uniform design of this work, all chapters are subdivided into ‘Introduction’, ‘Results and Discussion’, ‘Conclusion’, ‘References’, and ‘Supporting Information’. Furthermore, all chapters have the same text settings and the compound numeration begins anew. Due to different requirements of the journals and different article types, the presentation of figures for single crystal X-ray structures or the ‘Supporting Information’ may differ. In addition, a general introduction is given at the beginning and a comprehensive conclusion of all chapters is presented at the end of this thesis.

Contents

1. Introduction 1

1.1 Weakly coordinating anions 1

1.2 E_n ligand complexes — selected examples and their reactivity 5

1.3 Trimeric (perfluoro-*ortho*-phenylene)mercury — an unusual Lewis acid 12

1.4 References 14

2 Research objectives 19

3 Redox and coordination behavior of the hexaphosphabenzene $[(Cp^*Mo)_2(\mu,\eta^6{:}\eta^6\text{-}P_6)]$ towards the "naked" cations Cu^+, Ag^+ and Tl^+ 23

3.1 Introduction 23

3.2 Results and Discussion 23

3.3 Conclusion 30

3.4 References 31

3.5 Supporting Information 33

4 Interaction of 'naked' silver cations towards aromatic *cyclo*-P_5 and *cyclo*-As_5 ligands: from mixed σ and π bonding up to weakly π bonding 59

4.1 Introduction 59

4.2 Results and Discussion 61

4.3 Conclusion 66

4.4 References 67

4.5 Supporting Information 69

5 $[\{CpMo(CO)_2\}_4(\mu_4,\eta^2{:}\eta^2{:}\eta^2\text{-}P_4)]^{2+}$ a substituent-free dicationic P_4 chain complex obtained by oxidation of $[\{CpMo(CO)_2\}_2(\mu,\eta^2{:}\eta^2\text{-}P_2)]$ 77

5.1 Introduction 77
5.2 Results and Discussion 78
5.3 Conclusion 84
5.4 References 84
5.5 Supporting Information 86
6 Stabilization of oxidized E_n ligand complexes with the help of weakly coordinating anions 95
6.1 Introduction 95
6.2 Results and Discussion 96
6.3 Conclusion 108
6.4 References 109
6.5 Supporting Information 112
7 Organometallic polyphosphorus and -arsenic ligands as linkers between pre-assembled linear Cu^{I} fragments 123
7.1 Introduction 123
7.2 Results and Discussion 124
7.3 Conclusion 127
7.4 References 128
7.5 Supporting Information 130
8 Self-assembly of reactive linear Cu_3 building blocks for supramolecular coordination chemistry and their reactivity towards E_n ligand complexes 139
8.1 Introduction 139
8.2 Results and Discussion 142
8.3 Conclusion 156
8.4 References 157
8.5 Supporting Information 161

9 A comparative study of the coordination behavior of *cyclo*-P_5 and *cyclo*-As_5 ligand complexes towards the trinuclear Lewis acid complex (perfluoro-*ortho*-phenylene)mercury 171

9.1 Introduction 171

9.2 Results and Discussion 173

9.3 Conclusion 183

9.4 References 184

9.5 Supporting Information 186

10 Supramolecular adducts based on weak interactions between the trimeric Lewis acid complex (perfluoro-*ortho*-phenylene)mercury and polypnictogenyl complexes 207

10.1 Introduction 207

10.2 Results and Discussion 209

10.3 Conclusion 217

10.4 References 217

10.5 Supporting Information 219

11 Thesis Treasury 225

11.1 Coordination chemistry including WCAs 225

11.2 Oxidation chemistry including WCAs 237

11.3 Synthesis of new E_n ligand complexes 241

11.4 Experimental Part 245

11.5 References 254

12 Conclusion 257

12.1 Coordination chemistry of E_n ligand complexes towards monovalent cations 257

12.2 Oxidation chemistry of E_n ligand complexes 261

12.3 Reactivity of E_n ligand complexes towards pre-assembled Cu^I building blocks 263

12.4 Reactivity of E_n ligand complexes towards the unusual Lewis acid [(*o*-$C_6F_4Hg)_3$] 266

12.5 New E_n ligand complexes 267

12.6 References 267

13 Appendices 269

13.1 Alphabetic List of Abbreviations 269

13.2 Acknowledgments 271

1. Introduction

1.1 Weakly coordinating anions

“Non-coordinating anions: Fact or Fiction?” — This question as easy as it sounds is the topic of several discussions in the scientific community.[1,2,3] In the following paragraphs some basic concepts and famous examples of suitable candidates, especially the aluminates which are of great importance for this work will be introduced. Additionally, selected examples of interesting cations which could be stabilized with the help of these anions will be presented.

While some years ago chemists talked about ‘non-coordinating anions’ when halide anions were exchanged for small complex anions like $[CF_3SO_3]^-$, $[BF_4]^-$, $[ClO_4]^-$ or $[MF_6]^-$ (M = P, As, Sb), it has been shown that these anions can in fact very often coordinate to unsaturated Lewis acidic centers. Therefore, today the term ‘Weakly Coordinating Anion’ (WCA) is commonly used in the literature. This class of anions is not only found in fundamental research but has also found its way to applications in polymerization reactions, catalysis and electrochemistry just to mention a few.[3]

The perfect ‘non-coordinating anion’ would exhibit no cation-anion interaction. This is physically impossible, since opposite charges attract each other and the resulting force is expressed by the Coulomb equation (1).[4]

$$F = \frac{1}{4\pi\varepsilon_0}\frac{q_1 \cdot q_2}{r^2} = \frac{1}{4\pi\varepsilon_0}\frac{z_1 z_2 \cdot e^2}{r^2} \qquad (1)$$

q_1, q_2 = point charges, z_1, z_2 = ionic charges, e = elementary charge, r = distance between charges, ε_0 = dielectric constant.

The force is dependent on the ionic charges (z_1 and z_2) and it decreases with increasing distance between the charges (r). This means in order to get the best WCA, the negative charge should be small (usually –1) and delocalized over as many atoms as possible. Therefore, the size of the anion is usually large, which increases the distance between the charges, thus minimizing the Coulomb force. Another concept for WCAs is the exclusion of any Lewis basic groups on the exterior of the anion. (The anion is only as weakly coordinating as its most basic site.)[3] This is often realized by fluorination. The small and hard fluorine atom is regarded as a very weak Lewis base and its electron shell can’t be polarized easily.

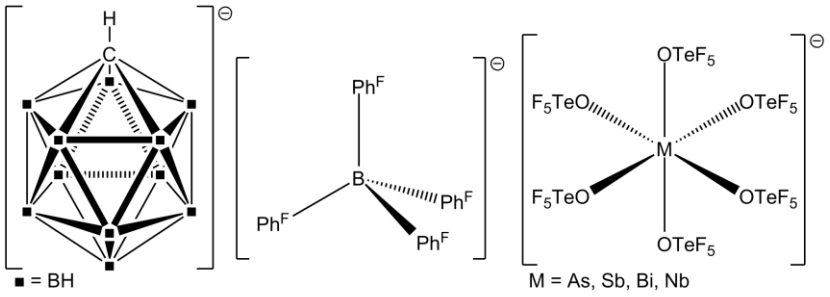

A **B** **C**

Scheme 1. Representation of the WCA classes of carborates (**A**), [BAr^F] anions (**B**) and teflate-based anions (**C**).

The first group of anions which will be introduced are borates. The anion $[BPh_4]^-$ which is formally obtained by exchanging the F atoms of $[BF_4]^-$ with phenyl groups represents a well-known anion. However, fluorination or substitution of the Ph groups results in more stable and better performing WCAs. This group of anions is referred to in the chemist's jargon as the [BAr^F] anions (see Scheme 1 **B**). Among these, the most prominent representatives are $[B(C_6F_5)_4]^-$ and $[B\{3,5\text{-}(CF_3)_2C_6H_3\}_4]^-$. Several salts of these anions are commercially available and they are widely used. The second group of WCAs is derived from the anion *closo*-$[CB_{11}H_{12}]^-$ (**A**). The carborates[5] are weakly coordinating and synthetic procedures are known for partially and fully halogenated derivatives. Although their chemical stability and weakly coordinating nature seem promising their applications are quite limited due to their multi-step syntheses. The third group of large WCAs that is mentioned here consists of the teflate-based anions which can be regarded as derived from the hexafluorometallates in which the F atoms are substituted by (-$OTeF_5$) groups $[M(OTeF_5)_6]^-$ (**C**). These anions are known for M = As, Sb, Bi, Nb. Although it was demonstrated that these anions can stabilize electrophilic cations like $[AsX_4]^+$ and $[SbX_4]^+$ (X = Cl, Br),[6,7] they are not commonly used.

The aluminates [TEF] and [FAl]

The frequent application of the weakly coordinating aluminate anion $[Al\{OC(CF_3)_3\}_4]^-$ (= [TEF]) has been especially promoted by *Krossing et al.* during the last years.[4] The anions [TEF] and [FAl] are easily prepared as their Li^+ salts starting from $Li[AlH_4]$ and four equivalents of the appropriate fluorinated alcohol R^FOH (R^F = $C(CF_3)_3$, $C_6F_{10}(C_6F_5)$).[8,9,10] The large [TEF] anion (57 atoms) contains four identical perfluoro-*tert*-butoxy groups bound to the central Al atom. The larger [FAl] anion (86 atoms) contains three bulky alkoxy groups each with an aliphatic and an aromatic six-membered ring. The fourth coordination site of Al is saturated by a fluoride anion which is cleaved from the last equivalent of R^FOH during the synthesis.

Monovalent M^+ salts of [TEF] can be prepared by metathesis reactions (Ag^+,[9] Cu^+,[11,12,13] Tl^+,[14] In^+[15]) starting from Li[TEF] or by oxidation of the neat metal by Ag[TEF] (In^+,[16] Ga^+[17]). For [FAl], only the Li^+ and the Ag^+ salts have been prepared so far.[10]

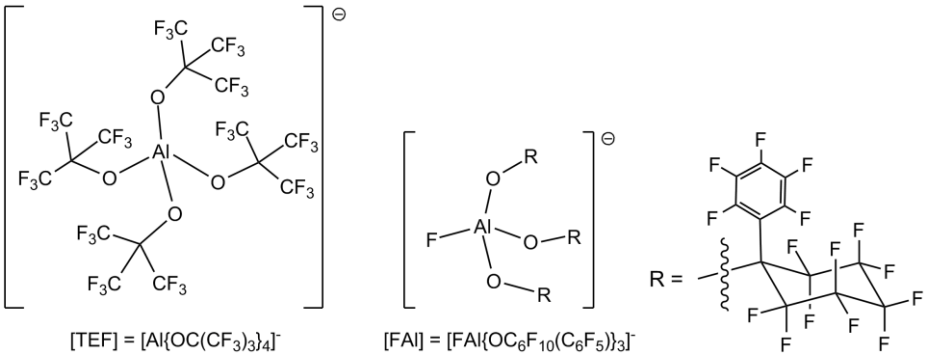

Scheme 2. Representation of the WCAs [TEF] and [FAl].

The [TEF] anion exhibits a very uniform fluorinated surface and is considered to be very weakly coordinating and chemically robust. In some exceptional cases it shows coordination via the O atoms of its tert-butoxy groups or decomposition.[14,18,19] In most cases, the [FAl] anion can also be considered as weakly coordinating. However, single crystal X-ray diffraction analysis revealed, that the [FAl] anion can adopt two different conformations in the solid state, related to each other by rotation around a C-O single-bond (see Scheme 3). In its weakly coordinating conformation, the Ph^F groups are shielding the Al-F bond of the [FAl] anion. In contrast, the Cy^F groups ($-C_6F_{10}$) can be arranged in a way that the Al-F bond is exposed and the [FAl] anion was shown to coordinate to Ag^+.[10] In addition, the [FAl] anion can be reactive and the Al bound F atom can be substituted (shown for Cl^-).[20]

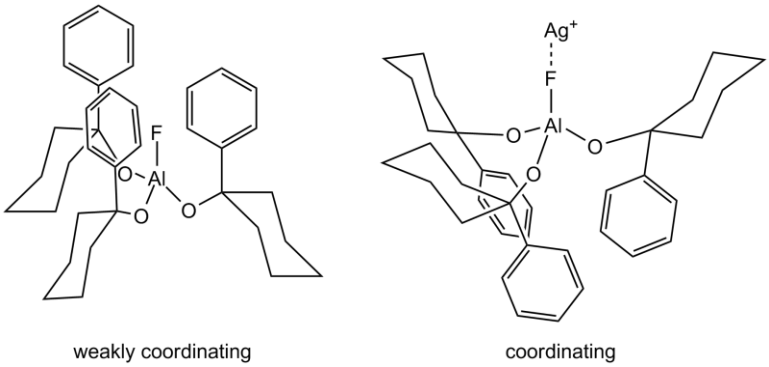

Scheme 3. Illustration of the weakly coordinating and the coordinating conformation of the [FAl] anion. All fluorine atoms except the coordinating one are omitted for clarity.

Using the [TEF] anion, a variety of reactive electrophilic cations could be stabilized in solution and structurally characterized in the solid state, like the trigonal planar $[CI_3]^+$.[21] In addition, the [TEF] anion also enabled the isolation of the binary phosphorus halide cations $[PX_4]^+$, $[P_2X_5]^+$ and $[P_5X_2]^+$ (X = Br, I),[22] the insertion of $[NO]^+$ into a P-P bond of P_4 to form $[P_4NO]^+$[23] as well as the subsequent isolation of the first homopolyatomic phosphorus cation $[P_9]^+$.[24] The latter could only be stabilized by [TEF] so far, since it readily reacts with more basic WCAs like $[SbF_6]^-$ under fluoride abstraction to form PF_3. The stability of the [TEF] anion can be explained by its super weak basicity and the exclusive presence of very strong C-F bonds on its exterior.

The weakly coordinating nature of the [TEF] anion also enabled the coordination of ligands exhibiting very low basicity to Cu^+ and Ag^+ like S_8,[25,11,13] P_4,[11,26] and As_4,[27] as well as unsubstituted C_2H_4[12] and C_2H_2,[28] just to mention a few. Following this approach, several metastable molecules and coordination of unusual Lewis bases could be observed in the coordination sphere of monovalent metal cations demonstrated by the characterization of the complexes $[Ag(As_4)_2]^+$,[27] $[Ag_2(cyclo\text{-}Se_6)(OSO)_4]^{2+}$,[29] $[Ag_2(cyclo\text{-}Se_{12})]^{2+}$,[10] $[Cu_2(cyclo\text{-}Se_{19})]^{2+}$[30] and $[Ag\{Fe(CO)_5\}_2]^+$.[31] Recently, the exceptional coordination behavior of the main group cations In^+ and Ga^+ could be investigated under weakly coordinating conditions with the aid of the [TEF] anion. While reactions with the bulky phosphane P^tBu_3 lead to carbene analogues complexes $[M(P^tBu_3)_2]^+$, N-heterocyclic carbenes (NHC) exhibit an unusual tilted coordination in the complexes $[M(NHC)_2]^+$ (M = Ga, In).[16,32] Recently, it was demonstrated that Ga^+ shows disproportionation while In^+ forms the tri- and tetranuclear clusters $[In_3(bipy)_6]^{3+}$ and $[In_4(bipy)_6]^{4+}$ stabilized by metal-metal bonds when reacted with bipy (= 2,2'-bipyridine). The latter complex exhibits a rhombic structure of four In^+ cations containing the shortest In^I-In^I bond described in the literature.[33] The previously published reactivity of monocations towards E_n ligand complexes will be described in the following chapter.

Single crystal X-ray diffraction analysis of compounds containing the anion [TEF]

Due to its weakly coordinating nature, the anion [TEF] shows a high tendency to be disordered. Therefore, the structural characterization by single crystal X-ray diffraction analysis of its compounds is often challenging. The CF_3- as well as whole $(CF_3)_3CO$-groups frequently exhibit rotational disorder by rotation of C–O or C–C bonds. In some cases even a positional disorder of the whole anion can be observed. During the refinement of these solid state structures it is common that a series of least-square restraints has to be applied. Very recently, a new program called DSR (disordered structure refinement) was developed which performs semi-automatic modeling of

disordered structures.[34] Although it was not used during this work, this will significantly simplify future structural analyses.

1.2 E_n ligand complexes — selected examples and their reactivity

The term E_n ligand complexes used throughout this work describes organometallic complexes containing a limited number *n* (*n* = 2, 3, 5, 6) of substituent-free pnictogen atoms E (E = P, As, Sb, Bi) which are only bonded to other pnictogen atoms or transition metals.[35,36,37,38,39] In 1981, Nobel Laureate *Roald Hoffmann* described that the isolobal analogy is building bridges between inorganic and organic chemistry.[40] It implies that numerous organometallic or inorganic compounds can be related to analogues organic molecules. In this context, the isolation of the *cyclo*-E_6 complexes $[(Cp^*Mo)_2(\mu,\eta^6{:}\eta^6\text{-}E_6)]$ (**1**) and the *cyclo*-E_5 complexes $[Cp^*Fe(\eta^5\text{-}E_5)]$ (E = P, As) by *Scherer et al.* during the 1980s can be viewed as a milestone in inorganic chemistry.[41,42,43,44] The complexes **A1**, **A2**, **B1** and **B2** represent the all-phosphorus and the all-arsenic analogues of benzene and the cyclopentadienide anion stabilized in the coordination sphere of transition metal complexes illustrated in Scheme 4. In the same manner one can explain the relation of the tetrahedrane complexes **D1, D2** and **C1**-**C4** (E = P, As, Sb, Bi) to white phosphorus by exchanging one or two atoms of the group 15 element P by the isolobal 15 VE complex fragment $[CpM(CO)_2]$ (M = Mo, Cr). For the heavier congeners **C2**-**C4**, the remaining two P atoms of **C1** are also formally substituted by the heavier group 15 elements As, Sb or Bi.

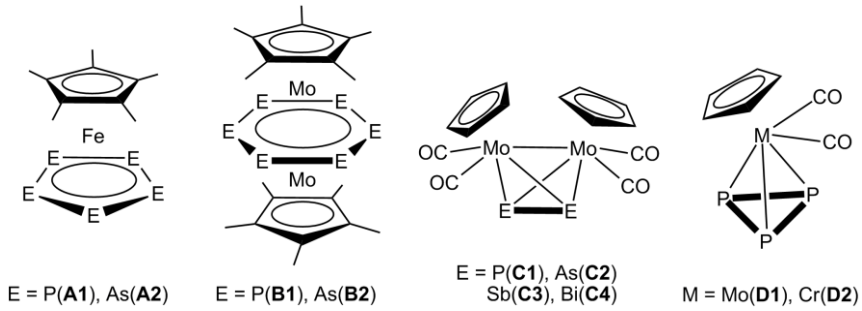

Scheme 4. Representation of selected E_n ligand complexes.

The *cyclo*-E_5 complexes A1 and A2

While numerous complexes containing *cyclo*-E_5 ligands (E = P, As, Sb) have been described in the literature[45,46,47,48,49,50,51,52] the current work is focusing on the ferrocene analogues sandwich complexes of Fe.[53] These complexes $[Cp^*Fe(\eta^5\text{-}E_5)]$ which are obtained from thermolytic reactions[41,42] of $[Cp^*Fe(CO)_2]_2$ with P_4 or As_4 will be referred

to as pentaphosphaferrocene (E = P(**A1**)) and pentaarsaferrocene (E = As(**A2**)) throughout this work.

Reactivity of pentaphosphaferrocene vs. pentaarsaferrocene

Although the chemistry of the *cyclo*-P_5 complex **A1** has been intensely studied during the last decades, a direct comparison of its reactivity towards the As analog **A2** is limited to three examples. It was shown that both *cyclo*-E_5 ligands can act in a bridging η^5:η^5-coordination mode resulting in the formation of the 30 VE (valence electron) triple-decker complexes [Cp*Fe(μ,η^5:η^5-E_5)M(CO)$_3$] (M = Cr, Mo) when reacted with [M(CO)$_3$(MeCN)$_3$] (see Scheme 5 right).[54] Both *cyclo*-E_5 complexes also show similar η^2-coordination by an E-E bond towards the 16 VE complex fragments [Cp*M(CO)] (M = Ir, Rh) (see Scheme 5 left).[55]

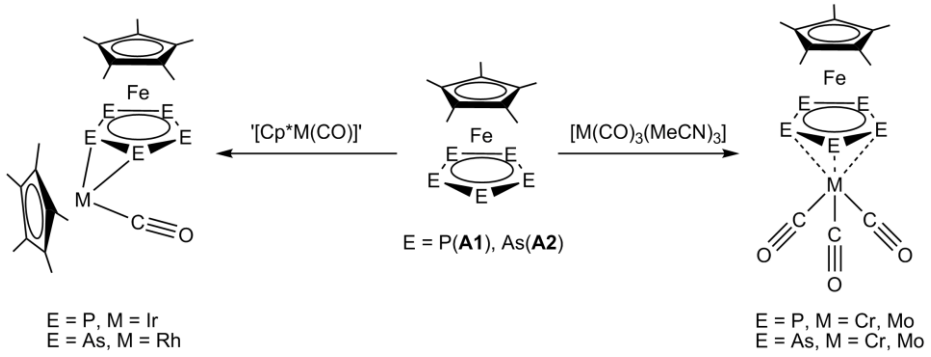

Scheme 5. Similar reactivity of the *cyclo*-E_5 complexes **A1** and **A2** towards 16 VE and 12 VE complex fragments.

However, when **A1** and **A2** are reacted with Cu^I halides, their coordination behavior differs significantly. During the last decade, **A1** has been shown to yield an abundance of one- and two-dimensional coordination polymers.[56,57] Additionally, from these reactions spherical[58,59,60,61,62,63] and capsule-like[64] supramolecules can be isolated, resembling the topology of fullerenes with five-membered *cyclo*-P_5 ligands and six-membered Cu_2P_4 rings illustrated in Scheme 6. The use of Cp ligands with higher steric demand like Cp^{Bn} (=C_5Bn_5)[65] and Cp^{BIG} (=C_5(4-^{n}Bu-C_6H_4)$_5$)[66] gave access to even lager and well soluble related supramolecules.[67,68,69,70] For similar reactions of [Cp*Fe(η^5-As_5)] (**A2**) with Cu^I halides, only the formation of one-dimensional coordination polymers was observed so far (see Scheme 6). For all Cu^I complexes σ coordination of **A1** via the lone pairs of the P atoms is preferred, while **A2** prefers a π donation via As-As bonds. Very recently, the reaction of **A1** with the planar trinuclear macrocycle [Cu{3,5-(CF$_3$)$_2$Pz}]$_3$ (Pz = pyrazolate, [N_2C_3H-3,5(CF$_3$)$_2$]$^-$) was reported, yielding a new coordination compound in which the *cyclo*-P_5 ligand is bridging two of the three Cu centers in a η^2:η^2-coordination mode.[71] This π coordination results in a folding of the

initially planar Cu_3 macrocycle of 89° across the Cu-Cu axis of the coordinated Cu atoms. It was shown that the *cyclo*-P_5 ligand simultaneously acts as an electron donor, as well as an electron acceptor towards Cu in this complex. The electron acceptor properties of the *cyclo*-P_5 complex **A1** have been demonstrated extensively by reactions with anionic nucleophiles.[72]

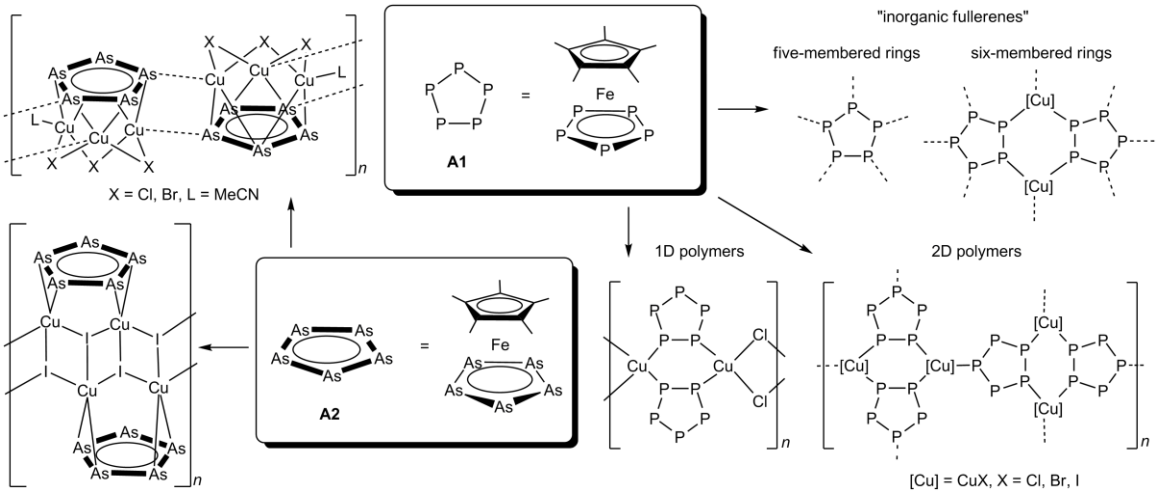

Scheme 6. Reactivity of **A1** and **A2** towards Cu^{I} halides.

Reactivity of A1 and A2 towards monovalent metal cations

Reactions of **A1** and coinage metal cations with small anions like halides, $[BF_4]^-$ or $[PF_6]^-$ often lead to precipitation of the poorly soluble products,[73] which limits further characterization. Previous results demonstrated, that reacting **A1** with Ag[TEF] instead, leads to a well soluble compound which forms a one-dimensional coordination polymer (see Scheme 7 **IV**) exhibiting a bridging 1,2,3-η^2:η^1-coordination mode of the *cyclo*-P_5 ligand in the solid state.[74] Very recently, the reactivity of **A1** towards 'naked' Cu^+ could be investigated.[75] Although the reaction yields a one-dimensional coordination polymer as well, the connectivity inside the chains differs significantly from its Ag^+ analog. While three complexes **A1** are bridging two Cu^+ cations in a 1,2-η^1:η^1-coordination mode to form a paddle-wheel unit, these units are further interconnected by one additional complex **A1** in a bridging 1,3-η^1:η^1-mode (see Scheme 7 **III**). For this compound the exchange of the anion [TEF] for [FAl] does not significantly change the arrangement in the solid state, but this way a satisfactory single crystal X-ray diffraction analysis can be performed. Although being polymeric in nature, these compounds are very well soluble, even in weakly donating solvents like CH_2Cl_2 and were characterized in solution. In case of $[Cp^{BIG}Fe(\eta^5\text{-}P_5)]$ and Ag[TEF] a one-dimensional coordination polymer with bridging σ-1,3-coordination mode of the *cyclo*-P_5 ligand is observed in the solid state.[66] Preliminary investigations showed

that introduction of organic linker molecules to these dynamic coordination compounds also give access to organometallic-organic hybrid materials containing the *cyclo*-P_5 complex **A1**.[76,77] Recently, it was also demonstrated that reactions of [$Cp^{Bn}Fe(\eta^5\text{-}P_5)$] and Ag^+ salts containing the small anions $[BF_4]^-$ or $[CF_3SO_3]^-$ also lead to spherical supramolecules comparable to their Cu^I halide congeners.[78]

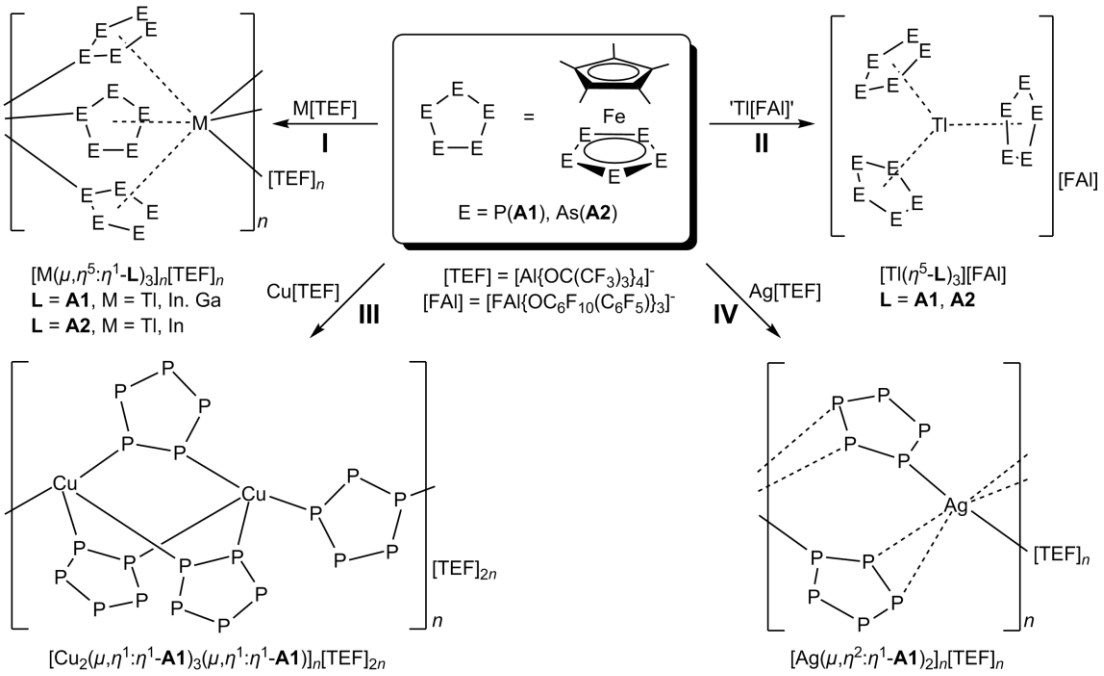

Scheme 7. Reactivity of the *cyclo*-E_5 complexes **A1** and **A2** towards the monovalent cations Ag^+, Cu^+, Tl^+, In^+ and Ga^+.

By using the WCA [TEF], the coordination chemistry of E_n ligand complexes could successfully be extended to the monovalent group 13 cations Tl^+, In^+ and Ga^+.[76] Reactions of Tl^+ and In^+ with **A1** and **A2** lead to the formation of isostructural one-dimensional coordination polymers exhibiting a unique bridging η^5:η^1-coordination mode of the *cyclo*-E_5 complexes with very weak σ interactions (see Scheme 7 **I**).[79,80] By exchanging the WCA [TEF] for the even larger [FAl] in reactions of **A1** and **A2** with 'in situ' generated Tl[FAl] it was demonstrated that these coordination polymers can be separated into isolated $[Tl(\eta^5\text{-}\mathbf{L})_3]^+$ (**L** = **A1**, **A2**) complex cations (see Scheme 7 **II**).[80,75] The first Ga^I compound of P_n ligand complexes which is isostructural to its Tl^I and In^I congeners can be obtained from the reaction of Ga^+ and **A1**, while only the formation of a dark precipitate is observed when the *cyclo*-As_5 complex **A2** is reacted with Ga^+.[80]

Redox chemistry of A1

The redox chemistry of **A1** was studied by electrochemical methods in 1999 showing both, irreversible one-electron oxidation and reduction.[81] In the same publication a dimerization was proposed for the resulting 17 VE cation (oxidation) and for the 19 VE anion (reduction), respectively. In 2013, these dimerized products and also the dianionic doubly reduced **A1** $[Cp^*Fe(\eta^4\text{-}P_5)]^{2-}$ could be isolated and fully characterized including their structural determination illustrated in Scheme 8.[82] Reduction of the *cyclo*-P_5 complex **A1** could also be realized by reactions with divalent lanthanide complexes leading to mixed d/f-triple-decker complexes[83] or reductive P-P bond formation.[84]

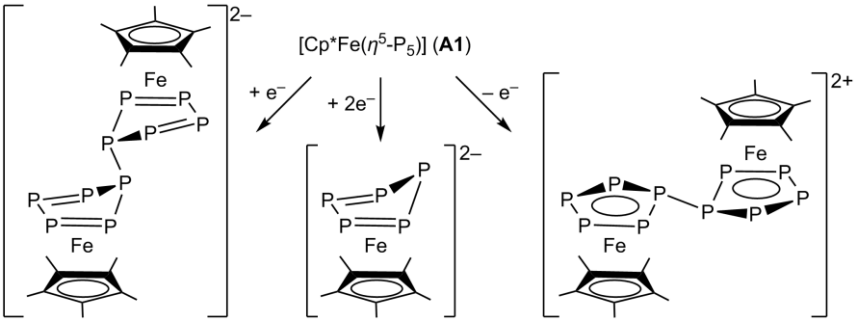

Scheme 8. Redox chemistry of **A1**.

The *cyclo*-E_6 complexes B1 and B2

While *cyclo*-P_6 triple-decker complexes are known for Ti, Nb, V, W and Mo, only the group 6 metal complexes of W and Mo exhibit perfectly hexagonal planar P_6 rings.[85,86,87,88,89] Up to this date the isolation of a *cyclo*-P_6 end deck ligand has not been reported. The current work is focusing on the Mo triple-decker complex **B1** which is obtained from a thermolytic reaction of $[Cp^*Mo(CO)_2]_2$ and P_4 in 1% yield after separation from several side-products described in 1985.[43] Most probably, due to the low yield as well as the need for chromatographic workup, no studies of its reactivity were published during the last 30 years. The analogues *cyclo*-As_6 complex **B2** was isolated in 1989.[44]

The tetrahedrane complexes C1-C4, D1 and D2

The E_2 complexes **C1**-**C3** are obtained in thermolytic reactions of $[CpMo(CO)_{2/3}]_2$ with P_4, $(AsC_6H_5)_6$, As_4S_4, grey As, grey Sb or *cyclic* $[Sb^tBu]_4$.[90,91,92,93,94,95] The *cyclo*-P_3 complex **D1** is formed in the same reaction with P_4. The Bi_2 complex **C4** is obtained in a two-step reaction (see Scheme 9).[96,97] At first, $[Bi\{MoCp(CO)_3\}_3]$ is formed from $BiCl_3$ and $Na[MoCp(CO)_3]$. Under photolytic activation, this complex releases $[CpMo(CO)_3]_2$ and CO under formation of the desired tetrahedrane complex **C4**.

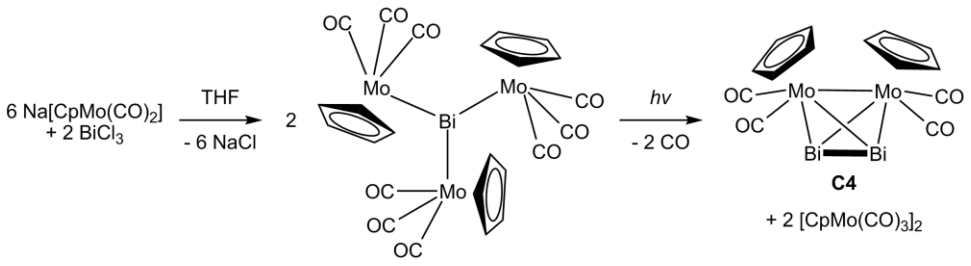

Scheme 9. Synthesis of the Bi_2 complex **C4**.

Reactions of the P_2 complex **C1** with Cu^I halides lead to one-dimensional polymers exhibiting six-membered Cu_2P_4 rings.[98,99,100] Similar reactions of the Sb_2 complex **C3** with CuX lead to dimeric species for X = Cl, Br and also a polymeric compound for X = I.[95] When **C3** is reacted with $Cu[GaCl_4]$ instead, the dicationic complex cation $[Cu(\mathbf{C3})_4]^{2+}$ containing a Cu_2-dumbbell is obtained.[95]

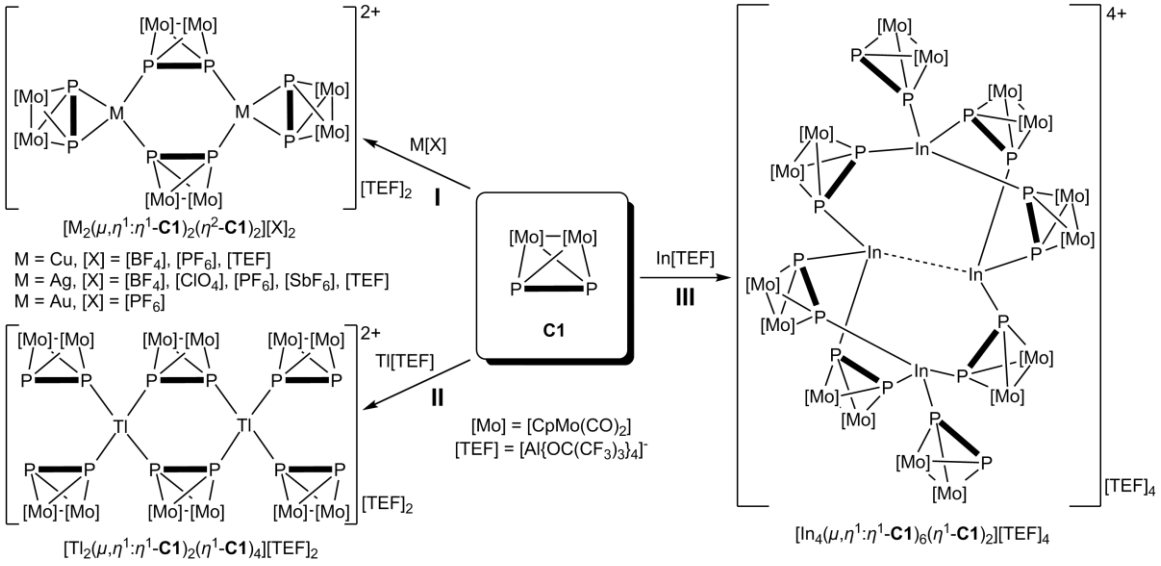

Scheme 10. Reactivity of the P_2 complex **C1** towards M^+ cations.

When the P_2 complex **C1** was reacted with coinage metal salts of different WCAs the formation of the dinuclear complex $[M_2(\mu,\eta^1\text{:}\eta^1\text{-}\mathbf{C1})_2(\eta^2\text{-}\mathbf{C1})_2]^{2+}$ (M = Cu, Ag, Au) exhibiting a central six-membered M_2P_4 ring has been observed regularly (see Scheme 10 **I**).[100,75] The introduction of organic linker molecules to these coordination compounds gave also access to organometallic-organic hybrid materials.[101,102,103] The reaction of **C1** and Tl[TEF] leads to the formation of a related dinuclear complex $[Tl_2(\mu,\eta^1\text{:}\eta^1\text{-}\mathbf{C1})_2(\eta^1\text{-}\mathbf{C1})_4]^{2+}$ featuring a central six-membered Tl_2P_4 ring, exhibiting four instead of two terminally bound ligands **C1** (see Scheme 10 **II**). The analogues In[TEF] salt enables the isolation of an unprecedented tetranuclear

complex $[In_4(\mu,\eta^1\text{-}\mathbf{C1})_6(\eta^1\text{-}\mathbf{C1})_2]^{4+}$ exhibiting a weak In^I-In^I interaction (see Scheme 10 **III**).[15]

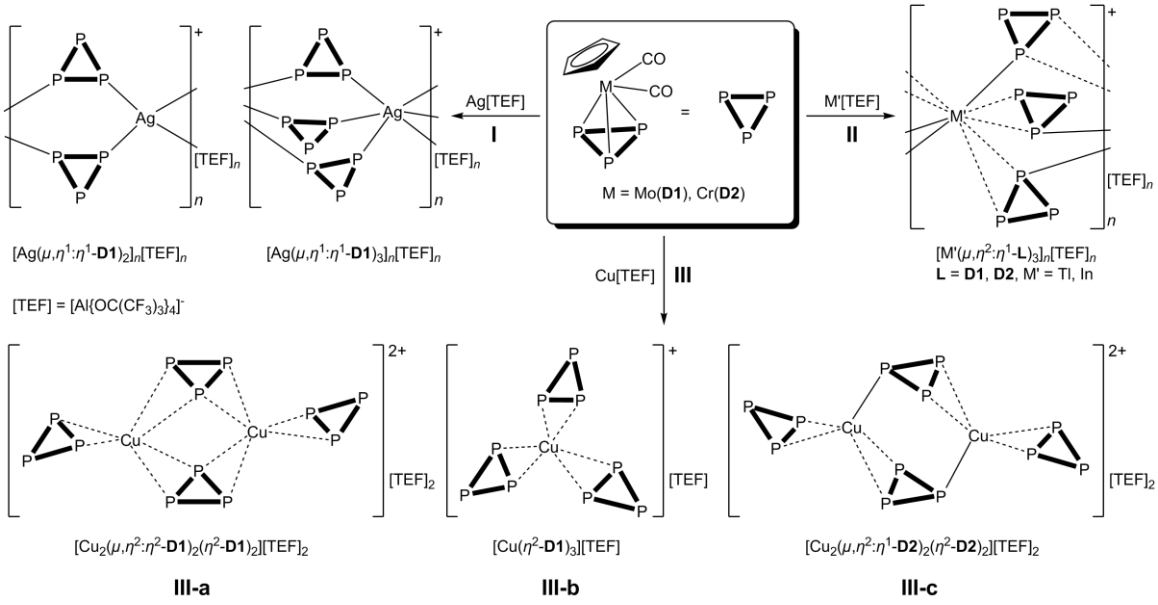

Scheme 11. Reactivity of the *cyclo*-P_3 complexes **D1** and **D2** towards the monovalent cations Ag^+, In^+, Tl^+ and Cu^+.

Reactions of the *cyclo*-P_3 complexes **D1** or **D2** with Ag^+, In^+ or Tl^+ salts of the WCA [TEF] lead to well soluble compounds showing highly dynamic coordination behavior in solution, although they form one-dimensional coordination polymers in the solid state (see Scheme 11 **I**, **II**). While Ag[TEF] forms polymers with **D1** in different molar ratios (2:1 and 3:1), reactions of the group 13 cations In^+ and Tl^+ exclusively yield four isostructural polymers with a molar ratio of 3:1 (see Scheme 11 **II**). The *cyclo*-P_3 ligand **D1** exhibits a bridging σ-1,2-coordination mode in both Ag^+ compounds, while for In^+ and Tl^+ in contrast, **D1** and **D2** show a mixed σ and π coordination inside the one-dimensional coordination polymers.[104] Very recently, our group could also investigate reactions of the *cyclo*-P_3 complexes **D1** and **D2** towards 'naked' Cu^+ with the help of the WCA [TEF] (see Scheme 11 **III**).[75] Although the formed compounds are well soluble and show a similar highly dynamic coordination behavior in solution like their Ag^+ analogs, the determined solid state structures differ significantly from the Ag^+ containing coordination polymers. In case of the *cyclo*-P_3 complex **D1** the formation of the dinuclear complex **III-a** and also the mononuclear complex **III-b** is observed. By adjusting the molar ratios of the reactants with an excess of **D1** or Cu^+ respectively, **III-a** or **III-b** can be obtained selectively as the only product. In contrast, the reaction of **D2** and Cu^+ always leads to the dinuclear complex **III-c** regardless of the used ratios. The complexes **III-a** and **III-c** are closely related. However, in **III-a** the *cyclo*-P_3 complex **D1** is bridging the two Cu^+ cations in a η^2:η^2-coordination mode, while

in **III-c** the *cyclo*-P_3 complex **D2** exhibits a η^2:η^1-coordination mode. Interestingly, the arrangements of the *cyclo*-P_3 complexes and the metal cations found for the complexes **III-a** - **III-c** in the solid state are predicted to be present in solution of the related Ag^+ complexes by DFT methods (density functional theory). Therefore, these structures are proposed to be snapshots of species present in solution of the related Ag^+ complexes.

1.3 Trimeric (perfluoro-*ortho*-phenylene)mercury — an unusual Lewis acid

The first organomercurials were prepared by *Frankland et al.* more than 150 years ago.[105,106] Although, their chemistry is extensively studied and they are less sensitive to air and moisture than most organometallic reagents, their applications have been drastically reduced due to their high toxicity.[107,108] This work includes the investigation of trimeric (perfluoro-*ortho*-phenylene)mercury. The chemistry of this unusual Lewis acid has been the topic of two review articles.[109,110] This planar trinuclear organomercurial is obtained in a very simple two-step decarboxylation of Hg^{II}(tetrafluorophtalate) illustrated in Scheme 12.[111] While the first decarboxylation yields a supposed trimeric or polymeric compound, the second decarboxylation results exclusively in the formation of the desired trinuclear Lewis acid which is obtained in analytical purity upon sublimation under constantly reduced pressure at ~300 °C.

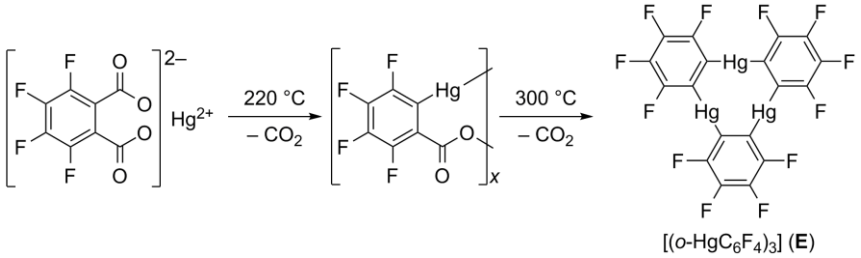

Scheme 12. Two-step decarboxylation of Hg^{II}(tetrafluorophtalate).

Due to its planar geometry this molecule contains three sterically accessible mercury centers, whose naturally low Lewis acidity is significantly increased by the fluorinated molecular backbone. DFT calculations show that the lowest unoccupied molecular orbital (LUMO) of [(*o*-$HgC_6F_4)_3$] (**E**) is situated in the center of the molecule with large contributions (44%) of the 6p orbitals of the Hg atoms.[112] In agreement with the position of the LUMO, **E** forms weak Lewis acid/base adducts with a variety of O, N and S donors as well as anions which simultaneously interact with all three Hg atoms (see Scheme 13 **I**).[113,110,114] However, these interactions are very weak and the high

energy of the LUMO (HOMO-LUMO gap ~3.357 eV) renders a population by electron donation of the Lewis base uncertain in these adducts. In accordance with this, no electrochemical reduction of **E** is observed in the solvent window of THF.[112]

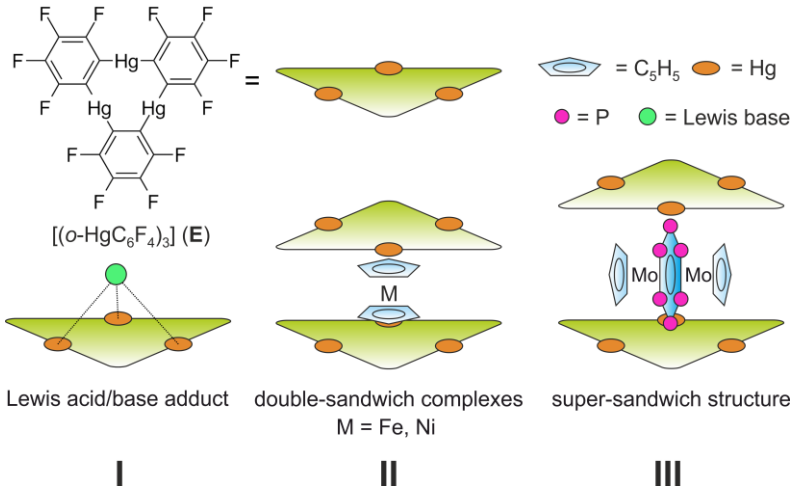

Scheme 13. Reactivity of [(*o*-$HgC_6F_4)_3$] (**E**) forming Lewis acid/base adducts (**I**), double-sandwich complexes with metallocenes Cp_2M (**II**) and super-sandwich compounds with $[(CpMo)_2(\mu,\eta^6{:}\eta^6\text{-}P_6)]$ (**III**).

Although these weak adducts may only arise from electrostatic and dispersion forces one can for example record a significant decrease (33 cm^{-1}) of the CO stretching frequency in the IR spectrum of the acetone adduct [E●(acetone)] compared to neat acetone.[115] Some additional evidence for the good interaction with organic carbonyls is the quantitative shift of the keto-enol-equilibrium of acetylacetone to the less stable keto form in the crystal lattice formed from CH_2Cl_2 solution by simultaneous bonding to two molecules of **E**.[116] The bonding between Lewis bases and **E** is significantly strengthened by cooperative effects arising from three simultaneous interactions with the Hg centers. In addition, **E** readily builds up alternating binary stacks with aromatic hydrocarbons.[117,118,119,120] By the formation of adducts with coranulenes it could be shown that this interaction of the mercury Lewis acid is not strictly limited to planar hydrocarbons.[121] Finally, it was demonstrated that **E** forms double-sandwich complexes featuring Hg···Cp interactions when reacted with the metallocenes Cp_2Fe and Cp_2Ni (see Scheme 13 **II**).[122] During the last years this chemistry was successfully extended to polyphosphorus complexes. It was proven that despite of their noted weakness, only P···Hg interactions are observed instead of potential Hg···Cp interactions in the reactions of **E** and the *cyclo*-P_6 triple-decker complex $[(CpMo)_2(\mu,\eta^6{:}\eta^6\text{-}P_6)]$ (Scheme 13 **III**).[123] A very recent study of the four structurally characterized polymorphs[124] of **E** claims that the solid state structures are mainly stabilized by Hg···C, C···C, F···C and Hg···F interactions, while the contribution of

mercuriophilic and F···F interactions can be neglected.[125] Similar observations are reported for adducts of **E**.

In addition to its chemical reactivity, the trinuclear Lewis acid **E** and its hydrogen substituted analog[126] [(*o*-$HgC_6H_4)_3$] were investigated in a joint research project by atomic force microscopy and scanning tunneling microscopy adsorbed on a clean Cu(111) surface by *Florian Albrecht* under the supervision of *Jascha Repp* of the surface physics department of the University of Regensburg.[127]

1.4 References

[1] M. R. Rosenthal, *J. Chem. Educ.* **1973**, *50*, 331-335.
[2] S. H. Strauss, *Chem. Rev.* **1993**, *93*, 927-942.
[3] I. Krossing, I. Raabe, *Angew. Chem. Int. Ed.* **2004**, *43*, 2066-2090; *Angew. Chem.* **2004**, *116*, 2116-2142.
[4] N. Trapp, I. Krossing, *Nachrichten aus der Chemie* **2009**, *57*, 632-637.
[5] C. A. Reed, *Acc. Chem. Res.* **1998**, *31*, 133-139.
[6] M. Gerken, P. Kolb, A. Wegner, H. P. A. Mercier, H. Borrmann, D. A. Dixon, G. J. Schrobilgen, *Inorg. Chem.* **2000**, *39*, 2813-2824.
[7] W. J. Casteel, P. Kolb, N. LeBlond, H. P. A. Mercier, G. J. Schrobilgen, *Inorg. Chem.* **1996**, *35*, 929-942.
[8] S. M. Ivanova, B. G. Nolan, Y. Kobayashi, S. M. Miller, O. P. Anderson, S. H. Strauss, *Chem. Eur. J.* **2001**, *7*, 503-510.
[9] I. Krossing, *Chem. Eur. J.* **2001**, *7*, 490-502.
[10] T. Köchner, N. Trapp, T. A. Engesser, A. J. Lehner, C. Röhr, S. Riedel, C. Knapp, H. Scherer, I. Krossing, *Angew. Chem. Int. Ed.* **2011**, *50*, 11253-11256; *Angew. Chem.* **2011**, *123*, 11449-11452.
[11] G. Santiso-Quiñones, R. Brückner, C. Knapp, I. Dionne, J. Passmore, I. Krossing, *Angew. Chem. Int. Ed.* **2009**, *48*, 1133-1137; *Angew. Chem.* **2009**, *121*, 1153-1157.
[12] G. Santiso-Quiñones, A. Reisinger, J. Slattery, I. Krossing, *Chem. Commun.* **2007**, 5046-5048.
[13] G. Santiso-Quiñones, A. Higelin, J. Schaefer, R. Brückner, C. Knapp, I. Krossing, *Chem. Eur. J.* **2009**, *15*, 6663-6677.
[14] M. Gonsior, I. Krossing, N. Mitzel, *Z. Anorg. Allg. Chem.* **2002**, *628*, 1821-1830.
[15] S. Welsch, M. Bodensteiner, M. Dušek, M. Sierka, M. Scheer, *Chem. Eur. J.* **2010**, *16*, 13041-13045.
[16] A. Higelin, U. Sachs, S. Keller, I. Krossing, *Chem. Eur. J.* **2012**, *18*, 10029-10034.
[17] J. M. Slattery, A. Higelin, T. Bayer, I. Krossing, *Angew. Chem. Int. Ed.* **2010**, *49*, 3228-3231; *Angew. Chem.* **2010**, *122*, 3297-3301.
[18] A. Decken, C. Knapp, G. B. Nikiforov, J. Passmore, J. M. Rautiainen, X. Wang, X. Zeng, *Chem. Eur. J.* **2009**, *15*, 6504-6517.
[19] A. Bihlmeier, M. Gonsior, I. Raabe, N. Trapp, I. Krossing, *Chem. Eur. J.* **2004**, *10*, 5041-5051.
[20] L. Dütsch, Master's thesis, Universität Regensburg (Regensburg), **2015**.
[21] I. Krossing, A. Bihlmeier, I. Raabe, N. Trapp, *Angew. Chem. Int. Ed.* **2003**, *42*, 1531-1534; *Angew. Chem.* **2003**, *115*, 1569-1572.
[22] M. Gonsior, I. Krossing, L. Müller, I. Raabe, M. Jansen, L. van Wüllen, *Chem. Eur. J.* **2002**, *8*, 4475-4492.
[23] T. Köchner, S. Riedel, A. J. Lehner, H. Scherer, I. Raabe, T. A. Engesser, F. W. Scholz, U. Gellrich, P. Eiden, R. A. Paz Schmidt, D. A. Plattner, I. Krossing, *Angew. Chem. Int. Ed.* **2010**, *49*, 8139-8143; *Angew. Chem.* **2010**, *122*, 8316-8320.
[24] T. Köchner, T. A. Engesser, H. Scherer, D. A. Plattner, A. Steffani, I. Krossing, *Angew. Chem. Int. Ed.* **2012**, *51*, 6529-6531; *Angew. Chem.* **2012**, *124*, 6635-6637.
[25] T. S. Cameron, A. Decken, I. Dionne, M. Fang, I. Krossing, J. Passmore, *Chem. Eur. J.* **2002**, *8*, 3386-3401.
[26] I. Krossing, L. van Wüllen, *Chem. Eur. J.* **2002**, *8*, 700-711.
[27] C. Schwarzmaier, M. Sierka, M. Scheer, *Angew. Chem. Int. Ed.* **2013**, *52*, 858-861; *Angew. Chem.* **2013**, *125*, 891-894.

[28] A. Reisinger, N. Trapp, I. Krossing, S. Altmannshofer, V. Herz, M. Presnitz, W. Scherer, *Angew. Chem. Int. Ed.* **2007**, *46*, 8295-8298; *Angew. Chem.* **2007**, *119*, 8445-8449.

[29] D. Aris, J. Beck, A. Decken, I. Dionne, J. Schmedt auf der Gunne, W. Hoffbauer, T. Kochner, I. Krossing, J. Passmore, E. Rivard, F. Steden, X. Wang, *Dalton Trans.* **2011**, *40*, 5865-5880.

[30] J. Schaefer, A. Steffani, D. A. Plattner, I. Krossing, *Angew. Chem. Int. Ed.* **2012**, *51*, 6009-6012; *Angew. Chem.* **2012**, *124*, 6112-6115.

[31] P. J. Malinowski, I. Krossing, *Angew. Chem. Int. Ed.* **2014**, *53*, 13460-13462; *Angew. Chem.* **2014**, *126*, 13678-13680.

[32] A. Higelin, S. Keller, C. Göhringer, C. Jones, I. Krossing, *Angew. Chem. Int. Ed.* **2013**, *52*, 4941-4944; *Angew. Chem.* **2013**, *125*, 5041-5044.

[33] M. R. Lichtenthaler, F. Stahl, D. Kratzert, L. Heidinger, E. Schleicher, J. Hamann, D. Himmel, S. Weber, I. Krossing, *Nat. Commun.* **2015**, DOI: 10.1038/ncomms9288.

[34] D. Kratzert, J. J. Holstein, I. Krossing, *J. Appl. Crystallogr.* **2015**, *48*, 933-938.

[35] O. J. Scherer, *Chem. unserer Zeit* **2000**, *34*, 374-381.

[36] O. J. Scherer, *Acc. Chem. Res.* **1999**, *32*, 751-762.

[37] O. J. Scherer, *Angew. Chem. Int. Ed. Engl.* **1990**, *29*, 1104-1122; O. J. Scherer, *Angew. Chem.* **1990**, *102*, 1137-1155.

[38] B. M. Cossairt, N. A. Piro, C. C. Cummins, *Chem. Rev.* **2010**, *110*, 4164-4177.

[39] M. Caporali, L. Gonsalvi, A. Rossin, M. Peruzzini, *Chem. Rev.* **2010**, *110*, 4178-4235.

[40] R. Hoffmann, *Angew. Chem. Int. Ed. Engl.* **1982**, *21*, 711-724; *Angew. Chem.* **1982**, *94*, 725-739.

[41] O. J. Scherer, T. Brück, *Angew. Chem. Int. Ed.* **1987**, *26*, 59-59; O. J. Scherer, T. Brück, *Angew. Chem.* **1987**, *99*, 59-59.

[42] O. J. Scherer, C. Blath, G. Wolmershäuser, *J. Organomet. Chem.* **1990**, *387*, C21-C24.

[43] O. J. Scherer, H. Sitzmann, G. Wolmershäuser, *Angew. Chem. Int. Ed.* **1985**, *24*, 351-353; *Angew. Chem.* **1985**, *97*, 358-359.

[44] O. J. Scherer, H. Sitzmann, G. Wolmershäuser, *Angew. Chem. Int. Ed.* **1989**, *28*, 212-213; *Angew. Chem.* **1989**, *101*, 214-215.

[45] O. J. Scherer, J. Schwalb, G. Wolmershäuser, W. Kaim, R. Gross, *Angew. Chem. Int. Ed.* **1986**, *25*, 363-364; *Angew. Chem.* **1986**, *98*, 349-350.

[46] O. J. Scherer, W. Wiedemann, G. Wolmershäuser, *J. Organomet. Chem.* **1989**, *361*, C11-C14.

[47] O. J. Scherer, W. Wiedemann, G. Wolmershäuser, *Chem. Ber.* **1990**, *123*, 3-6.

[48] B. Rink, O. J. Scherer, G. Wolmershäuser, *Chem. Ber.* **1995**, *128*, 71-73.

[49] H. J. Breunig, N. Burford, R. Rösler, *Angew. Chem. Int. Ed.* **2000**, *39*, 4148-4150; *Angew. Chem.* **2000**, *112*, 4320-4322.

[50] E. Urne˙žius, W. W. Brennessel, C. J. Cramer, J. E. Ellis, P. v. R. Schleyer, *Science* **2002**, *295*, 832-834.

[51] A. L. Rheingold, M. J. Foley, P. J. Sullivan, *J. Am. Chem. Soc.* **1982**, *104*, 4727-4729.

[52] B. M. Gardner, F. Tuna, E. J. L. McInnes, J. McMaster, W. Lewis, A. J. Blake, S. T. Liddle, *Angew. Chem. Int. Ed.* **2015**, *54*, 7068-7072; *Angew. Chem.* **2015**, *127*, 7174-7178.

[53] K. B. Dillon, F. Mathey, J. F. Nixon, *Phosphorus: the carbon copy: from organophosphorus to phospha-organic chemistry, Vol. 1*, Wiley, Toronto, **1998**.

[54] B. Rink, O. J. Scherer, G. Heckmann, G. Wolmershauser, *Chem. Ber.* **1992**, *125*, 1011-1016.

[55] M. Detzel, G. Friedrich, O. J. Scherer and G. Wolmershäuser, *Angew. Chem. Int. Ed.*, 1995, **34**, 1321-1323; *Angew. Chem.* **1995**, *107*, 1454-1456.

[56] J. Bai, A. V. Virovets, M. Scheer, *Angew. Chem. Int. Ed.* **2002**, *41*, 1737-1740; *Angew. Chem.* **2002**, *114*, 1808-1811.

[57] F. Dielmann, A. Schindler, S. Scheuermayer, J. Bai, R. Merkle, M. Zabel, A. V. Virovets, E. V. Peresypkina, G. Brunklaus , H. Eckert, M. Scheer, *Chem. Eur. J.* **2012**, *18*, 1168-1179.

[58] J. Bai, A. V. Virovets, M. Scheer, *Science* **2003**, *300*, 781-783.

[59] M. Scheer, J. Bai, B. P. Johnson, R. Merkle, A. V. Virovets, C. E. Anson, *Eur. J. Inorg. Chem.* **2005**, *2005*, 4023-4026.

[60] M. Scheer, A. Schindler, C. Gröger, A. V. Virovets, E. V. Peresypkina, *Angew. Chem. Int. Ed.* **2009**, *48*, 5046-5049; *Angew. Chem.* **2009**, *121*, 5148-5151.

[61] M. Scheer, A. Schindler, J. Bai, B. P. Johnson, R. Merkle, R. Winter, A. V. Virovets, E. V. Peresypkina, V. A. Blatov, M. Sierka, H. Eckert, *Chem. Eur. J.* **2010**, *16*, 2092-2107.

[62] A. Schindler, C. Heindl, G. Balázs, C. Gröger, A. V. Virovets, E. V. Peresypkina, M. Scheer, *Chem. Eur. J.* **2012**, *18*, 829-835.

[63] C. Schwarzmaier, A. Schindler, C. Heindl, S. Scheuermayer, E. V. Peresypkina, A. V. Virovets, M. Neumeier, R. Gschwind, M. Scheer, *Angew. Chem. Int. Ed.* **2013**, *52*, 10896-10899; *Angew. Chem.* **2013**, *125*, 11097-11100.
[64] S. Welsch, C. Gröger, M. Sierka, M. Scheer, *Angew. Chem. Int. Ed.* **2011**, *50*, 1435-1438; *Angew. Chem.* **2011**, *123*, 1471-1474.
[65] F. Dielmann, R. Merkle, S. Heinl, M. Scheer, *Z.Naturforsch.* **2009**, *64b*, 3-10.
[66] C. Heindl, S. Heinl, D. Lüdeker, G. Brunklaus, W. Kremer, M. Scheer, *Inorg. Chim. Acta* **2014**, *422*, 218-223.
[67] F. Dielmann, C. Heindl, F. Hastreiter, E. V. Peresypkina, A. V. Virovets, R. M. Gschwind, M. Scheer, *Angew. Chem. Int. Ed.* **2014**, *53*, 13605-13608; *Angew. Chem.* **2014**, *126*, 13823-13827.
[68] F. Dielmann, M. Fleischmann, C. Heindl, E. V. Peresypkina, A. V. Virovets, R. M. Gschwind, M. Scheer, *Chem. Eur. J.* **2015**, *21*, 6208-6214.
[69] S. Heinl, PhD-thesis, Universität Regensburg (Regensburg), **2014**.
[70] C. Heindl, PhD-thesis, Universität Regensburg (Regensburg), **2015**.
[71] O. A. Filippov, A. A. Titov, E. A. Guseva, D. A. Loginov, A. F. Smol'yakov, F. M. Dolgushin, N. V. Belkova, L. M. Epstein, E. S. Shubina, *Chem. Eur. J.* **2015**, *21*, 13176–13180.
[72] E. Mädl, M. V. Butovskii, G. Balázs, E. V. Peresypkina, A. V. Virovets, M. Seidl, M. Scheer, *Angew. Chem. Int. Ed.* **2014**, *53*, 7643-7646; *Angew. Chem.* **2014**, *126*, 7774-7777.
[73] M. Scheer, *Dalton Trans.* **2008**, 4372-4386.
[74] M. Scheer, L. J. Gregoriades, A. V. Virovets, W. Kunz, R. Neueder, I. Krossing, *Angew. Chem. Int. Ed.* **2006**, *45*, 5689-5693; *Angew. Chem.* **2006**, *118*, 5818-5822.
[75] M. Fleischmann, S. Welsch, E. V. Peresypkina, A. V. Virovets, M. Scheer, *Chem. Eur. J.* **2015**, *21*, 14332-14336.
[76] S. Welsch, PhD-thesis, Universität Regensburg (Regensburg), **2010**.
[77] M. Scheer, unpublished results.
[78] B. Krämer, Master's thesis, Universität Regensburg (Regensburg), **2014**.
[79] S. Welsch, L. J. Gregoriades, M. Sierka, M. Zabel, A. V. Virovets, M. Scheer, *Angew. Chem. Int. Ed.* **2007**, *46*, 9323-9326; *Angew. Chem.* **2007**, *119*, 9483-9487.
[80] M. Fleischmann, S. Welsch, H. Krauss, M. Schmidt, M. Bodensteiner, E. V. Peresypkina, M. Sierka, C. Gröger, M. Scheer, *Chem. Eur. J.* **2014**, *20*, 3759-3768.
[81] R. F. Winter, W. E. Geiger, *Organometallics* **1999**, *18*, 1827-1833.
[82] M. V. Butovskiy, G. Balázs, M. Bodensteiner, E. V. Peresypkina, A. V. Virovets, J. Sutter, M. Scheer, *Angew. Chem. Int. Ed.* **2013**, *52*, 2972-2976; *Angew. Chem.* **2013**, *125*, 3045-3049.
[83] T. Li, J. Wiecko, N. A. Pushkarevsky, M. T. Gamer, R. Köppe, S. N. Konchenko, M. Scheer, P. W. Roesky, *Angew. Chem. Int. Ed.* **2011**, *50*, 9491-9495; *Angew. Chem.* **2011**, *123*, 9663-9667.
[84] T. Li, M. T. Gamer, M. Scheer, S. N. Konchenko, P. W. Roesky, *Chem. Commun.* **2013**, *49*, 2183-2185.
[85] O. J. Scherer, H. Swarowsky, G. Wolmershäuser, W. Kaim, S. Kohlmann, *Angew. Chem. Int. Ed.* **1987**, *26*, 1153-1155; *Angew. Chem.* **1987**, *99*, 1178-1179.
[86] O. J. Scherer, J. Schwalb, H. Swarowsky, G. Wolmershäuser, W. Kaim, R. Gross, *Chem. Ber.* **1988**, *121*, 443-449.
[87] A. C. Reddy, E. D. Jemmis, O. J. Scherer, R. Winter, G. Heckmann, G. Wolmershaeuser, *Organometallics* **1992**, *11*, 3894-3900.
[88] O. J. Scherer, J. Vondung, G. Wolmershäuser, *Angew. Chem. Int. Ed.* **1989**, *28*, 1355-1357; *Angew. Chem.* **1989**, *101*, 1395-1397.
[89] M. Herberhold, G. Frohmader, W. Milius, *J. Organomet. Chem.* **1996**, *522*, 185-196.
[90] O. J. Scherer, H. Sitzmann, G. Wolmershäuser, *J. Organomet. Chem.* **1984**, *268*, C9-C12.
[91] P. J. Sullivan, A. L. Rheingold, *Organometallics* **1982**, *1*, 1547-1549.
[92] M. L. Ziegler, K. Blechschmitt, B. Nuber, T. Zahn, *Chem. Ber.* **1988**, *121*, 159-171.
[93] I. Bernal, H. Brunner, W. Meier, H. Pfisterer, J. Wachter, M. L. Ziegler, *Angew. Chem. Int. Ed.* **1984**, *23*, 438-439; *Angew. Chem.* **1984**, *96*, 428-429.
[94] J. R. Harper, A. L. Rheingold, *J. Organomet. Chem.* **1990**, *390*, C36-C38.
[95] H. V. Ly, M. Parvez, R. Roesler, *Inorg. Chem.* **2006**, *45*, 345-351.
[96] W. Clegg, N. A. Compton, R. J. Errington, N. C. Norman, *Polyhedron* **1988**, *7*, 2239-2241.
[97] W. Clegg, N. A. Compton, R. J. Errington, G. A. Fisher, N. C. Norman, T. B. Marder, *J. Chem. Soc., Dalton Trans.* **1991**, 2887-2895.

[98] J. Bai, E. Leiner, M. Scheer, *Angew. Chem. Int. Ed.* **2002**, *41*, 783-786; *Angew. Chem.* **2002**, *114*, 820-823.
[99] M. Scheer, L. J. Gregoriades, J. Bai, M. Sierka, G. Brunklaus, H. Eckert, *Chem. Eur. J.* **2005**, *11*, 2163-2169.
[100] M. Scheer, L. J. Gregoriades, M. Zabel, J. Bai, I. Krossing, G. Brunklaus, H. Eckert, *Chem. Eur. J.* **2008**, *14*, 282-295.
[101] B. Attenberger, PhD-thesis, Universität Regensburg (Regensburg), **2014**.
[102] B. Attenberger, E. V. Peresypkina, M. Scheer, *Inorg. Chem.* **2015**, *54*, 7021-7029.
[103] B. Attenberger, S. Welsch, M. Zabel, E. Peresypkina, M. Scheer, *Angew. Chem., Int. Ed.* **2011**, *50*, 11516; *Angew. Chem.* **2011**, *123*, 11718-11722.
[104] M. Fleischmann, S. Welsch, L. J. Gregoriades, C. Gröger, M. Scheer, *Z. Naturforsch.* **2014**, *69b*, 1348-1356.
[105] E. Frankland, B. F. Duppa, *J. Chem. Soc.* **1863**, *16*, 415-425.
[106] D. Seyferth, *Organometallics* **2001**, *20*, 2940-2955.
[107] C. Elschenbroich, in *Organometallchemie, Vol. 6*, B. G. Teubner Verlag, Wiesbaden, **2008**, pp. 77-83.
[108] A. F. Holleman, E. Wiberg, N. Wiberg, in *Lehrbuch der Anorganischen Chemie, Vol. 102*, Walter de Gruyter, Berlin, **2007**, pp. 1497-1498.
[109] M. R. Haneline, R. E. Taylor, F. P. Gabbaï, *Chem. Eur. J.* **2003**, *9*, 5188-5193.
[110] T. J. Taylor, C. N. Burress, F. P. Gabbaï, *Organometallics* **2007**, *26*, 5252-5263.
[111] P. Sartori, A. Golloch, *Chem. Ber.* **1968**, *101*, 2004-2009.
[112] M. R. Haneline, F. P. Gabbaï, *Inorg. Chem.* **2005**, *44*, 6248-6255.
[113] M. C. Ball, D. S. Brown, A. G. Massey, D. A. Wickens, *J. Organomet. Chem.* **1981**, *206*, 265-277.
[114] M. Tsunoda, F. P. Gabbaï, *J. Am. Chem. Soc.* **2003**, *125*, 10492-10493.
[115] J. B. King, M. R. Haneline, M. Tsunoda, F. P. Gabbaï, *J. Am. Chem. Soc.* **2002**, *124*, 9350-9351.
[116] I. A. Tikhonova, A. A. Yakovenko, K. I. Tugashov, F. M. Dolgushin, V. V. Novikov, M. Y. Antipin, V. B. Shur, *Organometallics* **2006**, *25*, 6155-6158.
[117] M. Tsunoda, F. P. Gabbaï, *J. Am. Chem. Soc.* **2000**, *122*, 8335-8336.
[118] C. N. Burress, M. I. Bodine, O. Elbjeirami, J. H. Reibenspies, M. A. Omary, F. P. Gabbaï, *Inorg. Chem.* **2007**, *46*, 1388-1395.
[119] M. R. Haneline, M. Tsunoda, F. P. Gabbaï, *J. Am. Chem. Soc.* **2002**, *124*, 3737-3742.
[120] I. A. Tikhonova, D. A. Gribanyov, K. I. Tugashov, F. M. Dolgushin, A. S. Peregudov, D. Y. Antonov, V. I. Rosenberg, V. B. Shur, *J. Organomet. Chem.* **2010**, *695*, 1949-1952.
[121] A. S. Filatov, E. A. Jackson, L. T. Scott, M. A. Petrukhina, *Angew. Chem. Int. Ed.* **2009**, *48*, 8473-8476; *Angew. Chem.* **2009**, *121*, 8625-8628.
[122] M. R. Haneline, F. P. Gabbaï, *Angew. Chem., Int. Ed.* **2004**, *43*, 5471-5474; *Angew. Chem.* **2004**, *116*, 5587-5590.
[123] M. Fleischmann, C. Heindl, M. Seidl, G. Balázs, A. V. Virovets, E. V. Peresypkina, M. Tsunoda, F. P. Gabbaï, M. Scheer, *Angew. Chem. Int. Ed.* **2012**, *51*, 9918-9921; *Angew. Chem.* **2012**, *124*, 10056-10059.
[124] M. R. Haneline, F. P. Gabbaï, *Z. Naturforsch.* **2004**, *59b*, 1483-1487.
[125] F. Dolgushin, A. Smol'yakov, K. Suponitsky, A. Vologzhanina, I. Fedyanin, S. Shishkina, *Struct. Chem.* **2015**, 1-13.
[126] G. Wittig, F. Bickelhaupt, *Chem. Ber.* **1958**, *91*, 883-894.
[127] F. Albrecht, J. Repp, M. Fleischmann, M. Scheer, M. Ondráček, P. Jelínek, *Phys. Rev. Lett.* **2015**, *115*, 076101.

2 Research objectives

Coordination chemistry

The current work is focusing on the reactivity of E_n ligand complexes under weakly coordinating conditions. The coordination chemistry of E_n ligand complexes towards monovalent cations should be investigated regarding the nature of the pnictogen atom (P or As) and the impact of the used anions on the assemblies in the solid state. Therefore, the following objectives arise:

- Synthesis of new M^+ salts containing the WCA [FAl]
- Investigation of the coordination chemistry of [Cp*Fe(η^5-E_5)] (E = P, As)
- Investigation of the coordination chemistry of [{CpMo$(CO)_2$}$_2$(μ,η^2:η^2-E_2)] (E = P, As)
- Comparison of the complexes containing [TEF] or [FAl] as the anion
- Investigation of the coordination chemistry of [(Cp*Mo)$_2$(μ,η^6:η^6-P_6)]

Oxidation chemistry

The oxidation chemistry of selected E_n ligand complexes will be investigated under weakly coordinating conditions. In order to accomplish this goal the following steps will be taken:

- Synthesis of new oxidizing agents containing the WCAs [TEF] and [FAl]
- Synthesis and characterization of the single-electron oxidation products of the *cyclo*-E_6 complexes [(Cp^{R}Mo)$_2$(μ,η^6:η^6-E_6)] (E = P, Cp^R = Cp, Cp*, $C_5(CH_2Ph)_5$; E = As, Cp^R = Cp*)
- Selective synthesis and characterization of the single-electron oxidation product of [{CpMo$(CO)_2$}$_2$(μ,η^2:η^2-P_2)]

Reactivity of pre-assemble Cu^I building blocks towards E_n ligand complexes

During this work the coordination chemistry of E_n ligand complexes towards trinuclear Cu^I complexes will be investigated in close collaboration with Dr. Christophe Lescop (Université de Rennes 1). The work on this topic focusses on the complexes [Cu_3(μ-X)$_2$(μ-dpmp)$_2$]$^+$ (X = Cl, Br, I) stabilized by the polyphosphine ligand bis(diphenylphosphinomethyl)phenylphosphine (dpmp). An introduction on this subject is presented at the beginning of the respective chapters. For the systematic investigation of this chemistry the following challenges arise:

- Development of an improved synthesis of the parent trinuclear Cu^{I} complexes $[Cu_3X_2]^+$ based on self-assembly
- Structural characterization of the pre-assemble $[Cu_3X_2]^+$ building blocks in the solid state
- Synthesis of reactive $[Cu_3X_2]^+$ building blocks containing vacant coordination sites
- NMR characterization of the $[Cu_3X_2]^+$ building blocks at variable temperatures
- Investigation of the reactivity towards a variety E_n ligand complexes
- Structural characterization of the obtained products in the solid state

Reactivity of E_n ligand complexes towards the unusual Lewis acid $[(o\text{-}C_6F_4Hg)_3]$

During this work the chemistry of E_n ligand complexes towards the trinuclear Lewis acid (perfluoro-*ortho*-phenylene)mercury should be investigated in collaboration with the group of Prof. Dr. François Gabbaï (Texas A&M University). Previous reports from this group demonstrated the isolation of the first adducts of phosphorus based Lewis bases with this unusual Lewis acid. In order to extend this chemistry based on weak interactions, the following topics have to be investigated:

- Comparison of the interaction with the planar *cyclo*-E_5 ligands of the sandwich complexes $[Cp^*Fe(\eta^5\text{-}E_5)]$
  (E = P, As)
- Reaction with the *cyclo*-P_3 ligand $[CpMo(CO)_2(\eta^3\text{-}P_3)]$
- Synthesis and comparison of the products obtained from reactions with the tetrahedrane complexes $[\{CpMo(CO)_2\}_2(\mu,\eta^2\text{:}\eta^2\text{-}E_2)]$
  (E = P, As, Sb, Bi)

Proceedings of this thesis

In chapter 3 the oxidation and coordination chemistry of the *cyclo*-P_6 complex $[(Cp^*Mo)_2(\mu,\eta^6\text{:}\eta^6\text{-}P_6)]$ is presented. Chapter 4 focusses on the coordination chemistry of the *cyclo*-E_5 complexes $[Cp^*Fe(\eta^5\text{-}E_5)]$ (E = P, As) towards Ag^+. The oxidation and characterization of the tetrahedrane complex $[\{CpMo(CO)_2\}_2(\mu,\eta^2\text{:}\eta^2\text{-}P_2)]$ is reported in chapter 5. The following chapter 6 presents a comparative study of the single-electron oxidation of several *cyclo*-E_6 triple-decker complexes $[(Cp^RMo)_2(\mu,\eta^6\text{:}\eta^6\text{-}E_6)]$ and other E_n ligand complexes. The coordination chemistry of E_n ligand complexes towards pre-assembled trinuclear Cu^{I} complexes is discussed in chapter 7 and 8. Chapter 9 and 10 describe the investigations of the reactivity of E_n ligand complexes towards the unusual trinuclear Lewis acid $[(o\text{-}C_6F_4Hg)_3]$. Finally, chapter 11 contains the thesis treasury and describes additional results which were obtained during the preparation of this work.

Preface

The following chapter has already been published: The article is reprinted with permission of Wiley-VCH. License Number: 3730780905824

English version

Angew. Chem. Int. Ed. **2015**, *54*, 13110-13115.

German version

Angew. Chem. **2015**, *127*, 13303-13308.

Authors

Martin Fleischmann, Fabian Dielmann, Laurence J. Gregoriades, Eugenia V. Peresypkina, Alexander V. Virovets, Sebastian Huber, Alexey Y. Timoshkin, Gábor Balázs and Manfred Scheer*

Author contributions

The preparation and characterization of all compounds including the single crystal X-ray structure determination and the preparation of the manuscript was done by the first author. Among them, the description of compound **6** and preliminary results on the reactivity of **1** with Cu^+ have been part of the Master's thesis. Fabian Dielmann developed and described the high-yield synthesis of **1** in his PhD-thesis. Laurence J. Gregoriades described the reaction of **1** with Ag[TEF] for the first time in his PhD-thesis including the description of the X-ray structure of **4b**. Eugenia V. Peresypkina, and Alexander V. Virovets were significantly involved in the X-ray structural characterization of all compounds and revised the experimental part for the X-ray structural analyses. Sebastian Huber conducted and analyzed the powder XRD measurements of **4a** and **5**. Alexey Y. Timoshkin and Gábor Balázs performed supporting DFT calculations. Manfred Scheer supervised the research and revised the manuscript prior to publication.

Acknowledgements

Arno Pfitzner is acknowledged for use of the X-ray powder diffraction device. Moritz Modl is acknowledged for the measurement of the EPR spectra of **3a** and **3b**. Christian Gröger is acknowledged for measuring the MAS NMR spectra. This work was supported by the Deutsche Forschungsgemeinschaft. The COST action CM1302 SIPs is gratefully acknowledged.

3 Redox and coordination behavior of the hexaphosphabenzene $[(Cp^*Mo)_2(\mu,\eta^6{:}\eta^6\text{-}P_6)]$ towards the "naked" cations Cu^+, Ag^+ and Tl^+

Abstract: Though the *cyclo*-P_6 complex $[(Cp^*Mo)_2(\mu,\eta^6{:}\eta^6\text{-}P_6)]$ (**1**) was reported 30 years ago, little is known about its chemistry. Herein, we report a high-yield synthesis of **1**, the complex **2**, containing an unprecedented *cyclo*-P_{10} ligand and the reactivity of **1** towards the 'naked' cations Cu^+, Ag^+ and Tl^+. Besides the formation of the single oxidation products **3a,b** showing a bis-allylic distorted *cyclo*-P_6 middle-deck the $[M(\mathbf{1})_2]^+$ complexes are described showing distorted square planar (M = Cu(**4a**), Ag(**4b**)) or distorted tetrahedral coordinated (M = Cu(**5**)) M^+ cations. The used solvents enable the control of the reaction outcome for Cu^+ proved by powder XRD and supported by DFT calculations. The reaction with Tl^+ affords a layered two-dimensional coordination network in the solid state.

3.1 Introduction

In 1981, Nobel Laureate Roald Hoffmann described how the isolobal analogy was building bridges between inorganic and organic chemistry.[1] In this context, the isolation of the all-phosphorus analog of one of the most prominent organic molecules – *benzene* – stabilized in the complex $[(Cp^*Mo)_2(\mu,\eta^6{:}\eta^6\text{-}P_6)]$ (**1**) in 1985 by Scherer et al. can be viewed as a milestone in inorganic chemistry.[2] *Cyclo*-P_6 triple-decker complexes have also been described for Ti, V, Nb and W.[3,4,5,6,7] Over the last decade, isolation of inorganic supramolecules resembling fullerenes,[8, 9, 10] was realized by coordination of the *cyclo*-P_5 complexes $[Cp^RFe(\eta^5\text{-}P_5)]$ to Cu^I halides. Intrigued by the idea to interconnect *cyclo*-P_6 complexes **1** to build up a supramolecular inorganic analog of graphene, we decided to investigate the coordination chemistry of **1**. The described yield of **1** after separation from several other products was only 1%, which is probably the reason why no studies on the reactivity of **1** had been carried out over the last 30 years.

3.2 Results and Discussion

Increasing the reaction temperature of the thermolysis of $[Cp^*Mo(CO)_{2/3}]_2$ with P_4 to approximately 205 °C in boiling *di*-isopropylbenzene gives **1** in analytically pure form in an astonishing 64% yield. Additionally, a novel phosphorus rich complex

$[(Cp^*Mo)_2(\mu\text{-}P_{10})]$ (**2**) is obtained in trace amounts in crystalline form during the isolation of **1**.[11] The reaction energy calculated by DFT for the reaction **2** → **1** + P_4 (ΔE = –19.6 kJ mol^{-1}) shows that **1** is the thermodynamic product.[12] The molecular structure of **2** (Figure 1) displays a strongly folded *cyclo*-P_{10} ligand that has four shorter bonds between P1-P2 and P4-P5 with 2.140(2) Å, while the remaining P-P bonds are longer with an average length of 2.2 Å. Therefore, an adequate description of the complex **2** would be a formal *cyclo*-decaphospha-tetraene-diide dianionic P_{10} ligand (Figure ***1*** c) stabilized by two $[Cp^*Mo]^+$ fragments.

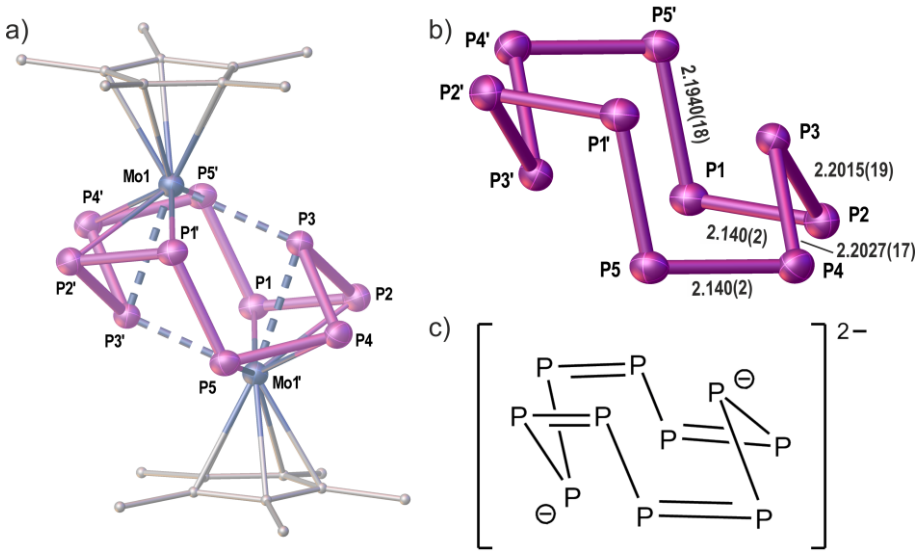

Figure 1. a) Molecular structure of complex **2**. C atoms are depicted as small spheres and H atoms are omitted for clarity. Thermal ellipsoids are drawn at 50% probability. Selected bond lengths [Å]: Mo1-P3 2.4965(15), Mo1-P3' 2.5109(12), b) Illustration of the *cyclo*-P_{10} ligand of **2**. c) Illustration of P_{10}^{2-}.

The polyphosphido ligand binds to each Mo center via a η^2:η^2 mode of the P-P double bonds and by additional η^1 coordination of P3 and P3'. This suggests an oxidation state of +2 for Mo. The Mo-Mo distance of 3.7018(8) Å is too long for any metal-metal interaction. DFT calculations show that Mo engages in a bonding interaction to P3 above as well as to its symmetry equivalent P3' atom through the phosphorus ring with Wiberg bonding indexes (WBI) of 0.70 and 0.76, respectively. The intramolecular P-P distances P2-P4, P3-P1' and P3-P5' are below the sum of the van der Waals radii (~3.13-3.17 Å). The respective WBIs of 0.05 and 0.06 indicate no bonding interactions. The molecular ion peak for $[\mathbf{2}]^+$ at *m*/*z* = 772.0 (g mol^{-1}) was clearly identified next to the peak for $[\mathbf{1}]^+$ at 647.9 (g mol^{-1}) in the EI-MS.

There is a substantial variety of polyphosphorus frameworks containing up to 24 P atoms[13] described in the literature that are stabilized as Zintl anions,[14] by main group substituents,[15,16] or in the coordination sphere of transition metals.[17,18] The unprecedented P_{10}^{2-} ligand of **2** represents the largest polyphosphorus cycle known

so far. The isolobal dianion $C_{10}H_{10}^{2-}$ has been exclusively studied by theoretical methods.[19]

In addition to characterizing complex **2**, we were able to study the reactivity of **1** in detail and initiated these studies with reaction of **1** with M^+ salts (M = Ag, Cu) of the weakly coordinating anion (WCA) $[Al\{OC(CF_3)_3\}_4]^-$ (=[TEF]).[20,21,22] When a CH_2Cl_2 solution of Ag[TEF] or Cu[TEF] is added to a CH_2Cl_2 solution of **1** oxidation takes place which can easily be followed by an immediate color change from light brown to dark teal and the formation of a metal mirror or black precipitate (see Scheme 1). The cyclic voltammogram of **1** shows a reversible oxidation at –0.24 V vs $Cp_2Fe^{0/+}$ while the second oxidation at ~ +0.59 V is irreversible.[23] The ^{1}H NMR spectrum of the paramagnetic complex **3a** in CD_2Cl_2 shows one broad singlet ($\omega_{1/2}$ = 16 Hz) at 4.08 ppm, while no signal can be resolved in the ^{31}P NMR spectrum between –1200 and +1200 ppm. The ^{19}F NMR spectrum shows the presence of the WCA [TEF]. The X-band EPR spectrum of $[\mathbf{1}]^+$ shows no signal at room temperature but upon cooling to 77 K, one broad signal can be resolved without any hyperfine coupling at g_{iso} = 2.024 (solid state) or g_{iso} = 2.019 (CD_2Cl_2).[24] The magnetic moment of **3a** (μ_{eff} = 1.67 μ_B) was determined by the Evans NMR method, which is consistent with one unpaired electron.[24] In the ESI mass spectrum a peak assignable to $[\mathbf{1}]^+$ is detected. The dark teal crystals of **3a** were not suitable for an X-ray structure analysis.[24] By exchanging the anion [TEF] for another WCA $[FAl\{OC_6F_{10}(C_6F_5)\}_3]^-$ (=[FAl]),[25] we were able to determine the crystal structure of the oxidized P_6 complex **3b** (Figure 2).

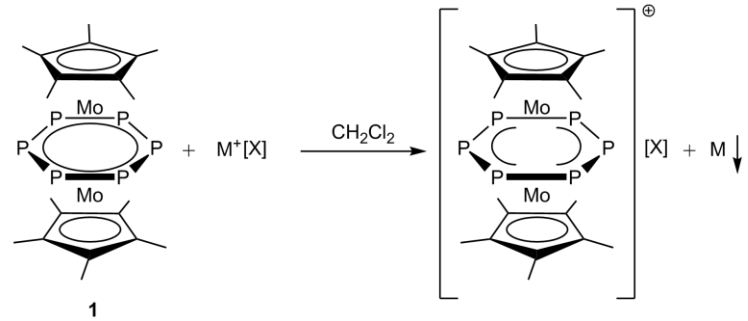

Scheme 1. Oxidation of **1** by M^+ salts.

The structure of **3b** shows that the triple-decker geometry is retained during the one-electron oxidation of **1**. The Mo-Mo' bond length of the cation $[\mathbf{1}]^+$ is almost identical with 2.6617(4) Å compared to 2.6463(3) Å of **1**.[24] The P-P bond lengths on the other hand are strongly affected by the oxidation. While the bonds P1-P1' and P3-P3' are elongated, the remaining P-P bonds are shortened compared to the P-P bond average

of ~2.183 Å of the starting material. Therefore, the middle-deck of $[\mathbf{1}]^+$ can best be described as a bis-allylic distorted *cyclo*-P_6 ligand. DFT calculations show that this distortion is due to depopulation of the P-P bonding orbitals in the oxidized complex cation $[\mathbf{1}]^+$.[24]

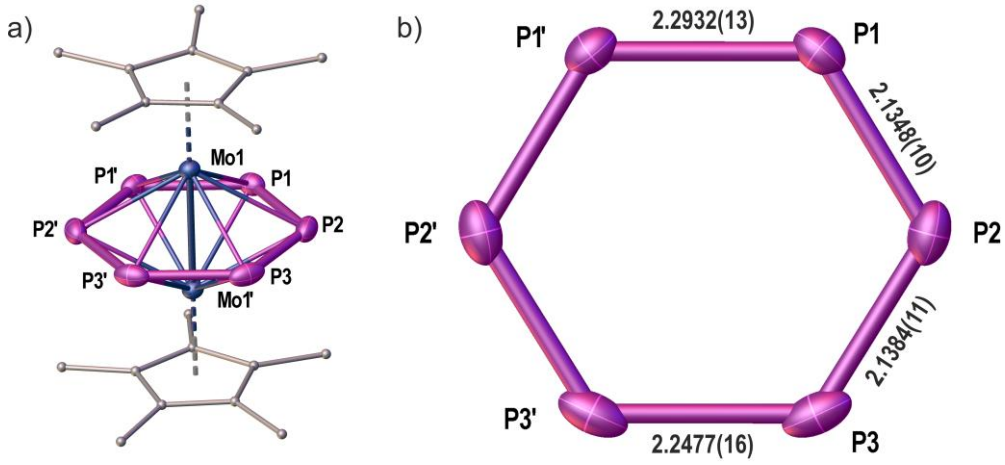

Figure 2. a) Molecular structure of the cation $[\mathbf{1}]^+$ in **3b**.[26] Thermal ellipsoids are drawn at 50% probability. Carbon atoms are depicted as small spheres, H atoms are omitted for clarity. Mo1-Mo1‘ 2.6617(4) Å. b) bis-allylic distorted *cyclo*-P_6 ligand.

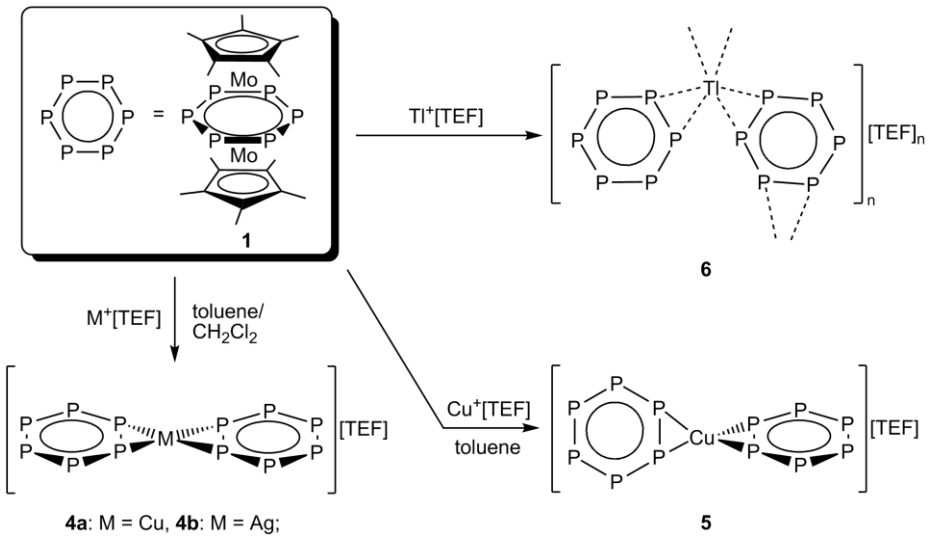

Scheme 2. Reactivity of **1** towards the cations Cu^+ and Tl^+.

To avoid oxidation of **1** by the M^+[TEF] salts, we reduced the redox potential of the cations by addition of toluene. While constantly obtaining a mixture of the dark teal oxidation (**3a**) and bright orange coordination product (**4b**) for Ag, we were able to completely avoid the oxidation and only obtain bright orange **4a** for Cu (Scheme 2). The $^{31}P\{^1H\}$ NMR spectrum of **4a** in CD_2Cl_2 shows a broad singlet at –290.4 ppm ($\omega_{½}$ = 126 Hz) at room temperature, which is shifted 24 ppm to lower field compared to **1**. At 193 K, the signal gets sharper ($\omega_{½}$ = 71 Hz) and moves slightly

to –293.4 ppm, but no splitting of this singlet could be resolved. The $^{31}P\{^{1}H\}$ MAS NMR spectrum (293 K, f = 30 kHz) shows only one broad singlet at –288.8 ppm ($\omega_{½}$ = 937 Hz). The solution NMR characterization of crystalline **4b** proved to be challenging due to low solubility in CD_2Cl_2 and fast decomposition. Nevertheless, a broad signal ($\omega_{1/2}$ = 155 Hz) at –294.0 ppm could be resolved in the $^{31}P\{1H\}$ NMR spectrum at 253 K when warming a crystalline sample in CD_2Cl_2. This suggests a highly dynamic coordination behavior of **1** towards Cu^+ and Ag^+.

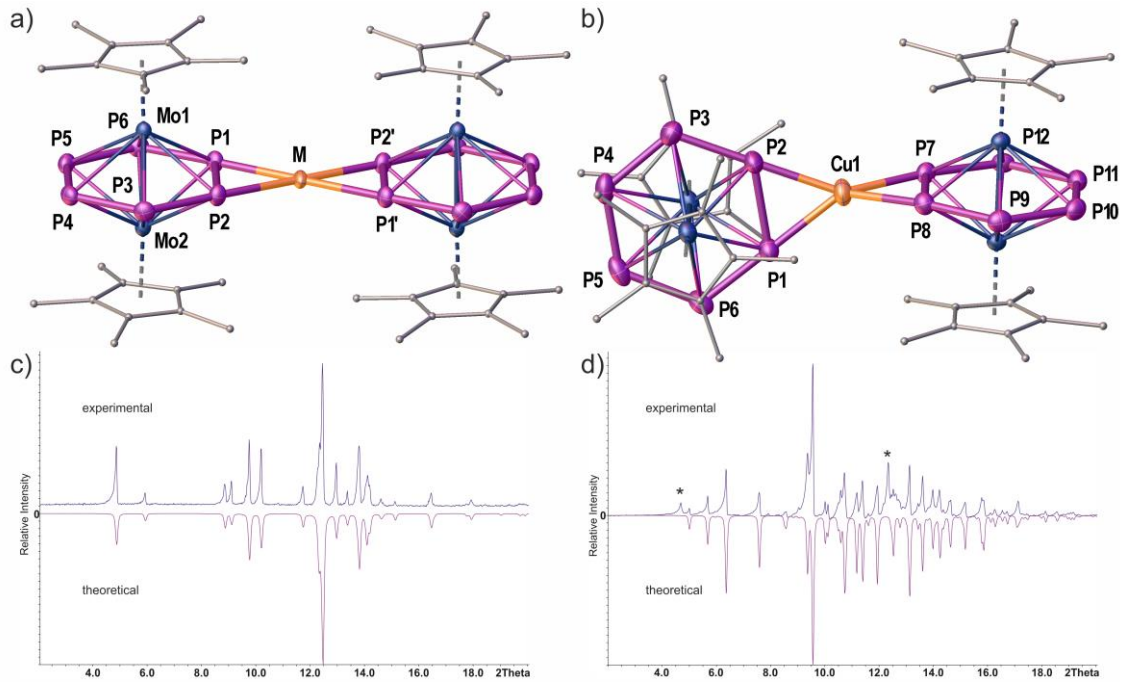

Figure 3. Solid state structure of the cations of **4a** (M = Cu), **4b** (M = Ag) a) and the cation of **5** b). Thermal ellipsoids are drawn at 50% probability. Selected bond lengths [Å]: **4a**: Cu1-P1 2.4354(12), Cu1-P2 2.3927(12), P1-P2 2.2694(16); **4b**: Ag1-P1 2.5793(10), Ag1-P2 2.6196(10), P1-P2 2.2915(14); **5**: Cu1-P1 2.3546(16), Cu1-P2 2.3343(16), Cu1-P7 2.3483(16), Cu1-P8 2.3383(16), P1-P2 2.286(2), P7-P8 2.2876(19). Angle between the planes P1P2Cu1 and P7P8Cu1 93.5°; C atoms are depicted as small spheres and H atoms are omitted for clarity. XRD pattern (positive intensities: measured, negative intensities: simulated) of **4a** c) and **5** d) (measured diagram of **5** is background corrected). * peaks arising from unknown impurities.

Single crystal X-ray analysis reveals that **4a** and **4b** are isostructural showing a distorted square planar coordination environment around the central cation by two side-on coordinating P-P bonds shown in Figure 3a). The Ag-P distances of **4b** (~2.6 Å) are shorter than the Ag-P distances observed of η^2-coordination by [Cp*Fe(η^5-P_5)] (~2.8 Å)[27] or [Cp*Mo(CO)$_2$(η^3-P_3)] (~2.7 Å)[28]. The Cu-P distances of **4a** (~2.4 Å) are a little longer than for the η^2-coordination by [Cp_2Mo_2(μ,η^2:η^2-P_2)] (~2.35 Å) but can be compared well to [CpMo(CO)$_2$(η^3-P_3)] (~2.4 Å).[29] The P-P bonds are elongated with 2.2694(16) Å (**4a**) and 2.2915(14) Å (**4b**) upon coordination while the remaining P-P bonds are not affected. Examination of the crystal packing reveals that **4a** and **4b** are layered compounds crystallizing in the monoclinic space group *C*2/*c* with alternating

negatively charged layers of the [TEF] anions and positively charged layers of isolated $[M(\mathbf{1})_2]^+$ complexes.[24] The layers lie inside the *bc*-plane and alternate along the *a*-axis (see Figure 4a) + c)). When Cu[TEF] is allowed to react with **1** in pure toluene the solution shows the bright orange color of the complex cation $[Cu(\mathbf{1})_2]^+$. To our surprise, analysis of crystals of **5** from this solution reveals a distorted tetrahedral coordination environment around Cu (Figure 3b). The resulting Cu-P distances of **5** are somewhat shorter than their counterparts in **4a**, while the coordinating P-P bonds are a little longer. This can be explained by less steric crowding of the tetrahedral coordination geometry around Cu in **5**.

To gain further insight into the equilibrium between 'tetrahedral' and 'square planar' coordination of **1** towards Cu^+ and Ag^+ DFT calculations were performed for different media. The results are presented in Table 1 and show that the enthalpy for the isomerization tetrahedral → square planar is positive for both metals, which means that the tetrahedral coordination should be favored. When the entropy is taken into account by calculating the Gibbs energy, small positive values for Cu^+ and larger, but negative, values for Ag^+ are observed. This means that for Cu^+ the tetrahedral geometry is predominant, but a significant percentage of the complexes adopt a square planar geometry in solution. For Ag^+, the equilibrium is significantly shifted to the right side (~98% for CH_2Cl_2 solution), which is probably the reason a tetrahedral coordination of **1** and Ag^+ was not yet observed. With the help of powder XRD analysis, shown in Figure 3 c) + d), we were able to prove that we can isolate the cation $[Cu(\mathbf{1})_2]^+$ selectively either as its tetrahedral isomer in **5** or as its square planar isomer in **4a**.

Table 1. Standard enthalpies ΔH^o_{298} and Gibbs energies ΔG^o_{298} (kJ mol^{-1}), standard entropies ΔS^o_{298} (J mol^{-1}K^{-1}) and equilibrium constants K_{298} for the isomerization process *tetrahedral* → *square planar* in different media.

metal	medium	ΔH^0_{298}	ΔS^o_{298}	ΔG^o_{298}	K_{298}
Cu	gas phase	22.5	57.5	5.34	0.12
	toluene	20.7	57.5	3.55	0.24
	CH_2Cl_2	19.5	57.5	2.39	0.38
Ag	gas phase	8.3	43.9	-4.8	7.0
	toluene	4.8	43.9	-8.3	28.3
	CH_2Cl_2	3.0	43.9	-10.1	59.1

Although **4a** and **4b** can be described as consisting of alternating layers, the $[M(\mathbf{1})_2]^+$ (M = Cu, Ag) cations as well as the [TEF] anions do not form a two-dimensional network. Prior studies have demonstrated the possibility to obtain an abundance of coordination compounds from Tl^+ and polyphosphorus and -arsenic ligands; therefore, we reacted **1** with Tl[TEF].[30,31,32] When Tl[TEF] is added to a CH_2Cl_2 solution of **1** an immediate color change occurs from light brown (**1**) to the deep red color of compound **6**. No signal can

be resolved in the $^{31}P\{^{1}H\}$ NMR spectrum of **6** in CD_2Cl_2 solution at room temperature. Upon cooling to 193 K, a very broad signal ($\omega_{1/2}$ = 1303 Hz) appears at –305.5 ppm, shifted ~8 ppm to lower field compared with **1**. The $^{31}P\{^{1}H\}$ MAS NMR spectrum of **6** at 293 K (f = 27 kHz) shows one broad singlet at –291.1 ppm ($\omega_{1/2}$ = 1530 Hz) while at 343 K (f = 25 kHz) two broad signals at –289.6 ($\omega_{1/2}$ = 300 Hz) and at –309.2 ($\omega_{1/2}$ = 260 Hz) can be resolved in a ratio of about 1:12.[24] Elemental analysis is consistent with a molar ratio of 2:1 of the P_6 complex **1** to Tl^+, while the crystal structure reveals a trigonal pyramidal coordination of Tl^+ by three side-on coordinating P-P bonds of the *cyclo*-P_6 ligands (Figure 5).

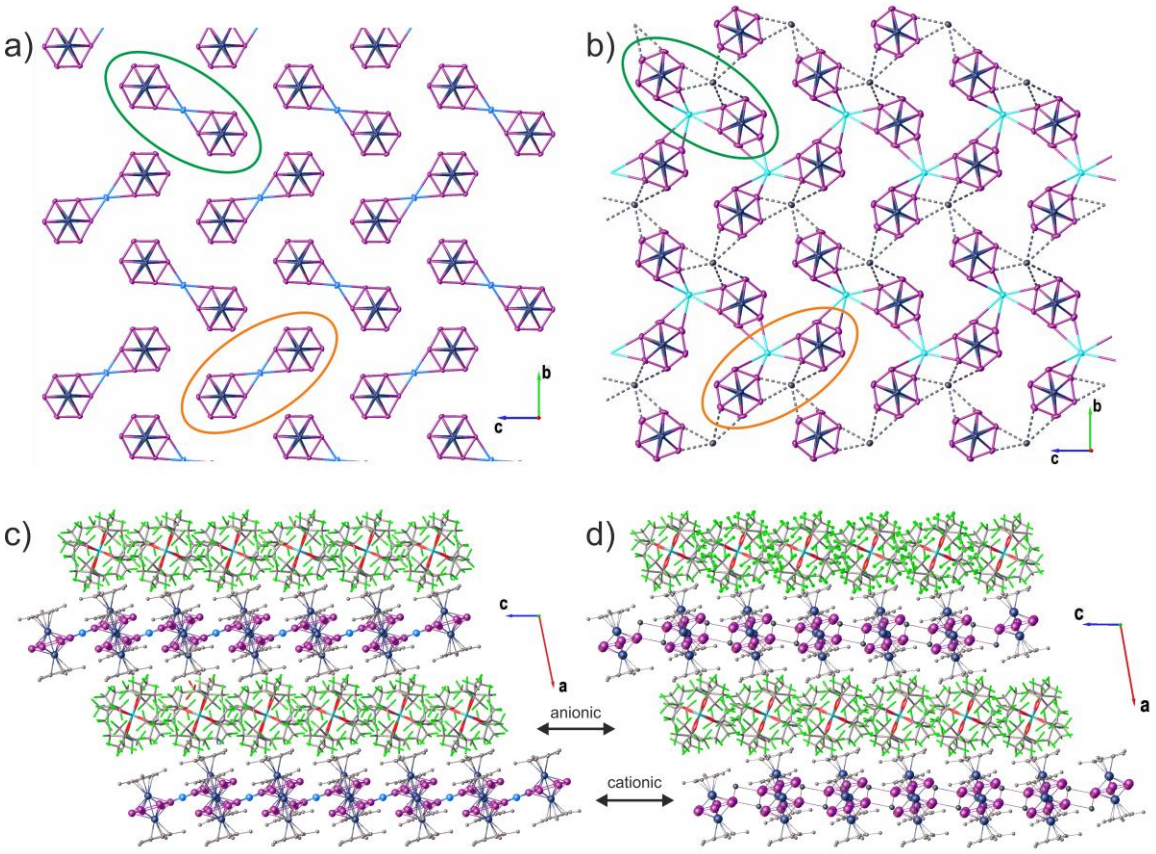

Figure 4. Cationic layers inside the *bc*-plane of **4b** a) and **6** b). Tl^+ positions (light and dark) in b) are half-occupied. For a) and b) anions, C and H atoms are omitted for clarity. c) + d) Illustration of the crystal packing of **4b** c) and **6** d) with viewing direction along the *b*-axis showing the alternation of cationic and anionic layers along the *a*-axis. The P_6 planes include a tilt angle of 16.3° (**4a**), 16.3° (**4b**) and 13.8° (**6**) to the *bc*-plane.

The P-P bonds P1-P2 and P8-P9 show shorter and uniform Tl-P distances of 3.2-3.3 Å, which are shorter than the Tl-P distances observed for the η^5-coordination of [Cp*Fe(η^5-P_5)] towards Tl^+ (~3.5-3.9 Å).[30,31] This coordination results in a slight elongation of these P-P bonds to about 2.22 Å while the third molecule of **1** (P5'-P6') shows an unsymmetrical coordination with long Tl-P distances of ~3.42 and 3.69 Å and no P-P bond elongation.

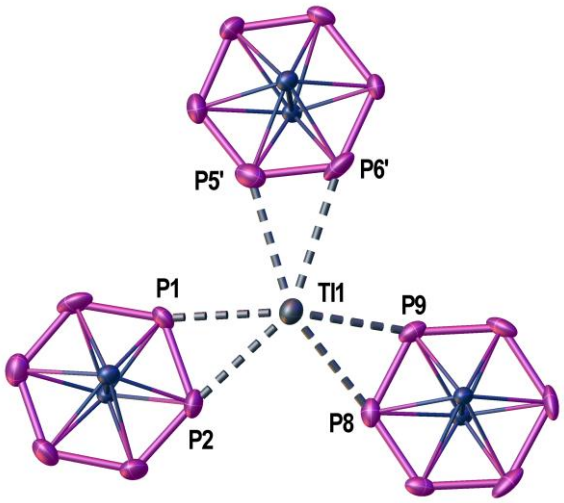

Figure 5. Coordination environment of Tl^+ in **6**. Ellipsoids are drawn at 50% probability. Cp* ligands are omitted. Sum of coordination angles = 343.5°.

Although the environment of Tl^+ in **6** is distinctly different from Cu^+ and Ag^+ in **4a** and **4b**, their structures are related.[33]. In Figure 4a) the isolated $[M(\mathbf{1})_2]+$ complex cations are shown for **4a** and **4b**, and in Figure 4b), the two-dimensional coordination network that propagates inside the *bc*-plane of **6** is displayed. The green and orange ellipses are directly corresponding to each other. Please note, that the Tl cations depicted in light blue and dark grey are symmetry equivalent positions and only half-occupied. Indeed, there is a statistical distribution of the Tl^+ cations inside the two-dimensional coordination network with the restriction that one of the ellipses can only be occupied by one Tl^+ cation. Herein structural similarities to graphene–like structures can be observed. Figure 4c) and d) illustrate the equal crystal packing with alternating positively charged 'coordination' layers and negatively charged 'anion' layers when going along the crystallographic *a*-axis.

3.3 Conclusion

In summary, we have presented a facile synthesis of the *cyclo*-P_6 complex **1** which enabled us to study its reactivity for the first time. Additionally, the by-product $[(Cp^*Mo)_2(\mu\text{-}P_{10})]$ (**2**) containing the largest known cyclic polyphosphorus ligand has been structurally characterized. We have demonstrated that the bis-allylic distortion of the *cyclo*-P_6 middle-deck occurs upon one-electron oxidation of **1**. By reacting **1** with Cu^+, Ag^+ and Tl^+ salts of the WCA [TEF], the highly dynamic coordination behavior of the cations was monitored in solution. The product distribution of the reaction of **1** with Cu^+ can be controlled by changing the solvent and, surprisingly, two isomers with distorted square planar or distorted tetrahedral coordination geometry at Cu^+ were selectively obtained. The results demonstrate further the potential of the *cyclo*-P_6 complex **1** to act

as a multidentate ligand in supramolecular chemistry for the formation of layered coordination compounds (**4a**, **4b** and **6**). While Cu^+ and Ag^+ (**4a**, **4b**) form layered structures with isolated $[M(\mathbf{1})_2]^+$ complex cations, Tl^+ shows further interconnection of the *cyclo*-P_6 ligands to form an extended 2D network that can be regarded as a supramolecular analog of graphene.

3.4 References

[1] R. Hoffmann, *Angew. Chem. Int. Ed. Engl.* **1982**, *21*, 711-724; *Angew. Chem.* **1982**, *94*, 725-739.

[2] O. J. Scherer, H. Sitzmann, G. Wolmershäuser, *Angew. Chem. Int. Ed. Engl.* **1985**, *24*, 351-353; *Angew. Chem.* **1985**, *97*, 358-359.

[3] O. J. Scherer, H. Swarowsky, G. Wolmershäuser, W. Kaim, S. Kohlmann, *Angew. Chem. Int. Ed. Engl.* **1987**, 26, 1153-1155; *Angew. Chem.* **1987**, *99*, 1178-1179.

[4] M. Herberhold, G. Frohmader, W. Milius, *J. Organomet. Chem.* **1996,** *522*, 185-196.

[5] O. J. Scherer, J. Schwalb, H. Swarowsky, G. Wolmershäuser, W. Kaim, R. Gross, *Chem. Ber.* **1988**, *121*, 443-449.

[6] O. J. Scherer, J. Vondung, G. Wolmershäuser, *Angew. Chem. Int. Ed. Engl.* **1989**, *28*, 1355-1357; *Angew. Chem.* **1989**, *101*, 1395-1397.

[7] O. J. Scherer, R. Winter, G. Heckmann, G. Wolmershäuser, *Organometallics* **1992,** *11*, 3894-3900.

[8] J. Bai, A. V. Virovets, M. Scheer, *Science* **2003**, *300*, 781-783.

[9] F. Dielmann, C. Heindl, F. Hastreiter, E. V. Peresypkina, A. V. Virovets, R. M. Gschwind, M. Scheer, *Angew. Chem. Int. Ed.* **2014**, *53*, 13605-13608; *Angew. Chem.* **2014**, *126*, 13823-13827.

[10] A. Schindler, C. Heindl, G. Balázs, C. Gröger, A. V. Virovets, E. V. Peresypkina, M. Scheer, *Chem. Eur. J.* **2012**, *18*, 829-835.

[11] Therefore no NMR studies could be performed.

[12] Level of theory: B3LYP, def2-TZVP. Please see ESI for details.

[13] F. Dielmann, M. Sierka, A. V. Virovets, M. Scheer, *Angew. Chem. Int. Ed.* **2010**, *49*, 6860-6864; *Angew. Chem.* **2010**, 122, 7012-7016.

[14] S. Scharfe, F. Kraus, S. Stegmaier, A. Schier, T. F. Fässler, *Angew. Chem. Int. Ed.* **2011**, *50*, 3630-3670; *Angew. Chem.* **2011**, *123*, 3712-3754.

[15] M. Scheer, G. Balázs, A. Seitz, *Chem. Rev.* **2010**, *110*, 4236-4256.

[16] M. Feierabend, C. von Hänisch, *Chem. Commun.* **2014**, *50*, 4416-4419.

[17] B. M. Cossairt, N. A. Piro, C. C. Cummins, *Chem. Rev.* **2010**, *110*, 4164-4177.

[18] M. Caporali, L. Gonsalvi, A. Rossin, M. Peruzzini, *Chem. Rev*. **2010**, *110*, 4178-4235.

[19] E.-K. Mucke, B. Schönborn, F. Köhler, R. Herges, *J. Org. Chem.* **2011**, *76*, 35-41.

[20] I. Krossing, *Chem. Eur. J.* **2001**, *7*, 490-502.

[21] G. Santiso-Quiñones, A. Higelin, J. Schaefer, R. Brückner, C. Knapp, I. Krossing, *Chem. Eur. J.* **2009**, *15*, 6663-6677.

[22] M. Gonsior, I. Krossing, N. Mitzel, *Z. Anorg. Allg. Chem.* **2002**, *628*, 1821-1830.

[23] CH_2Cl_2, 0.1 M $[NBu_4][PF_6]$, T = 298 K, v = 100 mV/s, Pt electrode.

[24] Please see supporting information for details.

[25] T. Köchner, N. Trapp, T. A. Engesser, A. J. Lehner, C. Röhr, S. Riedel, C. Knapp, H. Scherer, I. Krossing, *Angew. Chem. Int. Ed.* **2011**, *50*, 11253-11256; *Angew. Chem.* **2011**, *123*, 11449-11452.

[26] There are two independent cations in the unit cell. Cf. ESI for details.

[27] M. Scheer, L. J. Gregoriades, A. V. Virovets, W. Kunz, R. Neueder, I. Krossing, *Angew. Chem. Int. Ed.* **2006**, *45*, 5689-5693; *Angew. Chem.* **2006**, *118*, 5818-5822.

[28] L. J. Gregoriades, B. K. Wegley, M. Sierka, E. Brunner, C. Gröger, E. V. Peresypkina, A. V. Virovets, M. Zabel, M. Scheer, *Chem. Asian J.* **2009**, *4*, 1578-1587.

[29] M. Fleischmann, S. Welsch, E. V. Peresypkina, A. V. Virovets, M. Scheer, *Chem. Eur. J.* **2015**, *21*, 14332-14336.

[30] S. Welsch, L. J. Gregoriades, M. Sierka, M. Zabel, A. V. Virovets, M. Scheer, *Angew. Chem. Int. Ed.* **2007**, *46*, 9323-9326; *Angew. Chem.* **2007**, *119*, 9483-9487.

[31] M. Fleischmann, S. Welsch, H. Krauss, M. Schmidt, M. Bodensteiner, E. V. Peresypkina, M. Sierka, C. Gröger, M. Scheer, *Chem. Eur. J.* **2014**, *20*, 3759-3768.

[32] M. Fleischmann, S. Welsch, L. J. Gregoriades, C. Gröger, M. Scheer, *Z. Naturforsch.* **2014**, *69b*, 1348-1356.

[33] The compounds **4a**, **4b** and **6** crystallize in the same space group *C*2/*c* with similar unit cells. See Supporting information for details.

3.5 Supporting Information

General information

All experiments were performed under an atmosphere of dry argon or nitrogen using standard Schlenk and drybox techniques. Commercially available reagents were used as received without further purification. Solvents were freshly distilled under nitrogen from CaH_2 (CH_2Cl_2, CD_2Cl_2, CH_3CN ,CD_3CN), Na (toluene) or Na/K-alloy (*n*-pentane, *n*-hexane). Solution NMR spectra were recorded on a Bruker Avance 400 spectrometer (^1H: 400.130 MHz, ^{31}P: 161.976 MHz, ^{13}C: 100.613 MHz). The chemical shifts δ are presented in parts per million ppm and coupling constants *J* in Hz. The following samples were used for external reference: TMS (^1H, ^{13}C), $CFCl_3$ (^{19}F), H_3PO_4 85 % (^{31}P). $^{31}P\{^1H\}$ MAS NMR spectra were recorded on a Bruker Avance 300 (^{31}P: 121.495 MHz) by Dr. Christian Gröger of the Physics department of the University of Regensburg. The chemical shifts of the MAS NMR spectra are also presented in the δ scale using NaH_2PO_4 as an external standard. X-Band EPR spectra were recorded on a MiniScope MS400 device from Magnettech GmbH with a frequency of 9.5 GHz equipped with a rectangular resonator TE102. ESI-MS spectra were measured on a Finnigan Thermoquest TSQ 7000 mass-spectrometer. EI-MS spectra were recorded on a Finnigan MAT 95 mass spectrometer .IR spectra were recorded on a VARIAN FTS-800 FT-IR spectrometer in CH_2Cl_2 solution or the solid substances were grinded together with dried KBr and pressed to pellets. The starting materials $[Cp^*Mo(CO)_2]_2$,[1] Ag[TEF],[2] Ag[FAl],[3] [Cu(*o*-DFB)$_2$][TEF][4] (*o*-DFB = *ortho*-difluorobenzene), Tl[TEF][5] were prepared according to the literature procedure.

Syntheses of described compounds

Synthesis of [(Cp*Mo)$_2$(μ,η^6:η^6-P$_6$)] (**1**) and [(Cp*Mo)$_2$(μ-P$_{10}$)] (**2**): The synthesis of **1** was reported in the literature with 1% yield after chromatographic work up.[6] During this investigation we developed a new high yield synthesis that is described below.

$[Cp^*Mo(CO)_2]_2$ 1.94 g (3.38 mmol, 1eq.) and P_4 1.96 g (15.8 mmol, 3.1eq.) are dissolved in 100 mL of diisopropylbenzene (DIB) and heated to reflux. IR spectroscopy showed the disappearance of any CO stretching bands after 90 minutes. (Complex **1** is thermally stable. Therefore, a reaction time of 24 h reflux gives similar results.) The heating was removed and the reaction was slowly cooled down to room temperature whereby a light brown solid precipitated from the solution. The crude product (1.88 g) was filtered off, washed with *n*-pentane (3 × 30 mL) and dried in vacuum. Recrystallization from warm CH_2Cl_2 affords **1** as medium brown crystals. Yield: 1.88 g (crude), 1.41 g (64%, pure). ^1H NMR (CD_2Cl_2) δ/ppm = 0.56 (s; C_5Me_5); $^{31}P\{^1H\}$-NMR (CD_2Cl_2) δ/ppm = −314.3 (s). Anal. calcd. for $C_{20}H_{30}Mo_2P_6$: C, 37.06; H, 4.67. Found: C, 37.00; H, 4.83.
After recrystallization of **1** from CH_2Cl_2, we were able to identify very few tiny dark red crystals adhered to large crystals of **1**. Single crystal X-ray analysis revealed the molecular structure of [(Cp*Mo)$_2$(μ-P$_{10}$)] (**2**). Unfortunately, we were not able to isolate enough of this compound for NMR characterization. Yield: very few crystals (not determinable ~ below 0.1%) EI-MS (CH_2Cl_2) *m/q* (%) = 647.9 (100) $[(Cp^*Mo)_2P_6]^+$, 772.0 (5) $[(Cp^*Mo)_2P_{10}]^+$.

Synthesis of [(Cp*Mo)$_2$(μ,η^6:η^6-P$_6$)][TEF] (**3a**): The *cyclo*-P_6 ligand complex **1** is easily oxidized by Ag^+ or Cu^+ in pure CH_2Cl_2.

Method 1: A mixture of $Ag[Al\{OC(CF_3)_3\}_4]\bullet CH_2Cl_2$ (135 mg, 0.12 mmol), [(Cp*Mo)$_2$(μ,η^6:η^6-P$_6$)] (**1**) (75 mg, 0.12 mmol) and CH_2Cl_2 (20 mL) was stirred for 72 h at room temperature in the dark. The dark teal solution was filtered over diatomaceous earth, which was subsequently washed with CH_2Cl_2 (2 × 2 ml), and the combined filtrate and washings were concentrated to about one fifth of

the original volume (~ 5 mL). The concentrated solution was carefully layered with *n*-pentane (5 mL) and stored in a freezer (–28 °C). Compound **3a** can be isolated as dark teal plates. Yield 160 mg (86%).

Method 2: [Cu(*o*-DFB)$_2$][TEF] (50 mg; 1 eq., 0.04 mmol) and [(Cp*Mo)$_2$(μ,η^6:η^6-P$_6$)] (**1**) (26 mg, 1eq., 0.04 mmol) were weighed together as solids. The addition of CH_2Cl_2 (~ 10 mL) lead to an immediate color change from brown to a dark teal solution. After stirring for 3 h the solution was filtered over diatomaceous earth. The dark teal clear solution was carefully layered with *n*-pentane and stored at +4 °C. Compound **3a** was isolated as dark teal plates. The crystals were filtered off, washed with *n*-pentane (3 × 5 mL) and dried in vacuum. Yield 62 mg (80%). ^{1}H NMR (CD_2Cl_2) δ/ppm = 4.08 (br, ω½ = 16 Hz, CH_3); ^{13}C{^{1}H} NMR (CD_2Cl_2) δ/ppm = 90.28 (s, Cp*), 4.92 (s, CH_3), 121.64 (q, $^1J_{C,F}$ = 294 Hz, CF_3); ^{19}F{^{1}H} NMR (CD_2Cl_2) δ/ppm = –75.03 (s, CF_3); ^{31}P{^{1}H} NMR (CD_2Cl_2) δ/ppm = no signal detectable between –1200 and +1200 ppm (paramagnetic); ^{27}Al NMR (CD_2Cl_2) δ/ppm = 33.62 (s, [Al(OC(CF$_3$)$_3$)$_4$]$^-$). Anal. calcd. for $C_{36}H_{30}Mo_2P_6AlO_4F_{36}$ C, 26.77; H, 1.87. Found: C, 26.49; H, 1.99. X-band EPR (77 K, CD_2Cl_2) g_{iso} = 2.019. Evans-method μ_{eff} = 1.67 μ_B (one unpaired electron). ESI-MS (CH_2Cl_2) cations: *m/q* (%) = 647.9 (100) [(Cp*Mo)$_2$P$_6$]$^+$; anions: *m/q* (%) 966.9 (100) [Al(OC(CF$_3$)$_3$)$_4$]$^-$. IR (KBr) $\tilde{\nu}$/cm^{-1} = 2983 (w), 2924 (w), 1482 (w), 1451 (w), 142 (w), 1383 (m), 1353 (m), 1302 (s), 1277 (s), 1242 (s), 1220 (s), 1170 (m), 1101 (m), 1028 (m), 974 (s), 838 (w), 756 (w), 728 (s), 560 (w), 537 (m), 448 (m).

Synthesis of [(Cp*Mo)$_2$(μ,η^6:η^6-P$_6$)][FAl] (**3b**): Ag[FAl] (79 mg, 1eq., 0.05 mmol) is dissolved in 5 mL of CH_2Cl_2 to yield a clear colorless solution. [(Cp*Mo)$_2$(μ,η^6:η^6-P$_6$)] (**1**) (33 mg, 1eq., 0.05 mmol) is dissolved in 10 mL of CH_2Cl_2 to yield a clear medium brown solution. When the Ag^+ solution is slowly added to the stirred solution of **1** the color changes to dark green and a black precipitate of Ag^0 is formed. After stirring for 3 h the solution is filtered and subsequently carefully layered with *n*-hexane. After storage at +4 °C for some days compound **3b** can be obtained as dark green blocks. The solution is decanted off. The crystals are washed with *n*-hexane (3 × 10 mL) and dried in vacuum. Yield 59 mg (58%). ^{1}H NMR (CD_2Cl_2) δ/ppm = 4.21 (br, ω½ = 17 Hz, CH_3); ^{13}C{^{1}H} NMR (CD_2Cl_2) δ/ppm = 89.82 (s, Cp*), 4.55 (s, CH_3); ^{19}F{^{1}H} NMR (CD_2Cl_2) δ/ppm = –112.3 (d, $J_{F,F}$ = 275 Hz, 2F), –117.1 (d, $J_{F,F}$ = 279 Hz, 2F), –121.5 (d, $J_{F,F}$ = 277 Hz, 2F), –127.7 (s, 2F), –130.4 (d, $J_{F,F}$ = 275 Hz, 2F), –136.8 (d, $J_{F,F}$ = 276 Hz, 2F), –140.7 (d, $J_{F,F}$ = 277 Hz, 1F), –153.9 (t, $J_{F,F}$ = 22 Hz, 1F), –164.6 (t, $J_{F,F}$ = 18 Hz, 1F), –172.0 ppm (s, AlF); ^{31}P{^{1}H} NMR (CD_2Cl_2) δ/ppm = no signal detectable between –1200 and +1200 ppm (paramagnetic). Anal. calcd. for $C_{56}H_{30}Mo_2P_6AlO_3F_{46}$ C, 33.14; H, 1.49. Found: C, 33.35; H, 1.58. X-band EPR (77 K, solid) g_{iso} = 2.024. ESI-MS (CH_2Cl_2) cations: *m/q* (%) 647.9 (100) [(Cp*Mo)$_2$P$_6$]$^+$; anions: *m/q* (%) 1381 (100) [AlO$_3$C$_{36}$F$_{46}$]$^-$. IR (KBr) $\tilde{\nu}$/cm^{-1} = 2973 (w), 2924 (w), 2870 (vw), 1652 (m), 1533 (m), 1486 (vs), 1422 (vw), 1383 (m), 1323 (m), 1308 (m), 1267 (m), 1224 (m), 1203 (vs), 1187 (m), 1153 (m), 1134 (w), 1105 (m), 1019 (s), 1005 (m), 955 (vs), 910 (m), 849 (vw), 809 (vw), 769 (m), 750 (w), 730 (m), 634 (m), 528 (w), 496 (vw), 467 (w).

Synthesis of [Ag{(Cp*Mo)$_2$(μ,η^6:η^6:η^2-P$_6$)}$_2$][TEF] (**4b**): Ag[Al{OC(CF$_3$)$_3$}$_4$]•CH_2Cl_2 (87 mg, 1eq., 0.075 mmol) and [(Cp*Mo)$_2$(μ,η^6:η^6-P$_6$)] (**1**) (110 mg, 2.2eq., 0.165 mmol) were combined as solids. Addition of 15 mL toluene afforded a medium brown suspension. Upon slow addition of a small amount of CH_2Cl_2 (~ 3 mL) under constant stirring the solution turned bright orange and most of the precipitate dissolved. After 30 minutes the brown precipitate was filtered off ant the clear orange solution was layered with the fivefold amount of toluene and subsequently stored at +4 °C. Compound **4b** can be obtained as light orange crystals forming on the glass walls after a few days. The crystals are freed from the mother liquor, washed with toluene (2 × 50 mL) and dried in vacuum. The crystals show a rather low solubility in CH_2Cl_2 compared to the analogues Cu^+ compound **4a** and decomposes quickly to the oxidized compound **3a** and elemental Ag. Yield 29 mg (16 %). ^{1}H NMR (CD_2Cl_2, 253 K) δ/ppm = 0.77 (s, CH_3); ^{19}F{^{1}H} NMR (CD_2Cl_2) δ/ppm = –75.6 (s, CF_3); ^{31}P{^{1}H} NMR (CD_2Cl_2, 253 K) δ/ppm = –294.0 (ω½ = 155 Hz, P$_6$). Anal. calcd. for

$C_{56}H_{60}AgMo_4P_{12}AlO_4F_{36}$ C, 28.36; H, 2.55. Found: C, 28.37; H, 2.63. ESI-MS (CH_2Cl_2) cations: *m/q* (%) = 648.0 (100) $[(Cp^*Mo)_2P_6]^+$; anions: *m/q* (%) 967.1 (100) $[Al(OC(CF_3)_3)_4]^-$. IR (KBr) $\tilde{\nu}$/cm^{-1} = 2966 (w), 2917 (w), 2851 (w), 1627 (vw), 1482 (vw), 1378 (w), 1353 (w), 1301 (s), 1277 (s), 1242 (s), 1219 (vs), 1163 (vw), 1028 (w), 974 (vs), 727 (s), 445 (vw).

Synthesis of [Cu{$(Cp^*Mo)_2(\mu,\eta^6{:}\eta^6{:}\eta^2\text{-}P_6)$}$_2$][TEF] (**4a**, **5**): The addition of toluene or MeCN to this reaction is necessary to prevent the oxidation of $[(Cp^*Mo)_2(\mu,\eta^6{:}\eta^6\text{-}P_6)]$ (**1**) by Cu^+.

Isolation of [Cu{$(Cp^*Mo)_2(\mu,\eta^6{:}\eta^6{:}\eta^2\text{-}P_6)$}$_2$][TEF] as dist. square planar form **4a**: [Cu(*o*-DFB)$_2$][TEF] (100 mg, 1eq., 0.079 mmol) was dissolved in 10 mL toluene and 2 mL of CH_2Cl_2 affording a clear colorless solution. $[(Cp^*Mo)_2(\mu,\eta^6{:}\eta^6\text{-}P_6)]$ (**1**) (104 mg, 2eq., 0.159 mmol) was suspended in 5 mL toluene and 1 mL CH_2Cl_2. The Cu^+ solution was slowly added to the solution of **1** while stirring, resulting in a bright orange solution with very few precipitate. After 30 minutes, the solution was filtered and carefully layered with the twofold amount of *n*-pentane. After 3 days storage at +4 °C, compound **4a** can be isolated as orange needles. These were filtered off, washed with *n*-pentane (3 × 10 mL) and dried in vacuum. Yield 65 mg (35%).

Isolation of [Cu{$(Cp^*Mo)_2(\mu,\eta^6{:}\eta^6{:}\eta^2\text{-}P_6)$}$_2$][TEF] as dist. tetrahedral form **5**: [Cu(*o*-DFB)$_2$][TEF] (63 mg, 1eq., 0.05 mmol) and $[(Cp^*Mo)_2(\mu,\eta^6{:}\eta^6\text{-}P_6)]$ (**1**) (65 mg, 2eq., 0.1 mmol) were combined as solids. The addition of pristine toluene (~ 80 mL) while stirring resulted in the formation of a bright orange solution while most of the solids were dissolved and only a small amount of dark brown to black residue remained. After 30 minutes the solution was filtered and subsequently layered with the fivefold amount of *n*-hexane. Storage of this layered system at +4 °C for several days affords orange blocks as the main product next to a few very thin orange needles and some white precipitate. The orange needles and the white precipitate were not suitable for X-ray diffraction analysis. The fine orange needles and the precipitate can easily be removed from the orange crystals by washing them with *n*-hexane (3 × 50 mL) and decanting off the washings while the larger orange crystals settle on the ground. After this washing the crystals are dried in vacuum. Yield 35 mg (30%). ^{1}H NMR (CD_2Cl_2) δ/ppm = 0.93 (s, CH_3); ^{13}C{^{1}H} NMR (CD_2Cl_2) δ/ppm = 97.28 (s, Cp*), 12.05 (s, CH_3), 121.65 (q, $^1J_{C,F}$ = 295 Hz, CF_3); ^{19}F{^{1}H} NMR (CD_2Cl_2) δ/ppm = –75.75 (s, CF_3); ^{31}P{^{1}H} NMR (CD_2Cl_2, 300 K) δ/ppm = –290.4 (br, ω½ = 126 Hz, P_6); ^{31}P{^{1}H} NMR (CD_2Cl_2, 213 K) δ/ppm = –293.4 (br, ω½ = 71 Hz, P_6); ^{31}P{^{1}H}-MAS NMR (293 K, *f* = 30 kHz) δ/ppm = –288.8 (br, ω½ = 937 Hz, P_6). Anal. calcd. for $C_{56}H_{60}CuMo_4P_{12}AlO_4F_{36}$ C, 28.90; H, 2.60. Found: C, 28.71; H, 2.59. ESI-MS (CH_2Cl_2) cations: *m/q* (%) = 647.9 (100) $[(Cp^*Mo)_2P_6]^+$, 751.9 (42) $[Cu\{(Cp^*Mo)_2P_6\}(MeCN)]^+$, 1360.7 (11) $[Cu\{(Cp^*Mo)_2P_6\}_2]^+$; anions: *m/q* (%) 966.9 (100) $[Al(OC(CF_3)_3)_4]^-$. IR (KBr) $\tilde{\nu}$/cm^{-1} = 2970 (w), 2911 (w), 2859 (w), 1481 (w), 1449 (w), 1424 (w), 1379 (m), 1352 (m), 1301 (s), 1277 (s), 1241 (s), 1218 (s), 1164 (m), 1025 (m), 974 (s), 831 (w), 728 (s), 560 (w), 537 (m), 446 (m).

Synthesis of [Tl{$(Cp^*Mo)_2(\mu,\eta^6{:}\eta^6{:}\eta^2\text{-}P_6)$}$_2$]$_n$[TEF]$_n$ (**6**): $[(Cp^*Mo)_2(\mu,\eta^6{:}\eta^6\text{-}P_6)]$ (**1**) (50 mg, 2 eq., 0.08 mmol) and Tl[TEF] (45 mg, 1eq., 0.04 mmol) were combined as solids in a flask. Immediately upon the addition of CH_2Cl_2 (10 mL) a dark red solution formed. After 2 h of stirring at room temperature, the solution was filtered and carefully layered with the fivefold amount of *n*-pentane. After storage at +4 °C for several days compound **6** can be obtained as dark red plates. The crystals are filtered off, washed with *n*-pentane (3 × 5 mL) and dried in vacuum. Yield 65 mg (68%). ^{1}H NMR (CD_2Cl_2) δ/ppm = 0.83 (s; Cp*); ^{13}C{^{1}H} NMR (CD_2Cl_2) δ/ppm = 12.05 (s; $C_5(\underline{C}H_3)_5$), 97.28 (s; $\underline{C}_5(CH_3)_5$), 121.65 (q, $^1J_{F,C}$ = 296 Hz; CF_3); ^{19}F{^{1}H} NMR (CD_2Cl_2) δ/ppm = −75.7 (s; CF_3); ^{31}P{^{1}H} NMR (CD_2Cl_2, RT) no signal can be resolved; ^{31}P{^{1}H} NMR (CD_2Cl_2, 193 K) δ/ppm = –305.5 (br, ω½ = 1303 Hz); ^{31}P{^{1}H}-MAS NMR (293 K, 27 kHz) δ/ppm –291.1 (br, ω½ = 1530 Hz); ^{31}P{^{1}H}-MAS NMR (343 K, 25 kHz) δ/ppm –289.6 (br, ω½ = 300 Hz, small signal), –309.2 (br, ω½ = 260 Hz, large signal). Anal. calcd. for $TlAlO_4Mo_4P_{12}C_{56}F_{36}H_{60}$ C, 27.25; H, 2.45. Found: C, 27.62; H, 2.30. ESI-MS (CH_2Cl_2) cations: *m/q* (%) = 204.38 (100) Tl^+,

648.17 (98) $[(Cp^*Mo)_2P_6]^+$, 852.56 (3) $[Tl\{(Cp^*Mo)_2P_6\}]^+$; anions: 967.0 (100) $[Al\{OC(CF_3)_3\}_4]^-$. IR (KBr) $\tilde{\nu}$/cm^{-1} = 2960 (w), 2917 (w), 2851 (vw), 1636 (m), 1384 (w), 1302 (s), 1277 (s), 1242 (s), 1220 (vs), 1166 (m), 1025 (m), 974 (vs), 728 (s), 669 (m).

Determination of the magnetic moment of 3a by the Evans method

The magnetic moment μ_{eff} of the oxidized *cyclo*-P_6 complex [**1**]$^+$ in the compound [**1**][TEF] (**3a**) was determined by the Evans NMR method,[7,8,9,10] using equation (1).[11] The measurement resulted in a μ_{eff} of 1.67 μ_B for **3a** which is in good agreement with one unpaired electron.

$$\mu_{eff} = 798\sqrt{T \cdot \chi_m} \qquad (1)$$

$$\chi_m = \frac{3 \cdot \Delta f}{1000 \cdot f \cdot c}$$

χ_m = molar susceptibility of the sample in m^3 mol^{-1}, Δf = chemical shift difference of the residual solvent signal inside and outside of the capillary in Hz, f = frequency of the NMR spectrometer, c = concentration of the sample in mol dm^{-3}, T is the measurement temperature in K.

Representation of the X-Band EPR spectra of 3a and 3b

The oxidized *cyclo*-P_6 complex cation $[(Cp^*Mo)_2(\mu,\eta^6{:}\eta^6\text{-}P_6)]^+$ (= [**1**]$^+$) is paramagnetic and X-band EPR spectra (f = 9.5 GHz) were recorded for. [**1**][TEF] (**3a**) in CD_2Cl_2 solution and for [**1**][FAl] (**3b**) in the solid state. For both compounds we were unable to resolve any signal at room temperature, but upon cooling to 77 K we could resolve one broad signal for each sample without any hyperfine coupling at g_{iso} = 2.024 (**3b**) or g_{iso} = 2.019 (**3a**).

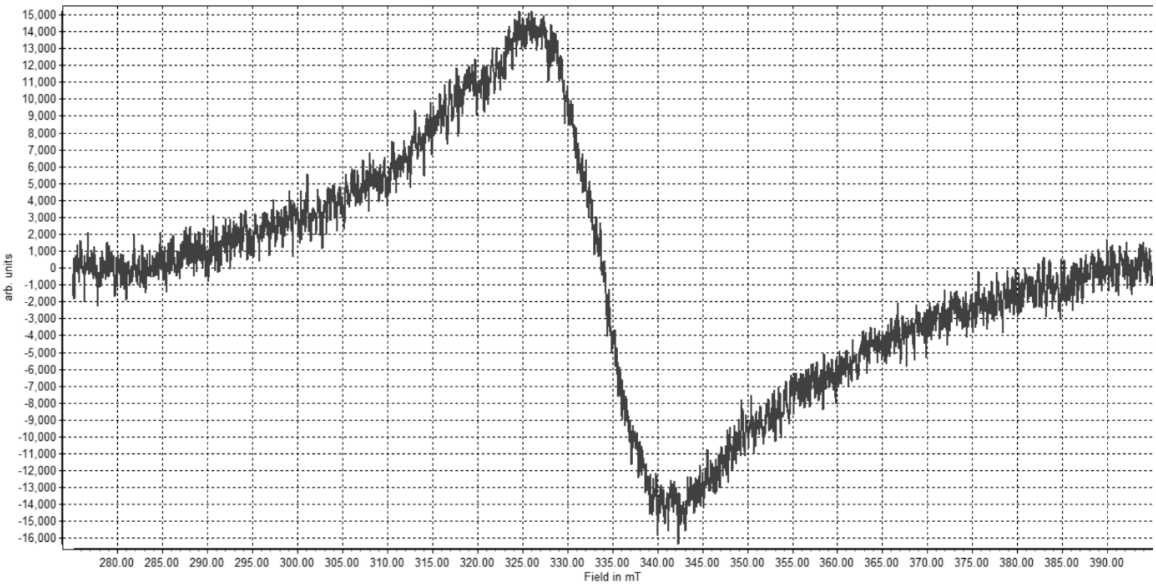

Figure 1. EPR spectrum of compound **3a** in CD_2Cl_2 measured at 77 K.

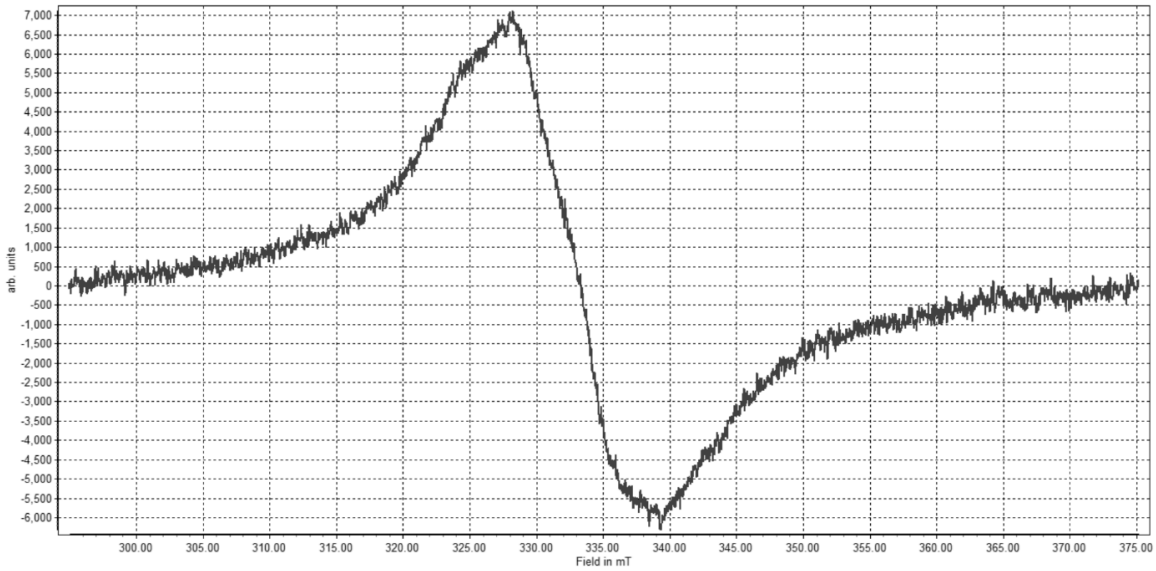

Figure 2. EPR spectrum of compound **3b** as crystalline sample cooled to 77 K.

Selected VT and MAS NMR spectra

MAS NMR of [Cu{(Cp*Mo)$_2$(μ,η^6:η^6:η^2-P$_6$)}$_2$][TEF] (**4a**):

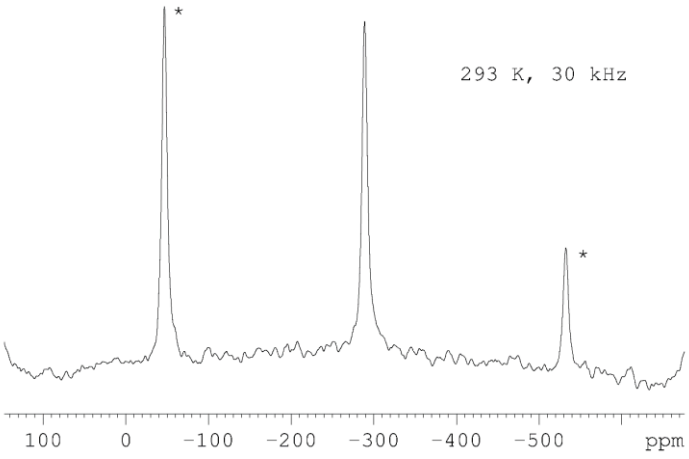

Figure 3. ^{31}P{^{1}H} MAS NMR spectra of the Cu$^+$ compound isolated as its square planar isomer **4a**. The absolute signal positions were confirmed by measurement at different rotation frequencies. * rotation side bands.

MAS NMR of [Tl{(Cp*Mo)$_2$(μ,η^6:η^6:η^2-P$_6$)}$_2$]$_n$[TEF]$_n$ (**6**):

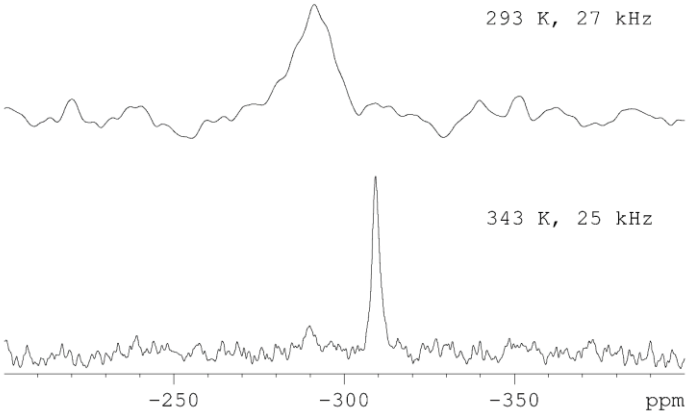

Figure 4. $^{31}P\{^1H\}$ MAS NMR spectra of compound **6**. The absolute signal positions were confirmed by measurement at different rotation frequencies.

VT NMR of [Cu{(Cp*Mo)$_2$(μ,η^6:η^6:η^2-P$_6$)}$_2$][TEF] (**4a**, **5**):

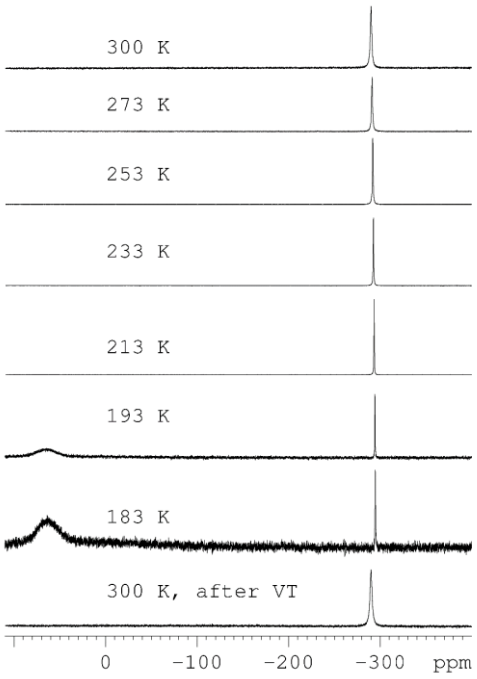

Figure 5. $^{31}P\{^1H\}$ VT NMR experiment of [Cu(**1**)$_2$][TEF] in CD_2Cl_2 cooling from 300 K to 183 K and warming up again to 300 K.

The Cu compounds **4a** and **5** show a broad singlet at –290.4 ppm in the $^{31}P\{^1H\}$ NMR spectrum at room temperature revealing the chemical and magnetic equivalence of all P atoms of the *cyclo*-P$_6$ ligands on the NMR timescale. This is most probably caused by fast underlying equilibria including fast rotation of the P$_6$ rings. Upon cooling the singlet remains almost unchanged

showing the highly dynamic coordination behavior persists even at low temperatures. When the solution is cooled below 193 K a new very broad signal arises next to the singlet at +66 ppm which may arise from precipitation of the product. After warming the sample up again, the new signal vanishes and only the singlet of the pure compound **4a** or **5** can be observed.

VT NMR of [Ag{(Cp*Mo)$_2$(μ,η^6:η^6:η^2-P$_6$)}$_2$][TEF] (**4b**):

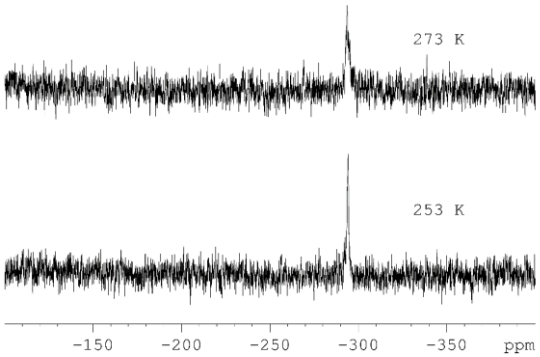

Figure 6. ^{31}P{^{1}H} VT NMR spectrum of **4b** recorded upon warming a crystalline sample of **4b** in CD_2Cl_2. The spectra for temperatures below 253 K or above 273 K did not show any signal because of the limited solubility and the fast decomposition.

VT NMR of [Tl{(Cp*Mo)$_2$(μ,η^6:η^6:η^2-P$_6$)}$_2$]$_n$[TEF]$_n$ (**6**):

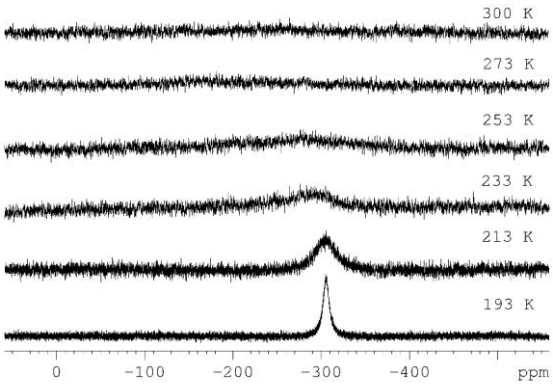

Figure 7. ^{31}P{^{1}H} VT NMR spectrum of compound **6** in CD_2Cl_2.

At room temperature no signal can be resolved in the ^{31}P{^{1}H} NMR spectrum of compound **6** in CD_2Cl_2. Upon cooling below 213 K a very broad signal can be observed at –305.5 ppm.

X-ray structure determination

General considerations

All crystal manipulations were performed under mineral oil or perfluorinated oil. The diffraction experiments were performed at 123 K on an Agilent Technologies Gemini R Ultra diffractometer

or an Agilent SuperNova diffractometer with Cu-K_α or Mo- K_α radiation. Crystallographic data together with the details of the experiments are given in Table 1 and Table 2. The cell determination, data reduction and absorption correction for all compounds were performed with the help of the CrysAlis PRO software by Agilent Technologies Ltd. The full-matrix least-square refinement against F^2 was done with ShelXL. During the refinement several restraints and constraints had to be applied. For the description of the refinement strategy we list the commonly used syntax for the ShelXL program (DFIX, SADI, SIMU, ISOR, EADP). All atoms except hydrogen were refined anisotropically if not described otherwise. The H atoms were calculated geometrically and a riding model was used during refinement process. Graphical material was created with the free software Olex2. CCDC-1411077-1411083 contain the supplementary crystallographic data for this paper. These data can be obtained free of charge from The Cambridge Crystallographic Data Centre via www.ccdc.cam.ac.uk/data_request/cif.

Special comments on the weakly coordinating anion [TEF]

Due to its weakly coordinating nature, the anion [TEF] tends to be disordered in a lot of its solid state structures. The CF_3- as well as whole $(CF_3)_3CO$-groups frequently exhibit rotational disorder by rotation of C–O or C–C bonds, respectively. In some cases even a positional disorder of the whole anion can be observed. To resolve these kinds of disorder which are still present at 100 K good data sets with high resolution are needed. In addition, most of the compounds containing the anion [TEF] show a rather weak diffraction at high angles which proves the X-ray crystallography of these compounds to be a very challenging task. During the refinement of these solid state structures it is common that a series of least-square restraints has to be applied to prevent the results to display an unrealistic geometry or displacement parameters. In rare cases, even good data sets do not enable the refinement of all disorders which usually results in large displacement parameters, especially of the fluorine atoms.

Crystallographic tables

Table 1. Crystallographic details for the compounds **1**, **2**, **3b** and **4b**.

Identification code	**1**	**2**	**3b**	**4b**
formula	$C_{20}H_{30}Mo_2P_6$	$C_{19}H_{28.5}Mo_2P_{9.8}$	$C_{56}H_{30}AlF_{46}Mo_2O_3P_6$	$C_{57}H_{62}AgAlCl_2F_{36}Mo_4O_4P_{12}$
weight [g·mol^{-1}]	648.14	752.30	2029.48	2456.21
T [K]	123.00(14)	123.00(10)	123.1(4)	123.01(10)
crystal system	triclinic	monoclinic	monoclinic	monoclinic
space group	$P\bar{1}$	$P2_1/n$	$C2/c$	$C2/c$
a [Å]	8.25280(10)	8.0528(4)	30.6081(3)	36.3787(4)
b [Å]	8.65580(10)	15.3282(6)	21.83616(15)	16.16213(17)
c [Å]	10.12920(10)	11.4000(6)	21.7617(3)	14.51853(16)
α [°]	101.1590(10)	90	90	90
β [°]	106.0070(10)	104.970(5)	110.4429(13)	101.5137(10)
γ [°]	113.5080(10)	90	90	90
V [Å^3]	598.789(13)	1359.41(12)	13628.7(3)	8364.49(16)
Z	1	2	8	4
ρ_{calc} [g·cm^{-3}]	1.797	1.838	1.978	1.950
μ [mm^{-1}]	1.454	13.087	6.080	10.624
absorption correction	gaussian	gaussian	gaussian	gaussian
T_{min}/T_{max}	0.820 / 0.855	0.301 / 0.707	0.434 / 0.727	0.435 / 0.617
F(000)	324.0	747.0	7928.0	4808.0
crystal size [mm^3]	0.185 × 0.180 × 0.141	0.202 × 0.082 × 0.030	0.212 × 0.120 × 0.058	0.110 × 0.076 × 0.062
radiation [Å]	MoK_α	CuK_α	CuK_α	CuK_α
diffractometer	Gemini R Ultra	SuperNova	Gemini R Ultra	SuperNova,
2 Θ range [°]	5.852 to 60.088	9.89 to 152.33	5.944 to 133.2	8.28 to 147.416
reflns collected / unique	54934 / 3339	4563 / 2718	56018 / 11876	23765 / 8226
R_{int} / R_{sigma}	0.0324 / 0.0182	0.0320 / 0.0350	0.0461 / 0.0326	0.0286 / 0.0212
data / restraints/ parameters	3339 / 0 / 132	2718 / 15 / 166	11876 / 36 / 1092	8226 / 109 / 738
GOF on F^2	1.106	1.069	0.946	1.067
R_1 / wR_2 [$I \geq 2\,\sigma(I)$]	0.0191 / 0.0491	0.0474 / 0.1279	0.0299 / 0.0728	0.0413 / 0.1149
R_1 / wR_2 [all data]	0.0210 / 0.0495	0.0549 / 0.1324	0.0357 / 0.0747	0.0440 / 0.1167
max / min $\Delta\rho$ [e·Å^{-3}]	1.40 / –0.48	1.20 / –0.89	0.61 / –0.67	1.24 / –0.85

Table 2. Crystallographic details for the compounds **4a**, **5** and **6**.

Identification code	**4a**	**5**	**6**
formula	$C_{57}H_{62}AlCl_2CuF_{36}Mo_4O_4P_{12}$	$C_{147}H_{160}Al_2Cu_2F_{72}Mo_8O_8P_{24}$	$C_{56.45}H_{60.9}AlCl_{0.9}F_{36}Mo_4O_4P_{12}Tl$
weight [g·mol^{-1}]	2411.88	5114.58	2506.00
T [K]	122.99(13)	123(1)	123.15
crystal system	monoclinic	triclinic	monoclinic
space group	*C*2/*c*	*P*–1	*C*2/*c*
a [Å]	36.4679(6)	16.7510(5)	36.1206(14)
b [Å]	16.1466(3)	17.2703(7)	16.4296(5)
c [Å]	14.4134(2)	18.8355(6)	14.5113(7)
α [°]	90	109.136(3)	90
β [°]	101.863(2)	97.750(3)	100.380(4)
γ [°]	90	108.799(3)	90
V [Å^3]	8305.8(2)	4693.8(3)	8470.8(6)
Z	4	1	4
ρ_{calc} [g·cm^{-3}]	1.929	1.809	1.965
μ [mm^{-1}]	9.123	7.604	11.921
absorption correction	analytical	multi-scan	gaussian
T_{min}/T_{max}	0.187 / 0.509	0.75936 / 1.000	0.270 / 0.870
F(000)	4736.0	2534.0	4851.6
crystal size [mm^3]	0.332 × 0.216 × 0.101	0.147 × 0.102 × 0.075	0.164 × 0.121 × 0.011
radiation [Å]	$CuK_α$	$CuK_α$	$CuK_α$
diffractometer	SuperNova	SuperNova	SuperNova
2 *Θ* range [°]	6.008 to 136.476	5.886 to 150.866	8.244 to 146.086
reflns collected / unique	68860 / 7599	34771 / 18870	14650 / 8068
R_{int} / R_{sigma}	0.0478 / 0.0166	0.0362 / 0.0472	0.0383 / 0.0464
data / restraints/ parameters	7599 / 123 / 758	18870 / 241 / 1261	8068 / 162 / 730
GOF on F^2	1.112	1.053	1.083
R_1 / wR_2 [$I \geq 2\ \sigma(I)$]	0.0472 / 0.1088	0.0665 / 0.1781	0.0836 / 0.2195
R_1 / wR_2 [all data]	0.0474 / 0.1090	0.0736 / 0.1867	0.0973 / 0.2272
max / min Δ*ρ* [e·Å^{-3}]	1.39 / –1.22	1.82 / –1.11	1.24 / –2.05

X-ray structure refinement of [(Cp*Mo)$_2$(μ,η^6:η^6-P$_6$)] (**1**): The solid state structure of **1** was reported earlier in the literature.[6] The measurement was performed at room temperature (R_1 = 4.1%), therefore we performed another X-ray experiment at low temperature. The solid state structure is depicted in Figure 8.

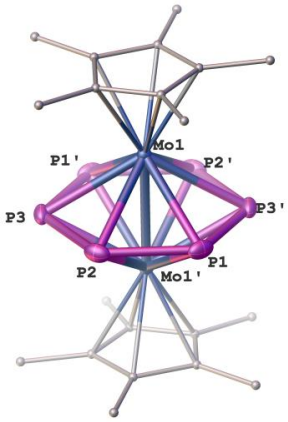

Figure 8. Molecular structure of **1**. P purple, Mo blue, C grey; H atoms are omitted and C atoms are depicted as small balls for clarity. Selected bond lengths [Å]: Mo1-Mo1‘ 2.6463(3), P1-P3‘ 2.1822(8), P1-P2 2.1833(8), P2-P3 2.1840(8).

X-ray structure refinement of [(Cp*Mo)$_2$(μ-P$_{10}$)] (**2**): Compound **2** crystallizes in the monoclinic space group *P*2$_1$/*n* with the molecule occupying the center of inversion. Figure 9 shows the *cyclo*-P$_{10}$ ligand of compound **2**. When the structural model containing only the complex with a *cyclo*-P$_{10}$ ligand was refined we observed a residual density peak of ~4 electrons situated at

about 0.8 Å next to Mo1. The position and environment of this peak as well as the electron count is in contradiction with the whole molecular complex. Therefore we interpreted it as the second minor position of Mo atom (Mo2). Its occupancy was refined to 5%. Subsequently, we found three additional electron density peaks at reasonable distances to each other and to Mo2 and assigned them as P6, P7 and P8. The Mo and P atoms of the minor part were refined in isotropic approximation. We were unable to localize the minor position of the Cp* ligand due to its negligible contribution to the electron density. Thus, the final model corresponds to a substitutional solid solution of two complexes, a *cyclo*-P_{10} complex **2** and a *cyclo*-P_6 complex **1** mixed in a 95:5 ratio. The model of the disorder is depicted in Figure 10.

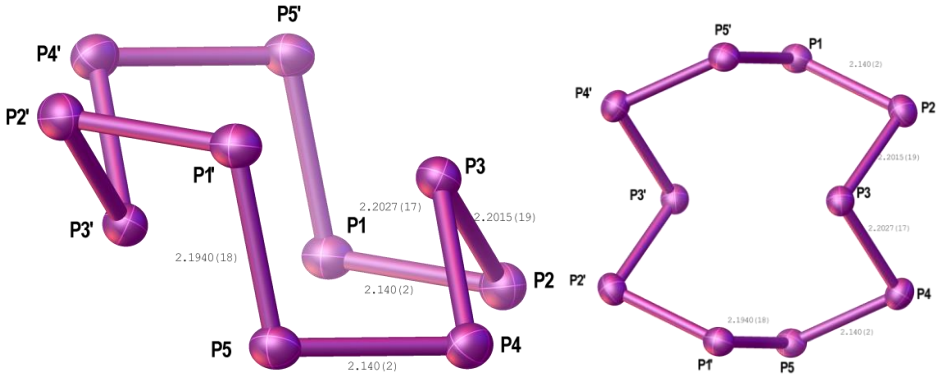

Figure 9. A greatly folded *cyclic* P_{10} ligand of compound **2**. Cp*Mo fragments were omitted for clarity. (left) side view (right) front view. Selected atomic distances [Å]: P1-P5' 2.1930(18), P1-P2 2.140(2), P2-P3 2.2015(19), P3-P4 2.2027(17), P4-P5 2.140(2), P2-P4 3.1279(19), P3-P2' 3.174(2), P3-P5' 3.1605(17). Mo1-Mo1' 3.7018(8); Interplanar angle P2-P3-P4-plane to P1-P2-P4-P5-plane 68.18(7)°, interplanar angle P1-P2-P4-P5-plane to P1-P5-P1'-P5'-plane 103.94(7)°.

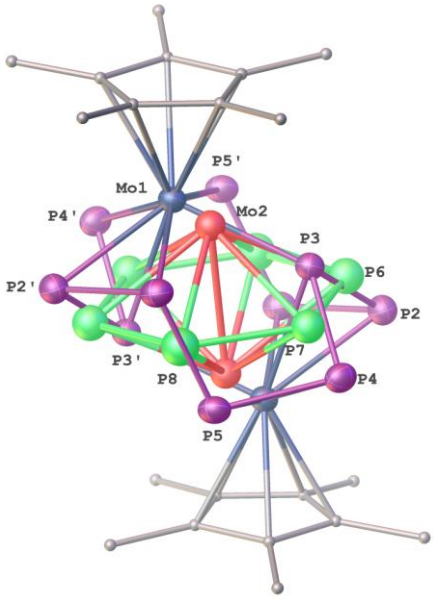

Figure 10. The disordering *cyclo*-P_{10} and *cyclo*-P_6 complexes in the crystal structure of compound **2**. H atoms are omitted and C atoms are depicted as small balls for clarity. The *cyclo*-P_{10} complex (P purple, Mo blue, C grey) with its Cp* ligands is occupied for 95%, the *cyclo*-P_6 complex (P green, Mo red) is occupied for 5% without Cp* ligands. Selected bond lengths [Å]: Mo2-Mo2' 2.613(18), average P-P bond lengths of *cyclo*-P6 ~2.16 (geometry was restrained by SADI instructions in SHELX!).

X-ray structure refinement of [(Cp*Mo)$_2$(μ,η^6:η^6-P_6)][FAl] (**3b**): Crystals of compound **3b** suitable for X-ray diffraction analysis can be obtained by layering a CH_2Cl_2 solution with *n*-hexane and storage at +4 °C for several days. Compound **3b** crystallizes in the monoclinic space group *C*2/*c*.

There are two complex cations occupying the position of a twofold rotation axis (see Figure 11) and one [FAl] anion occupying a general position. One of the P_6 rings shows a re-orientational disorder over three close positions (Figure 11 middle, right) while the other one is ordered (Figure 11 left). All P_6 rings show a bisallylic distortion with two opposing P-P bonds being significantly elongated (P1-P1', P3-P3', P5-P6, P9-P10, P12-P13). All atoms except hydrogen were refined anisotropically. The displacement parameters of the P atoms with 20% occupancy (P8-P13) had to be restrained with ISOR instruction in SHELX.

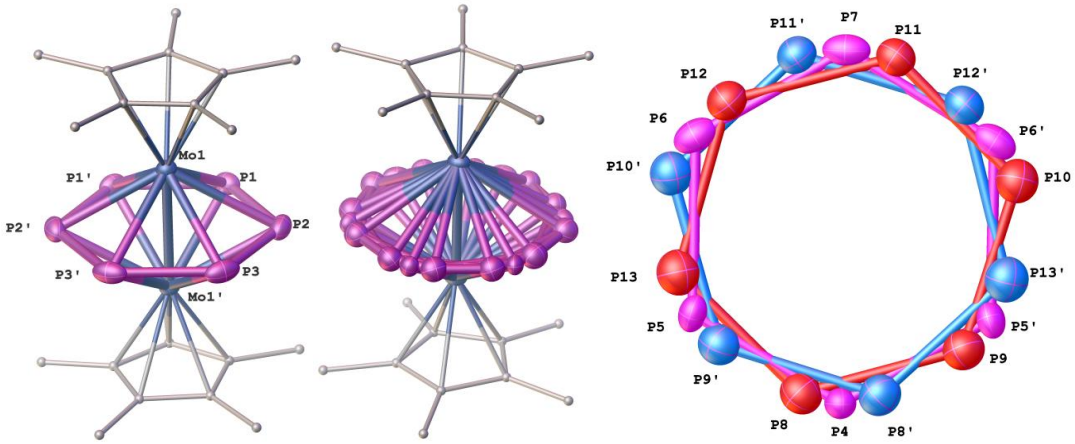

Figure 11. The complex cations in the crystal structure of compound **3b**. P purple, Mo blue, C grey; H atoms are omitted and C atoms are depicted as small balls for clarity. (left) Structure of the ordered complex cation. (middle) Structure of the second complex cation exhibiting a re-orientational disorder of the P_6 ring over three positions. (right) The model of the disorder for the P_6 ring. The P_6 ring is disordered over three positions in a ratio of 60:20:20. The major orientation (P4 - P7, pink) lie on the twofold axis. The two minor parts are symmetrically equivalent (P8 - P13, red and blue). Selected bond lengths [Å]: Mo1-Mo1‘ 2.6617(4), P1-P1‘ 2.2932(13), P1-P2 2.1348(10), P2-P3 2.1384(11), P3-P3‘ 2.2477(16), Mo2-Mo2‘ 2.671(2), P4-P5 2.157(3), P5-P6 2.220(3), P6-P7 2.176(3), P8-P9 2.105(9), P9-P10 2.215(8), P10-P11 2.163(7), P11-P12 2.181(8), P12-P13 2.235(8).

X-ray structure refinement of [Ag{(Cp*Mo)$_2$(μ,η^6:η^6:η^2-P$_6$)}$_2$][TEF] (**4b**) and [Cu{(Cp*Mo)$_2$(μ,η^6:η^6:η^2-P$_6$)}$_2$][TEF] in its square planar form **4a**:

The X-ray analysis of the compounds **4a** and **4b** will be discussed together since they are isostructural. Suitable crystals of both compounds can be obtained by layering a concentrated solution in CH_2Cl_2/toluene with *n*-hexane and storage at +4 °C for several days. The compounds crystallize in the monoclinic space group *C*2/*c*. The cationic complex $[M(P_6)_2]^+$ (M =Ag, Cu; P_6 = **1**) is occupying the center of inversion. The anion and one CH_2Cl_2 solvent molecule are situated each on a twofold rotation axis. Both independent fluorinated tert-butoxy groups of the aluminate anion are disordered over two positions (with probability 52:48, 51:49 (Ag); 53:47, 52:48 (Cu)). At the initial stages of the structure refinement most bond distances of the anion were restrained by several DFIX instructions, which were gradually replaced by SADI restraints, which number was maximally reduced, but a lot of them had to be kept even in the final model in order to keep reasonable geometry of the WCA [TEF]. The final model of the anions are shown in Figure 12 and Figure 13 on the right hand side. The displacement parameters of some of the disordered C and F atoms had to be restrained by ISOR, SIMU or DELU or constrained by EADP instructions as well. Some disordered atoms (1 for M = Cu, 7 for M = Ag) were refined in isotropic approximation. The CH_2Cl_2 solvent molecule is disordered over three positions for M = Ag (43:29:28) and two positions for M = Cu (70:30) The C-Cl distances were restrained in both cases by DFIX instructions. The methylene carbon atoms were refined isotropically and the displacement parameters were equated for M = Ag. The Cl-Cl distances for M = Cu were restrained by DFIX instructions and the displacement parameters of the less occupied Cl atoms were equated. The cationic complexes $[M(\mathbf{1})_2]^+$ were refined unconstrained (Figure 12 (Ag), Figure 13 (Cu), left hand side).

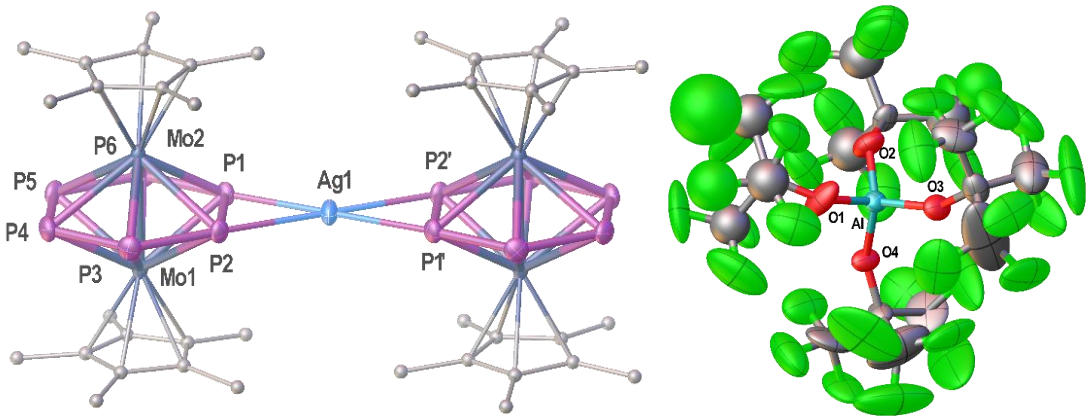

Figure 12. (left) The complex cation from the crystal structure of compound **4b**. P purple, Ag light blue, Mo blue, C grey; H atoms are omitted and C atoms are depicted as small balls for clarity. Selected bond lengths [Å]: Ag1-P1 2.5793(10), Ag1-P2 2.6196(10), P1-P2 2.2915(14), P2-P3 2.1653(14), P3-P4 2.1726(15), P4-P5 2.1630(15), P5-P6 2.1671(15), P6-P1 2.1667(14); (right) The final model of the [TEF] anion from the crystal structure of compound **4b**.

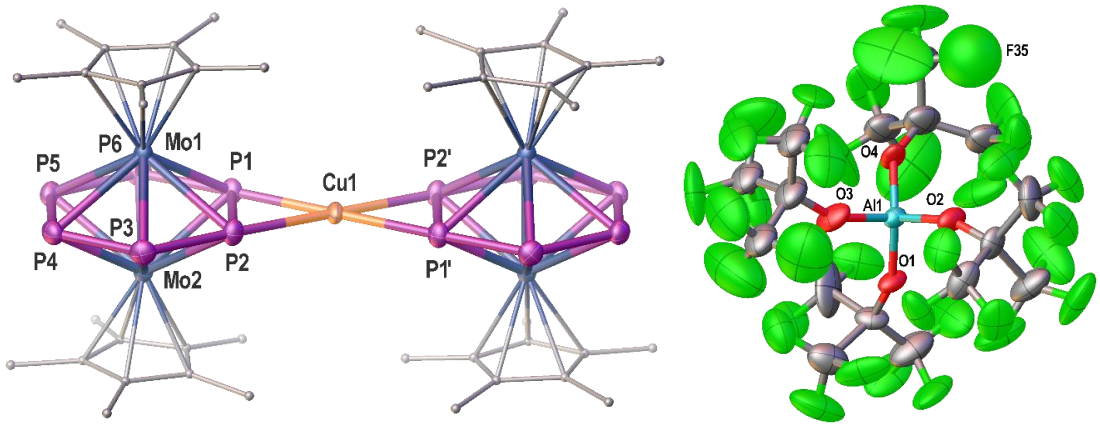

Figure 13. (left) The complex cation in the crystal structure of compound **4a**. P purple, Cu orange, Mo blue, C grey; H atoms are omitted and C atoms are depicted as small balls for clarity. Selected bond lengths [Å]: Cu1-P1 2.4354(12), Cu1-P2 2.3927(12), P1-P2 2.2694(16), P2-P3 2.1765(17), P3-P4 2.1685(18), P4-P5 2.1729(18), P5-P6 2.1677(17), P1-P6 2.1808(17); (right) The final model of the [TEF] anion from the crystal structure of compound **4a**.

X-ray structure refinement of [Cu{(Cp*Mo)$_2$(μ,η^6:η^6:η^2-P$_6$)}$_2$][TEF] in its tetrahedral form **5**: Suitable crystals of compound **5** for X-ray crystallography can be obtained by layering a toluene solution of **5** with *n*-hexane and storage at +4 °C for several days. Compound **5** crystallizes in the triclinic space group *P*-1 with two *cyclo*-P$_6$ ligands **1** coordinated to one Cu atom in a distorted tetrahedral geometry occupying a general position. The [TEF] anion and two toluene solvent molecules are also situated on general positions. Additionally there is another toluene molecule which occupies the center of inversion. The cationic complex [Cu(P$_6$)$_2$]$^+$ is shown in Figure 14 on the left. In the WCA [TEF] two tert-butoxy groups (containing O1 and O2) showed slight tendency for disorder that was not possible to resolve. The remaining two tert-butoxy groups show a disorder over two positions each related by a rotation around an O-C bond (depicted in Figure 14 right hand side). The occupancies of the two disordered groups were refined to 61:39 and 57:43. The C and F atoms with occupacies below 50% were refined isotropically. The bond distances of the disordered tert-butoxy groups were restrained by several DFIX commands. These DFIX restrains could only partly be replaced by SADI restraints during the final refinement. The displacement parameters of some of these atoms had to be also restrained by ISOR, SIMU and DELU restraints. The geometry of the two toluene solvent molecules on general positions was restrained

to be symmetric by SAME commands with the same ring atoms in opposite order as a reference. The third toluene solvent molecule is 50% occupied being disordered over an inversion center. The C atoms were refined isotropically and their displacement parameters were equated by EADP instructions.

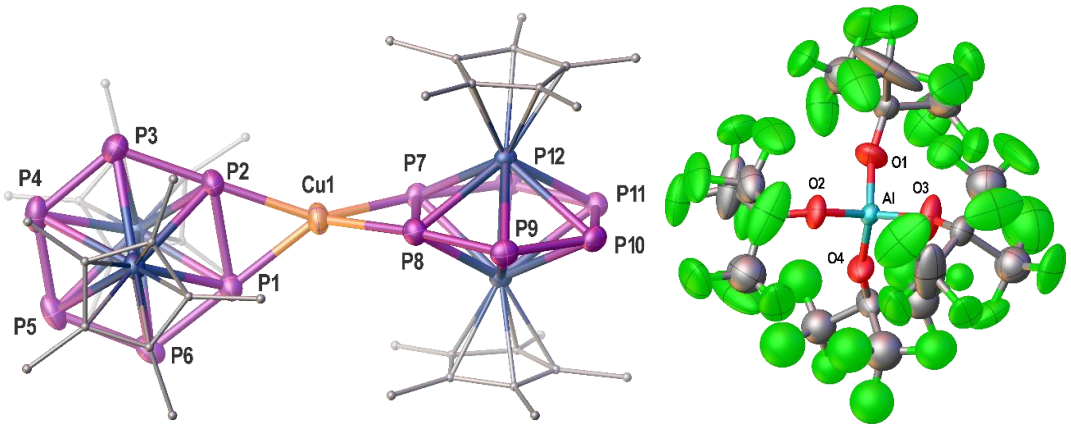

Figure 14. (left) The distorted tetrahedral complex cation in the crystal structure of compound **5**. P purple, Cu orange, Mo blue, C grey; H atoms are omitted and C atoms are depicted as small balls for clarity. Selected bond lengths [Å]: Cu1-P1 2.3546(16), Cu1-P2 2.3343(16), Cu1-P7 2.3483(16), Cu1-P8 2.3383(16), P1-P2 2.286(2), P2-P3 2.165(2), P3-P4 2.176(2), P4-P5 2.151(3), P5-P6 2.168(2), P6-P1 2.163(2), P7-P8 2.2876(19), P8-P9 2.1664(19), P9-P10 2.171(2), P10-P11 2.157(2), P11-P12 2.168(2), P12-P7 2.1666(19); Interplanar angle between P1-P2-Cu1 and P7-P8-Cu1 planes 93.5°; (right) The [TEF] anion in the crystal structure of compound **5**. For the tert-butoxy groups at O3 and O4 only one orientation is depicted here.

X-ray structure analysis of $[Tl\{(Cp^*Mo)_2(\mu,\eta^6{:}\eta^6{:}\eta^2\text{-}P_6)\}_2]_n[TEF]_n$ (6)

Details of the X-ray structure refinement: Compound **6** crystallizes in the monoclinic space group *C*2/*c* with a very similar unit cell like the Cu^+ and Ag^+ compounds **4a** and **4b** (**6** can be regarded as isostructural). The direct coordination environment of Tl^+ can be described as a cationic complex $[Tl(P_6)_2]^+$ (cf. Ag^+ and Cu^+) which is occupying the center of inversion. The anion and 90% of a CH_2Cl_2 solvent molecule are situated each on a twofold rotation axis. The structure is severely disordered. The Tl^+ cation is disordered around the inversion center. The *cyclo*-P_6 ring is disordered over two positions in a 1:1 ratio. The ratio is also in agreement with the distances to the Tl^+ cation for both its alternative positions (see Figure 16). One of the Cp* ligands is also disordered by rotation in a 75:25 ratio. The C-C distances of the minor Cp ring position were fixed during the refinement. The hydrogen atoms of the disordered Cp* ligands were refined in geometrically calculated positions for an ordered and in one case for a disordered methyl group. The [TEF] anion is disordered over two positions (1:1 ratio, disorder was refined similar to compound **4a**, see Figure 13 right hand side and exhibits a high thermal motion. During the refinement the geometry of this highly disordered anion had to be restrained by several DFIX, DANG and SADI commands. The number of these restraints was maximally reduced at the end of the refinement. Additionally some displacement parameters of these groups had to be restrained or constrained.

Analysis of the crystal structure: The X-ray structure of **6** is closely related to the crystal structures of the distorted square planar Cu^+ and Ag^+ compounds **4a** and **4b**. The coordination environment around Tl^+ is depicted in Figure 15.

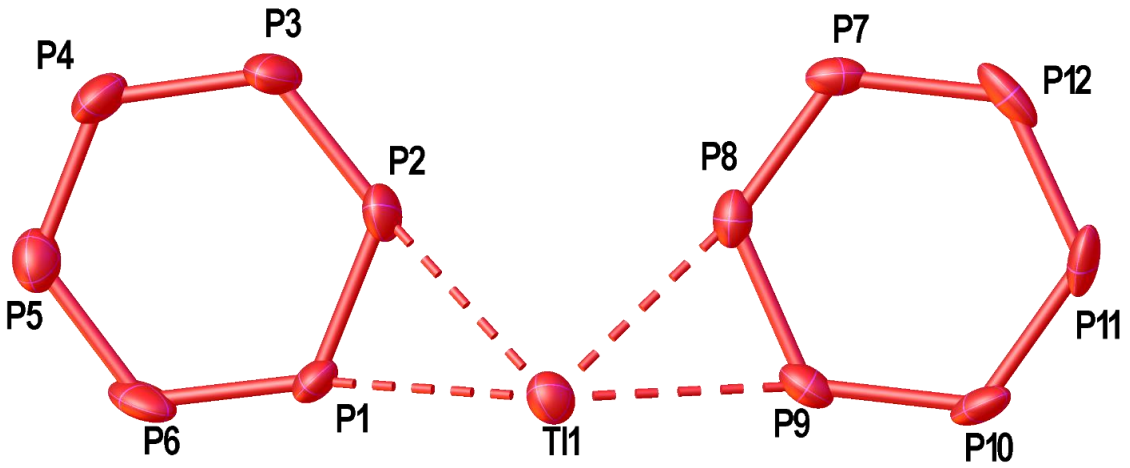

Figure 15. Direct coordination environment of Tl^+ in the crystal structure of compound **6** can be described as cationic $[Tl(P_6)_2]^+$ unit. Cp*Mo fragments are omitted for clarity. Selected bond lengths [Å]: Tl1-P1 3.23284(12), Tl1-P2 3.28516(15), Tl1-P8 3.23938(8), Tl1-P9 3.24129(14).

Tl1 is disordered over a center of inversion and cannot occupy it like Cu^+ or Ag^+ (see section 6.7, distance Tl1-Tl1' = 4.4448(19) Å). If this is caused by the larger atomic radius of Tl^+ or by the tendency to form complexes with a higher coordination number than 2 cannot be further elucidated. Nevertheless, the exchange of the central metal can be done without serious change of the structure type. As a consequence, the *cyclo*-P_6 ligand shows two orientations in the solid state with a 1:1 ratio when it is coordinated to Tl1 or Tl1', respectively.(1)

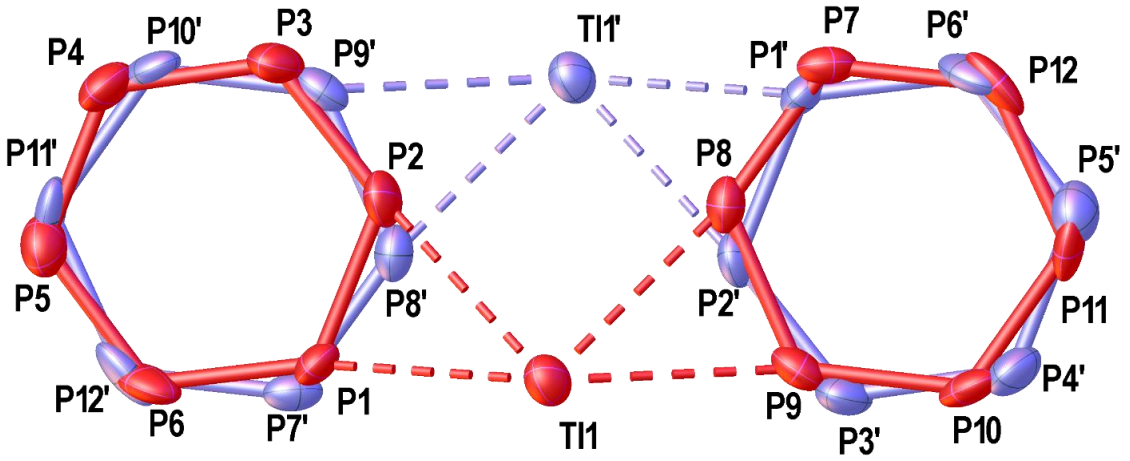

Figure 16. The model of the disorder of the $[Tl(P_6)_2]^+$ complex over the center of symmetry, where two *cyclo*-P_6 ligands in different orientations are coordinated to every Tl cation. Cp*Mo fragments of the P_6 ligands are omitted for clarity. A coordination of the Tl cation to the other orientation of the *cyclo*-P_6 ligand can be ruled out since it would result in too short Tl-P distances (e.g. Tl1-P8' 2.882 Å vs. Tl1 P2' 3.022 Å).

The present coordination forms $[Tl(P_6)_2]^+$ coordination units (see Figure 15) with Tl-P distances ranging from ~3.23 – 3.28 Å, but the large Tl^+ cation shows also elongated contacts to the P_6 rings of the next $[Tl(P_6)_2]^+$ coordination unit (see Figure 17) which results in a distorted trigonal

(1) A coordination to the other orientation of the *cyclo*-P6 ligand can be excluded since it would result in too short Tl-P distances which are not in accordance with the weak Tl^I-P interactions present in this compound. (e.g. Tl1-P8' 2.882 Å or Tl1 P2' 3.022 Å).

pyramidal coordination of three P-P bonds to Tl^+. The two possible orientations of the third *cyclo*-P_6 ligand around Tl^+ result in two pairs of Tl-P distances (either Tl1-P5' 3.42008(19), Tl1-P6' 3.69009(11) or Tl1-P12' 3.43(3), Tl1-P11' 3.743(19) which are not shown in Figure 17). These distances are close to each other and therefore no preferred orientation of the third P_6 ring can be assumed. The crystal packing of **6** (see Figure 18) consists of alternating layers of cationic complexes and negatively charged layers of the [TEF] anions. The 2D cationic layer expands along the crystallographic *bc* plane. The P atoms of all *cyclo*-P_6 ligands of a layer are turned by 14.9°.

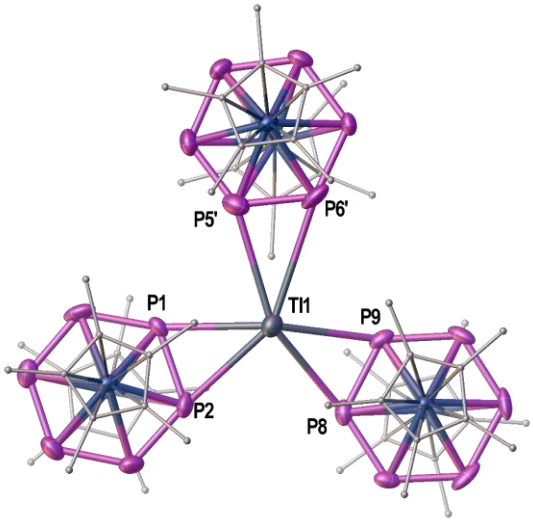

Figure 17. Coordination environment of Tl cation (view along the *a* axis). Selected bond lengths [Å]: Tl1-P1 3.23284(12), Tl1-P2 3.28516(15), Tl1-P8 3.23938(8), Tl1-P9 3.24129(14), Tl1-P5'3.42008(19), Tl1-P6' 3.69009(11), not shown here: Tl1-P12' 3.43(3), Tl1-P11' 3.743(19).

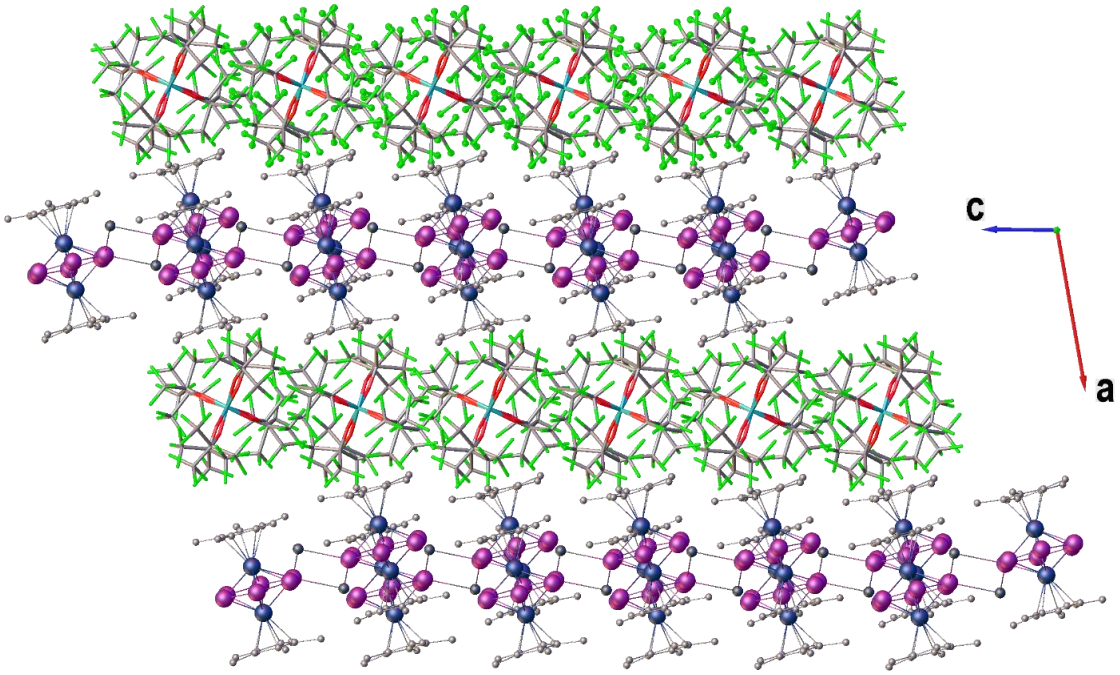

Figure 18. Crystal packing of **6** with viewing direction along the *b*-axis showing alternating layers of the 2D-coordination polymer and the WCAs [TEF].

Figure 19 shows the cationic layer of compound **6** viewed along the crystallographic a axis. Since only Tl1 or Tl1' can be occupied at once (light blue or dark grey, distance Tl-Tl1' = 4.4448(19) Å) and the respective Tl cation is coordinated by an additional *cyclo*-P_6 ligand the resulting assembly, if only one Tl is occupied in an ordered manner (always Tl1 or Tl1'), is presented in Figure 20. The assembly in Figure 20 shows parallel one-dimensional coordination strands of Tl^+ and *cyclo*-P_6 complexes inside the coordination layers. (*This is only one possibility! The Tl cations could also be occupied in a pure statistical manner which would also result in further interconnection of the coordination units. This means that the coordination layers are not completely closed sheets. Additionally this also implies that there would be cavities in the described coordination layers which could be filled by additional metal centers. However, this was unfortunately not possible during this study, since the large anions are necessary in this case to afford a* Tl^I *coordination to these cyclo-*P_6 *ligands.)*

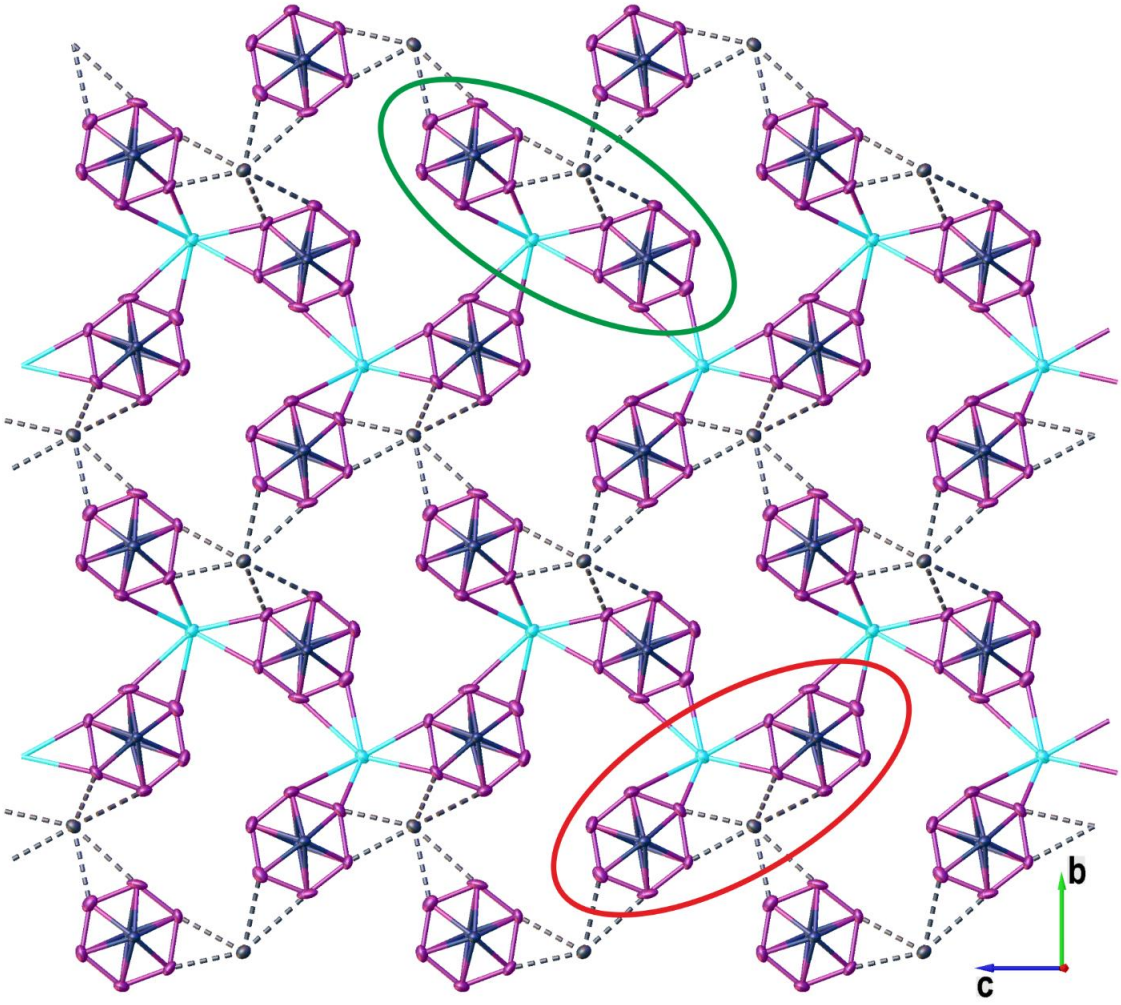

Figure 19. Viewing direction along the crystallographic *a* axis. The half-occupied Tl cations are depicted in dark and light grey and the $[Tl(P_6)_2]^+$ coordination units with shorter Tl-P distances are circumscribed by ellipses. Cp* ligands are omitted for clarity.

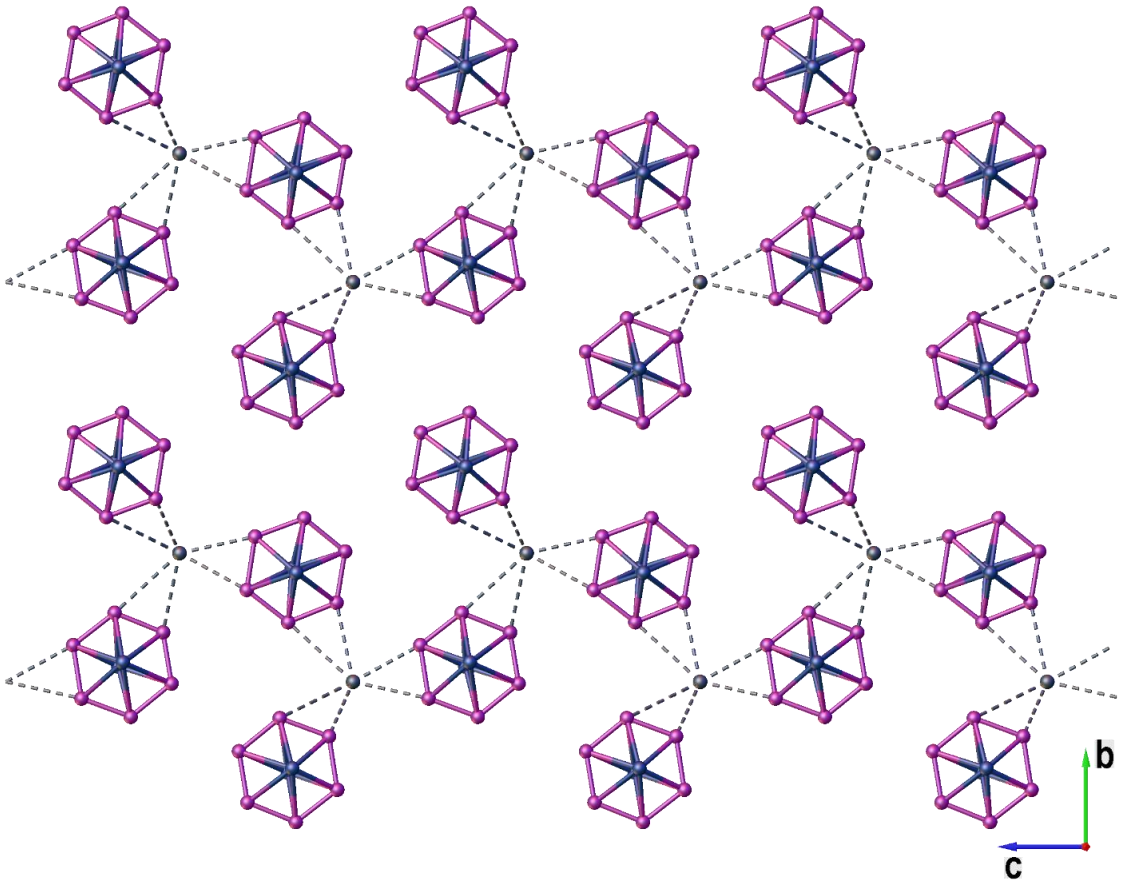

Figure 20. Possible one-dimensional coordination polymer found inside the cationic layers of compound **6** in the solid state. Viewing direction along the *a*-axis.

Similarity of the crystal structures of 4a, 4b and 6

The compounds **6**, **4a** and **4b** show very similar unit cells and crystallize in the same space group *C*2/*c*. The assembly in the solid state is also very similar with alternating negative layers of the [TEF] anions and positively charged coordination layers along the crystallographic *a* axis shown in Figure 21 c) and d). The similarity of the coordination layers of **6** and **4a-b** are visualized in Figure 21 a) and b). The $[Tl(P_6)_2]^+$ coordination units of **6** (see Figure 15) directly correspond to the complex cations $[M(P_6)_2]^+$ of **4a** (M =Cu, see Figure 13) and **4b** (M = Ag, see Figure 12).

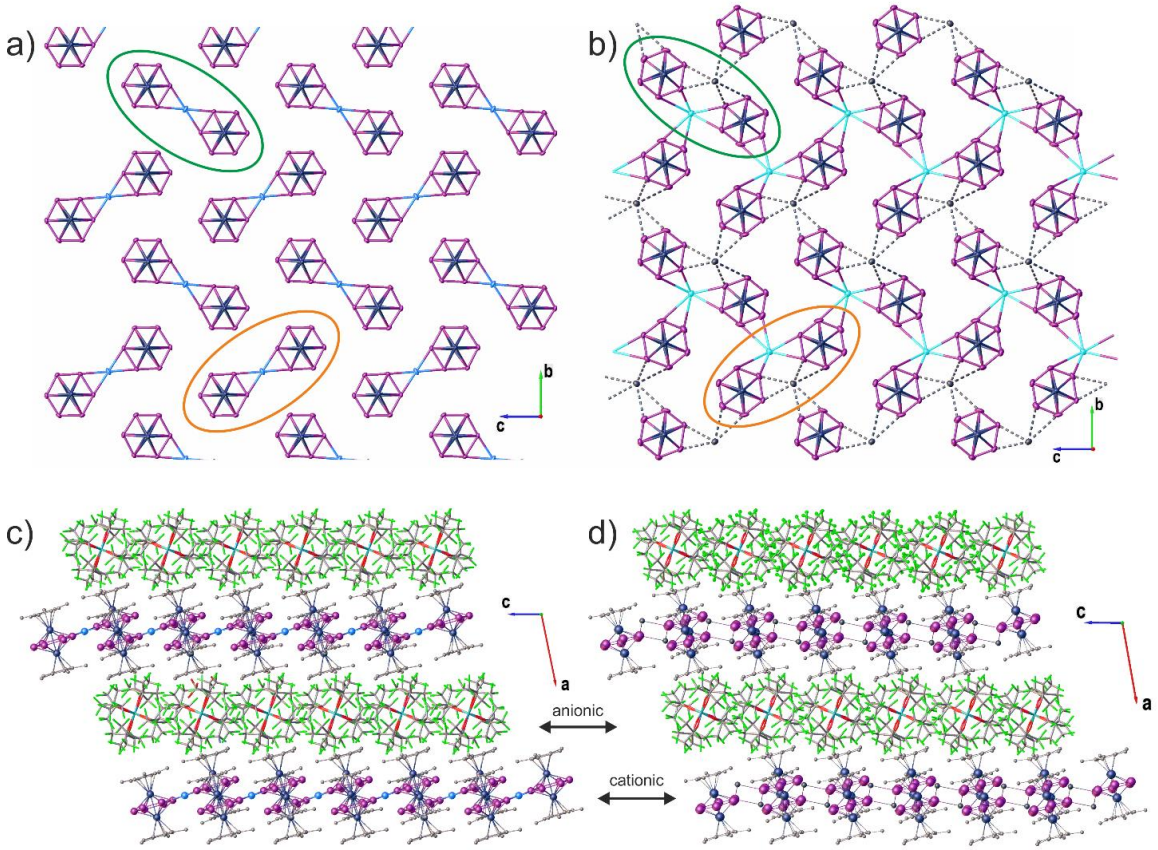

Figure 21. Cationic layers inside the *bc*-plane of **4b** a) and **6** b). Tl^+ positions (light and dark) in b) are half-occupied. For a) and b) anions, C and H atoms are omitted for clarity. c) + d) Illustration of the crystal packing of **4b** c) and **6** d) with viewing direction along the *b*-axis showing the alternation of cationic and anionic layers along the *a*-axis. The P_6 planes include a tilt angle of 16.3° (**4a**), 16.3° (**4b**) and 13.8° (**6**) to the *bc*-plane.

X-ray powder diffraction analysis

X-ray powder diffraction measurements were carried out with a STOE Stadi P diffractometer with monochromatic Cu-$K_{\alpha1}$-radiation (λ = 1.540598 Å, Ge-monochromator) and a Mythen 1 K detector at 293 K. The 2Θ-range was 2.000° to 93.335° for **4a** and 2.000° to 71.825° for **5**. Diffraction data were analyzed with WINXPOW. The cell constants determined with X-ray powder diffraction at room temperature differs slightly from single crystal data (123 K) and were refined to *a* = 36.812(9) Å, *b* = 16.307(6) Å, *c* = 14.61(2) Å, β = 100.74(3)° and *V* = 8615(9) Å^3 (**4a**) and *a* = 16.995(8) Å, *b* = 17.51(1) Å, *c* = 19.41(1) Å, α = 109.42(4)°, β = 97.65(4)°, γ = 108.44(3)° and *V* = 4981(7) Å^3 (**5**), see Table 3. The powder diffraction patterns were simulated with the unit cell parameters which were obtained from the 293 K powder measurement.

Table 3. Refined unit cells of the compounds **4a** and **5** by single crystal X-ray diffraction at 123 K and X-ray powder diffraction at 293 K.

compound	**4a**		**5**	
	single crystal (123 K)	powder (293 K)	single crystal (123 K)	powder (293 K)
a [Å]	36.4679(6)	36.812(9)	16.7510(5)	16.995(8)
b [Å]	16.1466(3)	16.307(6)	17.2703(7)	17.51(1)
c [Å]	14.4134(2)	14.61(2)	18.8355(6)	19.41(1)
α [°]	90	90	109.136(3)	109.42(4)
β [°]	101.863(2)	100.74(3)	97.750(3)	97.65(4)
γ [°]	90	90	108.799(3)	108.44(3)
V [Å^3]	8305.8(2)	8615(9)	4693.8(3)	4981(7)

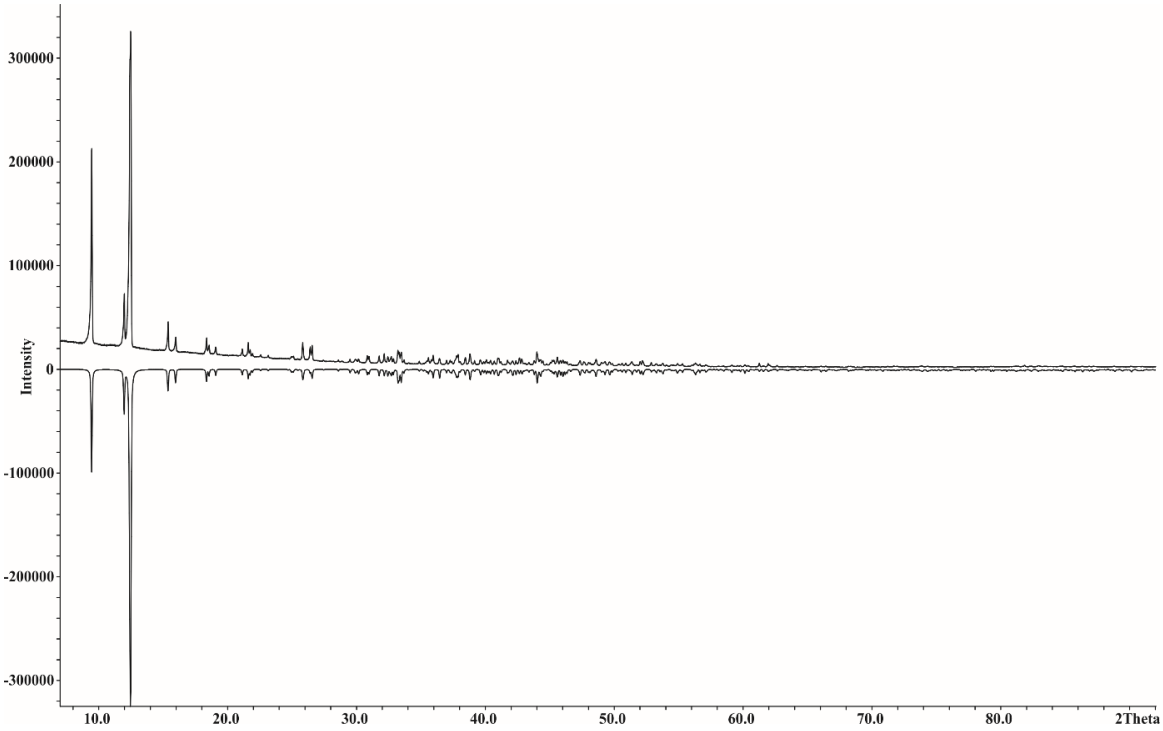

Figure 22. X-ray powder pattern for the pure *cyclo*-P_6 complex **1**. Positive intensities (measured), negative intensities (simulated).

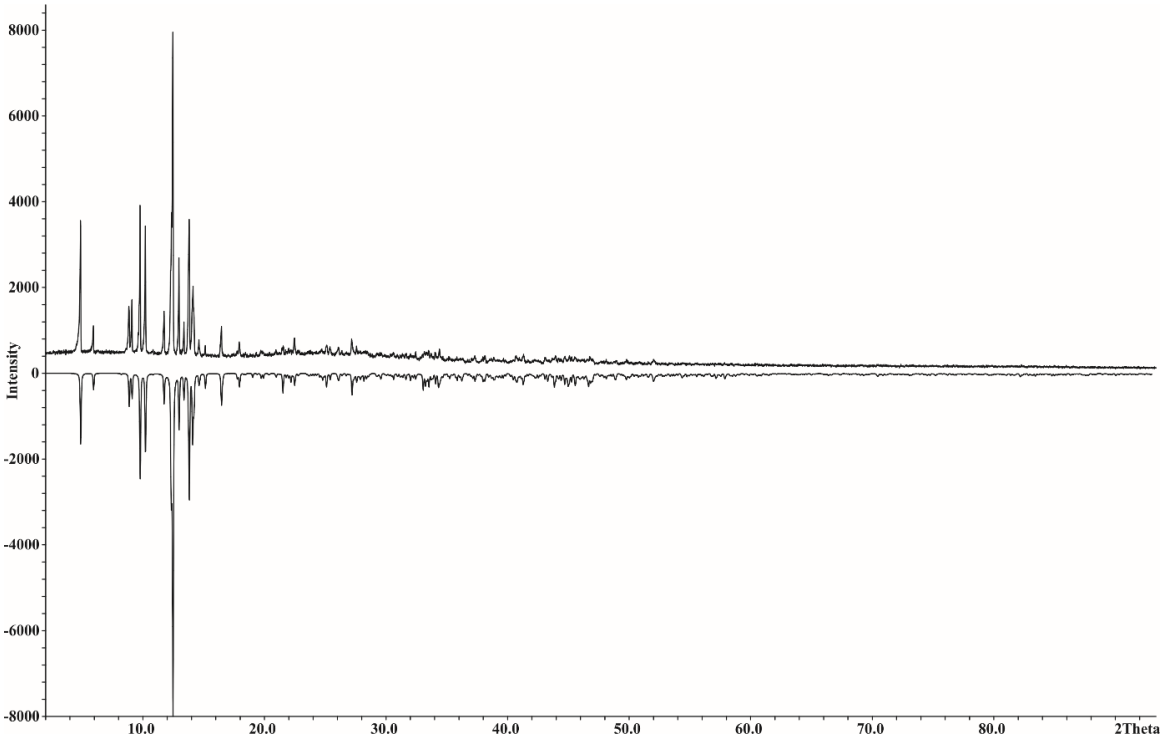

Figure 23. X-ray diffraction pattern for compound **4a**. Positive intensities (measured), negative intensities (simulated).

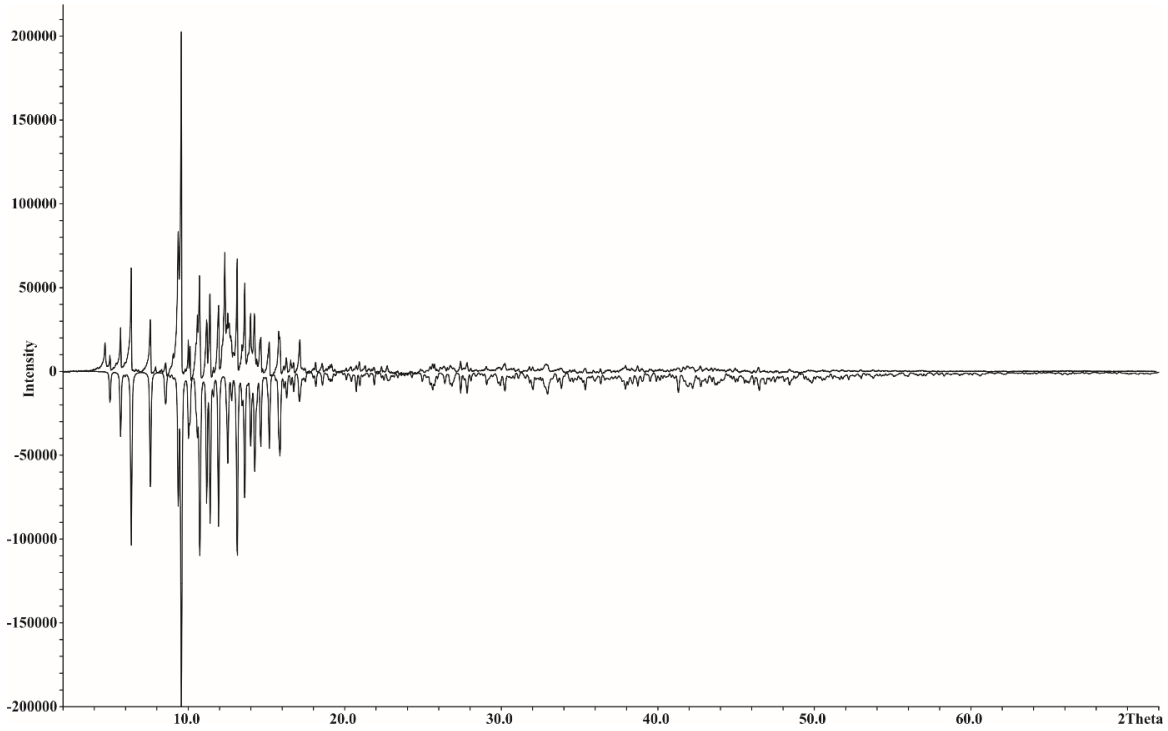

Figure 24. Xray powder diffraction pattern for compound **5**. Positive intensities (measured), negative intensities (simulated).

DFT calculation

DFT calculations for [(Cp*Mo)$_2$(μ-P$_{10}$)] (**2**): All calculations have been performed with the TURBOMOLE program package[12]. For the analysis of the bonding situation in [(Cp*Mo)$_2$(P$_{10}$)] the BP86 functional together with the def2-TZVP basis set has been used. The reaction energies has been calculated at the B3LYP[13]/def2-TZVP[14] level of theory. The nature of the stationary point was checked by calculating the vibration frequencies. All complexes show no negative frequencies, except [(Cp*Mo)$_2$(P$_{10}$)] for which one negative frequency (5.24 cm^{-1}) corresponding to the rotation of the Cp* ligand was observed. Repeated geometry optimizations did not lead to the elimination of this negative frequency. For calculating the reaction energies, this negative frequency has been ignored. The reported population analysis[15] was performed as implemented in TURBOMOLE. The reaction energy of the transformation [(Cp*Mo)$_2$(P$_{10}$)] → [(Cp*Mo)$_2$(P$_6$)] + P$_4$ is −19.64 kJ·mol^{-1} (corrected for zero point vibration energy; −13.26 kJ·mol^{-1} not corrected)

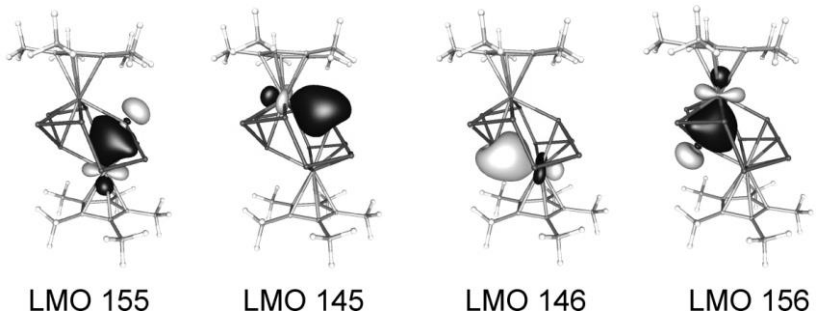

Figure 25. Isosurfaces of Localized Molecular Orbitals (LMO) representing the Mo-P bonding interactions, calculated at the BP86/def2-TZVP level of theory.

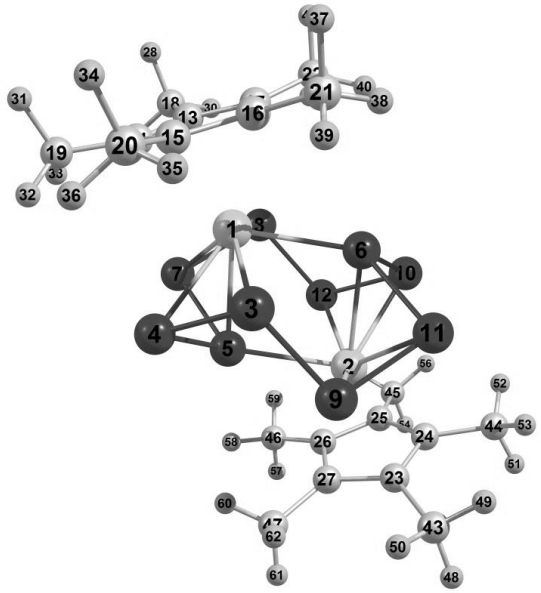

Figure 26. Atom labeling in $[(Cp^*Mo)_2(\mu\text{-}P_{10})]$. Optimized geometry of **2**.

Tables reporting on the calculated Wiberg bond indices in **2** and the cartesian coordinates can be found in the electronic form of the supporting information on the provided DVD.

DFT calculations for $[(Cp^*Mo)_2(\mu\text{-}\eta^6\text{:}\eta^6\text{-}P_6)]^{0/+}$ (**1**, **3a**, **3b**): All calculations have been performed with the TURBOMOLE program package[12] at the RI-[16]BP86[13]/def2-TZVP[14] level of theory, followed by single point calculations without the RI approximation. The Multipole Accelerated Resolution of Identity (MARI-J)[17] approximation was used in the geometry optimization steps. The nature of the stationary point was checked by the frequency calculations. For $[(Cp^*Mo)_2(P_6)]$ a negative frequency of $-2.26\ cm^{-1}$ corresponding to the rotation of the Cp* ligand was observed. Although the geometry has been optimized repeatedly using different methods and different input geometries, this negative frequency persisted.

The inspection of the frontier molecular orbitals in $[(Cp^*Mo)_2(\mu,\eta^6\text{:}\eta^6\text{-}P_6)]$ (**1**) shows, that the HOMO and HOMO-1 orbitals are basically degenerate and represent P-P bonding with contribution of molybdenum d orbitals. By elimination of one electron the HOMO-1 orbital in **1** is converted to the Single Occupied Molecular Orbital (SOMO) in $[\mathbf{1}]^+$ (Figure 27 and Figure 28). This leads to the reduction of the P-P bond order (two opposite P-P bonds) and to the observed bis-allylic distortion. This behavior is also nicely described by the Wiberg Bond Indices. The WBI for all P-P bonds in **1** is the same and equals to 0.86 whereas in $[\mathbf{1}]^+$ the WBI corresponding to the elongated P-P bonds are 0.67 and while it is 0.95 for the other P-P bonds. The WBI for the Mo-Mo bond (2.669 Å and 2.698 Å in **1** and $[\mathbf{1}]^+$, respectively) is 0.86 in **1** and 0.95 in $[\mathbf{1}]^+$.

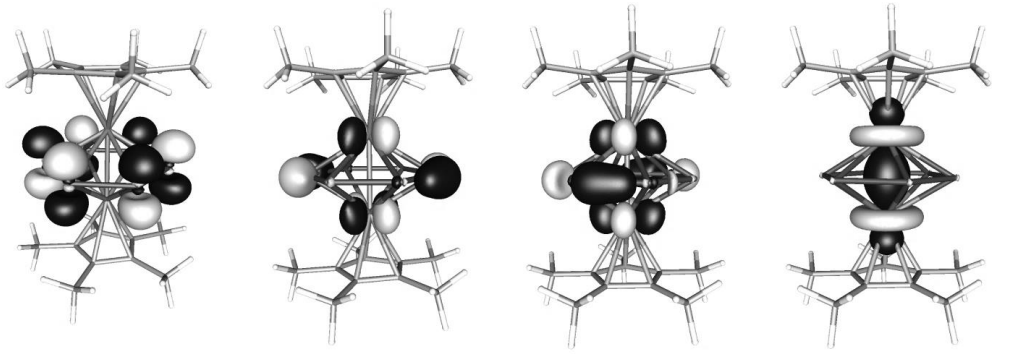

Figure 27. Isosurfaces of selected molecular orbitals in $[(Cp^*Mo)_2(\mu,\eta^6{:}\eta^6\text{-}P_6)]$ (**1**) calculated at the BP86/def2-TZVP level of theory.

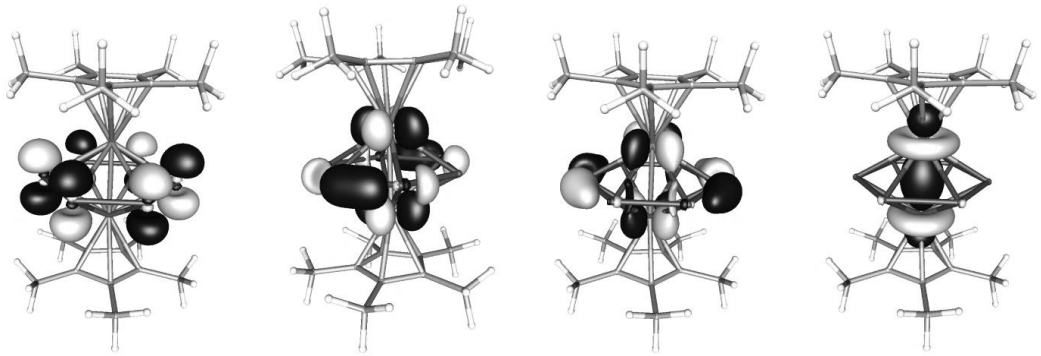

Figure 28. Isosurfaces of selected molecular orbitals in $[(Cp^*Mo)_2(\mu,\eta^6{:}\eta^6\text{-}P_6)]^+$ (= $[\mathbf{1}]^+$) calculated at the BP86/def2-TZVP level of theory.

Tables reporting on the cartesian coordinates can be found in the electronic form of the supporting information on the provided DVD.

DFT calculations for the equilibria of square planar and tetrahedral isomers of the complex cations $[M(1)_2]^+$ M = Cu, Ag

The geometries of the compounds have been fully optimized with gradient-corrected density functional theory (DFT) in form of Becke's three-parameter hybrid method B3LYP[18] with def2-SVP all electron basis set (ECP on Mo,Ag).[19] Gaussian 03 program package[20] was used throughout. All structures correspond to minima on their respective potential energy surfaces. Solvent effects have been estimated by performing single point energy computation of gas-phase optimized geometries using polarisable continuum model (PCM) as implemented in Gaussian 03.
For Cu compounds, optimization of a planar isomer in framework of C_i point group (inversion center) resulted in transition state structure, which is only by 0.7 kJ mol^{-1} higher than asymmetric minimum. Planar isomer is predicted to be energetically less stable than tetrahedral (24.6 kJ mol^{-1} in the gas phase), but has larger standard entropy. Values for the equilibrium constant for the isomerization reaction *tetrahedral* → *square planar* are 0.12, 0.24, and 0.38 for the gas phase, toluene and dichloromethane solutions, respectively. Thus, from the thermodynamic point of view, both isomers should be present in solution at room temperature (with tetrahedral isomer having the higher concentration). The influence of the solvent on the energetic of isomerization processes is rather small. However, changing from the gas phase to toluene and dichloromethane solutions increases concentration of the less stable planar isomer, but tetrahedral one remains dominant in all cases.

For Ag analogs, energetically the tetrahedral isomer is also more stable, but the difference is only 9.5 kJ mol^{-1} in the gas phase and 6.0 and 4.2 kJ mol^{-1} in toluene and dichloromethane. Due to entropy factor, planar isomer is predicted to be dominant in solution: values for the equilibrium constant for the isomerization reaction *tetrahedral* → *square planar* are 7.0, 28.3, and 59.1 for the gas phase, toluene and dichloromethane solutions, respectively. Thus, molar fraction of tetrahedral isomer with respect to planar is predicted to be below 4% in toluene and below 2% in dichloromethane. Thus, planar isomer should be dominant in solution.
Tables reporting on the total energies can be found in the electronic form of the supporting information on the provided DVD. A table of the reaction energies can be found in the main text of chapter 3.

References

[1] R. B. King, M. Z. Iqbal, A. D. King Jr, *J. Organomet. Chem.* **1979**, *171*, 53-63.
[2] I. Krossing, *Chem. Eur. J.* **2001**, *7*, 490-502.
[3] T. Köchner, N. Trapp, T. A. Engesser, A. J. Lehner, C. Röhr, S. Riedel, C. Knapp, H. Scherer, I. Krossing, *Angew. Chem. Int. Ed.* **2011**, *50*, 11253-11256; *Angew. Chem.* **2011**, *123*, 11449-11452.
[4] G. Santiso-Quiñones, A. Higelin, J. Schaefer, R. Brückner, C. Knapp, I. Krossing, *Chem. Eur. J.* **2009**, *15*, 6663-6677.
[5] M. Gonsior, I. Krossing, N. Mitzel, *Z. Anorg. Allg. Chem.* **2002**, *628*, 1821-1830.
[6] O. J. Scherer, H. Sitzmann, G. Wolmershäuser, *Angew. Chem. Int. Ed.* **1985**, *24*, 351-353; *Angew. Chem.* **1985**, *97*, 358-359.
[7] D. F. Evans, *J. Chem. Soc.* **1959**, 2003-2005.
[8] D. F. Evans, G. V. Fazakerley, R. F. Phillips, *J. Chem. Soc. A* **1971**, 1931-1934.
[9] T. H. Crawford, J. Swanson, *J. Chem. Educ.* **1971**, *48*, 382.
[10] D. H. Grant, *J. Chem. Educ.* **1995**, *72*, 39.
[11] G. J. P. Britovsek, V. C. Gibson, S. K. Spitzmesser, K. P. Tellmann, A. J. P. White, D. J. Williams, *J. Chem. Soc., Dalton Trans.* **2002**, 1159-1171.
[12] a) R. Ahlrichs, M. Bär, M. Häser, H. Horn, C. Kölmel, *Chem. Phys. Lett.***1989**, *162*, 165–169; b) O. Treutler, R. Ahlrichs, *J. Chem. Phys.***1995**, *102*, 346–354.
[13] a) P. A. M. Dirac, *Proc. Royal Soc.A*,**1929**, *123*, 714. b) J. C. Slater, *Phys. Rev.***1951**, *81*, 385. c) S. H. Vosko, L. Wilk, M. Nusair, *Can. J. Phys.***1980**, *58*, 1200. d) A. D. Becke, *Phys. Rev. A*, **1988**, *38*, 3098. e) C. Lee, W. Yang, R. G. Parr, *Phys. Rev. B*,**1988**, *37*, 785. f) A. D. Becke, *J. Chem. Phys.* **1993**, *98*, 5648.
[14] a) A. Schäfer, C. Huber, R. Ahlrichs, *J. Chem. Phys.***1994**, *100*, 5829; b) K. Eichkorn, F. Weigend, O. Treutler, R. Ahlrichs, *Theor. Chem. Acc.***1997**, *97*, 119.
[15] A. E. Reed, R. B. Weinstock, F. Weinhold, *J. Chem. Phys.*, **1985**, *83*, 735-746.
[**16**] a) K. Eichkorn, O. Treutler, H. Oehm, M. Häser, R. Ahlrichs, *Chem. Phys. Lett.*1995, 242, 652–660; b) K. Eichkorn, F. Weigend, O. Treutler, R. Ahlrichs, *Theor. Chem. Acc.*1997, 97, 119.
[**17**] M. Sierka, A. Hogekamp, R. Ahlrichs, *J. Chem. Phys.*2003, 118, 9136.
[18] a) A.D. Becke, *J. Chem. Phys.* **1993**, *98*, 5648. b) C. Lee, W. Yang, R.G. Parr, *Phys. Rev. B.* **1988**, *37*, 785.
[19] a) F. Weigend, R. Ahlrichs, *Phys.Chem.Chem.Phys.*, **2005**, *7*, 3297-3305. b) D. Andrae, U. Haeussermann, M.Dolg, H.Stoll, H.Preuss, *Theor.Chim.Acta,* **1990**, *77*, 123-141. .
[20] M. J. Frisch, G. W. Trucks, H. B. Schlegel, G. E. Scuseria, M. A. Robb, J. R. Cheeseman, J. A. Montgomery, Jr., T. Vreven, K. N. Kudin, J. C. Burant, J. M. Millam, S. S. Iyengar, J. Tomasi, V. Barone, B. Mennucci, M. Cossi, G. Scalmani, N. Rega, G. A. Petersson, H. Nakatsuji, M. Hada, M. Ehara, K. Toyota, R. Fukuda, J. Hasegawa, M. Ishida, T. Nakajima, Y. Honda, O. Kitao, H. Nakai, M. Klene, X. Li, J. E. Knox, H. P. Hratchian, J. B. Cross, V. Bakken, C. Adamo, J. Jaramillo, R. Gomperts, R. E. Stratmann, O. Yazyev, A. J. Austin, R. Cammi, C. Pomelli, J. W. Ochterski, P. Y. Ayala, K. Morokuma, G. A. Voth, P. Salvador, J. J. Dannenberg, V. G. Zakrzewski, S. Dapprich, A. D. Daniels, M. C. Strain, O. Farkas, D. K. Malick, A. D. Rabuck, K. Raghavachari, J. B. Foresman, J. V. Ortiz, Q. Cui, A. G. Baboul, S. Clifford, J. Cioslowski, B. B. Stefanov, G. Liu, A. Liashenko, P. Piskorz, I. Komaromi, R. L. Martin, D. J. Fox, T. Keith, M. A. Al-Laham, C. Y. Peng, A. Nanayakkara, M. Challacombe, P. M. W. Gill, B. Johnson, W. Chen, M. W. Wong, C. Gonzalez, and J. A. Pople, Gaussian03, revision B.05. Gaussian, Inc., Wallingford CT, 2004.

Preface

The following chapter has not been published until the submission of this thesis.

Authors

Martin Fleischmann, Alexander V. Virovets, Eugenia V. Peresypkina, Marek Sierka and Manfred Scheer*

Author contributions

The preparation and characterization of all compounds including the single crystal X-ray structure determination and the preparation of the manuscript was done by the first author. Alexander V. Virovets and Eugenia V. Peresypkina were significantly involved in the X-ray structural characterization of the compounds. Alexander V. Virovets conducted the structure refinement of the disordered Ag^+ cations in **1b** and wrote the corresponding section of the manuscript. Marek Sierka is performing supporting DFT calculations. Manfred Scheer supervised the research and revised the manuscript.

Acknowledgements

This work was supported by the Deutsche Forschungsgemeinschaft.

4 Interaction of 'naked' silver cations towards aromatic *cyclo*-P_5 and *cyclo*-As_5 ligands: from mixed σ and π bonding up to weakly π bonding

Abstract: Reaction of the *cyclo*-E_5 sandwich complexes [Cp*Fe(η^5-E_5)] (E = P(**A**), As(**B**)) containing the WCAs [TEF] and [FAl] are presented. These reactions afford the first Ag^+ complexes containing the *cyclo*-As_5 ligand **B**. The formation of the 1:2 compound [Ag(**B**)$_2$][TEF] (**1a**) is presented although the structural characterization could not be completed due to severe disorder of the anion [TEF]. The analogues compound [Ag(**B**)$_2$][FAl] (**1b**) of the larger anion [FAl] shows an interesting disorder of the central Ag^+ cation between two π coordinating *cyclo*-As_5 ligands. This phenomenon is either caused by thermal movement or by static disorder of the central Ag atom. The introduction of a third equivalent of **B** to Ag[FAl] results in the formation of isolated trigonal paddle-wheel [Ag(η^2-**B**)$_3$]$^+$ complex cations in the solid state via π coordination of an As-As bond. Finally, the reaction of Ag[FAl] and [Cp*Fe(η^5-P_5)] (**A**) results in the formation of a tetranuclear Ag^+ complex exhibiting four different coordination modes of the *cyclo*-P_5 ligand **A** among which two have only been predicted by DFT calculations before.

4.1 Introduction

The isolobal analogy helps to build bridges between inorganic and organic chemistry.[1] For example the preparation of the all-phosphorus analog of the well-known Cp ligand in [Cp*Fe(η^5-P_5)] (**A**) in 1987 by *Scherer et al.* can be viewed as a benchmark.[2] In the following decades, the reactivity of the pentaphosphaferrocene **A** towards Cu^I halides,[3,4,5,6,7,8,9,10,11] strong oxidants and reductants[12] and also nucleophiles[13] was more and more investigated. Although the all-arsenic analog [Cp*Fe(η^5-As_5)] (**B**) was isolated only three years later in 1990 investigations of its reactivity and comparison to its phosphorus analog are scarce.[14] While **A** and **B** show the same reactivity towards the 16 valence electron (VE) complex fragments [Cp*M(CO)] (M = Ir, Rh)[15] or the 12 VE fragments [M(CO)$_3$] (M = Cr, Mo)[16] they generally yield different products when reacted with Cu^I halides. In the recent years it was possible to isolate a variety of coordination polymers[3,4] and also fullerene-like supramolecules[5,6,7,8,9,10] in the case of **A** from these reactions where complex **A** is usually σ coordinating via the lone pairs of the P_5 ring. Complex **B** on the other hand is mainly π donating and prefers the side-on coordination of an As-As bond to Cu^+.[17]

A similar bonding preference of **A** and **B** could also be observed towards the Hg atoms of perfluoro-*ortho*-phenylenemercury $[(o\text{-}C_6F_4Hg)]_3$ although the adducts are primarily based on electrostatic forces instead of dative bonds.[18] Recently, we were able to demonstrate, that complex **B** can be forced to σ donation towards Cu^I by sterical shielding of the metal center in the trinuclear complexes $[Cu_3(\mu\text{-}Cl)_2(dpmp)_2]^+$ (dpmp = bis(diphenylphosphinomethyl)phenylphosphine).[19] In order to investigate the donor characteristics of the E_5 complexes towards different metal centers we chose to react them with monocations bearing weakly coordinating anions (WCA) which mimic pseudo-gas phase conditions.[20,21] When both complexes are reacted with the very weak and soft Lewis acid Tl^+ bearing the WCA [TEF] ([TEF] = $[Al\{OC(CF_3)_3\}_4]^-$)[22] both E_5 ligands show the same bridging η^5:η^1-coordination (see Scheme 1, top right).[23,24] By increasing the size of the WCA from [TEF] (57 atoms) to [FAl] (86 atoms) ([FAl] = $[FAl\{OC_6F_{10}(C_6F_5)\}_3]^-$)[25,26,27] a change of the coordination mode is observed and only the η^5-coordination towards Tl^+ remains (see Scheme 1, bottom right) affording isolated $[Tl(\mathbf{L})_3]^+$ (**L** = **A**, **B**) complex cations. In the case of Ag^+ from Ag[TEF] and complex **A** the one-dimensional coordination polymer $[Ag(\mu,\eta^2\text{:}\eta^1\text{-}\mathbf{A})_2]_n[TEF]_n$ is formed exhibiting a bridging coordination mode of complex **A** with mixed σ and π coordination towards Ag (see Scheme 1, bottom left).[28]

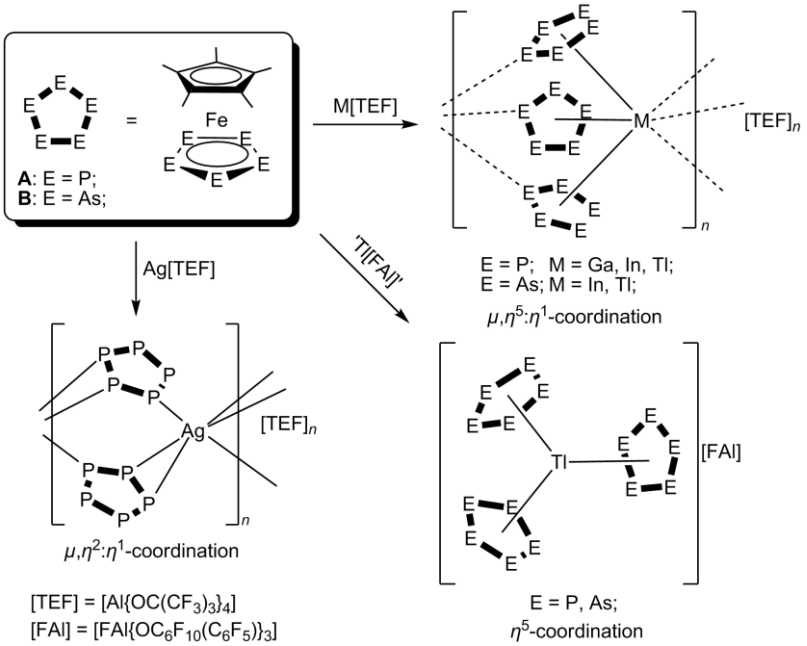

Scheme 1. Reported reactivity of $[Cp^*Fe(\eta^5\text{-}E_5)]$ towards M^+ cations featuring the WCAs [TEF] and [FAl]. The P_5 ring of **A** shows a bridging η^2:η^1-coordination towards Ag^+, while both E_5 complexes exhibit a bridging η^5:η^1-coordination towards the group 13 metal cations Tl^+, In^+ and Ga^+ (only **A**) with the [TEF] anion and a η^5-coordination towards Tl^+ featuring the anion [FAl].

Since the coordination ability of the complexes **A** and **B** is very flexible and hard to predict, the question arises which coordination mode complex **B** would adopt towards

Ag^+ and if the reaction outcome is dependent on the stoichiometry of the reactants. In order to answer these questions we reacted complex **B** with Ag[TEF] and Ag[FAl] in different molar ratios and thoroughly investigated the products by single crystal X-ray structural analysis. DFT calculations are currently performed but since these highly dynamic coordination compounds represent tremendous challenges they could not be finished in the scope of this work. Additionally, we investigated the impact of exchanging the WCA [TEF] for the WCA [FAl] in the reaction of complex **A** with Ag^+.

4.2 Results and Discussion

[Cp*Fe(η^5-As_5)] (**B**) is reacted with Ag[TEF] in CH_2Cl_2 in a 2:1 ratio. The initially green solution immediately turns red upon the addition of Ag^+ to complex **B**. NMR characterization of compound **1a** shows the presence of the Cp* ligands of **B** in the ^{1}H NMR spectrum and the anion [TEF] in the ^{19}F{^{1}H} NMR spectrum but unfortunately does not give any conclusions about the species in solution. From this reaction we were able to obtain dark red single crystals. The X-ray analysis revealed a monoclinic unit cell with a volume of 25566 Å^3 containing four independent [Ag(**B**)$_2$][TEF] formula units in the asymmetric unit. During the refinement process we encountered several problems which we initially accredited to the WCA [TEF] which is known to have a high tendency to be disordered in its solid state structures. This prevented a satisfying determination of the solid state structure of compound **1a**.[29] Nevertheless, the desired 2:1 composition of **1a** was confirmed by elemental analysis of the isolated and dried crystals. In the next step, we reacted complex **B** with Ag[FAl] in a 2:1 molar ratio. This reaction yields the analogues product [Ag(**B**)$_2$][FAl] (**1b**) (see Scheme 2) and proceeds similar to the synthesis of **1a**.

When the solid state structure of **1b** was determined by single crystal X-ray diffraction analysis (measurement at 123 K, Cu-K_α radiation) the final model[29] by anisotropic refinement with ShelX contains two independent [Ag(**B**)$_2$][FAl] formula units in which Ag is situated between two π coordinating As_5 rings. The unit cell additionally contains CH_2Cl_2 and *n*-pentane solvent molecules as well as two [FAl] anions. The outstanding characteristics of this structural model are the thermal displacement parameters of the Ag atoms. While all light atoms of the anions, as well as the solvent molecules show small ellipsoids with expected orientations of the thermal motion, the central Ag atoms show pronounced oblate deformation parallel to the As_5 planes. In order to minimize the influences of thermal motion and absorption the data collection was repeated at 90 K with Mo-K_α radiation.[30]

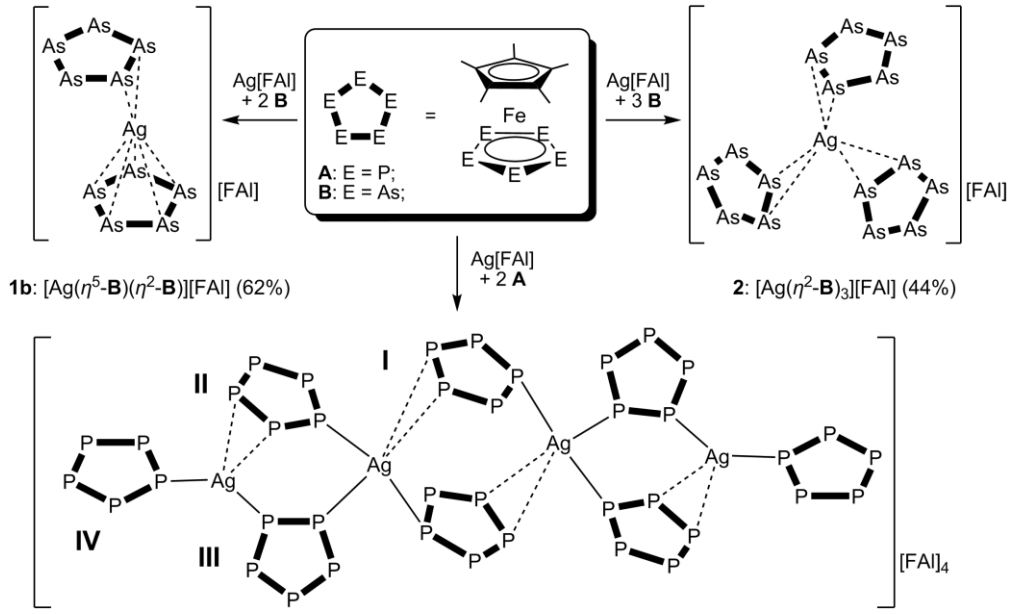

Scheme 2. Reactivity of the *cyclo*-E_5 complexes [Cp*Fe(η^5-E_5)] (E = P(**A**), As(**B**)) towards Ag[FAl]. Yields of the reactions are reported in parentheses.

Low-temperature high-angle diffraction experiment revealed disorder of Ag^+ cations similar to found in several sulfides like, e.g., $Ag_2Ti_2P_2S_{11}$ and $Ag_2MnP_2S_6$[31,32] minerals[33,34] and fast ionic conductors like, e.g., Ag_8SiTe_6[35], γ-Ag_8GeTe_6[36] or Ag_7PSe_6[37]. Two crystallographically unique Ag atoms are located near to inversion centers between parallel η^5-As_5 rings (Figure 1a) and c)). Anisotropic refinement of single Ag position reveals a large positive residual density peak directly on the center of inversion while both Ag positions (symmetry equivalent) show a negative residual density. This suggests a possible disorder of Ag although it is the central atom of the $[Ag(\mathbf{B})_2]^+$ complex cation. Among different approaches that were previously used to describe electron density near disordered Ag^+ cations we have chosen four: split atom model (Ag is splitted over six close positions), and anisotropic as well as first- and second-order anharmonic approximation for one (non-splitted) crystallographically unique Ag position. Therefore, six structural models for **1b** were generated in total. The refinements were performed by ShelX-2014 (split atom **U1s** and anisotropic model **U2s**) and XD2006 (split atom **U1x**, anisotropic **U2x** and anharmonic models **U3**, **U4**).[29] The best description of the determined electron density around Ag was achieved by split positions of isotropic Ag atoms (vide infra). (The anisotropic refinement done with ShelX-2014 (**U2s**) also ends with quite satisfactory residuals of R_1 = 0.0394, wR_2 = 0.0925.) Both Ag atoms were splitted into six independent positions (see Figure 2c and d) until no significant residual electron density remained.[29]

The resulting complexes are shown in Figure 2a) and b). It has to be emphasized at this point, that the rest of the structure determination could be done without any difficulties. There is even one *n*-pentane solvent molecule shown in Figure 2e) (50% occupancy, situated near the center of inversion) which could be refined without any restraints.

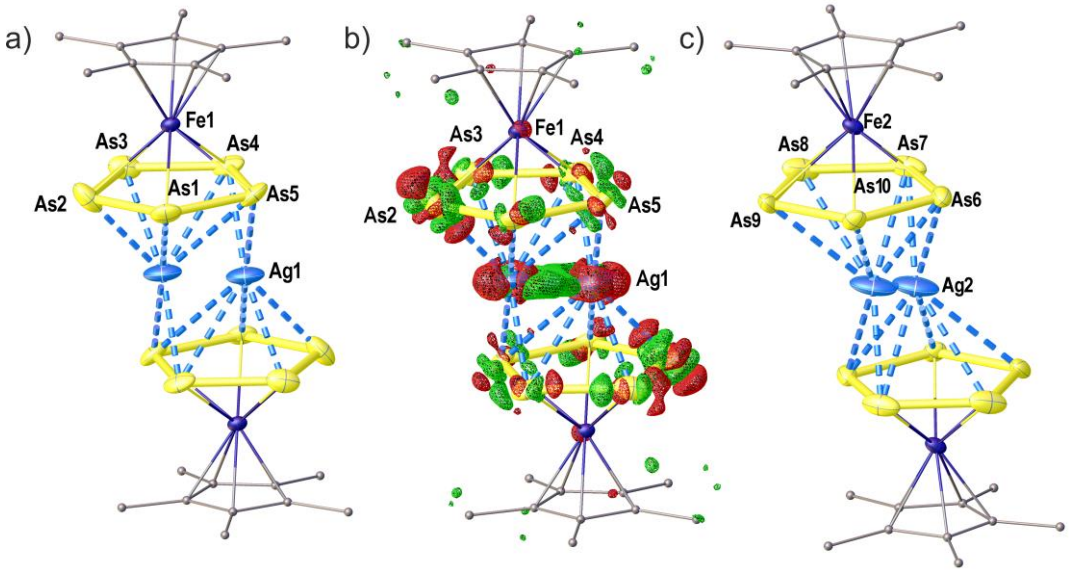

Figure 1. Illustration of the complex cations found in the solid state structure of compound **1b**. Measurement at 90 K, Mo-K_α radiation, anisotropic refinement of Ag atoms (50% occupancy, close to center of inversion). H atoms are omitted and C atoms are represented by small spheres for clarity. a) Illustration of the first $[Ag(\mathbf{B})_2]^+$ complex cation showing the coordination environment of Ag1. b) Representation of the residual electron density map of the same complex cation. Green: positive residual density, red: negative residual density. c) Solid state structure of the second $[Ag(\mathbf{B})_2]^+$ complex cation.

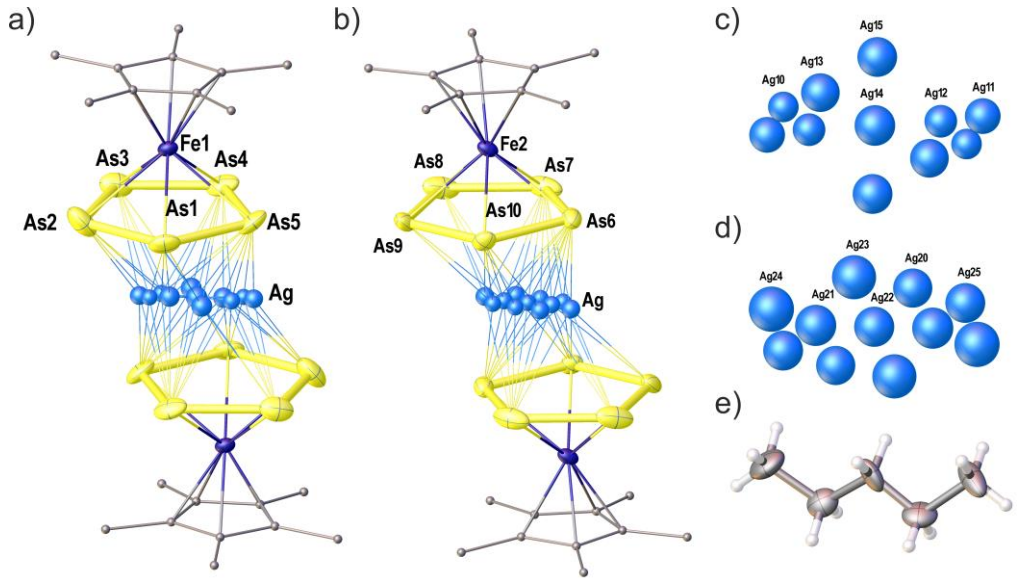

Figure 2. Illustration of the complex cations found in the solid state structure of compound **1b** (from the same measurement like in Fig. 1, but with refinement of the Ag atoms on split positions in an isotropic approximation). a) Representation of the first $[Ag(\mathbf{B})_2]^+$ complex cation. b) Representation of the second $[Ag(\mathbf{B})_2]^+$ complex cation. c) Representation of all split positions and their symmetry equivalents of Ag1 with Uiso represented in their respective radii. d) Representation of all split positions and their symmetry equivalents of Ag2 with Uiso represented in their respective radii. e) Pentane solvent molecule found in the unit cell (50% occupancy, occupying center of inversion) refined without any geometrical or ADP restraints.

Because of severe disorder of Ag^+ cations we refrain from describing the Ag-As distances of compound **1b**. In order to better understand the bonding situation in **1b** DFT calculations are performed for the species in solution as well as for the solid state structures. Due to the weakly interacting moieties containing several heavy elements, these calculations represent a tremendous effort and could not be finished until the submission of this PhD-thesis but will be included in an upcoming publication.

Questions that should be answered:

1. How does the optimized geometry of **1b** look in the gas phase and in solution?
2. What are the species present in solution?
3. How big are the energy barriers between different positions for Ag in the crystal?
4. Is there a static positional disorder of Ag on different opositions or is there a movement of the Ag^+ cation in a cavity of constructed by two parallel *cyclo*-As_5 ligands even at low temperature in the solid state?

The analysis of compound **1b** suggests that Ag^+ is very weakly coordinated by the *cyclo*-As_5 ligand **B**. Therefore, the question arises whether the introduction of an additional ligand to compound **1b** might have an impact on the coordination. Consequently, we reacted Ag[FAl] with three equivalents of the ligand **B** in CH_2Cl_2. The solution showed a similar color change from green to dark red upon addition of Ag^+ to complex **B**. NMR characterization of the reaction product once again could only ascertain the presence of the Cp* ligands of complex **B** and the [FAl] anion. When the CH_2Cl_2 solution is layered with alkanes compound **2** can be obtained as dark red crystals. The X-ray diffraction analysis (R_1 = 0.0318, wR_2 = 0.0859) reveals that **2** crystallizes in the trigonal space group *P*-3. The cationic part of **2** is depicted in Figure 3a) and shows a η^2-coordination of three ligands **B** towards a central Ag atom to form $[Ag(\eta^2\text{-}\mathbf{B})_3]^+$ paddle-wheel complex cations. The atomic displacement parameters of the Ag atom show no peculiarities and its environment can be best described as a trigonal planar geometry created by three side-on coordinating As-As bonds. The trigonal symmetry of the complex cation resembles the compound $[Tl(\mathbf{B})_3][FAl]$ (see Scheme 1), however in that case there is a η^5-coordination present towards Tl^+.[23, 24] The resulting Ag-As bonds in **2** show very similar lengths of Ag1-As1 2.8183(6) Å and Ag1-As2 2.7719(5) Å, respectively. The π coordinating As1-As2 bond is marginally elongated with 2.3718(7) Å compared to the remaining As-As bonds which show uniform lengths close to 2.327(6) Å the average As-As bond length of the free ligand **B**. In Figure 3b) it can be seen that the arrangement of two consecutive $[Ag(\eta^2\text{-}\mathbf{B})_3]^+$ paddle-wheels show a staggered conformation, but the rotational direction remains the same when going along the crystallographic *c*-axis.

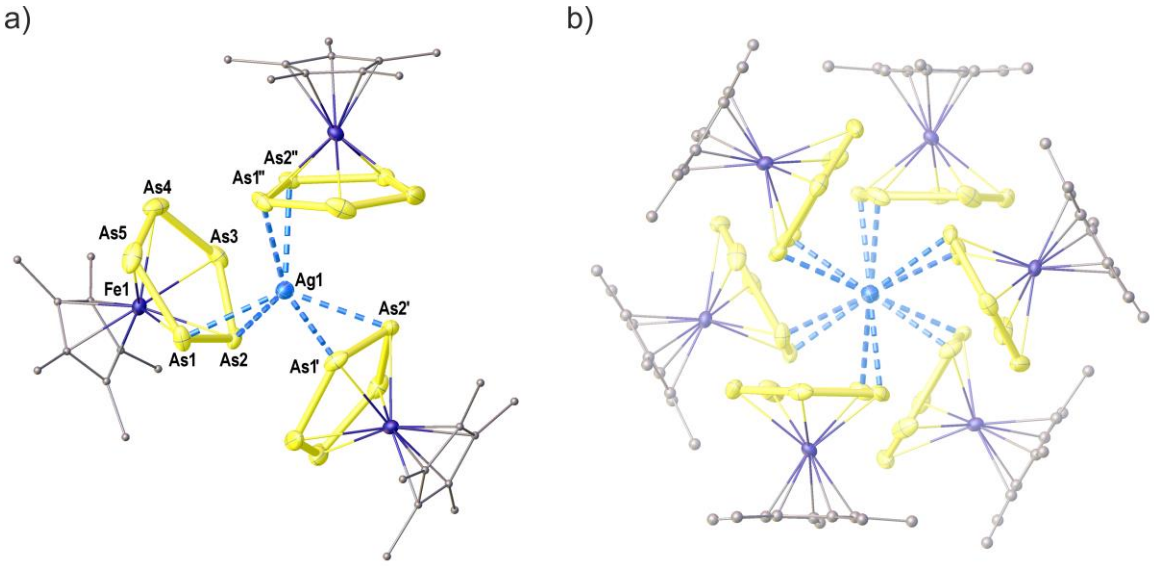

Figure 3. a) Illustration of the complex cation in the solid state structure of compound **2**. b) Viewing direction along the crystallographic c-axis of the trigonal crystal system showing the staggered arrangement of two consecutive $[Ag(\eta^2\text{-}\mathbf{B})_3]^+$ complexes. H atoms are omitted and C atoms are represented by small spheres for clarity. Selected bond lengths [Å]: Ag1-As1 2.8183(6), Ag1-As2 2.7719(5), As1-As2 2.3718(7), As2-As3 2.3384(7), As3-As4 2.3235(8), As4-As5 2.3251(9), As1-As5 2.3460(8). Sum of coordination angles Cent(As1-As2)-Ag1-Cent(As1'-As2)' = 359.3°.

The characterization of **2** clearly demonstrates that Ag^+ is weakly bound by the As_5 plane of complex **B** in **1b** and the introduction of another equivalent of **B** results in a change of the coordination mode in **1b** to mere η^2-coordination in **2**.

The current investigation shows different coordination abilities of the P_5 complex **A** and the As_5 complex **B** towards Ag^+. While the As complex **B** clearly prefers π coordination and the formation of isolated complex cations the analogues P_5 complex **A** has been reported to form the coordination polymer $[Ag(\mu,\eta^2\text{:}\eta^1\text{-}\mathbf{A})_2]_n[TEF]_n$ with Ag[TEF] exhibiting mixed σ and π coordination. In order to check, that the differences in the bonding preferences of **A** and **B** towards Ag^+ are not only caused by increasing the size of the anion from [TEF] (57 atoms) to [FAl] (86 atoms) we consequently also reacted **A** with Ag[FAl] in a 2:1 ratio. Upon addition of Ag[FAl] to a stirred CH_2Cl_2 solution of complex **A** the initially dark green solution turned to olive and finally to brown in the course of about one minute. The $^{31}P\{^1H\}$ NMR spectrum from CD_2Cl_2 solution shows a singlet at δ = 154.1 ppm slightly shifted to lower field compared to the free ligand **A** (δ = 152.2 ppm). This suggests fast dynamics in solution as expected. The ^1H and $^{19}F\{^1H\}$ NMR spectra show the characteristic signals for the Cp* ligand as well as the [FAl] anion. By layering the CH_2Cl_2 solution with alkanes compound **3** can be obtained as light brown crystalline plates. The determined X-ray structure (R_1 = 0.0338, wR_2 = 0.0690) presented in Figure 4 shows a tetranuclear complex cation containing eight P_5 ligands **A** which show mixed σ and π coordination towards Ag^+. The asymmetric unit contains four independent P_5 ligands (**I**-**IV**) while the

others are their symmetry equivalents by inversion. Taking a closer look at the bonding we can identify that all independent P_5 ligands show a different coordination mode. While ligand **IV** is only end-on σ coordinating one Ag atom ligand **III** is bridging two Ag atoms in a bridging 1,2-η^1:η^1-coordination mode. The ligand **II** shows a 1,2,3-η^2:η^1-coordination mode bridging two Ag atoms which was the only experimentally observed coordination mode known from the previously described coordination polymer $[Ag(\mu,\eta^2{:}\eta^1\text{-}\mathbf{A})_2]_n[TEF]_n$.[28] Finally, the ligand **I** shows a bridging 1,2,4-η^2:η^1-coordination mode. Interestingly, the coordination modes towards Ag^+ of the ligands **I** and **IV** were previously predicted to be present in in the gas phase and in solution by DFT calculations, but were not experimentally observed prior to this investigation.[28] The lengths of the Ag-P bonds are strongly dependent on the bonding mode, while σ coordination results in Ag-P bond lengths of ~2.5 Å, π coordination results in Ag-P distances of 2.7-2.8 Å in average. The P-P bond lengths of compound **3** are relatively uniform (2.11-2.12 Å) which is in good agreement to the average P-P bond length of 2.120(5) Å determined for the free complex **A**.[28] Only the π coordinating P-P bonds are slightly elongated with P3-P4 at 2.1704(14) Å and P7-P8 at 2.1539(14) Å.

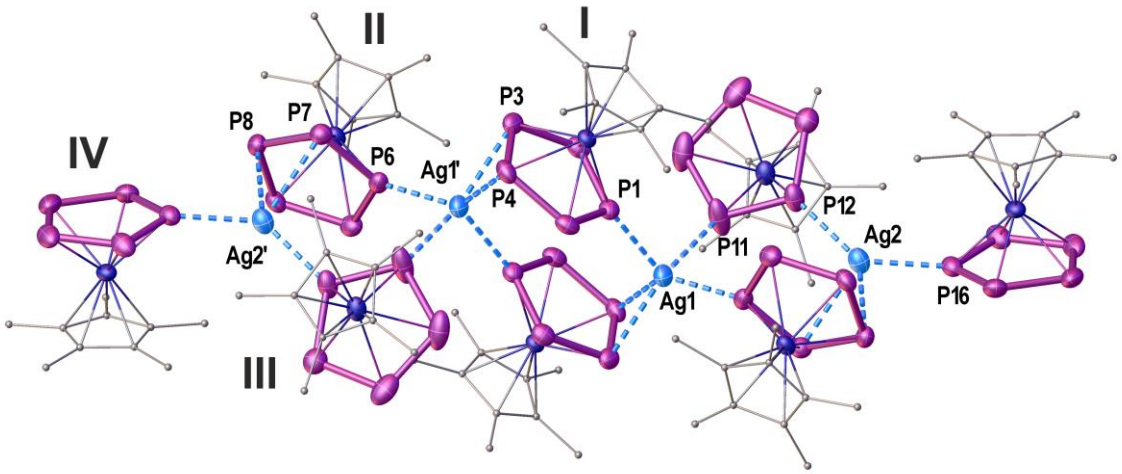

Figure 4. Excerpt of the solid state structure of compound **3** showing the tetranuclear complex cation. H atoms are omitted and C atoms are represented by small spheres for clarity. Selected bond lengths [Å]: P1-Ag1 2.5348(10), P3-Ag1‘ 2.6627(10), P4-Ag1‘ 2.7887(10), P6-Ag1‘ 2.4926(9), P7-Ag2‘ 2.8266(10), P8-Ag2‘ 2.8097(10), P11-Ag1 2.6100(11), P12-Ag2 2.4781(11), P16-Ag2 2.4719(10).

4.3 Conclusion

The presented results demonstrate the facile preparation of Ag^+ coordination compounds with the sandwich complexes $[Cp^*Fe(\eta^5\text{-}E_5)]$ (E = P(**A**), As(**B**)) containing the WCAs [TEF] and [FAl]. While the coordination of **A** to Ag^+ was reported before it was unprecedented for ligand **B**. The experiments show exclusive π coordination

via As-As bonds or the As_5 plane of ligand **B**. The coordination compound $[Ag(\mathbf{B})_2][FAl]$ (**1b**) exhibits an intriguing complex containing two parallel *cyclo*-As_5 ligands and a central Ag atom which cannot be clearly located. Whether this disorder is static or caused by a possible movement of the Ag cation inside a small cavity constructed by the *cyclo*-As_5 ligands cannot be answered and will be further investigated by DFT calculations. The introduction of a third equivalent of **B** to Ag[FAl] results in a change to a solely η^2-coordination mode of one As-As bond of **B** and the formation of trigonal paddle-wheel $[Ag(\eta^2\text{-}\mathbf{B})_3]^+$ complex cations in the solid state.

The increased size of the [FAl] anion compared to [TEF] results in the formation of a tetranuclear Ag^+ complex cation in **3** instead of the previously described polymer in the reaction with $[Cp^*Fe(\eta^5\text{-}P_5)]$ (**A**). Among the four independent *cyclo*-P_5 ligands **A** in **3**, one shows an end-on and one a bridging 1,2,4-η^2:η^1-coordination mode of the P_5 ring. These two bonding modes of ligand **A** towards Ag^+ were predicted by DFT calculations before and could now be verified experimentally. The investigation of the reactivity of these very flexible multidentate P_n and As_n ligand complexes and their behavior towards 'naked' cations under weakly coordinating conditions is a challenging and ongoing task.

4.4 References

[1] R. Hoffmann, *Angew. Chem. Int. Ed.* **1982**, *21*, 711-724; *Angew. Chem.* **1982**, *94*, 725-739.

[2] O. J. Scherer, J. Schwalb, G. Wolmershäuser, W. Kaim, R. Gross, *Angew. Chem. Int. Ed.* **1986**, *25*, 363-364; *Angew. Chem.* **1986**, *98*, 349-350.

[3] J. Bai, A. V. Virovets, M. Scheer, *Angew. Chem. Int. Ed.* **2002**, *41*, 1737-1740; *Angew. Chem.* **2002**, *114*, 1808-1811.

[4] F. Dielmann, A. Schindler, S. Scheuermayer, J. Bai, R. Merkle, M. Zabel, A. V. Virovets, E. V. Peresypkina, G. Brunklaus , H. Eckert, M. Scheer, *Chem. Eur. J.* **2012**, *18*, 1168-1179.

[5] J. Bai, A. V. Virovets, M. Scheer, *Science* **2003**, *300*, 781-783.

[6] M. Scheer, J. Bai, B. P. Johnson, R. Merkle, A. V. Virovets, C. E. Anson, *Eur. J. Inorg. Chem.* **2005**, *2005*, 4023-4026.

[7] M. Scheer, A. Schindler, C. Gröger, A. V. Virovets, E. V. Peresypkina, *Angew. Chem. Int. Ed.* **2009**, *48*, 5046-5049; *Angew. Chem.* **2009**, *121*, 5148-5151.

[8] M. Scheer, A. Schindler, J. Bai, B. P. Johnson, R. Merkle, R. Winter, A. V. Virovets, E. V. Peresypkina, V. A. Blatov, M. Sierka, H. Eckert, *Chem. Eur. J.* **2010**, *16*, 2092-2107.

[9] A. Schindler, C. Heindl, G. Balázs, C. Gröger, A. V. Virovets, E. V. Peresypkina, M. Scheer, *Chem. Eur. J.* **2012**, *18*, 829-835.

[10] C. Schwarzmaier, A. Schindler, C. Heindl, S. Scheuermayer, E. V. Peresypkina, A. V. Virovets, M. Neumeier, R. Gschwind, M. Scheer, *Angew. Chem. Int. Ed.* **2013**, *52*, 10896-10899; *Angew. Chem.* **2013**, *125*, 11097-11100.

[11] S. Welsch, C. Gröger, M. Sierka, M. Scheer, *Angew. Chem. Int. Ed.* **2011**, *50*, 1435-1438; *Angew. Chem.* **2011**, *123*, 1471-1474.

[12] M. V. Butovskiy, G. Balázs, M. Bodensteiner, E. V. Peresypkina, A. V. Virovets, J. Sutter, M. Scheer, *Angew. Chem. Int. Ed.* **2013**, *52*, 2972-2976; *Angew. Chem.* **2013**, *125*, 3045-3049.

[13] E. Mädl, M. V. Butovskii, G. Balázs, E. V. Peresypkina, A. V. Virovets, M. Seidl, M. Scheer, *Angew. Chem. Int. Ed.* **2014**, *53*, 7643-7646; *Angew. Chem.* **2014**, *126*, 7774-7777.

[14] O. J. Scherer, C. Blath, G. Wolmershäuser, *J. Organomet. Chem.* **1990**, *387*, C21-C24.

[15] M. Detzel, G. Friedrich, O. J. Scherer, G. Wolmershäuser, *Angew. Chem. Int. Ed.* **1995**, *34*, 1321-1323; *Angew. Chem.* **1995**, *107*, 1454-1456.

[16] B. Rink, O. J. Scherer, G. Heckmann, G. Wolmershauser, *Chem. Ber.* **1992**, *125*, 1011-1016.
[17] H. Krauss, G. Balázs, M. Bodensteiner, M. Scheer, *Chem. Sci.* **2010**, *1*, 337-342.
[18] M. Fleischmann, J. S. Jones, F. P. Gabbaï, M. Scheer, *Chem. Sci.* **2015**, *6*, 132-139.
[19] M. Fleischmann, L. Dütsch, M. E. Moussa, A. Schindler, G. Balázs, C. Lescop, M. Scheer, *Chem. Commun.* **2015**, *51*, 2893-2895.
[20] I. Krossing, I. Raabe, *Angew. Chem. Int. Ed.* **2004**, *43*, 2066-2090; *Angew. Chem.* **2004**, *116*, 2116-2142.
[21] N. Trapp, I. Krossing, *Nachr. Chem.* **2009**, *57*, 632-637.
[22] M. Gonsior, I. Krossing, N. Mitzel, *Z. Anorg. Allg. Chem.* **2002**, *628*, 1821-1830.
[23] S. Welsch, L. J. Gregoriades, M. Sierka, M. Zabel, A. V. Virovets, M. Scheer, *Angew. Chem. Int. Ed.* **2007**, *46*, 9323-9326; *Angew. Chem.* **2007**, *119*, 9483-9487.
[24] M. Fleischmann, S. Welsch, H. Krauss, M. Schmidt, M. Bodensteiner, E. V. Peresypkina, M. Sierka, C. Gröger, M. Scheer, *Chem. Eur. J.* **2014**, *20*, 3759-3768.
[25] T. Köchner, N. Trapp, T. A. Engesser, A. J. Lehner, C. Röhr, S. Riedel, C. Knapp, H. Scherer, I. Krossing, *Angew. Chem. Int. Ed.* **2011**, *50*, 11253-11256; *Angew. Chem.* **2011**, *123*, 11449-11452.
[26] Here ,Tl[FAl] was formed *in situ* by metathesis of Li[FAl] and Tl[PF6] in case of ligand **B** and the mixed salt [Tl(CH2Cl2)*x*][{FAl}2Li] was used in the case of ligand **A**.
[27] M. Fleischmann, S. Welsch, E. V. Peresypkina, A. V. Virovets, M. Scheer, *Chem. Eur. J.* **2015**, *21*, 14332-14336.
[28] M. Scheer, L. J. Gregoriades, A. V. Virovets, W. Kunz, R. Neueder, I. Krossing, *Angew. Chem. Int. Ed.* **2006**, *45*, 5689-5693; *Angew. Chem.* **2006**, *118*, 5818-5822.
[29] For a detailed discussion please see the supporting information.
[30] 90 K is the lowest possible temperature for our experimental setup.
[31] A. van der Lee, F. Boucher, M. Evain, R. Brec, Z. Kristallogr. **1993**, *203*, 247–264.
[32] E. Gaudin, L. Fischer, F. Boucher, M. Evain, V. Petricek, *Acta Cryst. B* **1997**, *53*, 67-75.
[33] L. Bindi, M. Evain, *Am. Mineral.* **2007**, *92*, 886-891.
[34] L. Bindi, M. Evain, A. Pradel, S. Albert, M. Ribes, S. Menchetti, *Phys. Chem. Miner.* **2006**, *33*, 677-690.
[35] F. Boucher, M. Evain, R. Brec, *J. Solid State Chem.* **1992**, *100*, 341-355.
[36] F. Boucher, M. Evain, R. Brec, *J. Solid State Chem.* **1993**, *107*, 332-346.
[37] M. Evain, E. Gaudin, F. Boucher, V. Petricek, F. Taulelle, *Acta Cryst. B* **1998**, *54*, 376-383.

4.5 Supporting Information

General infomation

All experiments were performed under an atmosphere of dry argon or nitrogen using standard Schlenk and drybox techniques. Commercially available reagents were used as received without further purification. Solvents were freshly distilled under nitrogen from commonly used drying agents or purified by a solvent purification system of MBraun. Solution NMR spectra were recorded on a Bruker Avance 400 spectrometer (^{1}H: 400.130 MHz, ^{31}P: 161.976 MHz, ^{13}C: 100.613 MHz). The chemical shifts δ are presented in parts per million ppm and coupling constants J in Hz. The following samples were used for external reference: TMS (^{1}H, ^{13}C), $CFCl_3$ (^{19}F), H_3PO_4 85 % (^{31}P). ESI-MS spectra were measured on a Finnigan Thermoquest TSQ 7000 mass-spectrometer. IR spectra were recorded on a VARIAN FTS-800 FT-IR spectrometer. The solid substances were grinded together with dried KBr and pressed to pellets. The starting materials [Cp*Fe(η^5-P_5)] (**A**),[1] [Cp*Fe(η^5-As_5)] (**B**),[2] Ag[TEF][3] and Ag[FAl][4] were prepared according to the literature procedure.

Syntheses of described coordination compounds

Synthesis of [Ag(**B**)$_2$][TEF] (**1a**): 70 mg (0.12 mmol, 2.1eq.) [Cp*Fe(η^5-As_5)] (**B**) is dissolved in 3 mL CH_2Cl_2. In a separate Schlenk vessel 58 mg (0.05 mmol, 1eq.) Ag(CH_2Cl_2)[TEF] are dissolved in 5 mL CH_2Cl_2. While stirring, the Ag[TEF] solution is slowly added to the initially green solution of [Cp*Fe(η^5-As_5)]. The color of the solution immediately turned dark red upon this addition. The clear solution was stirred for 2 h at room temperature. The filtered solution is carefully layered with *n*-hexane and kept at +4 °C. In the course of one day compound **1a** can be obtained as dark red crystals. The product is filtered off, washed with *n*-hexane (3 × 10 mL) and dried in vacuum. Elemental analysis shows, that this completely removes the solvent from the crystals. Yield 82 mg (75%). ^{1}H NMR (CD_2Cl_2) δ/ppm = 1.17 (s; C_5Me_5); ^{13}C{^{1}H} NMR (CD_2Cl_2) δ/ppm = 90.8 (s; C_5Me_5), 11.9 (s; CH_3); ^{19}F{^{1}H} NMR (CD_2Cl_2) δ/ppm = −75.6 (s; CF_3). Anal. calcd. for [Ag{Cp*FeAs$_5$}$_2$][TEF]: C, 19.60; H, 1.37. Found: C, 19.65; H, 1.39. ESI-MS (CH_2Cl_2) cations: *m/z* (%) = 756.8 (100) [Cp*$_2$Fe$_2$As$_5$]$^+$, 1238.2 (20) [Ag{Cp*FeAs$_5$}$_2$]$^+$; anions: 967.0 (100) [TEF]$^-$. IR (KBr) $\tilde{\nu}$/cm^{-1} = 2970 (vw), 2912 (vw), 1478 (vw), 1428 (vw), 1378 (vw), 1353 (w), 1302 (vs), 1277 (vs), 1241 (vs), 1219 (vs), 1157 (m), 1022 (w), 974 (vs), 831 (vw), 756 (vw), 728 (s).

Synthesis of [Ag(**B**)$_2$][FAl] (**1b**): 79 mg (0.05 mmol, 1eq.) Ag(CH_2Cl_2)[FAl] and 57 mg (0.1 mmol, 2eq.) [Cp*Fe(η^5-As_5)] are dissolved in 25 mL CH_2Cl_2 in separate Schlenk vessels. Upon addition of the Ag^+ solution to the stirred [Cp*Fe(η^5-As_5)] solution, the initial green color turned to dark red. After 2 h of stirring at room temperature, the solution remained slightly turbid. The filtered solution is carefully layered with the fivefold volume of *n*-pentane. After one week compound **1b** can be obtained as dark red crystals. The crystals are filtered off, washed with *n*-pentane (3 × 10 mL) and dried in vacuum. Yield 82 mg (62%). ^{1}H NMR (CD_2Cl_2) δ/ppm = 1.22 (s; C_5Me_5); ^{13}C{^{1}H} NMR (CD_2Cl_2) δ/ppm = 90.3 (s; C_5Me_5), 11.95 (s; CH_3); ^{19}F{^{1}H} NMR (CD_2Cl_2) δ/ppm = –112.6 (d, $J_{F,F}$ = 280 Hz, 2F), –117.1 (d, $J_{F,F}$ = 279 Hz, 2F), –121.5 (d, $J_{F,F}$ = 277 Hz, 2F), –127.7 (s, 2F), –130.4 (d, $J_{F,F}$ = 275 Hz, 2F), –136.8 (d, $J_{F,F}$ = 276 Hz, 2F), –140.7 (d, $J_{F,F}$ = 277 Hz, 1F), –153.9 (t, $J_{F,F}$ = 22 Hz, 1F), –164.6 (t, $J_{F,F}$ = 18 Hz, 1F), –172.0 ppm (s, AlF). Anal. calcd. for [Ag{Cp*FeAs$_5$}$_2$][FAl]: C, 25.67; H, 1.15. Found: C, 25.45.17; H, 1.33. ESI-MS (CH_2Cl_2) cations: *m/z* (%) = 1238.1 (100) [Ag{Cp*FeAs$_5$}$_2$]$^+$; anions: 1381.0 (100) [FAl]$^-$. IR (KBr) $\tilde{\nu}$/cm^{-1} = 2962 (w), 2916 (w), 2851 (vw), 1650 (m), 1532 (m), 1483 (vs), 1427 (m), 1377 (m), 1323 (m), 1307 (m), 1267 (s), 1242 (s), 1203 (vs), 1186 (s), 1156 (s), 1134 (m), 1104 (s), 1033 (m), 1018 (s), 1000 (m), 956 (vs), 908 (m), 849 (w), 811 (w), 766 (m), 750 (w), 729 (m).

Synthesis of [Ag(**B**)$_3$][FAl] (**2**): 53 mg (0.034 mmol, 1eq.) Ag(CH_2Cl_2)[FAl] and 57 mg (0.1 mmol, 3eq.) [Cp*Fe(η^5-As_5)] (**B**) are dissolved in 25 mL CH_2Cl_2 in separate Schlenk vessels. Upon addition of the Ag^+ solution to the stirred [Cp*Fe(η^5-As_5)] solution, the initial green color turned to dark red. After 2 h of stirring at room temperature, the solution remained slightly turbid. The filtered solution is carefully layered with the fivefold volume of *n*-pentane. After one week compound **2** can be obtained as dark red crystals. The crystals are filtered off, washed with *n*-pentane (3 × 10 mL) and dried in vacuum. Yield 46 mg (44%). ^{1}H NMR (CD_2Cl_2) δ/ppm = 1.23 (s; C_5Me_5); ^{13}C{^{1}H} NMR (CD_2Cl_2) δ/ppm = 90.1 (s; C_5Me_5), 12.0 (s; CH_3); ^{19}F{^{1}H} NMR (CD_2Cl_2) δ/ppm = –112.6 (d, $J_{F,F}$ = 280 Hz, 2F), –117.1 (d, $J_{F,F}$ = 279 Hz, 2F), –121.5 (d, $J_{F,F}$ = 277 Hz, 2F), –127.7 (s, 2F), –130.4 (d, $J_{F,F}$ = 275 Hz, 2F), –136.8 (d, $J_{F,F}$ = 276 Hz, 2F), –140.7 (d, $J_{F,F}$ = 277 Hz, 1F), –153.9 (t, $J_{F,F}$ = 22 Hz, 1F), –164.6 (t, $J_{F,F}$ = 18 Hz, 1F), –172.0 ppm (s, AlF). Anal. calcd. for [Ag{Cp*FeAs$_5$}$_3$][FAl]: C, 24.87; H, 1.42. Found: C, 24.84; H, 1.49. ESI-MS (CH_2Cl_2) cations: *m/z* (%) = 674.6 (7) [Ag{Cp*FeAs$_5$}]$^+$, 756.8 (11) [Cp*$_2$Fe$_2$As$_5$]$^+$, 1238.5 (100) [Ag{Cp*FeAs$_5$}$_2$]$^+$;anions: 1381.2 (100) [FAl]$^-$. IR (KBr) $\tilde{\nu}$/cm^{-1} = 2976 (vw), 2916 (vw), 2854 (vw), 1650 (m), 1532 (m), 1483 (vs), 1427 (m), 1377 (m), 1323 (m), 1307 (m), 1267 (s), 1242 (s), 1203 (vs), 1186 (s), 1156 (s), 1135 (m), 1105 (s), 1033 (m), 1018 (s), 1000 (m), 956 (vs), 909 (m), 849 (w), 811 (w), 766 (m), 752 (w), 729 (m).

Synthesis of [Ag(**A**)$_2$][FAl] (**3**): 79 mg (0.05 mmol, 1eq.) Ag(CH_2Cl_2)[FAl] and 35 mg (0.1 mmol, 2eq.) [Cp*Fe(η^5-P_5)] (**A**) are each dissolved in 5 mL CH_2Cl_2 in separate Schlenk vessels. Upon addition of the Ag^+ solution to the stirred [Cp*Fe(η^5-P_5)] solution, the initial dark green color turned to olive green and subsequently to light brown. After 3 h of stirring at room temperature, the solution was filtered and carefully layered with the fivefold volume of *n*-pentane. In the course of minutes the formation of small amounts of crystalline product was observed at the mixing zone of CH_2Cl_2 and *n*-pentane. The layered system was stored at +4 °C and in the course of one week compound **3** can be obtained as small brown crystalline plates. The crystals are filtered off, washed with *n*-pentane (3 × 10 mL) and dried in vacuum. Yield 62 mg (57%). ^{1}H NMR (CD_2Cl_2) δ/ppm = 1.37 (s; C_5Me_5); ^{13}C{^{1}H} NMR (CD_2Cl_2) δ/ppm = 11.07 (s, Me); ^{19}F{^{1}H} NMR (CD_2Cl_2) δ/ppm = –112.6 (d, $J_{F,F}$ = 280 Hz, 2F), –117.1 (d, $J_{F,F}$ = 279 Hz, 2F), –121.5 (d, $J_{F,F}$ = 277 Hz, 2F), –127.7 (s, 2F), –130.4 (d, $J_{F,F}$ = 275 Hz, 2F), –136.8 (d, $J_{F,F}$ = 276 Hz, 2F), –140.7 (d, $J_{F,F}$ = 277 Hz, 1F), –153.9 (t, $J_{F,F}$ = 22 Hz, 1F), –164.6 (t, $J_{F,F}$ = 18 Hz, 1F), –172.0 ppm (s, AlF); ^{31}P{^{1}H} NMR (CD_2Cl_2) δ/ppm = 153.8 (s). Anal. calcd. for [Ag{Cp*FeP$_5$}$_2$][FAl]: C, 30.83; H, 1.39. Found: C, 30.74; H, 1.54. ESI-MS (CH_2Cl_2) cations: *m/z* (%) = 798.8 (100) [Ag{Cp*FeP$_5$}$_2$]$^+$; anions: 1381.3 (100) [FAl]$^-$. IR (KBr) $\tilde{\nu}$/cm^{-1} = 2971 (vw), 2919 (vw), 2851 (vw), 1652 (m), 1533 (m), 1485 (vs), 1427 (w), 1379 (m), 1323 (m), 1308 (m), 1267 (m), 1244 (s), 1205 (vs), 1186 (s), 1154 (s), 1134 (m), 1105 (s), 1033 (m), 1018 (vs), 1006 (m), 956 (vs), 910 (m), 849 (w), 810 (w), 766 (m), 750 (w), 729 (m).

X-ray structure determination

General considerations

All crystal manipulations were performed under mineral oil or perfluorinated oil. The diffraction experiments were performed at 123 K and at 90 K either on a Rigaku (former Agilent Technologies or Oxford Diffraction) Gemini Ultra, on a SuperNova diffractometer using either Cu-K_α or Mo-K_α radiation. Crystallographic data together with the details of the experiments are given in Table 1 and Table 2. The cell determination, data reduction and absorption correction for all compounds were performed with the help of the CrysAlis PRO software. The full-matrix least-square refinement against F^2 for **2** and **3** was done with ShelXL. It was also done with ShelXL for **1b** measured at 123 K with Cu radiation (**1b** (**Cu**)), measured at 90 K with Mo radiation with an isotropic approximation for Ag **1b** (**U1s**) and also with an anisotropic approximation for Ag **1b** (**U2s**). The crystal structure of **1b** was also refined with the help of the program XD2006 with isotropic approximation of the Ag atoms (**1b** (**U1x**)) and anisotropic approximation (**1b** (**U2x**)). In

addition, the crystal structure of **1b** was also refined with first- (**1b** (**U3**)) and second-order anharmonic (**1b** (**U4**)) approximation of the Ag atoms by XD2006. The details about the different refinements of **1b** are described in the respective section below. For the description of the refinement strategy we list the commonly used syntax for the ShelXL program (DFIX, SADI, SIMU, ISOR, EADP) when restraints or constraints were applied. If not stated otherwise, all atoms except hydrogen were refined anisotropically. The H atoms were calculated geometrically and a riding model was used during refinement process. Graphical material was created with the free software Olex2.

Crystallographic tables

Table 1. Crystallographic details for **1a** and **1b** measured at 90 K with Mo-K_α radiation (**U1s, U2s**). The structure of **1a** could not be refined, so we report here only the determined unit cell for future reference.

Identification code	**1a**	**1b (U1s)**	**1b (U2s)**
formula	$[Ag(\mathbf{B})_2][TEF]$	$C_{60}H_{39}AgAlAs_{10}Cl_3F_{46}Fe_2O_3$	
weight [g·mol^{-1}]		2784.01	
Temperature [K]		89.9(6)	
crystal system	monoclinic	triclinic	
space group	$P2_1/c$	P–1	
a [Å]	37.1854(9)	13.5516(3)	
b [Å]	21.0878(5)	18.3330(3)	
c [Å]	36.2951(8)	19.6764(4)	
α [°]	90	64.6454(17)	
β [°]	116.120(3)	78.2813(17)	
γ [°]	90	68.8173(16)	
Volume [Å^3]	25554.5(12)	4112.28(15)	
Z	16	2	
ρ_{calc} [g·cm^{-3}]		2.248	
μ [mm^{-1}]		4.834	
F(000)		2660	
crystal size [mm^3]		0.448 × 0.161 × 0.082	
diffractometer		SuperNova (Mo)	
absorption correction		gaussian	
T_{min}/T_{max}		0.233 / 0.682	
radiation [Å]		MoK_α	
2Θ range [°]		6.082 to 73.118	
completeness		0.998	
reflns collected/unique		91699 / 37670	
R_{int}/R_{sigma}		0.0313 / 0.0892	
data/restraints/parameters		37670 / 1 / 1216	37620 / 7 / 1192
GOF on F^2		0.884	0.898
R_1/wR_2 [$I \geq 2\sigma(I)$]		0.0394 / 0.0883	0.0410 / 0.0958
R_1/wR_2 [all data]		0.0869 / 0.0925	0.0877 / 0.1003
max/min $\Delta\rho$ [e·Å^{-3}]		2.08 / –1.89	2.23 / –2.03

Table 2. Crystallographic details for **1b** measured at 123 K with Cu-K_α radiation (**Cu**), **2** and **3**.

Identification code	**1b (Cu)**	**2**	**3**
formula	$C_{60}H_{39}AgAlAs_{10}Cl_3F_{46}Fe_2O_3$	$C_{67}H_{47}AgAlAs_{15}Cl_2F_{46}Fe_3O_3$	$C_{226}H_{124}Ag_4Al_4Cl_4F_{184}Fe_8O_{12}P_{40}$
weight [g·mol^{-1}]	2784.01	3271.14	8894.04
Temperature [K]	123(1)	123.00(14)	122.9(3)
crystal system	triclinic	trigonal	monoclinic
space group	*P*–1	*P*–3	$P2_1/n$
a [Å]	13.5805(2)	20.3981(4)	23.46603(13)
b [Å]	18.4093(3)	20.3981(4)	19.73024(9)
c [Å]	19.7628(4)	12.9725(3)	34.51847(19)
α [°]	64.7970(18)	90	90
β [°]	78.3502(16)	90	108.1596(6)
γ [°]	68.6517(16)	120	90
Volume [Å^3]	4157.29(15)	4674.5(2)	15185.70(15)
Z	2	2	2
ρ_{calc} [g·cm^{-3}]	2.224	2.324	1.945
μ [mm^{-1}]	11.415	6.135	8.976
F(000)	2660.0	3108	8696
crystal size [mm^3]	0.110 × 0.072 × 0.047	0.382 × 0.121 × 0.099	0.122 × 0.104 × 0.047
diffractometer	SuperNova (Cu)	Gemini Ultra	Gemini Ultra
absorption correction	gaussian	gaussian	gaussian
T_{min}/T_{max}	0.444 / 0.666	0.257 / 0.639	0.473 / 0.699
radiation [Å]	CuK_α	MoK_α	CuK_α
2*Θ* range [°]	7 to 147.462	6.864 to 52.736	5.982 to 133.312
completeness	0.991	0.978	0.991
reflns collected/unique	46833 / 16069	15480 / 6246	104872 / 26626
R_{int}/R_{sigma}	0.0283 / 0.0270	0.0295 / 0.0501	0.0565 / 0.0761
data/restraints/ parameters	16069 / 7 / 1192	6246 / 8 / 432	26626 / 8 / 2212
GOF on F^2	1.088	0.948	0.783
R_1/wR_2 [$I \geq 2\sigma(I)$]	0.0460 / 0.1257	0.0318 / 0.0839	0.0338 / 0.0653
R_1/wR_2 [all data]	0.0547 / 0.1296	0.0471 / 0.0859	0.0595 / 0.0690
max/min $\Delta\rho$ [e·Å^{-3}]	4.07 / –1.77	1.32 / –1.41	1.88 / –1.07

X-ray structure refinement of [Ag(**B**)$_2$][TEF] (**1a**): Compound **1a** crystallizes in the monoclinic space group $P2_1/c$ with four independent formula units in the asymmetric unit. The X-ray structure determination of this particular compound proves to be very challenging, due to severe disorder caused, by the weakly coordinating nature of the [TEF] anion, as well as solvent molecules in the unit cell. In addition, the crystal slowly loses its crystallinity even at 123 K during the measurement.

During the refinement of the structural model we observed large oblate displacement parameters for the Ag atoms (*c.f.* compound **1b**). Finally we decided to not pursue a structure determination of compound **1a** any longer, since it would not result in a structural model suitable for publication. However, for future reference we report the determined unit cell as well provide a ball and stick representation of the complex cations of the 'final' model (R_1 ~19%, wR_2 ~50%).

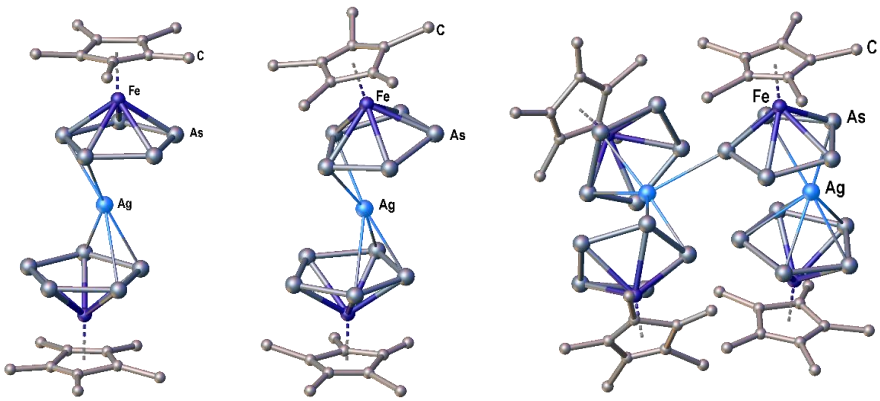

Figure 1. Representation of the four independent [Ag(**B**)$_2$]$^+$ complex cations of the final model of **1a**.

X-ray structure refinement of $[Ag(B)_2][FAl]$ (1b)

General comments on the X-ray structure of 1b

Compound **1b** crystallizes in the triclinic space group *P*–1 with two independent [Cp*Fe(η^5-As_5)] complexes coordinated to one Ag atom in the asymmetric unit. There is also the [FAl] anion and one CH_2Cl_2 molecule in general positions, as well as one CH_2Cl_2 molecule and one *n*-pentane molecule each occupying a center of inversion. We will describe the refinement strategy for each model of **1b** separately. Finally we will compare the different refinements for the measurement performed at 90 K with Mo-K_α radiation.

1b (Cu): During the start of our investigation we collected single crystal X-ray data by Cu-K_α radiation at 123K. The structure refinement could be done without any difficulty (to our surprise, *n*-pentane and one CH_2Cl_2 molecule are ordered). Only the geometry of the half-occupied CH_2Cl_2 molecule was restrained by SADI commands. The Ag atoms are both situated close to a center of inversion. The final model was refined with an anisotropic approximation for Ag and all other atoms except for H atoms which were refined using a riding model. The thermal displacement parameters of these half-occupied Ag atoms are larger than all other ADP's of the lighter atoms (Ag is the heaviest atom) and the ellipsoids show a pronounced oblate deformation. There is one large residual density peak close to Ag1 with approximately 4e⁻.

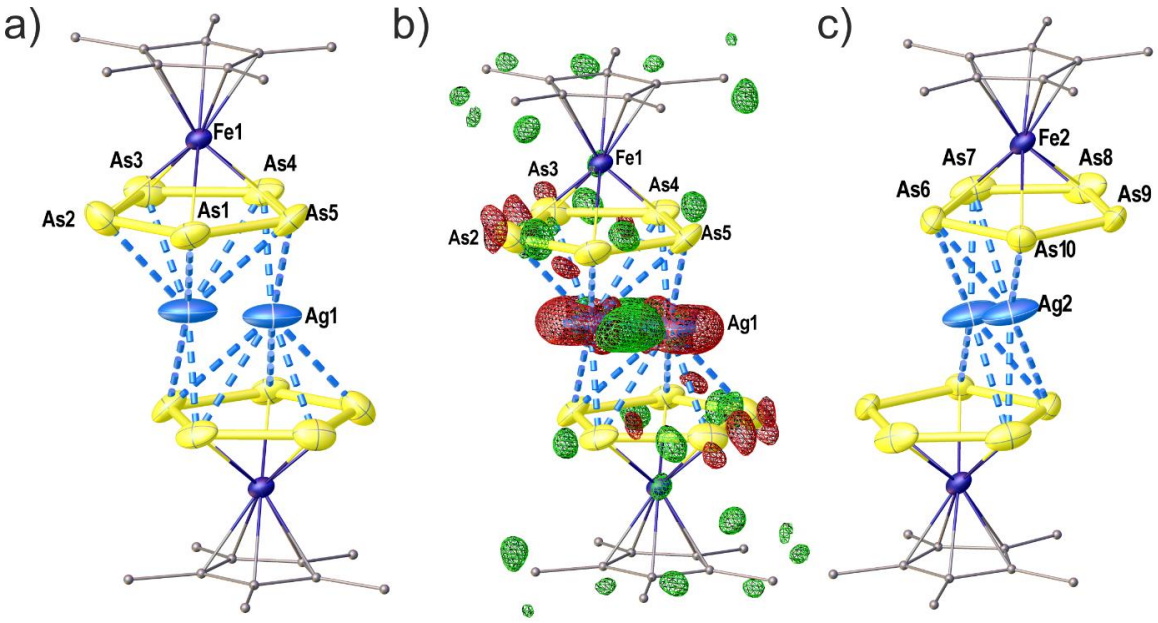

Figure 2. a) Illustration of the $[Ag(\mathbf{B})_2]^+$ complex cation containing Ag1. b) residual electron density map of complex 1. green = positive electron density (Q peaks), red = negative electron density (holes). c) Illustration of the $[Ag(\mathbf{B})_2]^+$ complex cation containing Ag2. Ellipsoids are drawn with 50% probability. H atoms are omitted and C atoms are represented by small spheres for clarity.

Refinement of the crystal structure of 1b measured at 90 K with Mo-K_α radiation

The diffuse electron density near two crystallographically unique Ag^+ positions, Ag(1) and Ag(2), can be explained by different models. The refinement strategy for each model is explained below.

U1-model (isotropic model): Both Ag(1) and Ag(2) are split over 6 positions each, Ag(10), Ag(11)…Ag(15) and Ag(20), Ag(21)…Ag(25) respectively. All positions were subsequently located one after another from the different electron density ($\Delta\rho$) maps during the preliminary refinement by SHELXL-2014 program. At the first stage of the final refinement the site occupancy

factors (sofs) together with *xyz* for all 12 positions were refined assuming the charge balance requirements (SUMP instruction in SHELXL-2014 program), the U_{iso}(Ag) being fixed at 0.03 $Å^{-2}$. After this the refined sofs values were fixed and U_{iso}(Ag) were refined together with *xyz*. The resulting sofs vary from 0.01556 to 0.18402.

U2-model (anisotropic model): Both Ag^+ positions were approximated as single atoms, Ag(1) and Ag(2), that were refined anisotropically.

U3-model: As in the **U2**-model, both Ag^+ positions were approximated as single atoms, Ag(1) and Ag(2). For both of them *xyz*, anisotropic (harmonic) a.d.p. ellipsoid (U2) and first-order anharmonic tensor (U3) were refined.

U4-model: The same as **U3**-model, but in addition second-order anharmonic tensors (U4) were refined for both Ag(1) and Ag(2).

The refinement of **U1**- and **U2**-models was performed against F^2 with SHELXL-2014 (**U1s**, **U2s**) and XD2006 (**U1x**, **U2x**) program sets. In the XD2006 refinement the atomic scattering factors from the VM (PBE-QZ4P-ZORA) databank were used, taking anomalous dispersion into account. In the SHELXL-2014 refinement all reflections were used, while in the XD2006 refinement only reflections with $Fo^2 \geq 3\sigma(Fo^2)$ were taken into account. During the refinement of **U1-model** by XD2006 (**U1x**) the values of sofs(Ag) were taken from the SHELXL-2014 refinement (**U1s**). The results are summarized in the Table 3. Details about the data collection can be found in Table 1 for **1b** (**U1s**).

model	**U1s**	**U2s**	**U1x**	**U2x**	**U3**	**U4**
atomic positions	12	2	12	2	2	2
parameters	48 [1]	18	48 [2]	18	38	68
peak at Ag^+, [$e/Å^3$]	1.10	2.23	1.49	2.42	2.06	<0.86
hole at Ag^+, [$e/Å^3$]	–0.99	–1.63	–1.85	–2.17	–1.73	–1.73
R_1 for observed reflections	0.040	0.044	0.041	0.043	0.041	0.040
wR_2 for all reflections	0.093	0.101	0.110	0.117	0.113	0.111
program	SHELXL-2014	SHELXL-2014	XD2006	XD2006	XD2006	XD2006

[1] The disorder of Ag^+ can be described by total 60 parameters, {*x*, *y*, *z*, sof, U_{iso}} (sof = site occupancy factor), but only 48 of them were independently refined, either {*x*, *y*, *z*, sof} or {*x*, *y*, *z*, U_{iso}}

[2] During the refinement by *XD2006* the values of site occupancy factors for disordered Ag^+ were taken from *SHELX2014* refinement, while {x, y, z, U_{iso}} were refined.

Description of the diffuse electron density near Ag^+ positions by different models requires different number of parameters to refine (parameters, Table 3). In the case of **U1** model it is 60 (12 positions by 5 parameters, {*x*, *y*, *z*, sof and U_{iso}}), but only 48 of them, either {*x*, *y*, *z*, sof} or {*x*, *y*, *z*, U_{iso}}, can be refined independently to avoid the correlation between sof and U_{iso}. In the case of anisotropic model, **U2**, one has to refine *xyz* and six U_{ij} for both of Ag(1) and Ag(2) (total 12 parameters). The anharmonic models require even more parameters (Table 3). The goodness of the model can be evaluated by values of residual electron density ($\Delta\rho$) around Ag^+ positions and by the least-squares residuals, R_1 and wR_2.

Analysis of the data from Table 3 and the $\Delta\rho$ maps shows that **U1** and **U4** models are significantly better than **U2** and **U3**. At that, isotropic (**U1**) model requires less number of parameters and gives more symmetrical peak/hole distribution of $\Delta\rho$ than **U4** model. Therefore the **U1** model can be called more synergetic. In the same time, it can be criticized because some of the Ag^+ positions appear to be very close one from another having low sof values. The splitting of Ag^+ in **U1** also complicates the interpretation of Ag-As distances.

The problem to clearly locate the central Ag atom in the $[Ag(\mathbf{B})_2]^+$ complex cations of **1b** renders a direct determination of the resulting Ag-As distances challenging or even impossible. Therefore

we refrain from discussion of these distances. They generally range from ~2.5 to 3.3 Å. The main text contains representations of the isotropic and anisotropic models **U1s** und **U2s**.

X-ray structure refinement of [Ag(**B**)$_3$][FAl] (**2**): Compound **2** crystallizes in the trigonal space group *P*–3 with the Ag atom, the anion and one CH_2Cl_2 solvent molecule occupying the threefold rotational axis and one complex **B** in general position. The refinement could be done without any problems. One of the Cl atoms of the CH_2Cl_2 molecule is situated directly on the rotational axis while the other Cl atom and the methylene carbon atom are situated next to the axis in general position (33% occupancy). Both C-Cl distances were restrained by DFIX commands and the ADPs of the methylene carbon atom were restrained by an ISOR command.

X-ray structure refinement of [Ag(**A**)$_2$][FAl] (**3**): Compound **3** crystallizes in the monoclinic space group $P2_1/n$ with two Ag atoms, four independent complexes **A** and two independent [FAl] anions in the asymmetric unit. Additionally, there is a disordered CH_2Cl_2 solvent molecule in the asymmetric unit. Both parts (56:44 ratio) were restrained by SADI commands and the carbon atom (56% occupancy) was restrained anisotropically restrained by an ISOR command or isotropically (44% occupancy). The next Q-peaks might show a second orientation of one *cyclo*-P_5 ligand of a complex **A**. When we performed a free refinement of the second position of the complex **A**, the occupancies were all below 8% and the distances between splitted positions were shorter 0.4 Å. Additionally, following this refinement strategy would lead to the necessity of refining a model with complete positional disorder of the whole cationic part of the crystal structure not only one complex **A**. The refinement of the final model (without this disorder) shows good *R* values (R_1 = 0.0338, wR_2 = 0.0653). Therefore, we finally decided to neglect this disorder.

References

[1] O. J. Scherer, T. Brück, *Angew. Chem. Int. Ed.* **1987**, *26*, 59-59; O. J. Scherer, T. Brück, *Angew. Chem.* **1987**, *99*, 59-59.
[2] O. J. Scherer, C. Blath, G. Wolmershäuser, *J. Organomet. Chem.* **1990**, *387*, C21-C24.
[3] A. Bihlmeier, M. Gonsior, I. Raabe, N. Trapp, I. Krossing, *Chem. Eur. J.* **2004**, *10*, 5041-5051.
[4] T. Köchner, N. Trapp, T. A. Engesser, A. J. Lehner, C. Röhr, S. Riedel, C. Knapp, H. Scherer, I. Krossing, *Angew. Chem. Int. Ed.* **2011**, *50*, 11253-11256; *Angew. Chem.* **2011**, *123*, 11449-11452.

Preface

The following chapter has not been published until the submission of this thesis.

Authors

Martin Fleischmann, Stefan Welsch, Gábor Balázs, Werner Kremer, Florian Pevny, Rainer Winter and Manfred Scheer*

Author contributions

The preparation and characterization of all compounds including the single crystal X-ray structure determination and the preparation of the manuscript was done by the first author. Compound **2** was previously obtained as a side-product in trace amounts and has been structurally characterized by Stefan Welsch. The description of the X-ray structure of **2**, DFT calculations and the spectroelectrochemistry have been described by Stefan Welsch in his PhD-thesis. Gábor Balázs performed supporting DFT calculations. Werner Kremer recorded MAS NMR spectra. Florian Pevny and Rainer Winter conducted cyclovoltammetric and spectroelectrochemical measurements of **A**. Manfred Scheer supervised the research and revised the manuscript.

Acknowledgements

Valentin Vass is gratefully acknowledged for MS measurements. David Konieczny is thanked for support of the preparation of [Thia][TEF] (**1**) This work was financially supported by the Deutsche Forschungsgemeinschaft.

5 $[\{CpMo(CO)_2\}_4(\mu_4,\eta^2{:}\eta^2{:}\eta^2{:}\eta^2\text{-}P_4)]^{2+}$ a substituent-free dicationic P_4 chain complex obtained by oxidation of $[\{CpMo(CO)_2\}_2(\mu,\eta^2{:}\eta^2\text{-}P_2)]$

Abstract: A simple one-step synthesis of the well-soluble strong oxidant [Thia][TEF] (**1**) (Thia = thianthrene, $S_2C_{12}H_8$, [TEF] = $[Al\{OC(CF_3)_3\}_4]^-$) is presented. The reaction of **1** with the P_2 ligand complex $[\{CpMo(CO)_2\}_2(\mu,\eta^2{:}\eta^2\text{-}P_2)]$ (**A**) leads to the dicationic complex $[\{CpMo(CO)_2\}_4(\mu_4,\eta^2{:}\eta^2{:}\eta^2{:}\eta^2\text{-}P_4)]^{2+}$ as dark green powder (**2cr**) or dark red crystals (**2**). Single crystal X-ray diffraction of **2** reveals a zigzag P_4 chain. All attempts to identify the formation of the monocation $[\mathbf{A}]^+$ by spectroelectrochemistry (SEC), Cyclovoltametry (CV), EPR spectroscopy and Evans NMR failed suggesting that $[\mathbf{A}]^+$ dimerizes very fast to the dication $[(\mathbf{A})_2]^{2+}$. Solution NMR studies of the dicationic species reveal a highly dynamic behavior rendering all P atoms as well as Cp and CO ligands equivalent on the NMR timescale. The $^{31}P\{^1H\}$ MAS NMR spectra of **2** and **2cr** show no dynamic behavior in the solid state. All analytical data suggest that depending on the conditions the dicationic reaction product can be obtained selectively as a symmetric (**2cr**) or asymmetric (**2**) P_4 chain complex. These isomeric forms can easily be converted into each other.

5.1 Introduction

During the last years, the catenation of phosphorus containing compounds and their heavier congeners has gained increasing interest in chemical research.[1,2,3,4] The majority of these cations bear organic substituents which significantly increases their stability. One prominent representative, the $[(P_4)(AsPh_3)_2]^{2+}$ dication however, exhibits a central P_4 butterfly moiety which is only bonded to As atoms.[5] Its bonding situation is vividly discussed in the current literature.[6,7,8] The side product $[Ph_3AsAsPh_3]^{2+}$ is one example for a pnictogen-pnictogen bond formation via oxidation. Our research focus on the reactivity of substituent-free polypnictogen ligand complexes[9,10,11,12,13] includes the investigation of their oxidation chemistry. Preliminary studies demonstrated that oxidation of $[(Cp^*Mo)_2(\mu,\eta^6{:}\eta^6\text{-}P_6)]$ results in the bis-allylic distortion of the hexaphosphabenzene[14] ligand (Scheme 1 **I**).[15] Additionally, it was reported before that single-electron oxidation of the thoroughly studied pentaphosphaferrocene[16] $[Cp^*Fe(\eta^5\text{-}P_5)]$ leads to an initial oxidation[17] of Fe^{II} to Fe^{III} followed by an internal redox process and a P-P bond formation. This finally yields a formally neutral bicylic P_{10} ligand stabilized by two $[Cp^*Fe^{II}]^+$ fragments (Scheme 1 **II**)

which could be structurally characterized in 2013.[18] Recently, *Krossing et al.* accomplished the preparation of the first homoatomic P cation $[P_9]^+$ by initial insertion of $[NO]^+$ into a P-P bond of P_4 with the help of the WCA (=weakly coordinating anion) $[Al\{OC(CF_3)_3\}_4]^-$ (=[TEF]).[19,20] This was the impulse to investigate the oxidation chemistry of the tetrahedrane complex $[\{CpMo(CO)_2\}_2(\mu,\eta^2{:}\eta^2\text{-}P_2)]$ (Scheme 1 **A**).[21] This P_2 complex has frequently been used as a multidentate ligand in supramolecular chemistry due to its flexible coordination ability.[22,23,24,25] It can be viewed as an analog of P_4 in which two P atoms are exchanged by the isolobal 15 VE complex fragments $[CpMo(CO)_2]$. However its oxidation chemistry has not been investigated, yet.

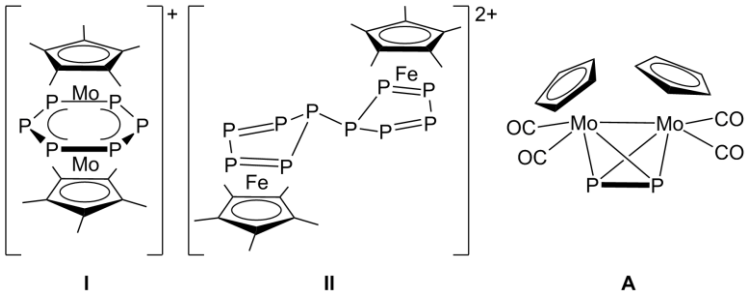

Scheme 1. Bis-allylic distorted *cyclo*-P_6 ligand in $[(Cp^*Mo)_2(\mu,\eta^6{:}\eta^6\text{-}P_6)]^+$ (**I**), bicyclic P_{10} ligand in $[(Cp^*Fe)_2(\mu,\eta^4{:}\eta^4\text{-}P_{10})]$ (**II**) and representation of $[\{CpMo(CO)_2\}_2(\mu,\eta^2{:}\eta^2\text{-}P_2)]$ (**A**).

5.2 Results and Discussion

Salts of Ag^+ are valuable one electron oxidants (E^0 = 0.65 V vs $Cp_2Fe^{0/+}$ in CH_2Cl_2).[26] The oxidation potential of Ag^+ is strongly dependent on the used solvent and it can also be significantly reduced if coordination of the substrate is a competing reaction pathway. Therefore, in reactions of Ag[TEF] with several substrates (P_4,[27] As_4,[28] S_8,[29] Se,[30] $[Fe(CO)_5]$[31]) the formation of coordination compounds or clusters is observed instead of oxidation. This is also true for the complex $[\{CpMo(CO)_2\}_2(\mu,\eta^2{:}\eta^2\text{-}P_2)]$ (**A**) which only acts as a ligand towards Ag^+ without being oxidized.[32,33] In order to accomplish the oxidation of **A**, the preparation of a stronger single-electron oxidant containing the WCA [TEF] was necessary. Therefore, the isolation of the organic radical cation of thianthrene $[C_{12}H_8S_2]^+$ (=[Thia]) having a high oxidation potential (E^0 = 0.86 V vs $Cp_2Fe^{0/+}$ in MeCN)[26] seemed to be a valuable goal. Two synthetic procedures were developed affording the desired deep purple salt [Thia][TEF] (**1**) in good yields (see Scheme 2). It can either be prepared from $[Thia][SbF_6]$ in a metathesis reaction with Li[TEF] (method 1) or by direct oxidation of thianthrene by $[NO]^+$ in the presence of the anion [TEF] (method 2). Thereby, method 2 represents a simple one-step synthesis starting from commercially available reagents. The reaction is performed in liquid SO_2 to ensure

the solubility of Li[TEF]. The product [Thia][TEF] however, is readily soluble in CH_2Cl_2 and can be obtained as dark purple single crystals from CH_2Cl_2/*n*-hexane.[34]

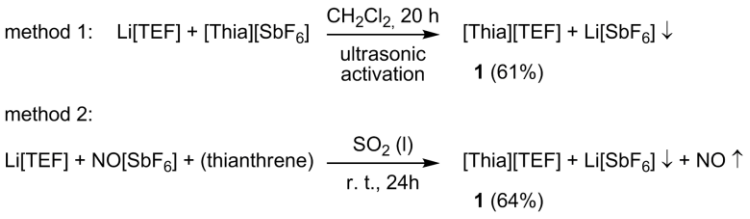

Scheme 2. Syntheses of [Thia][TEF].

With the strong oxidant [Thia][TEF] (**1**) in hand the reactivity of the P_2 complex **A** upon one-electron oxidation was investigated. When light orange solution of **A** in CH_2Cl_2 is reacted with **1** in CH_2Cl_2 an immediate color change to dark red-brown without formation of any precipitate is observed. Precipitation with toluene affords the crude ionic reaction product as a dark green powder (**2cr**). Surprisingly, recrystallization from CH_2Cl_2/*n*-hexane results in the formation of dark red single crystals of **2** which are suitable for X-ray diffraction analysis. The crystal structure of **2** is shown in Figure 1 and will be discussed below. The possibility to determine the structure of **2** helped us significantly to understand the formed species, however, the nature of the dark green powder **2cr** will be discussed in detail afterwards.

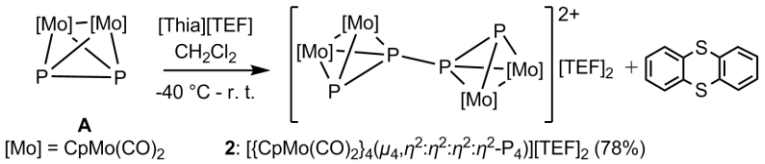

Scheme 3. Oxidation of the P_2 complex **A** forming the dication **2**.

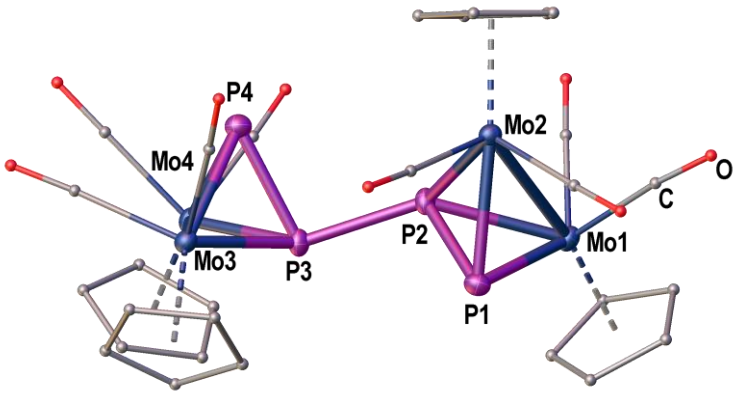

Figure 1. Crystal structure of the dication in **2**. Ellipsoids are drawn at 50% probability. H atoms are omitted and C as well as O atoms are drawn as small spheres for clarity. Selected bond-lengths [Å] and angles [°]: P1-P2 2.1277(11), P2-P3 2.2090(10), P3-P4 2.1641(10), Mo1-Mo2 3.1373(3), Mo3-Mo4 3.1669(3), P1P2P3 104.91(4), P2P3P4 98.96(4) dihedral angle P1P2P3P4 133.83(5).

Compound **2** crystallizes in the monoclinic space group $P2_1/n$ with the dicationic complex $[\{CpMo(CO)_2\}_4(\mu_4,\eta^2{:}\eta^2{:}\eta^2{:}\eta^2\text{-}P_4)]^{2+}$ and two independent [TEF] anions in the asymmetric unit. The central structural motif of the cation consist of a zigzag P_4 chain (PPP angles 98.96(4)° and 104.91(4)°) in a gauche conformation exhibiting a dihedral angle of 133.83(5)°. The P-P bonds in **2** are significantly elongated compared to complex **A** (2.079(2) Å) with the central P2-P3 bond being the longest one (2.2090(10) Å)[21] which directly correspond to the calculated Wiberg bond indexes (WBI) of 1.06(P1-P2), 0.80(P2-P3) and 1.01(P3-P4).[35] The Mo-Mo bonds are elongated compared to **A** as well (3.022(1) Å).[21] The tendency of increasing bond lengths in **2** compared to **A** is also shown by DFT calculations. All Mo-P bonds are within the range of 2.4031(7) Å up to 2.5088(7) Å with slightly shorter values for the central P atoms P2 and P3. A particularly interesting feature of the crystal structure of **2** is the relative orientation of the Cp rings on the Mo atoms. For all coordination compounds of **A**, as well as the free complex **A** and the analogues E_2 complexes of the heavier group 15 elements (E = As, Sb, Bi), the Cp rings on the Mo-Mo bond persistently point to opposite sides of the Mo-Mo bond (trans arrangement). In contrast, the Cp ligands on Mo3 and Mo4 in **2** point to the same side (cis) exhibiting an almost eclipsed arrangement. The Cp ligands on the remaining Mo atoms show different orientations with the ligand on Mo2 pointing away from the P1-P2 bond while the ligand is rotated towards the P1-P2 bond on Mo1. This arrangement suggests a possible free rotation of the ligands Cp, and the two CO ligands around the Mo atoms. This molecular motion was also described to be responsible for the chemical equivalence of the Cp ligands in the heteronuclear PAs analog of complex **A** $[\{CpMo(CO)_2\}_2(\mu,\eta^2{:}\eta^2\text{-}PAs)]$.[36,37,38]

Compound **2** represents the product obtained from single-electron oxidation of **A** and intramolecular P-P bond formation. This reaction was subsequently studied by cyclic voltammetry. The CV of **A** in CH_2Cl_2 solution is depicted in Figure 2 a. The complex undergoes a pseudo-reversible oxidation with the peak of the anodic wave (**I**) at +0.24 V vs. $Cp_2Fe^{0/+}$ while the corresponding cathodic wave (**II**) is significantly shifted to –0.21 V vs. $Cp_2Fe^{0/+}$. The second (+0.81 V vs. $Cp_2Fe^{0/+}$) and third oxidation (+1.09 V vs. $Cp_2Fe^{0/+}$) are irreversible (not shown here). This suggests that after the first oxidation of **A**, the shifted peak for the reduction corresponds to the dication of **2**. During this study, no decline of the cathodic wave of **2** or the observation of any reduction assignable to the monocation $[\mathbf{A}]^+$ could be observed in the CV regardless of the scan rates, the temperature and the concentration of **A**. This points to a rapid formation of the dication. This transformation can also be followed by IR spectroscopy

shown in Figure 2 b. During the oxidation the intensities of the CO stretching bands at 1913, 1962 and 1987 cm^{-1} for neutral **A** decrease while three new signals at higher energies (~2028, 2044 and 2053 cm^{-1}) evolve. The higher CO stretching frequencies for **2** can easily be explained by a decrease in π back bonding from the Mo atoms which are more electron poor compared to **A**. This process is fully reversible as long as **A** is only oxidized once.

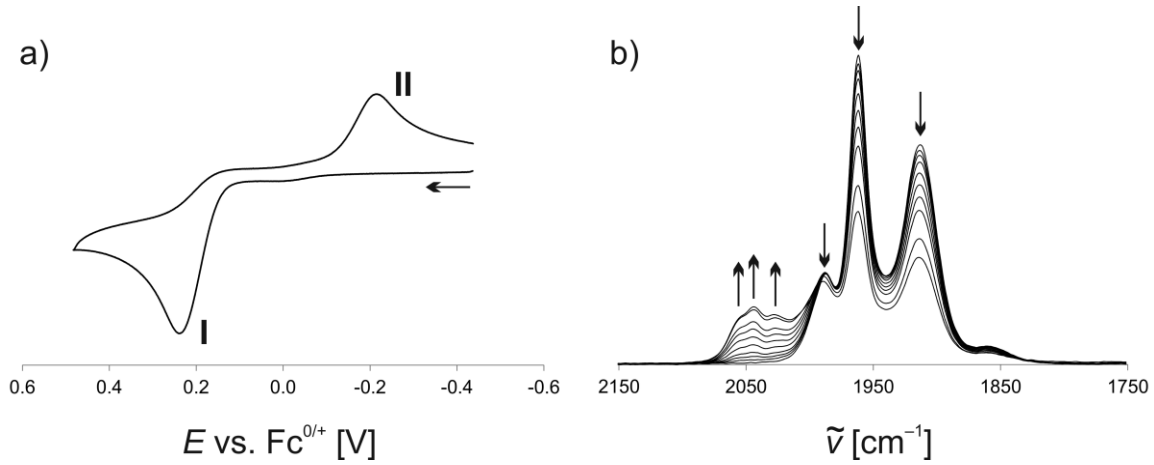

Figure 2. a) CV of **A** in CH_2Cl_2 (v = 200 $mV \cdot s^{-1}$, c([NBu_4][PF_6]) = 0.1 $mol \cdot L^{-1}$). b) IR spectrum of **A** during the oxidation obtained from spectroelectrochemical analysis.

To further elaborate the nature of the green powder **2cr** in comparison to crystalline **2** we thoroughly characterized the products in solution and in the solid state. When crystalline **2** is dissolved in CH_2Cl_2 the solution cannot be distinguished from dissolved **2cr** by IR and NMR spectroscopy (vide infra).[35] Additionally, the dissolved crystals of **2** can be precipitated by addition of toluene to afford a dark green powder which cannot be distinguished from **2cr** by IR spectroscopy (vide infra). The ^1H NMR spectra of **2** and **2cr** in CD_2Cl_2 solution show only one singlet at δ = 4.55 ppm for the Cp ligands. The $^{13}C\{^1H\}$ NMR spectra consistently show only one singlet for the Cp ligands at δ = 92.26 ppm and one singlet for the CO ligands at δ = 218.92 ppm. The $^{31}P\{^1H\}$ NMR spectra of **2** and **2cr** show only one broad signal at δ = –0.1 ppm (ω1/2 = 193 Hz) which moves to higher field (δ = –26.5 ppm) and significantly broadens upon cooling ($\omega_{1/2}$ > 10000 Hz at 213 K) but no signal splitting can be resolved before precipitation starts. Characteristic signals assignable to the [TEF] anion can be observed in the $^{19}F\{^1H\}$ and the $^{13}C\{^1H\}$ NMR spectra. Solutions in CD_2Cl_2 and solid samples of **2** and **2cr** are silent in the X-band EPR spectra and no paramagnetic shift is observed by the Evans NMR method suggesting only diamagnetic species in solution. This suggests that the diamagnetic dication in **2** does not dissociate in solution, which is in good agreement with calculations. DFT analysis at the BP86/def2-TZVP level of theory show

that the dissociation of **2** in two $[\{CpMo(CO)_2\}_2(\mu,\eta^2{:}\eta^2\text{-}P_2)]^+$ fragments is favored in the gas phase by 82.2 kJ·mol^{-1}, however it is disfavored by 52.8 kJ·mol^{-1} in solution.[35] The ESI mass spectrum of a CH_2Cl_2 solution clearly shows signals assignable to the monocationic species $[\mathbf{A}]^+$, $[\mathbf{A}–2(CO)]^+$, $[\mathbf{A}–3(CO)]^+$ and $[\mathbf{A}–4(CO)]^+$ which suggests dissociation in the gas phase in accordance with DFT.[35] However, some small peaks (~50:1 intensity, shifted by ~0.5 Da) can be observed in the same *m*/*z* region than $[\mathbf{A}]^+$ which are located in between the major signals for $[\mathbf{A}]^+$. These signals may arise from a small percentage of a dicationic species but the isotopic distribution cannot clearly be resolved due to the small percentage.[35] The behavior of **2** and **2cr** in solution conclusively show that the dication of **2** does not dissociate in solution and exhibits fast dynamic processes rendering all P atoms, all Cp ligands and all CO ligands chemically equivalent on the NMR timescale. This dynamic behavior can best be compared to the butadiene-like P_4 middle deck of $[(Cp''Fe)_2(\mu,\eta^4{:}\eta^4\text{-}P_4)]$ (Cp'' = 1,3-^{t}Bu$_2$H$_3$Cp) which also shows only one broad resonance in the $^{31}P\{^1H\}$ NMR spectrum at room temperature.[39]

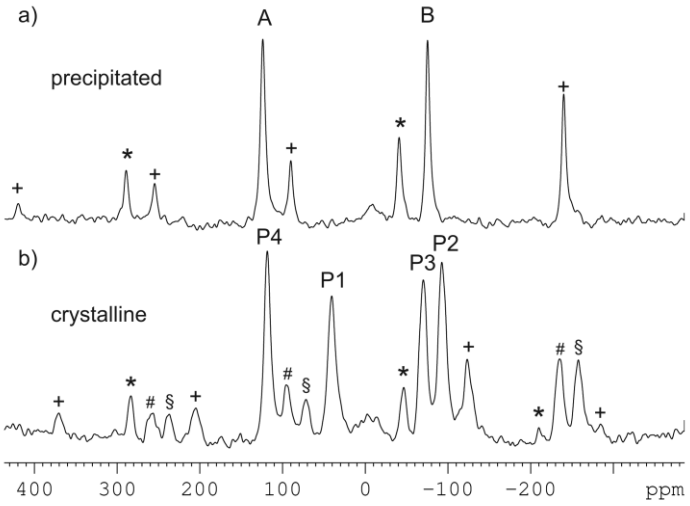

Figure 3. $^{31}P\{^1H\}$ MAS NMR spectra of **2** at f = 20 kHz as precipitated powder **2cr** (a) and in crystalline form **2** (b), respectively. Rotation side bands are marked corresponding to the signals *(A, P4) +(B, P1), #(P3) and §(P2).

Unfortunately, the exact nature of the species present in solutions of **2** and **2cr** still remains unclear. Therefore, we precipitated the ionic product from the solution with toluene and recorded $^{31}P\{^1H\}$ MAS NMR spectra of the dark green precipitate **2cr** as well as the dark red crystals **2** shown in Figure 3. Precipitated **2cr** (Figure 3 a) exhibits two distinctly different singlets at δ = 124.7 ppm (A) and δ = –75.9 ppm (B) in a 1:1 ratio. In contrast, the $^{31}P\{^1H\}$ MAS NMR spectrum of crystalline **2** (Figure 3 b) shows four signals at δ = 118.7, 40.7, –70.0 and –92.5 ppm in a 1:1:1:1 ratio which can easily be explained by the four independent P atoms of the crystal structure. Our signal

assignment is corroborated by DFT calculations determining the isotropic magnetic shielding for the P atoms P1-P4.[35] The calculated natural charges also correspond to the observed shifts in the $^{31}P\{^1H\}$ MAS NMR spectrum and reveal a positive charge accumulation on the terminal P atoms P1(+0.30 e) and P4(+0.40 e) while the central P atoms P2(+0.21 e) and P3(+0.22 e) show a lower positive charge. Scheme 4 shows possible resonance structures of the dicationic P_4 complex. Based on the charge distribution and the observed P-P bond lengths the dication in **2** can best be described as a mixture of the resonance structure **II** and **III** shown in Scheme 4.

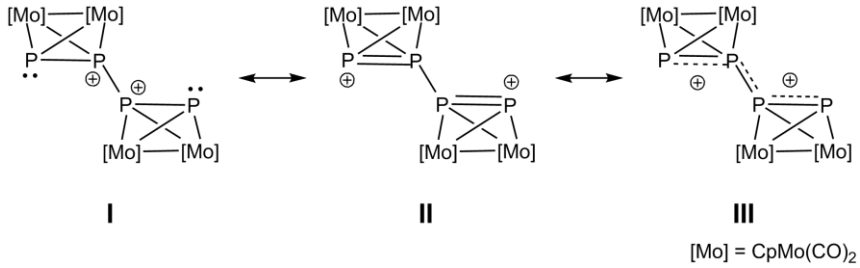

Scheme 4. Possible resonance structures for the dication in **2**.

In addition, the dicationic reaction products **2** and **2cr** contain several CO ligands which are excellent probes for IR spectroscopy. The IR spectrum of crystalline **2** in the solid state shows at least six strong resonances for the CO stretching frequencies (2069, 2060, 2043, 2028, 2016, 1994 cm^{-1}) for the eight different ligands of the unsymmetrical P_4 chain complex.[35] The IR spectrum of the dark green **2cr** in the solid state shows only three strong resonances (2048, 2030, 2002 cm^{-1}) for the CO stretching frequencies.[35] However, the solution IR spectra of **2** and **2cr** in CH_2Cl_2 are identical.[35]

The current investigation suggests a very fast dimerization of the initially formed monocation $[\mathbf{A}]^+$ in solution which does not dissociate back in solution and exhibits very fast dynamics. During crystallization however, the P_4 chain of **2** is obtained in an asymmetric form (see Figure 1) and the $^{31}P\{^1H\}$ MAS NMR spectrum consistently shows four signals for the inequivalent P atoms. Taking all evidence into account we assume that the dark green powder **2cr** consists of a similar dicationic P_4 chain complex with a more symmetric geometry. This would explain the appearance of two singlets in the $^{31}P\{^1H\}$ MAS NMR spectrum (see Figure 3 a) with A corresponding to the terminal and B corresponding to the internal P atoms. The fact that **2** can be reversibly converted into **2cr** and back and the fewer observed CO stretching frequencies of **2cr** compared to **2** in the solid state would also be in accordance with this assumption.

5.3 Conclusion

In summary we have presented a simple one-step synthesis of the strong oxidant [Thia][TEF] (**1**). This well-soluble salt enabled the oxidation of the P_2 complex **A** which could not be performed with Ag^+ as reactant. The oxidation affords the dicationic complex $[\{CpMo(CO)_2\}_4(\mu_4,\eta^2{:}\eta^2{:}\eta^2{:}\eta^2\text{-}P_4)]^{2+}$ (**2**). No monocation $[\mathbf{A}]^+$ could be identified in solution or the solid state. The presented results successfully expand the chemistry of polypnictogenyl cations. Complex **2** contains the first unsubstituted cationic P_4 chain stabilized in the coordination sphere of transition metals. In contrast to well-known polypnictogenyl cations with organic substituents or the homoatomic $[P_9]^+$ cation, this P_4 chain exhibits very fast dynamics in solution which could not be frozen by cooling. The dicationic P_4 chain complex can selectively be obtained in a symmetric form as dark green **2cr** when precipitated and in the asymmetric form **2** as dark red crystals upon crystallization. These two isomeric forms **2** and **2cr** can be converted reversibly from one to the other.

Additionally, [Thia][TEF] represent a well-soluble strong oxidant, that can be easily prepared and enables the stabilization of reactive cationic species by the almost inert WCA [TEF]. It allows reactions in solvents with low polarity like CH_2Cl_2 even at low temperatures and significantly increases the solubility of the ionic products. Therefore, it presents a valuable synthetic tool for future studies and may be used whenever Ag^+ salts do not afford the desired oxidation products.

5.4 References

[1] N. Burford, P. J. Ragogna, *J. Chem. Soc., Dalton Trans.* **2002**, 4307-4315.
[2] C. A. Dyker, N. Burford, *Chem. Asian J.* **2008**, *3*, 28-36.
[3] A. P. M. Robertson, P. A. Gray, N. Burford, *Angew. Chem. Int. Ed.* **2014**, *53*, 6050-6069; *Angew. Chem.* **2014**, *126*, 6162-6182.
[4] B. D. Ellis, C. L. B. Macdonald, *Coord. Chem. Rev.* **2007**, *251*, 936-973.
[5] M. Donath, E. Conrad, P. Jerabek, G. Frenking, R. Fröhlich, N. Burford, J. J. Weigand, *Angew. Chem. Int. Ed.* **2012**, *51*, 2964-2967; *Angew. Chem.* **2012**, *124*, 3018-3021.
[6] D. Himmel, I. Krossing, A. Schnepf, *Angew. Chem. Int. Ed.* **2014**, *53*, 370-374; *Angew. Chem.* **2014**, *126*, 378-382.
[7] G. Frenking, *Angew. Chem. Int. Ed.* **2014**, *53*, 6040-6046; *Angew. Chem.* **2014**, *126*, 6152-6158.
[8] D. Himmel, I. Krossing, A. Schnepf, *Angew. Chem. Int. Ed.* **2014**, *53*, 6047-6048; *Angew. Chem.* **2014**, *126*, 6159-6160.
[9] B. M. Cossairt, N. A. Piro, C. C. Cummins, *Chem. Rev.* **2010**, *110*, 4164-4177.
[10] M. Caporali, L. Gonsalvi, A. Rossin, M. Peruzzini, *Chem. Rev.* **2010**, *110*, 4178-4235.
[11] B. P. Johnson, G. Balázs, M. Scheer, *Coord. Chem. Rev.* **2006**, *250*, 1178-1195.
[12] O. J. Scherer, *Angew. Chem. Int. Ed.* **1990**, *29*, 1104-1122; *Angew. Chem.* **1990**, *102*, 1137-1155.
[13] O. J. Scherer, *Acc. Chem. Res.* **1999**, *32*, 751-762.
[14] O. J. Scherer, H. Sitzmann, G. Wolmershäuser, *Angew. Chem. Int. Ed.* **1985**, *24*, 351-353; *Angew. Chem.* **1985**, *97*, 358-359.

[15] M. Fleischmann, F. Dielmann, L. J. Gregoriades, E. V. Peresypkina, A. V. Virovets, S. Huber, A. Y. Timoshkin, G. Balázs, M. Scheer,

[16] O. J. Scherer, T. Brück, *Angew. Chem. Int. Ed.* **1987**, *26*, 59-59; *Angew. Chem.* **1987**, *99*, 59-59.

[17] R. F. Winter, W. E. Geiger, *Organometallics* **1999**, *18*, 1827-1833.

[18] M. V. Butovskiy, G. Balázs, M. Bodensteiner, E. V. Peresypkina, A. V. Virovets, J. Sutter, M. Scheer, *Angew. Chem. Int. Ed.* **2013**, *52*, 2972-2976; *Angew. Chem.* **2013**, *125*, 3045-3049.

[19] T. Köchner, S. Riedel, A. J. Lehner, H. Scherer, I. Raabe, T. A. Engesser, F. W. Scholz, U. Gellrich, P. Eiden, R. A. Paz Schmidt, D. A. Plattner, I. Krossing, *Angew. Chem. Int. Ed.* **2010**, *49*, 8139-8143; *Angew. Chem.* **2010**, *122*, 8316-8320.

[20] T. Köchner, T. A. Engesser, H. Scherer, D. A. Plattner, A. Steffani, I. Krossing, *Angew. Chem. Int. Ed.* **2012**, *51*, 6529-6531; *Angew. Chem.* **2012**, *124*, 6635-6637.

[21] O. J. Scherer, H. Sitzmann, G. Wolmershäuser, *J. Organomet. Chem.* **1984**, *268*, C9-C12.

[22] M. Scheer, L. J. Gregoriades, M. Zabel, J. Bai, I. Krossing, G. Brunklaus, H. Eckert, *Chem. Eur. J.* **2008**, *14*, 282-295.

[23] S. Welsch, L. J. Gregoriades, M. Sierka, M. Zabel, A. V. Virovets, M. Scheer, *Angew. Chem. Int. Ed.* **2007**, *46*, 9323-9326; *Angew. Chem.* **2007**, *119*, 9483-9487.

[24] B. Attenberger, S. Welsch, M. Zabel, E. Peresypkina, M. Scheer, *Angew. Chem. Int. Ed.* **2011**, *50*, 11516-11519; *Angew. Chem.* **2011**, *123*, 11718-11722.

[25] B. Attenberger, E. V. Peresypkina, M. Scheer, *Inorg. Chem.* **2015**, *54*, 7021-7029.

[26] N. G. Connelly, W. E. Geiger, *Chem. Rev.* **1996**, *96*, 877-910.

[27] I. Krossing, L. van Wüllen, *Chem. Eur. J.* **2002**, *8*, 700-711.

[28] C. Schwarzmaier, M. Sierka, M. Scheer, *Angew. Chem. Int. Ed.* **2013**, *52*, 858-861; *Angew. Chem.* **2013**, *125*, 891-894.

[29] T. S. Cameron, A. Decken, I. Dionne, M. Fang, I. Krossing, J. Passmore, *Chem. Eur. J.* **2002**, *8*, 3386-3401.

[30] T. Köchner, N. Trapp, T. A. Engesser, A. J. Lehner, C. Röhr, S. Riedel, C. Knapp, H. Scherer, I. Krossing, *Angew. Chem. Int. Ed.* **2011**, *50*, 11253-11256; *Angew. Chem.* **2011**, *123*, 11449-11452.

[31] P. J. Malinowski, I. Krossing, *Angew. Chem. Int. Ed.* **2014**, *53*, 13460-13462; *Angew. Chem.* **2014**, *126*, 13678-13680.

[32] J. Bai, E. Leiner, M. Scheer, *Angew. Chem. Int. Ed.* **2002**, *41*, 783-786; *Angew. Chem.* **2002**, *114*, 820-823.

[33] M. Scheer, L. J. Gregoriades, M. Zabel, J. Bai, I. Krossing, G. Brunklaus, H. Eckert, *Chem. Eur. J.* **2008**, *14*, 282-295.

[34] The determined crystal structure from single crystal X-ray diffraction analysis is described in the SI.

[35] please see supporting information.

[36] J. E. Davies, L. C. Kerr, M. J. Mays, P. R. Raithby, P. K. Tompkin, A. D. Woods, *Angew. Chem. Int. Ed.* **1998**, *37*, 1428-1429; *Angew. Chem.* **1998**, *110*, 1473-1475.

[37] J. E. Davies, M. J. Mays, P. R. Raithby, G. P. Shields, P. K. Tompkin, A. D. Woods, *J. Chem. Soc., Dalton Trans.* **2000**, 1925-1930.

[38] In addition we could not resolve any signal splitting of the singlet for the CO ligands of free **A** in the $^{13}C\{^1H\}$ NMR spectrum upon cooling in CD_2Cl_2 until precipitation starts.

[39] O. J. Scherer, G. Schwarz, G. Wolmershäuser, *Z. Anorg. Allg. Chem.* **1996**, *622*, 951-957

5.5 Supporting Information

General considerations

All manipulations were carried out under an inert atmosphere of dried nitrogen using standard Schlenk and drybox techniques. CH_2Cl_2 and CD_2Cl_2 were dried over CaH_2, alkanes were distilled from K or Na/K alloy. Dried solvents were also taken from a solvent purification system from MBraun. NMR spectra were recorded in CD_2Cl_2 on a Bruker Avance 300 MHz NMR spectrometer (^{1}H: 300.132 MHz, ^{31}P: 121.495 MHz, ^{13}C: 75.468 MHz, ^{19}F: 282.404 MHz) or a Bruker Avance 400 MHz NMR spectrometer (^{1}H: 400.130 MHz, ^{31}P: 161.976 MHz, ^{13}C: 100.613 MHz) with external references of $SiMe_4$ (^{1}H, ^{13}C), CCl_3F (^{19}F) and H_3PO_4 (85%, ^{31}P). ^{31}P{^{1}H} MAS NMR spectra were recorded on a Bruker Avance 300 (^{31}P: 121.495 MHz) by Prof. Dr. Werner Kremer of the Physics department of the University of Regensburg. The chemical shifts of the MAS NMR spectra are also presented in the δ scale using NaH_2PO_4 as an external standard. X-Band EPR spectra were recorded on a MiniScope MS400 device from Magnettech GmbH with a frequency of 9.5 GHz equipped with a rectangular resonator TE102. ESI-MS spectra were either measured on a Finnigan Thermoquest TSQ 7000 mass-spectrometer by the MS department of the University of Regensburg or on a Waters Micromass LCT ESI-TOF mass-spectrometer by Valentin Vass. IR spectra were recorded as KBr discs of in CH_2Cl_2 solution using a Varian FTS-800 FT-IR spectrometer. Elemental analyses were performed by the micro analytical laboratory of the University of Regensburg.

Preparation of the compounds 1 and 2

Preparation of $[Thia]^+[TEF]^-$ (**1**):

Method 1: Thia[SbF_6] (135 mg, 0.30 mmol, 1 eq.) and Li[TEF] (330 mg, 0.34 mmol, 1.1 eq.) were placed in a Schlenk flask equipped with a Young valve. Subsequently ~10 mL of CH_2Cl_2 (stored over CaH_2) were condensed onto the solids at –196 °C. The flask was closed under reduced pressure. Upon dissolution of the compounds the formation of a deep violet solution could be observed. The flask was sonicated for 20 h. In order to precipitate the ionic product the reaction mixture was filtered over diatomaceous earth directly into ~100 mL of stirred *n*-hexane. The blackish blue precipitate was freed from the colorless supernatant solution, washed with 100 mL of *n*-hexane and dried in vacuum. The solid was dissolved in 15 mL of CH_2Cl_2 and the deep violet solution was carefully layered with 80 mL of *n*-hexane. After storage at +4 °C compound **1** can be obtained as dark violet crystals in the course of three days. Yield 215 mg (61%).

Method 2: A Fisher-Porter flask was equipped with a stirring bar, thianthrene (260 mg, 1.2 mmol, 1.2 eq.), NO[SbF_6] (266 mg, 1.0 mmol, 1 eq.) and Li[TEF] (998 mg, 1.0 mmol, 1 eq.). SO_2 (~50 mL) was condensed onto these solids under reduced pressure at –196 °C. The flask was closed under reduced pressure and the cooling was removed. Upon dissolution the reaction turns from light blue to dark blue and finally to dark violet when everything is dissolved. After stirring at room temperature over night the SO_2 was removed and 30 mL of CH_2Cl_2 were added. The deep violet suspension was filtered over diatomaceous earth directly into ~100 mL of stirred toluene and washed with small amounts of pure CH_2Cl_2. The solvent mixture was reduced to ~50 mL which resulted in the precipitation of the crude product. The supernatant solution was decanted off. The solid washed three times with 100 mL of toluene and subsequently dried in vacuum. The crude product was dissolved in 15 mL of CH_2Cl_2. The resulting deep purple solution is filtered and carefully layered with the fivefold amount of *n*-hexane. Storage at +4 °C affords **1** as dark violet to black blocks. Yield 760 mg (64%).

^{1}H NMR (400 MHz, CD_2Cl_2, 300 K) no signal can be resolved for [Thia]$^+$. Additionally, the residual solvent signal of CD_2Cl_2 is significantly broadened and usual splitting to a triplet is not observed. ^{27}Al{^{1}H} NMR (104.3 MHz, CD_2Cl_2, 300 K) δ/ppm 34.8 [TEF]; ^{19}F{^{1}H} NMR (282.4 MHz, CD_2Cl_2, 300 K) δ/ppm = –75.4 (s, CF_3). X-band EPR (293 K, solid) g_{iso} = 2.007. Anal. calcd. for [Thia][TEF]: C, 28.42; H, 0.68, S, 5.42. Found: C, 28.82; H, 0.81, S, 5.47.

Preparation of **2cr** and **2**: Light orange [{CpMo(CO)$_2$}$_2$(μ,η^2:η^2-P_2)] (**A**) (109 mg, 0.22 mmol, 2.2 eq.) and dark purple [Thia][TEF] (**1**) (237 mg, 0.2 mmol, 2 eq.) were combined as solids and grinded together affording a dark brown powder. IR spectroscopy from KBr pellets did show the CO stretching frequencies of pure **A** (no reaction of Thia[TEF] and **A** in the solid state). The solid was transferred into a schlenk-flask and pre-cooled CH_2Cl_2 (~30 mL) was added at –50 °C and the resulting turbid dark red to brown solution was stirred in a cooling bath for 30 min while the solvent temperature reached –20 °C. The cooling bath was removed and the reaction was stirred for additional 10 minutes at room temperature. The dark solution was transferred to a larger flask containing ~100 mL of stirred toluene. The crude product **2cr** is precipitated as a fine dark green to black powder leaving a clear light orange solution (small excess of pure **A**). The supernatant solution was removed and the precipitate washed two times with 50 mL of pure toluene. The crude product was dried in vacuum yielding 250 mg (85%) of dark green powder. Recrystallization from CH_2Cl_2/hexane affords pure **2** as dark red blocks which are suitable for single crystal X-ray diffraction in 227 mg (78%) yield. ^{1}H NMR (400 MHz, CD_2Cl_2, 300 K) δ/ppm 4.55 (s, Cp); ^{31}P{^{1}H} NMR (162.0 MHz, CD_2Cl_2, 300 K) δ/ppm –0.1 (br, ω1/2 = 193 Hz [(**C**)$_2$]$^{2+}$); ^{13}C{^{1}H} NMR (100.6 MHz, CD_2Cl_2, 300 K) δ/ppm 218.92 (s, CO), 121.65 (q, $^{1}J_{CF}$ = 293 Hz; CF_3), 92.26 (s, Cp); ^{19}F{^{1}H} NMR (282.4 MHz, CD_2Cl_2, 300 K) δ/ppm = –75.5 (s, CF_3). ^{31}P{^{1}H} MAS NMR (121.6 MHz, 293 K, f = 20 kHz, precipitated) δ/ppm = 124.7 (s, ω1/2 = 790 Hz, P_{ex}), –74.9 (s, ω1/2 = 730 Hz, P_{int}); ^{31}P{^{1}H} MAS NMR (121.6 MHz, 293 K, f = 20 kHz, crystalline) δ/ppm = 118.7 (s, ω1/2 = 960 Hz, P_{ex1}), 40.7 (s, ω1/2 = 1220 Hz, P_{ex2}), –70.0 (s, ω1/2 = 1180 Hz, P_{int1}), –92.5 (s, ω1/2 = 1170 Hz, P_{int2}). The Evans NMR method of **2** in CD_2Cl_2 solution does not show any paramagnetic shifted solvent signal (suggests diamagnetic [(**A**)$_2$]$^{2+}$ in solution without dissociation). The compounds **2** and **2cr** are ESR silent in the solid state and in CH_2Cl_2 solution. Anal. calcd. for [($C_{14}H_{10}O_4Mo_2P_2$)$_2$][TEF]$_2$: C, 24.63; H, 0.69. Found: (crude product **2cr**, contains thianthrene) C, 27.33; H, 1.10; (crystalline product **2**) C, 24.99; H, 0.81. Positive ion MS, *m/q* (%): 495.8 (10) [**A**]$^+$, 439.8 (30) [**A**–2(CO)]$^+$, 411.8 (100) [**A**–3(CO)]$^+$, 383.8 (88) [**A**–4(CO)]$^+$. **2cr**:IR(KBr) cm^{-1}: 3128 (w), 2958 (vw), 2924 (w), 2853 (vw), 2048 (vs), 2039 (s), 2001 (vs), 1969 (vw), 1426 (vw), 1354 (m), 1303 (vs), 1277 (vs), 1244 (vs), 1219 (vs), 1168 (m), 973 (vs), 840 (m), 835 (m), 728 (s). **2**:IR(KBr) cm^{-1}: 3140(w), 2962 (vw), 2919 (vw), 2851 (vw), 2069 (s), 2060 (vs), 2043 (s), 2028 (s), 2016 (s), 1994 (s), 1963 (m), 1426 (vw), 1353 (m), 1303 (vs), 1277 (vs), 1243 (vs), 1219 (vs), 1173 (m), 973 (vs), 843 (m), 728 (s).

IR spectroscopic characterization of 2 and 2cr:

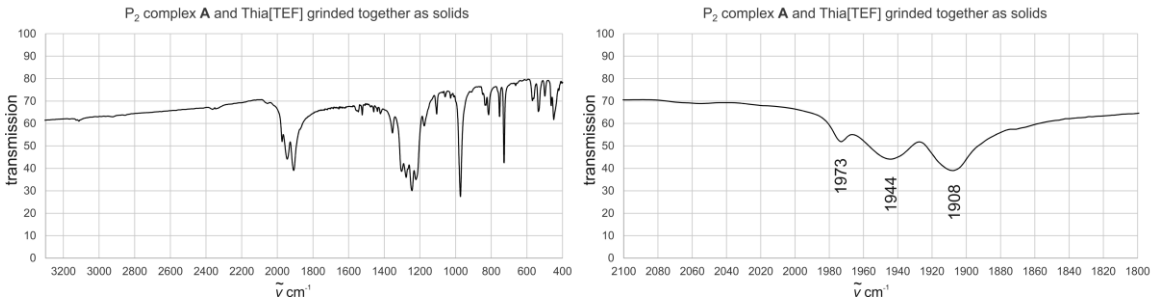

Figure 1. IR(KBr) before reaction.

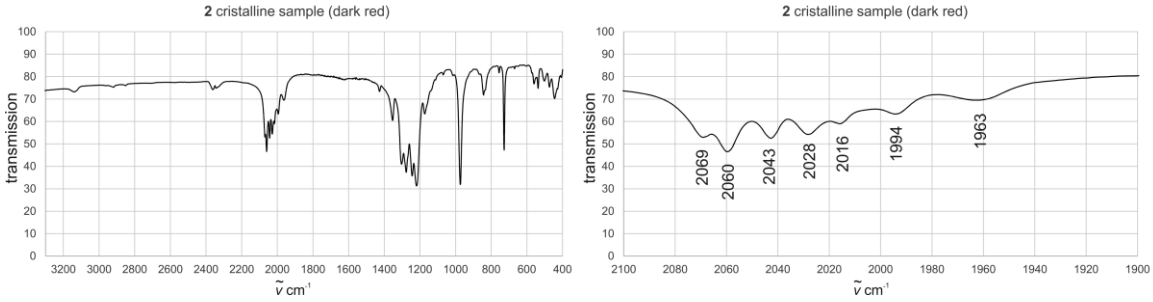

Figure 2. IR(KBr) of crystalline **2**.

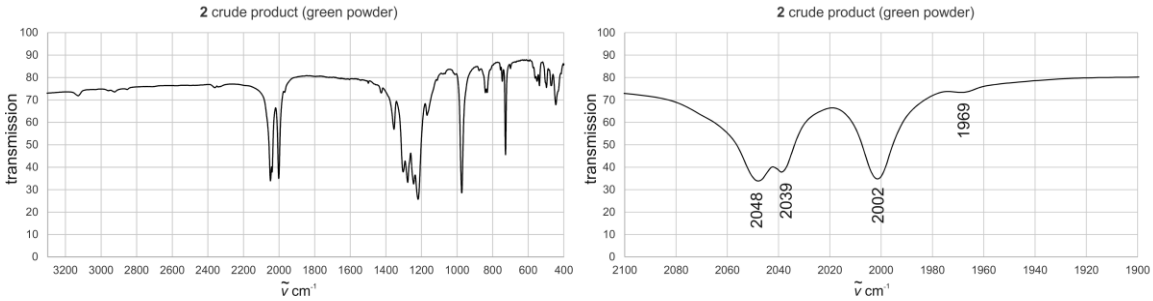

Figure 3. IR(KBr) of dark green powder **2cr**.

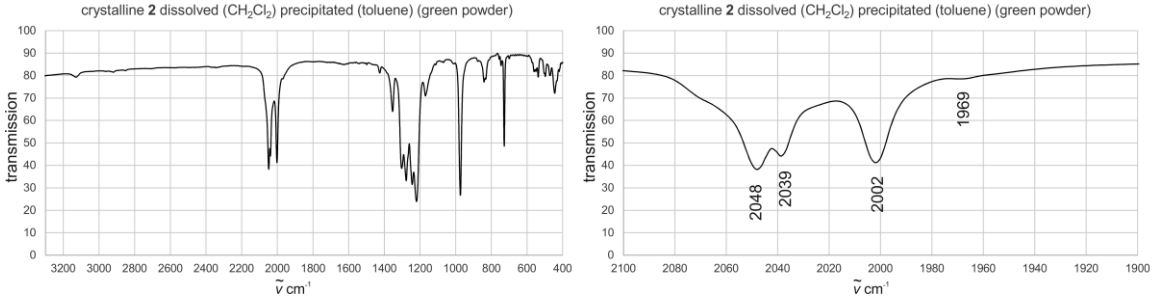

Figure 4. IR(KBr) of dissolved crystals of **2** in CH_2Cl_2 which were subsequently precipitated as dark green powder (identical to **2cr**).

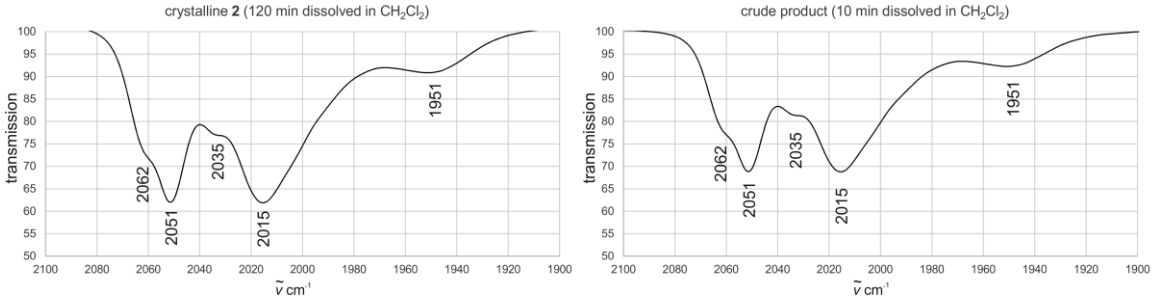

Figure 5. IR(CH_2Cl_2) of dissolved crystals of **2** (left) and dissolved **2cr** (right).

The solution IR spectra of **2** and **2cr** are identical and no evolution of the signals can be observed depending with time (10, 30, 120 min).

ESI mass spectrometry of 2

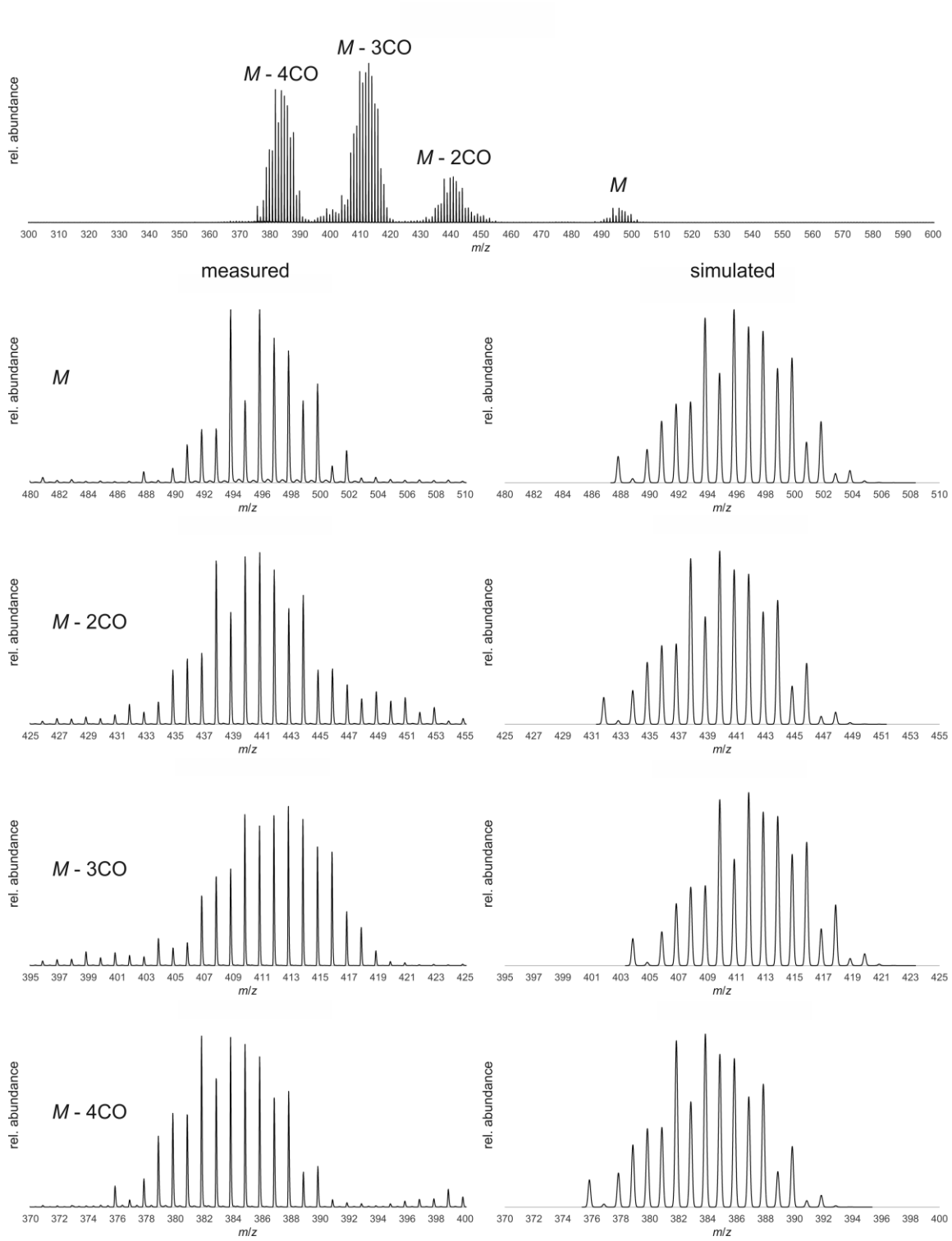

Figure 6. (top) ESI MS spectrum of **2cr** from CH_2Cl_2. Measured (left) and simulated (right) isotopic distribution for the assignable peaks. *M* = **A**.

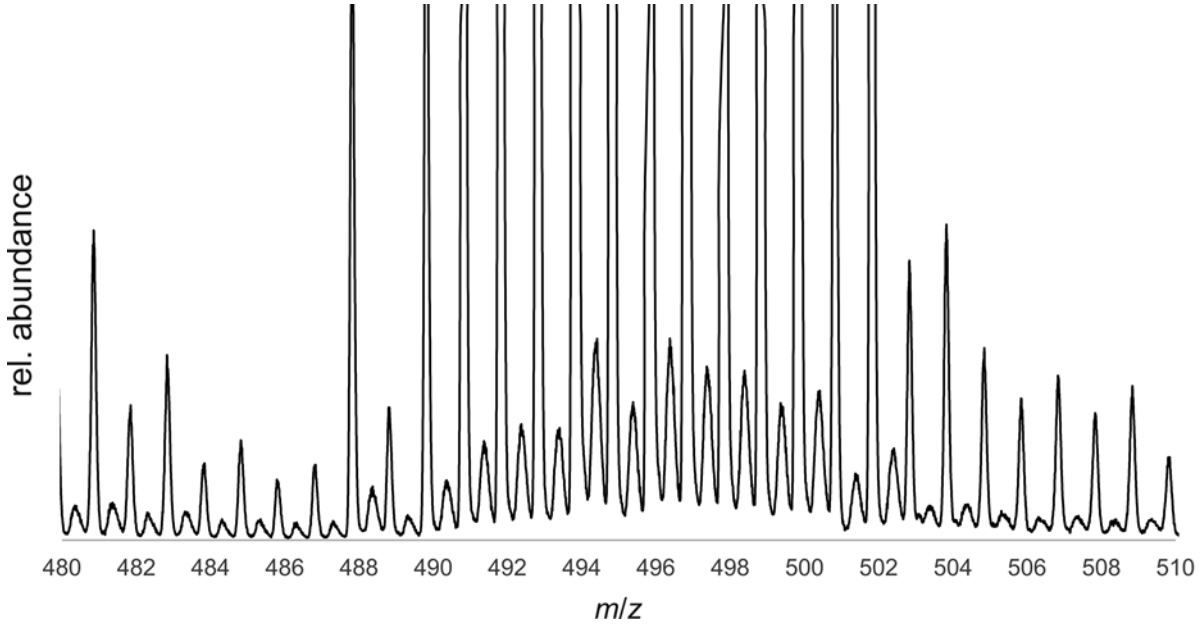

Figure 7. Magnification of the measured peaks for $[M]^+$ (=$[\mathbf{A}]^+$), showing the small peaks shifted by ~0.5 Da compared to the major signal. These probably arise from a dicationic species.

X-ray crystallography

General considerations

All crystal manipulations were performed under mineral oil. The diffraction experiments were performed at 123 K on a Rigaku (former Agilent Technologies or Oxford Diffraction) Gemini Ultra diffractometer using Cu-K_α radiation. Crystallographic data together with the details of the experiments are given in Table 1. The cell determination, data reduction and absorption correction for all compounds were performed with the help of the CrysAlis PRO software. The full-matrix least-square refinement against F^2 was done with ShelXL. If not stated otherwise, all atoms except hydrogen were refined anisotropically. The H atoms were calculated geometrically and a riding model was used during refinement process. For the description of the refinement strategy, the restraint command ISOR and SADI of the ShelX program package are used. Graphical material was created with the free software Olex2. All cif files are also saved on the provided DVD.

Table 1. Crystallographic details for the compounds **1** and **2**.

Identification code	**1**	**2**
formula	$C_{28}H_8AlF_{36}O_4S_2$	$C_{60}H_{20}Al_2F_{72}Mo_4O_{16}P_4$
weight [g·mol^{-1}]	1183.44	2926.36
Temperature [K]	123.00(14)	123.1(2)
crystal system	triclinic	monoclinic
space group	*P*–1	$P2_1/n$
a [Å]	11.6645(2)	15.43561(8)
b [Å]	14.21758(15)	21.49774(12)
c [Å]	14.28912(15)	26.97813(15)
α [°]	91.0927(9)	90
β [°]	112.6095(14)	89.2667(5)
γ [°]	113.5492(14)	90
Volume [Å^3]	1963.21(6)	8951.44(8)
Z	2	4
ρ_{calc} [g·cm^{-3}]	2.002	2.171
μ [mm^{-1}]	3.446	7.350
F(000)	1154.0	5640.0
crystal size [mm^3]	0.385 × 0.325 × 0.207	0.348 × 0.193 × 0.059
diffractometer	Gemini Ultra	Gemini Ultra
absorption correction	gaussian	gaussian
T_{min}/T_{max}	0.365 / 0.576	0.283 / 0.684
radiation [Å]	CuK_α	CuK_α
2*Θ* range [°]	6.928 to 135.572	7.738 to 132.072
completeness	0.988	0.994
reflns collected/unique	34878 / 7003	66712 / 15518
R_{int}/R_{sigma}	0.0272 / 0.0140	0.0283 / 0.0191
data/restraints/parameters	7003 / 12 / 748	15518 / 3 / 1471
GOF on F^2	1.080	1.043
R_1/wR_2 [$I \geq 2\sigma(I)$]	0.0555 / 0.1629	0.0305 / 0.0808
R_1/wR_2 [all data]	0.0565 / 0.1637	0.0338 / 0.0823
max/min $\Delta\rho$ [e·Å^{-3}]	1.29 / –0.54	1.09 / –0.50

Refinement details for **1**: The refinement of the crystal structure of **1** could be done without any difficulty. One -C_4F_9 group of the [TEF] anion shows a rotational disorder with a 50:50 ratio. Both parts were refined anisotropically. The ADPs of two half-occupied F atoms were restrained by ISOR commands. The crystal structure of **1** is shown in Figure 8 (disorder omitted).

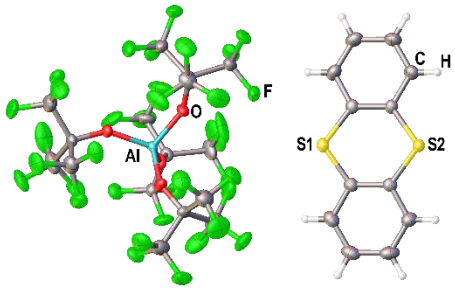

Figure 8. X-ray structure of [Thia][TEF].

Refinement details for **2**: The refinement of the crystal structure of **2** could be done without any difficulty. One -C_4F_9 group of one anion shows a rotational disorder with a 60:40 ratio. The minor part was refined isotropically and one of these -CF_3 groups was restrained during the refinement by SADI commands.

DFT calculations

The DFT calculations were performed with the TURBOMOLE[1] program package at the (RI-)[2]BP86[3]/def2-TZVP[2b,4] level of theory. The Multipole Accelerated Resolution of Identity (MARI-J)[5] approach was used to speed up the geometry optimizations which were performed

without any symmetry restrains. The total energies were calculated by single point calculations without using the RI formalism. The solvent effect were incorporated via the Conductor-like Screening Model[6] (COSMO) using the dielectric constant of CH_2Cl_2 (ε = 8.930) as single point calculations on the gas-phase optimized geometries. The SCF energies were used without corrections and the entropic effects are not considered.

The optimized geometry (see Figure 9) of $[\{CpMo(CO)_2\}_2(\mu,\eta^2{:}\eta^2\text{-}P_2)]^+$ (**A**$^+$) shows slightly elongated bond lengths compared to the neutral complex $[\{CpMo(CO)_2\}_2(\mu,\eta^2{:}\eta^2\text{-}P_2)]$ (**A**). According to the calculations the unpaired electron in **A**$^+$ is mainly located on both molybdenum atoms (70%) and only 20% is located on both phosphorus atoms. The dimerization of **A**$^+$ via Mo-Mo bond formation is probably inhibited by the steric repulsion. The dimerization of **A**$^+$ via P-P bond formation is thermodynamically favored by 52.8 kJ·mol^{-1}. The Wiberg bond index (WBI) of both Mo-Mo and P-P bonds decreases upon oxidation of **A** to **A**$^+$ from 0.43 and 1.22 to 0.38 and 1.12, respectively.

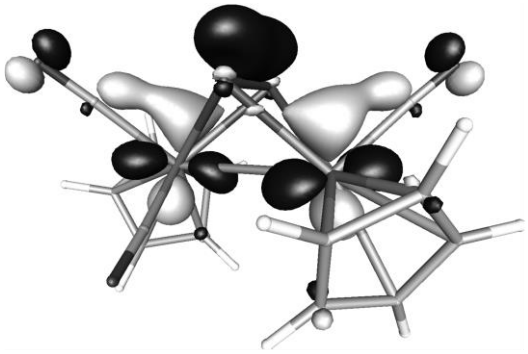

Figure 9. Single occupied molecular orbital in $[\{CpMo(CO)_2\}_2(\mu,\eta^2{:}\eta^2\text{-}P_2)]^+$ (**A**$^+$). Calculated at the BP86/def2-TZVP level.

In the optimized geometry (see Figure 10) of $[\{CpMo(CO)_2\}_4(\mu_4,\eta^2{:}\eta^2{:}\eta^2{:}\eta^2\text{-}P_4)]^{2+}$ (**2**), the central P-P bond is slightly elongated (2.286 Å) compared to the other two P-P bonds (2.139 Å and 2.187 Å). This is also nicely reflected in the corresponding Wiberg bond indices (0.80, 1.01 and 1.06, respectively) shown in Table 2. The natural population analysis show a positive charge accumulation on the peripheral phosphorus atoms (0.30 and 0.40e), whereas the internal phosphorus atoms are less charged (0.21 and 0.22e).

The highest occupied molecular orbital (HOMO) is mainly centered on molybdenum with smaller contributions from phosphorus. The LUMO is the central P-P antibonding orbital.

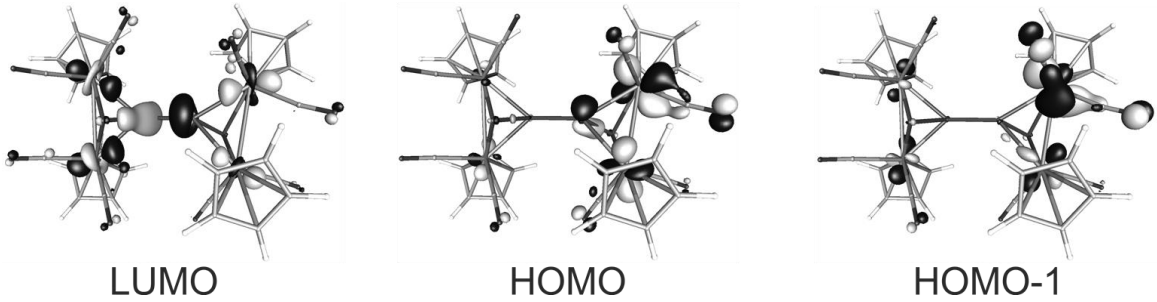

Figure 10. Frontier molecular orbitals of **2** calculated at the BP86/def2-TZVP level.

Table 2. Calculated natural charges, Wiberg bond indices and isotropic magnetic shielding at the BP86/def2-TZVP level of theory. Labeling of the toms according to the Labeling in the X-ray Structure (Figure 1 of the main text)

Atom	Natural Charge	Isotropic magnetic shielding	Bond	WBI
P1	0.30	120	P1-P2	1.06
P2	0.21	176	P2-P3	0.80
P3	0.22	132	P3-P4	1.01
P4	0.40	39		

Cartesian coordinates of the optimized geometries of **A**, $[\mathbf{A}]^+$ and **2** can be found on the provided DVD.

References

[1] a) F. Furche, R. Ahlrichs, C. Hättig, W. Klopper, M. Sierka, F. Weigend, *WIREs Comput. Mol. Sci.* **2014**, *4*, 91-100. b) R. Ahlrichs, M. Bär, M. Häser, H. Horn, C. Kölmel, *Chem. Phys. Lett.* **1989**, *162*, 165–169; c) O. Treutler, R. Ahlrichs, *J. Chem. Phys.* **1995**, *102*, 346–354.

[2] a) K. Eichkorn, O. Treutler, H. Oehm, M. Häser, R. Ahlrichs, *Chem. Phys. Lett.* **1995**, *242*, 652–660; b) K. Eichkorn, F. Weigend, O. Treutler, R. Ahlrichs, *Theor. Chem. Acc.* **1997**, *97*, 119.

[3] a) P. A. M. Dirac *Proc. Royal Soc. A*, **1929**, *123*, 714–733. b) J. C. Slater *Phys. Rev.*, **1951**, *81*, 385-390. c) S. Vosko; L. Wilk; M. Nusair, *Can. J. Phys.*, **1980**, *58*, 1200–1211. d) A. D. Becke *Phys. Rev. A*, **1988**, *38*, 3098–3100. e) J. P. Perdew. *Phys. Rev. B*, **1986**, *33*, 8822–8824.

[4] a) A. Schäfer, C. Huber, R. Ahlrichs, *J. Chem. Phys.* **1994**, *100*, 5829; b) K. Eichkorn, F. Weigend, O. Treutler, R. Ahlrichs, *Theor. Chem. Acc.* **1997**, *97*, 119. c) F. Weigend, R. Ahlrichs, *Phys. Chem. Chem. Phys.* **2005**, *7*, 3297. d) F. Weigend, *Phys. Chem. Chem. Phys.* **2006**, *8*, 1057.

[5] M. Sierka, A. Hogekamp, R. Ahlrichs, *J. Chem. Phys.* **2003**, *118*, 9136.

[6] a) A. Klamt; G. Schüürmann, *J. Chem. Soc. Perkin Trans.2*, **1993**, 799–805. b) A. Klamt; V. Jonas, *J. Chem. Phys.*, **1996**, 105, 9972–9981.

Preface

The following chapter has not been published until the submission of this thesis.

Authors

Martin Fleischmann, Fabian Dielmann, Luis Dütsch, Stefan Welsch, Gábor Balázs and Manfred Scheer*

Author contributions

The preparation and characterization of all compounds (except **1**, **2c** and **4e**) including the single crystal X-ray structure determination and the preparation of the manuscript was done by the first author. Fabian Dielmann developed and described the synthesis and characterization of the compounds **1**, **2c** and **4e**. Luis Dütsch reacted [Thia][FAl] (**10c**) with the P_2 complex **6** and will be involved in future investigations concerning upcoming publications. Stefan Welsch observed and described the compound **11b** for the first time in his PhD-thesis. Gábor Balázs performed supporting DFT calculations. Manfred Scheer supervised the research and revised the manuscript.
A detailed discussion about the oxidation of the P_2 complex **6** can be found in chapter 5. The oxidation of **2b** has been described in chapter 3.

Acknowledgements

Valentin Vass is gratefully acknowledged for MS measurements, Werner Kremer for MAS NMR measurements, Florian Pevny und Rainer Winter for spectroelectrochemical measurements and Moritz Modl for measurement of EPR spectra. This work was financially supported by the Deutsche Forschungsgemeinschaft.

6 Stabilization of oxidized E_n ligand complexes with the help of weakly coordinating anions

Abstract: Herein, we report investigations of single-electron oxidation products starting from neutral E_n ligand complexes. The oxidation of the 28 VE *cyclo*-E_6 triple-decker complexes $[(Cp^RMo)_2(\mu,\eta^6{:}\eta^6\text{-}E_6)]$ (E = P, Cp^R = Cp, Cp*, $C_5(CH_2Ph)_5$; E = As, Cp^R = Cp*) by Cu^+ or Ag^+ leads to isolated cationic 27 VE complexes which retain their general triple-decker geometry in the solid state. The *cyclo*-E_6 middle decks of the complexes are distorted from the initially perfect hexagonal geometry during oxidation. From reactions of Ag^+ with the P_2 complex $[\{CpMo(CO)_2\}_2(\mu,\eta^2{:}\eta^2\text{-}P_2)]$ no oxidation products could be obtained but three new coordination compounds with molar ratios of Ag^+ and the P_2 complex of 1:1, 1:2 and 2:3. The latter represents the first homoleptic coordination polymer of Ag^+ and $[\{CpMo(CO)_2\}_2(\mu,\eta^2{:}\eta^2\text{-}P_2)]$. A facile synthesis of the strong oxidants [Thia][TEF] and [Thia][FAl] ([Thia] = $[C_{12}H_8S_2]^+$, [TEF] = $[Al\{OC(CF_3)_3\}_4]^-$) is presented. Finally, the strong oxidant $[Thia]^+$ enabled the oxidation of the P_2 complex $[\{CpMo(CO)_2\}_2(\mu,\eta^2{:}\eta^2\text{-}P_2)]$ which forms a dicationic complex containing a central P_4 chain. From this cation we could structurally characterize a symmetrical and an unsymmetrical isomer.

6.1 Introduction

The chemistry of (poly)cationic frameworks containing pnictogen atoms has been intensively explored during the last years.[1,2,3,4] Following a catenation approach by halide abstractions from Pn-X bonds (Pn = pnictogen atom, X = halide) a large variety of polypnictogenyl cations are accessible. The majority of these catena cations bear organic substituents which contribute to the stabilization of these compounds. Recently, it was demonstrated that redox processes can also take place resulting for example in the facile formation of $[P_4(AsPh_3)_2]^{2+}$ bearing a central P_4 butterfly structural motif bonded only to As atoms.[5] Interestingly, this compound initiated a vivid discussion about describing the electronic structure of main group compounds by arrows in analogy to coordination chemistry of transition metals, which however will not be the focus of this work.[6,7,8] Additionally, oxidation of P_4 via initial $[NO]^+$ insertion gave access to the first substituent-free homoatomic phosphorus cation $[P_9]^+$.[9,10] This reaction could only be realized in the presence of the weakly coordinating anion $[Al\{OC(CF_3)_3\}_4]^-$ (=[TEF]), which can be regarded as inert in most of its reactions. Unfortunately, a structural characterization by single crystal diffraction studies could not be performed

for $[P_9][TEF]$ so far. The contribution of our group to this field includes the oxidation of substituent-free polypnictogenyl ligands in the coordination sphere of transition metals.[11,12,13,14,15] Preliminary studies include the one-electron oxidation of pentaphosphaferrocene[16] $[Cp^*Fe(\eta^5\text{-}P_5)]$ and the haxaphosphabenzene[17] complex $[(Cp^*Mo)_2(\mu,\eta^6\text{:}\eta^6\text{-}P_6)]$. One-electron oxidation of the *cyclo*-P_5 complex results in the formation of a diamagnetic dication $[(Cp^*Fe)_2(\mu,\eta^4\text{:}\eta^4\text{-}P_{10})]^{2+}$ (Scheme 1 **I**) by P-P bond formation. The formation of this product was predicted in 1999 with the help of electrochemical and theoretical investigations.[18] It could finally be isolated and structurally characterized in 2013.[19] In contrast to this dimerization, the single-electron oxidation of $[(Cp^*Mo)_2(\mu,\eta^6\text{:}\eta^6\text{-}P_6)]$ yields a paramagnetic 27 VE (valence electron) triple-decker complex with a bis-allylic distorted *cyclo*-P_6 middle deck (Scheme 1 **II**).[20] In this context, we got interested in the investigation and comparison of the reactivity of polypnictogenyl complexes upon oxidation depending on the organic ligands of the complexes, the nature (P or As) and the number of pnictogen atoms, as well as the influence of the used anions.

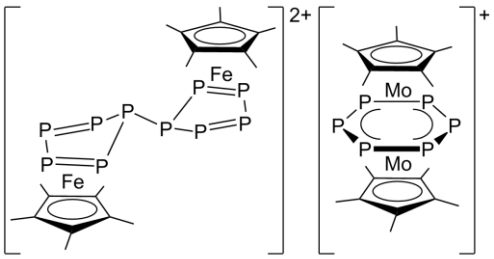

Scheme 1. Oxidation products **I** and **II**.

The current study includes the synthesis of a new hexaphosphabenzene complex containing the large Cp^{Bn} ligand (Cp^{Bn} = $C_5(CH_2Ph)_5$). The single-electron oxidation of four triple-decker complexes containing a *cyclo*-E_6 (E = P, As) middle deck as well as the reactivity of the P_2 complex $[\{CpMo(CO)_2\}_2(\mu,\eta^2\text{:}\eta^2\text{-}P_2)]$ towards Ag^+ will be described.

6.2 Results and Discussion

Preparation of $[(Cp^{Bn}Mo)_2(\mu,\eta^6\text{:}\eta^6\text{-}P_6)]$

The all-phosphorus and all-arsenic analogues of benzene have been stabilized by *Scherer et al.* several years ago in the triple-decker complexes $[(Cp^*Mo)_2(\mu,\eta^6\text{:}\eta^6\text{-}E_6)]$ (E = P(**2b**), As(**3**)).[14,21] The subtle steric and electronic differences by introducing substituted Cp ligands often has a dramatic effect on the reactivity of E_n complexes. For example the Cp analogues complex $[(CpMo)_2(\mu,\eta^6\text{:}\eta^6\text{-}P_6)]$ (**2a**) was prepared in 2012 and shows a poor solubility in all common solvents in contrast to the Cp* complex **2b** which is

known since 1985.[22] It was demonstrated previously that the pentabenzyl substituted Cp^{Bn} ligand significantly increases solubility of spherical supramolecules formed from [$Cp^{Bn}Fe(\eta^5\text{-}P_5)$] and Cu^I halides or even leads to new products compared to its Cp* derivative [$Cp^*Fe(\eta^5\text{-}P_5)$].[23,24,25,26,27,28,29] Therefore, the preparation of E_n complexes with varying Cp ligands offers an incentive.

The reaction of [$Mo(CO)_6$] and $Cp^{Bn}H$ in boiling decalin, yields [{$Cp^{Bn}Mo(CO)_2$}$_2$] (**1**) in 58% crystalline yield after chromatographic workup and subsequent recrystallization. Compound **1** is isolated as a red, slightly air-sensitive solid, which is nearly insoluble in hexane, but shows good solubility in CH_2Cl_2 and toluene. The IR spectrum of **1** (KBr) reveals two strong bands at 1870 cm^{-1} and 1834 cm^{-1} for the CO stretching frequencies (*c.f.* 1867 cm^{-1} and 1842 cm^{-1} for Cp* analog).[30,31] In the ^1H NMR spectrum of **1** in C_6D_6 solution two multiplets in the aromatic region for the Ph groups (δ = 6.93 - 7.03 and 6.67 - 6.71 ppm) as well as a sharp singlet at δ = 3.89 ppm for the CH_2 groups can be detected. The $^{13}C\{^1H\}$ NMR spectrum shows four signals for the Ph groups (δ = 139.5, 129.2, 128.4 and 126.4 ppm), one for the Cp ring (δ = 109.1 ppm), one for the CH_2 groups (δ = 31.9 ppm) and only one signal for the CO groups at δ = 239.0 ppm. Field desorption MS (FD-MS) reveals the molecular ion peak $[\mathbf{1}]^+$ while electron impact-MS (EI-MS) shows loss of CO and fragmentation. When **1** is reacted with an excess of P_4 in boiling diisopropylbenzene (DIB) at ~205 °C the hexaphosphabenzene complex [$(Cp^{Bn}Mo)_2(\mu,\eta^6\text{:}\eta^6\text{-}P_6)$] (**2c**) is obtained. After chromatographic workup and subsequent recrystallization **2c** can be isolated in 48% crystalline yield (orange color). Long reaction times are needed, since after 24 h unreacted **1** can still be detected by IR spectroscopy in the reaction mixture. Therefore, **1** is less reactive than its Cp* counterpart [{$Cp^*Mo(CO)_2$}$_2$] which yields [$(Cp^*Mo)_2(\mu,\eta^6\text{:}\eta^6\text{-}P_6)$] (**2b**) in 64% yield after 90 min.[20] The ^1H NMR spectrum of **2c** in CD_2Cl_2 solution shows a singlet at δ = 2.49 ppm for the CH_2 groups significantly upfield shifted compared to **1**. Additionally, three separate signals can be resolved for the *ortho* (d, δ = 5.95 ppm), *meta* (dd, δ = 6.57 ppm) and *para* protons (t, δ = 6.72 ppm) of the Ph groups. The $^{13}C\{^1H\}$ NMR spectrum shows four signals for the Ph groups (δ = 139.3, 128.9, 127.8 and 126.0 ppm), one signal for the Cp ring (δ = 101.4 ppm) and one signal for the CH_2 groups (δ = 35.1 ppm). The $^{31}P\{^1H\}$ NMR spectrum of **2c** in CD_2Cl_2 solution shows a sharp singlet at δ = −316.0 ppm, which is very similar to its Cp* analog **2b** (δ = –314.3 ppm).[17,20] FD and EI-MS show the molecular ion peak for $[\mathbf{2c}]^+$.

The crystal structures of **1** and **2c** were determined by single crystal X-ray diffraction analysis, and their structures are shown in Figure 1. Compound **1** crystallizes in the monoclinic space group $P2_1/c$ with half a molecule in the asymmetric unit. The second half is generated by inversion. The two Cp^{Bn} ligands show a trans arrangement.

In contrast to its Cp* analog, the carbonyl ligands in **1** bind to the Mo atoms in a semi-bridging coordination mode, comparable to the Cp analog, with short Mo–C bond distances of 1.968(3) and 1.972(4) Å while the distances of the carbonyl C atoms to the other Mo atom are 2.686(3) and 2.703(4) Å, respectively (*c.f.* average 2.56 Å for the Cp analog).[32] The Mo1-Mo1' bond (2.5213(3) Å) is consistent with a Mo-Mo triple bond although it is slightly elongated compared to its Cp* (2.488(3) Å) or its Cp (2.4477(12) Å) derivative.[30,32] The Ph rings of the flexible Bn groups are pointing away from the Mo atom. This arrangement is regularly observed for the Cp^{Bn} ligand and is stabilized by several intra- and intermolecular π π interaction.[23]

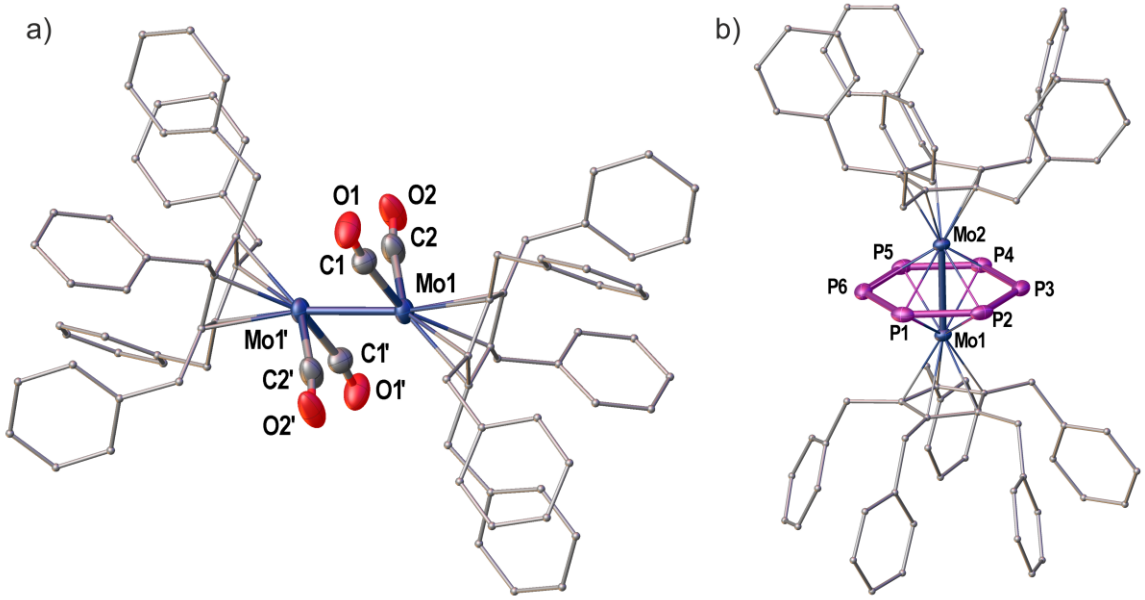

Figure 1. Crystal structures of **1** a) and **2c** b). Selected bond lengths [Å] and angles [°]: **1**: Mo1-Mo1' 2.5186(7), Mo1-C1 1.968(3), Mo1-C2 1.972(4), Mo1-C1' 2.686(3), Mo1-C2' 2.703(4), Cp^{Bn}_{cent}-Mo1 1.9978(11), Cp^{Bn}_{cent}-Mo1-Mo1' 162.9(1); **2c**: Mo1-Mo2 2.6650(1), P1-P2 2.1875(1), P2-P3 2.1776(1), P3-P4 2.1875(1), P4-P5 2.1740(1), P5-P6 2.1841(1), P6-P1 2.1644(1).

The *cyclo*-P_6 triple-decker complex **2c** crystallizes in the monoclinic space group $P2_1/c$ with one independent molecule in the asymmetric unit shown in Figure 1 b). The middle deck can be regarded as an almost perfect hexagonal planar *cyclo*-P_6 ligand with an average P-P bond length of 2.1792(1) Å (see Figure 1 b) and all P-P-P angles close to 120°. The Mo-Mo bond length in **2c** measures 2.6650(1) Å. The whole triple-decker geometry can be compared very well to the Cp and the Cp* analogs **2a** and **2b**.[17,20,22] The Ph rings of the Bn groups are oriented away from the Mo atoms comparable to the arrangement found in **1**.

Oxidation of *cyclo*-E_6 complexes

CV study of the *cyclo*-E_6 complexes

During the current study the electrochemistry of the *cyclo*-P_6 complexes **2a-c** was investigated by cyclovoltammetry in CH_2Cl_2. The results are presented in Table 1 and show the first oxidation of each of the 28 VE (valence electron) triple-decker complexes to a 27 VE species to be reversible. However, the second oxidation to a 26 VE species is irreversible for each *cyclo*-P_6 complex.[33,34,35] The redox potentials reveal that the Cp* complex **2b** is more easily oxidized than its Cp analog while the Cp^{Bn} congener is least prone to oxidation. Nevertheless, all *cyclo*-P_6 complexes **2a-c** should be readily oxidized by Ag^+ in CH_2Cl_2 with a formal potential of +0.65 V vs $Fc^{0/+}$ (Fc = ferrocene).[36]

Table1. Oxidations of the *cyclo*-E_6 complexes **2a-c** and **3** established by cyclovoltammetry (CV). The position of the peaks in the CV are presented with $Fc^{0/+}$ as a reference (Fc = ferrocene). The annotations (r) and (i) describe if the oxidations are reversible or irreversible.

complex	1. oxidation	2. oxidation
2a (Cp^R = Cp)	–35.5 mV (r)	693 mV (i)
2b (Cp^R = Cp*)	–240 mV (r)	587 mV (i)
2c (Cp^R = Cp^{Bn})	+40 mV (r)	730 mV (i)

When the *cyclo*-P_6 complexes **2a-c** are reacted with Ag^+ salts of the WCAs [TEF] (=$[Al\{OC(CF_3)_3\}_4]^-$) and [FAl] (=$[FAl\{OC_6F_{10}(C_6F_5)\}_3]^-$) in CH_2Cl_2 solution (see Scheme 2), an immediate color change to dark purple (**2a**) or dark teal (**2b**, **2c**) can be observed accompanied by the formation of a silver mirror or black precipitate of Ag^0. The *cyclo*-As_6 complex **3** is readily oxidized by $[Cu(MeCN)_4][BF_4]$ in CH_2Cl_2 solution resulting in a color change to dark green and formation of black precipitate (presumably Cu^0). Diffusion of alkanes into the filtered solutions affords the products obtained by single-electron oxidation as dark purple (**4a**, **4b**), dark teal (**4c-e**) or dark green (**5**) crystals, respectively. The ^1H NMR spectra of the oxidized *cyclo*-P_6 complexes **2a-c** in CD_2Cl_2 solution show a broad peak at δ = 11.55 ppm (ω1/2 = 35 Hz) for the Cp ligand of the cation [**2a**]$^+$ in **4a**, a broad peak at δ = 4.08 ppm (ω1/2 = 17 Hz) for the Cp* ligand of the cation [**2b**]$^+$ in **4c** and a broad peak at δ = 5.94 ppm (ω1/2 = 48 Hz) for the CH_2 groups of the Cp^{Bn} ligand of the cation [**2c**]$^+$ in **4e**, all significantly shifted to lower field compared to the neutral 28 VE complexes **2a-c**. In addition **4e** shows three separate signals for the *ortho* (δ = 6.45 ppm), *meta* (δ = 6.92 ppm) *para* protons (δ = 6.97 ppm) of the Ph groups. For all oxidized *cyclo*-P_6 complexes **4a-e**, no signals can be observed in the $^{31}P\{^1H\}$ NMR spectra in the range from δ = –1200 to 1200 ppm. The ^1H NMR spectra of the oxidized *cyclo*-As_6 complex **5** shows one broad signal at δ = 2.64 ppm (ω1/2 = 14 Hz) for

the Cp* ligand shifted significantly to lower field by 2.74 ppm compared to neutral **3** (–0.1 ppm).[21] The $^{19}F\{^1H\}$ NMR spectra show characteristic signal patterns of the weakly coordinating anions (WCAs) [TEF] (**4a**, **4c**, **4e**), [FAl] (**4b**, **4d**) and $[BF_4]^-$ (**5**), respectively. The X-band EPR spectra of the paramagnetic polyphosphorus cations [**2a-c**]$^+$ show no signal at room temperature but upon cooling to 77 K one broad signal can be observed for each complex. Specifically, it can be found at g_{iso} = 2.025 (solid state) or g_{iso} = 2.003 (CD_2Cl_2) for [**2a**]$^+$, at g_{iso} = 2.024 (solid state) or g_{iso} = 2.019 (CD_2Cl_2) for [**2b**]$^+$ and at g_{iso} = 2.023 (CD_2Cl_2) for [**2c**]$^+$ without resolving any hyperfine coupling.[37] No signal could be detected in the X-band EPR spectrum for a CD_2Cl_2 solution of [**3**]$^+$ neither at room temperature nor at 77 K. With the help of the Evans NMR method the magnetic moments of **4a** (μ_{eff} = 1.68 μ_B), **4b** (μ_{eff} = 1.59 μ_B), **4c** (μ_{eff} = 1.68 μ_B), **4e** (μ_{eff} = 1.57 μ_B) and **5** (μ_{eff} = 1.66 μ_B) could be determined.[38] The magnetic moments are in good agreement with the expected values for one unpaired electron for all 27 VE cations. ESI-MS of CH_2Cl_2 solutions of **4a-5** show the molecular ion peaks for the 27 VE cations $[(Cp^RMo)_2(\mu,\eta^6{:}\eta^6\text{-}E_6)]^+$ in all cases.

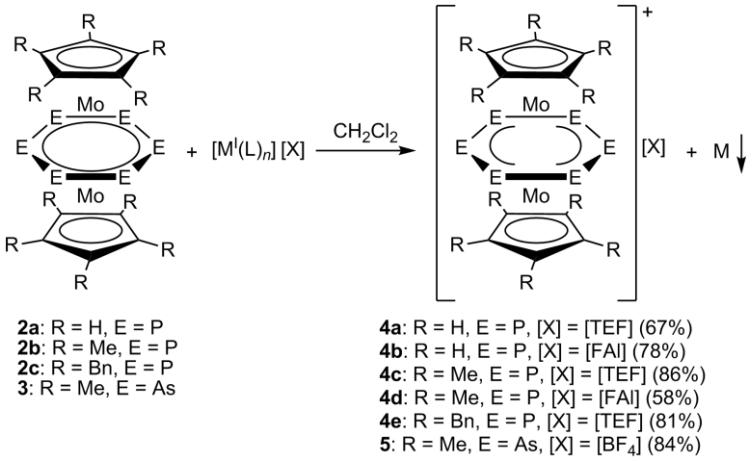

Scheme 2. Oxidation of the *cyclo*-E_6 complexes **2a-d** and **3** by M^+ cations to 27 VE triple-decker complexes. The cation $[M^+(L)_n]^+$ is $[Ag(CH_2Cl_2)]^+$ for E = P and $[Cu(MeCN)_4]^+$ for E = As.

Crystal structures of the oxidized *cyclo*-E_6 complexes

For **4a** and **4c**, respectively, the obtained crystals are not suitable for single crystal X-ray diffraction analysis.[39] However, the crystal structure of the cations [**2a**]$^+$ and [**2b**]$^+$ could be determined with the help of the WCA [FAl] in **4b** and **4d**, respectively.[40] Single crystal X-ray structure determination reveals, that the *cyclo*-E_6 complexes **2a-c** and **3** retain the triple-decker geometry upon one-electron oxidation.[41] The crystal structures of **4b**, **4d**, **4e** and **5** are shown in Figure 2. The Mo-Mo bond lengths of the oxidized complexes (2.6745(5) Å (**4b**), 2.6614(8) Å (**4d**), 2.683(1) Å (**4e**) and

2.6773(12) Å (**5**)) are very uniform and close to the Mo-Mo bond distances of the corresponding neutral *cyclo*-E_6 complexes suggesting a Mo-Mo single-bond. The planes of the two Cp ligands show small tilt angles in respect to each other (2.07(14)° (**4d**), 7.50(1)° (**4e**)) or adopt a perfectly planar arrangement (**4b** and **5**). The Ph rings of the Cp^{Bn} ligand in **4e** are pointing away from Mo resembling the structures of **1** and **2c**.

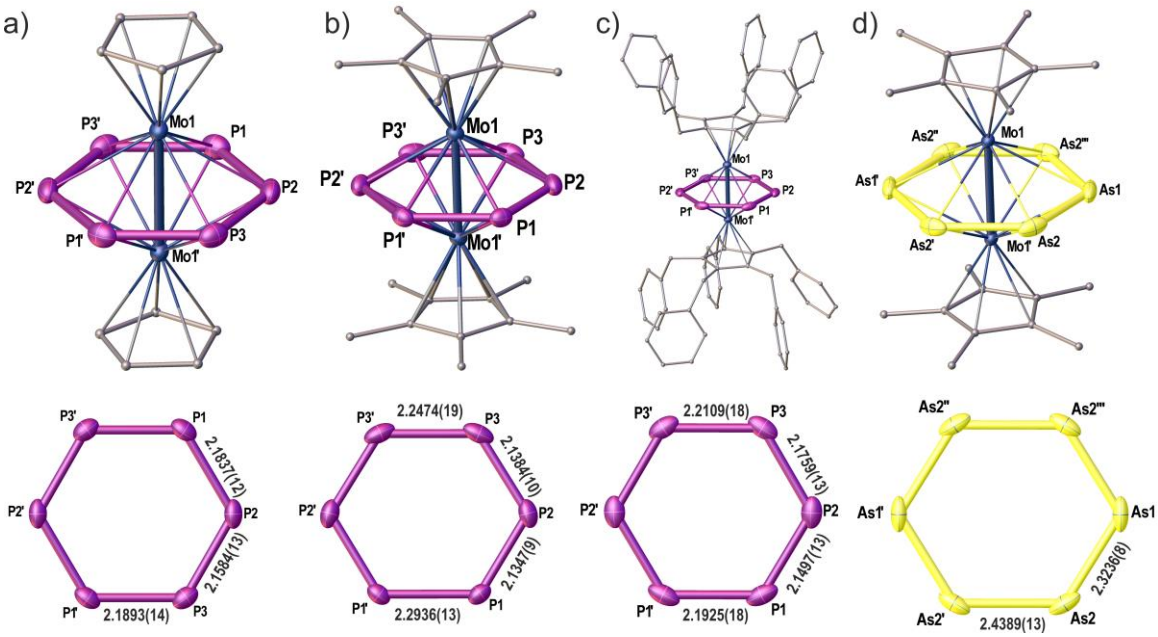

Figure 2. (top) Crystal structures of the oxidized *cyclo*-E_6 complexes in **4b** a) **4d** b), **4e** c) and **5** d). Ellipsoids are drawn at 50% probability. H atoms are omitted for clarity. Only one of two independent molecules are depicted for **4b** and **4d**.[41] (bottom) Illustration of the corresponding *cyclo*-E_6 ligands with their respective E-E bond lengths. Symmetry equivalent E-E bond lengths are omitted. Space groups are *C*2/*c* (**4b**, **4d**, **4e**) and *Ibam* (**5**). Selected bond lengths [Å]: **4b**: Mo1-Mo1' 2.6745(5); **4d**: Mo1-Mo1' 2.6614(8); **4e**: Mo1-Mo1' 2.683(1); **5**: Mo1-Mo1' 2.6773(12).

Although the crystal structures of the cationic triple-decker complexes containing planar *cyclo*-E_6 middle decks are similar to each other, distinct differences can be observed for the E-E bond lengths (see Figure 2). The *cyclo*-P_6 ligand of the purple **4b** can be described as a planar hexagon showing a small deviation from the ideal hexagonal geometry with two opposing P-P bonds (P2-P3 and P2'-P3') being slightly shortened with 2.1584(13) Å. The average P-P bond length in **4b** is 2.177 Å which is unchanged to neutral **2a**.[22] In contrast, the dark teal **4d** exhibits two significantly elongated P-P bonds (P1-P1' and P3-P3') with 2.2474(19) Å and 2.2936(13) Å while the remaining P-P bonds are shortened with 2.1384(10) Å and 2.1347(9) Å compared to the neutral hexaphosphabenzene **2b** ($P\text{-}P_{av}$ 2.183 Å).[17,20] This geometry can best be described as a bis-allylic distortion of the *cyclo*-P_6 ligand. A similar bis-allylic distortion could be observed in the structurally characterized single-electron oxidized benzene derivatives $[C_6F_6]^+$ and [H_2N-2,4,6-tri-^{t}Bu-benzene]$^+$.[42,43] This distortion is by far less pronounced in **4e** (max. P-P bond length deviation 0.06 Å), while it can clearly be

observed for the *cyclo*-As_6 ligand in **5** with elongated As-As bonds of 2.4389(13) Å and shortened As-As bonds of 2.3236(8) Å (neutral **3**: As-As_{av} 2.349 Å).

DFT calculations

In order to investigate the electronic structure of the $[(Cp^RMo)_2P_6]$ and $[(Cp^RMo)_2P_6]^+$ (Cp^R = C_5H_5 and C_5Me_5) complexes, DFT calculations have been performed at the BP86[44]/def2-TZVP[45] level of theory. Qualitatively, the geometric parameters are well reproduced for the neutral complexes as well as for the oxidized species $[(Cp^RMo)_2P_6]^+$. While the neutral species **2a,b** shows a symmetric P_6 unit, in the oxidized species [**2a,b**]$^+$ a bis-allylic distortion is observed (P-P 2.155 Å and 2.295 Å for [**2a**]$^+$ as well as for [**2b**]$^+$), however it is more pronounced than in the experimental geometry (see Figure 2) determined by X-ray diffraction. Since the experimental and calculated geometry of the cation [**2a**]$^+$ show a pronounced deviation one from another, we additionally performed single point calculation of [**2a**]$^+$ containing the symmetric *cyclo*-P_6 middle deck (optimized geometry of neutral **2a**). These calculations reveal that the bis-allylic distortion of the *cyclo*-P_6 middle deck is thermodynamically favored by 23.5 kJ/mol in the gas phase. The reason for the bis-allylic distortion of the *cyclo*-P_6 ring upon oxidation is the depopulation of the practically degenerate P-P bonding HOMO and HOMO-1 in **2a** (highest occupied molecular orbital, see SI Figure X). In the oxidized species [**2a**]$^+$ the SOMO (singly occupied molecular orbital) is also P-P bonding, hence leads to a P-P bond order of only 0.5 (only for two opposite P-P bonds). The WBI (Wiberg bond index) for these P-P bonds (0.66) is considerably lower than that of the other P-P bonds (0.94), leading to the elongation of these bonds. The WBI for the Mo-P bonds in [**2a**]$^+$ are 0.58 while in **2a** they vary from 0.65 to 0.67. The Mo-Mo WBI do not change upon oxidation of **2a** to [**2a**]$^+$ (0.76 and 0.77, respectively). The arsenic derivative **3** and **5** shows a similar behavior (see SI).

Reactions of the tetrahedrane complex [{CpMo(CO)$_2$}$_2$(μ,η^2:η^2-P$_2$)] (6)

The P_2 complex [{CpMo(CO)$_2$}$_2$(μ,η^2:η^2-P$_2$)] (**6**) (see Scheme 3) is related to white phosphorus by exchanging two P atoms by two isolobal 15 VE [CpMo(CO)$_2$] complex fragments. Since oxidation[9,10] of P_4 with [NO][TEF] leads to catenation under formation of $[P_9]^+$ the question arises how complex **6** behaves upon oxidation. Cyclic voltammetry of **6** shows the first oxidation to be quasi-reversible with its oxidation peak at +0.24 V and its reduction peak significantly shifted to –0.21 V vs. $Fc^{0/+}$ (Fc = ferrocene) while the second (+0.81 V) and third (+1.09 V) oxidation are irreversible. A more detailed description of the CV can be found in the previous chapter. Therefore, Ag^+ salts with a formal potential of +0.65 V vs. $Fc^{0/+}$ in CH_2Cl_2 solution should be strong

enough to readily oxidize **6**.[36] However, from several reactions of Ag[TEF] or Ag[FAl] with **6** in CH_2Cl_2 solution with varying reactant ratios, no precipitate of Ag^0 can be observed. By layering the solutions with toluene the coordination compounds **7-9** could be isolated from separate reactions as light orange to red crystals (see Scheme 3).

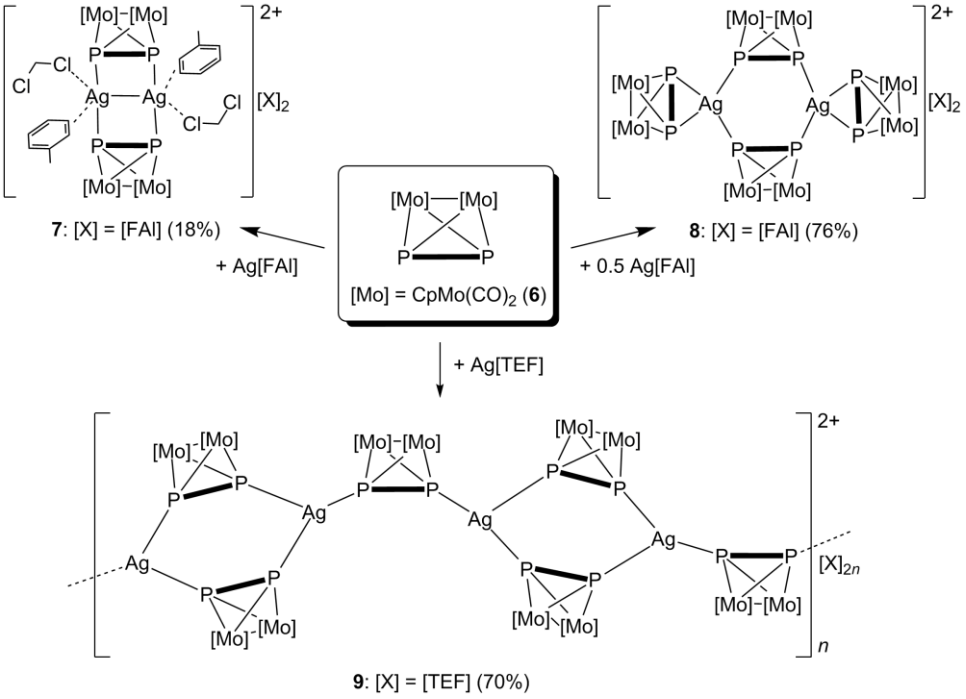

Scheme 3. Products from the reactions of the P_2 complex **6** with Ag[TEF] and Ag[FAl].

Crystal-structures of the coordination compounds 7-9

Single crystal X-ray diffraction analysis clearly reveals that the obtained coordination compounds contain varying ratios of Ag^+ and **6** in the solid state, with 1:1(**7**), 1:2(**8**) and 2:3(**9**), respectively resulting in the formation of different structural motifs in the solid state (see Figure 3). Among these, **7** contains a dicationic complex of two Ag^+ ions showing a short Ag-Ag contact of 3.0532(11) Å, stabilized by two bridging η^1:η^1-coordinating P_2 complexes **6** to form a central $P_2Ag_2P_2$ ladder-shaped motif with nearly identical P-Ag bond lengths (2.4524(15) and 2.4550(13) Å). The P1-P2 bond (2.1338(19) Å) is slightly elongated compared to free **6** (2.079(2) Å).[46] Additionally, each Ag ion is η^2-coordinated by a toluene molecule (Ag-CC_{cent} 3.010(6) Å) and η^1-coordinated by a CH_2Cl_2 molecule (Ag-Cl 3.402(3) Å). These labile ligands can easily be substituted by addition of another equivalent of **6** which is realized in the dicationic complex of **8** (Figure 3 b). Here, a central Ag_2P_4 six-membered ring showing a slight distortion towards a chair conformation (fold angle 20.53(10)°) can be observed which is stabilized by two bridging η^1:η^1-coordinating complexes **6**. Each Ag atom is additionally coordinated by an end-on η^2-coordinating ligand **6** and no Ag-Ag interaction is observed

in **8** (*d*(Ag-Ag) > 4.85 Å). The Ag-P distances inside the six-membered Ag_2P_4 ring (2.4878(15) and 2.4831(15) Å) are significantly shorter than the Ag-P distances to the end-on coordinated complexes **6** (2.7112(18) and 2.5977(15) Å). The η^2-coordinating P1-P2 bond (2.1373(17) Å) is slightly elongated and the η^1:η^1-coordinating bonds P3-P3' and P4-P4' (2.089(3) Å) are almost unchanged to the free complex **6** (2.079(2) Å).[46] Similar dinuclear complexes $[M_2(\mathbf{6})_4]^{2+}$ have been described for all coinage metals (M = Cu, Ag, Au) and several WCAs.[47,48,49] Additionally, the central M_2P_4 six-membered ring motif of **8** has been also described for Tl^+ and it is regularly observed as a repeating unit of polymeric organometallic-organic hybrid materials built from Ag^+ salts and **6** including organic linker molecules.[50,51,52,53]

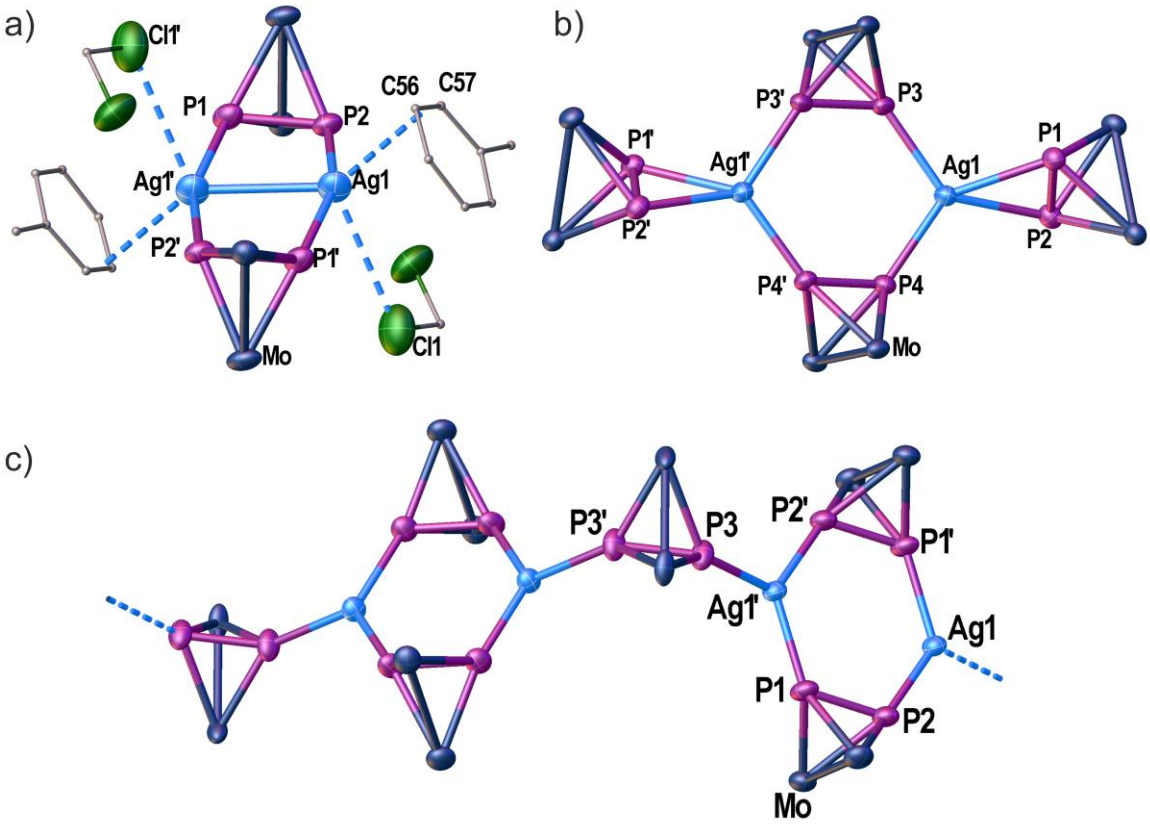

Figure 3. Crystal structures of the cationic parts of the coordination compounds **7** a) **8** b) and **9** c). Ellipsoids are drawn at 50% probability. The P_2 complexes **6** are represented only by their central tetrahedral Mo_2P_2 cores. For **7**, the coordinated solvent molecules CH_2Cl_2 and toluene are depicted with small spheres for C and without H atoms for clarity. Selected bond lengths [Å] and angles [°]: **7**: Ag1-Ag1' 3.0532(11), Ag1-P1' 2.4524(15), Ag1-P2 2.4550(13), P1-P2 2.1338(19), Ag1-Cl1 3.402(3), Ag1-C56 3.195(9), Ag1-C57 2.978(8); **8**: Ag1-P1 2.7112(18), Ag1-P2 2.5977(15), Ag1-P3 2.4878(15), Ag1-P4 2.4831(15), P1-P2 2.1373(17), P3-P3'2.089(3), P4-P4' 2.089(3), interplanar angle P3Ag1P4 – P3P3'P4P4' 20.53(10); **9**: Ag1-P1' 2.4465(15), Ag1-P2 2.4642(17), Ag1'-P3 2.4425(17), P1-P2 2.097(2), P3-P3' 2.082(3), interplanar angle P1'Ag1P2 – P1P2P1'P2' 12.54(12), interplanar angle between the mean planes of two consecutive Ag_2P_4 repeating units 49.96(4).

The structure of **9** (see Figure 3 c) exhibits a one-dimensional zigzag coordination polymer consisting of the aforementioned Ag_2P_4 six-membered ring repeating units interconnected by an additional bridging η^1:η^1-coordinating ligand **6**. The Ag-P distances

to the connecting ligands **6** Ag1‘-P3 (2.4425(17) Å) are almost identical to the Ag-P distances inside the rings Ag1-P1‘ and Ag1-P2 with 2.4465(15) Å and 2.4642(17) Å, respectively. The P-P distances in **9** (P1-P2 2.097(2) Å and P3-P3‘ 2.082(3) Å) are almost unchanged to the free complex **6**.[46] Two consecutive Ag_2P_4 repeating units along the polymeric chain of **9** are oriented in an angle of 49.96(4)° towards each other (mean planes). The Ag_2P_4 ring itself is almost planar showing only a slight distortion towards a chair conformation (fold angle 12.54(12)°). Although the coordination chemistry of **6** towards Ag^+ has been extensively studied, **9** represents the first homoleptic polymeric compound of **6** and Ag^+. A related structure was reported for the product of reaction of **6** with $Ag[NO_3]$, however, the $[NO_3]^-$ anion is acting as an additional bridging ligand to connect the Ag_2P_4 repeating units.[47,48]

The compounds **7-9** demonstrate the flexible coordination ability of **6** and present an interesting extension of its chemistry towards Ag^+. No oxidation products could be isolated from these reactions so far. The formation of Ag^+ coordination compounds instead of oxidation product has been observed before for P_4,[54] As_4,[55] S_8,[56] $[Fe(CO)_5]$,[57] Se.[40] A strong oxidant is needed for this task. The intensive purple radical cation of thianthrene $[S_2C_{12}H_8]^+$ (=[Thia]) seems to be a suitable candidate (formal potential +0.86 V vs $Fc^{0/+}$ in MeCN).[36] It can easily be prepared as its $[SbF_6]^-$ salt (**10a**) from $[NO][SbF_6]$ and colorless $S_2C_{12}H_8$.[58] When it is reduced again during subsequent reactions it reforms neutral colorless thianthrene which can simply be removed from the ionic products by washing with toluene.

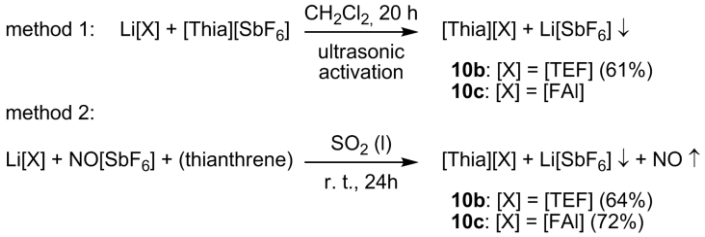

Scheme 4. Two synthetic routes for the preparation of **10b** and **10c**.

During this study two synthetic routes were developed to obtain the strong oxidant [Thia][X] ([X] = [TEF](**10b**), [FAl](**10c**)) (see Scheme 4). While the first route is a metathesis reaction of $[Thia][SbF_6]$ and Li[TEF] or Li[FAl], the second route is a direct synthesis starting from $S_2C_{12}H_8$, $NO[SbF_6]$ and Li[TEF] or Li[FAl] in liquid SO_2. This solvent was chosen to ensure the solubility of the Li^+ salts of the WCAs [TEF] and [FAl]. [Thia][TEF] is obtained as dark purple crystals or powder and is readily soluble in CH_2Cl_2, while [Thia][FAl] is obtained as a pink powder which shows low solubility in CH_2Cl_2 but readily forms intensively purple solutions in MeCN. No signal can be

observed for $[Thia]^+$ in the ^1H NMR spectra of **10b** and **10c** while the $^{19}F\{^1H\}$ NMR spectra show the characteristic signal pattern for the anions [TEF] (**10b**) and [FAl] (**10c**).

Crystal structures of [Thia][TEF] and [Thia][FAl]

The results of the single crystal X-ray diffraction analysis of **10b** and **10c** are shown in Figure 4. The structures clearly show the $[S_2C_{12}H_8]^+$ cation next to the respective WCAs. The cations show average S-C bond lengths of ~1.73 Å.

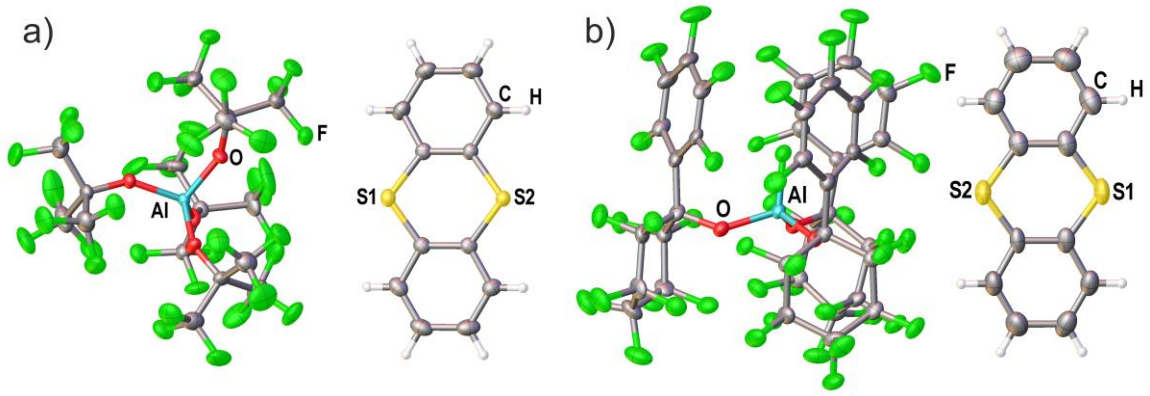

Figure 4. Crystal structures of **10b** a) and **10c** b) (only one independent molecule depicted). Ellipsoids are drawn at 50% probability.

With this simple preparation of the strong oxidants **10b** and **10c**, their reactivity towards the P_2 complex **6** could be investigated. When bright orange **6** is reacted with **10a-c** in CH_2Cl_2, a turbid dark reaction mixture is formed for [X] = $[SbF_6]$(**11a**) and [FAl](**11c**)[59] while an immediate color change to dark red is observed for [TEF](**11b**). The reaction product **11b** can be precipitated by addition of toluene. When the stirring is stopped a dark green to black precipitate is settling to the ground of the flask (**11a-c**) while the supernatant solution exhibits a pale orange color (small excess of **6**). By removing the solution and washing with toluene, the reaction products **11a-c** can be obtained as dark green powders. Compound **11b** is readily soluble in CH_2Cl_2 while **11a** and **11c** are almost insoluble in CH_2Cl_2. The latter are readily soluble in MeCN but the oxidation products are slowly decomposing (presumably reforming **6**). The $^{31}P\{^1H\}$ NMR spectrum of **11b** in CD_2Cl_2 solution shows only one broad signal at δ = –0.1 ppm ($\omega_{1/2}$ = 193 Hz), which does not split into different signals at low temperatures (up to 213 K) but moves to higher field (~ –26.5 ppm) and broadens significantly ($\omega_{1/2}$ > 10000 Hz). The ^1H NMR spectrum shows only one singlet at δ = 4.55 ppm for the Cp rings. The solution is ESR silent and no paramagnetic shift is observed by applying the Evans NMR method. The NMR spectra of **11a** and **11c** in CD_3CN solution are similar, however the evolution of new signals due to decomposition is observed. Therefore, the full characterization of **11a** and **11c** could not be completed during the

preparation of this work. A promising prospect for future work in this field of chemistry will be the use of liquid SO_2 or $MeNO_2$ as solvents.

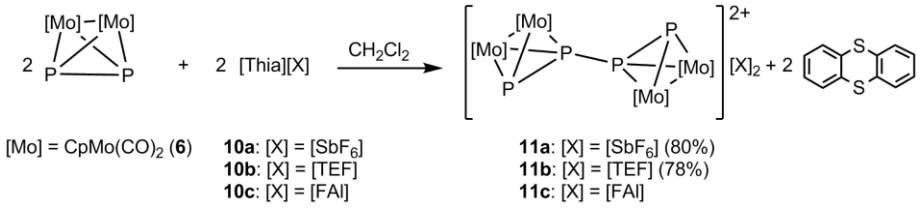

Scheme 5. Oxidation of the P_2 complex **6** by [Thia][X] ([X] = $[SbF_6]$(**10a**), [TEF](**10b**), [FAl](**10c**)).

MeCN obviously reacts with these oxidized species **11a-c**. Nevertheless, we were able to obtain some dark red single crystals of **11a** from MeCN/Et_2O solution at –30°C. Dark red single crystals of **11b** suitable for X-ray diffraction analysis can be obtained from CH_2Cl_2/hexane. For **11c** no crystals could be obtained during this work. The crystal structures of **11a** and **11b** are shown in Figure 5.

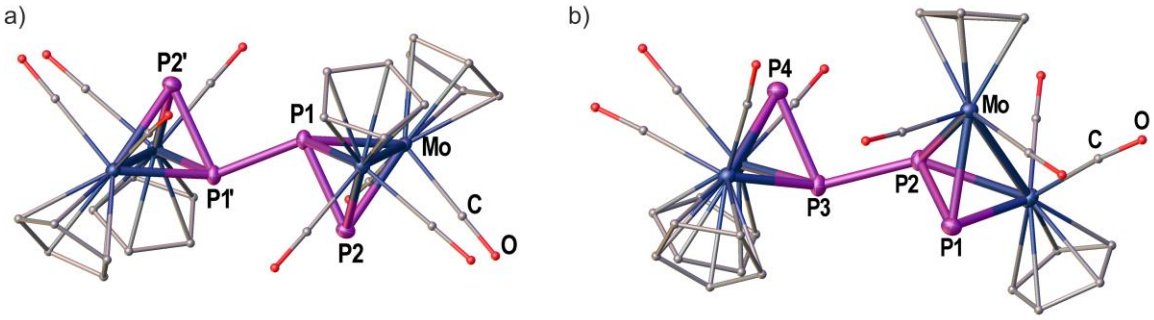

Figure 5. Crystal structures of the dicationic P_4 complexes in **11a** and **11b**. Ellipsoids are drawn at 50% probability. H atoms are omitted and C as well as O atoms are drawn as small spheres for clarity. Selected bond-lengths [Å] and angles [°]: **11a**: P1-P2 2.1751(8), P1-P1' 2.220(1), Mo1-Mo2 3.1794(6), P2P1P1' 93.00(3), dihedral angle P2P1P1'P2' 180.00(4); **11b**: P1-P2 2.1277(11), P2-P3 2.2090(10), P3-P4 2.1641(10), Mo1-Mo2 3.1373(3), Mo3-Mo4 3.1669(3), P1P2P3 104.91(4), P2P3P4 98.96(4) dihedral angle P1P2P3P4 133.83(5).

Crystal structures of 11a and 11b

The compounds **11a** and **11b** show analogues dicationic $[\{CpMo(CO)_2\}_4(\mu_4,\eta^2{:}\eta^2{:}\eta^2{:}\eta^2\text{-}P_4)]^{2+}$ complexes exhibiting a central zigzag P_4 chain in the solid state. While **11a** contains the smaller $[SbF_6]^-$ anion, **11b** contains the large WCA [TEF]. The crystal structure of **11b** has already been reported in detail in the previous chapter. Therefore, the following paragraph will focus on the description of **11a** highlighting only significant differences to **11b**. Compound **11a** crystallizes in the monoclinic space group $P2_1/n$ with one half of the dicationic $[\{CpMo(CO)_2\}_4(\mu_4,\eta^2{:}\eta^2{:}\eta^2{:}\eta^2\text{-}P_4)]^{2+}$ complex, one $[SbF_6]^-$ anion in general position and one MeCN solvent molecule in general position inside the asymmetric unit. The second

half of the complex cation is crystallographically generated by inversion. Therefore, the P_4 chain in **11a** shows a symmetrical geometry with PPP angles of 93.00(3)° and a dihedral angle of exactly 180.00(4)°. In contrast, the zigzag P_4 chain in **11b** shows larger PPP angles of 98.96(4)° and 104.91(4)° and adopts a gauche conformation with a dihedral angle of 133.83(5)°. The P-P bond lengths in **11a** are 2.1751(8) Å for P1-P2 and 2.220(1) Å for P1-P1'. For **11b**, the observed P-P bond lengths are somewhat shorter than for **11a** but the longest P-P bond is also situated in the center of the complex cation resembling a 1,3-butadiene-like chain in both compounds. The P-P bond lengths of **11a** and **11b** are significantly elongated compared to the starting material **6** (2.079(2) Å).[46] All Mo-P bonds in **11a** are within the range of 2.4113(6) Å up to 2.4876(6) Å with the shorter values to the central P atom P1. Due to the symmetrical geometry of **11a** compared to **11b**, there is also an obvious difference concerning the orientation of the Cp ligands on the Mo atoms. For **11a** the Cp ligands on each Mo-Mo bond adopt an almost ecliptic arrangement while for **11b** they adopt an ecliptic arrangement on the left side and an almost trans arrangement on the right side of Figure 5. It was described in the previous chapter that the dicationic species in **11b** exhibits very fast dynamic behavior in solution and can be obtained in an unsymmetrical form during crystallization (see Figure 5) while it is obtained in a symmetrical form upon precipitation from solution (derived from $^{31}P\{^1H\}$ MAS NMR spectra). Consequently, the symmetric cation of **11a** may correspond to the symmetrical form of the dicationic species of **11b** which can be precipitated from solution. This isomerization mechanism has to be further elucidated in the future and the characterization of **11c** featuring the WCA [FAl] may also give more insight into this dynamic process.

6.3 Conclusion

In summary, the current study demonstrated that one-electron oxidation of the 28 VE *cyclo*-E_6 triple-decker complexes $[(Cp^RMo)_2(\mu,\eta^6{:}\eta^6\text{-}E_6)]$ (E = P, Cp^R = Cp(**2a**), Cp*(**2b**), $C_5(CH_2Ph)_5$(**2c**); E = As, Cp^R = Cp*(**3**)) is easily achieved by Ag^+ (E = P) or Cu^+ (E = As) leading to isolated cationic 27 VE complexes which retain their triple-decker geometry. However, the *cyclo*-E_6 middle decks show a distortion from the hexagonal geometry with two opposite E-E bonds either slightly shortened (**2a**) or elongated (**2b**, **2c**, **3**). This distortion from a hexagonal geometry has also been observed for oxidized derivatives of benzene.

Reactions of Ag^+ salts with the P_2 complex $[\{CpMo(CO)_2\}_2(\mu,\eta^2{:}\eta^2\text{-}P_2)]$ (**6**) yield three coordination compounds with a Ag:**6** ratio of 1:1 (**11**), 1:2 (**12**) and 2:3 (**13**). While the structural motif of **12** is well-known for several anions, **11** shows an unprecedented

dicationic complex exhibiting labile CH_2Cl_2 and toluene ligands which makes it a potential starting material for the preparation of organometallic-organic hybrid materials by introducing organic linkers. Additionally, **13** represents the first homoleptic coordination polymer of Ag^+ and **6**.

Singe Ag^+ could not oxidize the P_2 complex **6** we developed two synthetic routes which yield the strong oxidants [Thia][TEF] (**10b**) and [Thia][FAl] (**10c**) in good yields. With the help of $[Thia]^+$ we could successfully oxidize the P_2 complex which was shown to dimerize via P-P bond formation yielding a dicationic complex $[\{Cp_2Mo_2(CO)_4\}_2(\mu_4,\eta^2{:}\eta^2{:}\eta^2{:}\eta^2\text{-}P_4)]^{2+}$ showing a central zigzag P_4 chain in the solid state. This cationic P_4 chain could be structurally characterized as a symmetric (C_i) and an unsymmetric isomer in **11a** and **11b**. The cationic P_4 chain complex shows a very dynamic behavior and the exact nature of the species in solution has to be further elucidated.

6.4 References

[1] N. Burford, P. J. Ragogna, *J. Chem. Soc., Dalton Trans.* **2002**, 4307-4315.
[2] C. A. Dyker, N. Burford, *Chem. Asian J.* **2008**, *3*, 28-36.
[3] A. P. M. Robertson, P. A. Gray, N. Burford, *Angew. Chem. Int. Ed.* **2014**, *53*, 6050-6069; *Angew. Chem.* **2014**, *126*, 6162-6182.
[4] B. D. Ellis, C. L. B. Macdonald, *Coord. Chem. Rev.* **2007**, *251*, 936-973.
[5] M. Donath, E. Conrad, P. Jerabek, G. Frenking, R. Fröhlich, N. Burford, J. J. Weigand, *Angew. Chem. Int. Ed.* **2012**, *51*, 2964-2967; *Angew. Chem.* **2012**, *124*, 3018-3021.
[6] D. Himmel, I. Krossing, A. Schnepf, *Angew. Chem. Int. Ed.* **2014**, *53*, 370-374; *Angew. Chem.* **2014**, *126*, 378-382.
[7] G. Frenking, *Angew. Chem. Int. Ed.* **2014**, *53*, 6040-6046; *Angew. Chem.* **2014**, *126*, 6152-6158.
[8] D. Himmel, I. Krossing, A. Schnepf, *Angew. Chem. Int. Ed.* **2014**, *53*, 6047-6048; *Angew. Chem.* **2014**, *126*, 6159-6160.
[9] T. Köchner, S. Riedel, A. J. Lehner, H. Scherer, I. Raabe, T. A. Engesser, F. W. Scholz, U. Gellrich, P. Eiden, R. A. Paz Schmidt, D. A. Plattner, I. Krossing, *Angew. Chem. Int. Ed.* **2010**, *49*, 8139-8143; *Angew. Chem.* **2010**, *122*, 8316-8320.
[10] T. Köchner, T. A. Engesser, H. Scherer, D. A. Plattner, A. Steffani, I. Krossing, *Angew. Chem. Int. Ed.* **2012**, *51*, 6529-6531; *Angew. Chem.* **2012**, *124*, 6635-6637.
[11] B. M. Cossairt, N. A. Piro, C. C. Cummins, *Chem. Rev.* **2010**, *110*, 4164-4177.
[12] M. Caporali, L. Gonsalvi, A. Rossin, M. Peruzzini, *Chem. Rev.* **2010**, *110*, 4178-4235.
[13] B. P. Johnson, G. Balázs, M. Scheer, *Coord. Chem. Rev.* **2006**, *250*, 1178-1195.
[14] O. J. Scherer, *Angew. Chem. Int. Ed.* **1990**, *29*, 1104-1122; *Angew. Chem.* **1990**, *102*, 1137-1155.
[15] O. J. Scherer, *Acc. Chem. Res.* **1999**, *32*, 751-762.
[16] O. J. Scherer, T. Brück, *Angew. Chem. Int. Ed.* **1987**, *26*, 59-59; *Angew. Chem.* **1987**, *99*, 59-59.
[17] O. J. Scherer, H. Sitzmann, G. Wolmershäuser, *Angew. Chem. Int. Ed.* **1985**, *24*, 351-353; *Angew. Chem.* **1985**, *97*, 358-359.
[18] R. F. Winter, W. E. Geiger, *Organometallics* **1999**, *18*, 1827-1833.
[19] M. V. Butovskiy, G. Balázs, M. Bodensteiner, E. V. Peresypkina, A. V. Virovets, J. Sutter, M. Scheer, *Angew. Chem. Int. Ed.* **2013**, *52*, 2972-2976; *Angew. Chem.* **2013**, *125*, 3045-3049.
[20] M. Fleischmann, F. Dielmann, L. J. Gregoriades, E. V. Peresypkina, A. V. Virovets, S. Huber, A. Y. Timoshkin, G. Balázs, M. Scheer, *Angew. Chem. Int. Ed.* **2015**, *54*, 13110-13115; *Angew. Chem.* **2015**, *127*, 13303-13308.
[21] O. J. Scherer, H. Sitzmann, G. Wolmershäuser, *Angew. Chem. Int. Ed.* **1989**, *28*, 212-213; *Angew. Chem.* **1989**, *101*, 214-215.

[22] M. Fleischmann, C. Heindl, M. Seidl, G. Balázs, A. V. Virovets, E. V. Peresypkina, M. Tsunoda, F. P. Gabbaï, M. Scheer, *Angew. Chem. Int. Ed.* **2012**, *51*, 9918-9921; *Angew. Chem.* **2012**, *124*, 10056-10059.
[23] F. Dielmann, R. Merkle, S. Heinl, M. Scheer, *Z.Naturforsch.* **2009**, *64b*, 3-10.
[24] F. Dielmann, C. Heindl, F. Hastreiter, E. V. Peresypkina, A. V. Virovets, R. M. Gschwind, M. Scheer, *Angew. Chem. Int. Ed.* **2014**, *53*, 13605-13608; *Angew. Chem.* **2014**, *126*, 13823-13827.
[25] F. Dielmann, M. Fleischmann, C. Heindl, E. V. Peresypkina, A. V. Virovets, R. M. Gschwind, M. Scheer, *Chem. Eur. J.* **2015**, *21*, 6208-6214.
[26] J. Bai, A. V. Virovets, M. Scheer, *Science* **2003**, *300*, 781-783.
[27] M. Scheer, J. Bai, B. P. Johnson, R. Merkle, A. V. Virovets, C. E. Anson, *Eur. J. Inorg. Chem.* **2005**, *2005*, 4023-4026.
[28] A. Schindler, C. Heindl, G. Balázs, C. Gröger, A. V. Virovets, E. V. Peresypkina, M. Scheer, *Chem. Eur. J.* **2012**, *18*, 829-835.
[29] C. Heindl, E. V. Peresypkina, A. V. Virovets, W. Kremer, M. Scheer, *J. Am. Chem. Soc.* **2015**, *137*, 10938-10941.
[30] J.-S. Huang, L. F. Dahl, *J. Organomet. Chem.* **1983**, *243*, 57-68.
[31] R. B. King, M. Z. Iqbal, A. D. King Jr, *J. Organomet. Chem.* **1979**, *171*, 53-63.
[32] R. J. Klingler, W. M. Butler, M. D. Curtis, *J. Am. Chem. Soc.* **1978**, *100*, 5034-5039.
[33] The CV measurement of the *cyclo*-As6 complex **3** could not conducted until the submission of this thesis.
[34] The position of the irreversible oxidation was determined by the difference of the peaks.
[35] The first oxidation of **2b** has been reported as irreversible previously in O. J. Scherer, J. Schwalb, H. Swarowsky, G. Wolmershäuser, W. Kaim, R. Gross, *Chem. Ber.* **1988**, *121*, 443-449. This behavior could not be observed in the current study in at least two independent CV measurements.
[36] N. G. Connelly, W. E. Geiger, *Chem. Rev.* **1996**, *96*, 877-910.
[37] See supporting information for a representation.
[38] μ_{eff} of **4d** was not measured, but **4c** contains the same paramagnetic cation.
[39] In case of **4a**, the obtained crystals show strong diffraction, however, each reflection is situated on a ring of intensity (see supporting information for a representative data collection frame). This phenomenon is reproducible and no structure solution can be obtained from this data. In case of **4c**, the data collection shows features that can be indicative of a modulated structure. A satisfactory structure solution could not be obtained. For future references, the determined unit cells of **4a** and **4c** are given in the Supporting information. This problem has been reported for **4c** in chapter 3.
[40] T. Köchner, N. Trapp, T. A. Engesser, A. J. Lehner, C. Röhr, S. Riedel, C. Knapp, H. Scherer, I. Krossing, *Angew. Chem. Int. Ed.* **2011**, *50*, 11253-11256; *Angew. Chem.* **2011**, *123*, 11449-11452.
[41] **4b** and **4d** contain two independent molecules in the unit cell. For one molecule the *cyclo*-P6 ligand is disordered by rotation in each of these structures. The discussion of metric data is presented for the ordered molecule. It has to be noted, that the geometry of the disordered ligand is very similar.
[42] H. Shorafa, D. Mollenhauer, B. Paulus, K. Seppelt, *Angew. Chem. Int. Ed.* **2009**, *48*, 5845-5847; *Angew. Chem.* **2009**, *121*, 5959-5961.
[43] X. Chen, X. Wang, Y. Sui, Y. Li, J. Ma, J. Zuo, X. Wang, *Angew. Chem. Int. Ed.* **2012**, *51*, 11878-11881; *Angew. Chem.* **2012**, *124*, 12048-12051.
[44] a) P. A. M. Dirac *Proc. Royal Soc. A*, **1929**, *123*, 714–733. b) J. C. Slater *Phys. Rev.*, **1951**, *81*, 385-390. c) S. Vosko; L. Wilk; M. Nusair, *Can. J. Phys.*, **1980**, *58*, 1200–1211. d) A. D. Becke *Phys. Rev. A*, **1988**, *38*, 3098–3100. e) J. P. Perdew. *Phys. Rev. B*, **1986**, *33*, 8822–8824.
[45] a) K. Eichkorn, F. Weigend, O. Treutler, R. Ahlrichs, *Theor. Chem. Acc.* **1997**, *97*, 119; b) A. Schäfer, C. Huber, R. Ahlrichs, *J. Chem. Phys.* **1994**, *100*, 5829; c) K. Eichkorn, F. Weigend, O. Treutler, R. Ahlrichs, *Theor. Chem. Acc.* **1997**, *97*, 119. d) F. Weigend, R. Ahlrichs, *Phys. Chem. Chem. Phys.* **2005**, *7*, 3297. e) F. Weigend, *Phys. Chem. Chem. Phys.* **2006**, *8*, 1057.
[46] O. J. Scherer, H. Sitzmann, G. Wolmershäuser, *J. Organomet. Chem.* **1984**, *268*, C9-C12.
[47] J. Bai, E. Leiner, M. Scheer, *Angew. Chem. Int. Ed.* **2002**, *41*, 783-786; *Angew. Chem.* **2002**, *114*, 820-823.
[48] M. Scheer, L. J. Gregoriades, M. Zabel, J. Bai, I. Krossing, G. Brunklaus, H. Eckert, *Chem. Eur. J.* **2008**, *14*, 282-295.
[49] M. Fleischmann, S. Welsch, E. V. Peresypkina, A. V. Virovets, M. Scheer, *Chem. Eur. J.* **2015**, *21*, 14332-14336.

[50] S. Welsch, L. J. Gregoriades, M. Sierka, M. Zabel, A. V. Virovets, M. Scheer, *Angew. Chem. Int. Ed.* **2007**, *46*, 9323-9326; *Angew. Chem.* **2007**, *119*, 9483-9487.
[51] M. Fleischmann, S. Welsch, L. J. Gregoriades, C. Gröger, M. Scheer, *Z. Naturforsch.* **2014**, *69b*, 1348-1356.
[52] B. Attenberger, S. Welsch, M. Zabel, E. V. Peresypkina, M. Scheer, *Angew. Chem., Int. Ed.* **2011**, *50*, 11516; *Angew. Chem.* **2011**, *123*, 11718-11722.
[53] B. Attenberger, E. V. Peresypkina, M. Scheer, *Inorg. Chem.* **2015**, *54*, 7021-7029.
[54] I. Krossing, L. van Wüllen, *Chem. Eur. J.* **2002**, *8*, 700-711.
[55] C. Schwarzmaier, M. Sierka, M. Scheer, *Angew. Chem. Int. Ed.* **2013**, *52*, 858-861; *Angew. Chem.* **2013**, *125*, 891-894.
[56] T. S. Cameron, A. Decken, I. Dionne, M. Fang, I. Krossing, J. Passmore, *Chem. Eur. J.* **2002**, *8*, 3386-3401.
[57] P. J. Malinowski, I. Krossing, *Angew. Chem. Int. Ed.* **2014**, *53*, 13460-13462; *Angew. Chem.* **2014**, *126*, 13678-13680.
[58] B. Boduszek, H. J. Shine, *J. Org. Chem.* **1988**, *53*, 5142-5143.
[59] unpublished results Luis Dütsch and Manfred Scheer.

6.5 Supporting Information

Preparation of the described compounds

General considerations

All manipulations were carried out under an inert atmosphere of dried nitrogen using standard Schlenk and drybox techniques. CH_2Cl_2 and CD_2Cl_2 were dried over CaH_2, toluene and alkanes were distilled from Na, K or Na/K alloy. Dried solvents were also taken from a solvent purification system from MBraun. SO_2 was purchased from Linde and was condensed onto the reactants at –196 °C. NMR spectra were recorded in CD_2Cl_2 on a Bruker Avance 300 MHz NMR spectrometer (^{1}H: 300.132 MHz, ^{31}P: 121.495 MHz, ^{13}C: 75.468 MHz, ^{19}F: 282.404 MHz) or a Bruker Avance 400 MHz NMR spectrometer (^{1}H: 400.130 MHz, ^{31}P: 161.976 MHz, ^{13}C: 100.613 MHz) with external references of $SiMe_4$ (^{1}H, ^{13}C), CCl_3F (^{19}F) and H_3PO_4 (85%, ^{31}P). X-Band EPR spectra were recorded on a MiniScope MS400 device from Magnettech GmbH with a frequency of 9.5 GHz equipped with a rectangular resonator TE102. Mass spectra were recorded by the MS department of the University of Regensburg on a ThermoQuest Finnigan TSQ 7000 mass spectrometer (ESI) or a Finnigan MAT 95 mass spectrometer (EI, FD). The ESI mass spectrum of **11b** was measured on a Waters Micromass LCT ESI-TOF mass-spectrometer by Valentin Vass. IR spectra were recorded as KBr discs of in CH_2Cl_2 solution using a Varian FTS-800 FT-IR spectrometer. Elemental analyses were performed by the micro analytical laboratory of the University of Regensburg. Commercially available reagents were purchased and used without further purification. The synthesis and characterization of **1**, **2c** and **4e** have been performed by Dr. Fabian Dielmann and have been discussed before in his PhD-thesis. The crystal structure of **11b** has been described before by Dr. Stefan Welsch in his PhD-thesis. A detailed discussion about the oxidation of the P_2 complex **6** (**11b**) can be found in chapter 5. The oxidation of **2b** (**4c**, **4d**) has been described in chapter 3. The preparation of [Thia][TEF] (**10b**) has been described in chapter 5.

Preparation of [{$Cp^{Bn}Mo(CO)_2$}$_2$] (**1**): A mixture of [$Mo(CO)_6$] (4.09 g, 15.48 mmol, 1 eq.) and $Cp^{Bn}H$ (8.00 g, 15.48 mmol, 1 eq.) in decalin (100 mL) was heated to reflux with stirring in a round bottom flask. The reaction progress was monitored by IR spectroscopy. After 10 h the deep red solution was allowed to cool to room temperature. The solvent was removed under reduced pressure. Subsequent column chromatographic workup (silica gel, toluene, 3 × 25 cm) afforded a red oily product. For further purification, it was dissolved in CH_2Cl_2, layered with the threefold amount of *n*-hexane and stored in a freezer at –35 °C. The resulting red crystals of **1** were washed with warm *n*-pentane (4 × 20 mL) and dried in vacuum. Crystals of **1** suitable for a single crystal X-ray diffraction analysis were obtained from toluene. Yield 5.97 mg (58%). ^{1}H NMR (400 MHz, C_6D_6, 300 K) *δ*/ppm 6.84 - 6.89 (m, 15H, CH), 6.69 - 6.74 (m, 10H, CH), 4.16 (s, 10H, CH_2); ^{1}H NMR (400 MHz, CD_2Cl_2, 300 K) *δ*/ppm 6.93 – 7.03 (m, 15H, CH), 6.67 - 6.71 (m, 10H, CH), 3.89 (s, 10H, CH_2); ^{13}C{^{1}H} NMR (100.6 MHz, CD_2Cl_2, 300 K) *δ*/ppm 239.0 (CO), 139.5 (Ph), 129.2 (Ph), 128.4 (Ph), 126.4 (Ph), 109.1 (Cp), 31.9 (CH_2). Anal. calcd. for [{$Cp^{Bn}Mo(CO)_2$}$_2$]: C, 75.55; H, 5.28. Found: C, 75.31; H, 5.06. LIFDI-MS (toluene), *m/q* (%): 1335.5 (100) [*M*]$^+$; EI-MS (70 eV, toluene), *m/q* (%): = 1335.1 (3) [*M*]$^+$, 1307.1 (5) [*M*–CO]$^+$, 1278.1 (2) [*M*–$(CO)_2$]$^+$, 1249.1 (3) [*M*–$(CO)_3$]$^+$, 1221.2 (25) [*M*–$(CO)_4$]$^+$, 611.1 (66) [$Cp^{Bn}Mo$]$^+$, 91 (100) [C_7H_7]$^+$. IR(KBr) cm^{-1}: 3105 (vw), 3085 (w), 3061 (m), 3027 (m), 3004 (vw), 2922 (w), 1870 (vs), 1834 (vs), 1602 (m), 1584 (w), 1495 (s), 1454 (m), 1182 (w), 1076 (w), 1030 (m), 733 (s), 696 (s), 531 (w), 487 (m), 460 (w).

Preparation of [$(Cp^{Bn}Mo)_2(\mu,\eta^6{:}\eta^6\text{-}P_6)$] (**2c**): A stirred mixture of [{$Cp^{Bn}Mo(CO)_2$}$_2$] (**1**) (3.00 g, 2.25 mmol, 1eq.) and P_4 (1.54 g, 12.4 mmol, 5.5 eq.) in DIB (200 mL) was heated to reflux for 24 h. The yellow to brown reaction mixture was allowed to cool to room temperature. The solvent

was removed upon distillation under vacuum, and the resulting brown, oily residue was dried for another 2 h under reduced pressure. Column chromatographic workup on silica gel (*n*-hexane/toluene (1:1), 27 × 4 cm) afforded a first fraction of unreacted **1**. A solvent mixture of *n*-hexane/toluene (2:1) eluted a brown mixed fraction of **1** and **2c**. A final yellow fraction of **2c** was isolated using pure toluene as eluent. Further purification of the combined fraction was achieved by recrystallization from hot toluene. Crystals of **2c** suitable for single crystal X-ray diffraction analysis were obtained from toluene solutions. Yield 1.51 g (48%). ^{1}H NMR (400 MHz, CD_2Cl_2, 300 K) δ/ppm 6.72 (t, $^{3}J_{HH}$ = 7.7 Hz, 5H, H_{para}), 6.57 (dd, $^{3}J_{HH}$ = 7.7 Hz, 10H; H_{meta}), 5.95 (d, $^{3}J_{HH}$ = 7.7 Hz, 10H, H_{ortho}), 2.49 (s, 10H, CH_2); ^{31}P{^{1}H} NMR (162.0 MHz, CD_2Cl_2, 300 K) δ/ppm –316.0 (s, P_6); ^{31}P{^{1}H} NMR (162.0 MHz, C_6D_6, 300 K) δ/ppm –315.1 (s, P_6); ^{13}C{^{1}H} NMR (100.6 MHz, CD_2Cl_2, 300 K) δ/ppm 139.3 (Ph), 128.9 (Ph), 127.8 (Ph), 126.0 (Ph), 101.4 (Cp), 35.1 (CH_2). Anal. calcd. for [($Cp^{Bn}Mo)_2P_6$]: C, 68.19; H, 5.01. Found: C, 68.46; H, 5.04. LIFDI-MS (toluene), *m/q* (%): 1409.3 (100) [*M*]$^+$; EI-MS (70 eV, CH_2Cl_2/toluene), *m/q* (%): = 1408.8 (100) [*M*]$^+$, 1318.8 (11) [*M*–C_7H_7]$^+$, 1227.8 (5) [*M*–$(C_7H_7)_2$]$^+$, 705.0 (10) [*M*]$^{2+}$. IR(KBr) cm^{-1}: 3105 (vw), 3085 (w), 3059 (m), 3026 (m), 3002 (vw), 2914 (w), 1946 (w), 1879 (w), 1802 (w), 1602 (m), 1495 (s), 1451 (m), 1440 (m), 1182 (w), 1155 (w), 1076 (m), 1030 (m), 969 (w), 732 (s), 696 (s), 616 (w), 585 (w), 485 (m), 461 (w).

Preparation of [$(CpMo)_2(\mu,\eta^6{:}\eta^6\text{-}P_6)$][TEF] (**4a**): [$(CpMo)_2(\mu,\eta^6{:}\eta^6\text{-}P_6)$] (**2a**) (95 mg, 0.187 mmol, 1 eq.) was stirred for 3 h in 250 mL CH_2Cl_2 at room temperature which afforded a turbid light brown solution. [$Ag(CH_2Cl_2)$][TEF] (217 mg, 0.187 mmol, 1 eq.) was dissolved in 15 mL CH_2Cl_2 and slowly added to the stirred solution of [$(CpMo)_2(\mu,\eta^6{:}\eta^6\text{-}P_6)$]. The color of the solution turned to dark violet and the formation of a silver mirror could be observed. After 1 h of stirring the solution was filtered, concentrated to 20 mL and carefully layered with the fivefold amount of *n*-pentane. Storage at +4 °C afforded compound **4a** as violet needles in the course of a few days. The crystals are washed with *n*-pentane and dried in vacuum. Yield 185 mg (67%). ^{1}H NMR (400 MHz, CD_2Cl_2, 300 K) δ/ppm 11.55 (s, br, Cp); ^{31}P{^{1}H} NMR (162.0 MHz, CD_2Cl_2, 300 K) no signal can be resolved from 1200 to –1200 ppm; ^{13}C{^{1}H} NMR (100.6 MHz, CD_2Cl_2, 300 K) δ/ppm 121.61 (q, $^{1}J_{CF}$ = 293 Hz, CF_3), 79.40 (br, $\underline{C}(CF_3)_3$), 73.97 (s, Cp); ^{19}F{^{1}H} NMR (282.4 MHz, CD_2Cl_2, 300 K) δ/ppm = –75.31 (s, CF_3). X-band EPR (77 K, CD_2Cl_2) g_{iso} = 2.025, (77 K, solid) g_{iso} = 2.003. Evans-method μ_{eff} = 1.68 μ_B (one unpaired electron). Anal. calcd. for [$(CpMo)_2P_6$][TEF]: C, 21.17; H, 0.68. Found: C, 21.22; H, 0.76. ESI-MS (CH_2Cl_2): cations, *m/q* (%): 507.7 (100) [$(CpMo)_2P_6$]$^+$; anions, *m/q* (%): 967.1 (100) [TEF]$^-$. IR(KBr) cm^{-1}: 3134 (w), 3091 (vw), 3082 (vw), 1429 (w), 1352 (m), 1301 (s), 1276 (vs), 1242 (vs), 1219 (vs), 1170 (m), 1011 (w), 974 (vs), 835 (m), 819 (w), 756 (vw), 728 (s), 447 (w).

Preparation of [$(CpMo)_2(\mu,\eta^6{:}\eta^6\text{-}P_6)$][FAl] (**4b**): [$(CpMo)_2(\mu,\eta^6{:}\eta^6\text{-}P_6)$] (**2a**) (25 mg, 0.05 mmol, 1 eq.) was suspended in 20 mL CH_2Cl_2 to form a turbid light brown solution. [$Ag(CH_2Cl_2)$][FAl] (79 mg, 0.05 mmol, 1 eq.) was dissolved in 5 mL CH_2Cl_2 and slowly added to the stirred solution of [$(CpMo)_2(\mu,\eta^6{:}\eta^6\text{-}P_6)$]. The color of the solution turned to dark violet and the formation of a black precipitate (probably Ag^0) could be observed. After 3 h of stirring the solution was filtered and carefully layered with the twofold amount of *n*-pentane. Storage at +4 °C afforded compound **4b** as violet needles in the course of two days. The crystals were washed with *n*-pentane and dried in vacuum. Yield 74 mg (78%). ^{1}H NMR (300 MHz, CD_2Cl_2, 300 K) δ/ppm 11.54 (br, Cp); ^{31}P{^{1}H} NMR (162.0 MHz, CD_2Cl_2, 300 K) no signal can be resolved from 1200 to –1200 ppm; ^{13}C{^{1}H} NMR (100.6 MHz, CD_2Cl_2, 300 K) δ/ppm 74.27 (br, Cp); ^{19}F{^{1}H} NMR (282.4 MHz, CD_2Cl_2, 300 K) δ/ppm = –112.5 (d, $J_{F,F}$ = 274 Hz, 2F), –117.1 (d, $J_{F,F}$ = 279 Hz, 2F), –121.5 (d, $J_{F,F}$ = 277 Hz, 2F), –127.7 (s, 2F), –130.6 (d, $J_{F,F}$ = 273 Hz, 2F), –136.8 (d, $J_{F,F}$ = 277 Hz, 2F), –141.1 (d, $J_{F,F}$ = 277 Hz, 1F), –154.2 (t, $J_{F,F}$ = 22 Hz, 1F), –164.8 (t, $J_{F,F}$ = 18 Hz, 2F), –172.0 ppm (s, AlF). X-band EPR (77 K, CD_2Cl_2) g_{iso} = 2.026. Evans-method μ_{eff} = 1.59 μ_B (one unpaired electron). Anal. calcd. for [$(CpMo)_2P_6$][FAl]·(CH_2Cl_2): C, 28.59; H, 0.61. Found: C, 28.59; H, 0.66. ESI-MS (CH_2Cl_2): cations, *m/q* (%): 507.8 (100) [$(CpMo)_2P_6$]$^+$; anions, *m/q* (%): 1381.1 (100)

[FAl]$^-$. IR(KBr) cm^{-1}: 3125 (w), 1652 (m), 1532 (s), 1485 (vs), 1428 (w), 1323 (m), 1309 (w), 1267 (m), 1244 (m), 1204 (vs), 1185 (s), 1155 (m), 1136 (w), 1103 (m), 1034 (w), 1018 (vs), 954 (vs), 910 (m), 850 (vw), 833 (m), 810 (vw), 766 (m), 729 (m), 635 (w), 527 (w), 469 (w).

Preparation of [(Cp^{Bn}Mo)$_2$(μ,η^6:η^6-P$_6$)][TEF] (**4e**): A mixture of [(Cp^{Bn}Mo)$_2$(μ,η^6:η^6-P$_6$)] (**2c**) (60 mg, 0.0426 mmol, 1 eq.) and Ag[Al{OC(CF$_3$)$_3$}$_4$] (46 mg, 0.0426 mmol, 1 eq.) in CH_2Cl_2 (15 mL) was stirred in the absence of light for 15 h at room temperature. The resulting green solution was concentrated to 1.5 mL, filtered and layered with the same amount of a solvent mixture (CH_2Cl_2/*n*-pentane 4:1) and subsequently with the fourfold amount of *n*-pentane. Storage at –35 °C affords compound **4e** as dark green plates in the course of one month. The obtained crystals are washed with *n*-pentane (3 × 2 mL) and dried in vacuum. Yield 82 mg (81%). ^{1}H NMR (400 MHz, CD_2Cl_2, 300 K) δ/ppm 6.97 (m, 5H, H$_{para}$), 6.92 (m, 10H, H$_{meta}$), 6.45 (m, 10H, H$_{ortho}$), 5.94 (s, 10H; CH_2); ^{31}P{^{1}H} NMR (162.0 MHz, CD_2Cl_2, 300 K) no signal can be resolved from 1200 to –1200 ppm; ^{13}C{^{1}H} NMR (100.6 MHz, CD_2Cl_2, 300 K) δ/ppm 142.53 (Ph), 129.86 (Ph), 129.44 (Ph), 126.82 (Ph), 121.65 (q, $^1J_{CF}$ = 293 Hz; CF_3), 100.61 (Cp), 23.87 (CH_2); ^{19}F{^{1}H} NMR (282.4 MHz, CD_2Cl_2, 300 K) δ/ppm = –75.29 (s, CF_3). X-band EPR (77 K, CD_2Cl_2) g_{iso} = 2.023. Evans-method μ_{eff} = 1.57 μ_B (one unpaired electron). Anal. calcd. for [(Cp^{Bn}Mo)$_2$P$_6$][TEF]: C, 48.52; H, 2.97. Found: C, 48.59; H, 2.72. ESI-MS (CH_2Cl_2): cations, *m/q* (%): 1410.5 (100) [(Cp^{Bn}Mo)$_2$P$_6$]$^+$; anions, *m/q* (%): 967.2 (100) [TEF]$^-$. IR(KBr) cm^{-1}: 3105 (vw), 3090 (vw), 3065 (w), 3032 (w), 3002 (vw), 2917 (w), 1604 (w), 1497 (m), 1445 (w), 1352 (m), 1297 (s), 1277 (vs), 1240 (vs), 1220 (vs), 1166 (w), 1030 (w), 975 (vs), 831 (w), 728 (s), 696 (m), 537 (w), 485 (w), 447 (w).

Preparation of [(Cp*Mo)$_2$(μ,η^6:η^6-As$_6$)][BF$_4$] (**5**): [(Cp*Mo)$_2$(μ,η^6:η^6-As$_6$)] (**3**) (91 mg, 0.1 mmol, 1 eq.) was suspended in 10 mL CH_2Cl_2 to form a turbid brown solution. [Cu(MeCN)$_4$][BF$_4$] (32 mg, 0.1 mmol, 1 eq.) was dissolved in 5 mL CH_2Cl_2 and slowly added to the stirred solution of [(Cp*Mo)$_2$(μ,η^6:η^6-As$_6$)]. The color of the solution turned to dark green and the formation of a black precipitate (probably Cu^0) could be observed. After 3 h of stirring the solution was filtered and carefully layered with the fivefold amount of *n*-hexane. Storage at +4 °C afforded compound **5** as dark green crystals after several days. The crystals were washed with *n*-hexane and dried in vacuum. Yield 84 mg (84%). ^{1}H NMR (300 MHz, CD_2Cl_2, 300 K) δ/ppm 2.64 (br, Cp*); ^{11}B{^{1}H} NMR (128.4 MHz, CD_2Cl_2, 300 K) δ/ppm –1.39 (s, BF_4); ^{13}C{^{1}H} NMR (100.6 MHz, CD_2Cl_2, 300 K) δ/ppm 87.11 (s, $\underline{C}_5Me_5$), –0.81 (s, $C_5\underline{Me}_5$); ^{19}F{^{1}H} NMR (282.4 MHz, CD_2Cl_2, 300 K) δ/ppm = –151.6 ($^{10}BF_4$), –151.7 ($^{11}BF_4$). X-band EPR (77 K, CD_2Cl_2) no signal detectable. Evans-method μ_{eff} = 1.66 μ_B (one unpaired electron). Anal. calcd. for [(Cp*Mo)$_2$As$_6$][BF$_4$]: C, 24.05; H, 3.03. Found: C, 23.98; H, 3.07. ESI-MS (CH_2Cl_2): cations, *m/q* (%): 911.7 (100) [(Cp*Mo)$_2$As$_6$]$^+$; anions, *m/q* (%): 86.9 (100) [BF$_4$]$^-$. IR(KBr) cm^{-1}: 2951 (w), 2904 (w), 1474 (w), 1458 (vw), 1418 (w), 1377 (s), 1303 (vw), 1281 (vw), 1241 (vw), 1223 (vw), 1092 (m), 1054 (vs), 1038 (m), 1013 (m), 976 (vw), 801 (vw), 520 (vw).

Preparation of [Ag$_2$(μ,η^1:η^1-**6**)$_2$(η^1-CH$_2$Cl$_2$)(η^2-C$_7$H$_8$)$_2$][FAl]$_2$ (**7**): [{CpMo(CO)$_2$}$_2$(μ,η^2:η^2-P$_2$)] (**6**) (25 mg, 0.05 mmol, 1 eq.) was dissolved in 10 mL of CH_2Cl_2. [Ag(CH_2Cl_2)][FAl] (79 mg, 0.05 mmol, 1 eq.) was dissolved in 5 mL of CH_2Cl_2 and slowly added to the stirred solution of **6**. The red solution turns cloudy and some orange precipitate is formed. After stirring for 2 h at room temperature, the solution was filtrated and carefully layered with the fourfold amount of toluene. Storage at +4 °C affords orange crystals of **7** at the solvent mixing zone after several days. The crystals were washed with toluene and dried in vacuum. Yield 18 mg (18%). Anal. calcd. for [Ag(Cp$_2$Mo$_2$(CO)$_4$P$_2$)(CH_2Cl_2)(C$_7$H$_8$)$_{0.5}$][FAl]: C, 30.88; H, 0.76. Found: C, 30.88; H, 1.15. ESI-MS (CH_2Cl_2): cations, *m/q* (%): 1100.6 (100) [Ag(**6**)$_2$]$^+$; anions, *m/q* (%): 1381.2 (100) [FAl]$^-$. IR(KBr) cm^{-1}: 3122 (w), 2007 (vs), 1968 (vs), 1652 (w), 1533 (m), 1486 (vs), 1422 (w), 1323 (w), 1308 (w), 1267 (m), 1242 (m), 1204 (vs), 1187 (s), 1154 (m), 1135 (w), 1104 (m), 1033 (w), 1019 (s), 1006 (m), 955 (vs), 911 (w), 838 (w), 770 (w), 729 (w), 635 (vw), 625 (vw), 457 (vw).

Preparation of $[Ag_2(\mu,\eta^1{:}\eta^1\text{-}\mathbf{6})_2(\eta^2\text{-}\mathbf{6})][FAl]$ (**8**): $[\{CpMo(CO)_2\}_2(\mu,\eta^2{:}\eta^2\text{-}P_2)]$ (**6**) (50 mg, 0.1 mmol, 2 eq.) was dissolved in 10 mL of CH_2Cl_2. $[Ag(CH_2Cl_2)][FAl]$ (79 mg, 0.05 mmol, 1 eq.) was dissolved in 5 mL of CH_2Cl_2 and slowly added to the stirred solution of **6**. The clear red solution was stirred for 2 h at room temperature, filtrated and carefully layered with the fourfold amount of toluene. Storage at +4 °C affords compound **8** as clear red blocks in the course of one week. The crystals were washed with *n*-hexane and dried in vacuum. Yield 94 mg (76%). Anal. calcd. for $[Ag(Cp_2Mo_2(CO)_4P_2)_2][FAl]$: C, 30.98; H, 0.81. Found: C, 30.75; H, 1.02. ESI-MS (CH_2Cl_2): cations, *m/q* (%): 1100.7 (100) $[Ag(\mathbf{6})_2]^+$; anions, *m/q* (%): 1381.3 (100) $[FAl]^-$. IR(KBr) cm^{-1}: 3132 (w), 2008 (vs), 1981 (vs), 1940 (vs), 1652 (w), 1532 (m), 1485 (vs), 1424 (w), 1327 (w), 1309 (w), 1267 (m), 1243 (m), 1204 (vs), 1186 (s), 1154 (m), 1136 (w), 1105 (m), 1034 (w), 1018 (s), 956 (vs), 910 (w), 824 (w), 767 (w), 752 (vw), 729 (w), 635 (vw), 559 (vw), 522 (vw), 455 (vw).

Preparation of $[Ag_2(\mu,\eta^1{:}\eta^1\text{-}\mathbf{6})_2(\mu,\eta^1{:}\eta^1\text{-}\mathbf{6})]_n[TEF]_{2n}$ (**9**): $[\{CpMo(CO)_2\}_2(\mu,\eta^2{:}\eta^2\text{-}P_2)]$ (**6**) (50 mg, 0.1 mmol, 1 eq.) was dissolved in 5 mL of CH_2Cl_2. $[Ag(CH_2Cl_2)][TEF]$ (116 mg, 0.1 mmol, 1.5 eq.) was dissolved in 5 mL of CH_2Cl_2 and slowly added to the stirred solution of **6**. After 12 h stirring at room temperature a small amount of brown precipitate formed which could be dissolved again by adding 5 mL of CH_2Cl_2. The clear red solution was filtered and layered with the eightfold amount of toluene. After one day at room temperature compound **9** already crystallizes in the form of red plates at the solvent mixing zone. Storage at +4 °C for three weeks resulted in further crystalline product. The supernatant solution was decanted off, the crystals were washed two times with toluene and dried in vacuum. Yield 85 mg (70%). Anal. calcd. for $[Ag_2(Cp_2Mo_2(CO)_4P_2)_3][TEF]_2\cdot(C_7H_8)$: C, 26.00; H, 1.02. Found: C, 26.04; H, 1.09. ESI-MS (CH_2Cl_2): cations, *m/q* (%): 1100.7 (100) $[Ag(\mathbf{6})_2]^+$; anions, *m/q* (%): 967.1 (100) $[TEF]^-$. IR(KBr) cm^{-1}: 3129 (w), 1993 (vs), 1968 (vs), 1942 (s), 1426 (w), 1353 (m), 1303 (vs), 1276 (vs), 1242 (vs), 1219 (vs), 1172 (m), 1066 (vw), 974 (vs), 831 (m), 728 (s), 559 (vw), 510 (vw), 453 (w).

Preparation of [Thia][FAl] (**10c**):

Method 1: Thia$[SbF_6]$ (135 mg, 0.30 mmol, 1 eq.) and Li[FAl] (450 mg, 0.32 mmol, 1.1 eq.) were placed in a Schlenk flask equipped with a Young valve. Subsequently ~20 mL of CH_2Cl_2 (stored over CaH_2) were condensed onto the solids at –196 °C. The flask was closed under reduced pressure. Upon dissolution of the compounds the formation of a deep violet solution could be observed. The flask was sonicated for 2 h. In order to precipitate the ionic product the reaction mixture was filtered over diatomaceous earth directly into ~100 mL of stirred *n*-hexane. Thereby, the formation of a small amount of pink precipitate could be observed. The supernatant solution was decanted off, the solid was washed with 100 mL of *n*-hexane and dried in vacuum. The solid was dissolved in 20 mL of CH_2Cl_2 and the cloudy light pink solution was filtered and carefully layered with 80 mL of *n*-hexane. After storage at +4 °C compound **10c** was obtained as very thin pink needles in the course of several days. From these crystals we were able to determine the solid state structure of **10c** but the yield was very low since a large percentage of the product was lost during the process because of its low solubility in CH_2Cl_2. Therefore, no yield was determined for this preparation method.

Method 2: A double schlenk flask equipped with two Young valves and a G4 frit plate in the middle was loaded on one side with a stirring bar, thianthrene (151 mg, 0.7 mmol, 1.2 eq.), $NO[SbF_6]$ (160 mg, 0.6 mmol, 1 eq.) and Li[FAl] (1 g, 0.72 mmol, 1.2 eq.). SO_2 (~10 mL) was condensed onto these solids under reduced pressure at –196 °C. The flask was closed under reduced pressure and the cooling was removed. Upon dissolution the reaction turns from light blue to dark blue and finally to dark violet when everything is dissolved. After stirring at room temperature over night the dark violet solution was filtered over the G4 frit to the other side. The

SO_2 was condensed back onto the remaining dark purple residue by cooling to –196 °C and subsequently filtered again to the other side after stirring at room temperature for 10 min. This procedure was repeated four times until the stirred solution had only a light purple color. Finally, the SO_2 was removed and remaining solid was dissolved in 20 mL MeCN to form a deep violet solution. This solution was transferred into 200 mL of pure toluene which resulted in a clear purple solution. The amount of solvent was reduced under reduced pressure until a dark precipitate formed and a light pink solution remained. The supernatant solution was decanted off and the residue washed two times with 50 mL of toluene and one time with Et_2O and subsequently dried in vacuum to afford a pink to violet fine powder. Yield 683 mg (72%). ^{1}H NMR (400 MHz, CD_2Cl_2, 300 K) no signals detectable for $[Thia]^+$; $^{19}F\{^1H\}$ NMR (282.4 MHz, CD_3CN, 300 K) δ/ppm = –111.6 (d, $J_{F,F}$ = 277 Hz, 2F), –116.1 (d, $J_{F,F}$ = 279 Hz, 2F), –120.9 (d, $J_{F,F}$ = 278 Hz, 2F), –127.7 (s, 2F), –129.7 (d, $J_{F,F}$ = 275 Hz, 2F), –136.4 (d, $J_{F,F}$ = 277 Hz, 2F), –140.7 (d, $J_{F,F}$ = 277 Hz, 1F), –153.8 (t, $J_{F,F}$ = 22 Hz, 1F), –164.5 (t, $J_{F,F}$ = 18 Hz, 1F), –170.5 (s, AlF). Elemental analysis shows a possible impurity with thianthrene (~11%). Anal. calcd. for [Thia][FAl]: C, 36.09; H, 0.50, S, 4.01. Anal. calcd. for [Thia][FAl]·(thianthrene)$_{0.11}$: C, 36.53; H, 0.55, S, 4.39. Found: C, 36.54; H, 0.71, S, 4.49. Positive ion MS, *m/q* (%): 215.9 (100) $[Thia]^+$. Negative ion MS, *m/q* (%): 1381.2 (100) $[FAl]^-$. IR(KBr) cm^{-1}: 3620 (vw), 3165 (vw), 3089 (vw), 3039 (vw), 3005 (vw), 2967 (vw), 2928 (vw), 2850 (vw), 2866 (vw), 2537 (vw), 2490 (vw), 2411 (vw), 1653 (m), 1534 (m), 1522 (w), 1484 (vs), 1436 (vw), 1422 (vw), 1324 (m), 1307 (m), 1264 (s), 1244 (s), 1205 (vs), 1185 (s), 1155 (s), 1134 (m), 1105 (s), 1033 (m), 1019 (s), 1005 (m), 954 (vs), 910 (m), 850 (w), 810 (w), 766 (m), 748 (s), 730 (m), 666 (w), 648 (w), 635 (w), 625 (w), 600 (w), 536 (w), 525 (w), 498 (w), 428 (vw).

Preparation of $[\{CpMo(CO)_2\}_4(\mu_4,\eta^2{:}\eta^2{:}\eta^2{:}\eta^2\text{-}P_4)][SbF_6]_2$ (**11a**): $[\{CpMo(CO)_2\}_2(\mu,\eta^2{:}\eta^2\text{-}P_2)]$ (**6**) (99 mg, 0.2 mmol, 2 eq.) was dissolved in 15 mL of CH_2Cl_2 at –35 °C. [Thia][SbF_6] (90 mg, 0.2 mmol, 2 eq.) was dissolved in 40 mL of CH_2Cl_2 at –35 °C and slowly added to the stirred solution of **6**. The turbid dark reaction mixture was stirred at –30 °C for 20 min. When the stirring was stopped, a dark green precipitate and a clear light orange solution (small excess **6**) could be observed. The supernatant solution was decanted off and the crude product was washed two times with toluene (~30 mL) and dried in vacuum. This affords **11a** as a dark green powder. Yield 117 mg (80%). ^{1}H NMR (400 MHz, CD_3CN_2, 273 K, decomposition!) δ/ppm 5.74 (br, Cp), 3.15 (br), 1.93 (br); $^{31}P\{^1H\}$ NMR (162.0 MHz, CD_3CN_2, 273 K, decomposition!) δ/ppm 3.2 (br, ω½ = 1300 Hz), –42.2 (s, presumably **6**); $^{13}C\{^1H\}$ NMR (100.6 MHz, CD_3CN_2, 273 K, decomposition!) δ/ppm 220.53 (s, CO), 92.45 (s, Cp); Anal. calcd. for $[\{Cp_2Mo_2(CO)_4P_2\}_2][SbF_6]_2$: C, 22.98; H, 1.38. Found: C, 22.93; H, 1.54.

X-ray crystallography

General considerations

All crystal manipulations were performed under mineral oil. The diffraction experiments were performed at low temperatures accomplished by nitrogen cooling on either a Gemini (R) Ultra or a SuperNova or a GV1000 diffractometer from Rigaku (former Agilent Technologies or Oxford Diffraction) using either Cu-K_α or Mo-K_α radiation. Crystallographic data together with the details of the experiments are presented in Tables 1-4. The cell determination, data reduction and absorption correction for all compounds were performed with the help of the CrysAlis PRO software.[1] The full-matrix least-square refinement against F^2 was done with ShelXL.[2] Graphical material was created with the free software Olex2.[3] All cif files are provided on the provided DVD. The crystal structure of **4d** has been reported before.[4] Details of the crystal structures determinations of **10b** and **11b** are presented in chapter 5.

Table 1. Crystallographic details for **1**, **2c** and **4a**.

Identification code	**1**	**2c**	**4a**
formula	$C_{98}H_{86}Mo_2O_4$	$C_{80}H_{70}Mo_2P_6$	
weight [g·mol^{-1}]	1519.54	1409.06	
Temperature [K]	123.0(3)	123.00(14)	
crystal system	monoclinic	monoclinic	hexagonal *P*
space group	$P2_1/c$	$P2_1/c$	
a [Å]	16.0635(7)	10.33712(12)	20.3534(8)
b [Å]	13.5669(9)	30.8196(3)	20.3660(8)
c [Å]	17.4719(7)	20.5929(3)	10.4626(4)
α [°]	90	90	90
β [°]	91.639(4)	102.4830(13)	90
γ [°]	90	90	120
Volume [Å^3]	3806.1(3)	6405.50(13)	3757.7(2)
Z	2	4	
ρ_{calc} [g·cm^{-3}]	1.326	1.461	
μ [mm^{-1}]	0.384	4.978	
F(000)	1580.0	2896.0	
crystal size [mm^3]	0.483 × 0.443 × 0.333	0.387 × 0.326 × 0.244	
diffractometer	Gemini R Ultra	Gemini R Ultra	
absorption correction	gaussian	gaussian	
T_{min}/T_{max}	0.862 / 0.902	0.273 / 0.469	
radiation [Å]	MoK_α	CuK_α	
2Θ range [°]	6.796 to 65.922	7.228 to 141.642	
completeness	0.997	0.996	
reflns collected/unique	47909 / 13094	44777 / 12017	
R_{int}/R_{sigma}	0.0726 / 0.0545	0.0425 / 0.0237	
data/restraints/parameters	13094 / 0 / 457	12017 / 0 / 793	
GOF on F^2	1.083	1.019	
R_1/wR_2 [$I \geq 2\sigma(I)$]	0.0581 / 0.1681	0.0331 / 0.0881	
R_1/wR_2 [all data]	0.0825 / 0.1770	0.0368 / 0.0908	
max/min $\Delta\rho$ [e·Å^{-3}]	2.39 / –1.37	0.91 / –0.38	

Table 2. Crystallographic details for **4b**, **4c** and **4e**.

Identification code	**4b**	**4c**	**4e**
formula	$C_{95}H_{26}Al_2Cl_6F_{92}Mo_4O_6P_{12}$		$C_{98}H_{74}AlCl_4F_{36}Mo_2O_4P_6$
weight [g·mol^{-1}]	4033.22		2546.05
Temperature [K]	123(1)		100.1(9)
crystal system	monoclinic	monoclinic *P*	monoclinic
space group	*C*2/*c*		*C*2/*c*
a [Å]	13.1706(1)	11.5938(3)	28.8769(4)
b [Å]	18.5816(2)	42.4088(10)	17.2960(2)
c [Å]	51.0054(5)	22.8996(6)	20.3093(3)
α [°]	90	90	90
β [°]	92.016(1)	104.18(1)	97.0217(13)
γ [°]	90	90	90
Volume [Å^3]	12474.9(2)	10916.0(5)	10067.5(2)
Z	4		4
ρ_{calc} [g·cm^{-3}]	2.148		1.680
μ [mm^{-1}]	7.779		5.072
F(000)	7792.0		5092.0
crystal size [mm^3]	0.382 × 0.321 × 0.247		0.409 × 0.275 × 0.233
diffractometer	Gemini R Ultra		Gemini R Ultra
absorption correction	analytical		gaussian
T_{min}/T_{max}	0.165 / 0.338		0.348 / 0.539
radiation [Å]	CuK_α		CuK_α
2Θ range [°]	8.24 to 131.64		7.18 to 141.908
completeness	0.984		0.998
reflns collected/unique	18288 / 10672		41482 / 9520
R_{int}/R_{sigma}	0.0300 / 0.0379		0.0551 / 0.0322
data/restraints/parameters	10672 / 73 / 1091		9520 / 0 / 681
GOF on F^2	1.033		1.037
R_1/wR_2 [$I \geq 2\sigma(I)$]	0.0325 / 0.0847		0.0464 / 0.1275
R_1/wR_2 [all data]	0.0363 / 0.0896		0.0502 / 0.1303
max/min $\Delta\rho$ [e·Å^{-3}]	0.71 / –0.72		1.36 / –0.81

Table 3. Crystallographic details for **5**, **7** and **8**.

Identification code	**5**	**7**	**8**
formula	$C_{20}H_{30}As_6BF_4Mo_2$	$C_{58}H_{20}AgAlCl_2F_{46}Mo_2O_7P_2$	$C_{159.22}H_{56.36}Ag_2Al_2Cl_{0.36}F_{92}Mo_8O_{22}P_8$
weight [g·mol^{-1}]	998.65	2162.31	5366.78
Temperature [K]	123.00(14)	123.00(10)	123.01(10)
crystal system	orthorhombic	monoclinic	monoclinic
space group	*Ibam*	$P2_1/c$	$C2/c$
a [Å]	11.5548(12)	12.8202(2)	29.9487(4)
b [Å]	15.4212(18)	19.0679(4)	21.10640(19)
c [Å]	15.239(2)	27.8091(4)	33.3294(4)
α [°]	90	90	90
β [°]	90	95.7340(10)	113.6367(15)
γ [°]	90	90	90
Volume [Å^3]	2715.3(6)	6764.0(2)	19300.4(4)
Z	4	4	4
ρ_{calc} [g·cm^{-3}]	2.443	2.123	1.847
μ [mm^{-1}]	8.217	8.286	7.829
F(000)	1892.0	4184.0	10391.0
crystal size [mm^3]	0.220 × 0.145 × 0.120	0.150 × 0.150 × 0.035	0.125 × 0.106 × 0.047
diffractometer	Gemini R Ultra	SuperNova	SuperNova
absorption correction	gaussian	analytical	gaussian
T_{min}/T_{max}	0.323 / 0.476	0.483 / 0.779	0.500 / 0.748
radiation [Å]	MoK_α	CuK_α	CuK_α
2*Θ* range [°]	6.892 to 58.576	6.93 to 146.238	6.616 to 144.528
completeness	0.988	0.986	0.987
reflns collected/unique	3641 / 1614	23992 / 13025	35811 / 18317
R_{int}/R_{sigma}	0.0341 / 0.0479	0.0419 / 0.0535	0.0286 / 0.0412
data/restraints/parameters	1614 / 0 / 85	13025 / 0 / 1073	18317 / 4 / 1357
GOF on F^2	1.112	1.021	1.042
R_1/wR_2 [$I \geq 2\sigma(I)$]	0.0384 / 0.1094	0.0513 / 0.1301	0.0484 / 0.1286
R_1/wR_2 [all data]	0.0496 / 0.1111	0.0647 / 0.1433	0.0609 / 0.1396
max/min Δ*ρ* [e·Å^{-3}]	2.12 / –0.93	2.74 / –1.34	1.51 / –1.11

Table 4. Crystallographic details for **9**, **10c** and **11a**.

Identification code	**9**	**10c**	**11a**
formula	$C_{80}H_{37.2}Ag_2Al_2Cl_{0.8}F_{72}Mo_6O_{20}P_6$	$C_{48}H_8AlF_{46}O_3S_2$	$C_{32}H_{26}F_{12}Mo_4N_2O_8P_4Sb_2$
weight [g·mol^{-1}]	3745.82	1597.64	1545.69
Temperature [K]	100.05(10)	122.99(19)	122.9(4)
crystal system	monoclinic	triclinic	monoclinic
space group	*I*2/*a*	*P*–1	$P2_1/n$
a [Å]	19.44134(16)	11.4701(7)	13.01592(16)
b [Å]	17.47231(13)	21.1297(5)	7.86686(8)
c [Å]	34.8842(2)	22.6211(8)	22.5280(2)
α [°]	90	103.452(3)	90
β [°]	101.9624(7)	98.248(4)	99.6948(11)
γ [°]	90	96.990(4)	90
Volume [Å^3]	11592.33(15)	5208.0(4)	2273.80(4)
Z	4	4	2
ρ_{calc} [g·cm^{-3}]	2.146	2.038	2.258
μ [mm^{-1}]	10.554	3.095	20.280
F(000)	7203.0	3116.0	1468.0
crystal size [mm^3]	0.215 × 0.154 × 0.138	0.315 × 0.039 × 0.024	0.162 × 0.076 × 0.051
diffractometer	Gemini Ultra	GV1000	Gemini Ultra
absorption correction	gaussian	gaussian	gaussian
T_{min}/T_{max}	0.229 / 0.406	0.601 / 0.933	0.105 / 0.517
radiation [Å]	CuK_α	CuK_α	CuK_α
2*Θ* range [°]	6.87 to 133.988	5.156 to 149.812	7.354 to 133.956
completeness	0.983	0.984	0.992
reflns collected/unique	26464 / 10155	32133 / 20011	20568 / 4035
R_{int}/R_{sigma}	0.0200 / 0.0212	0.0761 / 0.1056	0.0341 / 0.0287
data/restraints/parameters	10155 / 312 / 1180	20011 / 0 / 1801	4035 / 0 / 290
GOF on F^2	1.055	1.050	1.103
R_1/wR_2 [$I \geq 2\sigma(I)$]	0.0577 / 0.1662	0.0767 / 0.2202	0.0186 / 0.0407
R_1/wR_2 [all data]	0.0632 / 0.1711	0.1209 / 0.2342	0.0203 / 0.0415
max/min Δ*ρ* [e·Å^{-3}]	1.60 / –1.76	0.91 / –0.81	0.53 / –0.41

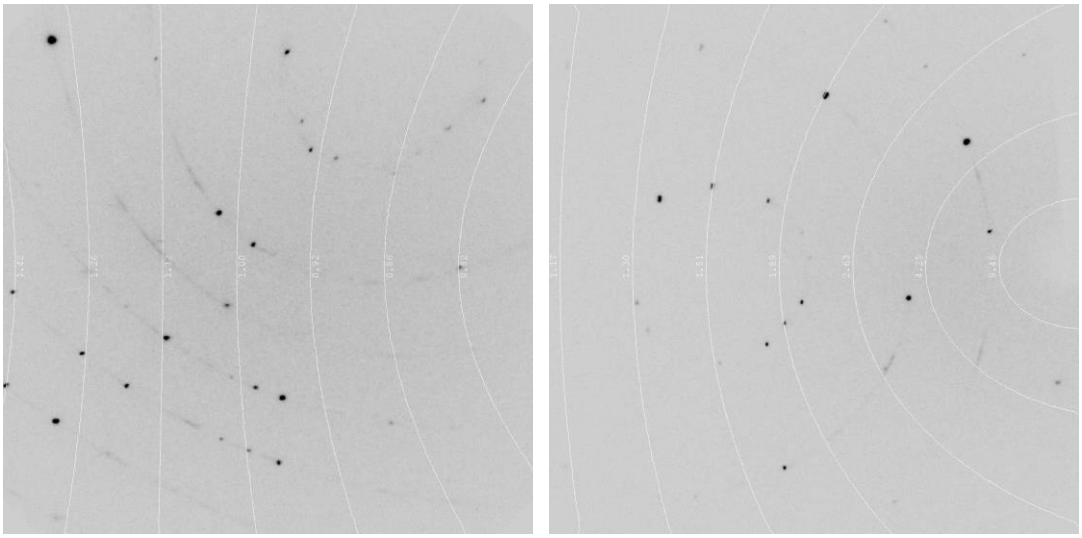

Figure 1. Data collection frames from the single crystal X-ray diffraction measurement of **4a**. Each reflection lies on a ring of X-ray intensity. From this data set no structure solution could be obtained. This phenomenon is reproducible for **4a**, even after recrystallization from CH_2Cl_2/alkanes.

Computational Details

Details about the computations of $[(Cp^*Mo)_2(\mu,\eta^6{:}\eta^6\text{-}P_6)]^{0/+}$ ([**2b**]$^{0/+}$) are presented in chapter 1. Figure 2 shows the isosurfaces of the frontier molecular orbitals for $[(CpMo)_2(\mu,\eta^6{:}\eta^6\text{-}P_6)]^{0/+}$ ([**2a**]$^{0/+}$). All calculations have been performed with the TURBOMOLE program package[5] at the RI-[6]BP86[7]/def2-TZVP[8] level of theory, followed by single point calculations without the RI approximation. The Multipole Accelerated Resolution of Identity (MARI-J)[9] approximation was used in the geometry optimization steps.

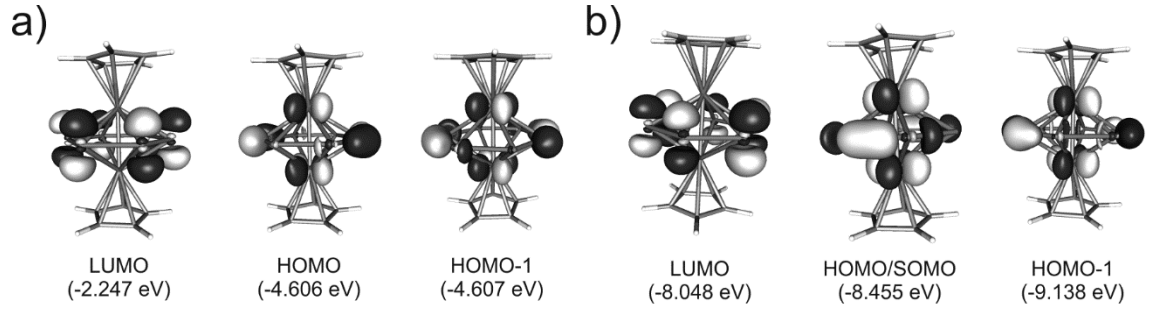

Figure 2. Isosurfaces of the frontier molecular orbitals in **2a** (a) and [**2a**]$^+$ (b) (α-spin).

The inspection of the frontier molecular orbitals in the model complex $[(CpMo)_2(\mu,\eta^6{:}\eta^6\text{-}As_6)]$ (**A**) shows, that the HOMO and HOMO-1 orbitals are basically degenerate and represent As-As bonding orbitals with contribution of molybdenum d orbitals. By elimination of one electron the HOMO-1 orbital in **A** is converted to the Singly Occupied Molecular Orbital (SOMO) in **A**$^+$ (see Figure 3). This leads to the reduction of the As-As bond order (two opposite As-As bonds) and to the observed bis-allylic distortion. This behavior is also nicely described by the Wiberg Bond Indices. The WBI for all As-As bonds in **A** (As-As distance 2.397 – 2.410 Å) are roughly the same and vary from 0.76 to 0.80 whereas in **A**$^+$ the WBI corresponding to the elongated As-As bonds (2.475 – 2.479 Å) are 0.58 – 0.60 and 0.85 – 0.88 for the other As-As bonds (As-As distance 2.360 – 2.363 Å). The WBI for the Mo-Mo bond (2.680 Å and 2.713 Å in **A** and **A**$^+$, respectively) is 0.94 in **A** and 0.95 in **A**$^+$. According to Mulliken population analysis the spin density in **A**$^+$ is mainly localized on both Mo centers (0.32 e each), with minor contribution from the As_6 middle deck. The behavior of the Cp* substituted analog $[(Cp^*Mo)_2(\mu,\eta^6{:}\eta^6\text{-}As_6)]$ (**B**) is very similar. The WBI of the As-As bonds in $[(Cp^*Mo)_2(\mu,\eta^6{:}\eta^6\text{-}As_6)]$ (**B**) vary from 0.77 to 0.79 (As-As distances: 2.401 – 2.402

Å) whereas for the Mo-Mo bond it is 0.96 (Mo-Mo 2.676 Å). In $[(Cp^*Mo)_2(\mu,\eta^6{:}\eta^6\text{-}As_6)]^+$ (**B**$^+$) the WBI of the shorter As-As bonds (2.361 Å) is 0.87 while for the longer As-As bonds (As-As 2.476 Å) is 0.60. The WBI of the Mo-Mo bond (WBI: 0.96) remains unchanged by going from **B** to **B**$^+$. Just like in the Cp derivative **A**$^+$, the spin density is evenly distributed on each Mo centers (0.34 e) with minor contribution from the As_6 middle deck. The DFT calculations of the *cyclo*-As_6 complexes always showed an imaginary frequency of low energy which was retained even after several calculations.

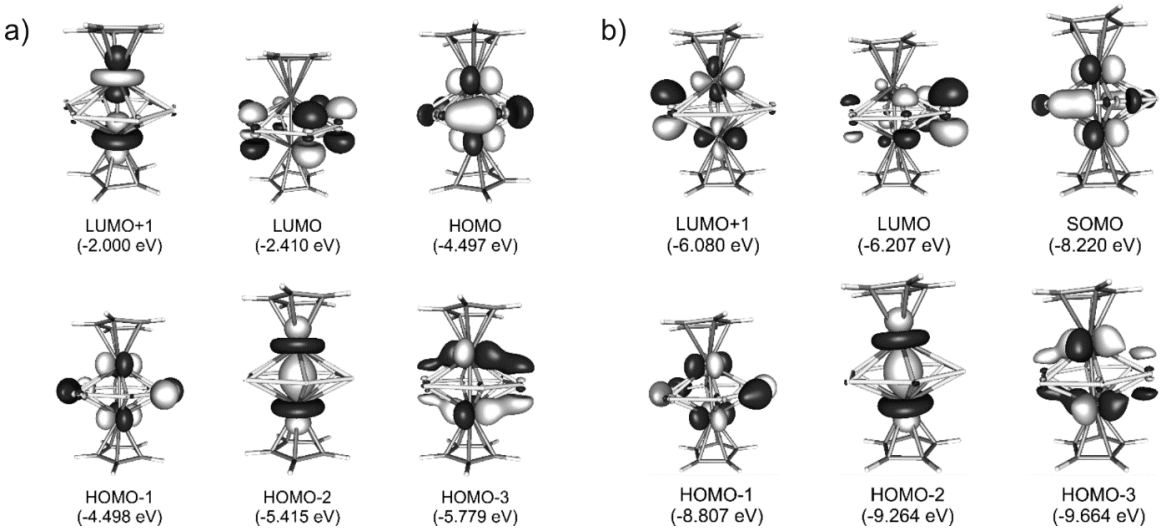

Figure 3. Isosurfaces of selected molecular orbitals of $[(CpMo)_2(\mu,\eta^6{:}\eta^6\text{-}As_6)]$ (a) and alpha-spin MOs of $[(CpMo)_2(\mu,\eta^6{:}\eta^6\text{-}As_6)]^+$ (b). Calculated at the BP86/def2-TZVP level of theory.

References

[1] different versions ed., Rigaku (former: Agilent Technologies Ltd. or Oxford Diffraction Ltd.)

[2] G. M. Sheldrick, *Acta Cryst. A* **2008**, *64*, 112-122.

[3] O. V. Dolomanov, L. J. Bourhis, R. J. Gildea, J. A. K. Howard, H. Puschmann, *J. Appl. Crystallogr.* **2009**, *42*, 339-341.

[4] M. Fleischmann, F. Dielmann, L. J. Gregoriades, E. V. Peresypkina, A. V. Virovets, S. Huber, A. Y. Timoshkin, G. Balázs, M. Scheer, *Angew. Chem. Int. Ed.* **2015**, *54*, 13110-13115; *Angew. Chem.* **2015**, *127*, 13303-13308.

[5] a) R. Ahlrichs, M. Bär, M. Häser, H. Horn, C. Kölmel, *Chem. Phys. Lett.***1989**, *162*, 165–169; b) O. Treutler, R. Ahlrichs, *J. Chem. Phys.***1995**, *102*, 346–354.

[6] a) K. Eichkorn, O. Treutler, H. Oehm, M. Häser, R. Ahlrichs, Chem. Phys. Lett.1995, 242, 652–660; b) K. Eichkorn, F. Weigend, O. Treutler, R. Ahlrichs, Theor. Chem. Acc.1997, 97, 119.

[7] a) P. A. M. Dirac, Proc. Royal Soc. A, 1929, 123, 714-733. b) J. C. Slater, Phys. Rev.1951, 81, 385-390. c) S. H. Vosko, L. Wilk, M. Nusair, Can. J. Phys. 1980, 58, 1200-1211. d). A. D. Becke, Phys. Rev. A, 1988, 38, 3098. e) J. P. Perdew, Phys. Rev. B 1986, 33, 8822-8824.

[8] a) A. Schäfer, C. Huber, R. Ahlrichs, *J. Chem. Phys.***1994**, *100*, 5829; b) K. Eichkorn, F. Weigend, O. Treutler, R. Ahlrichs, *Theor. Chem. Acc.***1997**, *97*, 119.

[9] M. Sierka, A. Hogekamp, R. Ahlrichs, J. Chem. Phys.2003, 118, 9136.

Preface

The following chapter has already been published. The article is reprinted with permission of the Royal Society of Chemistry.
Chem. Commun. **2015**, *51*, 2893–2895.

Authors

Martin Fleischmann, Luis Dütsch, Mehdi Elsayed Moussa, Andrea Schindler, Gábor Balázs, Christophe Lescop* and Manfred Scheer *

Author contributions

The preparation and characterization of all compounds including the single crystal X-ray structure determination and the preparation of the manuscript (in close collaboration with Christophe Lescop) was done by the first author. Luis Dütsch prepared and described some of the presented compounds in his Bachelor's thesis which was done under the supervision of Martin Fleischmann and Manfred Scheer. Mehdi Elsayed Moussa prepared the polyphosphine ligand dpmp. Andrea Schindler described the structure of compound 4 which was obtained as a side-product in trace amounts for the first time. Gábor Balázs performed supporting DFT calculations. Christophe Lescop and Manfred Scheer supervised the research and revised the manuscript.

Acknowledgements

This work was financially supported by the Deutsche Forschungsgemeinschaft.

7 Organometallic polyphosphorus and -arsenic ligands as linkers between pre-assembled linear Cu^{I} fragments

Abstract: A simple and straightforward synthesis of a new linear trinuclear Cu^{I} cluster with polyphosphine ligands is presented. The reaction of this pre-organized Cu_3 precursor with E_n ligand complexes (E = P, As; n = 2, 5) affords discrete complexes exhibiting end-on η^1-coordination of the E_2 ligands or one-dimensional coordination polymers featuring σ-1,3-bridging E_5 rings, respectively.

7.1 Introduction

In recent years, molecular wires have attracted increasing attention as promising nanostructured materials for molecular electronic, optical, and chemical devices.[1,2,3,4] Among these, homoleptic polymetallic linear arrays featuring multidentate bridging ligands and short intermetallic distances have been synthesized, bearing in some case conductive or semi-conductive behaviors.[5,6,7,8,9,10,11,12,13,14] Yet, the general access to such polymetallic molecular wires remains complicated as it is mostly hindered by the rather low structural control of the synthetic methods applied, which often led to polyhedral cluster cores instead of linear arrays. Therefore, there is interest to develop new synthetic approaches toward such polymetallic supramolecular arrays. The P_n organometallic ligand complexes **A1**, **B1** (Scheme 1)[15,16] have been used previously as very versatile linking moieties between monovalent metal centers to afford spherical nano-sized supramolecular aggregates[17,18,19,20,21] as well as 1D and 2D coordination polymers.[22,23,24] However, these ligand complexes as well as their arsenic As_n analogs **A2**, **B2** (Scheme 1)[25,26] have not yet been used to built-up extended molecular wires bearing polymetallic linear arrays with short metal-metal contacts. Herein we describe the reaction of E_n ligand complexes **A1**, **A2**, **B1** and **B2** (**A1**, **B1**: E = P; **A2**, **B2**: E = As, Scheme 1) with a new trimetallic Cu^{I} linear precursor bearing short intermetallic distances to produce linear molecular wires. In a field where organic N, O or S donor ligands are the most commonly used linkers, this heteroleptic approach gives the opportunity to investigate: *i*) the effect of the variation of the nuclearity and geometry of the organometallic E_n ligand complexes on the dimension of the supramolecular entities formed; *ii*) the nature of the coordination modes adopted by the E_n ligands in

such molecular assemblies; *iii*) how the variation of the pnictogen donor atom coordinated on Cu^{I} metal centers can alter intermetallic distances compared to the original linear trimetallic fragment.

7.2 Results and Discussion

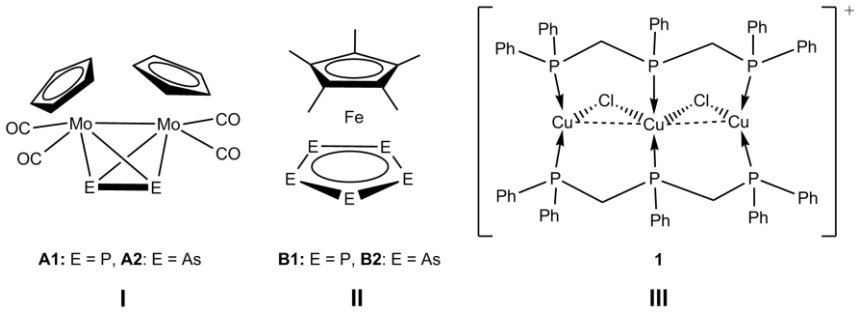

Scheme 1. Representation of the molecular structures of the used E_n ligand complexes **A1**, **A2** and **B1**, **B2** as well as the newly synthesized trimetallic Cu^{I} entity **1** $[Cu_3(\mu\text{-}Cl)_2(dpmp)_2]^+$.

A straightforward synthetic approach allowed us to obtain the new compound $[Cu_3(\mu\text{-}Cl)_2(dpmp)_2][BF_4]$ (**1**) by self-assembly of 2 eq. of dpmp (dpmp = bis(diphenylphosphinomethyl)phenylphosphine), 2 eq. of CuCl and 1 eq. of $[Cu(CH_3CN)_4][BF_4]$ in CH_2Cl_2. Subsequent vapor diffusion of *n*-pentane into the crude solution afforded **1** as colorless crystals. The ^{1}H as well as the $^{31}P\{^{1}H\}$ NMR spectra of isolated crystals of compound **1** dissolved in CD_2Cl_2 suggest dynamic coordination behavior of the dpmp ligand coordinated on Cu^{I} metal centers at room temperature.[27]

The solid state structure of **1** shows a $[Cu_3(\mu\text{-}Cl)_2(dpmp)_2]^+$ unit (see Figure 1a), containing an almost linear trinuclear Cu^{I} fragment (Cu1-Cu2-Cu3; 159.5°) stabilized by two bridging $\eta^1{:}\eta^1{:}\eta^1$-dpmp ligands and two additional bridging Cl atoms. The Cu-Cu distances in **1** are short (2.8386(4) and 2.8782(4) Å) suggesting intramolecular metallophilic interactions. The terminal Cu^{+} cations are coordinatively unsaturated and exhibit distorted trigonal planar geometries with the sum of the bond angles being 358.9° and 359.7°, respectively. Conversely, the internal Cu^{I} metal center has a distorted tetrahedral coordination sphere.

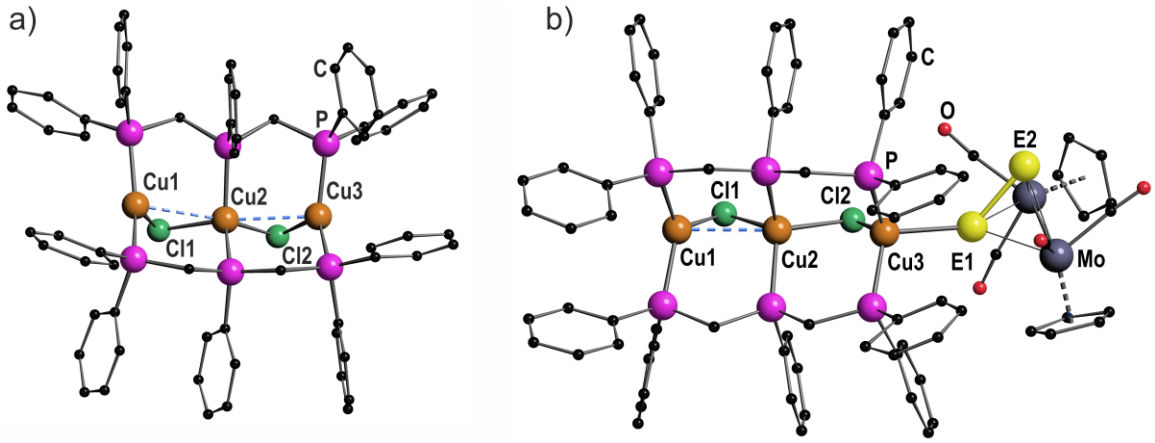

Figure 1. Crystal structures of the complexes **1** (a) and the isostructural complexes **2** (E = P) and **3** (E = As) (b). The anion, hydrogen atoms and solvent molecules are omitted for clarity. Selected distances [Å] **1/2/3**: Cu1-Cu2 2.8782(4)/2.8359(7)/2.8304(8), Cu2-Cu3 2.8386(4)/3.3572(6)/3.2176(8), 2: Cu3-P1 2.3693(10), P1–P2 2.0869(14), 3: Cu3–As1 2.5295(7), As1-As2 2.3097(8).

A related $[Cu_3]$ complex $[Cu_3(\mu\text{-}Cl)_2(dpmp)_2(MeCN)_2]^+[ClO_4]^-\bullet H_2O$ containing MeCN ligands coordinated to the terminal Cu^I metal centers (Cu1 and Cu3) was described previously, and shows larger intermetallic distances (ca. 3.2 Å).[28] This suggests that the terminal, trigonal planar Cu^I metal centers of **1** might be reactive and, therefore, compound **1** represents *a priori* an interesting linear $[Cu_3]$ building block for supramolecular chemistry exhibiting close Cu···Cu contacts and potentially free, reactive, terminal coordination sites. Inspired by these observations, we intended to connect the $[Cu_3]$ clusters of **1** by E_n ligand complexes **A1**, **A2**, **B1**, **B2** (Scheme 1) (E = P, As). The addition of the tetrahedrane complexes **A1** or **A2** to a solution of **1** in CH_2Cl_2 affords clear red solutions of the products **2** and **3**, respectively. Vapor diffusion of *n*-pentane into CH_2Cl_2 solutions afforded orange (**2**) or dark red (**3**) crystals which can be isolated in good yields. Interestingly, the reported MeCN containing trinuclear Cu^I complex[28] does not react with E_n ligand complexes, what underlines the need of vacant coordination sites for supramolecular aggregation. The ^1H NMR spectra of **2** and **3** show a set of signals for the dpmp ligands of the $[Cu_3]$ unit very similar to those recorded for **1** and one singlet assignable to the Cp rings of **A1** or **A2**. The $^{31}P\{^1H\}$ NMR spectra of **2** and **3** show a set of signals for the $[Cu_3]$ moiety slightly down field shifted compared to the signals registered for **1**. Additionally, **2** shows one singlet for the P_2 unit of **A1** at –65.6 ppm which is shifted 21 ppm upfield compared to the free ligand.[15] Single crystal X-ray diffraction analysis reveals isolated $[Cu_3(\mu\text{-}Cl)_2(dpmp)_2(\eta^1\text{-}L)]^+$ (L = **A1** (**2**), **A2** (**3**)) complexes (see Figure 1b). The isostructural compounds **2** and **3** bear one tetrahedrane complex **A1** or **A2**, coordinated to one terminal, distorted tetrahedral coordinated Cu atom of an almost linear $[Cu_3]$ unit (Cu1-Cu2-Cu3; **2**: 164.81°; **3**: 164.72°). Therefore, the overall structure of the trimetallic core present in **1** is preserved upon

these reactions. The other terminal Cu atom (Cu1 in Figure 1b) exhibits a distorted trigonal planar geometry with the sum of angles being 358.6°(**2**) or 358.7°(**3**), respectively. The coordination environment of the central Cu^+ cation can best be described as distorted tetrahedral. The coordination of **A1** or **A2** as terminal ligands results in an elongation of the adjacent Cu···Cu distance inside the [Cu_3] chain while the E–E bond lengths of the coordinated E_2 ligands are almost unchanged compared to those of the free complexes (**2**: 2.0869(14) Å, **A1**: 2.079(2) Å[15]; **3**: 2.3097(8) Å, **A2**: 2.305(3) Å[25]). Therefore, the intermetallic distances Cu1–Cu2/Cu2–Cu3 are distinctly different with 2.8359(7) /3.3572(6) Å in **2** and 2.8304(8) /3.2176(8) Å in **3**, respectively. To investigate the influence of the coordination of the E_2 ligand complexes on the intermetallic distances found in the [Cu_3] cluster of **2** and **3**, DFT calculations on the model compound $[Cu_3(dmmp)_2(\mu\text{-}Cl)_2(\eta^1\text{-}\mathbf{A1})]^+$ (dmmp = bis(dimethylphosphino)methyl-phosphane) were performed.[29] The results show that the closer ligand **A1** approaches the Cu3 atom, the longer the Cu2–Cu3 distance gets (labeling according to Figure 1b). In contrast, the Cu1–Cu2 distance is unaffected by the coordination of **A1** to Cu3 and can be very well compared with the starting compound **1**. The solid state structures of **2** and **3** show that the elongation of the Cu2–Cu3 distance is more pronounced in the case of the P_2 ligand **A1** instead of the As_2 ligand **A2**. Supporting this observation, the calculated dissociation energies of the E_n ligand in $[Cu_3(\mu\text{-}Cl)_2(dpmp)_2(\eta^1\text{-}L)]^+$ (L = **A1**(**2**): 36.5 kJ·mol^{-1}, **A2**(**3**) 31.7 kJ·mol^{-1}) are slightly higher for L = **A1** (**2**) suggesting a stronger interaction of the P_2 fragment with the [Cu_3] unit.

As a next step, we focused our attention on the use of the sandwich complexes $[Cp^*Fe(\eta^5\text{-}E_5)]$ (E = P (**B1**), As(**B2**)). The addition of complexes **B1** or **B2** to **1** in CH_2Cl_2 afforded a clear green solution of the product **4** and a clear brown solution of derivative **5**, respectively. Vapor diffusion of *n*-pentane into CH_2Cl_2 solutions afforded light green (**4**) or brown (**5**) crystals as needles. The ^{1}H NMR spectra of **4** and **5** in CD_2Cl_2 show in addition to the set of signals for the dpmp ligands one singlet assignable to the Cp* rings of **B1** or **B2** at a similar chemical shift compared to the free complexes. The $^{31}P\{^1H\}$ NMR spectra of the derivatives **4** and **5** in CD_2Cl_2 show a set of signals for the dpmp ligands of the [Cu_3] cluster slightly down field shifted compared to the signals observed for compound **1**. Only one singlet for the *cyclo*-P_5 ligand **B1** at 149.9 ppm is detected, which is shifted 3 ppm upfield compared to the free ligand.[16] Single crystal X-ray diffraction analysis reveals that **4** and **5** are isostructural and consist of a one-dimensional coordination polymer of almost linear [Cu_3] units (Cu1-Cu2-Cu3; **4**: 168.78°; **5**: 169.12°) connected by *cyclo*-E_5 complexes (see Figure 2) with the general formula $[Cu_3(dpmp)_2(\mu\text{-}Cl)_2\{\mu\text{-}L\}]_n[BF_4]_n$ (L = **B1** (**4**), **B2** (**5**)).

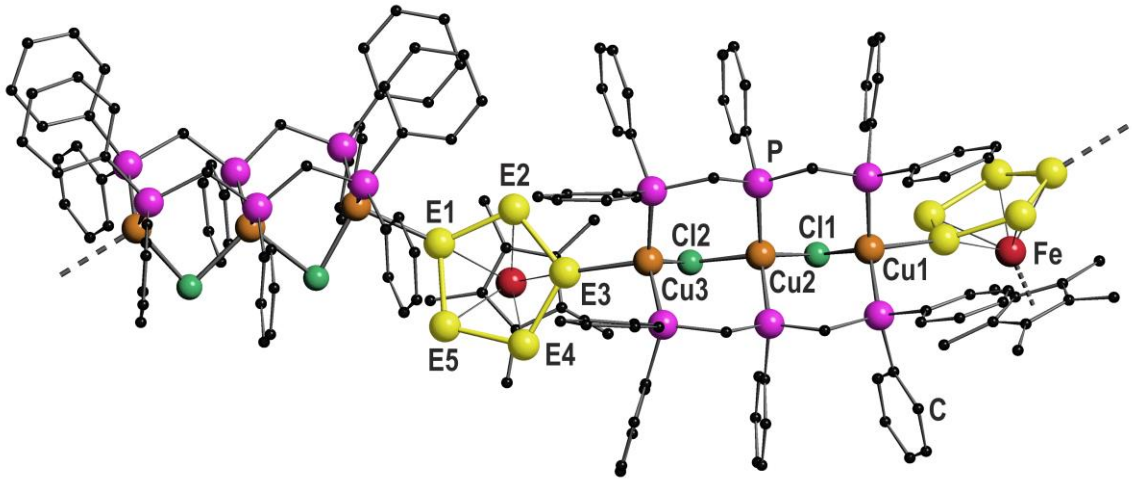

Figure 2. Section of the structures of the isostructural coordination polymers **4** (E = P) and **5** (E = As). The anion, hydrogen atoms and solvent molecules are omitted for clarity. Selected distances **4**/**5** [Å]: Cu1-Cu2 3.2975(8)/3.2135(8), Cu2-Cu3 3.3389(8)/3.0345(8), Cu1-E1 2.3743(11)/2.5036(7), Cu3-E3 2.3271(10)/2.5980(8).

The *cyclo*-E_5 ligands **B1** and **B2** are bridging two Cu centers in a σ-1,3-coordination mode. This σ coordination mode is unprecedented for the *cyclo*-As_5 ligand **B2**. For the phosphorus compound **B1** the 1,3-coordination mode was only observed towards coordination with $Cr(CO)_5$ and CuI.[24,30] The intermetallic distances Cu1–Cu2 /Cu2–Cu3 are different with 3.2975(8)/3.3389(8) Å in **4** and 3.2135(8)/3.0345(8) Å in **5**, revealing shorter Cu–Cu distances for the As_5 ligand complex **B2** as organometallic linker. The E-E bond lengths of the *cyclo*-E_5 ligands in both compounds are very uniform. The calculated energies for the dissociation of **B1** and **B2** for the monomeric complexes $[Cu_3(dpmp)_2(\mu\text{-}Cl)_2\{\eta^1\text{-}L\}]^+$ (L = **B1**, **B2**) of 41.2 kJ·mol^{-1} (**4**) and 31.9 kJ·mol^{-1} (**5**) are relatively low which is in agreement with the observed dynamic coordination behavior of the complexes in solution.[27] We previously described a preferred η^2-coordination mode of the $[Cp^*Fe(\eta^5\text{-}As_5)]$ ligand **B2** towards Cu^I cations.[31] The fact that **B2** exhibits a σ coordination mode is probably caused by steric repulsion of the phenyl substituents of the dpmp ligand and the Cp* ligand. According to DFT calculations, a η^2-coordination of **B2** to the $[Cu_3]$ cluster is disfavored by 17.0 kJ·mol^{-1}.[29]

7.3 Conclusion

In conclusion, a simple route to prepare the cationic building block $[Cu_3(dpmp)_2(\mu\text{-}Cl)_2]^+$ (**1**) is presented. The $[Cu_3]$ cluster **1** features two vacant coordination sites, which allows the reaction with the E_2 and E_5 ligand complexes resulting in the isolation of discrete complexes **2** and **3** and one-dimensional coordination polymers **4** and **5**, respectively. Surprisingly, the polyphosphorus and –arsenic complexes show the same η^1-coordination of the E_2 ligands **A1** and **A2**, and even more

astonishing, the same and rarely observed bridging σ-1,3-coordination of the E_5 ligands which is so far unprecedented for the *cyclo*-As_5 complex **B2**. The intermetallic Cu···Cu distances of the [Cu_3] cluster are dependent on the strength of the coordination to the terminal Cu atoms. The stronger the E-Cu coordination, the longer the adjacent Cu–Cu distance.

This study demonstrates the preparation of easily accessible extended metal atom chains and exemplifies the potential of E_n ligand complexes as connecting moieties resulting from their adjustable bonding modes. The solubility and dynamic coordination behavior of the isolated compounds show the features of the [Cu_3] cluster **1** as well as the E_n ligand complexes to act as building blocks in supramolecular chemistry. These observations will likely allow for a large variety of new supramolecular assemblies in the future. Parts of this development is presented in the following chapter.

7.4 References

[1] T. S. Arrhenius, M. Blanchard-Desce, M. Dvolaitzky, J-M. Lehn, J. Malthete, *Proc. Natl. Acad. Sci. USA* **1986**, *86*, 5355-5359.

[2] G. Sedghi, K. Sawada, L. J. Esdaile, M. Hoffmann, H. L. Anderson, D. Bethell, W. Haiss, S. J. Higgins, R. J. Nichols, *J. Am. Chem. Soc.* **2008**, *130*, 8582-8583. G. Sedghi, K. Sawada, L. J. Esdaile, M. Hoffmann, H. L. Anderson, D. Bethell, W. Haiss, S. J. Higgins, R. J. Nichols, *J. Am. Chem. Soc.* **2008**, *130*, 8582-8583.

[3] L. D. A. Siebbeles, F. G. Grozema, *Charge and Exciton Transport through Molecular Wires*, Wiley-VCH Verlag GmbH & Co., Weinheim, **2011**.

[4] F. Meng, Y.-M. Hervault, Q. Shao, B. Hu, L. Norel, S. Rigaut, X. Chen, *Nat. Commun.* **2014**, *5*, 3023.

[5] M. G. Campbell, D. C. Powers, J. Raynaud, M. J. Graham, P. Xie, E. Lee, T. Ritter, *Nat Chem* **2011**, *3*, 949-953.

[6] M. G. Campbell, S.-L. Zheng, T. Ritter, *Inorg. Chem.* **2013**, *52*, 13295-13297.

[7] K. Sakai, E. Ishigami, Y. Konno, T. Kajiwara, T. Ito, *J. Am. Chem. Soc.* **2002**, *124*, 12088-12089.

[8] I. W. P. Chen, M.-D. Fu, W.-H. Tseng, J.-Y. Yu, S.-H. Wu, C.-J. Ku, C.-h. Chen, S.-M. Peng, *Angew. Chem. Int. Ed.* **2006**, *45*, 5814-5818; *Angew. Chem.* **2006**, *118*, 5946-5950.

[9] R. H. Ismayilov, W.-Z. Wang, G.-H. Lee, C.-Y. Yeh, S.-A. Hua, Y. Song, M.-M. Rohmer, M. Bénard, S.-M. Peng, *Angew. Chem. Int. Ed.* **2011**, *50*, 2045-2048; *Angew. Chem.* **2011**, *123*, 2093-2096.

[10] T. Murahashi, M. Fujimoto, M.-a. Oka, Y. Hashimoto, T. Uemura, Y. Tatsumi, Y. Nakao, A. Ikeda, S. Sakaki, H. Kurosawa, *Science* **2006**, *313*, 1104-1107.

[11] Y. Tatsumi, K. Shirato, T. Murahashi, S. Ogoshi, H. Kurosawa, *Angew. Chem. Int. Ed.* **2006**, *45*, 5799-5803; *Angew. Chem.* **2006**, *118*, 5931-5935.

[12] Y. Tatsumi, T. Murahashi, M. Okada, S. Ogoshi, H. Kurosawa, *Chem. Commun.* **2008**, 477-479.

[13] Y. Takemura, H. Takenaka, T. Nakajima, T. Tanase, *Angew. Chem. Int. Ed.* **2009**, *48*, 2157-2161; *Angew. Chem.* **2009**, *121*, 2191-2195.

[14] E. Goto, R. A. Begum, S. Zhan, T. Tanase, K. Tanigaki, K. Sakai, *Angew. Chem. Int. Ed.* **2004**, *43*, 5029-5032; *Angew. Chem.* **2004**, *116*, 5139-5142.

[15] O. J. Scherer, H. Sitzmann, G. Wolmershäuser, *J. Organomet. Chem.* **1984**, *268*, C9-C12.

[16] O. J. Scherer, T. Brück, *Angew. Chem. Int. Ed.* **1987**, *26*, 59-59; *Angew. Chem.* **1987**, *99*, 59-59.

[17] J. Bai, A. V. Virovets, M. Scheer, *Science* **2003**, *300*, 781-783.

[18] M. Scheer, A. Schindler, C. Gröger, A. V. Virovets, E. V. Peresypkina, *Angew. Chem. Int. Ed.* **2009**, *48*, 5046-5049; *Angew. Chem.* **2009**, *121*, 5148-5151.

[19] M. Scheer, A. Schindler, J. Bai, B. P. Johnson, R. Merkle, R. Winter, A. V. Virovets, E. V. Peresypkina, V. A. Blatov, M. Sierka, H. Eckert, *Chem. Eur. J.* **2010**, *16*, 2092-2107.

[20]] S. Welsch, C. Gröger, M. Sierka, M. Scheer, *Angew. Chem. Int. Ed.* **2011**, *50*, 1435-1438; *Angew. Chem.* **2011**, *123*, 1471-1474.
[21] A. Schindler, C. Heindl, G. Balázs, C. Gröger, A. V. Virovets, E. V. Peresypkina, M. Scheer, *Chem. Eur. J.* **2012**, *18*, 829-835.
[22] M. Scheer, L. J. Gregoriades, M. Zabel, J. Bai, I. Krossing, G. Brunklaus, H. Eckert, *Chem. Eur. J.* **2008**, *14*, 282-295.
[23] J. Bai, A. V. Virovets, M. Scheer, *Angew. Chem. Int. Ed.* **2002**, *41*, 1737-1740; *Angew. Chem.* **2002**, *114*, 1808-1811.
[24] F. Dielmann, A. Schindler, S. Scheuermayer, J. Bai, R. Merkle, M. Zabel, A. V. Virovets, E. V. Peresypkina, G. Brunklaus , H. Eckert, M. Scheer, *Chem. Eur. J.* **2012**, *18*, 1168-1179.
[25] P. J. Sullivan, A. L. Rheingold, *Organometallics* **1982**, *1*, 1547-1549.
[26] O. J. Scherer, C. Blath, G. Wolmershäuser, *J. Organomet. Chem.* **1990**, *387*, C21-C24.
[27] For a detailed description of the dynamic coordination behavior in solution, see the supporting information.
[28] D. Li, H.-K. Yip, C.-M. Che, Z.-Y. Zhou, T. C. W. Mak, S.-T. Liu, *J. Chem. Soc., Dalton Trans.* **1992**, 2445-2449.
[29] A more detailed discussion of the DFT calculations is given in the supporting information.
[30] O. J. Scherer, T. Brück, G. Wolmershäuser, *Chem. Ber.* **1989**, *122*, 2049-2054.
[31] H. Krauss, G. Balázs, M. Bodensteiner, M. Scheer, *Chem. Sci.* **2010**, *1*, 337-342.

7.5 Supporting Information

Syntheses of the described compounds

General considerations

All manipulations were carried out under an inert atmosphere of dried nitrogen using standard Schlenk and drybox techniques. THF was dried with Na. MeCN, CH_2Cl_2 and CD_2Cl_2 were dried over CaH_2. NMR spectra were recorded in CD_2Cl_2 on a Bruker Avance 300 MHz NMR spectrometer (^{1}H: 300.132 MHz, ^{31}P: 121.495 MHz, ^{13}C: 75.468 MHz, ^{19}F: 282.404 MHz) or a Bruker Avance 400 MHz NMR spectrometer (^{1}H: 400.130 MHz, ^{31}P: 161.976 MHz, ^{13}C: 100.613 MHz, ^{11}B: 128.378 MHz). IR spectra were recorded as KBr discs using a Varian FTS-800 FT-IR spectrometer. Electron spray ionization mass spectra were recorded by the MS department of the University of Regensburg on a ThermoQuest Finnigan TSQ 7000 mass spectrometer. Elemental analyses were performed by the micro analytical laboratory of the University of Regensburg.

Preparation of $[Cu_3(\mu\text{-}Cl)_2(dpmp)_2]^+[BF_4]^-$ (**1**): 101 mg (2eq., 0.2 mmol) dpmp, 32 mg (1eq., 0.1 mmol) $[Cu(MeCN)_4][BF_4]$ and 20 mg (2eq., 0.2 mmol) CuCl were weighed into a Schlenk flask and 10 mL CH_2Cl_2 were added under constant stirring. The cloudy solution turns clear in the course of five minutes. After 24 hours of stirring at room temperature, this solution can either be used for further reaction with the desired P_n or As_n ligands or filtrated and layered with *n*-pentane. This affords colorless crystals in 73 % yield (99 mg). ^{1}H NMR (400 MHz, CD_2Cl_2) d 7.70 - 6.58 (m, 50H, Ph), 3.81 - 3.00 (multiple overlapping signals, CH_2); ^{31}P{^{1}H} NMR (162.0 MHz, CD_2Cl_2) d –6.54 (m, small signal), –11.17 (m, small signal), –14.30 (m, $RPPh_2$), –17.27 (br, R_2PPh); ^{11}B{^{1}H} NMR (128.4 MHz, CD_2Cl_2) d –0.95 ($^0BF_4$); ^{13}C{^{1}H} NMR (100.6 MHz, CD_2Cl_2) 133.65 - 127.49 (multiple signals, Ph), 28.16 (CH_2). IR(KBr) cm^{-1}:3072 (vw), 3052 (w), 3020 (vw), 2955 (vw), 2924 (vw), 2896 (vw), 2854 (vw), 1587 (vw), 1574 (vw), 1485 (m), 1436 (s), 1377 (m), 1333 (vw), 1310 (vw), 1278 (vw), 1189 (vw), 1159 (vw), 1099 (s), 1084 (m), 1065 (m), 1028 (m) 999 (m), 794 (m), 739 (s), 691 (s).

General preparation procedure of the compounds **2-5**: A solution of **1** was prepared as described above. After 24 hours of stirring the P_n or As_n ligand complex (0.1 mmol, 1eq.) was dissolved in a small amount of CH_2Cl_2 and added dropwise to this solution. This reaction was degassed five times and stirred for another 24 hours. Afterwards the solution was filtered and *n*-pentane diffusion into the solution afforded the crystalline products in a course of several days.

Isolation of $[Cu_3(\mu\text{-}Cl)_2(dpmp)_2\{(\mu_3,\eta^1{:}\eta^2{:}\eta^2\text{-}P_2)Mo_2(CO)_2Cp_2\}][BF_4]$ (**2**): 50 mg **A1** (1 eq., 0.1 mmol) added in a small amount of CH_2Cl_2 to a 1:1 stoichiometric solution of **1**. After 24 hours stirring, subsequent filtration and layering with *n*-pentane, compound **2** was isolated as orange to red plates in 51 % yield (95 mg, 0.051 mmol). ^{1}H NMR (300 MHz, CD_2Cl_2) d 7.70 - 6.55 (m, 50H, Ph), 5.11 (s, 9H, Cp), 3.63 (m, 3.5H, CH_2), 3.38 (m, 1H, CH_2), 3.10 (m, 3.5H, CH_2); ^{31}P{^{1}H} NMR (121.5 MHz, CD_2Cl_2) d –6.68 (br m, small signal), –11.35 (br m, small signal), –15.28 (m, $RPPh_2$), –19.72 (br, R_2PPh), –65.60 (s, P_2); ^{19}F NMR (282.4 MHz, CD_2Cl_2) d –148.75 ($^{10}BF_4$), –148.81 ($^{11}BF_4$); ^{13}C{^{1}H} NMR (75.5 MHz, CD_2Cl_2) 226.53 (CO), 134.61 - 128.15 (multiple signals, Ph), 87.52 (Cp), 30.48 (CH_2). Positive ion MS, *m/q* (%): 1273.2 (100) $[Cu_3Cl_2(dpmp)_2]^+$. Negative ion MS, *m/q* (%): 1447.3 (100) $[Cu_3Cl_2(dpmp)_2(BF_4)_2]^-$. IR(KBr) cm^{-1}: 3117 (vw), 3079 (vw), 3052 (w), 3005 (w), 2987 (w), 2954 (vw), 2917 (vw), 2851 (vw), 2000 (m), 1991 (m), 1965 (vs), 1925 (s), 1908 (s), 1848 (m), 1629 (w), 1485 (m), 1435 (s), 1377 (w), 1098 (s), 1084 (s). Anal. calcd for $Cu_3Cl_2(dpmp)_2\{Cp_2Mo_2(CO)_4P_2\}(BF_4)(CH_2Cl_2)_{0.3}$: C, 49.95; H, 3.67. Found: C, 49.98; H, 3.62.

Isolation of $[Cu_3(\mu\text{-}Cl)_2(dpmp)_2\{(\mu_3,\eta^1{:}\eta^2{:}\eta^2\text{-}As_2)Mo_2(CO)_2Cp_2\}][BF_4]$ (**3**): 59 mg **A2** (1 eq., 0.1 mmol) added in a small amount of CH_2Cl_2 to a 1:1 stoichiometric solution of **1**. After 24 hours stirring, subsequent filtration and layering with *n*-pentane, compound **3** was isolated as dark red blocks in 43 % yield (84 mg, 0.043 mmol). ^{1}H NMR (300 MHz, CD_2Cl_2) d 7.72 - 6.54 (m, 50H, Ph), 5.11 (s, 8H, Cp), 3.81 - 3.00 (multiple overlapping signals, CH_2); $^{31}P\{^1H\}$ NMR (121.5 MHz, CD_2Cl_2) d –7.12 (br m, small signal), –11.35 (br m, small signal), –14.53 (m, $RPPh_2$), –17.42 (br, R_2PPh); ^{19}F NMR (282.4 MHz, CD_2Cl_2) d –149.67 ($^{10}BF_4$), –149.73 ($^{11}BF_4$); $^{13}C\{^1H\}$ NMR (75.5 MHz, CD_2Cl_2), 131.05 - 126.25 (multiple signals, Ph), 84.99 (Cp). Positive ion MS, *m/q* (%): 1273.0 (100) $[Cu_3Cl_2(dpmp)_2]^+$, 1879.4 (0.55) $[Cu_4Cl_3(dpmp)_3]^+$, 1979.2 (0.25) $[Cu_5Cl_4(dpmp)_3]^+$. IR(KBr) cm^{-1}: 3081 (vw), 3053 (w), 2955 (vw), 2919 (vw) 2898 (vw), 2851 (vw), 1978 (w), 1954 (vs), 1913 (s), 1896 (s), 1630 (w), 1485 (w), 1435 (m), 1378 (w), 1098 (m), 1084 (m). Anal. calcd for $Cu_3Cl_2(dpmp)_2\{Cp_2Mo_2(CO)_4As_2\}(BF_4)(CH_2Cl_2)$: C, 46.74; H, 3.48. Found: C, 46.88; H, 3.65.

Isolation of $[Cu_3(\mu\text{-}Cl)_2(dpmp)_2\{(\mu_3,\eta^1{:}\eta^1{:}\eta^5\text{-}P_5)FeCp^*\}]_n[BF_4]_n$ (**4**): 35 mg **B1** (1 eq., 0.1 mmol) added in a small amount of CH_2Cl_2 to a 1:1 stoichiometric solution of **1**. After 24 hours stirring, subsequent filtration and layering with *n*-pentane, compound **4** was isolated as green rods in 47 % yield (81 mg, 0.047 mmol). ^{1}H NMR (300 MHz, CD_2Cl_2) d 7.72 - 6.55 (m, 50H, Ph), 3.81 - 3.01 (multiple overlapping signals, CH_2), 1.42 (s, 14H, Cp*); $^{31}P\{^1H\}$ NMR (121.5 MHz, CD_2Cl_2) d 149.91 (s, P_5), –6.92 (br m, small signal), –11.33 (br m, small signal), –14.62 (m, $RPPh_2$), –18.35 (br, R_2PPh); ^{19}F NMR (282.4 MHz, CD_2Cl_2) d –149.35 ($^{10}BF_4$), –149.40 ($^{11}BF_4$); $^{13}C\{^1H\}$ NMR (75.5 MHz, CD_2Cl_2) 134.84 - 128.31 (multiple signals, Ph), 91.82 (Cp*) 30.23 (CH_2), 11.06 (CH_3). Positive ion MS, *m/q* (%): 1272.9 (100) $[Cu_3Cl_2(dpmp)_2]^+$, 1782.3 (3.0) $[Cu_3Cl_2(dpmp)_3]^+$. Negative ion MS, *m/q* (%): 87.1 (100) $[BF_4]^-$. IR(KBr) cm^{-1}:3072 (vw), 3051 (w), 3017 (vw), 2954 (vw), 2908 (vw) 1436 (m), 1376 (w), 1124 (w), 1097 (w), 1084 (m), 1026 (w) 1000 (w), 791 (w), 738 (m), 690 (m), 669 (m). Anal. calcd for $Cu_3Cl_2(dpmp)_2\{Cp^*FeP_5\}(BF_4)(CH_2Cl_2)_{1.3}$: C, 49.76; H, 4.19. Found: C, 49.73; H, 4.26.

Isolation of $[Cu_3(\mu\text{-}Cl)_2(dpmp)_2\{(\mu_3,\eta^1{:}\eta^1{:}\eta^5\text{-}As_5)FeCp^*\}]_n[BF_4]_n$ (**5**): 57 mg **B2** (1 eq., 0.1 mmol) added in a small amount of CH_2Cl_2 to a 1:1 stoichiometric solution of **1** which resulted in an immediate color change from olive green color of complex **B2** to dark red. After 24 hours stirring, subsequent filtration and layering with *n*-pentane, compound 5 was isolated as brown blocks in 36 % yield (70 mg, 0.036 mmol). ^{1}H NMR (300 MHz, CD_2Cl_2) d 7.70 - 6.55 (m, 50H, Ph), 3.81 - 3.03 (multiple overlapping signals, CH_2), 1.37 (s, 13H, Cp*); $^{31}P\{^1H\}$ NMR (121.5 MHz, CD_2Cl_2) d –6.82 (br m, small signal), –11.34 (br m, small signal), –14.44 (m, $RPPh_2$), –17.25 (br, R_2PPh); ^{19}F NMR (282.4 MHz, CD_2Cl_2) d –149.36 ($^{10}BF_4$), –149.41 ($^{11}BF_4$); $^{13}C\{^1H\}$ NMR (75.5 MHz, CD_2Cl_2) 134.71 - 128.06 (multiple signals, Ph), 88.01 (Cp*) 30.32 (CH_2), 12.27 (CH_3). Positive ion MS, *m/q* (%): 2583.6, (20) $[Cu_6Cl_5(dpmp)_4]^+$; 1977.8, (10) $[Cu_5Cl_4(dpmp)_3]^+$; 1879.6, (5) $[Cu_4Cl_3(dpmp)_3]^+$; 1273.0, (100) $[Cu_3Cl_2(dpmp)_2]^+$; 665.1, (5) $[Cu_2Cl(dpmp)]^+$; 619.2, (17) $[Cu_3Cl(dpmp)_2]^{2+}$; 569.1, (3) $[Cu(dpmp)]^+$. Negative ion MS, *m/q* (%): 87.2, (100) $[BF_4]^-$. IR(KBr) cm^{-1}: 3072 (w), 3051 (m), 3019 (vw), 3005 (vw), 2986 (vw), 2952 (w), 2899 (w), 2360 (vw), 2342 (vw), 1625 (w), 1587 (w), 1574 (w), 1484 (m), 1435 (vs), 1375 (m), 1124 (m), 1098 (s), 1084 (vs), 1064 (s), 1026 (m), 999 (m). Anal. calcd for $Cu_3Cl_2(dpmp)_2\{Cp^*FeAs_5\}(BF_4)(CH_2Cl_2)$: C, 44.77; H, 3.76. Found: C, 44.80; H, 4.01.

Preparation of $[Cu_3(\mu\text{-}Cl)_2(dpmp)_2(MeCN)_2]^+[BF_4]^-$ (**6**): The literature reports of one structurally characterized related trinuclear Cu^I complex ($[Cu_3(\mu\text{-}Cl)_2(dpmp)_2(MeCN)_2]^+[ClO_4]^-\bullet H_2O$).[1] We were able to synthesize the same cationic complex with $[BF_4]^-$ as an anion. Therefore we followed a one-pot synthesis to obtain compound 1 with two terminal MeCN ligands.

101 mg (2eq., 0.2 mmol) dpmp, 32 mg (1eq., 0.1 mmol) $[Cu(MeCN)_4][BF_4]$ and 20 mg (2eq., 0.2 mmol) CuCl were weighed into a Schlenk flask and a solvent mixture of 8 mL THF and 2 mL MeCN were added under constant stirring. The compounds dissolved to form a clear and

colorless solution in about 30 to 60 seconds. After 24 hours of stirring at room temperature the solution was filtered vapor diffusion of Et_2O into the solution affords colorless crystal in the course of some days. The mother liquor is decanted off the crystals. The crystals are washed with Et_2O a few times and dried in vacuum for 30 minutes. After this time about 0.6 equivalents of the coordinated MeCN ligands could be removed from the crystals as indicated by elemental analysis. By grinding the sample and drying it in vacuum for another 2 hours, the MeCN could completely be removed. Yield 66% (95 mg). Sample dried for 30 minutes: Anal. calcd for $Cu_3Cl_2(dpmp)_2(MeCN)_{1.4}(BF_4)$: C, 56.55; H, 4.42; N, 1.38. Found: C, 56.55; H, 4.70; N, 1.35. Sample grinded and dried for 2 h: Anal. calcd for $Cu_3Cl_2(dpmp)_2(BF_4)$: C, 56.47; H, 4.29; N, 0.00. Found: C, 56.27; H, 4.35; N, 0.00. Positive ion MS, *m/q* (%): 1273.4 (100) $[Cu_3Cl_2(dpmp)_2]^+$, 1175.3 (7) $[Cu_2Cl_1(dpmp)_2]^+$, 669.0 (10) $[Cu_2Cl(dpmp)]^+$, 569.1 (8) $[Cu(dpmp)]^+$. Negative ion MS, *m/q* (%): 87.1 (100) $[BF_4]^-$. IR(KBr) cm^{-1}: 3052 (w), 2956 (vw), 2895 (vw), 1587 (vw), 1574 (vw), 1485 (m), 1436 (s), 1377 (m), 1333 (vw), 1309 (vw), 1278 (vw), 1189 (vw), 1159 (vw), 1099 (s), 1084 (s), 1028 (m) 1000 (m), 793 (m), 738 (s), 691 (s).

Dynamic coordination behavior of the parent $[Cu_3]$ building block (**1**): The parent compound $[Cu_3(\mu\text{-}Cl)_2(dpmp)_2]^+[BF_4]^-$ (**1**) is prepared in a straightforward manner by dissolving two equivalents dpmp and CuCl together with one equivalent of $[Cu(MeCN)_4][BF_4]$. The use of MeCN/THF (1:5) mixtures as solvent afforded the desired building block **1** with terminal MeCN ligands $[Cu_3(\mu\text{-}Cl)_2(dpmp)_2(MeCN)_2]^+[BF_4]^-$ (**6**) (see Figure 1 for a representation of the solid state structure). A related compound $[Cu_3(\mu\text{-}Cl)_2(dpmp)_2(MeCN)_2]^+[ClO_4]^-\bullet H_2O$ was described in the literature before, following a different synthetic approach.[1] When the substitution of the labile MeCN ligands by our P_n or As_n ligand complexes was tried in MeCN/THF mixtures we could never observe any coordination to the Cu ions.

Therefore, we prepared the parent compound **1** in pure CH_2Cl_2 without THF or MeCN addition. After stirring CuCl, dpmp and $[Cu(MeCN)_4][BF_4]$ in CH_2Cl_2 and subsequent vapor diffusion of *n*-pentane into the solution, we were able to isolate the parent cationic building block $[Cu_3(\mu\text{-}Cl)_2(dpmp)_2]^+[BF_4]^-$ (**1**) without MeCN ligands. This was an astonishing result, since the central cationic cluster $[Cu_3(\mu\text{-}Cl)_2(dpmp)_2]^+$ is still intact, but is now also exhibiting two vacant coordination sites on the outer Cu ions. Consequently, we performed our following coordination chemistry only in CH_2Cl_2 solution.

When crystals of the pure $[Cu_3(\mu\text{-}Cl)_2(dpmp)_2]^+$ building block (=$[Cu_3]$) are dissolved in CD_2Cl_2 at –80 °C the $[Cu_3]$ cluster remains intact and two broad signals can be identified in the $^{31}P\{^1H\}$ NMR spectrum at –15.3 ppm and at –17.4 ppm in a 2:1 ratio for the dpmp ligand. The ^1H NMR spectrum at –80 °C shows next to the aromatic protons of the phenyl rings two broad signals at 3.06 ppm and at 3.58 ppm for the diastereotopic atoms of the methylene groups of the bridging dpmp ligands. When the solution is warmed up in the NMR spectrometer the $[Cu_3]$ cluster seems to show some dynamic behavior above –20 °C which can be monitored by new signals arising next to the ones of the $[Cu_3]$ cluster which is still the major part in solution even at room temperature. When the same solution is cooled down again, the ^1H and the $^{31}P\{^1H\}$ NMR spectra do not change and do not show the initial signals for the pure $[Cu_3]$ cluster. Thus, we assume a dynamic coordination behavior that needs some thermal energy for breaking the dative Cu–P bonds and cooling down the solution of the dissociated compounds will not reverse the process to form the desired coordination complexes. This formation can be realized during the crystallization process by the addition of the investigated P_n and As_n ligand complexes to the $[Cu_3]$ building block in CH_2Cl_2 and subsequent vapor diffusion of *n*-pentane into the solution. This affords the desired coordination complexes formed from the $[Cu_3]$ cluster coordinated by the P or As atoms of the E_n ligands. The ^1H NMR spectra of the isolated products in CD_2Cl_2 at room temperature show the same set of signals as the pure $[Cu_3]$ building block and an additional singlet for the Cp rings of $[Cp_2Mo_2(CO)_4(\mu,\eta^2\text{:}\eta^2\text{-}E_2)]$ (E = P(**A1**), As(**A2**)) or the Cp* ring of $[Cp^*Fe(\eta^5\text{-}E_5)]$ (E = P(**B1**),

As(**B2**)). The $^{31}P\{^1H\}$ NMR spectrum of complex **2** additionally shows a singlet at –65.6 ppm for the P_2 ligand **A1** which is shifted 21 ppm upfield compared to the free complex **1**. The $^{31}P\{^1H\}$ NMR spectrum of the one-dimensional coordination polymer **4** also shows a singlet at 149.9 ppm for the P_5 ring of complex **B1** which is shifted **3** ppm upfield compared to the free ligand **B1**. The observed singlets for the P_n ligands in the $^{31}P\{^1H\}$ NMR spectra of the products **2** and **4** show that the P atoms are equivalent on the NMR timescale and show a dynamic behavior.

All isolated compounds (**1-6**) always exhibit the cationic building block $[Cu_3(\mu\text{-}Cl)_2(dpmp)_2]^+$ and we never saw any other combination of Cu^+ and the dpmp ligand in the solid state. The ^1H NMR as well as the ^{31}P NMR spectra of isolated crystals of the compounds **1-5** dissolved in CD_2Cl_2 at room temperature show a dynamic coordination behavior and suggest that the well-defined arrangement of the described coordination units in the solid state structures are formed during the crystallization process. From these observations we can conclude, that the $[Cu_3(\mu\text{-}Cl)_2(dpmp)_2]^+$ building block is a very stable aggregate, since it is exclusively observed in the solid state, but in solution different Cu^+ species with dpmp and Cl^- ligands are in equilibrium.

X-ray Crystallography

All crystal preparations were done under mineral oil. The data collection was either performed on an Agilent Technologies SuperNova diffractometer equipped with a micro focus Cu X-ray source, an Agilent Technologies Gemini R Ultra equipped with sealed tube Mo and Cu X-ray sources or on a Bruker Apex II difractometer equipped with a Mo X-ray source. All measurements were performed at 150 K or at 123 K by nitrogen cooling. The structure least square refinement was done with the SHELX program package[2] against F^2.

Table 1. Crystallographic details for the compounds **1-3**.

Identification code	**1**	**2**	**3**
Empirical formula	$C_{66}H_{62}BCl_6Cu_3F_4P_6$	$C_{80}H_{72}BCl_6Cu_3F_4Mo_2O_4P_8$	$C_{80}H_{72}As_2BCl_6Cu_3F_4Mo_2O_4P_6$
M [gmol^{-1}]	1531.14	2027.18	2115.08
Crystal size [mm]	0.18 × 0.13 × 0.04	0.17 × 0.10 × 0.02	0.27 × 0.14 × 0.03
T [K]	123(1)	123(1)	123(1)
λ [Å]	1.54178	1.54178	1.54178
crystal system	monoclinic	monoclinic	monoclinic
space group	$P2_1/n$	$P2_1/c$	$P2_1/c$
a [Å]	12.4596(1)	12.8855(1)	12.8880(2)
b [Å]	27.6079(2)	43.5442(4)	43.5784(5)
c [Å]	20.0624(2)	14.9499(1)	15.0001(2)
α [°]	90	90	90
β [°]	104.466(1)	95.216(1)	95.152(2)
γ [°]	90	90	90
V [Å^3]	6682.34(10)	8353.49(12)	8390.6(2)
Z	4	4	4
ρ_{calc} [gcm^{-3}]	1.522	1.612	1.674
μ [mm^{-1}]	5.096	6.923	7.403
diffractometer	SuperNova	SuperNova	SuperNova
radiation	CuK_α	CuK_α	CuK_α
θ range [°]	3.20 – 70.07	3.14 – 73.67	3.13 – 66.59
absorption correct.	analytical	analytical	analytical
T_{min} / T_{max}	0.548 / 0.832	0.515 / 0.887	0.262 / 0.791
reflns collect / unique	38396 / 12632	60821 / 16362	62003 / 14787
reflns obs [$I > 2\,\sigma(I)$]	10855	15012	12776
R_{int}	0.0236	0.0462	0.0513
parameters / restraints	781 / 0	1055 / 110	1078 / 103
GOF on F^2	1.123	1.065	1.037
R_1 / wR_2 [$I > 2\,\sigma(I)$]	0.0299 / 0.0869	0.0506 / 0.1293	0.0465 / 0.1178
R_1 / wR_2 (all data)	0.0369 / 0.0950	0.0548 / 0.1315	0.0534 / 0.1214
max / min $\Delta\rho$ [eÅ^{-3}]	0.866 / –0.764	1.732 / –1.124	0.784 / –1.024

Table 2. Crystallographic details for the compounds **4-6**.

Identification code	**4**	**5**	**6**
Empirical formula	$C_{74}H_{73}BCl_2Cu_3F_4FeP_{11}$	$C_{76}H_{77}As_5BCl_6Cu_3F_4FeP_6$	$C_{68}H_{64}BCl_2Cu_3F_4N_2P_6$
M [gmol^{-1}]	1707.21	2096.81	1443.39
Crystal size [mm]	0.43 × 0.17 × 0.11	0.13 × 0.11 × 0.06	0.60 × 0.45 × 0.33
T [K]	123(1)	123(1)	150(1)
λ [Å]	0.71073	1.54178	0.71073
crystal system	monoclinic	monoclinic	triclinic
space group	$P2_1/c$	$P2_1/c$	P–1
a [Å]	12.5098(3)	12.5858(1)	12.7414(4)
b [Å]	25.2944(6)	24.4849(2)	13.4211(4)
c [Å]	27.8308(5)	27.9362(2)	21.4040(7)
α [°]	90	90	85.562(3)
β [°]	97.692(2)	98.748(1)	72.949(3)
γ [°]	90	90	79.079(3)
V [Å^3]	8727.2(3)	8508.73(12)	3435.0(2)
Z	4	4	2
ρ_{calc} [gcm^{-3}]	1.299	1.637	1.395
μ [mm^{-1}]	1.443	7.545	1.190
diffractometer	Gemini R Ultra	Gemini R Ultra	Bruker Apex II
radiation	MoK_α	CuK_α	MoK_α
θ range [°]	3.04 – 27.10	3.20 – 66.64	2.49 – 27.38
absorption correct.	analytical	analytical	multi-scan
T_{min} / T_{max}	0.705 / 0.878	0.541 / 0.792	0.6342 / 0.7456
reflns collect / unique	64795 / 19018	61670 / 14620	24359 / 15299
reflns obs [$I > 2\ \sigma(I)$]	13117	10588	10562
R_{int}	0.0283	0.0337	0.0418
parameters / restraints	890 / 48	924 / 0	807 / 266
GOF on F^2	1.046	0.960	1.026
R_1 / wR_2 [$I > 2\ \sigma(I)$]	0.0384 / 0.1220	0.0379 / 0.1016	0.0539 / 0.1417
R_1 / wR_2 (all data)	0.0559 / 0.1272	0.0549 / 0.1065	0.0831 / 0.1549
max / min $\Delta\rho$ [eÅ^{-3}]	0.930 / –0.541	1.234 / –1.191	2.045 / –2.093

Structure refinement details

compound **1**: The asymmetric unit contains one cationic [Cu_3] coordination unit, consisting of three Cu, two Cl atoms and two dpmp ligands as well as the $[BF_4]^-$ anion and two CH_2Cl_2 solvent molecules. The structure solution and refinement could be done without difficulty.

compound **2**: The asymmetric unit contains one unit of the coordination compound **2** consisting of the cationic [Cu_3] complex of two dpmp ligands, three Cu and two Cl atoms coordinated to a P atom of the Mo complex **A1**. It also contains a $[BF_4]^-$ anion and two CH_2Cl_2 molecules. The solvent molecules are disordered over two positions (50:50) or three positions (49:28:23). The anion is disordered over two positions (67:33) and the minor part is refined isotropically. During the refinement process the tetrahedral geometry of the anion was restrained by SADI commands and several DFIX commands and some EADP constraints were applied to the disordered solvent molecules.

compound **3**: The asymmetric unit contains one [Cu_3] coordination unit, consisting of three Cu, two Cl atoms and two dpmp ligands coordinated to one As_2 ligand complex **A2**, two disordered CH_2Cl_2 solvent molecules and one $[BF_4]^-$ anion. One phenyl ring of the dpmp ligand is disordered over two positions with a ratio of 61 % to 39 %. The two solvent molecules are disordered over two or three positions, respectively with the occupancies of 54:46 and 50:25:25. SADI restraints as well as EADP constraints were used for the refinement of the solvent molecules.

compound **4**: With the aid of PLATON a solvent accessible area was found. The residual difference Fourier peaks exhibit a geometrical environment resembling the molecular geometry of

CH_2Cl_2 molecules. Unfortunately, the refinement of disordered (and restrained) CH_2Cl_2 molecules did not lead to a satisfactory structure solution. Therefore we treated the residual electron density with the program SQUEEZE[3] which showed a solvent accessible void. The midpoint, the size and the number of electrons in that void were refined and the contribution to the calculated structure factors of the disordered solvent is taken into account by back-Fourier transformation. The void is found around (0 0.5 0), the size is 779 A^3, and 172 e^- were detected. This electron number corresponds roughly to four CH_2Cl_2 molecules. These four CH_2Cl_2 molecules are not taken into account for the empirical formula and the calculated density, but for the analytical absorption correction and the given absorption coefficient. The disordered $[BF_4]^-$ anion was restrained with SADI commands to form a tetrahedron. Several disordered phenyl rings were fixed using the AFIX 66 command. Otherwise, the refinement was not stable or the resulting C-C bonds did not show physically correct lengths.

compound **5**: The asymmetric unit contains one cationic $[Cu_3]$ coordination unit, consisting of three Cu, two Cl atoms and two dpmp ligands coordinated to one *cyclo*-As_5 sandwich complex **B2** as well as the $[BF_4]^-$ anion and two CH_2Cl_2 solvent molecules. The structure solution and refinement could be done without difficulty.

compound **6**:

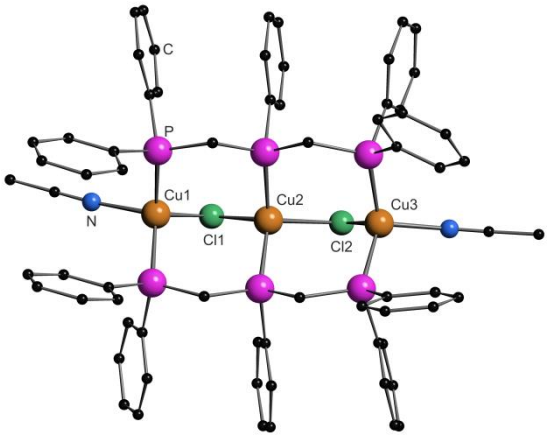

Figure 1. Crystal structure of compound **6**. The $[BF_4]^-$ anion, hydrogen atoms and solvent molecules are omitted for clarity. Selected bond lengths [Å] and angles [°]: Cu1-Cu2 3.230(6), Cu2-Cu3 3.3239(6), Cu1-Cl1 2.3333(11), Cu2-Cl1 2.4282(10), Cu2-Cl2 2.3862(10), Cu3-Cl2 2.3612(11), Cu1–N1 2.143(4), Cu3–N3 2.065(4), Cu1-Cu2-Cu3 164.73(2).

Figure 1 shows a representation of the cationic complex in compound **6** in the solid state. The geometry of the coordination compound is in good agreement with the formerly described complex $[Cu_3(\mu\text{-}Cl)_2(dpmp)_2(MeCN)_2]^+[ClO_4]^-\bullet H_2O$.[1] The intramolecular Cu-Cu distances are distinctly elongated compared to the novel $[Cu_3]$ coordination unit of compound **1** with vacant coordination sites on the external Cu cations.

structure solution: With the aid of PLATON a solvent accessible area was found, but it was impossible to refine any reasonable molecule from difference Fourier peaks. Therefore the midpoint, the size and the number of electrons in that void were refined and the contribution to the calculated structure factors of the disordered solvent is taken into account by back-Fourier transformation with the program SQUEEZE[3] The void is found around (–0.192 0.052 0.173), the size is 133 A^3 and 45 e^- were detected. The void most likely contains one THF molecule. The geometry of the disordered phenyl rings on the dpmp ligand was fixed to regular hexagons (AFIX 66). The displacement parameters of these carbon atoms were restrained by ISOR commands. Otherwise, the refinement was not stable or the resulting C-C bonds did not show physically correct lengths.

DFT calculations

The results of the calculation concerning the Cu-Cu distances in 1 will presented in the following chapter. Details of the DFT calculations of this chapter are included in electronic form on the provided DVD.

References

[1] D. Li, H.-K. Yip, C.-M. Che, Z.-Y. Zhou, T. C. W. Mak, S.-T. Liu, *J. Chem. Soc., Dalton Trans.,* **1992**, 2445-2449.
[2] G. M. Sheldrick, *Acta Cryst. A*, **2008**, *64*, 112-122.
[3] a) A. Spek, *J. Appl. Cryst.,* **2003**, *36*, 7-13; b) P. van der Sluis, A. Spek, *Acta Cryst.*, **1990**, *A46*, 194-201.

Preface

The following chapter has recently been submitted for publication.

Authors

Martin Fleischmann, Luis Dütsch, Mehdi Elsayed Moussa, Gábor Balász, Christophe Lescop* and Manfred Scheer*

Author contributions

The preparation and characterization of all compounds including the single crystal X-ray structure determination and the preparation of the manuscript was done by the first author. Luis Dütsch prepared and described some of the presented compounds in his Bachelor's thesis which was written under the supervision of Martin Fleischmann and Manfred Scheer. Mehdi Elsayed Moussa prepared the polyphosphine ligand dpmp and supported the work with helpful advice. Gábor Balázs performed supporting DFT calculations and supported the work with helpful advice. Christophe Lescop and Manfred Scheer supervised the research and revised the manuscript.

Acknowledgements

This work was supported by the Deutsche Forschungsgemeinschaft and the European Research Council (ERC) (Projekt SELFPHOS AdG-2013-339072). The COST action CM1302 SIPs is gratefully acknowledged. This work was supported by the Ministère de l'Enseignement Supérieur et de la Recherche and the CNRS.

8 Self-assembly of reactive linear Cu_3 building blocks for supramolecular coordination chemistry and their reactivity towards E_n ligand complexes

Abstract: The current study describes the selective and easy one-pot synthesis of linear trinuclear halide bridged Cu^I complexes $[Cu_3(\mu\text{-}X)_2(\mu\text{-dpmp})_2(MeCN)_2]^+$ (**1a**: X = Cl; **1b**: X = Br; **1c**: X = I), stabilized by the tridentate dpmp ligand, and two terminally coordinated MeCN ligands obtained by self-assembly reaction in THF/MeCN. By drying these complexes the MeCN ligands can be removed and the complexes are directly transformed to the reactive parent trinuclear $[Cu_3(\mu\text{-}X)_2(\mu\text{-dpmp})_2]^+$ (**2a-c**) building blocks with two vacant coordination sites on the terminal Cu atoms. An alternative synthesis in CH_2Cl_2 directly yields **2a-c**. In the course of this srudy two related isomeric compound **2a*** and **2c*** as well as two complexes containing two weakly coordinating CH_2Cl_2 molecules $[Cu_3(\mu\text{-}X)_2(\mu\text{-dpmp})_2(CH_2Cl_2)_2]^+$ (X = Br(**3b**), I(**3c**)) could be structurally characterized. The frameworks of the $[Cu_3(\mu\text{-}X)_2(\mu\text{-dpmp})_2]^+$ complex cations are stable in solution when dissolved at low temperatures and show dynamic coordination behavior at elevated temperatures involving equilibria between different species as proved by new signals arising in VT NMR studies. These equilibria cannot be shifted back by simply decreasing the temperature but the $[Cu_3(\mu\text{-}X)_2(\mu\text{-dpmp})_2]^+$ (X = Cl, Br, I) complex cations can be obtained selectively in the solid state upon crystallization. While reactions of **2a-c** with the E_2 complexes **A1** and **A2** lead to unsymmetrically substituted $[Cu_3(\mu\text{-}X)_2(\mu\text{-dpmp})_2(\eta^1\text{-}L)]^+$ (**4a-c**: X = Cl-I, L = **A1**; **5**: X = Cl, L = **A2**) complexes, the reactions with the *cyclo*-P_3 complex **B** afford zigzag chain polymers $[Cu_3(\mu\text{-}X)_2(\mu\text{-dpmp})_2(\mu,\eta^1\text{:}\eta^1\text{-}\mathbf{B})]_n[BF_4]_n$ (**6a**: X = Cl; **6b**: X = Br) and the symmetrically substituted complex $[Cu_3(\mu\text{-}I)_2(\mu\text{-dpmp})_2(\eta^1\text{-}\mathbf{B})_2]^+$ (**7**). Reactions of **2a-c** with the *cyclo*-E_5 complexes **C1** and **C2** lead to the isolation of the one-dimensional coordination polymers $[Cu_3(\mu\text{-}X)_2(\mu\text{-dpmp})_2(\mu,\eta^1\text{:}\eta^1\text{-}L)]_n[BF_4]_n$ (**8a-b**: X = Cl-Br, L = **C1**; **9**: X = Cl, L = **C2**) and the symmetrically substituted complex $[Cu_3(\mu\text{-}I)_2(\mu\text{-dpmp})_2(\eta^1\text{-}\mathbf{C1})_2]^+$ (**10**). All products exhibit the trinuclear $[Cu_3(\mu\text{-}X)_2(\mu\text{-dpmp})_2]^+$ complex cations as the central structural motif. The variation of the intramolecular Cu-Cu distances inside the Cu_3 complexes is discussed and supporting DFT computations for the model complex $[Cu_3(\mu\text{-}Cl)_2(dmmp)_2\{(\eta^1\text{-}\mathbf{A1})\}]^+$ (**4a'**) are presented.

8.1 Introduction

Extended linear arrays of transition metals are currently discussed for their potential application in molecular electronics. Some examples include self-aggregation of

dinuclear precursor complexes via intermolecular M–M bond formation (M = Pd,[1,2] Pt,[3,4,5] Rh,[6,7,8,9,10,11] Ir[12,13]). These linear metal chains however feature various supporting ligands (see Scheme 1). The most famous and thoroughly studied group of extended metal atom chains (EMACs) includes up to eleven metal atoms (homo- or heterometallic) in one linear array containing polypyridylamide ligands or their derivatives (Scheme 1 **I**).[14,15,16,17,18,19,20,21,22,23] Molecular chains of Pd atoms can be stabilized by neutral unsaturated or aromatic organic ligands (Scheme 1 **II**).[24,25,26,27,28,29,30,31] Polydentate phosphines like the tridentate ligand bis(diphenylphosphinomethyl)-phenylphosphine (dpmp, see Scheme 2) can also stabilize multimetallic complexes. Especially their Au^{I} complexes have been thoroughly investigated due to their luminescent properties.[32,33,34,35,36,37,38] Complexes of the dpmp ligand have also been described for different metals like Ag,[39] Rh[40] and Pt[41,42,43,44,45] including the formation of a hexanuclear Pt string complex.[46] It was recently reported that the luminescence intensity of heterometallic Ag^{I}/Au^{I} complexes stabilized by polyphosphine ligands increases with increasing gold content.[47] Utilization of the analogues tetraphosphine ligand gave access to heterometallic trinuclear complexes[48] as well as linear chains of four M^{+} (M = Ag, Au) cations (Scheme 1 **III**)[49,50] and multinuclear complexes of up to eight metal centers.[51,52,53] Recently, it was demonstrated that hydride bridged Cu^{I} complexes stabilized by tetraphosphine ligands undergo facile CO_2 insertion.[54] In 1992, the preparation of the trinuclear halide bridged Cu^{I} complexes $[Cu_3(\mu\text{-}X)_2(\mu\text{-dpmp})_2(MeCN)_2]^{+}$ (X = Cl, I) was described (Scheme 1 **IV**).[55] Although the intermolecular Cu-Cu distances of 3.3 Å do not suggest metal-metal interactions these complexes exhibit photoluminescence in the solid state and may be valuable building blocks in supramolecular chemistry. In 2009 the analogues tetranuclear complexes have also been prepared.[56]

The main challenges in the chemistry of molecular metal chains lies in the development of rational synthetic methods based on self-assembly which lead to linear metal arrays instead of polyhedral clusters or product mixtures. Another intriguing goal is the introduction of additional ligands of varying nature on the terminal metal atoms in order to form heteroleptic linear metal clusters or extended coordination polymers in a controllable manner. In this context, the current investigation includes the introduction of the organometallic E_n ligand complexes **A1-C2** (see Scheme 2) which contain substituent free pnictogen atoms (E = P, As), instead of more commonly used organic linker molecules with N, O or S donor atoms.

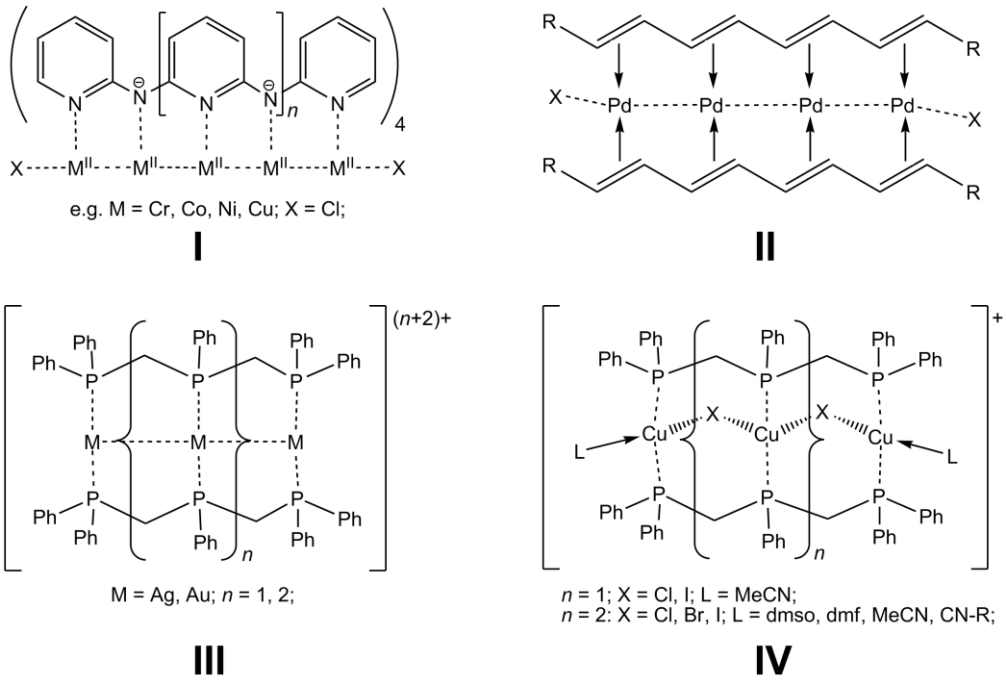

Scheme 1. (**I**) Model complexes of linear transition metal arrays supported by polypyridylamide ligands; (**II**) Pd chains sandwiched by conjugated polyene molecules. (**III**) Polymetallic Ag^{+} and Au^{+} clusters stabilized by polyphosphine ligands; (**IV**) Multinuclear Cu^{I} chains stabilized by polyphosphine ligands and bridging halides.

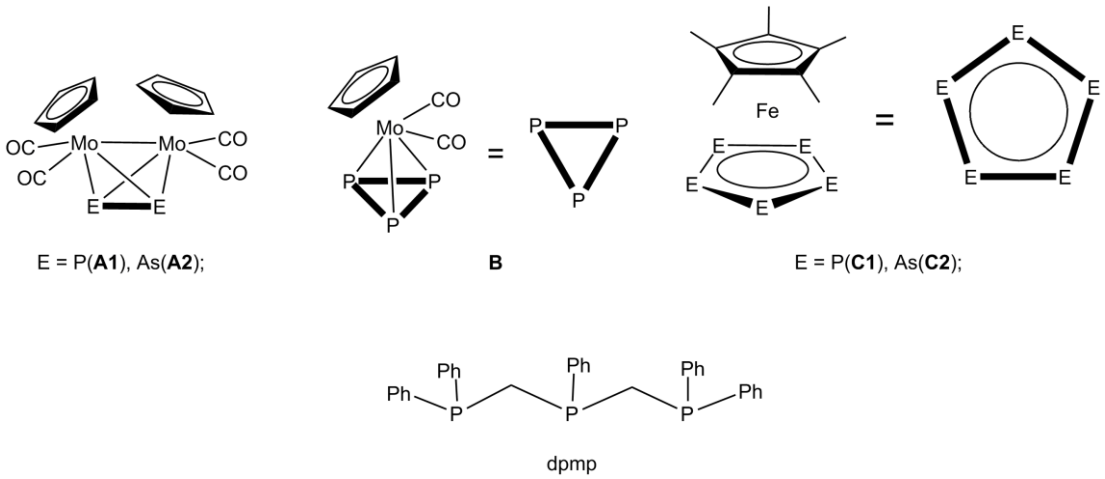

Scheme 2. Illustration of the used E_n ligand complexes **A1**-**C2** and the polyphosphine ligand dpmp.

It was shown that these E_n ligand complexes are excellent multidentate ligands for supramolecular chemistry allowing a broad variety of possible coordination modes. Reactions of the *cyclo*-P_5 complex **C1** with Cu^{I} halides result in the formation of coordination polymers[57,58] and spherical supramolecules which are referred to as 'inorganic fullerenes' due to their analogues topology.[59,60,61,62,63,64] When $[Cp^{R}Fe(\eta^5\text{-}P_5)]$ complexes with sterically demanding Cp ligands (Cp^{Bn} = $C_5(CH_2Ph)_5$,[65] Cp^{BIG} = $C_5(4\text{-}^{n}Bu\text{-}C_6H_4)_5$)[66] are reacted with Cu^{I} halides, well-soluble and very large supramolecules are obtained.[67,68,69,70] The P_2 complex **A1** readily forms homoleptic

dinuclear complexes $[M_2(\mathbf{A1})_4]^{2+}$ with the monovalent coinage metal cations M^+ (M = Cu, Ag, Au) which exhibit dynamic coordination behavior in solution.[71] Addition of organic linker molecules to solutions of these complexes gives access to heteroleptic organometallic-organic hybrid materials forming polymers, extended frameworks or isolated rectangles.[72,73] Additionally, it was demonstrated that introduction of **A1** to di- and trinuclear Cu^{I} complexes containing bridging mixed P,N ligands or polyphosphine ligands affords original coordination modes for **A1** without collapse of the pre-assembled multimetallic fragments.[74] Introduction of the weakly coordinating anion $[Al\{OC(CF_3)_3\}_4]^-$ enables the isolation and characterization of a variety of compounds showing highly dynamic coordination behavior of E_n ligand complexes towards the Lewis acidic cations Cu^+,[75] Ag^+,[76,77] Tl^+,[78,79,80] In^+[80,81] and Ga^+.[79]

The current study focuses on trinuclear Cu^{I} complexes (see Scheme 1 **IV**) stabilized by the tridentate phosphine ligand dpmp (see Scheme 2) and their reactivity. Herein we describe a simple straightforward synthesis of the trinuclear $[Cu_3(\mu\text{-}X)_2(\mu\text{-}dpmp)_2(MeCN)_2]^+$ (X = Cl, Br, I) cationic complexes **1a-c** containing terminal MeCN ligands. It is shown that the terminal MeCN ligands can be removed and these derivatives can easily be transformed to $[Cu_3(\mu\text{-}X)_2(\mu\text{-}dpmp)_2]^+$ **2a-c** cationic units exhibiting two vacant terminal coordination sites. Additionally, a direct synthesis of **2a-c** will be presented. These reactive trinuclear complexes are investigated by VT NMR experiments to get more insight into the existing species in solution. Subsequently, the coordination chemistry of the E_n ligand complexes **A1-C2** towards the parent trinuclear complexes is investigated. The results of this study which have been partly reported in a preliminary communication,[82] give access to a rational synthesis of discrete and infinite supramolecular compounds containing the linear parent trinuclear Cu^{I} building blocks $[Cu_3(\mu\text{-}X)_2(\mu\text{-}dpmp)_2]^+$, as well as the possibility of a direct comparison of the coordination behavior of P_n and their analogues As_n ligand complexes.

8.2 Results and Discussion

The parent Cu_3 complexes

Syntheses of 1a-c:

The $[Cu_3(\mu\text{-}Cl)_2(dpmp)_2(MeCN)_2]^+$ complex cation was previously prepared as the $[ClO_4]^-$ salt after recrystallization of the crude product obtained from heating dpmp and CuCl in MeOH at 60°C and subsequent metathesis with $LiClO_4$.[55] Herein we present a simple synthesis (see Scheme 3) based on self-assembly under mild conditions to yield the trinuclear complexes $[Cu_3(\mu\text{-}X)_2(\mu\text{-}dpmp)_2(MeCN)_2]^+$ (X = Cl(**1a**), Br(**1b**), I(**1c**))

as $[BF_4]^-$ salts as the only products in good yields (65-80%). Dissolution of 2 equiv. CuX (X = Cl, Br, I), 2 equiv. dpmp and 1 equiv. $[Cu(MeCN)_4][BF_4]$ in a THF/MeCN (80:20) mixture affords clear colorless solutions in a few minutes. Diffusion of Et_2O into the filtered solutions affords colorless single crystals which were used to establish the X-ray structures of **1a-c**. Elemental analysis reveals complete removal of the terminal MeCN ligands upon drying in vacuum overnight already at room temperature. This gives access to the parent complexes $[Cu_3(\mu\text{-}X)_2(\mu\text{-dpmp})_2]^+$ (X = Cl(**2a**), Br(**2b**), I(**2c**)) as colorless powders in the solid state. Our investigations revealed an increased reactivity of **2a-c** compared to **1a-c** as the relatively weak E_n ligand complexes were not able to substitute the terminal MeCN ligands of **1a-c** in THF/MeCN solutions. Therefore, we subsequently developed a direct synthesis of **2a-c** in CH_2Cl_2.

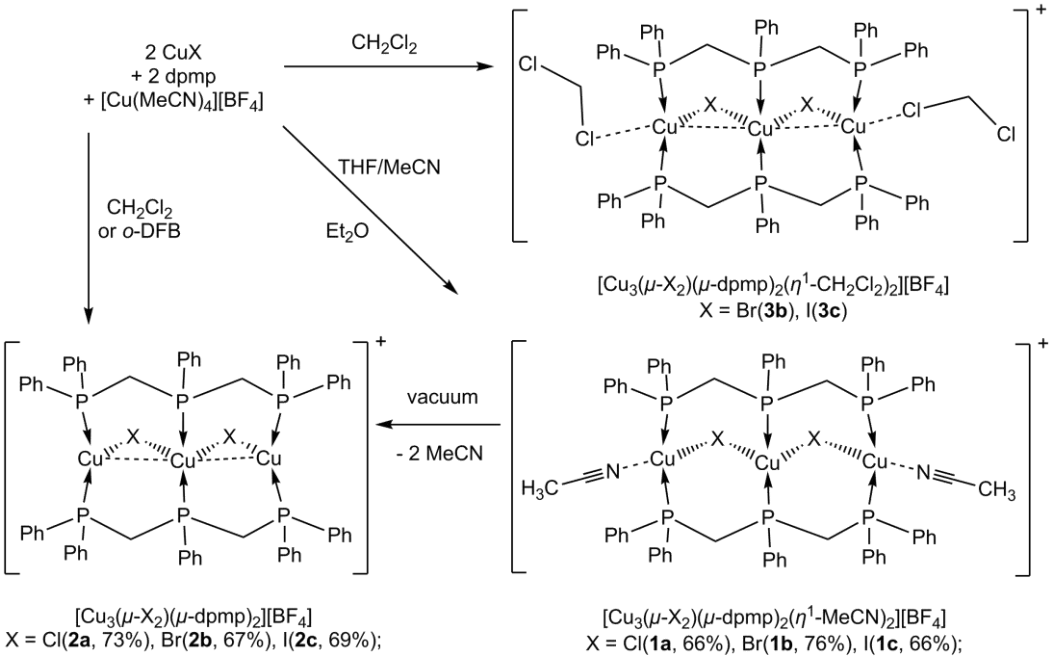

Scheme 3. Syntheses of the trinuclear complexes **1a-c**, containing terminal MeCN ligands, the parent complexes **2a-c** as well as the complexes **3b** and **3c** containing two coordinating CH_2Cl_2 solvent molecules. Yields are given in parentheses.

Direct synthesis of 2a-c:

When the reactants (2 equiv. CuX (X = Cl, Br, I), 2 equiv. dpmp and 1 equiv. $[Cu(MeCN)_4][BF_4]$) are suspended in pure CH_2Cl_2 or *ortho*-difluorobenzene (*o*-DFB) and stirred at room temperature, the formation of clear colorless solutions can be observed after 5 min (X = Cl), 30 min (X = Br) or 5-6 h (X = I). Subsequent diffusion of alkanes into the filtered solution yields the parent trinuclear complexes $[Cu_3(\mu\text{-}X)_2(\mu\text{-dpmp})_2]^+$ (X = Cl(**2a**), Br(**2b**), I(**2c**)) as colorless crystals in good yields (65-75%).[83] Additionally, $[Cu_3(\mu\text{-}X)_2(\mu\text{-dpmp})_2(CH_2Cl_2)_2]^+$ (X = Br(**3b**), I(**3c**)) (identified by single crystal X-ray

structural analysis) which show two terminal η^1-coordinating CH_2Cl_2 molecules could also be observed from these reactions.[84] These CH_2Cl_2 solvent molecules are removed by drying the crystals.

X-ray structural analysis of 1a-3c:

Single crystal X-ray diffraction analysis (see Figure 1a) clearly reveals that monocationic **1a-c** bearing $[BF_4]^-$ as counter ions show very similar structures of their central trinuclear Cu^{I} complexes $[Cu_3(\mu\text{-}X)_2(\mu\text{-dpmp})_2(MeCN)_2]^+$.[85] These discrete alignments of three Cu^{I} centers are stabilized by two bridging dpmp ligands and two additional bridging halide anions in the molecular backbone. The coordination environment of all Cu atoms in **1a-c** can be described as distorted tetrahedral. The distance of the MeCN ligands towards the terminal Cu atoms are very similar for **1a-c** with ~2.06 Å except for N1-Cu1 in **1a** which is slightly longer with 2.1425(1) Å. The intramolecular Cu-Cu distances in the MeCN ligated complexes **1a-c** are too long for d^{10}-d^{10} metallophilic interactions (3.2330(1) Å - 3.4388(1) Å) and increase with the size of the halides from **1a-c**. The Cu_3 chains can be viewed as almost linear with Cu-Cu-Cu angles between 163° to 165°.

The parent compounds $[Cu_3(\mu\text{-}X)_2(\mu\text{-dpmp})_2]^+$ **2a-c** are obtained either by removal of the terminal MeCN ligands from **1a-c**, or from the direct synthesis in CH_2Cl_2 solutions. In the latter case two different isomers of the central Cu_3 building blocks $[Cu_3(\mu\text{-}X)_2(\mu\text{-dpmp})_2]^+$ can be present (**2a-c** and **2a*-c***, respectively) related to each other by a slightly different configuration of one dpmp ligand. Among the six possible isomers four of them could be structurally characterized during this study, **2a**, **2a***, **2b** and **2c*** which will be discussed together.[86] It has to be noted, that for all compounds containing any terminal ligands only one isomer of the parent Cu_3 building blocks (corresponding to **2a-c**) is observed. The crystal structures of **2a**, **2b** and **2c*** are depicted Figure 1b while **2a*** is shown in Figure 2a. The removal of the terminal MeCN ligands of **1a-b** results in a drastic shortening of the intramolecular Cu-Cu distances in **2a** (2.7827(5) - 2.8244(4) Å) and **2b** (2.8470(1) - 2.8995(1) Å), while the general arrangement of the central $[Cu_3(\mu\text{-}X)_2(\mu\text{-dpmp})_2]^+$ (X = Cl, Br) complex cations is preserved. Similar short Cu-Cu distances are observed for **2a*** and **2c***. Table 1 summarizes all observed intramolecular Cu-Cu distances for the described compounds. The aforementioned Cu-Cu distances are within the expected range for possible d^{10}-d^{10} metallophilic interactions of Cu^{I}. The central Cu atom exhibits a distorted tetrahedral coordination environment. In contrast, the terminal Cu atoms show a distorted trigonal planar coordination environment. The Cu-Cu-Cu angles of **2a** and **2b** are close to 163° while they are a little smaller and close to 159° for **2a*** and **2c***.

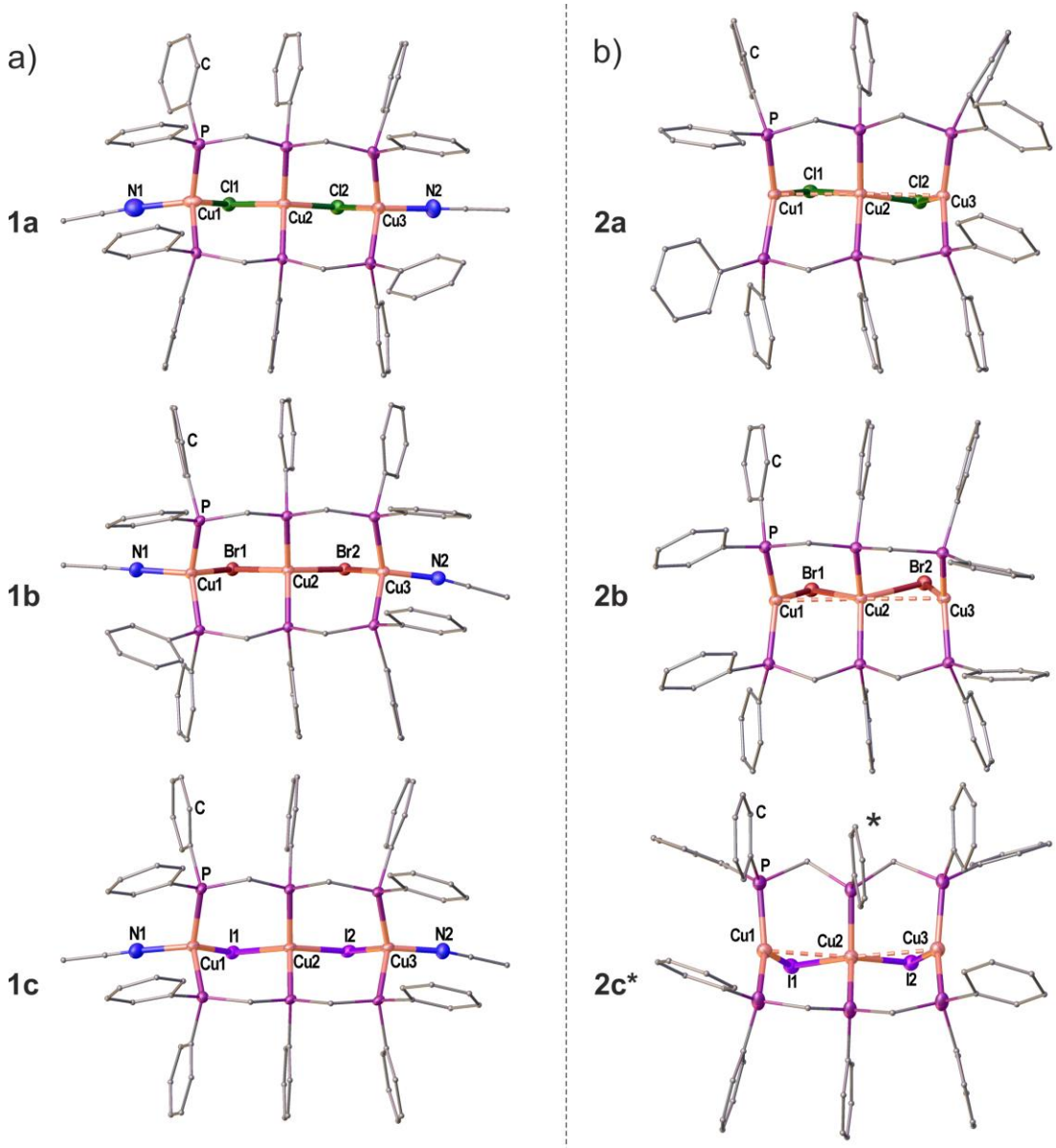

Figure 1. a) Crystal structures of the complex cations in **1a-c**. b) Crystal structures of the parent compounds **2a**, **2b** and **2c***.[83] H atoms are omitted and C atoms are drawn as small spheres for clarity. Ph ring marked with * is pointing towards the reader. Selected bond lengths [Å] and angles [°]: **1a**: Cu1-Cu2 3.2330(1), Cu2-Cu3 3.3239(1), Cu1-N1 2.1425(1), Cu3-N2 2.0651(1), Cu1-Cu2-Cu3 164.73(1); **1b**: Cu1-Cu2 3.4095(7), Cu2-Cu3 3.3702(7), Cu1-N1 2.057(4), Cu3-N2 2.063(3), Cu1-Cu2-Cu3 163.42(2); **1c**: Cu1-Cu2 3.3954(1), Cu2-Cu3 3.4388(1), Cu1-N1 2.0676(1), Cu3-N2 2.0561(1), Cu1-Cu2-Cu3 164.25(1); **2a**: Cu1-Cu2 2.8244(4), Cu2-Cu3 2.7827(5), Cu1-Cu2-Cu3 163.36(1); **2b**: Cu1-Cu2 2.8470(1), Cu2-Cu3 2.8995(1), Cu1-Cu2-Cu3 163.13(1); **2c***: Cu1-Cu2 2.8903(1), Cu2-Cu3 2.8836(1), Cu1-Cu2-Cu3 159.38(1).

The crystal structures of **3b** and **3c** are illustrated in Figure 2b and c.[84] The complexes contain a central $[Cu_3(\mu\text{-}X)_2(\mu\text{-dpmp})_2]^+$ (X = Br(**3b**), I(**3c**)) building block which shows two terminal CH_2Cl_2 molecules in a η^1-coordination mode. The intramolecular Cu-Cu distances of **3b** and **3c** are slightly elongated (~0.1 Å) compared to the parent compounds **2b** and **2c***. However, they are notably shorter (~0.5 Å) compared those observed in the MeCN ligated complexes **1b** and **1c**.

The resulting Cu-Cl distances are rather long (~3.2 – 3.3 Å), except for Cu1-Cl1 in **3b** which is only 2.8765(1) Å. The Cu-Cu-Cu angles of **3b** and **3c** are close to 163°.

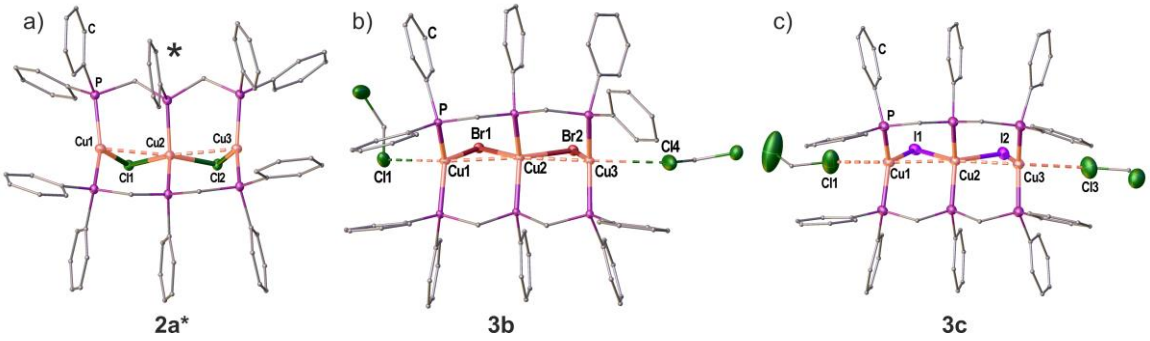

Figure 2. Crystal structure of **2a***(a), **3b**(b) and **3c**(c). H atoms are omitted and C atoms are drawn as small spheres for clarity. Ph ring marked with * is pointing towards the reader. Selected bond lengths [Å] and angles [°]:**2a***: Cu1-Cu2 2.8782(1), Cu2-Cu3 2.8386(1), Cu1-Cu2-Cu3 159.49(1); **3b**: Cu1-Cu2 3.0061(1), Cu2-Cu3 2.9341(1), Cu1-Cl1 2.8765(1), Cu3-Cl4 3.2425(1), Cu1-Cu2-Cu3 163.00(1); **3c**: Cu1-Cu2 2.9493(10), Cu2-Cu3 2.9167(10), Cu1-Cl1 3.202(3), Cu3-Cl3 3.295(2), Cu1-Cu2-Cu3 162.82(4).

Table1. Summary of the intramolecular Cu-Cu distances and the bond lengths of terminally bound ligands for all described products.

Compound	ligand 1	E1	E1-Cu1	Cu1-Cu2	Cu2-Cu3	E2-Cu3	E2	ligand2
1a	MeCN	N	2.1425(1)	3.2330(1)	3.3239(1)	2.0651(1)	N	MeCN
1b	MeCN	N	2.057(4)	3.4095(7)	3.3702(7)	2.063(3)	N	MeCN
1c	MeCN	N	2.0676(1)	3.3954(1)	3.4388(1)	2.0561(1)	N	MeCN
2a	–	–	–	2.8244(4)	2.7827(5)	–	–	–
2a*	–	–	–	2.8782(1)	2.8386(1)	–	–	–
2b	–	–	–	2.8470(1)	2.8995(1)	–	–	–
2c*	–	–	–	2.8903(1)	2.8836(1)	–	–	–
3b	CH_2Cl_2	Cl	2.8765(1)	3.0061(1)	2.9341(1)	3.2425(1)	Cl	CH_2Cl_2
3c	CH_2Cl_2	Cl	3.202(3)	2.9493(10)	2.9167(10)	3.295(2)	Cl	CH_2Cl_2
4a	–	–	–	2.8359(1)	3.3572(1)	2.3693(1)	P	**A1**
4b	–	–	–	2.8570(1)	3.4616(1)	2.3554(1)	P	**A1**
4c	–	–	–	3.0658(15)	3.5190(14)	2.3582(18)	P	**A1**
5	–	–	–	2.8302(1)	3.2176(1)	2.5295(1)	As	**A2**
6a	**B**	P	2.4573(13)	3.1743(9)	3.2227(9)	2.3670(14)	P	**B**
6b	**B**	P	2.4829(2)	3.2825(2)	3.3769(2)	2.3515(2)	P	**B**
7	**B**	P	2.3433(1)	3.4393(1)	3.4373(1)	2.4041(1)	P	**B**
8a	**C1**	P	2.3743(1)	3.2975(1)	3.3389(1)	2.3271(1)	P	**C1**
8b	**C1**	P	2.3689(1)	3.3536(1)	3.3903(1)	2.3276(1)	P	**C1**
10	**C1**	P	2.407(5)	3.520(3)	3.612(3)	2.331(5)	P	**C1**
9	**C2**	As	2.5980(1)	3.0345(1)	3.2135(1)	2.5036(1)	As	**C2**

NMR characterization of the parent complexes $[Cu_3(\mu\text{-}X)_2(\mu\text{-}dpmp)_2]^+$ 2a-c in solution

When crystals of **1a-c** are dried in vacuum, the terminal MeCN ligands can be removed completely, proved by elemental analysis. While heating or grinding the

samples leads to a mixture of products (visible in the $^{31}P\{^{1}H\}$ NMR spectrum at low temperature) drying in vacuum for several hours at room temperature cleanly converts the MeCN ligated complexes **1a-c** directly to **2a-c** in the solid state without destroying the central $[Cu_3(\mu\text{-}X)_2(\mu\text{-dpmp})_2]^+$ complex cations. The solvent loss turns the crystals of **1a-c** to fine powder of **2a-c**. This can be concluded from the observed behavior of the dried samples of **1a-c** in VT NMR experiments shown in Figure 3.

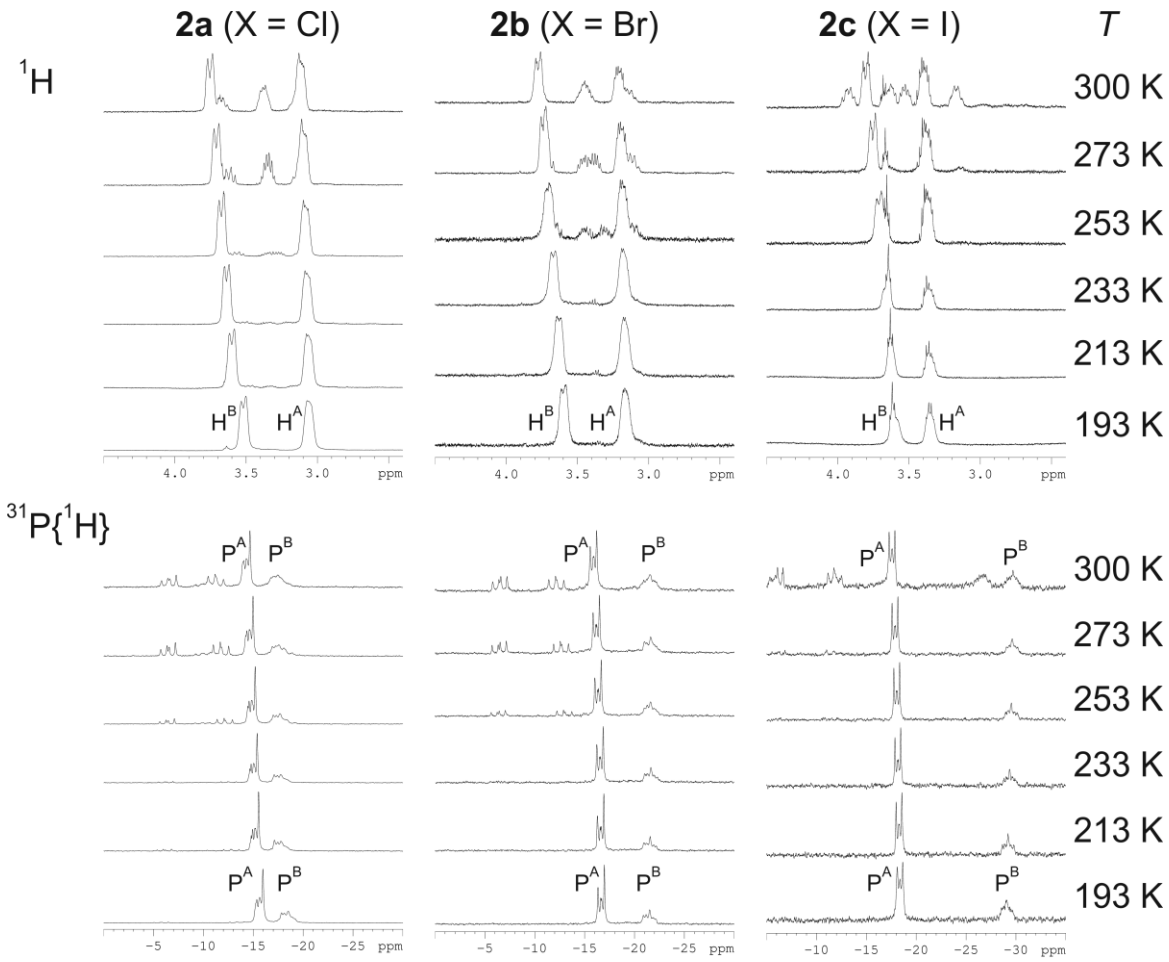

Figure 3. ^{1}H and $^{31}P\{^{1}H\}$ VT NMR experiments for **2a-c** starting from 193 K up to 300 K in CD_2Cl_2 solution. The diastereotopic H atom H^A and H^B were assigned tentatively. The sharp signals on top of the broad signals in the ^{1}H NMR spectrum of **2c** arise from residual THF and Et_2O from the initial synthesis of **1c**. The compounds **2a-c** represent a AA'A''A'''BB' spin system illustrated in Scheme 4 which result in higher-order $^{31}P\{^{1}H\}$ NMR spectra.

When the powders of **2a-c** (obtained from drying **1a-c**) are dissolved at –80°C in cold CD_2Cl_2 the ^{1}H NMR spectra of **2a-c** show each two broad signals for the diastereotopic H atoms H^A and H^B of the four chemically equivalent CH_2 groups illustrated in Scheme 4. The $^{31}P\{^{1}H\}$ NMR spectra of **2a-c** show two broad signals in a 2:1 ratio for the $RPPh_2$ (P^A) and R'_2PPh (P^B) groups, respectively. When the samples are warmed up in the spectrometer the formation of new signals in the ^{1}H as well as the $^{31}P\{^{1}H\}$ NMR spectra of **2a-c** can be observed above 253 K which is caused by increasing dynamic processes

of the complex cations in solution. The $^{31}P\{^{1}H\}$ NMR spectra of **2a-c** at 300 K can be viewed as characteristic since they do not change significantly upon the addition of E_n ligands (see below). Notably, these thermal evolutions are not reversible as upon cooling from room temperature solutions, the NMR spectra do not evolve and return to the initial pattern. This suggests equilibria of different species in solution. However, the NMR spectra of **2a** and **2b** at room temperature still show the initial signal patterns of the parent $[Cu_3(\mu\text{-}X)_2(\mu\text{-dpmp})_2]^+$ complexes (X = Cl(**2a**), Br(**2b**)) as the major species (~80%). For X = I(**2c**), the initial signals of $[Cu_3(\mu\text{-}I)_2(\mu\text{-dpmp})_2]^+$ (**2c**) can still be observed at room temperature, although they only represent about 50% or less of the species in solution. It has to be emphasized at this point, that by following our synthetic strategy of pre-assembled $[Cu_3(\mu\text{-}X)_2(\mu\text{-dpmp})_2]^+$ building blocks, no other combination of CuX, dpmp and $[Cu^+][BF_4]$ could ever be observed in the solid-sate. This conclusively suggests dynamic coordination behavior of the Cu_3 building blocks at elevated temperatures in solution but exclusive formation of the parent $[Cu_3(\mu\text{-}X)_2(\mu\text{-dpmp})_2]^+$ complexes upon crystallization.

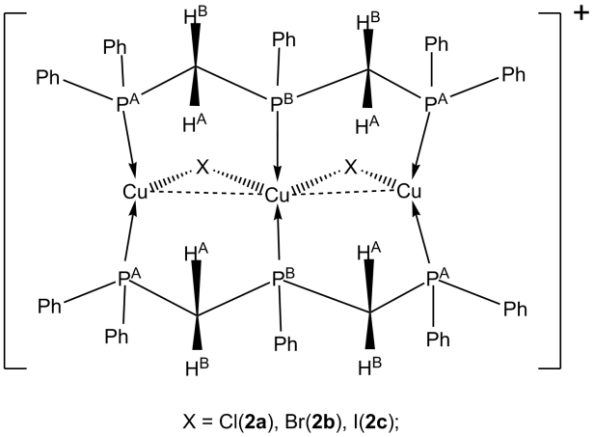

X = Cl(**2a**), Br(**2b**), I(**2c**);

Scheme 4. Schematic representation of the complex cations of **2a-c** for NMR assignments.

Compounds containing the E_2 ligands A1 and A2

Syntheses and characterization of 4a-5:

The P_2 complex **A1** has been reported to bridge monocationic metal centers in a $\mu,\eta^1{:}\eta^1$-mode in several compounds.[71] Therefore, the interconnection of the $[Cu_3(\mu\text{-}X)_2(\mu\text{-dpmp})_2]^+$ building blocks **2a-c** was attempted by reacting them with the E_2 complexes **A1** and **A2**. The ligands **A1** or **A2** are dissolved in small amount of CH_2Cl_2 and directly added to a in situ prepared clear CH_2Cl_2 solution of the parent trinuclear complexes $[Cu_3(\mu\text{-}X)_2(\mu\text{-dpmp})_2]^+$ **2a-c**. (see Scheme 5). Diffusion of alkanes into the filtered CH_2Cl_2 solutions affords light red crystals of the products **4a-c** or dark red crystals

of **5**. The ^{1}H and $^{31}P\{^{1}H\}$ NMR spectra of **4a-c** and **5** in CD_2Cl_2 solution show sets of signals which are almost identical to the signals assigned to the $[Cu_3(\mu\text{-}X)_2(\mu\text{-dpmp})_2]^+$ complex cations **2a-c**. In addition a singlet can be observed in the ^{1}H NMR spectra for the Cp rings of **A1** or **A2** respectively. The signal corresponding to the P_2 ligand of **A1** in the $^{31}P\{^{1}H\}$ NMR spectra of **4a-c** is significantly broadened and shifted to higher field ($\Delta\delta$ = 21 ppm for **4a**, 30 ppm for **4b** and 34 ppm for **4c**), compared to the free ligand **A1** (δ = –42.9 ppm).[87]

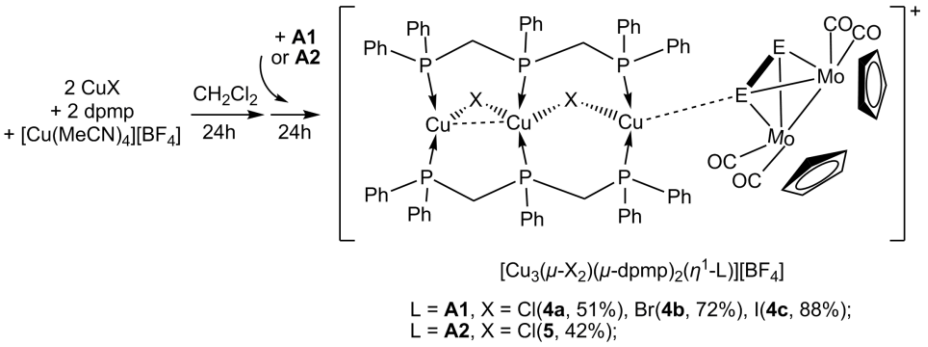

Scheme 5. One-pot synthesis of the compounds **4a-c** and **5**. Yields are given in parentheses.

X-ray structural analysis of 4a-c and 5

Single crystal X-ray structural analysis (see Figure 4) clearly reveals that the compounds **4a-c** and **5** show very similar structures. The compounds exhibit central $[Cu_3(\mu\text{-}X)_2(\mu\text{-dpmp})_2]^+$ building blocks with no terminal ligand on Cu1 while Cu3 is additionally coordinated in a η^1-mode by the E_2 complexes **A1** or **A2**, respectively. Therefore, the coordination geometry of Cu1 can be described as distorted trigonal planar while Cu3 adopt a distorted tetrahedral geometry. The intermolecular Cu-Cu distances Cu1-Cu2 and Cu2-Cu3 of each $[Cu_3(\mu\text{-}X)_2(\mu\text{-dpmp})_2]^+$ building block differ significantly due to the coordination of **A1** or **A2** to Cu3. The Cu1-Cu2 distances for all complexes **4a-c** (~2.84 Å) and **5** (3.0658(15) Å) are quite short suggesting cuprophilic interactions and can be compared well to the parent complex cations **2a**, **2b** and **2c***. While the Cu2-Cu3 distance is the shortest for **5** containing the As_2 ligand **A2** with 3.2176(1) Å it increases in the series **4a** (X = Cl), **4b** (X = Br), **4c** (X = I) from 3.3572(1) Å to 3.5190(14) Å with increasing size of the halides. The Cu_3 chains can be viewed as almost linear with Cu-Cu-Cu angles between 160° to 164° which are not significantly changed compared to **2a-c***. The Cu3-P1 as well as the P1-P2 bond lengths of **4a-c** are identical with ~2.36 Å (Cu3-P1) and ~2.08 Å (P1-P2, 2.079(2) Å for free **A1**), respectively.[87] The As-As distance in **5** (2.3097(1) Å) is also unchanged to free **A2** (2.305(3) Å).[88] In conclusion, it can be noted that the introduction of the

E_2 complexes **A1** and **A2** to the pre-assembled $[Cu_3(\mu\text{-}X)_2(\mu\text{-}dpmp)_2]^+$ building blocks did not afford an interconnection, but **4a-c** and **5** can be obtained as the only products by crystallization without the formation of any other isomers or different combinations of the starting materials in the solid state. All complexes **4a-5** can be recrystallized without alteration of the assemblies in the solid state.

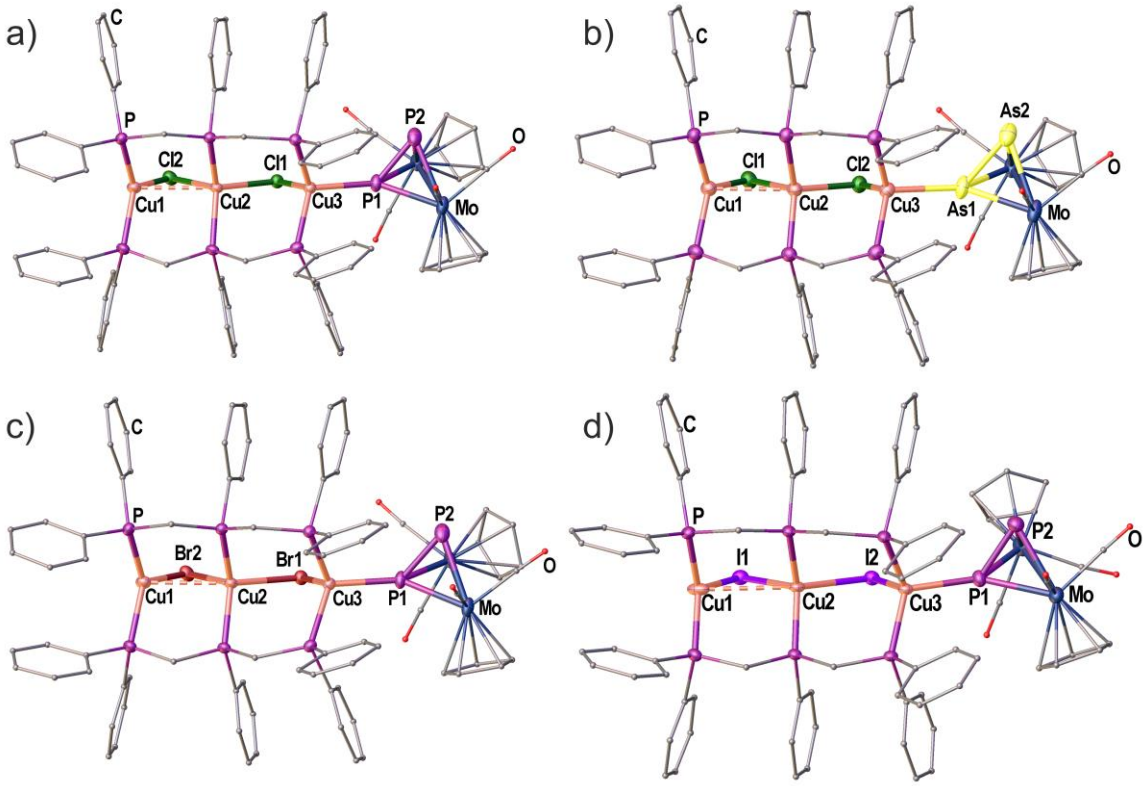

Figure 4. Crystal structures of the complex cations in **4a** a), **5** b), **4b** c) and **4c** d). H atoms are omitted and C and O atoms are drawn as small spheres for clarity. Selected bond lengths [Å] and angles [°]: **4a**: Cu1-Cu2 2.8359(1), Cu2-Cu3 3.3572(1), Cu3-P1 2.3693(1), P1-P2 2.0869(1), Cu1-Cu2-Cu3 164.81(1), Cu3-P1-P2 128.87(1), Cl1-Cu3-P1-P2 106.54(1); **5**: Cu1-Cu2 2.8302(1), Cu2-Cu3 3.2176(1), Cu3-As1 2.5295(1), As1-As2 2.3097(1), Cu1-Cu2-Cu3 164.73(1), Cu3-As1-As2 128.86(1), Cl2-Cu3-As1-As2 106.53(1); **4b**: Cu1-Cu2 2.8570(1), Cu2-Cu3 3.4616(1), Cu3-P1 2.3554(1), P1-P2 2.0826(1), Cu1-Cu2-Cu3 163.65(1), Cu3-P1-P2 130.35(1), Br1-Cu3-P1-P2 108.82; **4c**: Cu1-Cu2 3.0658(15), Cu2-Cu3 3.5190(14), Cu3-P1 2.3582(18), P1-P2 2.084(3), Cu1-Cu2-Cu3 160.7(1), Cu3-P1-P2 126.2(1), I2-Cu3-P1-P2 105.6(1).

DFT calculations

All the above described compounds **1a-5** demonstrate that the intramolecular Cu-Cu distances are drastically affected upon coordination of any ligand to the terminal Cu atoms. Since the compounds **4a-5** represent the first unsymmetrically substituted $[Cu_3(\mu\text{-}X)_2(\mu\text{-}dpmp)_2]^+$ building blocks it is interesting to investigate the geometrical effects induced by coordination of only one terminal ligand. Therefore, we performed DFT calculations on the model compound $[Cu_3(\mu\text{-}X)_2(\mu\text{-}dmmp)_2(\eta^1\text{-}\mathbf{A1})]^+$ (**4a'**) (dmmp = bis(dimethylphosphinomethylene)methylphosphine)) (calculated by restrained geometry optimizations).[89] Figure 5a shows the relative energy of the model compound **4a'** with

the variation of the Cu3-P1 distance (labels according to **4a**). The calculations reveal a minimum at a Cu3-P1 bond length around 2.35 Å which is in good agreement to the determined X-ray structure of **4a**. Figure 5b shows the evolution of the intramolecular Cu-Cu distances (Cu1-Cu2 and Cu2-Cu3) as well as the Cu3-Cl1 distance with variation of the Cu3-P1 distance. From this graph it can be clearly seen that an approach of the P1 atom of **A1** towards the Cu3 atom induces a drastic increase in the adjacent Cu3-Cu2 distance while the Cu1-Cu2 distance is not changed at all. The Cu3-Cl1 distance is only slightly affected.

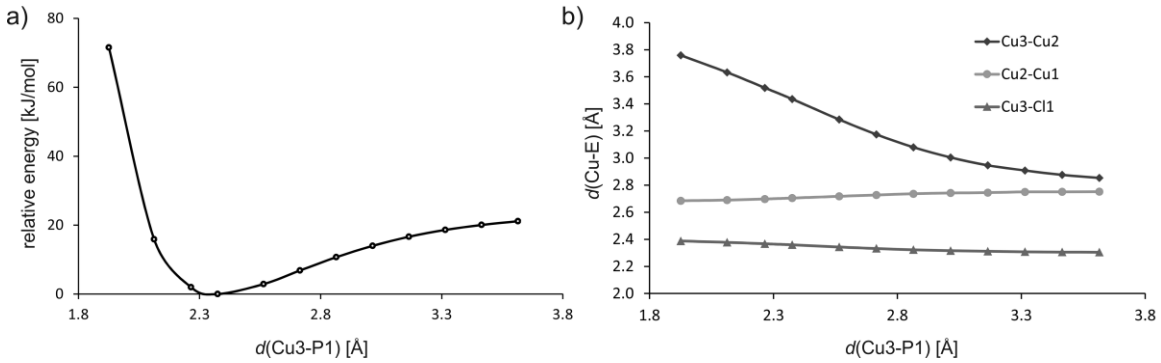

Figure 5. a) Variation of the relative energy of $[Cu_3(\mu\text{-}Cl)_2(\mu\text{-}dmmp)_2(\eta^1\text{-}A1)]^+$ (4a') (dmmp = bis(dimethylphosphino) methylenephosphine) with the Cu3-P1 distance (restrained geometry optimization). b) Variations of the Cu1-Cu2, Cu2-Cu3 and Cu3-Cl1 distances in 4a' with the Cu3-P1 distance. Calculated at the BP86/def2-SVP level of theory.

Compounds containing the *cyclo*-P_3 ligand B

Syntheses and characterization of 6a-7

The E_2 ligands **A1** and **A2** did not afford an interconnection of the $[Cu_3(\mu\text{-}X)_2(\mu\text{-}dpmp)_2]^+$ building blocks **2a-c** but the isolated complexes **4a-c** and **5**, instead. In order to realize the connection of **2a-c** via P_n ligand complexes, the less sterically demanding *cyclo*-P_3 complex **B** was introduced. The complexes **A1** and **B** are closely related and their analogy can easily be described by exchanging one 15 VE complex fragment $[CpMo(CO)_2]$ of **A1** for an isolobal P atom in **B** (see Scheme 2). Complex **B** was added to in situ prepared clear colorless CH_2Cl_2 solutions of **2a-c** in an equimolar ratio (see Scheme 6). The clear yellow solutions were stirred and subsequently filtered. Diffusion of alkanes into these solutions afforded clear yellow needles of **6a** (X = Cl), and yellow blocks of **6b** (X = Br) or **7** (X = I). Subsequent analysis of **7** revealed a 1:2 stoichiometry of the $[Cu_3(\mu\text{-}I)_2(\mu\text{-}dpmp)_2]^+$ building block and the complex **B** and the synthesis was subsequently reproduced with this ratio to afford **7** as the only product.[90] The ^1H and $^{31}P\{^1H\}$ NMR spectra of **6a**, **6b** and **7** in CD_2Cl_2 suggest dissociation in solution and show characteristic signals for the $[Cu_3(\mu\text{-}X)_2(\mu\text{-}dpmp)_2]^+$ complex cations. The ^1H NMR spectra of **6a**, **6b** and **7** show an additional singlet for the

Cp ring of **B**. The $^{31}P\{^{1}H\}$ NMR spectra in CD_2Cl_2 solution reveal an additional sharp singlet at δ = –350.7 ppm (**6a**), –350.7 ppm (**6b**) and –351.2 ppm (**7**) which is almost identical to the free complex **B** (δ = –351.1 ppm).[87]

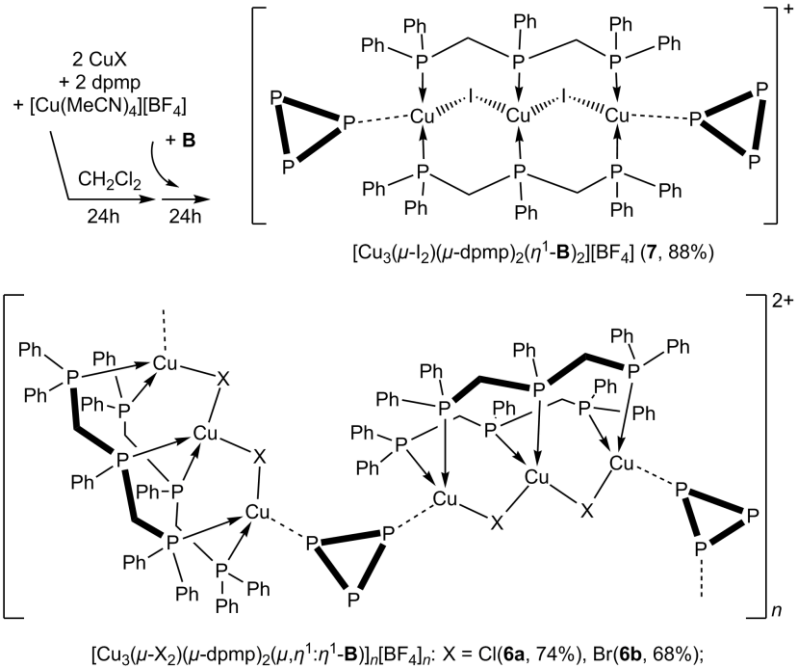

Scheme 6. One-pot syntheses of the one-dimensional polymers **6a**, **6b** and the isolated complex **7**. Yields are given in parentheses.

X-ray structural analysis of 6a, 6b and 7

Single crystal X-ray structure determination (see Figure 6 a, b) revealed an isostructural one-dimensional polymeric structure of the compounds **6a** (X = Cl) and **6b** (X = Br), respectively in which the central $[Cu_3(\mu\text{-}X)_2(\mu\text{-dpmp})_2]^+$ building blocks are connected by a *cyclo*-P_3 ligand of the complex **B** bridging in a η^1:η^1-coordination mode.[91] The coordination polymers **6a** and **6b** describe a zig-zag chain with alternating orientations of the $[Cu_3(\mu\text{-}X)_2(\mu\text{-dpmp})_2]^+$ building blocks. Surprisingly, the structure determination of **7** shows a finite complex cation consisting of a central $[Cu_3(\mu\text{-}I)_2(\mu\text{-dpmp})_2]^+$ building block terminated by an η^1-coordinating *cyclo*-P_3 complex on each end instead of a coordination polymer (see Figure 6 c).[90] The intramolecular Cu-Cu distances of **6a**, **6b** and **7** are all above 3.17 Å and increase with increasing size of the bridging halides up to ~3.44 Å for **7**. The Cu-P bond lengths of the terminal Cu atoms to the P atom of the complex B are not identical on both sides of the $[Cu_3(\mu\text{-}X)_2(\mu\text{-dpmp})_2]^+$ building blocks with average values ranging from 2.35 Å to 2.45 Å. The Cu-Cu-Cu angles are between 162° and 167°. In conclusion it can be noted that the *cyclo*-P_3 complex **B** facilitates the interconnection of the pre-assembled $[Cu_3(\mu\text{-}X)_2(\mu\text{-dpmp})_2]^+$ building blocks (for X = Cl, Br) while it acts as a terminal η^1-ligand

towards $[Cu_3(\mu\text{-}I)_2(\mu\text{-}dpmp)_2]^+$. Although dissociation takes place in solution, **6a**, **6b** and **7** can be obtained as the only products by crystallization without the observation of any other isomers or different combinations of the starting materials in the solid state. All complexes **6a-7** can be recrystallized without alteration of the assemblies in the solid state.

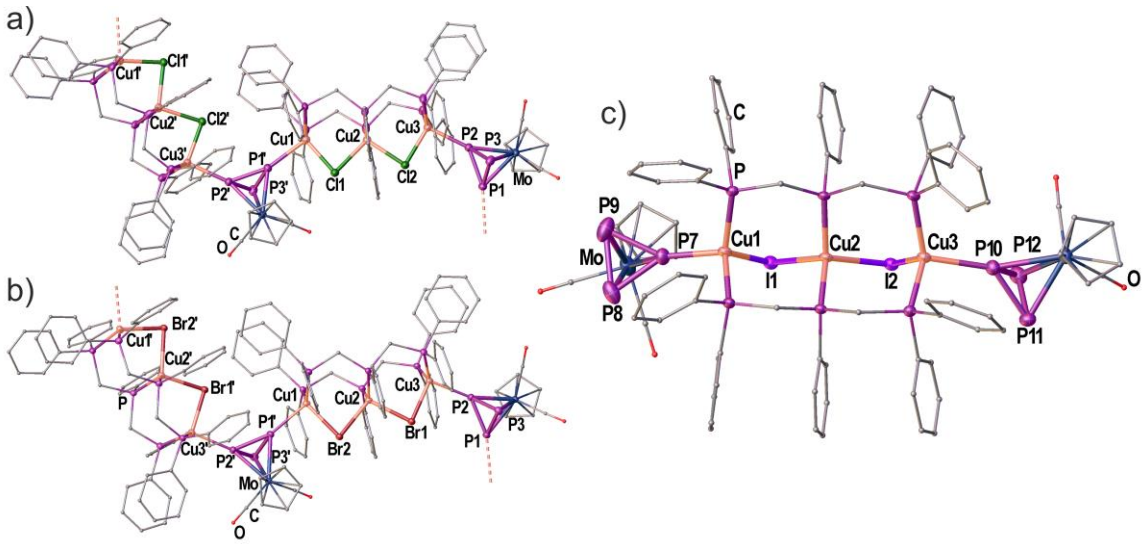

Figure 6. Crystal structures of the cationic one-dimensional coordination polymers **6a** a) and **6b** b) and the complex cation of **7** c). H atoms are omitted and C and O atoms are drawn as small spheres for clarity. Selected bond lengths [Å] and angles [°]: **6a** (final model)[91]: Cu1-Cu2 3.1743(9), Cu2-Cu3 3.2227(9), Cu1-P1' 2.4573(13), Cu3-P2 2.3670(14), P1-P2 2.1540(17), P2-P3 2.1470(18), P1-P3 2.1426(18), Cu1-Cu2-Cu3 167.69(3), Cu1-P1'-P2' 163.01(7), Cu3-P2-P1 135.83(7); **6b**: Cu1-Cu2 3.2825(2), Cu2-Cu3 3.3769(2), Cu1-P1' 2.4829(2), Cu3-P2 2.3515(2), P1-P2 2.1496(1), P2-P3 2.1458(1), P1-P3 2.1396(2), Cu1-Cu2-Cu3 164.94(1), Cu1-P1'-P2' 162.39(1), Cu3-P2-P1 134.56(1); **7**: Cu1-Cu2 3.4393(1), Cu2-Cu3 3.4373(1), Cu1-P7 2.3433(1), Cu3-P10 2.4041(1), P7-P8 2.1272(1), P7-P9 2.1429(1), P8-P9 2.1552(1), P10-P11 2.1541(1), P10-P12 2.1302(1), P11-P12 2.1536(1), Cu1-Cu2-Cu3 162.18(1), Cu2-Cu1-P7 150.34(1), Cu2-Cu3-P10 152.53(1).

Compounds containing the *cyclo*-E$_5$ complexes C1 and C2

Syntheses and characterization of 8a-10

After successful characterization of the finite coordination compounds **4a-c**, **5**, **7** and the one-dimensional coordination polymers **6a** and **6b** from reactions with E_2 and *cyclo*-P_3 ligand complexes, subsequently, the larger *cyclo*-E_5 complexes **C1** and **C2** (see Scheme 2) were introduced to the pre-assembled $[Cu_3(\mu\text{-}X)_2(\mu\text{-}dpmp)_2]^+$ building blocks. Therefore, **C1** or **C2** were added to a in situ prepared clear colorless CH_2Cl_2 solutions of **2a-c** in an equimolar ratio (see Scheme 7). The clear green (E = P) or brown (E = As) solutions were stirred for additional 24 h. After filtration and subsequent alkane diffusion into these solutions, compounds **8a**, **8b** and **10** can be isolated as rod-like green crystals while **9** crystallizes as brown blocks. Analysis of **10** revealed a 1:2 stoichiometry of the $[Cu_3(\mu\text{-}I)_2(\mu\text{-}dpmp)_2]^+$ building block and the complex **C1**.[92] The synthesis was subsequently reproduced with this ratio to afford pure **10**. The ^{1}H and

$^{31}P\{^{1}H\}$ NMR spectra of **8a**, **8b**, **9**, and **10** in CD_2Cl_2 suggest dissociation in solution and show characteristic signals for the $[Cu_3(\mu\text{-}X)_2(\mu\text{-dpmp})_2]^+$ complex cations. The ^{1}H NMR spectra show an additional singlet for the Cp* rings of **C1** or **C2**. The $^{31}P\{^{1}H\}$ NMR spectra of **8a**, **8b** and **10** in CD_2Cl_2 solution show an additional sharp singlet at δ = 149.9 ppm (**8a**), 149.9 ppm (**8b**) and 151.2 ppm (**10**) similar to the free *cyclo*-P_5 complex **C1** (δ = 153.0 ppm).[93]

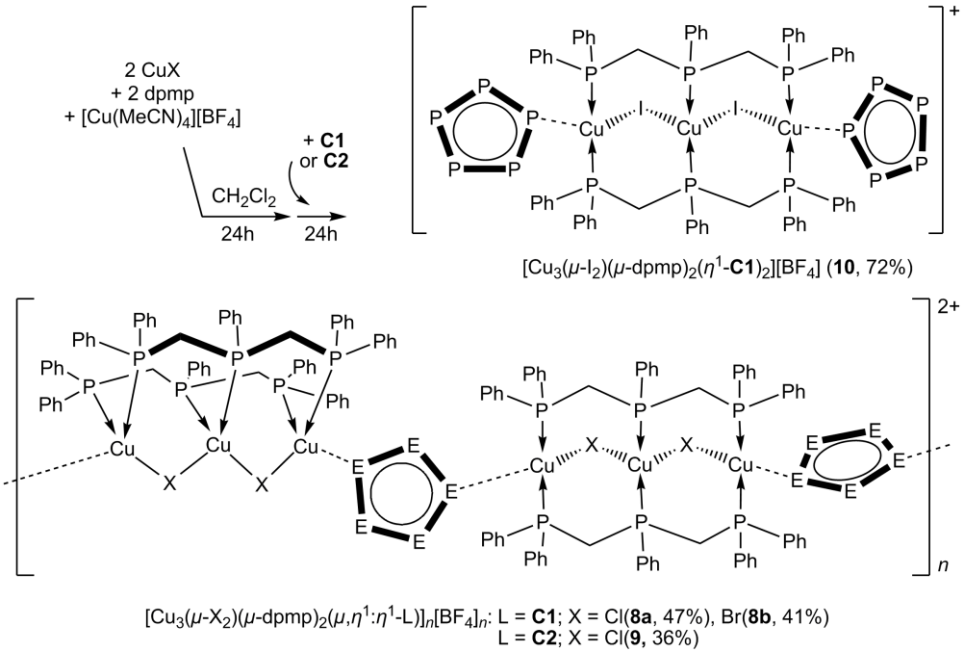

Scheme 7. One-pot syntheses of the cationic one-dimensional polymers **8a**, **8b**, **9** and the isolated complex cation **10**. Yields are given in parentheses.

X-ray structural analysis of 8a, 8b, 9 and 10

Single crystal X-ray structure determination reveals isostructural one-dimensional coordination polymers of **8a**, **8b** and **9** (see Figure 7 a-c) with alternating $[Cu_3(\mu\text{-}X)_2(\mu\text{-dpmp})_2]^+$ building blocks (**8a**, **9**: X = Cl; **8b**: X = Br) and bridging σ-1,3-coordinating *cyclo*-E_5 ligand complexes (**8a**, **8b**: E = P; **9**: E = As). This bridging coordination mode has been described previously for **C1** towards Cu^{I} centers but was unprecedented for **C2** prior to the characterization of **9**.[58,82] Two consecutive $[Cu_3(\mu\text{-}X)_2(\mu\text{-dpmp})_2]^+$ building blocks along the one-dimensional polymeric chain are rotated by roughly 90°. In contrast, the crystal structure of **10** shows a finite complex cation with a central $[Cu_3(\mu\text{-}I)_2(\mu\text{-dpmp})_2]^+$ building block and two terminal η^1-coordinating *cyclo*-P_5 complexes **C1** (*cf*. *cyclo*-P_3 complexes **B** in **7**).[94] The intramolecular Cu-Cu distances inside the Cu_3 units coordinated to the *cyclo*-P_5 complex **C1** are all above 3.29 Å and increase with increasing size of the bridging halides in the order **8a**, **8b**, **10** from 3.2975(1) Å up to 3.612(3) Å. The isostructural one-dimensional polymer **9**

containing the *cyclo*-As_5 complex **C2** instead exhibits the shortest Cu-Cu distances in this series with 3.0345(1) Å and 3 3.2135(1) Å, respectively. The Cu-Cu-Cu angles of the one-dimensional polymers **8a**, **8b** and **9** are similar and between 168° and 169°. In contrast, the complex **10** exhibits a Cu-Cu-Cu angle of only 159.62(8)°. In conclusion it can be noted that the *cyclo*-P_5 complex **C1** facilitates the interconnection of the pre-assembled $[Cu_3(\mu\text{-}X)_2(\mu\text{-dpmp})_2]^+$ building blocks (for X = Cl, Br).[92] Surprisingly, the *cyclo*-As_5 complex **C2** shows the same connectivity towards $[Cu_3(\mu\text{-}Cl)_2(\mu\text{-dpmp})_2]^+$ in the crystal structure of **9**, however, resulting in shorter intermolecular Cu-Cu distances than observed for the analogous *cyclo*-P_5 polymer **8a**. In case of the iodine bridged $[Cu_3(\mu\text{-}I)_2(\mu\text{-dpmp})_2]^+$ building block, a discrete complex featuring two η^1-coordinating *cyclo*-P_5 ligands **C1** is formed.[92] Although the obtained products of the $[Cu_3(\mu\text{-}Cl)_2(\mu\text{-dpmp})_2]^+$ building blocks and the *cyclo*-E_5 complexes **C1** and **C2** dissociate in solution they can be isolated as the only products by crystallization without the formation of any other isomers or different combinations of the starting materials in the solid state. All complexes **8a-10** can be recrystallized without alteration of the assemblies in the solid state.

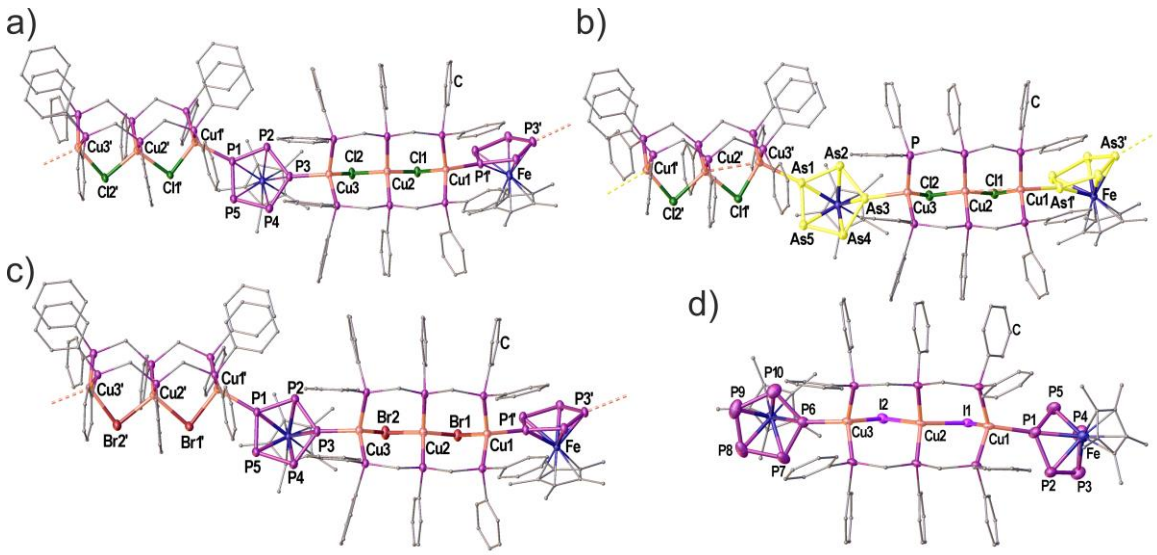

Figure 7. Crystal structures of the one-dimensional coordination polymers **8a** a), **9** b), **8b** c) and the complex cation of **10** d). H atoms are omitted and C atoms are drawn as small spheres for clarity. Selected bond lengths [Å] and angles [°]: **8a**: Cu1-Cu2 3.2975(1), Cu2-Cu3 3.3389(1), Cu1-P1' 2.3743(1), Cu3-P3 2.3271(1), P1-P2 2.1156(1), P2-P3 2.1180(1), P3-P4 2.1143(1), P4-P5 2.1120(1), P1-P5 2.1158(1), Cu1-Cu2-Cu3 168.78(1), P_5(plane)-P_5(plane) 61.09(1); **9**: Cu1-Cu2 3.0345(1), Cu2-Cu3 3.2135(1), Cu1-As1' 2.5980(1), Cu3-As3 2.5036(1), As1-As2 2.3212(1), As2-As3 2.3200(1), As3-As4 2.3223(1), As4-As5 2.3229(1), As1-As5 2.3189(1), Cu1-Cu2-Cu3 169.12(1), As_5(plane)-As_5(plane) 61.45(1); **8b**: Cu1-Cu2 3.3536(1), Cu2-Cu3 3.3903(1), Cu1-P1' 2.3689(1), Cu3-P3 2.3276(1), P1-P2 2.1150(1), P2-P3 2.1109(1), P3-P4 2.1139(1), P4-P5 2.1114(1), P1-P5 2.1126(1), Cu1-Cu2-Cu3 167.88(1), P_5(plane)-P_5(plane) 60.14(1); **10**: Cu1-Cu2 3.520(3), Cu2-Cu3 3.612(3), Cu1-P1 2.407(5), Cu3-P6 2.331(5), P1-P2 2.114(7), P2-P3 2.104(7), P3-P4 2.111(7), P4-P5 2.096(8), P1-P5 2.102(7), P6-P7 2.125(6), P7-P8 2.101(7), P8-P9 2.086(10), P9-P10 2.128(8), P10-P6 2.106(7), Cu1-Cu2-Cu3 159.62(8), P_5(plane)-P_5(plane) 63.1(1).

Comparison of intramolecular Cu-Cu distances

All described compounds **1a-10** contain cationic $[Cu_3(\mu\text{-}X)_2(\mu\text{-}dpmp)_2]^+$ building blocks in their crystal structures. Table 1 (vide supra) summarizes the intermolecular Cu-Cu distances as well as the distances to the respective donor atoms of the terminal ligands. The presented data clearly shows the direct influence of the coordination to the terminal Cu atoms on the adjacent Cu-Cu distances. The shortest Cu-Cu distances, which are in the range of d^{10}-d^{10} metallophilic interactions are observed for **2a-2c*** exhibiting no terminal ligands and two Cu atoms in distorted trigonal planar coordination geometry. An elongation of the Cu-Cu distances takes place if any ligand is introduced on the terminal Cu atoms. This phenomenon is even observed for the very weakly coordinating ligand CH_2Cl_2 in **3b** and **3c**. Structural analysis of **4a-c** and **5** clearly shows that coordination to only one end of the $[Cu_3(\mu\text{-}X)_2(\mu\text{-}dpmp)_2]^+$ building blocks results only in the elongation of the adjacent Cu-Cu distance, while the other is not affected resembling the short Cu-Cu distances of **2a-2c***. When the same ligands are coordinated on both sides of the Cu_3 units (**1a-c**, **3b**, **3c**, **6a-10**) the direct comparison allows the following conclusion: The shorter the bond length to the terminal ligand (Cu-E) becomes, the longer will be the respective adjacent Cu-Cu distance inside the Cu_3 unit. Whether this elongation is either caused by electronic effects via termination of any possible metallophilic d^{10}-d^{10} interactions or just by the change of the coordination environment of the terminal Cu atoms from trigonal planar to tetrahedral cannot be clearly answered at this point. Similar studies on the alteration of Cr-Cr distances upon coordination of different terminal ligands have been carried out for trinuclear Cr EMACS.[95]

8.3 Conclusion

In conclusion, the easily feasible and selective preparation of the trinuclear $[Cu_3(\mu\text{-}X)_2(\mu\text{-}dpmp)_2]^+$ building blocks and their potential use in supramolecular chemistry is described. Reactions with selected E_n ligand complexes and full characterization of the products demonstrated the following: 1. Although some of the characterized products exhibit finite complex cations, the used E_n ligand complexes are confirmed as valuable linking moieties for supramolecular chemistry, which are so far dominated by organic O, N and S donors. 2. The framework of the pre-assembled $[Cu_3(\mu\text{-}X)_2(\mu\text{-}dpmp)_2]^+$ complex cations are stable towards the introduction of varying E_n ligand complexes. Additionally, it has to be noted that although all described syntheses are based on self-assembly of multi-component systems, the reactions proceed very selectively and no formation of any side-product could be observed. The comparison of the intramolecular Cu-Cu distances inside the $[Cu_3(\mu\text{-}X)_2(\mu\text{-}dpmp)_2]^+$ complex cations for all compounds demonstrates that

coordination to the terminal Cu atoms results in an elongation of the adjacent aforementioned Cu-Cu distances. This behavior is supported by DFT computations for the model complex $[Cu_3(\mu\text{-}Cl)_2(dmmp)_2\{(\eta^1\text{-}\mathbf{A1})\}]^+$ (**4a'**). We expect that synthetic approaches via self-assembly based on the presented findings will lead to a broad variety of supramolecular coordination compounds containing the readily available $[Cu_3(\mu\text{-}X)_2(\mu\text{-}dpmp)_2]^+$ building blocks in the near future. Current investigations already include the determination of the photo-physical properties of the $[Cu_3(\mu\text{-}X)_2(\mu\text{-}dpmp)_2]^+$ complex cations and their adducts.

8.4 References

[1] M. G. Campbell, S.-L. Zheng, T. Ritter, *Inorg. Chem.* **2013**, *52*, 13295-13297.

[2] M. G. Campbell, D. C. Powers, J. Raynaud, M. J. Graham, P. Xie, E. Lee, T. Ritter, *Nat. Chem.* **2011**, *3*, 949-953.

[3] A. Guijarro, O. Castillo, A. Calzolari, P. J. S. Miguel, C. J. Gómez-García, R. di Felice, F. I. Zamora, *Inorg. Chem.* **2008**, *47*, 9736-9738.

[4] M. Mitsumi, H. Ueda, K. Furukawa, Y. Ozawa, K. Toriumi, M. Kurmoo, *J. Am. Chem. Soc.* **2008**, *130*, 14102-14104.

[5] K. Sakai, E. Ishigami, Y. Konno, T. Kajiwara, T. Ito, *J. Am. Chem. Soc.* **2002**, *124*, 12088-12089.

[6] K. Uemura, M. Ebihara, *Inorg. Chem.* **2013**, *52*, 5535-5550.

[7] F. A. Cotton, E. V. Dikarev, M. A. Petrukhina, *J. Organomet. Chem.* **2000**, *596*, 130-135.

[8] F. A. Cotton, E. V. Dikarev, M. A. Petrukhina, *J. Chem. Soc., Dalton Trans.* **2000**, 4241-4243.

[9] G. M. Finniss, E. Canadell, C. Campana, K. R. Dunbar, *Angew. Chem. Int. Ed.* **1996**, *35*, 2772-2774; *Angew. Chem.* **1996**, *108*, 2946-2948.

[10] F. Lafolet, S. Chardon-Noblat, C. Duboc, A. Deronzier, F. P. Pruchnik, M. Rak, *Dalton Trans.* **2008**, 2149-2156.

[11] F. P. Pruchnik, P. Jakimowicz, Z. Ciunik, K. Stanislawek, L. A. Oro, C. Tejel, M. A. Ciriano, *Inorg. Chem. Commun.* **2001**, *4*, 19-22.

[12] C. Tejel, M. A. Ciriano, B. E. Villarroya, J. A. López, F. J. Lahoz, L. A. Oro, *Angew. Chem. Int. Ed.* **2003**, *42*, 529-532; *Angew. Chem.* **2003**, *115*, 547-550.

[13] M. P. del Río, J. A. López, M. A. Ciriano, C. Tejel, *Chem. Eur. J.* **2013**, *19*, 4707-4711.

[14] J. F. Berry, in *Metal-Metal Bonding, Vol. 136* (Ed.: G. Parkin), Springer Berlin Heidelberg, **2010**, pp. 1-28.

[15] C. Yin, G.-C. Huang, C.-K. Kuo, M.-D. Fu, H.-C. Lu, J.-H. Ke, K.-N. Shih, Y.-L. Huang, G.-H. Lee, C.-Y. Yeh, C.-h. Chen, S.-M. Peng, *J. Am. Chem. Soc.* **2008**, *130*, 10090-10092.

[16] J. F. Berry, F. A. Cotton, C. S. Fewox, T. Lu, C. A. Murillo, X. Wang, *Dalton Transactions* **2004**, 2297-2302.

[17] F. Albert Cotton, L. M. Daniels, C. A. Murillo, X. Wang, *Chem. Commun.* **1999**, 2461-2462.

[18] J.-T. Sheu, C.-C. Lin, I. Chao, C.-C. Wang, S.-M. Peng, *Chem. Commun.* **1996**, 315-316.

[19] S.-J. Shieh, C.-C. Chou, G.-H. Lee, C.-C. Wang, S.-M. Peng, *Angew. Chem. Int. Ed.* **1997**, *36*, 56-59; *Angew. Chem.* **1997**, *109*, 57-59.

[20] S.-Y. Lai, T.-W. Lin, Y.-H. Chen, C.-C. Wang, G.-H. Lee, M.-h. Yang, M.-k. Leung, S.-M. Peng, *J. Am. Chem. Soc.* **1998**, *121*, 250-251.

[21] M.-M. Rohmer, I. P.-C. Liu, J.-C. Lin, M.-J. Chiu, C.-H. Lee, G.-H. Lee, M. Bénard, X. López, S.-M. Peng, *Angew. Chem. Int. Ed.* **2007**, *46*, 3533-3536; *Angew. Chem.* **2007**, *119*, 3603-3606.

[22] S.-M. Peng, C.-C. Wang, Y.-L. Jang, Y.-H. Chen, F.-Y. Li, C.-Y. Mou, M.-K. Leung, *J. Magn. Magn. Mater.* **2000**, *209*, 80-83.

[23] R. H. Ismayilov, W.-Z. Wang, G.-H. Lee, C.-Y. Yeh, S.-A. Hua, Y. Song, M.-M. Rohmer, M. Bénard, S.-M. Peng, *Angew. Chem. Int. Ed.* **2011**, *50*, 2045-2048; *Angew. Chem.* **2011**, *123*, 2093-2096.

[24] T. Murahashi, E. Mochizuki, Y. Kai, H. Kurosawa, *J. Am. Chem. Soc.* **1999**, *121*, 10660-10661.

[25] T. Murahashi, T. Otani, T. Okuno, H. Kurosawa, *Angew. Chem. Int. Ed.* **2000**, *39*, 537-540; *Angew. Chem.* **2000**, *112*, 547-550.

[26] T. Murahashi, Y. Higuchi, T. Katoh, H. Kurosawa, *J. Am. Chem. Soc.* **2002**, *124*, 14288-14289.
[27] T. Murahashi, T. Uemura, H. Kurosawa, *J. Am. Chem. Soc.* **2003**, *125*, 8436-8437.
[28] T. Murahashi, M. Fujimoto, M.-a. Oka, Y. Hashimoto, T. Uemura, Y. Tatsumi, Y. Nakao, A. Ikeda, S. Sakaki, H. Kurosawa, *Science* **2006**, *313*, 1104-1107.
[29] Y. Tatsumi, K. Shirato, T. Murahashi, S. Ogoshi, H. Kurosawa, *Angew. Chem. Int. Ed.* **2006**, *45*, 5799-5803; *Angew. Chem.* **2006**, *118*, 5931-5935.
[30] T. Murahashi, T. Nagai, T. Okuno, T. Matsutani, H. Kurosawa, *Chem. Commun.* **2000**, 1689-1690.
[31] Y. Tatsumi, T. Murahashi, M. Okada, S. Ogoshi, H. Kurosawa, *Chem. Commun.* **2008**, 477-479.
[32] L.-J. Xu, J.-Y. Wang, L.-Y. Zhang, L.-X. Shi, Z.-N. Chen, *Organometallics* **2013**, *32*, 5402-5408.
[33] I. S. Krytchankou, D. V. Krupenya, A. J. Karttunen, S. P. Tunik, T. A. Pakkanen, P.-T. Chou, I. O. Koshevoy, *Dalton Trans.* **2014**, *43*, 3383-3394.
[34] T. M. Dau, Y.-A. Chen, A. J. Karttunen, E. V. Grachova, S. P. Tunik, K.-T. Lin, W.-Y. Hung, P.-T. Chou, T. A. Pakkanen, I. O. Koshevoy, *Inorg. Chem.* **2014**, *53*, 12720-12731.
[35] T. M. Dau, J. R. Shakirova, A. Doménech, J. Jänis, M. Haukka, E. V. Grachova, T. A. Pakkanen, S. P. Tunik, I. O. Koshevoy, *Eur. J. Inorg. Chem.* **2013**, *2013*, 4976-4983.
[36] M. Bardají, A. Laguna, P. G. Jones, A. K. Fischer, *Inorg. Chem.* **2000**, *39*, 3560-3566.
[37] M. Bardají, A. Laguna, V. M. Orera, M. D. Villacampa, *Inorg. Chem.* **1998**, *37*, 5125-5130.
[38] D. Li, C.-M. Che, S.-M. Peng, S.-T. Liu, Z.-Y. Zhou, T. C. W. Mak, *J. Chem. Soc., Dalton Trans.* **1993**, 189-194.
[39] C.-M. Che, H.-K. Yip, D. Li, S.-M. Peng, G.-H. Lee, Y.-M. Wang, S.-T. Liu, *J. Chem. Soc., Chem. Commun.* **1991**, 1615-1617.
[40] A. L. Balch, L. A. Fossett, J. K. Nagle, M. M. Olmstead, *J. Am. Chem. Soc.* **1988**, *110*, 6732-6738.
[41] L.-Y. Zhang, L.-J. Xu, X. Zhang, J.-Y. Wang, J. Li, Z.-N. Chen, *Inorg. Chem.* **2013**, *52*, 5167-5175.
[42] W. Lu, M. C. W. Chan, N. Zhu, C.-M. Che, C. Li, Z. Hui, *J. Am. Chem. Soc.* **2004**, *126*, 7639-7651.
[43] S. C. F. Kui, I. H. T. Sham, C. C. C. Cheung, C.-W. Ma, B. Yan, N. Zhu, C.-M. Che, W.-F. Fu, *Chem. Eur. J.* **2007**, *13*, 417-435.
[44] T. Tanase, H. Takahata, H. Ukaji, M. Hasegawa, Y. Yamamoto, *J. Organomet. Chem.* **1997**, *538*, 247-250.
[45] T. Tanase, H. Ukaji, H. Takahata, H. Toda, Y. Yamamoto, *Organometallics* **1998**, *17*, 196-209.
[46] E. Goto, R. A. Begum, S. Zhan, T. Tanase, K. Tanigaki, K. Sakai, *Angew. Chem. Int. Ed.* **2004**, *43*, 5029-5032; *Angew. Chem.* **2004**, *116*, 5139-5142.
[47] M. T. Dau, J. R. Shakirova, A. J. Karttunen, E. V. Grachova, S. P. Tunik, A. S. Melnikov, T. A. Pakkanen, I. O. Koshevoy, *Inorg. Chem.* **2014**, *53*, 4705-4715.
[48] A. Yoshii, H. Takenaka, H. Nagata, S. Noda, K. Nakamae, B. Kure, T. Nakajima, T. Tanase, *Organometallics* **2012**, *31*, 133-143.
[49] Y. Takemura, T. Nakajima, T. Tanase, *Eur. J. Inorg. Chem.* **2009**, *2009*, 4820-4829.
[50] T. Tanase, R. Otaki, T. Nishida, H. Takenaka, Y. Takemura, B. Kure, T. Nakajima, Y. Kitagawa, T. Tsubomura, *Chem. Eur. J.* **2014**, *20*, 1577-1596.
[51] Y. Takemura, H. Takenaka, T. Nakajima, T. Tanase, *Angew. Chem. Int. Ed.* **2009**, *48*, 2157-2161; *Angew. Chem.* **2009**, *121*, 2191-2195.
[52] A. Yoshii, H. Takenaka, H. Nagata, S. Noda, K. Nakamae, B. Kure, T. Nakajima, T. Tanase, *Organometallics* **2012**, *31*, 133-143.
[53] K. Nakamae, Y. Takemura, B. Kure, T. Nakajima, Y. Kitagawa, T. Tanase, *Angew. Chem. Int. Ed.* **2015**, *54*, 1016-1021; *Angew. Chem.* **2015**, *127*, 1030-1035.
[54] K. Nakamae, B. Kure, T. Nakajima, Y. Ura, T. Tanase, *Chem. Asian J.* **2014**, *9*, 3106-3110.
[55] D. Li, H.-K. Yip, C.-M. Che, Z.-Y. Zhou, T. C. W. Mak, S.-T. Liu, *J. Chem. Soc., Dalton Trans.* **1992**, 2445-2449.
[56] Y. Takemura, T. Nakajima, T. Tanase, *Dalton Trans.* **2009**, 10231-10243.
[57] J. Bai, A. V. Virovets, M. Scheer, *Angew. Chem. Int. Ed.* **2002**, *41*, 1737-1740; *Angew. Chem.* **2002**, *114*, 1808-1811.
[58] F. Dielmann, A. Schindler, S. Scheuermayer, J. Bai, R. Merkle, M. Zabel, A. V. Virovets, E. V. Peresypkina, G. Brunklaus , H. Eckert, M. Scheer, *Chem. Eur. J.* **2012**, *18*, 1168-1179.
[59] J. Bai, A. V. Virovets, M. Scheer, *Science* **2003**, *300*, 781-783.
[60] M. Scheer, J. Bai, B. P. Johnson, R. Merkle, A. V. Virovets, C. E. Anson, *Eur. J. Inorg. Chem.* **2005**, *2005*, 4023-4026.
[61] M. Scheer, A. Schindler, C. Gröger, A. V. Virovets, E. V. Peresypkina, *Angew. Chem. Int. Ed.* **2009**, *48*, 5046-5049; *Angew. Chem.* **2009**, *121*, 5148-5151.

[62] A. Schindler, C. Heindl, G. Balázs, C. Gröger, A. V. Virovets, E. V. Peresypkina, M. Scheer, *Chem. Eur. J.* **2012**, *18*, 829-835.

[63] C. Schwarzmaier, A. Schindler, C. Heindl, S. Scheuermayer, E. V. Peresypkina, A. V. Virovets, M. Neumeier, R. Gschwind, M. Scheer, *Angew. Chem. Int. Ed.* **2013**, *52*, 10896-10899; *Angew. Chem.* **2013**, *125*, 11097-11100.

[64] S. Welsch, C. Gröger, M. Sierka, M. Scheer, *Angew. Chem. Int. Ed.* **2011**, *50*, 1435-1438; *Angew. Chem.* **2011**, *123*, 1471-1474.

[65] F. Dielmann, R. Merkle, S. Heinl, M. Scheer, *Z.Naturforsch.* **2009**, *64b*, 3-10.

[66] C. Heindl, S. Heinl, D. Lüdeker, G. Brunklaus, W. Kremer, M. Scheer, *Inorg. Chim. Acta* **2014**, *422*, 218-223.

[67] F. Dielmann, C. Heindl, F. Hastreiter, E. V. Peresypkina, A. V. Virovets, R. M. Gschwind, M. Scheer, *Angew. Chem. Int. Ed.* **2014**, *53*, 13605-13608; *Angew. Chem.* **2014**, *126*, 13823-13827.

[68] F. Dielmann, M. Fleischmann, C. Heindl, E. V. Peresypkina, A. V. Virovets, R. M. Gschwind, M. Scheer, *Chem. Eur. J.* **2015**, *21*, 6208-6214.

[69] S. Heinl, E. Peresypkina, J. Sutter, M. Scheer, *Angew. Chem. Int. Ed.* **2015**, 10.1002/anie.201505516; *Angew. Chem.* **2015**, 10.1002/ange.201505516.

[70] C. Heindl, E. V. Peresypkina, A. V. Virovets, W. Kremer, M. Scheer, *J. Am. Chem. Soc.* **2015**, *137*, 10938-10941.

[71] M. Scheer, L. J. Gregoriades, M. Zabel, J. Bai, I. Krossing, G. Brunklaus, H. Eckert, *Chem. Eur. J.* **2008**, *14*, 282-295.

[72] B. Attenberger, S. Welsch, M. Zabel, E. Peresypkina, M. Scheer, *Angew. Chem., Int. Ed.* **2011**, *50*, 11516; *Angew. Chem.* **2011**, *123*, 11718-11722.

[73] B. Attenberger, E. V. Peresypkina, M. Scheer, *Inorg. Chem.* **2015**, *54*, 7021-7029.

[74] S. Welsch, C. Lescop, G. Balázs, R. Réau, M. Scheer, *Chem. Eur. J.* **2011**, *17*, 9130-9141.

[75] M. Fleischmann, S. Welsch, E. V. Peresypkina, A. V. Virovets, M. Scheer, *Chem. Eur. J.* **2015**, *21*, 14332-14336.

[76] M. Scheer, L. J. Gregoriades, A. V. Virovets, W. Kunz, R. Neueder, I. Krossing, *Angew. Chem. Int. Ed.* **2006**, *45*, 5689-5693; *Angew. Chem.* **2006**, *118*, 5818-5822.

[77] L. J. Gregoriades, B. K. Wegley, M. Sierka, E. Brunner, C. Gröger, E. V. Peresypkina, A. V. Virovets, M. Zabel, M. Scheer, *Chem. Asian J.* **2009**, *4*, 1578-1587.

[78] S. Welsch, L. J. Gregoriades, M. Sierka, M. Zabel, A. V. Virovets, M. Scheer, *Angew. Chem. Int. Ed.* **2007**, *46*, 9323-9326; *Angew. Chem.* **2007**, *119*, 9483-9487.

[79] M. Fleischmann, S. Welsch, H. Krauss, M. Schmidt, M. Bodensteiner, E. V. Peresypkina, M. Sierka, C. Gröger, M. Scheer, *Chem. Eur. J.* **2014**, *20*, 3759-3768.

[80] M. Fleischmann, S. Welsch, L. J. Gregoriades, C. Gröger, M. Scheer, *Z. Naturforsch.* **2014**, *69b*, 1348-1356.

[81] S. Welsch, M. Bodensteiner, M. Dušek, M. Sierka, M. Scheer, *Chem. Eur. J.* **2010**, *16*, 13041-13045.

[82] M. Fleischmann, L. Dütsch, M. E. Moussa, A. Schindler, G. Balázs, C. Lescop, M. Scheer, *Chem. Commun.* **2015**, *51*, 2893-2895.

[83] The parent compounds **2a-c** can exhibit two different isomers regarding the orientation of the central Ph group of one dpmp ligand (see below for details) which are referred to as **2a-c** and **2a*-c***, respectively. This isomerism was only observed for the parent compounds with vacant coordination sites on the terminal atoms. During this study no single crystal structures of **2c** and **2a*** could be determined.

[84] The analogues complex for X = Cl(**3a**) could not be structurally characterized.

[85] The crystal structure of **1a** is in good agreement with the determined structure of the previously reported [ClO4]– salt.[55]

[86] While the central Ph ring in **2a** and **2b** are directed upwards in Figure 1, they are directed towards the reader in **2c*** and **2a*** in Figure 1 and 2.

[87] O. J. Scherer, H. Sitzmann, G. Wolmershäuser, *J. Organomet. Chem.* **1984**, *268*, C9-C12.

[88] P. J. Sullivan, A. L. Rheingold, *Organometallics* **1982**, *1*, 1547-1549.

[89] details can be found in the supporting information of [82].

[90] The dynamic coordination behavior of $[Cu_3(\mu\text{-}I)_2(\mu\text{-dpmp})_2]^+$ (see NMR characterization) is the reason, that in solution only ~50% of the parent Cu_3 building block are present next to other species. Therefore, we assume, that this trinuclear complex readily reacts with the *cyclo*-P_3 ligand **B** to form compound **7** with a 1:2 ratio instead of the analogues polymeric **6c** with a 1:1 ratio. When a solution of a 1:1 stoichiometry (**2c**:**B**) is kept for a long time, the formation of **7** (1:1 ratio) can be seen followed

by the formation of colorless crystals after some time (presumably pure **2c**). A similar behavior is observed in the reaction of **2c** with the *cyclo*-P_5 complex **C1**. For this reaction we have some indications, that we can actually prepare the analogues compound with a 1:1 ratio (**2c**:**C1**) (see below).

[91] Crystals of **6a** could only be obtained as very fine needles which lose their crystallinity immediately after removal from the mother liquor even when mounted in cooled oil. This significantly complicated the data collection and the structure refinement. The unit cell and space group were assigned to $P2_1$, a = 14.7809(3) Å, b = 20.9944(4) Å, c = 15.7059(3) Å, β = 95.416(2)°, V = 4852.04(16) Å3. The final model for this structure determination (R_1 = 4.0% wR_2 = 10.8%) clearly shows the similar arrangement of **6a** and **6b** in the solid-state (the structure solution and refinement of **6b** could be done without difficulty).

[92] The reactivity of **C1** towards **2c** closely resembles the reactivity of complex **B**. We assume this result because of the same reasons (see [90]) based on the dynamic coordination behavior of **2c** in solution. When **2c** is dissolved at –30°C (see VT NMR study: NMR shows almost 100% of the compound is present as the parent $[Cu_3(\mu\text{-}I)_2(\mu\text{-}dpmp)_2]^+$ complex) and reacted with an equimolar amount of **C1**, very tiny light green crystals are obtained upon diffusion of alkanes into this solution. X-ray diffraction allows the determination of a unit cell (monoclinic P, a = 12.4819(19) Å, b = 25.128(3), c = 27.818(7) Å, β = 97.68(2), V = 8647(3), 95.12% indexed, 164 reflections collected) but the diffraction was too weak to enable a structure determination. This unit cell is in good agreement with the determined unit cells of the three isostructural one-dimensional coordination polymers **8a**, **8b** and **9**. This conclusively suggests the formation of the analogues polymeric compound **8c**, although we were unable to structurally characterize it.

[93] O. J. Scherer, T. Brück, *Angew. Chem. Int. Ed.* **1987**, *26*, 59-59; *Angew. Chem.* **1987**, *99*, 59-59.

[94] All crystals that were obtained of compound **10** showed twinning. The central $[Cu_3(\mu\text{-}I)_2(\mu\text{-}dpmp)_2]^+$ building block and the *cyclo*-P_5 ligands **C1** could clearly be determined without any disorder. The data reduction by the CrysalisPro Software package lead to comparable results when the data was integrated for twinned crystals or as a single crystal. Therefore the structure solution of **10** was done by regular HKLF 4 refinement by ShelX. This may be the cause for the elevated R values, standard uncertainties and the residual electron density for **10**.

[95] J. F. Berry, F. A. Cotton, T. Lu, C. A. Murillo, B. K. Roberts, X. Wang, *J. Am. Chem. Soc.* **2004**, *126*, 7082-7096.

8.5 Supporting Information

Preparation of the described compounds

General considerations

All manipulations were carried out under an inert atmosphere of dried nitrogen using standard Schlenk and drybox techniques. THF was dried with Na. MeCN, CH_2Cl_2 and CD_2Cl_2 were dried over CaH_2. *ortho*-difluorobenzene (*o*-DFB) was distilled from P_4O_{10}. NMR spectra were recorded in CD_2Cl_2 on a Bruker Avance 300 MHz NMR spectrometer (^{1}H: 300.132 MHz, ^{31}P: 121.495 MHz, ^{13}C: 75.468 MHz, ^{19}F: 282.404 MHz) or on a Bruker Avance 400 MHz NMR spectrometer (^{1}H: 400.130 MHz, ^{31}P: 161.976 MHz, ^{13}C: 100.613 MHz, ^{11}B: 128.378 MHz) with external references of $SiMe_4$ (^{1}H, ^{13}C), CCl_3F (^{19}F), H_3PO_4 (85%, ^{31}P) and $Et_2O{\cdot}BF_3$ (^{11}B). IR spectra were recorded as KBr discs using a Varian FTS-800 FT-IR spectrometer. Electron spray ionization mass spectra were recorded by the MS department of the University of Regensburg on a ThermoQuest Finnigan TSQ 7000 mass spectrometer. Elemental analyses were performed by the micro analytical laboratory of the University of Regensburg. Commercially available reagents were used without further purification. Cu^{I} halides were recrystallized from MeCN prior to use. The E_n ligand complexes **A1**,[1] **A2**,[2] **B**,[1] **C1**[3] and **C2**[4] as well as the dpmp ligand were prepared according to the literature procedures including minor alterations. The preparation and full characterization of the compounds **1a**, **2a***, **4a**, **5**, **8a** and **9** was reported previously.[6]

NMR characterization of $[Cu_3(\mu\text{-}Cl)_2(dpmp)_2(MeCN)_2]^+[BF_4]^-$ (**1a**): Due to drying in vacuum the MeCN ligands are removed. ^{1}H NMR (400 MHz, CD_2Cl_2, 193 K) *δ*/ppm 8.20 – 6.16 (multiple signals, 50H, Ph), 3.52 (br, 4H, CH_2), 3.06 (br, 4H, CH_2); ^{31}P{^{1}H} NMR (162.0 MHz, CD_2Cl_2, 193 K) *δ*/ppm –15.6 (m, 4P, $RPPh_2$), –18.2 (br, 2P, R_2PPh); ^{1}H NMR (400 MHz, CD_2Cl_2, 300 K) *δ*/ppm 7.70 - 6.58 (m, 50H, Ph), 3.81 - 3.00 (multiple overlapping signals, CH_2); ^{31}P{^{1}H} NMR (162.0 MHz, CD_2Cl_2, 300 K) *δ*/ppm –6.5 (m, small signal), –11.2 (m, small signal), –14.3 (m, $RPPh_2$), –17.3 (br, R_2PPh); ^{11}B{^{1}H} NMR (128.4 MHz, CD_2Cl_2, 300 K) *δ*/ppm –0.95 (BF_4); ^{13}C{^{1}H} NMR (100.6 MHz, CD_2Cl_2, 300 K) *δ*/ppm 133.65 - 127.49 (multiple signals, Ph), 28.16 (CH_2).

Preparation of $[Cu_3(\mu\text{-}Br)_2(dpmp)_2(MeCN)_2]^+[BF_4]^-$ (**1b**): 101 mg (2eq., 0.2 mmol) dpmp, 32 mg (1eq., 0.1 mmol) $[Cu(MeCN)_4][BF_4]$ and 29 mg (2eq., 0.2 mmol) CuBr were weighed into a Schlenk flask and a solvent mixture of 8 mL THF and 2 mL MeCN were added under constant stirring. The compounds dissolved to form a clear and colorless solution. After 24 hours of stirring at room temperature the solution was filtered and subsequently layered with the fivefold amount of Et_2O. Storage at +4 °C affords colorless crystal in the course of some days. The mother liquor is decanted off the crystals. The crystals are washed with Et_2O a few times and dried in vacuum for 30 minutes. After this time the coordinated MeCN ligands could be removed from the crystals proved by elemental analysis. Yield 116 mg (76%). ^{1}H NMR (400 MHz, CD_2Cl_2, 193 K) *δ*/ppm 8.34 – 6.12 (multiple signals, 50H, Ph), 3.60 (br, 4H, CH_2), 3.17 (br, 4H, CH_2); ^{31}P{^{1}H} NMR (162.0 MHz, CD_2Cl_2, 193 K) *δ*/ppm –16.7 (m, 4P, $RPPh_2$), –21.5 (br, 2P, R_2PPh); ^{1}H NMR (400 MHz, CD_2Cl_2, 300 K) *δ*/ppm 7.87 - 6.57 (m, 50H, Ph), 3.85 - 3.07 (multiple overlapping signals, CH_2); ^{31}P{^{1}H} NMR (162.0 MHz, CD_2Cl_2, 300 K) *δ*/ppm –6.5 (m, small signal), –12.1 (m, small signal), –15.9 (m, $RPPh_2$), –21.5 (br, R_2PPh); ^{11}B{^{1}H} NMR (128.4 MHz, CD_2Cl_2, 300 K) *δ*/ppm –0.91 (BF_4); ^{13}C{^{1}H} NMR (100.6 MHz, CD_2Cl_2, 300 K) *δ*/ppm 135.32 - 127.65 (multiple signals, Ph), 31.05 - 28.76 (CH_2). Anal. calcd. for $Cu_3Br_2(dpmp)_2(BF_4)$: C, 53.00; H, 4.03. Found: C, 53.17; H, 4.09. Positive ion MS, *m/q* (%): 1363.2 (100) $[Cu_3Br_2(dpmp)_2]^+$, 1319.3 (17) $[Cu_3BrCl(dpmp)_2]^+$, 713.0 (13) $[Cu_2Br(dpmp)]^+$, 642.2 (10) $[Cu_3Br(dpmp)_2]^{2+}$, 569.0 (8) $[Cu(dpmp)]^+$. Negative ion MS, *m/q* (%): 87.1 (100) $[BF_4]^-$. IR(KBr) cm^{-1}: 3072 (w), 3052 (w),

3021 (vw), 3005 (vw), 2987 (vw), 2925 (vw), 2897 (vw), 2361 (w), 2333 (w), 1624 (w), 1587 (w), 1574 (w), 1484 (m), 1435 (s), 1384 (w), 1124 (m), 1097 (s), 1084 (vs), 1064 (m), 1028 (m), 1000 (w).

Preparation of $[Cu_3(\mu\text{-}I)_2(dpmp)_2(MeCN)_2]^+[BF_4]^-$ (**1c**): 101 mg (2eq., 0.2 mmol) dpmp, 32 mg (1eq., 0.1 mmol) $[Cu(MeCN)_4][BF_4]$ and 38 mg (2eq., 0.2 mmol) CuI were weighed into a Schlenk flask and a solvent mixture of 10 mL THF and 5 mL MeCN were added under constant stirring. The compounds dissolved to form a clear and colorless solution. After 24 hours of stirring at room temperature the solution was filtered and subsequently layered with the fivefold amount of Et_2O. Storage at +4 °C affords colorless crystal in the course of some days. The mother liquor is decanted off the crystals. The crystals are washed with Et_2O a few times and dried in vacuum for 30 minutes. After this time the coordinated MeCN ligands could be removed from the crystals proved by elemental analysis. Yield 107 mg (66%). ^{1}H NMR (400 MHz, CD_2Cl_2, 193 K) *δ*/ppm 7.30 - 6.43 (m, 50H, Ph), 3.60 (br, 4H, CH_2), 3.35 (br, 4H, CH_2); $^{31}P\{^1H\}$ NMR (162.0 MHz, CD_2Cl_2, 193 K) *δ*/ppm –18.4 (m, $RPPh_2$), –29.0 (br, R_2PPh); ^{1}H NMR (400 MHz, CD_2Cl_2, 300 K) *δ*/ppm 8.12 - 6.04 (m, 50H, Ph), 4.04 – 2.40 (m, 8H, CH_2); $^{31}P\{^1H\}$ NMR (162.0 MHz, CD_2Cl_2, 300 K) *δ*/ppm –6.5 (m, small signal), –11.2 (m, small signal), –17.8 (m, $RPPh_2$), –25.8 (br, R_2PPh), –30.5 (br, R_2PPh); $^{11}B\{^1H\}$ NMR (128.4 MHz, CD_2Cl_2, 300 K) *δ*/ppm –1.05 (s, BF_4); Anal. calcd. for $Cu_3I_2(dpmp)_2(BF_4)$: C, 49.78; H, 3.79. Found: C, 49.90; H, 3.84. Positive ion MS, *m/q* (%): 1836.8 (20) $[Cu_5I_4(dpmp)_2]^+$, 1746.9 (8) $[Cu_5I_3Cl(dpmp)_2]^+$, 1646.9 (32) $[Cu_4I_3(dpmp)2]^+$, 1555.0 (8) $[Cu_4I_2Cl(dpmp)_2]^+$, 1457.1 (100) $[Cu_3I_2(dpmp)_2]^+$, 1365.1 (40) $[Cu_3ICl(dpmp)_2]^+$, 1075.3 (2) $[Cu(dpmp)_2]^+$, 569.0 (3) $[Cu(dpmp)]^+$. Negative ion MS, *m/q* (%): 87.1 (100) $[BF_4]^-$. IR(KBr) cm^{-1}: 3072 (w), 3052 (w), 3021 (vw), 3005 (vw), 2988 (vw), 2949 (vw), 2894 (vw), 2359 (w), 2325 (w), 1624 (w), 1587 (w), 1574 (w), 1484 (m), 1435 (vs), 1381 (w), 1124 (m), 1097 (vs), 1084 (vs), 1060 (s), 1027 (m), 999 (m).

Preparation of $[Cu_3(\mu\text{-}Br)_2(dpmp)_2(CH_2Cl_2)_2]^+[BF_4]^-$ (**3b**) and $[Cu_3(\mu\text{-}Br)_2(dpmp)_2]^+[BF_4]^-$ (**2b**): 101 mg (2eq., 0.2 mmol) dpmp, 32 mg (1eq., 0.1 mmol) $[Cu(MeCN)_4][BF_4]$ and 29 mg (2eq., 0.2 mmol) CuBr were weighed into a Schlenk flask and 10 mL of CH_2Cl_2 (**3**) or 50 mL of *o*-DFB (**2b**) were added and the reaction stirred for 24 hours. The compounds dissolved to form a clear and colorless solution in ~30min. After 24 hours of stirring at room temperature the solution was filtered and subsequent layering with the fivefold amount of *n*-hexane (**2b**) or gas phase diffusion of *n*-pentane into the solution (**3**) afforded the product **2b** or **3** as clear colorless crystals in the course of some days. The mother liquor is decanted off the crystals. The crystals are washed with alkanes a few times and dried in vacuum for 30 minutes. Yield 97 mg (**3**, 67%). For analytical data see preparation of **1b**.

Preparation of $[Cu_3(\mu\text{-}I)_2(dpmp)_2]^+[BF_4]^-$ (**2c**): 101 mg (2eq., 0.2 mmol) dpmp, 32 mg (1eq., 0.1 mmol) $[Cu(MeCN)_4][BF_4]$ and 38 mg (2eq., 0.2 mmol) CuI were weighed into a Schlenk flask and 10 mL of CH_2Cl_2 were added and the reaction stirred for 24 hours. The compounds dissolved to form a clear and colorless solution in the course of 5-6 hours. After 24 hours of stirring at room temperature the solution was filtered and subsequent gas phase diffusion of *n*-pentane into the solution afforded **2c** as clear colorless crystals in the course of some days. The mother liquor is decanted off the crystals. The crystals are washed with *n*-pentane a few times and dried in vacuum for 30 minutes. Yield 107 mg (69%). For analytical data see preparation of **1c**.

Preparation of $[Cu_3(\mu\text{-}Br)_2(dpmp)_2(\eta^1\text{-}\mathbf{A1})]^+[BF_4]^-$ (**4b**): 101 mg (2eq., 0.2 mmol) dpmp, 32 mg (1eq., 0.1 mmol) $[Cu(MeCN)_4][BF_4]$ and 29 mg (2eq., 0.2 mmol) CuBr were weighed into a Schlenk flask and 10 mL of CH_2Cl_2 were added. The solids dissolved under constant stirring in the course of 30 min. to form a clear colorless solution. After 24 hours of stirring at room temperature 50 mg (1 eq., 0.1 mmol) of **A1** were added and the clear red solution was stirred for additional 24 hours. Vapor diffusion of *n*-pentane into the filtered solution at room temperature

affords **4b** as orange needles after several days. The crystals are freed from the mother liquor, washed with *n*-pentane a few times and dried in vacuum. Yield 140 mg (72%). ^{1}H NMR (300 MHz, CD_2Cl_2, 300 K) *δ*/ppm 7.75 – 6.54 (m, 50H, Ph), 5.09 (br, Cp), 3.78 (m, small signal, CH_2), 3.62 (m, CH_2), 3.46 (m, small signal, CH_2), 3.18 (m, CH_2); ^{31}P{^{1}H} NMR (121.5 MHz, CD_2Cl_2, 300 K) *δ*/ppm –6.4 (m, small signal), –12.2 (m, small signal), –17.3 (m, $RPPh_2$), –23.8 (br, R_2PPh) –74.4 (br, *ω½* ~ 500 Hz, P_2); ^{19}F{^{1}H} NMR (282.4 MHz, CD_2Cl_2, 300 K) *δ*/ppm –148.9 (br, BF_4); ^{13}C{^{1}H} NMR (75.5 MHz, CD_2Cl_2, 300 K) *δ*/ppm 135.61 – 127.20 (multiple signals, Ph), 87.88 (s, Cp). Anal. calcd. for $Cu_3Br_2(dpmp)_2$(**A1**)$(BF_4)\cdot(CH_2Cl_2)_{0.5}$: C, 47.41; H, 3.50. Found: C, 47.44; H, 3.54. Positive ion MS, *m/q* (%): 1363.1 (100) $[Cu_3Br_2(dpmp)_2]^+$, 1319.1 (11) $[Cu_3BrCl(dpmp)_2]^+$, 1506.9 (3) $[Cu_4Br_3(dpmp)_2]^+$, 1219.1 (6) $[Cu_2Br(dpmp)_2]^+$. Negative ion MS, *m/q* (%): 1537.2 (100) $[Cu_3Br_2(dpmp)_2(BF_4)_2]^-$, 1491.3 (14) $[Cu_3BrCl(dpmp)_2(BF_4)_2]^-$. IR(KBr) cm^{-1}: 3118 (vw), 3080 (vw), 3052 (w), 3005 (vw), 2987 (vw), 2951 (vw), 2894 (vw), 1990 (w), 1964 (vs), 1924 (s), 1911 (s), 1630 (w), 1485 (w), 1435 (m), 1419 (w), 1378 (w), 1098 (m), 1084 (m), 1027 (w), 1000 (w).

Preparation of $[Cu_3(\mu\text{-}I)_2(dpmp)_2(\eta^1$-**A1**$)]^+[BF_4]^-$ (**4c**): 101 mg (2eq., 0.2 mmol) dpmp, 32 mg (1eq., 0.1 mmol) $[Cu(MeCN)_4][BF_4]$ and 38 mg (2eq., 0.2 mmol) CuI were weighed into a Schlenk flask and 10 mL of CH_2Cl_2 were added. The solids dissolved under constant stirring in the course of 5 to 6 hours to form a clear colorless solution. After 24 hours of stirring at room temperature 50 mg (1 eq., 0.1 mmol) of **A1** were added and the clear red solution was stirred for additional 24 hours. Vapor diffusion of *n*-pentane into the filtered solution at room temperature affords **4c** as orange to red needles after several days. The crystals are freed from the mother liquor, washed with *n*-pentane a few times and dried in vacuum. Yield 180 mg (88%). ^{1}H NMR (300 MHz, CD_2Cl_2, 300 K) *δ*/ppm 8.57 - 6.03 (m, 50H, Ph), 5.09 (s, Cp), 3.58 (br, 4H, CH_2), 3.34 (br, 4H, CH_2); ^{31}P{^{1}H} NMR (121.5 MHz, CD_2Cl_2, 300 K) *δ*/ppm –20.2 (m, $RPPh_2$), –31.2 (br, R_2PPh), –78.4 (br, *ω½* ~ 450 Hz, P_2); ^{19}F{^{1}H} NMR (282.4 MHz, CD_2Cl_2, 300 K) *δ*/ppm –149.71 ($^{10}BF_4$), –149.76 ($^{11}BF_4$); ^{13}C{^{1}H} NMR (75.5 MHz, CD_2Cl_2, 300 K) *δ*/ppm 135.20 – 127.30 (multiple signals, Ph), 88.01 (s, Cp). Anal. calcd. for $Cu_3I_2(dpmp)_2$(**A1**)$(BF_4)\cdot(CH_2Cl_2)_{0.5}$: C, 45.27; H, 3.34. Found: C, 45.17; H, 3.37. Positive ion MS, *m/q* (%): 1457.2 (100) $[Cu_3I_2(dpmp)_2]^+$, 1365.2 (17) $[Cu_3ICl(dpmp)_2]^+$, 1838.8 (12) $[Cu_5I_4(dpmp)_2]^+$, 1747.0 (2) $[Cu_5I_3Cl(dpmp)_2]^+$, 1647.0 (43) $[Cu_4I_3(dpmp)_2]^+$, 1555.1 (4) $[Cu_4I_2Cl(dpmp)_2]^+$, 1267.2 (30) $[Cu_2I(dpmp)_2]^+$, 1175.3 (1.5) $[Cu_2Cl(dpmp)_2]^+$. Negative ion MS, *m/q* (%): 1631.2 (100) $[Cu_3I_2(dpmp)_2(BF_4)_2]^-$, 1539.3 (24) $[Cu_3ICl(dpmp)_2(BF_4)_2]^-$, 2012.6 (12) $[Cu_5I_4(dpmp)_2(BF_4)]^-$, 1922.0 (6) $[Cu_5I_3Cl(dpmp)_2(BF_4)_2]^-$, 1822.3 (40) $[Cu_4I_3(dpmp)_2(BF_4)_2]^-$, 1732.2 (5) $[Cu_4I_2Cl(dpmp)_2(BF_4)_2]^-$. IR(KBr) cm^{-1}: 3110 (vw), 3072 (vw), 3051 (w), 3005 (vw), 2988 (vw), 2953 (vw), 2923 (vw), 2891 (vw), 2852 (vw), 1995 (m), 1950 (vs), 1941 (vs), 1918 (vs), 1852 (m), 1635 (w), 1484 (w), 1435 (s), 1380 (w), 1097 (m), 1084 (m), 1063 (m), 1028 (w), 1000 (w).

Preparation of $[Cu_3(\mu\text{-}Cl)_2(dpmp)_2(\mu,\eta^1{:}\eta^1$-**B**$)]^+_n[BF_4]^-_n$ (**6a**): 101 mg (2eq., 0.2 mmol) dpmp, 32 mg (1eq., 0.1 mmol) $[Cu(MeCN)_4][BF_4]$ and 20 mg (2eq., 0.2 mmol) CuCl were weighed into a Schlenk flask and 10 mL of CH_2Cl_2 were added. The solids dissolved under constant stirring in the course of 5 min. to form a clear colorless solution. After 24 hours of stirring at room temperature 31 mg (1 eq., 0.1 mmol) of **B** were added and the clear yellow solution was stirred for additional 24 hours. Careful layering with the fivefold amount of *n*-pentane and subsequent storage at +4 °C affords **6a** as thin yellow needles after several days. The mother liquor is decanted off, the crystals are washed with *n*-pentane a few times and dried in vacuum. Yield 123 mg (74%). ^{1}H NMR (300 MHz, CD_2Cl_2, 300 K) *δ*/ppm 7.92 – 6.50 (m, 50H, Ph), 5.25 (s, Cp), 3.71 (br, CH_2), 3.38 (br, small signal, CH_2), 3.11 (br, CH_2); ^{31}P{^{1}H} NMR (121.5 MHz, CD_2Cl_2, 300 K) *δ*/ppm –6.6 (m, small signal), –11.4 (m, small signal), –14.5 (m, $RPPh_2$), –18.5 (br, R_2PPh), –350.7 (s, P_3); ^{19}F{^{1}H} NMR (282.4 MHz, CD_2Cl_2, 300 K) *δ*/ppm –149.35 ($^{10}BF_4$), –149.40 ($^{11}BF_4$); ^{13}C{^{1}H} NMR (75.5 MHz, CD_2Cl_2, 300 K) *δ*/ppm 135.01 – 128.04 (multiple signals, Ph), 86.31 (s, Cp). Anal. calcd. for $Cu_3Cl_2(dpmp)_2$(**B**)$(BF_4)\cdot(CH_2Cl_2)_{0.3}$: C, 50.48;

H, 3.78. Found: C, 50.39; H, 3.99. Positive ion MS, *m/q* (%): 1273.3 (100) $[Cu_3Cl_2(dpmp)_2]^+$. Negative ion MS, *m/q* (%): 86.7 (100) $[BF_4]^-$. IR(KBr) cm^{-1}: 3143 (vw), 3115 (vw), 3071 (vw), 3050 (w), 3017 (vw), 3005 (vw), 2986 (vw), 2950 (vw), 2889 (vw), 2017 (vs), 1955 (vs), 1587 (w), 1574 (w), 1484 (m), 1435 (vs), 1420 (vw), 1380 (m), 1332 (vw), 1310 (vw), 1279 (vw), 1186 (vw), 1150 (vw), 1098 (s), 1080 (vs), 1028 (m), 1000 (m), 838 (vw), 828 (vw), 792 (s), 766 (m), 717 (vs), 690 (vs), 555 (vw), 508 (s), 475 (s), 444 (w).

Preparation of $[Cu_3(\mu\text{-}Br)_2(dpmp)_2(\mu,\eta^1{:}\eta^1\text{-}\mathbf{B})]^+_n[BF_4]^-_n$ (**6b**): 101 mg (2eq., 0.2 mmol) dpmp, 32 mg (1eq., 0.1 mmol) $[Cu(MeCN)_4][BF_4]$ and 29 mg (2eq., 0.2 mmol) CuBr were weighed into a Schlenk flask and 10 mL of CH_2Cl_2 were added. The solids dissolved under constant stirring in the course of 30 min. to form a clear colorless solution. After 24 hours of stirring at room temperature 31 mg (1 eq., 0.1 mmol) of **B** were added and the clear yellow solution was stirred for additional 24 hours. Vapor diffusion of *n*-pentane into the filtered solution at room temperature affords **6b** as thin yellow needles after several days. The mother liquor is decanted off, the crystals are washed with *n*-pentane a few times and dried in vacuum. Yield 119 mg (68%). ^{1}H NMR (400 MHz, CD_2Cl_2, 300 K) *δ*/ppm 7.74 - 6.58 (m, 50H, Ph), 5.26 (s, Cp), 3.74 (br, CH_2), 3.45 (br, small signal, CH_2), 3.21 (br, CH_2); $^{31}P\{^1H\}$ NMR (162.0 MHz, CD_2Cl_2, 300 K) *δ*/ppm –6.3 (m, small signal), –12.1 (m, small signal), –15.9 (m, $RPPh_2$), –22.0 (br, R_2PPh), –350.7 (s, P_3); $^{13}C\{^1H\}$ NMR (100.6 MHz, CD_2Cl_2, 300 K) *δ*/ppm 222.24 (s, CO), 134.87 - 127.55 (multiple signals, Ph), 86.26 (s, Cp), 30.62 (br, CH_2). Anal. calcd. for $Cu_3Br_2(dpmp)_2(\mathbf{B})(BF_4)\cdot(CH_2Cl_2)_{0.5}$: C, 47.64; H, 3.58. Found: C, 47.71; H, 3.55. Positive ion MS, *m/q* (%): 1363.1 (100) $[Cu_3Br_2(dpmp)_2]^+$, 1319.1 (12) $[Cu_3BrCl(dpmp)_2]^+$, 2156.8 (0.2) $[Cu_5Br_4(dpmp)_3]^+$, 2112.9 (0.06) $[Cu_5Br_3Cl(dpmp)_3]^+$, 2013.1 (0.5) $[Cu_4Br_3(dpmp)_3]^+$, 1969.1 (0.15) $[Cu_4Br_2Cl(dpmp)_3]^+$, 1650.8 (0.75) $[Cu_5Br_4(dpmp)_2]^+$. Negative ion MS, *m/q* (%): 1537.4 (100) $[Cu_3Br_2(dpmp)_2(BF_4)_2]^-$, 1493.4 (14) $[Cu_3BrCl(dpmp)_2(BF_4)_2]^-$, 1681.2 (13) $[Cu_4Br_3(dpmp)_2(BF_4)_2]^-$. IR(KBr) cm^{-1}: 3118 (vw), 3072 (vw), 3050 (w), 3005 (vw), 2987 (vw), 2949 (vw), 2917 (vw), 2891 (vw), 2850 (vw), 2361 (w), 2342 (w), 2018 (vs), 1956 (vs), 1636 (m), 1484 (m), 1435 (vs), 1420 (w), 1384 (w), 1124 (m), 1098 (s), 1084 (vs), 1028 (m), 1000 (m).

Preparation of $[Cu_3(\mu\text{-}I)_2(dpmp)_2(\eta^1\text{-}\mathbf{B})_2]^+[BF_4]^-$ (**7**): 101 mg (2eq., 0.2 mmol) dpmp, 32 mg (1eq., 0.1 mmol) $[Cu(MeCN)_4][BF_4]$ and 38 mg (2eq., 0.2 mmol) CuI were weighed into a Schlenk flask and 10 mL of CH_2Cl_2 were added. The solids dissolved under constant stirring in the course of 5 to 6 hours to form a clear colorless solution. After 24 hours of stirring at room temperature 62 mg (2 eq., 0.2 mmol) of **B** were added and the clear yellow solution was stirred for additional 24 hours. The solution was filtered, carefully layered with pristine CH_2Cl_2 (~5 mL) and subsequently layered with the fivefold amount of *n*-pentane. Storage at +4 °C affords **7** as yellow blocks after some days. The mother liquor is decanted off, the crystals are washed with *n*-pentane a few times and dried in vacuum. Yield 191 mg (88%). ^{1}H NMR (300 MHz, CD_2Cl_2, 300 K) *δ*/ppm 8.60 - 6.02 (m, multiple overlapping signals, Ph), 5.29 (s, Cp), 3.72 – 2.21 (multiple overlapping signals, CH_2); $^{31}P\{^1H\}$ NMR (121.5 MHz, CD_2Cl_2, 300 K) *δ*/ppm –4.6 - –36.1 (multiple overlapping signals, dpmp) –351.2 (s, P_3); $^{19}F\{^1H\}$ NMR (282.4 MHz, CD_2Cl_2, 300 K) *δ*/ppm –151.38 ($^{10}BF_4$), –151.44 ($^{11}BF_4$); $^{13}C\{^1H\}$ NMR (75.5 MHz, CD_2Cl_2, 300 K) *δ*/ppm 135.40 - 127.69 (multiple signals, Ph), 86.29 (s, Cp). Anal. calcd. for $Cu_3I_2(dpmp)_2(\mathbf{B})_2(BF_4)\cdot(CH_2Cl_2)_{0.5}$: C, 42.73; H, 3.15. Found: C, 42.73; H, 3.18. Positive ion MS, *m/q* (%): 1457.1 (100) $[Cu_3I_2(dpmp)_2]^+$, 1365.2 (16) $[Cu_3ICl(dpmp)_2]^+$, 2344.6 (0.5) $[Cu_5I_4(dpmp)_3]^+$, 2153.8 (2.5) $[Cu_4I_3(dpmp)_3]^+$, 2031.2 (1) $[Cu_6I_5(dpmp)_2]^+$, 1837.0 (13) $[Cu_5I_4(dpmp)_2]^+$, 1746.9 (0.5) $[Cu_5I_3Cl(dpmp)_2]^+$, 1647.0 (30) $[Cu_4I_3(dpmp)_2]^+$, 1554.7 (2) $[Cu_4I_2Cl(dpmp)_2]^+$, 1267.3 (16) $[Cu_2I(dpmp)_2]^+$, 759.0 (6) $[Cu_2I(dpmp)]^+$, 665.1 (73) $[Cu_3I(dpmp)^2]^{2+}$. Negative ion MS, *m/q* (%):87.3 (100) $[BF_4]^-$. IR(KBr) cm^{-1}: 3108 (vw), 3072 (vw), 3050 (w), 3004 (vw), 2988 (vw), 2944 (vw), 2886 (vw), 2361 (vw), 2335 (vw), 2000 (vs), 1943 (vs), 1636 (w), 1484 (m), 1435 (s), 1420 (m), 1380 (w), 1096 (s), 1083 (s), 1061 (m), 1028 (m), 1000 (m).

Isolation of $[Cu_3(\mu\text{-}Br)_2(dpmp)_2(\mu,\eta^1{:}\eta^1\text{-}\mathbf{C1})]^+_n[BF_4]^-_n$ (**8b**): 101 mg (2eq., 0.2 mmol) dpmp, 32 mg (1eq., 0.1 mmol) $[Cu(MeCN)_4][BF_4]$ and 29 mg (2eq., 0.2 mmol) CuBr were weighed into a Schlenk flask and 10 mL of CH_2Cl_2 were added. The solids dissolved under constant stirring in the course of 30 min. to form a clear colorless solution. To this solution 35 mg (1 eq., 0.1 mmol) **C1** was added. After 24 hours stirring, subsequent filtration and gas-phase diffusion of *n*-pentane, compound **8b** can be obtained as fine green rods. Yield 74 mg (41%). ^{1}H NMR (300 MHz, CD_2Cl_2, 300 K) *δ*/ppm 7.76 – 6.56 (m, 50H, Ph), 3.74 (m, CH_2), 3.45 (br, small signal, CH_2), 3.22 (br, CH_2), 1.41 (s, Cp*); ^{31}P{^{1}H} NMR (121.5 MHz, CD_2Cl_2, 300 K) *δ*/ppm 149.9 (s, P_5), –6.4 (m, small signal), –12.2 (m, small signal), –16.2 (m, $RPPh_2$), –22.2 (br, R_2PPh); ^{19}F{^{1}H} NMR (282.4 MHz, CD_2Cl_2, 300 K) *δ*/ppm –148.81 ($^{10}BF_4$), –148.87 ($^{11}BF_4$); ^{13}C{^{1}H} NMR (75.5 MHz, CD_2Cl_2, 300 K) *δ*/ppm 135.50 – 127.15 (multiple signals, Ph), 11.06 (s, Cp*). Anal. calcd. for $Cu_3Br_2(dpmp)_2$(**C1**)$(BF_4)\cdot(CH_2Cl_2)_{1.2}$: C, 47.58; H, 4.00. Found: C, 47.57; H, 3.99. Positive ion MS, *m/q* (%): 1363.1 (100) $[Cu_3Br_2(dpmp)_2]^+$, 1319.2 (16) $[Cu_3BrCl(dpmp)_2]^+$. Negative ion MS, *m/q* (%):87.3 (100) $[BF_4]^-$. IR(KBr) cm^{-1}: 3144 (vw), 3072 (vw), 3049 (w), 3018 (vw), 3005 (vw), 2951 (vw), 2898 (vw), 1587 (vw), 1574 (vw), 1483 (m), 1435 (s), 1377 (m), 1323 (vw), 1309 (vw), 1278 (vw), 1264 (vw), 1189 (vw), 1161 (vw), 1096 (s), 1083 (s), 1026 (m), 992 (m), 917 (vw), 844 (vw), 790 (s), 764 (m), 737 (vs), 689 (vs), 651 (vw), 504 (m), 475 (m).

Isolation of $[Cu_3(\mu\text{-}I)_2(dpmp)_2(\eta^1\text{-}\mathbf{C1})_2][BF_4]$ (**10**): 101 mg (2eq., 0.2 mmol) dpmp, 32 mg (1eq., 0.1 mmol) $[Cu(MeCN)_4][BF_4]$ and 38 mg (2eq., 0.2 mmol) CuI were weighed into a Schlenk flask and 10 mL of CH_2Cl_2 were added and the reaction stirred for 24 hours. The solids dissolved under constant stirring in the course of 5-6 hours to form a clear colorless solution. To this solution 69 mg (2 eq., 0.2 mmol) **C1** was added. After 24 hours stirring, subsequent filtration and gas-phase diffusion of *n*-pentane, compound **9** can be obtained as fine green rods. Yield 162 mg (72%). ^{1}H NMR (300 MHz, CD_2Cl_2, 300 K) *δ*/ppm 8.59 - 6.02 (m, multiple overlapping signals, Ph), 4.03 – 2.21 (multiple overlapping signals, CH_2), 1.41 (s, Cp*); ^{31}P{^{1}H} NMR (121.5 MHz, CD_2Cl_2, 300 K) *δ*/ppm 151.2 (s, P_5), –4.7 - –31.1 (multiple overlapping signals, dpmp); ^{19}F{^{1}H} NMR (282.4 MHz, CD_2Cl_2, 300 K) *δ*/ppm –150.93 ($^{10}BF_4$), –150.98 ($^{11}BF_4$); ^{13}C{^{1}H} NMR (75.5 MHz, CD_2Cl_2, 300 K) *δ*/ppm 135.76 – 128.15 (multiple signals, Ph), 10.99 (s, Cp*). Anal. calcd. for $Cu_3I_2(dpmp)_2$(**B**)$_2(BF_4)\cdot(CH_2Cl_2)_{2.5}$: C, 42.43; H, 3.83. Found: C, 42.24; H, 3.85. Positive ion MS, *m/q* (%): 1457.3 (100) $[Cu_3I_2(dpmp)_2]^+$, 1365.3 (4) $[Cu_3ICl(dpmp)_2]^+$, 2725.9 (0.4) $[Cu_7I_6(dpmp)_3]^+$, 2635.0 (0.05) $[Cu_7I_5Cl(dpmp)_3]^+$, 2535.6 (0.3) $[Cu_6I_5(dpmp)]^+$, 2343.9 (0.4) $[Cu_5I_4(dpmp)_3]^+$, 2153.9 (2) $[Cu_4I_3(dpmp)_3]^+$, 2029.2 (1) $[Cu_6I_5(dpmp)_2]^+$, 1837.1 (12) $[Cu_5I_4(dpmp)_2]^+$, 1747.1 (0.4) $[Cu_5I_3Cl(dpmp)_2]^+$, 1647.1 (36) $[Cu_4I_3(dpmp)_2]^+$, 1552.7 (3) $[Cu_4I_2Cl(dpmp)_2]^+$, 1267.3 (16) $[Cu_2I(dpmp)_2]^+$, 761.1 (2) $[Cu_2I(dpmp)]^+$, 665.1 (49) $[Cu_3I(dpmp)_2]^{2+}$. Negative ion MS, *m/q* (%):87.2 (100) $[BF_4]^-$. IR(KBr) cm^{-1}: 3050 (w), 2950 (w), 2904 (w), 1962 (vw), 1890 (vw), 1810 (vw), 1586 (w), 1573 (vw), 1483 (m), 1434 (s), 1375 (m), 1332 (vw), 1309 (vw), 1277 (vw), 1137 (vw), 1158 (vw), 1139 (vw), 1095 (s), 1070 (s), 1025 (s), 992 (m), 914 (vw), 790 (m), 737 (vs), 689 (vs).

X-ray structural analysis

All crystal preparations were done under mineral oil. When the samples lose their crystallinity by solvent loss the crystals were prepared under a constant flow of cooled nitrogen at approximately 170-200 K. The data collection was either performed on an Agilent Technologies SuperNova diffractometer equipped with a micro focus Cu X-ray source, an Agilent Technologies Gemini R Ultra or Gemini Ultra equipped with sealed tube Mo and Cu X-ray sources or on a Bruker Apex II diffractometer equipped with a Mo X-ray source. All measurements were performed at 150 K or at 123 K by nitrogen cooling. The structure least square refinement was done with the SHELX program package[5] against F^2. All crystallographic data and details about the measurements can be found in the Table 1-4 at the end of the experimental section. The crystal structures of **1a**, **2a***, **4a**, **5**, **8a** and **9** have been reported previously.[6] Details can be found there.

Table 1. Crystallographic data for **1b**, **1c**, **2a** and **2b**.

Identification code	**1b**	**1c**	**2a**	**2b**
formula	$C_{72}H_{73.36}BBr_2Cu_3F_4N_2OP_6$	$C_{70}H_{67}BCu_3F_4I_2N_3P_6$	$C_{65}H_{60}BCl_4Cu_3F_4P_6$	$C_{64}H_{58}BBr_2Cu_3F_4P_6$
weight [g·mol^{-1}]	1605.75	1667.35	1446.18	1450.19
Temperature [K]	122.9(4)	123(1)	123.02(10)	123(1)
crystal system	triclinic	triclinic	monoclinic	monoclinic
space group	*P*–1	*P*–1	$P2_1/c$	*C*2/*c*
a [Å]	12.9373(2)	14.1918(2)	15.60512(13)	25.9617(2)
b [Å]	13.4542(2)	15.0336(3)	31.7652(2)	15.6931(1)
c [Å]	21.4483(2)	21.1593(4)	14.05170(13)	29.5724(3)
α [°]	88.2465(11)	94.291(2)	90	90
β [°]	73.3789(11)	107.910(2)	114.0862(11)	94.798(1)
γ [°]	77.9023(14)	102.175(2)	90	90
Volume [Å^3]	3496.17(9)	4151.42(15)	6358.95(11)	12006.15(17)
Z	2	2	4	8
ρ_{calc} [g·cm^{-3}]	1.525	1.334	1.511	1.605
μ [mm^{-1}]	4.147	8.283	4.565	4.738
F(000)	1631.0	1664.0	2944.0	5840.0
crystal size [mm^3]	0.257 × 0.189 × 0.117	0.205 × 0.076 × 0.058	0.367 × 0.195 × 0.161	0.284 × 0.175 × 0.108
diffractometer	Gemini Ultra	SuperNova	SuperNova	Gemini R Ultra
absorption correction	gaussian	analytical	gaussian	analytical
T_{min}/T_{max}	0.498 / 0.720	0.349 / 0.688	0.356 / 0.614	0.421 / 0.664
radiation	CuK_α	CuK_α	CuK_α	CuK_α
2*Θ* range [°]	6.722 to 132.584	6.08 to 141.54	6.8 to 134.134	6.58 to 148.44
completeness	0.987	0.970	1.000	0.994
reflns collected/unique	42446 / 12125	15495 / 15495	133342 / 11350	32633 / 11669
R_{int}/R_{sigma}	0.0462 / 0.0381	0.0406 / 0.0373	0.0659 / 0.0204	0.0214 / 0.0198
data/restraints/parameters	12125 / 19 / 837	15495 / 73 / 808	11350 / 4 / 824	11669 / 0 / 721
GOF on F^2	1.138	1.021	1.044	1.092
R_1/wR_2 [$I \geq 2\sigma(I)$]	0.0347 / 0.0967	0.0365 / 0.0960	0.0324 / 0.0888	0.0256 / 0.0715
R_1/wR_2 [all data]	0.0449 / 0.1157	0.0458 / 0.1017	0.0342 / 0.0899	0.0281 / 0.0726
max/min $\Delta\rho$ [e·Å^{-3}]	0.76 / –0.80	1.85 / –0.85	0.84 / –0.56	0.37 / –0.56

Table 2. Crystallographic data for **2c***, **3b** and **3c**.

Identification code	**2c***	**3b**	**3c**
formula	$C_{132}H_{124}B_2Cl_8Cu_6F_8I_4P_{12}$	$C_{67}H_{64}BBr_2Cl_6Cu_3F_4P_6$	$C_{66}H_{62}BCl_4Cu_3F_4I_2P_6$
weight [g·mol^{-1}]	3428.08	1704.97	1714
Temperature [K]	123(1)	123(1)	122.9(6)
crystal system	monoclinic	monoclinic	triclinic
space group	$P2_1/c$	$P2_1/n$	*P*–1
a [Å]	20.1590(2)	12.6490(4)	14.1533(2)
b [Å]	12.8028(1)	44.9781(15)	15.0547(2)
c [Å]	27.5537(2)	13.0564(4)	21.4267(3)
α [°]	90	90	95.7164(11)
β [°]	97.607(1)	111.149(3)	106.7947(13)
γ [°]	90	90	101.5198(12)
Volume [Å^3]	7048.80(10)	6927.8(4)	4222.06(11)
Z	2	4	2
ρ_{calc} [g·cm^{-3}]	1.615	1.635	1.348
μ [mm^{-1}]	11.012	6.282	9.193
F(000)	3400.0	3424.0	1700
crystal size [mm^3]	0.173 × 0.055 × 0.036	0.212 × 0.179 × 0.091	0.254 × 0.118 × 0.060
diffractometer	SuperNova	SuperNova	Gemini Ultra
absorption correction	analytical	analytical	gaussian
T_{min}/T_{max}	0.363 / 0.791	0.391 / 0.635	0.216 / 0.588
radiation	CuK_α	CuK_α	CuK_α
2*Θ* range [°]	6.48 to 130.16	7.52 to 136.5	6.72 to 131.98
completeness	0.991	0.986	0.993
reflns collected/unique	36500 / 11906	22543 / 12521	55752 / 14597
R_{int}/R_{sigma}	0.0265 / 0.0258	0.0289 / 0.0355	0.0558 / 0.0506
data/restraints/parameters	11906 / 109 / 817	12521 / 0 / 802	14597 / 8 / 788
GOF on F^2	1.057	1.127	0.956
R_1/wR_2 [$I \geq 2\sigma(I)$]	0.0419 / 0.1269	0.0375 / 0.0982	0.0553 / 0.1451
R_1/wR_2 [all data]	0.0487 / 0.1324	0.0484 / 0.1022	0.0666 / 0.1504
max/min $\Delta\rho$ [e·Å^{-3}]	2.46 / –0.96	1.29 / –1.07	2.41 / –1.09

Table 3. Crystallographic data for **4b**, **4c** and **6b**.

Identification code	**4b**	**4c**	**6b**
formula	$C_{80}H_{72}BBr_2Cl_4Cu_3F_4Mo_2O_4P_8$	$C_{81}H_{74}BCl_6Cu_3F_4I_2Mo_2O_4P_8$	$C_{72}H_{65}BBr_2Cl_2Cu_3F_4MoO_2P_9$
weight [g·mol^{-1}]	2116.08	2295.01	1845.07
Temperature [K]	123(1)	123(1)	123(1)
crystal system	monoclinic	orthorhombic	monoclinic
space group	$P2_1/c$	$P2_12_12_1$	$P2_1$
a [Å]	12.8572(2)	14.9976(2)	12.7309(7)
b [Å]	43.8609(9)	19.9846(3)	21.1741(15)
c [Å]	14.9221(4)	29.7143(5)	14.8684(13)
α [°]	90	90	90
β [°]	95.004(2)	90	110.373(7)
γ [°]	90	90	90
Volume [Å^3]	8382.9(3)	8906.0(2)	3757.3(5)
Z	4	4	2
ρ_{calc} [g·cm^{-3}]	1.677	1.712	1.631
μ [mm^{-1}]	7.429	11.946	2.384
F(000)	4216.0	4528.0	1844.0
crystal size [mm^3]	0.147 × 0.034 × 0.013	0.226 × 0.076 × 0.020	0.746 × 0.224 × 0.066
diffractometer	SuperNova	SuperNova	Gemini R Ultra
absorption correction	analytical	analytical	analytical
T_{min}/T_{max}	0.567 / 0.924	0.346 / 0.790	0.349 / 0.883
radiation	CuK_α	CuK_α	MoK_α
2*Θ* range [°]	6.9 to 130.16	6.6 to 142.12	6.42 to 53.68
completeness	0.990	0.981	0.976
reflns collected/unique	26227 / 14144	49296 / 16640	17526 / 11560
R_{int}/R_{sigma}	0.0464 / 0.0604	0.0544 / 0.0483	0.0722 / 0.0890
data/restraints/parameters	14144 / 27 / 1044	16640 / 0 / 1000	11560 / 1 / 865
GOF on F^2	0.988	1.027	1.027
R_1/wR_2 [$I \geq 2\sigma(I)$]	0.0497 / 0.1267	0.0480 / 0.1282	0.0378 / 0.0834
R_1/wR_2 [all data]	0.0613 / 0.1356	0.0513 / 0.1313	0.0438 / 0.0870
max/min *Δρ* [e·Å^{-3}]	1.10 / –0.66	1.90 / –0.94	0.74 / –0.80
Flack parameter	–	–0.014(4)	–0.012(5)

Table 4. Crystallographic data for **7**, **8b** and **10**.

Identification code	**7**	**8b**	**10**[7]
formula	$C_{86.6}H_{88}BCl_{3.2}Cu_3F_4I_2Mo_2O_4P_{12}$	$C_{74}H_{73}BBr_2Cu_3F_4FeP_{11}$	$C_{86.29}H_{92.58}BCl_{4.58}Cu_3F_4Fe_2I_2P_{16}$
weight [g·mol^{-1}]	2400.99	1796.11	2430.47
Temperature [K]	123(1)	150(2)	123.0(2)
crystal system	monoclinic	monoclinic	monoclinic
space group	$P2_1/n$	$P2_1/c$	$P2_1/n$
a [Å]	23.7223(2)	12.4888(3)	24.5036(5)
b [Å]	15.1243(1)	25.2517(7)	15.3314(3)
c [Å]	26.4420(2)	28.0939(11)	26.5971(6)
α [°]	90	90	90
β [°]	99.932(1)	97.053(3)	98.126(2)
γ [°]	90	90	90
Volume [Å^3]	9344.77(13)	8792.8(5)	9891.5(4)
Z	4	4	4
ρ_{calc} [g·cm^{-3}]	1.707	1.357	1.632
μ [mm^{-1}]	11.338	2.031	11.902
F(000)	4768.0	3624.0	4857.0
crystal size [mm^3]	0.290 × 0.074 × 0.047	0.181 × 0.074 × 0.063	0.188 × 0.068 × 0.034
diffractometer	SuperNova	Bruker Apex II	SuperNova
absorption correction	analytical	multi-scan	gaussian
T_{min}/T_{max}	0.206 / 0.672	0.886 / 1.000	0.322 / 0.700
radiation	CuK_α	CuK_α	CuK_α
2*Θ* range [°]	6.76 to 147.46	3.28 to 54.2	6.672 to 133.7
completeness	0.979	0.996	0.961
reflns collected/unique	65727 / 18479	79512 / 19309	51872 / 16887
R_{int}/R_{sigma}	0.0441 / 0.0268	0.0537 / 0.0410	0.0671 / 0.0456
data/restraints/parameters	18479 / 283 / 1157	19309 / 200 / 969	16887 / 55 / 1132
GOF on F^2	1.011	1.085	1.089
R_1/wR_2 [$I \geq 2\sigma(I)$]	0.0593 / 0.1659	0.0560 / 0.1555	0.1027 / 0.2593
R_1/wR_2 [all data]	0.0627 / 0.1688	0.0743 / 0.1696	0.1111 / 0.2633
max/min *Δρ* [e·Å^{-3}]	2.49 / –1.38	0.89 / –1.91	2.51 / –1.96

References

[1] O. J. Scherer, H. Sitzmann, G. Wolmershäuser, *J. Organomet. Chem.* **1984**, *268*, C9-C12.
[2] P. J. Sullivan, A. L. Rheingold, *Organometallics* **1982**, *1*, 1547-1549.
[3] O. J. Scherer, T. Brück, *Angew. Chem. Int. Ed.* **1987**, *26*, 59-59; *Angew. Chem.* **1987**, *99*, 59-59.
[4] O. J. Scherer, C. Blath, G. Wolmershäuser, *J. Organomet. Chem.* **1990**, *387*, C21-C24.
[5] G. M. Sheldrick, *Acta Cryst. A*, **2008**, *64*, 112-122.
[6] M. Fleischmann, L. Dütsch, M. E. Moussa, A. Schindler, G. Balázs, C. Lescop, M. Scheer, *Chem. Commun.* **2015**, *51*, 2893-2895.
[7] All crystals that were obtained of compound **10** showed twinning. The central $[Cu_3(\mu\text{-}I)_2(\mu\text{-}dpmp)_2]^+$ building block and the *cyclo*-P_5 ligands **C1** could clearly be determined without any disorder. The data reduction by the CrysalisPro Software package lead to comparable results when the data was integrated for twinned crystals or as a single crystal. Therefore the structure solution of **10** was done by regular HKLF 4 refinement by ShelX. This may be the cause for the elevated *R* values, standard uncertainties and the residual electron density for **10**.

Preface

The following chapter has already been published. The article is reprinted with the permission of the Royal Society of Chemistry.
Chem. Sci. **2015**, *6*, 132–139.

Authors

Martin Fleischmann, James S. Jones, François P. Gabbaï* and Manfred Scheer*

Author contributions

The preparation and characterization of all compounds including the single crystal X-ray structure determination, the Hirshfeld surface analysis and the preparation of the manuscript was done by the first author. James S. Jones performed and described supporting DFT calculations. François P. Gabbaï and Manfred Scheer supervised the research and revised the manuscript.

Acknowledgements

Christian Marquardt is gratefully acknowledged for recording the crystal data for [**3**•(CH_2Cl_2)] (**9**) (see supporting information). Bianca Attenberger is acknowledged for recording the analytical data for [Cp'FeP_5] **6 a**. This work was financially supported by the Deutsche Forschungsgemeinschaft (Sche 384/26-2), the National Science Foundation (CHE-1300371) and the Welch Foundation (A-1423).

9 A comparative study of the coordination behavior of *cyclo*-P_5 and *cyclo*-As_5 ligand complexes towards the trinuclear Lewis acid complex (perfluoro-*ortho*-phenylene)mercury

Abstract: Reactions of the *cyclo*-E_5 sandwich complexes [Cp*Fe(η^5-P_5)] (**1**) and [Cp*Fe(η^5-As_5)] (**2**) with the planar Lewis acid trimeric (perfluoro-*ortho*-phenylene)mercury [(*o*-$C_6F_4Hg)_3$] (**3**) afford compounds that show distinctly different assemblies in the solid state. The phosphorus ligand **1** forms dimeric coordination units with two molecules of **3**, with one P atom of each P_5 positioned in close proximity to the center of a molecule of **3**. In contrast to the coordination behavior of **1**, the arsenic analog **2** shows simultaneous interaction of three As atoms with the Hg atoms of **3**. A DFT study and subsequent AIM analyses of the products suggest that electrostatic forces are prevalent over donor-acceptor interactions in these adducts, and may play a role in the differences in the observed coordination behavior. Subsequently, a series of [Cp^RFe(η^5-P_5)] (Cp^R = $C_5H_{5-n}tBu_n$, n = 1-3, **6a-c**) sandwich complexes was prepared and also reacted with [(*o*-$C_6F_4Hg)_3$]. The obtained products **7a-c** with increasing steric demand of the Cp^R ligands show no significant change of the assembly in the solid state compared to the Cp* analog **4**. All products were characterized by single crystal X-ray structure analysis, mass spectrometry, and elemental analysis as well as NMR spectroscopy and IR spectrometry.

9.1 Introduction

The research area of substituent-free group 15 element ligands in the coordination sphere of transition metal complexes has shown to be a prosperous field in chemistry.[1,2,3,4,5] Some of these complexes possess planar E_3, E_4, E_5 and E_6 rings. From their appealing symmetry, to the lively discussion of their possible aromaticity,[6,7,8,9,10] these main group ligands induce a fascination to chemists on their own. Among these, the ferrocene analogues sandwich complexes [Cp*Fe(η^5-E_5)] (E = P (**1**), E = As (**2**))[11,12] bearing a planar E_5 ring as an end deck are even of special interest as ligands in supramolecular coordination chemistry, since they show a large variety of coordination modes of the *cyclo*-E_5 moieties depending on the nature of the used Lewis acid. While reactions of the *cyclo*-P_5 complex **1** with strongly coordinating Cu^I halides leads to an abundance of coordination polymers,[13,14] and also spherical aggregates,[15,16,17,18,19] the As analog **2** leads only to the isolation of coordination

polymers so far.[20] In these products the P atoms are mainly σ coordinating the Cu centers via their lone pairs while the As_5 ring mainly shows π coordination via As-As bonds. The reaction of **1** with Ag^+ ions under weakly coordinating conditions affords a soluble one-dimensional coordination polymer.[21] Recently, we were able to show that both E_5 complexes **1** and **2** reveal a similar η^5-coordination of the E_5 end deck to the group 13 cations Tl^+ and In^+.[22,23] Since investigations of the reactivity of *cyclo*-P_5 and *cyclo*-As_5 complexes including a direct comparison are rare, it seems worthwhile to analyze their coordination chemistry towards the unusual Lewis acid trimeric (perfluoro-*ortho*-phenylene)mercury $[(o\text{-}C_6F_4Hg)_3]$ (**3**).[24]

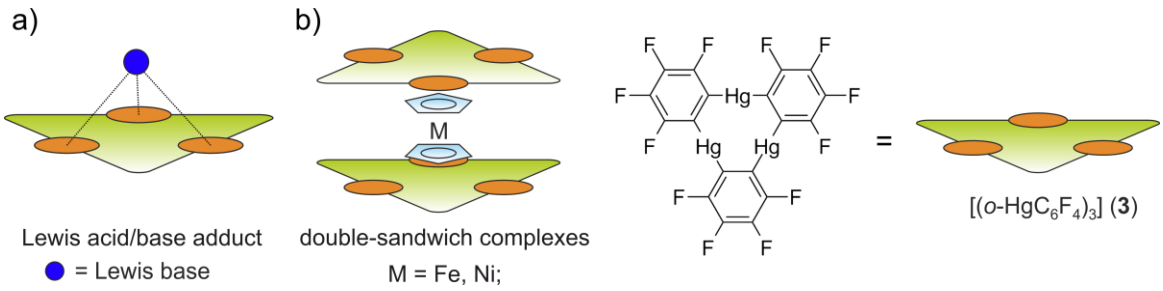

Scheme 1. a) The planar Lewis acid **3** can simultaneously interact through all three Hg atoms with Lewis bases; b) Double-sandwich complexes built from **3** and the simple metallocenes $[Cp_2Fe]$ and $[Cp_2Ni]$.

The latter is a planar, electron deficient molecule containing three sterically available Hg atoms in close proximity. Compound **3** forms weak Lewis acid/base adducts with a large variety of O, N and S-donor Lewis bases as well as some anions (scheme 1 a).[25,26] Additionally, it readily builds up alternating binary stacks with different electron rich aromatic hydrocarbons[27,28,29,30,31,32] and forms double-sandwich complexes with the metallocenes $[Cp_2Ni]$ and $[Cp_2Fe]$ (Scheme 1 b).[33] Accordingly, we reported the reaction of **3** with the triple-decker complex $[(CpMo)_2(\mu,\eta^6\text{:}\eta^6\text{-}P_6)]$ bearing two Cp rings and a *cyclo*-P_6 middle-deck.[34] In this case, the obtained products show a one-dimensional polymeric structure which are based on weak P-Hg interactions and no Hg-Cp interactions are observed.

The presented results raise the question how the ferrocene analog *cyclo*-E_5 complexes **1** and **2** will interact with the planar Lewis acid **3**. Will they form Lewis acid/base adducts via the lone pairs of the group 15 elements or will they show a π interaction of the aromatic E_5 ligands comparable to pure ferrocene? To address this question we reacted the *cyclo*-E_5 complexes **1** and **2** with $[(o\text{-}C_6F_4Hg)_3]$ (**3**) in CH_2Cl_2 and subsequently determined the solid state structure of the products. To gain further insight into the Hg–E interactions, the electrostatic potentials of the complexes **1-3** were obtained from DFT calculations. Additionally an atoms in molecules (AIM) analyses was performed at the experimentally determined geometries. To investigate the impact of

sterical demand to these compounds, we prepared a series of *cyclo*-P_5 sandwich complexes $[Cp^RFe(\eta^5\text{-}P_5)]$ ($Cp^R = C_5H_{5-n}tBu_n$, n = 1-3, **6a-c**) with increasing sizes of the Cp ligands and subsequently reacted them with compound **3**.† The resulting adducts were analysed by X-ray crystallography and a Hirshfeld surface analysis was performed to better compare the involved intermolecular contacts in the solid state.

9.2 Results and Discussion

Synthesis of the compounds 4, 5, 7a-c

Since $[(o\text{-}C_6F_4Hg)_3]$ (**3**) forms Lewis acid/base adducts with donor solvents like THF or MeCN, the syntheses were all conducted in CH_2Cl_2 to prevent any competition between the E_n ligand complexes and the solvent molecules. Nevertheless, in some other reactions we could isolate two solvates of $[(o\text{-}C_6F_4Hg)_3]$ containing only CH_2Cl_2 (see supporting information). For the current study, the E_n ligand complexes were combined with a stoichiometric (1:1) amount of $[(o\text{-}C_6F_4Hg)_3]$ and the mixture was dissolved in pure CH_2Cl_2. After filtration the solvent was evaporated to the limit of solubility. The supersaturated solution was stored at +4 °C or –30 °C which afforded crystals of the compounds **4**, **5**, **7a-c** in a matter of several hours to some days.

Synthesis of the sandwich complexes $[Cp^RFe(\eta^5\text{-}P_5)]$ ($Cp^R = C_5H_{5-n}tBu_n$, n = 1-3, 6a-c)

For the present work all three complexes were prepared by a thermolysis of $[Cp^RFe(CO)_2]_2$ with P_4 in decalin. Chromatographic workup afforded the pure compounds as dark green solids.

General considerations

The solid state structures of the formed assemblies are based on weak interactions of the Hg atoms of $[(o\text{-}C_6F_4Hg)_3]$ and the phosphorus or arsenic atoms of the sandwich complexes $[Cp^*Fe(\eta^5\text{-}E_5)]$. The van der Waals (vdW) radius of Hg in different compounds is discussed in the literature with reported values ranging from 1.7 Å up to 2.2 Å.[35,36,37,38] In the following discussion the shortest value of 1.7 Å is taking as a reference. Therefore, Hg–E distances that are within the sum of the vdW radii[39] of 3.6 Å for E = P or 3.7 Å for E = As are highlighted by fragmented blue lines in the Figures 1, 2 and 6.

When the starting compounds **1** and **3** are dissolved in CH_2Cl_2, the solution shows the dark green color of the pure complex **1**. The crystals which were obtained by storing a concentrated solution at –30 °C are pleochromic showing a green to brown color.

Compound **4** crystallizes in the triclinic space group *P*–1. The solid state structure is depicted in Figure 1.

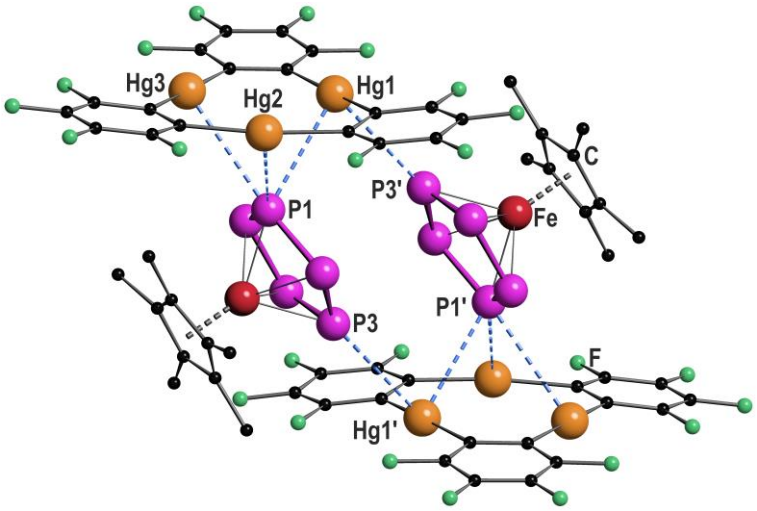

Figure 1 Solid state structure of **4**; selected bond lengths [Å] and angles [°]: Hg1-P1 3.2878(9), Hg2-P1 3.3592(9), Hg3-P3 3.5281(11), Hg1'-P3 3.5265(10), angle P_5-plane - Hg3-plane 62.29(2).

In **4** the P_5 ring of **1** is approaching the center of the three Hg atoms of **3** with the phosphorus atom P1 and on the other side, the atom P3 is coordinating to the second Hg_3-moiety. The P-P bond lengths are very uniform with an average value of 2.111(4) Å, which is the same as in the starting compound **1** with 2.120(5) Å.[21] The angle enclosed by the *cyclo*-P_5 plane and the Hg_3 plane constitutes 62.29(2) °. The observed assembly resembles the weak Lewis acid/base adducts that are formed from **3** with several Lewis bases and significantly differs from a cofacial arrangement that was found for the double-sandwich complexes formed by $[Cp_2Fe]$ and **3**.[33] The closest Hg-P distance Hg1-P1 of 3.2878(9) Å is a bit longer than the closest Hg-P contact (3.195(3) Å) found in the polymeric chains of $[(o\text{-}C_6F_4Hg)\bullet\{(CpMo)_2(\mu,\eta^6\text{:}\eta^6\text{-}P_6)\}]_n$ but the other found Hg-P distances can be compared well with this one.[34] The shortest intermolecular P···P distance is 3.9443(13) Å and all others lie above 4 Å. In summary, the best description of the solid state structure of **4** is the enclosure of two *cyclo*-P_5 sandwich complexes by two planar molecules of **3** held together by weak Hg···P interactions.

In CD_2Cl_2 solution at room temperature **4** shows a singlet in both the ^1H NMR spectrum and the $^{31}P\{^1H\}$ NMR spectrum. The signal is only shifted 0.04 ppm upfield in the case of the methyl protons and 2.5 ppm downfield in the case of the phosphorus atoms compared to the free complex **1**. When going to 193 K, these shifts increase to 0.13 ppm upfield for the ^1H and 7.6 ppm downfield for the ^{31}P nuclei. In all experiments we could not resolve any coupling to the NMR active ^{199}Hg (I = 1/2, 16.84% natural abundance) or ^{201}Hg (I = 3/2, 13.22% natural abundance) nuclei. The ^{19}F NMR spectrum

shows two multiplets that correspond to the fluorine atoms of **3** in *ortho* and *para* position to the Hg atoms.[40] The mass spectrum (FD or ESI) of **4** shows no adduct in the gas phase. Only the starting materials **1** and **3** can be detected. Thus, the small differences of the chemical shifts and the absence of any coupling in the NMR spectra as well as the absence of any product peaks in the mass spectrum are in good agreement with the expected weak Hg···P interactions.

During the further investigation we also added the *cyclo*-As_5 complex **2** to the Lewis acid **3**. The brown solution of both compounds in CH_2Cl_2 could easily be distinguished from the olive green color of the pure sandwich complex **2**. The obtained crystals of compound **5** show a medium brown color. The solid state structure is shown in Figure 2.

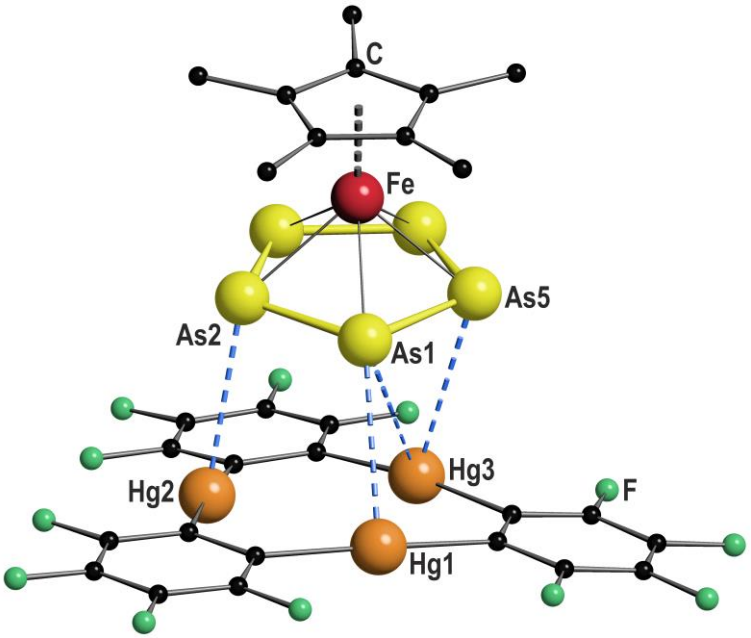

Figure 2. Solid state structure of **5**; selected bond lengths [Å] and angles [°]: Hg1-As1 3.4059(4), Hg2-As2 3.3014(4), Hg3-As1 3.6325(5), Hg3-As5 3.4201(5), angle As_5-plane - Hg3-plane 10.68(2).

Compound **5** crystallizes in the triclinic space group *P*–1. The As-As bond lengths are very uniform with an average value of 2.326(6) Å which is the same as 2.327(6) Å found in the starting compound **2**.[23] The assembly of the As_5 ring significantly differs from the P_5 ring in **4**. The angle enclosed by the As_5 plane and the Hg_3 plane of 10.68(2)° shows an almost parallel arrangement. The center of the Hg_3 triangle is not situated directly below the center of the As_5 ring, but rather to the arsenic atom As1. The resulting Hg-As distances show four contacts below the sum of the vdW radii with the closest one between Hg2 and As2 with 3.3014(4) Å. The assembly can best be described as a coordination of three As atoms to the Hg_3 platform. The observation of different assemblies for **1** and **2** with the weak Lewis acid **3** was surprising, since we observed a

similar η^5-coordination mode of the E_5 end-decks of **1** and **2** to the weak Lewis acids Tl^+ and In^+ before.[23] There is no second molecule of **3** stacked directly on top of the sandwich complex **2** to form a double-sandwich structure like it was observed for ferrocene. Nevertheless, there is a close contact (3.383(2) Å) of a carbon atom of the Cp* ring to a carbon atom of a fluorinated phenyl ring of the next molecule of **3** which may indicate possible stabilizing *π*-*π*-interaction of the electron rich Cp* ring to the electron deficient molecules of **3** or even F-H interaction to the methyl groups.

In order to better understand the difference in the nature of the Hg-E interactions in **4** and **5**, their constituent compounds **1**, **2**, and **3** were first subjected to optimization by DFT methods.†† The computed magnitudes of the respective HOMO-LUMO gaps between **1** and **3** and **2** and **3** of 3.70 and 3.36 eV suggest that efficient mixing of the HOMOs of **1** and **2** with the LUMO of **3** is not likely to be prevalent in **4** and **5**. Instead, we envisage that electrostatic and dispersion forces may play a large role in the stabilization of these adducts. To investigate the role played by electrostatic forces in **4** and **5**, we decided to inspect the electrostatic potential surfaces of the individual components shown in Figure 3. For **1** and **2**, a distinct accumulation of negative character is observed at the center of the E_5 ring. This feature is reminiscent of that observed for simple aromatic units such as benzene or the cyclopentadienide ligands of metallocenes.[41] A closer inspection of the surfaces shows a greater accumulation of negative character at the phosphorus atoms in **1**. This accumulation of negative character appears to be directly aligned with the phosphorus lone pairs that point outward from the center of the P_5 ring. Such areas of negative electrostatic potential concentrations are much less developed on the surface of the As_5 ring in **2**, a difference that we assign to the more electropositive character of arsenic and the more diffuse nature of its orbitals. Bearing in mind that the electrostatic potential surface at the center of the **3** is positive,[26,42] formation of the adducts **4** and **5** is driven, at least in part, by electrostatic forces as shown by the complementarity of the surfaces that come into contact in the adducts.

The side-on coordination of the phosphorus complex **1** to the center of **3** in adduct **4** can be correlated to the concentration of negative charges on each of the phosphorus atoms. Similarly, the more co-planar arrangement of the As_5 ring and Hg_3 plane in **5** is proposed to result from the complementarity of the negative and positive electrostatic potential concentration at the centers of the As_5 and Hg_3 units, respectively.

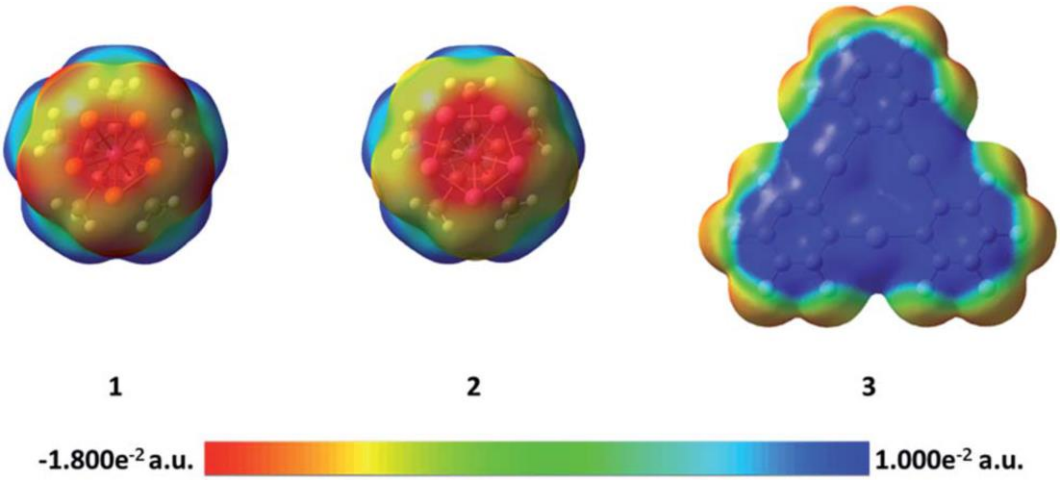

Figure 3. Electrostatic potential surfaces of compounds **1**, **2**, and **3**.

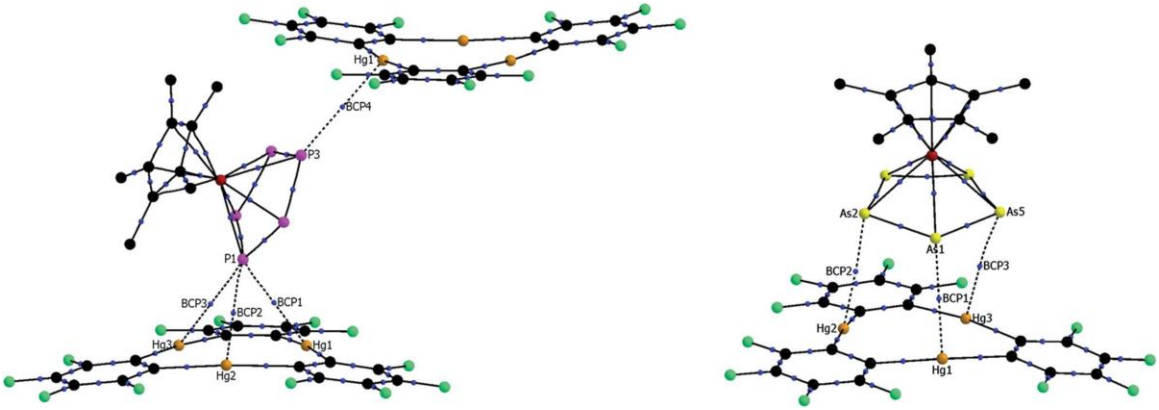

Figure 4. xyz plots of **4** (left) and **5** (right), including selected bond critical points located via AIM analysis. Bond critical points are shown in blue.

Table 1. Calculated features of the electron density distribution at selected BCPs in compound **4**.

BCP No. (A-B)	*d*(A-BCP) [Å]	*d*(B-BCP) [Å]	$\rho(r_{BCP})$ [e·Å^{-3}]	$\nabla^2\rho(r_{BCP})$ [e·Å^{-5}]	$H(r_{BCP})/\rho(r_{BCP})$ [E_h·e^{-1}]	ε
1 (Hg1-P1)	1.657	1.630	0.105	0.876	0.012	0.048
2 (Hg2-P1)	1.664	1.696	0.101	0.835	0.020	0.046
3 (Hg3-P1)	1.754	1.776	0.072	0.620	0.055	0.046
4 (Hg1'-P3)	1.737	1.789	0.072	0.622	0.065	0.051

Table 2. Calculated features of the electron density distribution at selected BCPs in compound **5**.

BCP No. (A-B)	*d*(A-BCP) [Å]	*d*(B-BCP) [Å]	$\rho(r_{BCP})$ [e·Å^{-3}]	$\nabla^2\rho(r_{BCP})$ [e·Å^{-5}]	$H(r_{BCP})/\rho(r_{BCP})$ [E_h·e^{-1}]	ε
1 (Hg1-As1)	1.698	1.707	0.091	0.757	0.044	0.031
2 (Hg2-As2)	1.654	1.648	0.109	0.885	0.018	0.052
3 (Hg3-As5)	1.695	1.731	0.096	0.762	0.027	0.344

In an effort to further investigate the nature of the Hg-E interactions in **4** and **5**, atoms in molecules (AIM)[43] analyses were carried out at the experimentally determined geometries. XYZ plots featuring selected bond critical points between the *cyclo*-E_5 units and **3** are shown in Figure 4. Relevant features of the calculated electron density distributions for selected Hg-E bond critical points (BCP) found in **4** and **5** are shown in

Tables **1** and **2**, respectively. Tables of the electron density distribution features at all bond critical points found between units of **1** and **3** and **2** and **3** are provided in the supporting information. In **4**, four bond critical points were found between the *cyclo*-P_5 moiety of **1** and the two molecules of **3**, as shown in Figure 4. P1, which is positioned above the center of a unit of **3**, shares a BCP with each of the proximal Hg atoms, with the electron densities at the critical points ranging from 0.072-0.105 e $Å^{-3}$. A critical point with similar electron density (0.072 e $Å^{-3}$) was also found between P3 and Hg1' of the second unit of **3**. In compound **5**, AIM analysis found three BCPs between the *cyclo*-As_5 moiety of **2** and **3**. The three As atoms closest to **3** (As1, As2, and As5) each share a single critical point with a proximal Hg atom, with the electron densities at these critical points ranging from 0.091-0.109 e $Å^{-3}$.

The values of the electron density, $\rho(r)$, found at the Hg-E BCPs in both **4** and **5** are relatively small, being similar in magnitude to those found for weak hydrogen bonds.[44] The positive values of the Laplacian of the electron density at the Hg-E BCPs, $\nabla^2\rho(r_{BCP})$, are also suggestive of closed shell interactions. The relatively small magnitude of the $\rho(r)$ and $\nabla^2\rho(r_{BCP})$ values found at the bond critical points are not conclusive evidence of the weakness of the Hg-E interactions, as $\rho(r)$ values tend to become smaller with increasing diffuseness of the electrons involved.[45] However, the positive values of $H(r_{BCP})/\rho(r_{BCP})$, the total energy density at the BCP relative to $\rho(r)$,[43] found at the Hg-E BCPs suggest that any donor-acceptor[46,47] contribution to the Hg-E bonding is weak.[48] Instead, we note that positive $H(r_{BCP})/\rho(r_{BCP})$ values are usually encountered in systems stabilized by electrostatic and/or van der Waals interactions.[45] Hence, while donor-acceptor bonding cannot be entirely neglected in **4** and **5**, electrostatic forces as supported by the preceding potential map analysis must play a prevalent role in the formation of these adducts. Dispersion forces, which are inherently more difficult to visualize, may also play an important role.

The ellipticity values (ε), which provide information on the anisotropy of electron density perpendicular to the bond path, at the Hg-P BCPs in **4** are small and uniform, indicating no preferential plane of electron density accumulation. This is a characteristic of σ interactions, in agreement with the orientation of the phosphorus lone pairs toward the mercury atoms. In contrast to those found in **4**, the ellipticities at the Hg-As BCPs in **5** are not uniform. The ellipticity value of 0.344 found at the BCP between Hg3 and As5 is substantially larger than the values obtained for the two other Hg-As BCPs. Considering the relative uniformity of the $\rho(r)$ values found for all three Hg-As BCPs, the large ellipticity value found for the Hg3-As5 BCP suggests the involvement of an As-As π bond in the interaction with Hg3.

Whether the different assembly of the *cyclo*-P_5 and the *cyclo*-As_5 complexes towards the planar Lewis acid **3** might be caused by packing effects due to the longer As-As bonds (≈2.33 Å) compared to the P-P bonds (≈2.12 Å) is hard to answer. Considering all the presented experimental data we can assume the Hg···P interactions found in **4** to be weak. Both E_5 complexes **1** and **2** exhibit two degenerate orbitals as their HOMO which are localized on the E_5 rings.[20] Consequently, we rationalized that it might be possible to direct the P_5 complex to also show an almost cofacial arrangement to the molecular plane of the Lewis acid **3**. Therefore, we followed a synthetic approach by increasing the steric bulk of the Cp^R ligand on the *cyclo*-P_5 sandwich complex to induce a change of its orientation towards the Hg_3 plane of **3** in the solid state. For this reason we decided to compare complexes with mono-, di- and trisubstituted *tert*-butyl-cyclopentadienyl ligands [Cp'Fe(η^5-P_5)] (**6a**), [Cp''Fe(η^5-P_5)] (**6b**), [Cp'''Fe(η^5-P_5)] (**6c**). The compounds are obtained by reacting the suitable Cp^R substituted dimeric iron-dicarbonyl complexes $[Cp^RFe(CO)_2]_2$ with white phosphorus at elevated temperature.

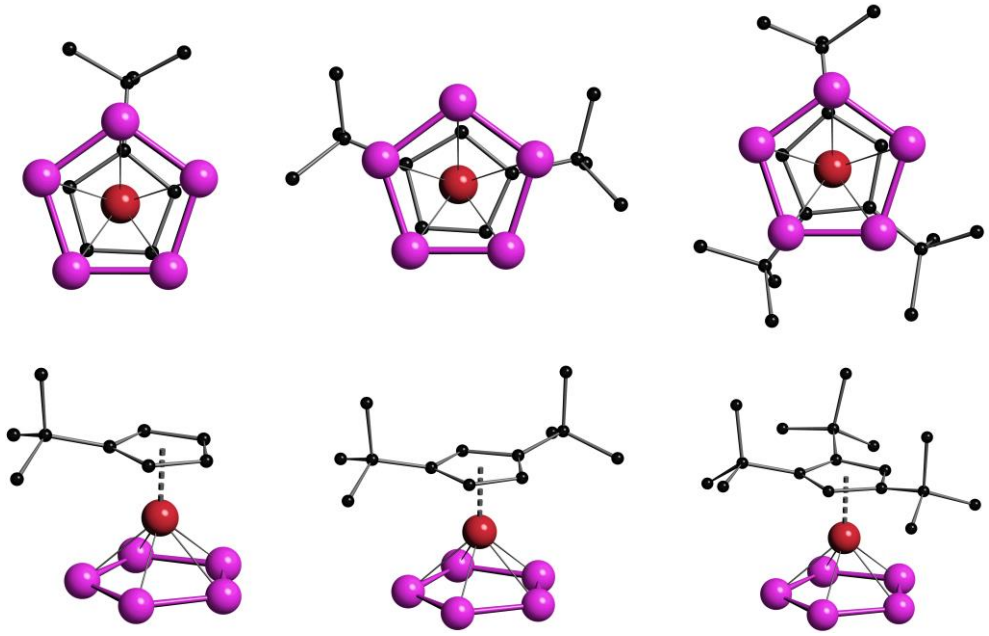

Figure 5. Solid state structures of the complexes [Cp'Fe(η^5-P_5)] **6a** (left), [Cp''Fe(η^5-P_5)] **6b** (middle), [Cp'''Fe(η^5-P_5)] **6c** (right); (top) viewing direction perpendicular to the P_5 plane revealing a nearly eclipsed arrangement of the Cp rings to the P_5 rings for all three complexes. (bottom) side view of the complexes **6a-c**.

The determined solid state structures of the compounds **6a-c** are shown in Figure 5. All three analyzed complexes **6a-c** show the expected sandwich structure with two parallel five-membered rings. Table 3 summarizes some geometric data for a better comparison. The distances between the Fe atom and the center of both rings are increasing very little when the size of the Cp ligand is increasing. When looking at the top

row in Figure 5 it can be seen that the P_5 rings are almost in eclipsed position with the Cp rings in all cases. This could be explained by steric effects when looking closer at the bottom row, since two methyl groups of each *tert*-butyl group are pointing between two P atoms of the P_5 rings. The volume of the complexes was determined by dividing the unit cell volume by the number of molecules within the cell. Here it can be seen, that each additional *tert*-butyl group adds about 100 Å³ to the size of the complexes.

Table 3. Selected lengths [Å]: *d*(P_5-Fe) and *d*(Cp-Fe) describe the distances of Fe to the center of the five-membered rings.

complex	*d*(P_5-Fe) [Å]	*d*(Cp-Fe) [Å]	volume [Å³]
6a	1.5396(2)	1.7026(2)	338.6
6b	1.5514(13)	1.7122(13)	436.5
6c	1.5615(2)	1.7174(2)	530.2

With these *cyclo*-P_5 complexes **6a-c** in hand, we prepared and fully characterized the compounds **7a-c** formed in the reaction of the *cyclo*-P_5 complex with $[(o\text{-}C_6F_4Hg)_3]$ in a 1:1 stoichiometry. The solid state structures of **7a-c** are shown in Figure 6. The obtained compounds each exhibit a similar assembly like it was found in **4** with two *cyclo*-P_5 complexes enclosed by two molecules of **3** held together by weak Hg···P interactions.

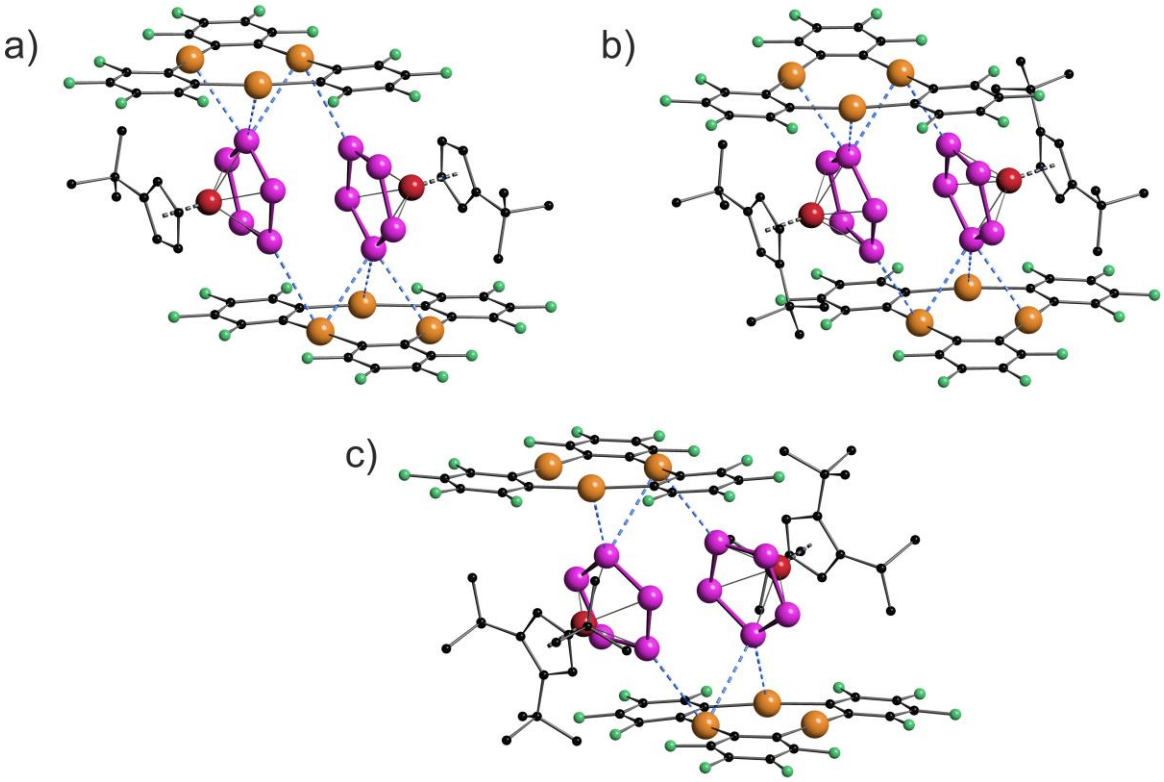

Figure 6. Solid state structures of $[\{Cp'Fe(\eta^5\text{-}P_5)\}\bullet\{(o\text{-}C_6F_4Hg)_3\}]$ (**7a**) (a), $[\{Cp''Fe(\eta^5\text{-}P_5)\}\bullet\{(o\text{-}C_6F_4Hg)_3\}]$ (**7b**) (b), $[\{Cp'''Fe(\eta^5\text{-}P_5)\}\bullet\{(o\text{-}C_6F_4Hg)_3\}]$ (**7c**) (c);

There are small differences in the assemblies caused by the steric demand of the Cp ligands, but the general arrangement of the *cyclo*-P_5 ring towards the molecular plane of **3** did not change dramatically, although the central phosphorus atom in **7c** (Figure 6c) shows only two contacts below the sum of the vdW radii to the Hg atoms of **3**.

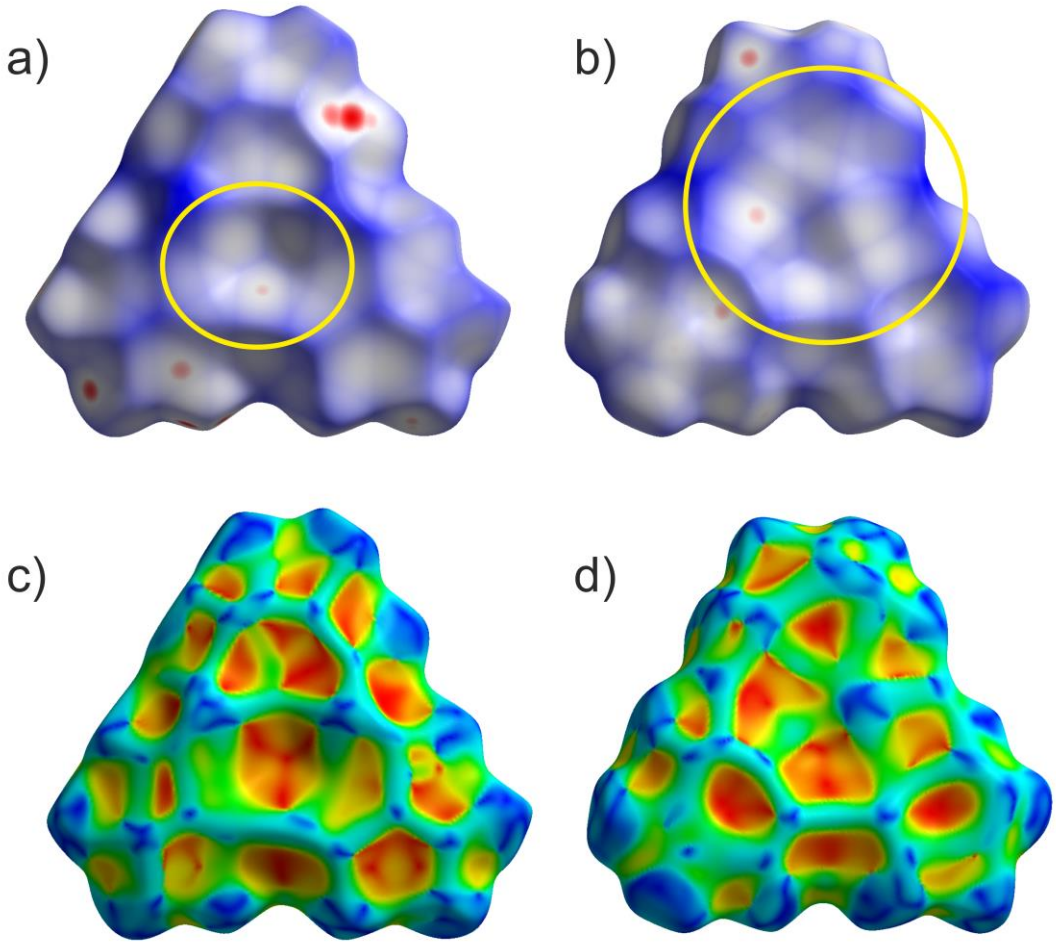

Figure 7. Representation of the Hirshfeld surfaces (HS) of the planar Lewis acid **3** in the compounds **4** (a + c) and **5** (b + d). The first row shows d_{norm} values mapped onto the HS while the second row shows the shape index. Highlighted in yellow are the contact areas of the planar molecule **3** with the *cyclo*-E_5 ligands of $[Cp^*Fe(\eta^5\text{-}P)_5]$ in a) and $[Cp^*Fe(\eta^5\text{-}As)_5]$ in b), respectively.

In order to better visualize the different interaction of the *cyclo*-P_5 and the *cyclo*-As_5 ligand towards the planar Lewis acid **3** we performed a Hirshfeld surface analysis[49,50,51,52] of all described compounds.[53] Figure 7 shows a representation of the Hirshfeld surfaces (HS) of the planar Lewis acid **3** which is facing the *cyclo*-E_5 ligands **1** or **2** derived from the solid state structures of compound **4** (a + c) and **5** (b + d), respectively. While the first row shows d_{norm} values which are used to identify close intermolecular contacts mapped onto the HS, the second row displays the corresponding shape index. The yellow ellipses highlight the contact regions to the pnictogen atoms of the *cyclo*-E_5 ligands. Figure 7a and c exhibit a pronounced indentation of the HS in the

center of the molecule for compound **4**. Figure 7a additionally shows three close contacts as white to red dots in this region on the HS which arise from interaction of the three Hg atoms of **3** with one P atom of the P_5 ring.[54] In Figure 7b we can identify a contact area, highlighted in yellow, which shows five small indentations for compound **5** instead. These can be seen even better in the representation of the respective shape index in Figure 7d, which resembles a rather face to face arrangement of the As_5 plane to the Hg_3 plane.

A detailed HS analysis including decomposed fingerprint plots of all described compounds enabled us to further analyze and compare important intermolecular distances. Figure 8 shows the fingerprint plots of the planar Lewis acid **3** in the compounds **4** and **5** with highlighted regions of contact atom pairs.[53]

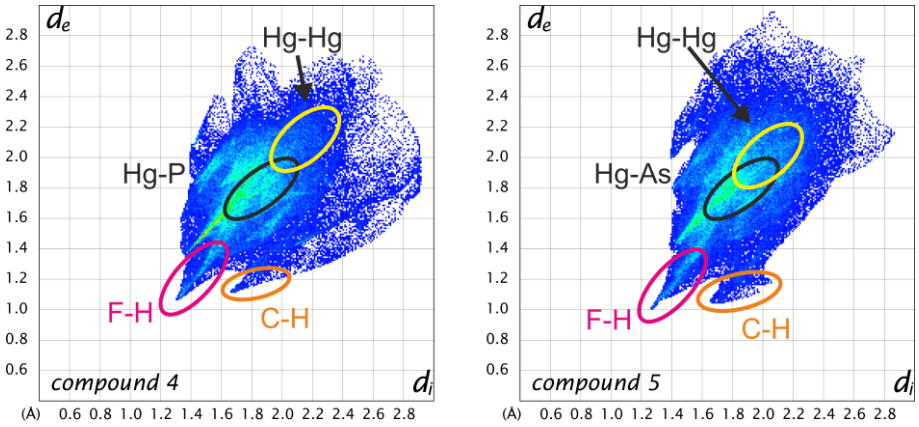

Figure 8. Fingerprint plots of the Hirshfeld surfaces of the planar Lewis acid **3** in the compounds **4** (left) and **5** (right); Regions of the shortest intermolecular distances depending on particular atom pairs are highlighted.

The fingerprint plots of the Lewis acid **3** show some similar features for all compounds. While F-H and C-H distances naturally represent the shortest intermolecular contacts, the Hg-Hg contacts are already at the edge of Hg-Hg interactions and only contribute less than 2% to the Hirshfeld surface. In compound **7c** there are no Hg-Hg contacts at all. However, the Hg-P and Hg-As distances represent short intermolecular contacts for their respective atom types below the sum of the vdW radii (see general considerations). The Hg-P contact area generally contributes about 4-5% to the Hirshfeld surface in all *cyclo*-P_5 compounds (**4**, **7a-c**) and does not change upon Cp ligand exchange of the P_5 complexes. In contrast, the F-H and F-F contacts for example are significantly influenced by the respective *cyclo*-P_5 complex (rising H content of the Cp ligand results in rising F-H contact area).[53] Therefore, in accordance with the single crystal X-ray structure analyses, it can be assumed, that the observed arrangement in the solid state of two *cyclo*-P_5 sandwich complexes enclosed by two

planar Lewis acidic molecules **3** is relatively stable and it can resists a considerable increase in size of the adjacent ligands on the *cyclo*-P_5 sandwich complexes.

9.3 Conclusion

A systematic comparison of the coordination behavior of the *cyclo*-E_5 complexes [Cp*Fe(η^5-P_5)] (**1**) and [Cp*Fe(η^5-As_5)] (**2**) towards the planar trinuclear Lewis acid [(*o*-$C_6F_4Hg)_3$] (**3**) is presented. While one phosphorus atom of the P_5 ring of **1** interacts simultaneously with all three Hg atoms of **3** resembling a weak Lewis acid/base adduct, the analogous *cyclo*-As_5 complex **2** is interacting with the Hg atoms of **3** via only three As atoms instead showing an almost cofacial arrangement of the As_5 plane to the Hg_3 plane of **3** in the solid state. The assemblies are supported by weak Hg-E interactions which are in agreement with the small shifts in the NMR spectra as well as the absence of any adduct signals in the mass spectra of **4** and **5**.

Large energy gaps between the HOMOs of **1** and **2** and the LUMO of **3**, along with the complementarity of their respective electrostatic potential surfaces, suggests that electrostatic forces play a prominent role in the stabilization and coordination behavior of **4** and **5**. AIM analyses of **4** and **5** corroborate the observed weakness of the Hg-E interactions, and suggest the involvement of an As-As π bond in the Hg-*cyclo*-As_5 interactions in **5**.

Subsequently, we prepared and fully characterized the *cyclo*-P_5 sandwich complexes **6a-c** as well as their adducts with the Lewis acid **3** (**7a-c**). By determining the solid state structure and performing a detailed Hirshfeld surface analysis for all compounds we could demonstrate that the general arrangement which was found for compound **4** is relatively stable and can resists a considerable increase of steric demand of the *cyclo*-P_5 complexes. A comparison of the HS of compound **4** and **5** shows quite different contact areas as expected.

In conclusion the presented results show that although the characterized compounds are only supported by weak interactions instead of strong covalent dative bonds we can observe the preference of σ interaction of the *cyclo*-P_5 complex **1** and π interaction of the *cyclo*-As_5 complex **2**.

Notes

† The complexes for n = 2, 3 were reported before.[55,56] During this work the first solid state structure for a complex with n = 2 and a new polymorph for n = 3 could be analyzed by X-ray diffraction analysis.

†† Calculations were performed using the Gaussian program with the B3LYP functional and mixed basis sets: Hg, cc-pVTZ-PP; P/Fe/As, 6-311++G**; F, 6-31G(d‘); C/H, 6-31G).

9.4 References

[1] B. M. Cossairt, N. A. Piro, C. C. Cummins, *Chem. Rev.* **2010**, *110*, 4164-4177.
[2] M. Caporali, L. Gonsalvi, A. Rossin, M. Peruzzini, *Chem. Rev.* **2010**, *110*, 4178-4235.
[3] B. P. Johnson, G. Balázs, M. Scheer, *Coord. Chem. Rev.* **2006**, *250*, 1178-1195.
[4] O. J. Scherer, *Angew. Chem. Int. Ed.* **1990**, *29*, 1104-1122; *Angew. Chem.* **1990**, *102*, 1137-1155.
[5] O. J. Scherer, *Acc. Chem. Res.* **1999**, *32*, 751-762.
[6] D. Y. Zubarev, A. I. Boldyrev, in *Encyclopedia of Inorganic and Bioinorganic Chemistry*, John Wiley & Sons, Ltd, **2011**.
[7] N. H. Martin, J. D. Robinson, *J. Mol. Graphics Modell.* **2012**, *38*, 26-30.
[8] Z. Li, C. Zhao, L. Chen, *J. Mol. Struct.* **2007**, *810*, 1-6.
[9] F. De Proft, P. W. Fowler, R. W. A. Havenith, P. v. R. Schleyer, G. Van Lier, P. Geerlings, *Chem. Eur. J.* **2004**, *10*, 940-950.
[10] E. J. P. Malar, *J. Org. Chem.* **1992**, *57*, 3694-3698.
[11] O. J. Scherer, T. Brück, *Angew. Chem. Int. Ed.* **1987**, *26*, 59-59; *Angew. Chem.* **1987**, *99*, 59-59.
[12] O. J. Scherer, C. Blath, G. Wolmershäuser, *J. Organomet. Chem.* **1990**, *387*, C21-C24.
[13] J. Bai, A. V. Virovets, M. Scheer, *Angew. Chem. Int. Ed.* **2002**, *41*, 1737-1740; *Angew. Chem.* **2002**, *114*, 1808-1811.
[14] F. Dielmann, A. Schindler, S. Scheuermayer, J. Bai, R. Merkle, M. Zabel, A. V. Virovets, E. V. Peresypkina, G. Brunklaus , H. Eckert, M. Scheer, *Chem. Eur. J.* **2012**, *18*, 1168-1179.
[15] J. Bai, A. V. Virovets, M. Scheer, *Science* **2003**, *300*, 781-783.
[16] M. Scheer, A. Schindler, C. Gröger, A. V. Virovets, E. V. Peresypkina, *Angew. Chem. Int. Ed.* **2009**, *48*, 5046-5049; *Angew. Chem.* **2009**, *121*, 5148-5151.
[17] M. Scheer, A. Schindler, J. Bai, B. P. Johnson, R. Merkle, R. Winter, A. V. Virovets, E. V. Peresypkina, V. A. Blatov, M. Sierka, H. Eckert, *Chem. Eur. J.* **2010**, *16*, 2092-2107.
[18] S. Welsch, C. Gröger, M. Sierka, M. Scheer, *Angew. Chem. Int. Ed.* **2011**, *50*, 1435-1438; *Angew. Chem.* **2011**, *123*, 1471-1474.
[19] A. Schindler, C. Heindl, G. Balázs, C. Gröger, A. V. Virovets, E. V. Peresypkina, M. Scheer, *Chem. Eur. J.* **2012**, *18*, 829-835.
[20] H. Krauss, G. Balázs, M. Bodensteiner, M. Scheer, *Chem. Sci.* **2010**, *1*, 337-342.
[21] M. Scheer, L. J. Gregoriades, A. V. Virovets, W. Kunz, R. Neueder, I. Krossing, *Angew. Chem. Int. Ed.* **2006**, *45*, 5689-5693; *Angew. Chem.* **2006**, *118*, 5818-5822.
[22] S. Welsch, L. J. Gregoriades, M. Sierka, M. Zabel, A. V. Virovets, M. Scheer, *Angew. Chem. Int. Ed.* **2007**, *46*, 9323-9326; *Angew. Chem.* **2007**, *119*, 9483-9487.
[23] M. Fleischmann, S. Welsch, H. Krauss, M. Schmidt, M. Bodensteiner, E. V. Peresypkina, M. Sierka, C. Gröger, M. Scheer, *Chem. Eur. J.* **2014**, *20*, 3759-3768.
[24] P. Sartori, A. Golloch, *Chem. Ber.* **1968**, *101*, 2004-2009.
[25] M. R. Haneline, R. E. Taylor, F. P. Gabbaï, *Chem. Eur. J.* **2003**, *9*, 5188-5193.
[26] T. J. Taylor, C. N. Burress, F. P. Gabbaï, *Organometallics* **2007**, *26*, 5252-5263.
[27] T. J. Taylor, C. N. Burress, L. Pandey, F. P. Gabbaï, *Dalton Trans.* **2006**, 4654-4656.
[28] C. N. Burress, M. I. Bodine, O. Elbjeirami, J. H. Reibenspies, M. A. Omary, F. P. Gabbaï, *Inorg. Chem.* **2007**, *46*, 1388-1395.
[29] A. S. Filatov, E. A. Jackson, L. T. Scott, M. A. Petrukhina, *Angew. Chem. Int. Ed.* **2009**, *48*, 8473-8476; *Angew. Chem.* **2009**, *121*, 8625-8628.
[30] M. Tsunoda, F. P. Gabbaï, *J. Am. Chem. Soc.* **2000**, *122*, 8335-8336.
[31] M. R. Haneline, M. Tsunoda, F. P. Gabbaï, *J. Am. Chem. Soc.* **2002**, *124*, 3737-3742.
[32] M. R. Haneline, J. B. King, F. P. Gabbaï, *Dalton Trans.* **2003**, 2686-2690.
[33] M. R. Haneline, F. P. Gabbaï, *Angew. Chem. Int. Ed.* **2004**, *43*, 5471-5474; *Angew. Chem.* **2004**, *116*, 5587-5590.
[34] M. Fleischmann, C. Heindl, M. Seidl, G. Balázs, A. V. Virovets, E. V. Peresypkina, M. Tsunoda, F. P. Gabbaï, M. Scheer, *Angew. Chem. Int. Ed.* **2012**, *51*, 9918-9921; *Angew. Chem.* **2012**, *124*, 10056-10059.
[35] A. J. Canty, G. B. Deacon, *Inorg. Chim. Acta* **1980**, *45*, L225-L227.
[36] S. S. Batsanov, *J. Chem. Soc., Dalton Trans.* **1998**, 1541-1546.
[37] P. Pyykko, M. Straka, *PCCP* **2000**, *2*, 2489-2493.

[38] K. R. Flower, V. J. Howard, S. Naguthney, R. G. Pritchard, J. E. Warren, A. T. McGown, *Inorg. Chem.* **2002**, *41*, 1907-1912.
[39] A. F. Holleman, E. Wiberg, N. Wiberg, *Lehrbuch der Anorganischen Chemie, Vol. 102*, Walter de Gruyter, Berlin, **2007**.
[40] R. E. Taylor, F. P. Gabbaï, *J. Mol. Struct.* **2007**, *839*, 28-32.
[41] J. Rodríguez-Otero, E. M. Cabaleiro-Lago, Á. Peña-Gallego, M. Merced Montero-Campillo, *Tetrahedron* **2009**, *65*, 2368-2371.
[42] A. Burini, J. P. Fackler, R. Galassi, T. A. Grant, M. A. Omary, M. A. Rawashdeh-Omary, B. R. Pietroni, R. J. Staples, *J. Am. Chem. Soc.* **2000**, *122*, 11264-11265.
[43] R. W. F. Bader, *Atoms in Molecules. A Quantum Theory*, Cambridge University Press, Oxford, UK, **1991**.
[44] R. Parthasarathi, V. Subramanian, N. Sathyamurthy, *J. Phys. Chem. A* **2006**, *110*, 3349-3351.
[45] P. Macchi, A. Sironi, *Coord. Chem. Rev.* **2003**, *238–239*, 383-412.
[46] G. Frenking, *Angew. Chem. Int. Ed.* **2014**, *53*, 6040-6046; *Angew. Chem.* **2014**, *126*, 6152-6158.
[47] D. Himmel, I. Krossing, A. Schnepf, *Angew. Chem. Int. Ed.* **2014**, *53*, 370-374; *Angew. Chem.* **2014**, *126*, 378-382.
[48] D. Cremer, E. Kraka, *Angew. Chem. Int. Ed.* **1984**, *23*, 627-628; D. Cremer, E. Kraka, *Angew. Chem.* **1984**, *96*, 612-614.
[49] J. J. McKinnon, D. Jayatilaka, M. A. Spackman, *Chem. Commun.* **2007**, 3814-3816.
[50] J. J. McKinnon, A. S. Mitchell, M. A. Spackman, *Chem. Eur. J.* **1998**, *4*, 2136-2141.
[51] M. A. Spackman, D. Jayatilaka, *CrystEngComm* **2009**, *11*, 19-32.
[52] A. S. Mark, *Phys. Scr.* **2013**, *87*, 048103.
[53] A detailed discussion of the Hirshfeld surface analyses for the compounds **4**, **5**, **7a-c** can be found in the supporting information including representations of discussed surfaces and selected decomposed fingerprint plots.
[54] Unfortunately, the close contacts are not very pronounced as red contact areas since the crystal explorer software uses shorter vdW radii as a reference. A detailed description of the matter can be found in the supporting information.
[55] M. Scheer, G. Friedrich, K. Schuster, *Angew. Chem. Int. Ed.* **1993**, *32*, 593-594; *Angew. Chem.* **1993**, *105*, 641-643.
[56] O. J. Scherer, T. Hilt, G. Wolmershäuser, *Organometallics* **1998**, *17*, 4110-4112.

9.5 Supporting Information

General considerations

All experiments were performed under an atmosphere of dry argon or nitrogen using standard Schlenk and drybox techniques. Commercially available reagents were used as received without further purification. Solvents were freshly distilled under nitrogen from CaH_2 (CH_2Cl_2, CD_2Cl_2), Solution NMR spectra were recorded on a Bruker Avance 400 spectrometer (^{1}H: 400.130 MHz, ^{31}P: 161.976 MHz, ^{13}C: 100.613 MHz). The chemical shifts δ are presented in parts per million ppm and coupling constants J in Hz. The following samples were used for external reference: TMS (^{1}H, ^{13}C), $CFCl_3$ (^{19}F), H_3PO_4 85 % (^{31}P). IR spectra were recorded on a VARIAN FTS-800 FT-IR spectrometer. Mass spectra were recorded by the MS department of the University of Regensburg on a ThermoQuest Finnigan TSQ 7000 mass spectrometer (ESI) or a Finnigan MAT 95 mass spectrometer (EI, FD). The solid substances were grinded together with dried KBr and pressed to pellets. The starting materials **1, 2** and **3** were prepared according to the literature procedure.[1]

Syntheses of the compound 6a-c

The preparation of the starting *cyclo*-P_5 sandwich complexes is easily done following the same procedure as it was done for the Cp* analogues complex. Table 1 shows the quantities and yields for the different reactions.

Procedure: Solid P_4 is weighed into a round bottom flask together with solid $[Cp^RFe(CO)_2]_2$ and decalene is added. The resulting mixture was refluxed for 3 h. During this time a color change from dark red to olive green to dark brown is observed. The solvent is evaporated under reduced pressure. The solid remainder was dissolved in a small amount of CH_2Cl_2, some silica gel added and the solvent removed until a free flowing brown powder remained. Column chromatographic workup on silica with pure *n*-hexane afforded only a green band. Other side products were not isolated for this work. The green solution was reduced to a minimum and stored at –30 °C. After one day **6a** and **6 c** form dark green blocks but **6b** can only be isolated as a light green powder. The mother liquor is removed and the crystals dried in vacuum. To grow crystals of **6b**, a saturated solution in Et_2O at room temperature was cooled to –30 °C.

Table 1. Summaryof the quantities used for the preparation of **6a-c**.

	$m([Cp^RFe(CO)_2]_2)$ [g]	$n([Cp^RFe(CO)_2]_2)$ [mmol]	$m(P_4)$ [g]	$n(P_4)$ [mmol]	V(decalene) [mL]	Yield [g]	Yield [%]
Cp'FeP5	3.8	8.2	4.1	33.1	200	0.46	8.5
Cp''FeP5	5.2	9.0	5.0	40.4	200	2.34	33.5
Cp'''FeP5	0.28	0.40	0.30	2.42	50	0.16	45

Analytical data for 6a-c

[Cp'Fe(η^5-P_5)] (**6a**): Yield 460 mg (8.5 %). ^{1}H NMR (C_6D_6) δ/ppm = 0.89 (s, Me, 9H), 3.41 (s, CpH, 2H), 3.55 (s, CpH, 2H); ^{13}C{^{1}H} NMR (C_6D_6) δ/ppm = 30.05 (s, Me), 31.05 (s, CMe3), 73.72 (s, CpH), 65.20 (s, CpH), 110.87 (s, Cp^{t}Bu); ^{31}P{^{1}H} NMR (C_6D_6) δ/ppm = 168.20 (s, P_5). Anal. calcd. for [$C_9H_{13}FeP_5$]: C, 32.57; H, 3.95. Found: C, 32.52; H, 3.98. EI-MS (CH_2Cl_2) *m/q* (%) = 331.9 (100) $[M]^+$, 269.9 (82) $[M–2P]^+$. IR (KBr) $\tilde{\nu}$/cm^{-1} = 3089 (w), 2956 (m), 2927 (w), 2898 (w), 2861 (w), 1480 (m), 1456 (w), 1396 (m), 1361 (m), 1273 (w), 1149 (w), 1037 (w), 905 (w), 842 (m).

[Cp''Fe(η^5-P_5)] (**6b**): Yield 2.34 g (33.5 %). ^{1}H NMR (C_6D_6) δ/ppm = 1.01 (s, Me, 18H), 3.63 (s, CpH, 2H), 3.65 (s, CpH, 1H); ^{13}C{^{1}H} NMR (C_6D_6) δ/ppm = 30.36 (s, Me), 31.52 (s, CMe_3), 70.34 (s, CpH), 72.10 (s, CpH), 109.79 (s, Cp^{t}Bu); ^{31}P{^{1}H} NMR (C_6D_6) δ/ppm = 166.44 (s, P_5); ^{31}P NMR (C_6D_6) δ/ppm = 166.43 (s, P_5). EI-MS (CH_2Cl_2) *m/q* (%) = 388.0 (100) [*M*]$^+$, 326.0 (98) [*M*–2P]$^+$. IR (KBr) $\tilde{\nu}$/cm^{-1} = 2957 (m), 2927 (vw), 2900 (w), 2862 (w), 1486 (w), 1458 (w), 1367 (w), 1360 (m), 1251 (w), 1163 (w), 1051 (w), 863 (m), 845 (m).

[Cp'''Fe(η^5-P_5)] (**6c**): Yield 160 mg (45 %). ^{1}H NMR (C_6D_6) δ/ppm = 1.08 (s, Me, 9H), 1.20 (s, Me, 18H), 3.95 (s, CpH, 2H); ^{13}C{^{1}H} NMR (C_6D_6) δ/ppm = 30.57 (m, Me), 31.62 (s, CMe_3), 33.28 (s, CMe_3), 33.42 (m, Me), 73.10 (s, CpH), 104.60 (s, Cp^{t}Bu), 106.66 (s, Cp^{t}Bu); ^{31}P{^{1}H} NMR (C_6D_6) δ/ppm = 165.24 (s, P_5). Anal. calcd. for [$C_{17}H_{29}FeP_5$]: C, 45.97; H, 6.58. Found: C, 45.96; H, 6.53. EI-MS: *m/q* (%): 444.0 (100) [*M*]$^+$, 382.0 (65) [*M*–2P]$^+$, 386.9 (12) [*M*–C_4H_9]$^+$. IR (KBr) $\tilde{\nu}$/cm^{-1} = 2957 (m), 2920 (w), 2864 (w), 1491 (vw), 1460 (vw), 1363 (w), 1247 (vw), 1169 (vw), 1020 (vw).

Syntheses of the compounds 4, 5 and 7a-c

Since CH_2Cl_2 is considered as a very weak donor, the reactions were performed in this solvent. Furthermore, all used *cyclo*-E_5 ligand complexes and also the Lewis acid $[(o\text{-}C_6F_4Hg)_3]$ show a good solubility in CH_2Cl_2.
For the preparation of the compounds **4**, **5** and **7a-c**, the *cyclo*-E_5 ligand complexes were weighed together with solid $[(o\text{-}C_6F_4Hg)_3]$. The used amounts for all reactions can be found in Table 2. CH_2Cl_2 was added while stirring the reaction until the solution turned clear (about 10 to 20 mL). This solution was filtered into another flask and the solvent was slowly evaporated while stirring. The solid that forms above the solvent was repeatedly dissolved again. When the solid starts to dissolve only very slowly, the solution is warmed to room temperature. When the solution is completely clear again, the flask is stored at +4 °C or –30 °C. The crystals usually form on the walls of the flask above the solvent at +4 °C or inside the solution at –30 °C.

Table 2. summary of the quantities used for the preparation of compounds **4**, **5**, and **7a-c**.

complex	*m*(Cp^RFeE_5) [mg]	*n*(Cp^RFeE_5) [mmol]	*m*($Hg_3C_{18}F_{12}$) [mg]	*n*($Hg_3C_{18}F_{12}$) [mmol]	Yield [mg]	Yield [%]
Cp*FeP5	35	0.1	105	0.1	87	62
Cp*FeAs5	57	0.1	105	0.1	124	77
Cp'FeP5	33	0.1	105	0.1	67	49
Cp''FeP5	39	0.1	105	0.1	76	53
Cp'''FeP5	45	0.1	105	0.1	94	63

Analytical data for the compounds 4, 5, 7a-c

[{Cp*Fe(η^5-P_5)}•{$(o\text{-}C_6F_4Hg)_3$}] (**4**): Yield 87 mg (62 %). ^{1}H NMR (CD_2Cl_2) δ/ppm = 1.38 (s, Cp*); ^{13}C{^{1}H} NMR (CD_2Cl_2) δ/ppm = 91.93 (s, C_{Cp}), 10.95 (s, CH_3); ^{19}F NMR (CD_2Cl_2) δ/ppm = –120.66 (m, *o*-F), –155.34 (m, *p*-F); ^{31}P{^{1}H} NMR (CD_2Cl_2) δ/ppm = 155.32 (s, P_5); ^{31}P NMR (CD_2Cl_2)δ/ppm = 155.32 (s, P_5). Anal. calcd. for [$Hg_3C_{18}F_{12}$][$C_{10}H_{15}FeP_5$]: C, 24.16; H, 1.09. Found: C, 24.18; H, 1.10. FD-MS (CH_2Cl_2) *m/q* (%) = 346.1 (100) [Cp^*FeP_5]$^+$, 1046.3 (50) [$Hg_3C_{18}F_{12}$]$^+$. IR (KBr) $\tilde{\nu}$/cm^{-1} = 2978 (vw), 2959 (vw), 2909 (vw), 1616 (w), 1583 (w), 1475 (vs), 1419 (s), 1377 (w), 1289 (m), 1088 (m), 1005 (m), 816 (w).

NMR spectra at different temperatures for compound **4**: ^{1}H NMR (CD_2Cl_2, 300 K) δ/ppm = 1.39 (s, CH_3); ^{1}H NMR (CD_2Cl_2, 193 K) δ/ppm = 1.22 (s, CH_3); ^{31}P NMR (CD_2Cl_2, 300 K) δ/ppm = 154.8 (s, P_5); ^{31}P NMR (CD_2Cl_2, 193 K) δ/ppm = 156.7 (s, P_5).

NMR spectra at different temperatures for the free ligand complex **1**: ^{1}H NMR (CD_2Cl_2, 300 K) δ/ppm = 1.43 (s, CH_3); ^{1}H NMR (CD_2Cl_2, 193 K) δ/ppm = 1.35 (s, CH_3); ^{31}P NMR (CD_2Cl_2, 300 K) δ/ppm = 152.3 (s, P_5); ^{31}P NMR (CD_2Cl_2, 193 K) δ/ppm = 149.1 (s, P_5).

[{Cp*Fe(η^5-As_5)}•{(o-$C_6F_4Hg)_3$}] (**5**): Yield 124 mg (77 %). ^{1}H NMR (CD_2Cl_2) δ/ppm = 1.27 (s, Cp*); ^{13}C{^{1}H} NMR (CD_2Cl_2) δ/ppm = 12.12 (s, Me), 88.75 (s, Cp); ^{19}F NMR (CD_2Cl_2) δ/ppm = –120.64 (m, o-F), –155.80 (m, p-F). Anal. calcd. for $[C_{10}H_{15}FeAs_5 \bullet Hg_3C_{18}F_{12}]$: C, 20.87; H, 0.94. Found: C, 20.89; H, 0.98. FD-MS (CH_2Cl_2) m/q (%) = 566.0 (18) $[Cp^*FeAs_5]^+$, 756.8 (100) $[Cp^*_2Fe_2As_5]^+$, 1045.8 (8) $[Hg_3C_{18}F_{12}]^+$. IR (KBr) $\tilde{\nu}$/cm^{-1} = 2963 (vw), 2910 (vw), 2858 (vw), 1614 (w), 1581 (w), 1472 (vs), 1417 (s), 1376 (w), 1287 (w), 1086 (m), 1004 (m), 814 (w).

[{Cp'Fe(η^5-P_5)}•{(o-$C_6F_4Hg)_3$}] (**7a**): Yield 67 mg (49 %). ^{1}H NMR (CD_2Cl_2) δ/ppm = 1.13 (s, Me, 9H), 4.06 (s, CpH, 2H), 4.21 (s, CpH, 2H); ^{19}F NMR (CD_2Cl_2) δ/ppm = –120.77 (m, o-F), –155.10 (m, p-F); ^{31}P{^{1}H} NMR (CD_2Cl_2) δ/ppm = 168.70 (s, P_5). Anal. calcd. for $[Hg_3C_{18}F_{12}][C_9H_{13}FeP_5]$: C, 23.54; H, 0.95. Found: C, 23.97; H, 1.16. FD-MS (CH_2Cl_2) m/q (%) = 332.0 (100) $[Cp'FeP_5]^+$, 1046.9 (8) $[Hg_3C_{18}F_{12}]^+$. IR (KBr) $\tilde{\nu}$/cm^{-1} = 3118 (vw), 2965 (w), 2955 (w), 2934 (vw), 2927 (w), 2906 (vw), 2868 (vw), 1615 (m), 1583 (m), 1471 (vs), 1420 (s), 1288 (s), 1252 (m), 1088 (s), 1004 (s), 850 (m), 814 (m), 771 (m).

[{Cp''Fe(η^5-P_5)}•{(o-$C_6F_4Hg)_3$}] (**7b**): Yield 76 mg (53 %). ^{1}H NMR (CD_2Cl_2) δ/ppm = 1.16 (s, Me, 18H), 3.90 (s, CpH, 1H), 4.05 (s, CpH, 2H); ^{19}F NMR (CD_2Cl_2) δ/ppm = –120.75 (m, o-F), –155.10 (m, p-F); ^{31}P{^{1}H} NMR (CD_2Cl_2) δ/ppm = 166.94 (s, P_5). Anal. calcd. for $[Hg_3C_{18}F_{12}][C_{13}H_{21}FeP_5]$: C, 25.97; H, 1.48. Found: C, 26.10; H, 1.58. FD-MS (CH_2Cl_2) m/q (%) = 388.1 (100) $[Cp''FeP_5]^+$, 1045.9 (30) $[Hg_3C_{18}F_{12}]^+$. IR (KBr) $\tilde{\nu}$/cm^{-1} = 2968 (w), 2959 (w), 2905 (vw), 2864 (vw), 1616 (w), 1582 (w), 1473 (vs), 1418 (s), 1289 (m), 1085 (m), 1006 (m), 814 (w).

[{Cp'''Fe(η^5-P_5)}•{(o-$C_6F_4Hg)_3$}] (**7c**): Yield 94 mg (63 %). ^{1}H NMR (CD_2Cl_2) δ/ppm = 1.17 (s, Me, 9H), 1.31 (s, Me, 18H), 4.08 (s, CpH, 2H); ^{19}F NMR (CD_2Cl_2) δ/ppm = –120.73 (m, o-F), –155.19 (m, p-F); ^{31}P{^{1}H} NMR (CD_2Cl_2) δ/ppm = 166.38 (s, P_5). Anal. calcd. for $[Hg_3C_{18}F_{12}][C_{17}H_{29}FeP_5]$: C, 28.21; H, 1.96. Found: C, 28.79; H, 2.13. FD-MS (CH_2Cl_2) m/q (%) = 444.2 (100) $[Cp'''FeP_5]^+$, 1046.1 (28) $[Hg_3C_{18}F_{12}]^+$. IR (KBr) $\tilde{\nu}$/cm^{-1} = 2965 (w), 2927 (vw), 2872 (vw), 1615 (vw), 1583 (vw), 1471 (vs), 1418 (s), 1289 (m), 1250 (w), 1082 (m), 1005(m), 815 (w), 770 (vw).

X-ray diffraction analysis

General considerations

All diffraction experiments were performed at 123 K. The different data sets were either collected on an Rigaku (former Agilent Technologies or Oxford Diffraction) Gemini R Ultra diffractometer with Cu-K_α or Mo-K_α radiation or an Agilent SuperNova diffractometer with Cu-K_α radiation. Crystallographic data together with the details of the experiments are given in the Tables 4-6. All crystal preparations were performed under mineral oil. The cell determination, data reduction and absorption correction for all other compounds were performed with the help of the CrysAlis PRO software.[2] The structure solution was done by direct methods with SIR97[3] or ShelXS.[4] The full-matrix least-square refinement against F^2 was done with ShelXL.[4] All fully occupied atoms except hydrogen were refined anisotropically. The H atoms were calculated geometrically and a riding model was used during the refinement process. Graphical material was created with the free software Schakal99.[5]

CCDC-1012615-1012624 contain the supplementary crystallographic data for this chapter These data can be obtained free of charge from the Cambridge Crystallographic Data Centre via www.ccdc.cam.ac.uk/data_request/cif. Additionally, all cif-files and the refined structures are saved on the provided DVD.

Crystal structure of [{(*o*-$C_6F_4Hg)_3$}•{Cp*Fe(η^5-As_5)}$_2$]•[Cp*Fe(η^5-As_5)]•(toluene) (**8**): When the *cyclo*-As_5 complex **2** was combined with [(*o*-$C_6F_4Hg)_3$] in CH_2Cl_2 in a small tube which was stored for several weeks in a closed jar with some toluene for gas phase diffusion, it was possible to isolate and analyze some crystals of the novel adduct **8**. Compound **8** crystallizes in the monoclinic space group *C*2/*c*. The asymmetric unit contains Three independent *cyclo*-As_5 sandwich complexes, one molecule of [(*o*-$C_6F_4Hg)_3$] and one and a half toluene molecules. Figure 1 shows the solid state structure of **8**. The As_5 ring As11-As15 is disordered over three positions with the occupancies of 53:28:19. Only the major part is shown here. Unfortunately, we were not able to reproduce this result in a selective manner. Nevertheless, the solid state structure will be presented since it shows the preference of the weak Hg-As interactions over the interactions of **3** with the electron rich toluene molecules which are also found in the crystal lattice.

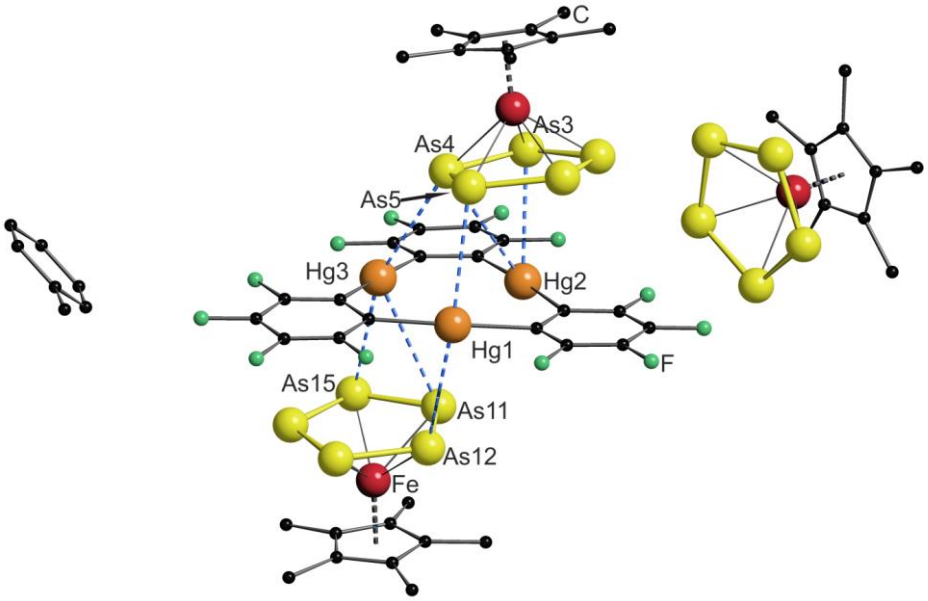

Figure 1. Solid state structure of **8**; The toluene molecule on the left and the pentaarsaferrocene molecule on the right show no short contacts to [(*o*-$C_6F_4Hg)_3$]. The As5 ring As11-As15 is disordered over three positions while only the major part is depicted here (53 % occupancy). Selected bond lengths [Å] and angles [°]: Hg1-As5 3.5329(7), Hg1-As12 3.579(5), Hg2-As3 3.2846(6), Hg2-As4 3.6852(5), Hg3-As4 3.4738(7), Hg3-As11 3.641(7) Hg3-As15 3.486(8), angle(As1-As5 plane to Hg_3 plane) 12.07(1), angle(As11-As15 plane to Hg_3 plane) 6.45(9).

CH_2Cl_2 solvates of [(*o*-$C_6F_4Hg)_3$]

X-ray of [{(*o*-$C_6F_4Hg)_3$}•CH_2Cl_2] (**9**): In another unrelated reaction, we were able to identify crystals of the CH_2Cl_2 solvate of the Lewis acid **3**. This result was surprising since no adduct of CH_2Cl_2 and **3** was either expected or reported so far, since the CH_2Cl_2 is supposed to be a very weak donor. Compound **9** crystallizes in the triclinic space group *P*–1. The asymmetric unit contains one molecule of [(*o*-$C_6F_4Hg)_3$] and one CH_2Cl_2 molecule. Figure 2 shows the solid state structure of **9**. The solvent molecule is not disordered. There is a short contact of Cl2 to Hg1 of 3.351(2) Å that is considerably shorter than the sum of the vdW radii for Hg and Cl (3.5 Å).

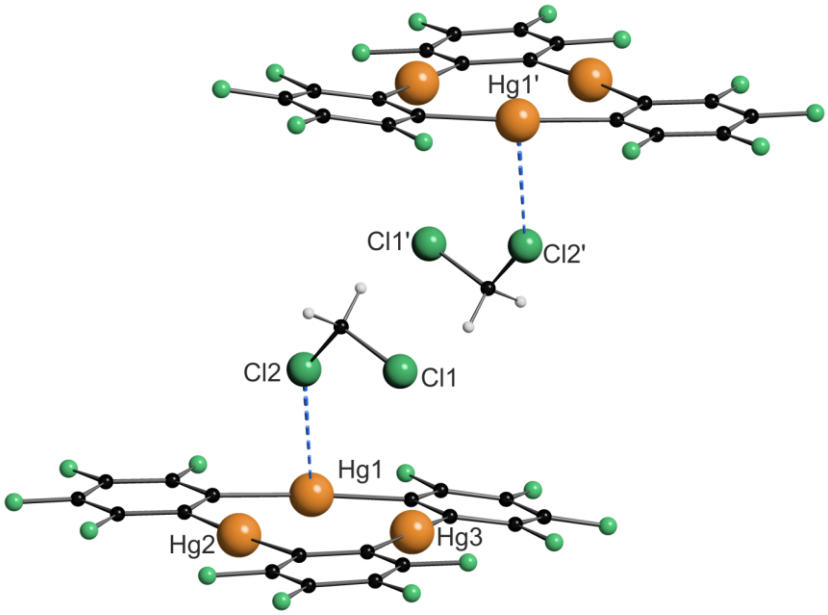

Figure 2. Solid state structure of compound **9**; Hg1-Cl2 3.351(2).

Additional unit cell for a CH_2Cl_2 solvate of [(o-C_6F_4Hg)$_3$]: In addition to the compound **9** another sort of crystals that only contain [(*o*-C_6F_4Hg)$_3$] and CH_2Cl_2 could be obtained from an unrelated reaction. Unfortunately, in this case the solvent molecules as well as one [(*o*-C_6F_4Hg)$_3$] molecule are severely disordered and no satisfactory structure solution could be obtained. Therefore, we just report the unit cell for future reference.

Table 3. Unit cell of a second CH_2Cl_2 solvate of [(*o*-C_6F_4Hg)$_3$].

crystal system	triclinic	*α* [°]	60.940(7)
a [Å]	12.5016(7)	*β* [°]	81.802(6)
b [Å]	14.1313(10)	*γ* [°]	87.573(5)
c [Å]	14.2267(11)	*V* [Å^3]	2173.4(2)

Table 4. Crystallographic data for the compounds **4**, **5**, **6a** and **6b**.

Identification code	**4**	**5**	**6a**	**6b**
Empirical formula	$C_{29}H_{17}Cl_2F_{12}FeHg_3P_5$	$C_{29}H_{17}As_5Cl_2F_{12}FeHg_3$	$C_9H_{13}FeP_5$	$C_{13}H_{21}FeP_5$
M [gmol^{-1}]	1476.80	1696.55	331.89	388.00
Crystal size [mm]	0.19 × 0.12 × 0.10	0.24 × 0.10 × 0.05	0.28 × 0.19 × 0.09	0.28 × 0.07 × 0.06
T [K]	123(1)	123(1)	123(1)	123(1)
λ [Å]	0.71073	0.71073	1.54178	1.54178
crystal system	triclinic	triclinic	orthorhombic	orthorhombic
space group	*P*–1	*P*–1	*Pnma*	*Pca*2$_1$
a [Å]	11.7330(2)	11.9982(2)	11.4347(1)	18.7588(8)
b [Å]	12.1852(2)	13.3448(2)	23.4865(2)	6.5778(3)
c [Å]	13.1641(2)	14.1016(2)	15.1315(1)	14.1509(6)
α [°]	85.129(1)	65.329(1)	90	90
β [°]	80.243(1)	78.072(1)	90	90
γ [°]	74.103(2)	66.415(2)	90	90
V [Å^3]	1782.43(5)	1878.24(6)	4063.73(6)	1746.10(13)
Z	2	2	12	4
ρ_{calc} [gcm^{-3}]	2.752	3.000	1.628	1.476
μ [mm^{-1}]	13.702	17.197	14.256	11.129
diffractometer	Gemini R Ultra	Gemini R Ultra	SuperNova	Gemini R Ultra
radiation	MoK_α	MoK_α	CuK_α	CuK_α
θ range [°]	3.14 – 27.10	3.00 – 27.48	3.47 – 73.60	4.71 – 67.00
absorption correct.	analytical	analytical	analytical	analytical
T_{min} / T_{max}	0.170 / 0.381	0.070 / 0.456	0.081 / 0.391	0.115 / 0.587
reflns collect / unique	43547 / 7854	22941 / 8567	41579 / 4180	3376 / 2274
reflns obs [$I > 2\,\sigma(I)$]	6612	6941	4068	1847
R_{int}	0.0362	0.0292	0.0568	0.0380
Flack parameter	—	—	—	0.025(8)
parameters / restraints	474 / 0	474 / 0	211 / 0	249 / 33
GOF on F^2	0.897	0.935	1.063	0.950
R_1 / wR_2 [$I > 2\,\sigma(I)$]	0.0170 / 0.0307	0.0200 / 0.0394	0.0213 / 0.0541	0.0427 / 0.0910
R_1 / wR_2 (all data)	0.0223 / 0.0311	0.0272 / 0.0400	0.0225 / 0.0549	0.0510 / 0.0929
max / min $\Delta\rho$ [eÅ^{-3}]	0.738 / –0.936	1.149 / –0.993	0.301 / –0.356	0.352 / –0.556

Table 5. Crystallographic data for the compounds **6c**, **7a** and **7b**.

Identification code	**6c**	**7a**	**7b**
Empirical formula	$C_{17}H_{29}FeP_5$	$C_{28}H_{15}Cl_2F_{12}FeHg_3P_5$	$C_{31}H_{21}F_{12}FeHg_3P_5$
M [gmol^{-1}]	444.10	1462.77	1433.95
Crystal size [mm]	0.29 × 0.24 × 0.16	0.41 × 0.28 × 0.16	0.42 × 0.18 × 0.11
T [K]	123(1)	123(1)	123(1)
λ [Å]	0.71073	0.71073	0.71073
crystal system	monoclinic	triclinic	triclinic
space group	*P*2$_1$/*c*	*P*–1	*P*–1
a [Å]	9.0507(1)	11.6373(4)	12.0744(2)
b [Å]	25.6020(3)	11.8015(3)	12.2486(2)
c [Å]	10.1648(2)	15.7005(5)	14.5238(3)
α [°]	90	89.754(2)	69.244(2)
β [°]	115.783(2)	68.252(3)	82.395(2)
γ [°]	90	66.286(3)	65.440(2)
V [Å^3]	2120.87(6)	1806.94(12)	1826.58(7)
Z	4	2	2
ρ_{calc} [gcm^{-3}]	1.391	2.688	2.607
μ [mm^{-1}]	1.085	13.551	13.261
diffractometer	Gemini R Ultra	Gemini R Ultra	Gemini R Ultra
radiation	MoK_α	MoK_α	MoK_α
θ range [°]	2.96 – 27.00	2.96 – 27.00	2.90 – 30.11
absorption correct.	analytical	analytical	analytical
T_{min} / T_{max}	0.794 / 0.875	0.081 / 0.243	0.034 / 0.400
reflns collect / unique	35725 / 5783	12948 / 8836	43916 / 9760
reflns obs [$I > 2\,\sigma(I)$]	4883	5940	8367
R_{int}	0.0264	0.0357	0.0297
parameters / restraints	217 / 0	463 / 0	475 / 0
GOF on F^2	1.059	0.807	0.982
R_1 / wR_2 [$I > 2\,\sigma(I)$]	0.0230 / 0.0609	0.0353 / 0.0529	0.0178 / 0.0344
R_1 / wR_2 (all data)	0.0283 / 0.0618	0.0549 / 0.0548	0.0230 / 0.0349
max / min $\Delta\rho$ [eÅ^{-3}]	0.360 / –0.295	2.006 / –1.743	1.717 / –0.953

Table 6. Crystallographic data for the compounds **7c**, **8** and **9**.

Identification code	**7c**	**8**	**9**
Empirical formula	$C_{73}H_{64}Cl_6F_{24}Fe_2Hg_6P_{10}$	$C_{55}H_{53}As_{15}F_{12}Fe_3Hg_3$	$C_{19}H_2Cl_2F_{12}Hg_3$
M [gmol^{-1}]	3234.88	2835.09	1130.88
Crystal size [mm]	0.26 × 0.20 × 0.16	0.29 × 0.09 × 0.05	0.25 × 0.10 × 0.06
T [K]	123(1)	123(1)	123(1)
λ [Å]	0.71073	0.71073	0.71073
crystal system	Monoclinic	monoclinic	triclinic
space group	$P2_1$	$C2/c$	P–1
a [Å]	12.3145(3)	48.2155(11)	9.2776(2)
b [Å]	26.4751(6)	14.1380(2)	9.7199(2)
c [Å]	14.4338(3)	22.3159(5)	12.7689(2)
α [°]	90	90	103.463(1)
β [°]	107.168(2)	109.887(2)	100.800(2)
γ [°]	90	90	97.447(2)
V [Å^3]	4496.14(18)	14304.9(5)	1081.75(4)
Z	2	8	2
ρ_{calc} [gcm^{-3}]	2.389	2.633	3.472
μ [mm^{-1}]	10.963	13.914	21.239
diffractometer	Gemini R Ultra	Gemini R Ultra	Gemini R Ultra
radiation	MoK_α	MoK_α	MoK_α
θ range [°]	2.74 – 27.10	2.81 – 27.48	2.86 – 28.50
absorption correct.	Analytical	analytical	analytical
T_{min} / T_{max}	0.136 / 0.369	0.129 / 0.510	0.081 / 0.403
reflns collect / unique	39551 / 19613	39165 / 15949	42673 / 6017
reflns obs [$I > 2\ \sigma(I)$]	16576	13516	4682
R_{int}	0.0313	0.0314	0.0507
Flack parameter	0.058(3)	—	—
parameters / restraints	1109 / 13	863 / 0	325 / 0
GOF on F^2	0.860	1.006	0.945
R_1 / wR_2 [$I > 2\ \sigma(I)$]	0.0237 / 0.0384	0.0267 / 0.0530	0.0243 / 0.0470
R_1 / wR_2 (all data)	0.0295 / 0.0387	0.0369 / 0.0561	0.0382 / 0.0485
max / min $\Delta\rho$ [eÅ^{-3}]	1.171 / –0.810	0.129 / –0.793	1.821 / –1.708

DFT studies and AIM analyses

DFT optimizations were performed using the Gaussian 09 program[6] (functional, B3LYP[7], mixed basis sets: Hg, cc-pVTZ-PP[8] with the Stuttgart relativistic small core ECP;[9] P/Fe/As, 6-311++G**;[10] F, 6-31G(d');[11] H/C, 6-31G[12]) The AIM analyses were performed with the AIMAll[13] program using the wavefunction files generated from a single point energy calculation at the experimentally determined solid state geometry. XYZ plots of compounds **4** and **5** featuring all bond critical points found between **1** and **3** and **2** and **3**, respectively, as well as Tables 7 and 8 showing the features of the electron distribution function of these critical points are shown below.

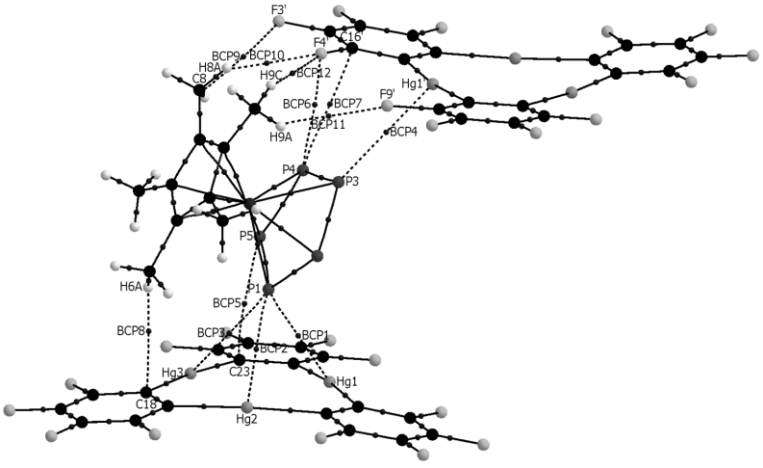

Figure 3. XYZ plot of compound **4**, featuring all bond critical points found between the units of **1** and **3**.

Table 7. Calculated features of the electron density distribution at the bond critical points between **1** and **3** in compound **4**.

BCP No. (A-B)	*d*(A-BCP) [Å]	*d*(B-BCP) [Å]	$\rho(r_{BCP})$ [e Å^{-3}]	$\nabla^2\rho(r_{BCP})$ [e Å^{-5}]	$H(r_{BCP})/\rho(r_{BCP})$ [E_h e^{-1}]	$G(r_{BCP})/\rho(r_{BCP})$ [E_h e^{-1}]	ε
1(Hg1-P1)	1.657	1.630	0.105	0.876	0.012	0.570	0.048
2(Hg2-P1)	1.664	1.696	0.101	0.835	0.020	0.553	0.046
3(Hg3-P1)	1.754	1.776	0.072	0.620	0.055	0.546	0.046
4(Hg1'-P3)	1.737	1.789	0.072	0.622	0.065	0.542	0.051
5(P5-C23)	1.965	1.820	0.033	0.328	0.142	0.551	8.215
6(P4-F4')	1.808	1.486	0.042	0.678	0.140	0.845	1.283
7(P4-C16')	1.849	1.572	0.050	0.533	0.133	0.613	0.132
8(C18-H6A)	3.238	2.213	0.038	0.453	0.192	0.631	0.501
9(C8-F3')	3.457	3.084	0.018	0.342	0.357	0.892	1.923
10(H8A-F4')	1.982	2.697	0.049	0.864	0.232	1.000	0.026
11(H9A-F9')	2.429	3.010	0.017	0.335	0.384	0.961	0.033
12(H9C-F4')	2.065	2.734	0.037	0.692	0.272	1.036	0.052

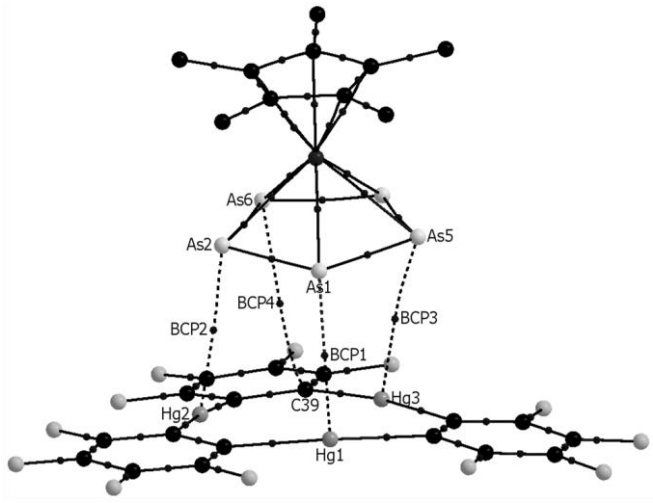

Figure 4. XYZ plot of compound **5**, featuring all bond critical points found between the units of **2** and **3**.

Table 7. Calculated features of the electron density distribution at the bond critical points between **2** and **3** in compound **5**.

BCP No. (A-B)	*d*(A-BCP) [Å]	*d*(B-BCP) [Å]	$\rho(r_{BCP})$ [e Å^{-3}]	$\nabla^2\rho(r_{BCP})$ [e Å^{-5}]	$H(r_{BCP})/\rho(r_{BCP})$ [E_h e^{-1}]	$G(r_{BCP})/\rho(r_{BCP})$ [E_h e^{-1}]	ε
1(Hg1-As1)	1.698	1.707	0.091	0.757	0.044	0.540	0.031
2(Hg2-As2)	1.654	1.648	0.109	0.885	0.018	0.524	0.052
3(Hg3-As5)	1.695	1.731	0.096	0.762	0.027	0.549	0.344
4(As3-C18)	2.024	1.771	0.036	0.325	0.111	0.518	4.005

Hirshfeld surface analyses

In order to further investigate the present interactions in the solid state a detailed Hirshfeld surface analysis[14] of the mercury containing compounds (**4**, **5**, **7a-c**) was performed using the free of charge crystal explorer software.[15] After some general considerations we will present representations of all discussed Hirshfeld surfaces on the following pages describing some highlighted features. Finally we will conclude the discussion with some selected fingerprint plots.

General considerations

All mercury containing compounds contain the same Lewis acid [(*o*-$HgC_6F_4)_3$] (**3**). Therefore, a detailed discussion of the Hirshfeld surface of **3** in these compounds (**4**, **5**, **7a-c**) is presented here. Since the Lewis acid **3** has the characteristic of an almost planar geometry it is possible to easily distinguish two faces of the molecule. To simplify the following discussion we define the side which shows an interaction with either P or As atoms as the front while the opposite side is defined as the back (see Scheme 1).

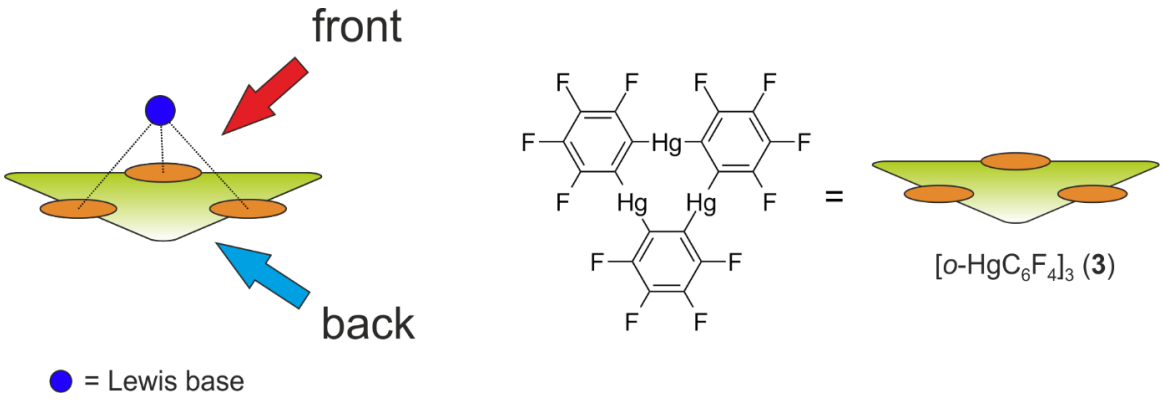

Scheme 1. Definition of front and back side of the planar Lewis acid **3**.

d_{norm} values and the van der Waals radii

The d_{norm} values (depicted in Figure 5-10 a) + b)) for Hirshfeld surfaces were defined[14a] to describe intermolecular contacts in normalized contact distances which are based on the van der Waals radii (vdW) of the involved atoms. The authors designed this very useful representation in a fashion, that: *"d_{norm} … is displayed using a red-white-blue colour scheme, where red highlights shorter contacts, white is used for contacts around the vdW separation, and blue is for longer contacts."*[14a] (page 3814, right column) This visual aid for close contacts is based on the vdW radii (for P 1.80 Å, As 1.85 Å and Hg 1.55 Å) which are also used by the CCDC and taken from the literature.[16] However, the author of this report states: *"the aforementioned metal radii are substantially smaller than predicted from ionization potentials … It is not certain, therefore, how best to estimate the van der Waals radii of metals in metal organic compounds."*[16] (page 448, right column) In the main text of this publication we state: *"The van der Waals (vdW) radius of Hg in different compounds is discussed in the literature with reported values ranging from 1.7 Å up to 2.2 Å*[17] *In the following discussion the shortest value of 1.7 Å is taking as a reference."* The vdW radii of P (1.9) and As (2.0) for our discussion are adopted from an established inorganic textbook (HoWi).[18]

Therefore, the sum of the vdW radii from the crystal explorer software[15] (3.35 for Hg-P and 3.40 for Hg-As) differ from our estimates (3.6 for Hg-P and 3.7 for Hg-As). As a result the following representations of the d_{norm} values on the Hirshfeld surfaces (Figures 5-10 a) clearly show close contacts of Hg to P and As atoms in the center of the molecule but these are unfortunately not highlighted as strongly as some close contacts (F-F and F-H for example) on the periphery.

Hirshfeld surface of compound 4

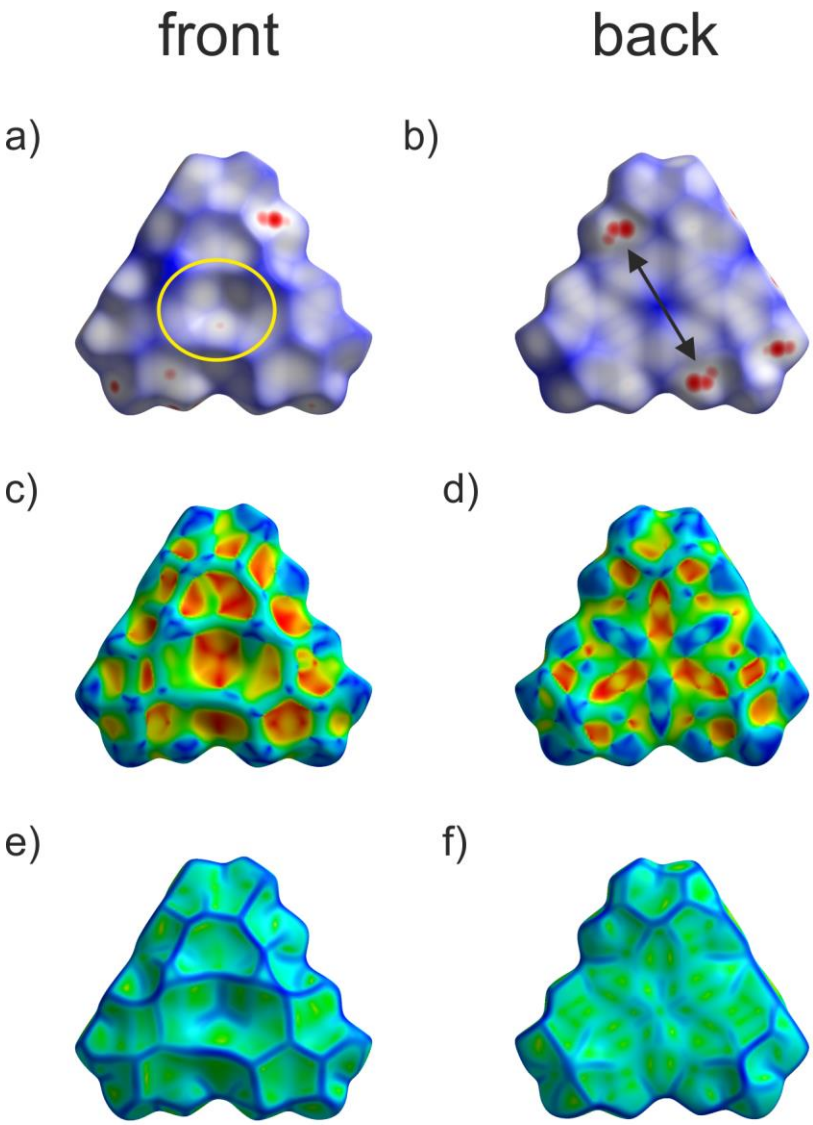

Figure 5. Representation of the Hirshfeld surface of the front (left) and the back (right) of the planar Lewis acid **3** in the compound [(Cp*FeP_5)•(**3**)] (**4**). The first row shows the d_{norm} values, while the second row shows the shape index values and the third row shows the curvedness, respectively.

When looking at the front side of the molecule, one can see a distinctive indentation in the center highlighted in yellow which arises from three short contacts of one P atom to the three mercury atoms (white to red spots). This close approximation is also clearly visible as a red region in the shape index (c) and the three connected blue lines in the curvedness (e). In contrast, the back side of the Hirshfeld surface is flat which arises of a face to face arrangement of two molecules of **3** in the crystal lattice (by an inversion center which is situated directly above the center of the molecule). This can clearly be seen by the shape index (d) which shows self-complementary surface areas around the center of the molecule. In (b) two corresponding close contact regions are highlighted by an arrow.

Hirshfeld surface of compound 5

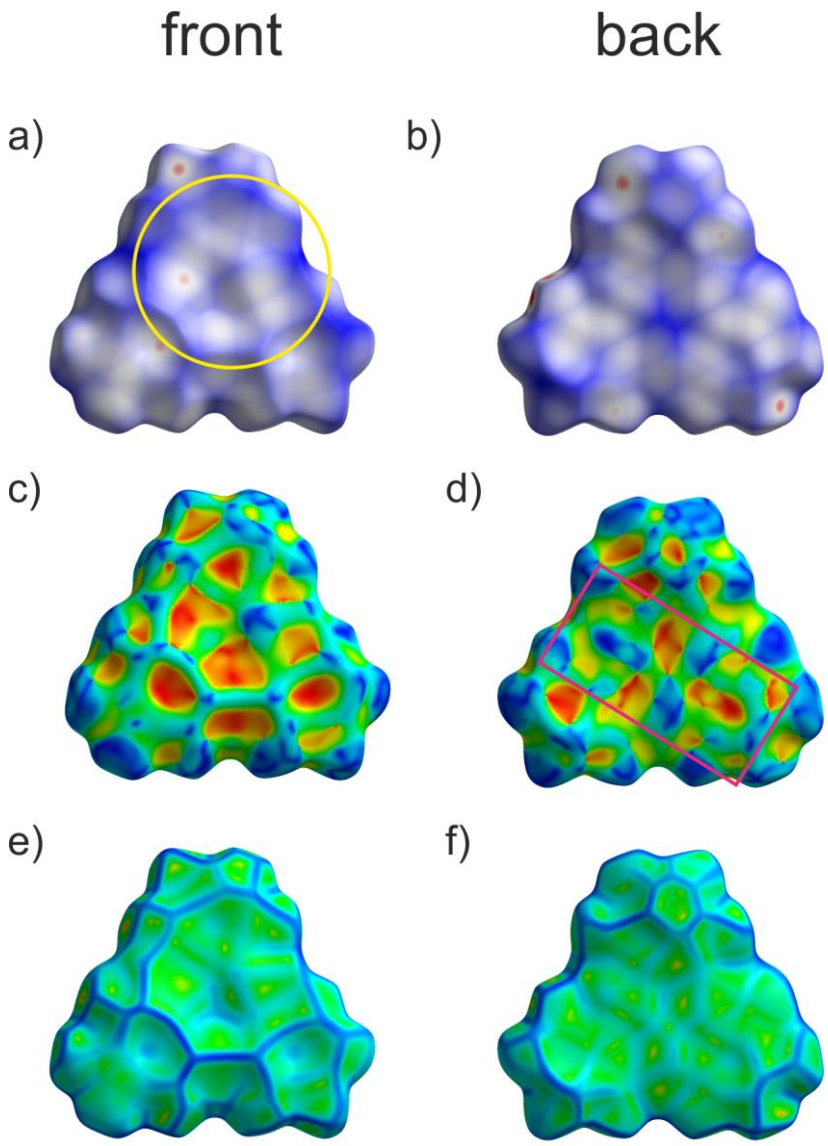

Figure 6. Representation of the Hirshfeld surface of the front (left) and the back (right) of the planar Lewis acid **3** in the compound [(Cp*$FeAs_5$)•(**3**)] (**5**). The first row shows the d_{norm} values, while the second row shows the shape index values and the third row shows the curvedness, respectively.

When looking at the front of the molecule in (a) one can also see a shallow indentation in the center of the molecule like it was found for compound **4** (compare Figure 5a), but this time it is not as pronounced. In this compound the *cyclo*-As_5 complex [Cp*Fe(η^5-$As)_5$] shows contacts to the front side of the Lewis acid **3** by all five As atoms resembling an almost face to face assembly highlighted in yellow. The fact that the Hirshfeld surface is greatly influenced by the five-membered As ring can be seen even more clearly when looking at the shape index (c) which exhibits five red spots or the curvedness (e) which shows a relatively smooth surface in the contact area.

The back side (b) of the molecule is flat. The shape index (d) shows large self-complementary surface regions highlighted in purple which reveal a face to face arrangement of two molecules of **3** by an inversion center which is situated slightly below the center of the molecule in this representation.

Hirshfeld surface of compound 7a

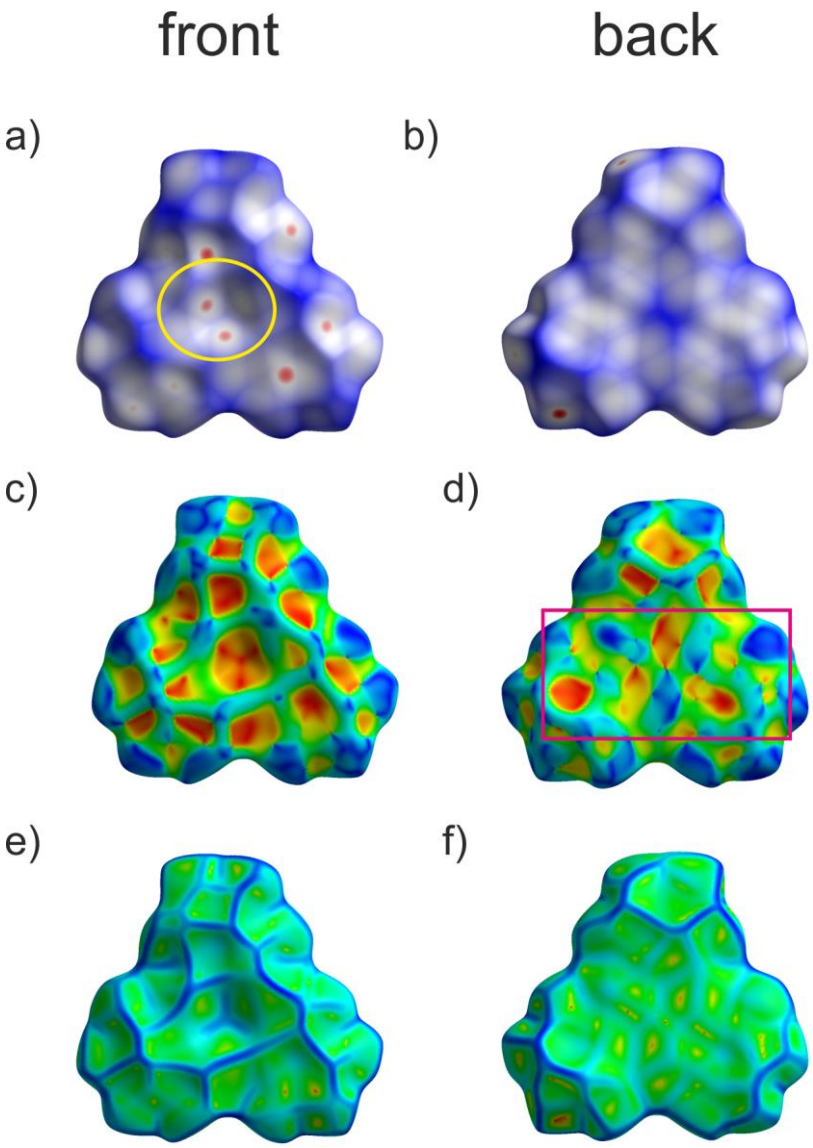

Figure 7. Representation of the Hirshfeld surface of the front (left) and the back (right) of the planar Lewis acid **3** in the compound [(Cp'FeP_5)•(**3**)] (**7a**). The first row shows the d_{norm} values, while the second row shows the shape index values and the third row shows the curvedness, respectively.

The Hirshfeld surface of the Lewis acid **3** in the compound **7a** exhibits features which are very reminiscent of the compound **4** (compare Figure 5). Namely, a distinctive indentation in the center of the front side highlighted in yellow showing three contacts and a flat back side with large self-complementary surface areas.

Hirshfeld surface of compound 7b

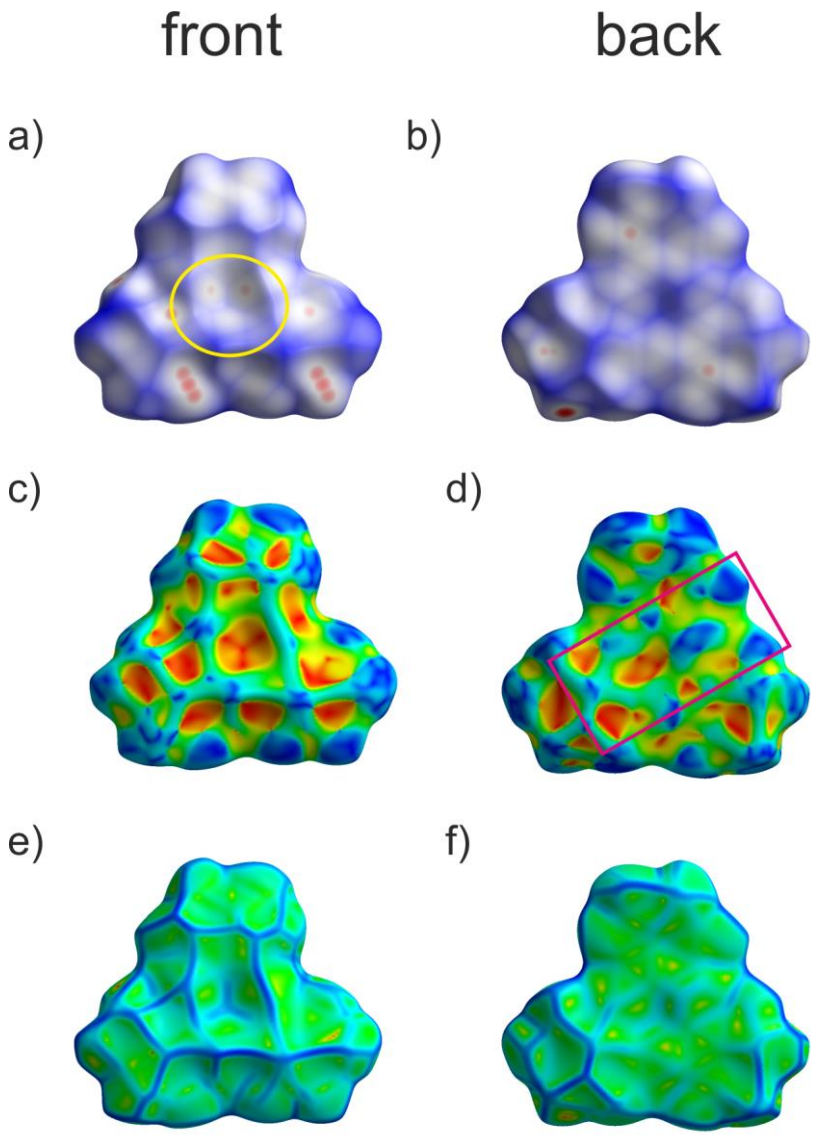

Figure 8. Representation of the Hirshfeld surface of the front (left) and the back (right) of the planar Lewis acid **3** in the compound [(Cp''FeP_5)•(**3**)] (**7b**). The first row shows the d_{norm} values, while the second row shows the shape index values and the third row shows the curvedness, respectively.

The Hirshfeld surface of the Lewis acid **3** in the compound **7b** is closely related to the one found in compound **7a** (compare Figure 7) and also exhibits features which are very reminiscent of compound **4** (compare Figure 5). Namely, a distinctive indentation in the center of the front side highlighted in yellow showing three contacts and a flat back side with large self-complementary surface areas.

Hirshfeld surface of compound 7c

The compound **7c** crystallizes with two independent molecules of the Lewis acid **3** in the asymmetric unit, but these show very similar environments. Therefore, the Hirshfeld surfaces for both molecules are presented separately, but the features will be discussed together.

Molecule 1

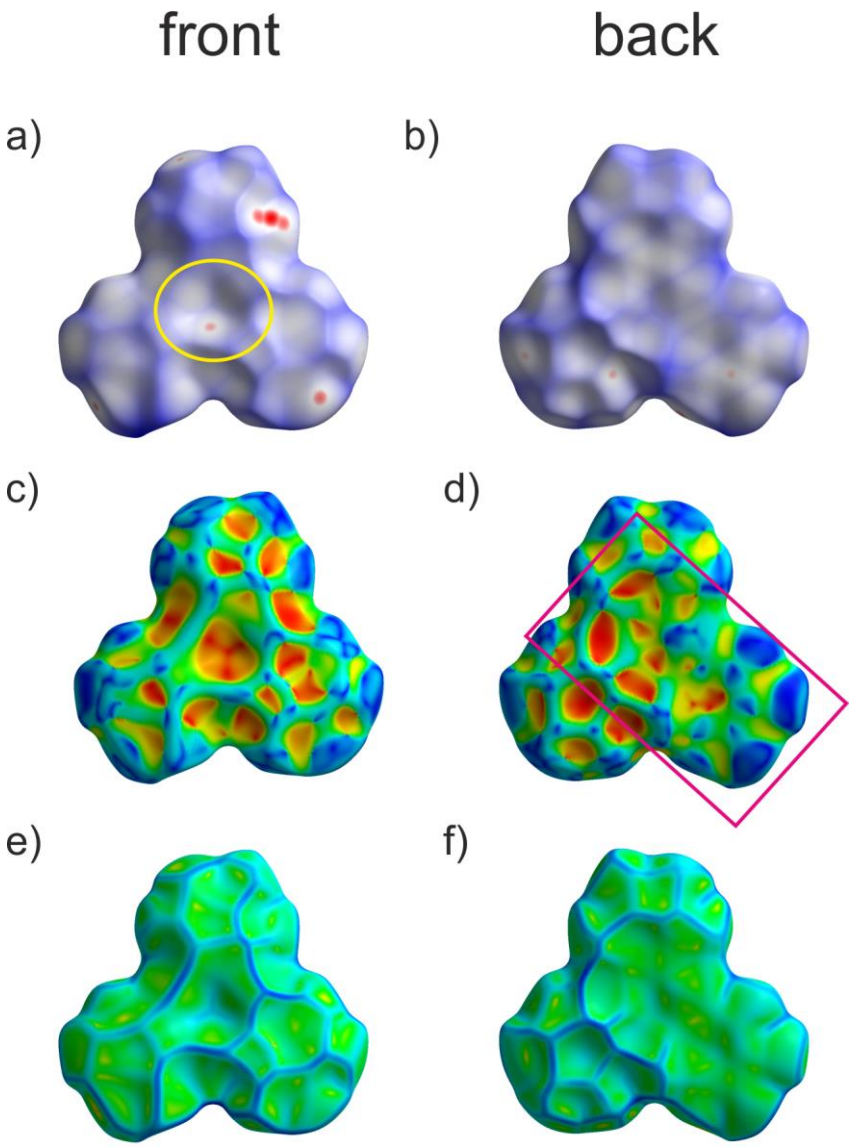

Figure 9. Representation of the Hirshfeld surface of the front (left) and the back (right) of molecule **1** in the compound $[(Cp'''FeP_5)\bullet(\mathbf{3})]$ (**7c**). The first row shows the *d*norm values, while the second row shows the shape index values and the third row shows the curvedness, respectively.

Molecule 2

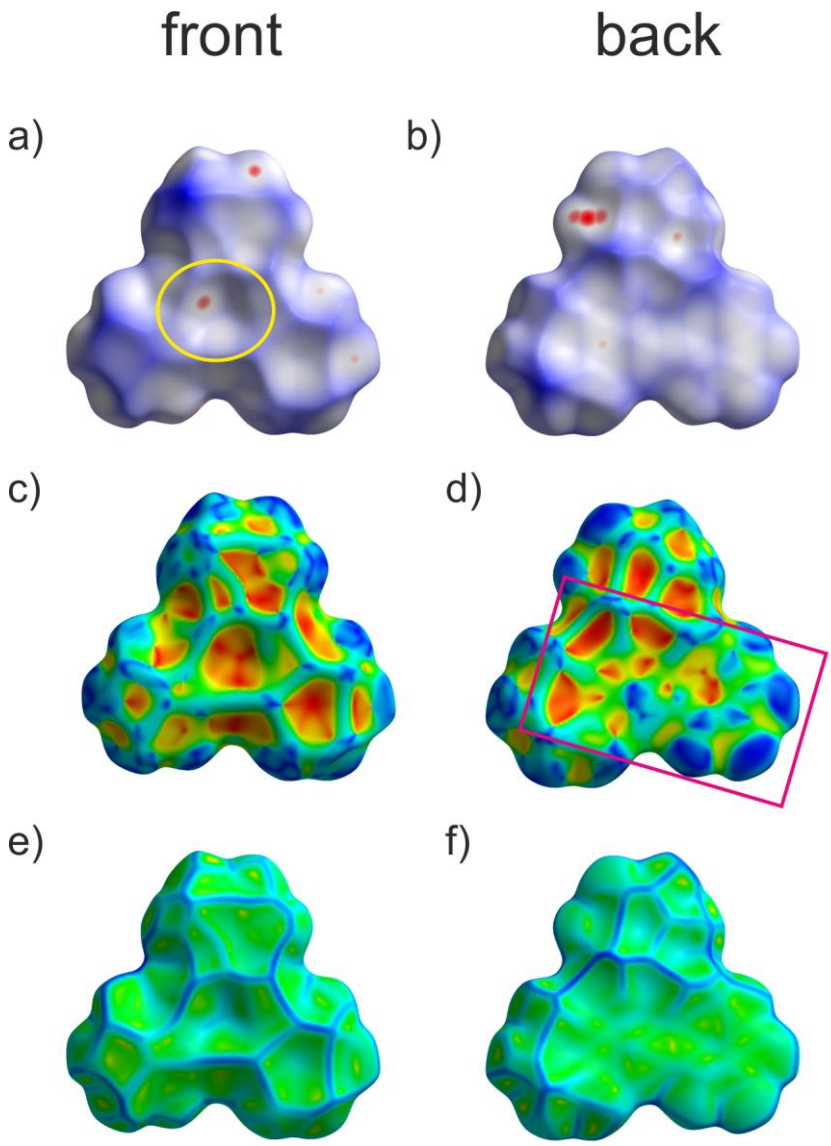

Figure 10. Representation of the Hirshfeld surface of the front (left) and the back (right) of molecule **2** in the compound [(Cp'''FeP_5)•(**3**)] (**7c**). The first row shows the d_{norm} values, while the second row shows the shape index values and the third row shows the curvedness, respectively.

The Hirshfeld surfaces of the Lewis acid **3** in the compound **7c** exhibit features which are very reminiscent of the compounds **4**, **7a** and **7b** (compare Figures. 5, 7 and 8). Namely, a distinctive indentation in the center of the front side highlighted in yellow showing three contacts and a flat back side. The only difference is the orientation of the next planar Lewis acid **3** in respect to the center of the molecule. In this case the next molecule of **3** is not created via an inversion center in the solid state but is an independent molecule (molecule **1** on top of molecule **2** and vice versa). Nevertheless, since the environment of the two molecules is very similar, their Hirshfeld surfaces show very similar features. When looking at Figure 9 and 10 (d) the purple rectangles highlight surface areas which show almost complementary shape indexes although they are not self-complementary.

Fingerprint plots of the compounds 4, 5 and 7a-c

On the following pages we present selected fingerprint plots of the planar Lewis acid **3** in the mercury containing coordination compounds **4**, **5** and **7a-c**. These plots visually present intermolecular contacts in d_i-d_e pairs which describe the distances of the nearest nuclei inside or outside the Hirsheld surface to one particular point on the surface. The plots are color coded to show the relative frequency of specific d_i-d_e pairs, but they do not take different atom sizes into account. Therefore, short Hg-P distances will be found in different regions than short C-H distances. The surface of the investigated Lewis acid **3** in all compounds roughly consists of 11.5% contribution from Hg atoms, 63% from F atoms and 25.5% from C atoms.

Decomposed fingerprint plots of compound 4

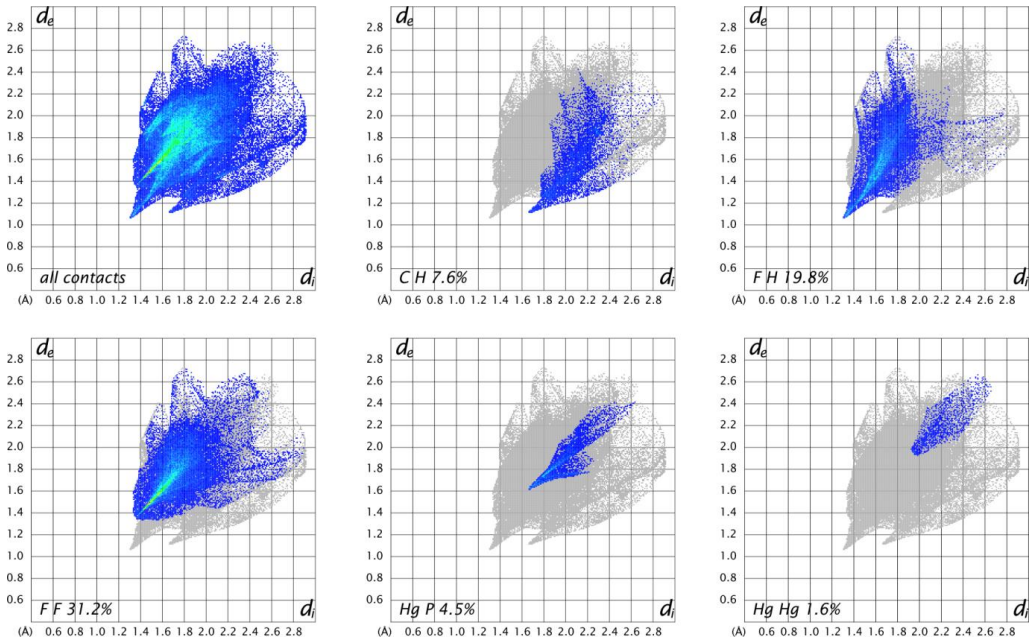

Figure 11. Selected fingerprint plots of compound **4**.

The decomposed fingerprint plots of compound **4** in Figure 11 reveal that the two tips at the bottom of the plot representing the shortest contacts arise from F-H and C-H contacts. While F-F contacts contribute the major part of contacts, Hg-Hg contacts only contribute 1.6% with rather long intermolecular distances. The Hg-P contacts contribute 4.5% with some of the contacts in a short region for these atoms.

Decomposed fingerprint plots of compound 5

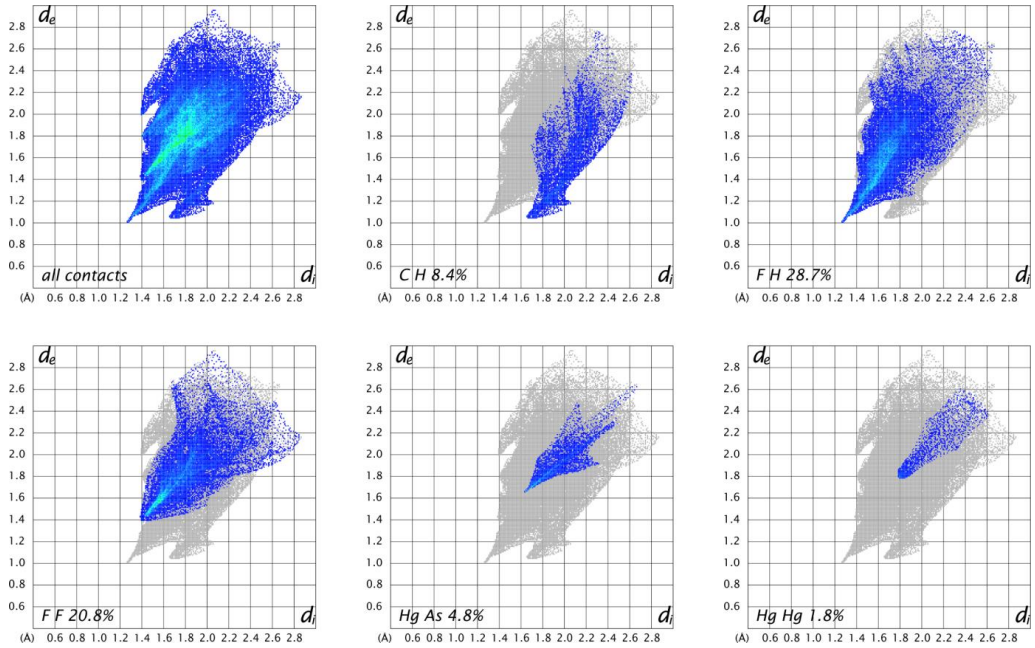

Figure 12. Selected fingerprint plots of compound **5**.

The decomposed fingerprint plots of compound **5** in Figure 12 exhibit some similar features like it was found for compound **4**. The closest contact regions arise from F-H and C-H contacts. While this time the F-H contacts contribute the major part, there are still 20.8% of F-F contacts. Hg-Hg contacts only contribute 1.8% with intermolecular distances which are a little shorter than for compound 4. The Hg-As contacts contribute 4.8% with some of the contacts in a short region for these atoms.

Decomposed fingerprint plots of compound 7a

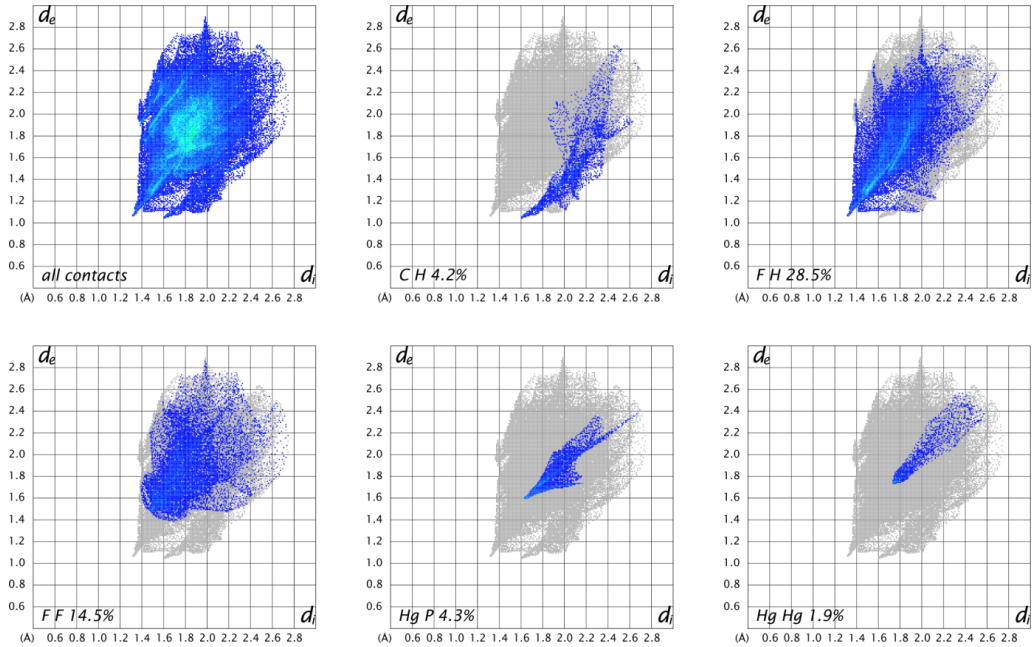

Figure 13. Selected fingerprint plots of compound **7a**.

The decomposed fingerprint plots for **7a** in Figure 13 show similar features like the plots for compound **4** (compare Figure 11), except the majority of the contacts arises from F-H contacts instead of F-F contacts. The Hg-P contact area contributes 4.3% and is therefore almost unchanged compared to compound **4**.

Decomposed fingerprint plots of compound 7b

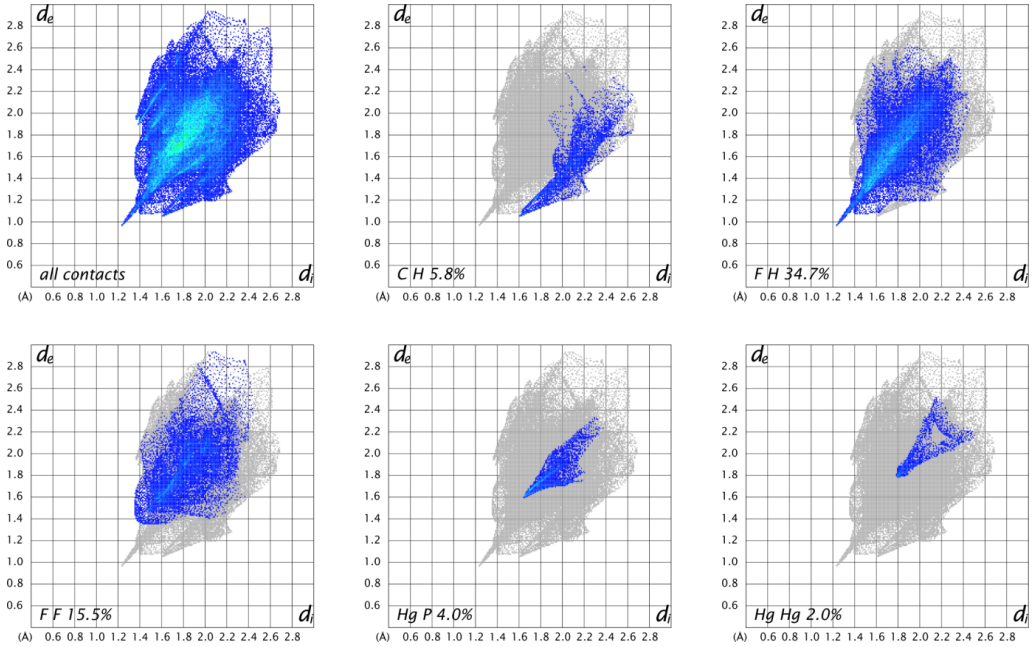

Figure 14. Selected fingerprint plots of compound **7b**.

The decomposed fingerprint plots for compound **7b** in Figure 14 show similar features like the plots for compound **4** (compare Figure 11), except the majority of the contacts arises from F-H contacts instead of F-F contacts and is even bigger than in compound **7a**. The Hg-P contact area contributes 4.0% and is therefore almost unchanged compared to compound **4**.

Decomposed fingerprint plots of compound 7c

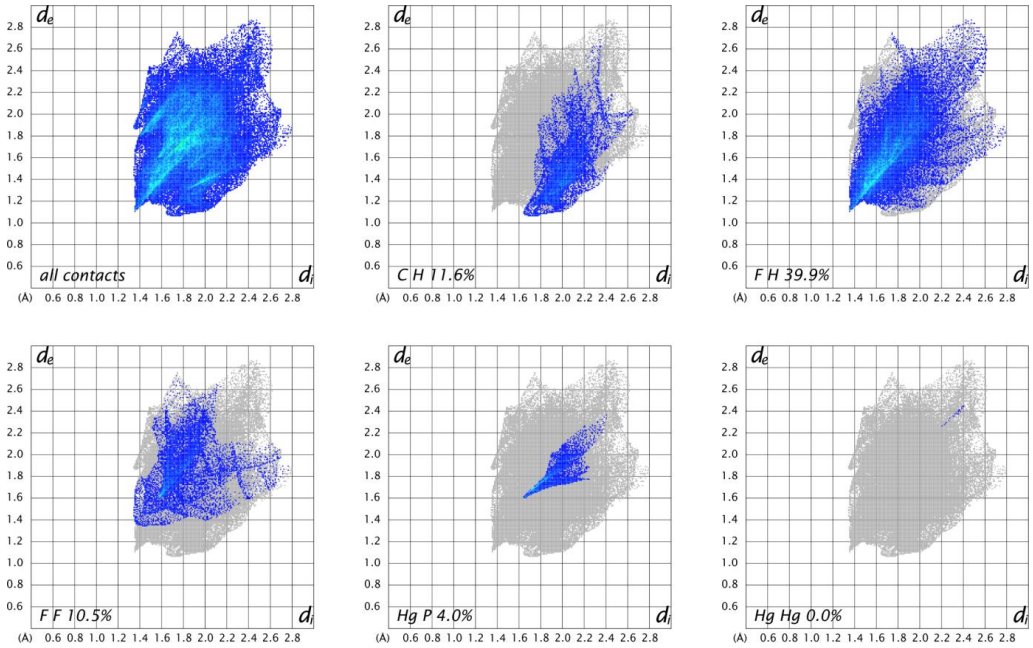

Figure 15. Selected fingerprint plots for compound **7c**.

Since the Hirshfeld surface analysis of the two independent molecules in compound **7c** showed almost no difference, we only present the fingerprint plots for one molecule. The decomposed fingerprint show that the shortest contacts arise again from F-H and C-H contacts. The majority of the contacts arises from F-H contacts. The percentage of F-H contacts is the highest for all described compounds. This can easily be rationalized by the increasing size of the Cp ligand and the increasing hydrogen content of the P_5 sandwich complex. Nevertheless, the Hg-P contact area still contributes 4.0% and is therefore almost unchanged compared to compound **4**. No Hg-Hg contacts are present in this compound. This is due to the fact, that different molecules of the planar Lewis acid **3** are not situated directly on each other (see Figure 9 and 10 for an explanation).

References

[1] a) O. J. Scherer, T. Brück, *Angew. Chem.* **1987**, *99*, 59-59; b) O. J. Scherer, T. Brück, *Angew. Chem. Int. Ed.* **1987**, *26*, 59-59; c) O. J. Scherer, C. Blath, G. Wolmershäuser, *J. Organomet. Chem.* **1990**, *387*, C21-C24; d) P. Sartori, A. Golloch, *Chem. Ber.* **1968**, *101*, 2004-2009.

[2] different versions, Agilent Technologies Ltd. (former Oxford Diffraction Ltd.), Oxford, UK.

[3] A. Altomare, M. C. Burla, M. Camalli, G. L. Cascarano, C. Giacovazzo, A. Guagliardi, A. G. G. Moliterni, G. Polidori, R. Spagna, *J. Appl. Cryst.* **1999**, *32*, 115-119.

[4] G. M. Sheldrick, *Acta Cryst. A* **2008**, *64*, 112-122.

[5] E. Keller, Freiburg, **1997**.

[6] M. J. Frisch, G. W. Trucks, H. B. Schlegel, G. E. Scuseria, M. A. Robb, J. R. Cheeseman, G. Scalmani, V. Barone, B. Mennucci, G. A. Petersson, H. Nakatsuji, M. Caricato, X. Li, H. P. Hratchian, A. F. Izmaylov, J. Bloino, G. Zheng, J. L. Sonnenberg, M. Hada, M. Ehara, K. Toyota, R. Fukuda, J. Hasegawa, M. Ishida, T. Nakajima, Y. Honda, O. Kitao, H. Nakai, T. Vreven, J. A. Montgomery Jr., J. E. Peralta, F. Ogliaro, M. J. Bearpark, J. Heyd, E. N. Brothers, K. N. Kudin, V. N. Staroverov, R. Kobayashi, J. Normand, K. Raghavachari, A. P. Rendell, J. C. Burant, S. S. Iyengar, J. Tomasi, M. Cossi, N. Rega, N. J. Millam, M. Klene, J. E. Knox, J. B. Cross, V. Bakken, C. Adamo, J. Jaramillo, R. Gomperts, R. E. Stratmann, O. Yazyev, A. J. Austin, R. Cammi, C. Pomelli, J. W. Ochterski, R. L. Martin, K. Morokuma, V. G. Zakrzewski, G. A. Voth,

P. Salvador, J. J. Dannenberg, S. Dapprich, A. D. Daniels, Ö. Farkas, J. B. Foresman, J. V. Ortiz, J. Cioslowski, D. J. Fox, Gaussian, Inc., Wallingford, CT, USA, **2009**.

[7] a) J. P. Perdew, W. Yue, *Phys. Rev. B,* **1986**, *33*, 8800-8802; b) A. D. Becke, *J. Chem. Phys.* **1993**, *98*, 5648-5652.

[8] K. A. Peterson, C. Puzzarini, *Theor Chem Acc* **2005**, *114*, 283-296.

[9] D. Figgen, G. Rauhut, M. Dolg, H. Stoll, *Chem. Phys.* **2005**, *311*, 227-244.

[10] a) A. J. H. Wachters, *J. Chem. Phys.* **1970**, *52*, 1033-1036; b) P. J. Hay, *J. Chem. Phys.* **1977**, *66*, 4377-4384.

[11] a) G. A. Petersson, A. Bennett, T. G. Tensfeldt, M. A. Al-Laham, W. A. Shirley, J. Mantzaris, *J. Chem. Phys.* **1988**, *89*, 2193-2218; bG. A. Petersson, M. A. Al-Laham, *J. Chem. Phys.* **1991**, *94*, 6081-6090.

[12] R. Ditchfield, W. J. Hehre, J. A. Pople, *J. Chem. Phys.* **1971**, *54*, 724-728.

[13] T. A. Keith, TK Gristmill Software, Overland Park KS, USA, **2014**.

[14] a) J. J. McKinnon, D. Jayatilaka and M. A. Spackman, *Chem. Commun.*, **2007**, 3814-3816; b) J. J. McKinnon, A. S. Mitchell and M. A. Spackman, *Chem. Eur. J.*, **1998**, *4*, 2136-2141; c) M. A. Spackman and D. Jayatilaka, *Crystengcomm*, **2009**, *11*, 19-32; d) M. A. Spackman, *Phys. Scr.*, **2013**, *87*, 048103.

[15] www.hirshfeldsurface.net

[16] A. Bondi, *J. Phys. Chem.*, **1964**, *68*, 441–452.

[17] a) A. J. Canty and G. B. Deacon, *Inorg. Chim. Acta*, **1980**, *45*, L225-L227. b) S. S. Batsanov, *J. Chem. Soc., Dalton Trans.*, **1998**, 1541-1546. c) P. Pyykko, M. Straka, *PCCP*, **2000**, *2*, 2489-2493. d) K. R. Flower, V. J. Howard, S. Naguthney, R. G. Pritchard, J. E. Warren, A. T. McGown, *Inorg. Chem.*, **2002**, *41*, 1907-1912.

[18] A. F. Holleman, E. Wiberg and N. Wiberg, *Lehrbuch der Anorganischen Chemie*, Walter de Gruyter, Berlin, **2007**.

Preface

The following chapter has not been published until the submission of this thesis.

Authors

Martin Fleischmann, James S. Jones, Gábor Balázs, François P. Gabbaï* and Manfred Scheer*

Author contributions

The preparation and characterization of all compounds (except **3c**) including the single crystal X-ray structure determination and the preparation of the manuscript was done by the first author. James S. Jones performed and described supporting DFT calculations. Gábor Balázs developed a new synthesis for **3c** and structurally characterized a new modification of **3c**. François P. Gabbaï and Manfred Scheer supervised the research and revised the manuscript.

Acknowledgements

Manfred Zabel is acknowledged for recording the X-ray dataset for **3c**. This work was financially supported by the Deutsche Forschungsgemeinschaft.

10 Supramolecular adducts based on weak interactions between the trimeric Lewis acid complex (perfluoro-*ortho*-phenylene)mercury and polypnictogenyl complexes

Abstract: Herein we report reactions of the trinuclear Lewis acid perfluoro-*ortho*-phenylene)mercury [(*o*-$HgC_6F_4)_3$] (**1**). With the polypnictogenyl complexes [$CpMo(CO)_2(\eta^3$-$P_3)$] (**2**) containing a *cyclo*-P_3 ligand and the series of E_2 complexes [{$CpMo(CO)_2$}$_2(\mu,\eta^2$:η^2-$E_2)$] (E = P(**3a**), As(**3b**), Sb(**3c**), Bi(**3d**)). In all cases, the reaction products show very weak interactions of the E_n ligand complexes and the Lewis acid **1** exhibiting highly dynamic behavior in solution and the formation of adducts in the solid state showing Hg-E contacts below the respective sum of the van der Waals radii. The complexes **2** (P_3), **3a** (P_2) and **3b**(As_2) show interaction of only one pnictogen atom with all three Hg atoms of **1**. The complex **3c**(Sb_2) forms two adducts with **1** showing either a side-on coordination of the Sb_2 dumbbell towards Hg or an end-on coordination of both Sb atoms towards two independent molecules of **1**. The Bi_2 complex **3d** shows an almost parallel alignment of the Bi_2 dumbbell situated above the center of the planar Lewis acid **1**. The arrangements of the E_2 complex series towards **1** are rationalized with the help of electrostatic potential maps obtained by DFT calculations. Finally we present the structural characterization of a new modification of the free Sb_2 complex **3c**, the Bi_2 complex **3d**, the starting material of its preparation [Bi{$CpMo(CO)_3$}$_3$] (**4**) and an unprecedented 'Cr_4As_5' cluster **5**.

10.1 Introduction

During the last decades supramolecular chemistry based on weakly interacting molecules instead of strong covalent bonds has gained more and more attention. The investigation of planar electron-deficient molecules has developed into a rich area of research with applications in anion recognition,[1,2] molecular machines,[3] or light emitting materials.[4] In this context, pyridinium cations,[3] or electron deficient aromatic compounds,[1,2] are prototypical representatives. During our investigations we became particularly interested in the chemistry of the trinuclear organometallic compound (perfluoro-*ortho*-phenylene)mercury (**1**).[5] Due to its planar geometry this molecule contains three sterically accessible mercury centers whose naturally low Lewis acidity is significantly increased by the fluorinated molecular backbone.[6,7] This unusual Lewis acid builds up alternating binary stacks with aromatic hydrocarbons[8,9,10,11] and forms

double-sandwich complexes featuring Hg···Cp interactions when reacted with the metallocenes Cp_2Fe and Cp_2Ni (Scheme 1a).[12] Additionally **1** forms weak Lewis acid/base adducts with a variety of O, N and S donors which simultaneously interact with all three Hg atoms (Scheme 1b).[6,7,13] During the last years we could extent this chemistry to polyphosphorus complexes and were able to prove that despite their noted weakness we only observed P···Hg interactions instead of potential Hg···Cp interactions in the reactions of **1** and the triple-decker complex $[(CpMo)_2(\mu,\eta^6\text{:}\eta^6\text{-}P_6)]$ (Scheme 1c).[14] Recently we reported the different coordination behavior of the aromatic *cyclo*-P_5 and *cyclo*-As_5 ligands from the ferrocene analogues complexes $[Cp^*Fe(\eta^5\text{-}E_5)]$ (E = P, As)[15,16] towards the Lewis acid **1**.[17] While the P_5 ring forms a weak Lewis acid/base adduct (Scheme 1d) with one P donor atom, the As_5 ring shows a rather cofacial arrangement towards the molecular plane of **1** with three As atoms interacting simultaneously with the Hg centers (Scheme 1e).

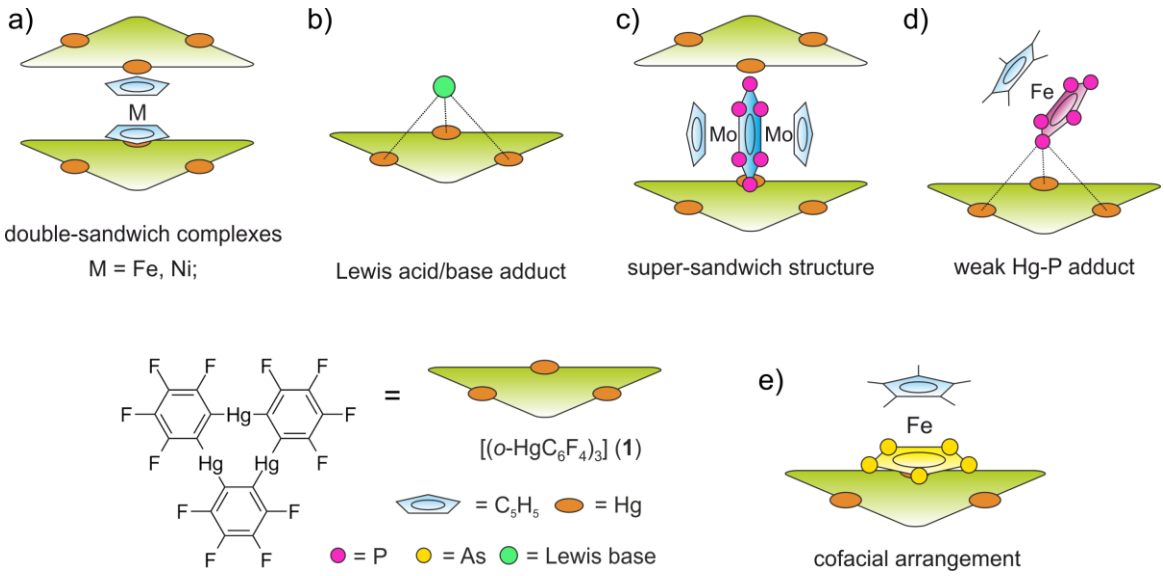

Scheme 1. a) Representation of the double-sandwich complexes formed from **1** and the metallocenes Cp_2Fe and Cp_2Ni. b) Illustration of Lewis acid/base adducts of **1** with the Lewis bases simultaneously interacting with all three Hg centers. c) Super-sandwich structures obtained from **1** and $[(CpMo)(\mu,\eta^6\text{:}\eta^6\text{-}P_6)]$. d) Coordination of $[Cp^*Fe(\eta^5\text{-}P_5)]$ to the three Hg atoms of **1** via one P atom. e) $[Cp^*Fe(\eta^5\text{-}As_5)]$ interacting with **1** via three As atoms showing an almost cofacial arrangement.

Since the nature of the polypnigtogenyl complexes has a dramatic effect on its reactivity towards **1** the question arose how the trinuclear Lewis acid might interact with a terminal *cyclo*-P_3 ligand and furthermore how its coordination may vary when reacting **1** with complexes of the heavier pnictogen atoms Sb and Bi. To address these questions we first investigated the reactivity of **1** towards the P_3 complex $[CpMo(CO)_2(\eta^3\text{-}P_3)]$ (**2**) and subsequently towards the E_2 complex series $[\{CpMo(CO)_2\}_2(\mu,\eta^2\text{:}\eta^2\text{-}E_2)]$ E = P(**3a**), As(**3b**), Sb(**3c**), Bi(**3d**) (Scheme 2). During our investigations we were able to structurally characterize a new modification of the Sb_2 complex **3c** and the Bi_2 complex **3d** and the

starting material of its synthesis [{CpMo(CO)$_3$}$_3$Bi] (**4**) for the first time. Additionally, an unprecedented Cr-As cluster [(CpCr)$_4$(μ,η^3:η^3-As$_2$)(μ,η^3:η^2:η^3-As$_3$)] (**5**) obtained from a related reaction could also be studied by single crystal X-ray diffraction.

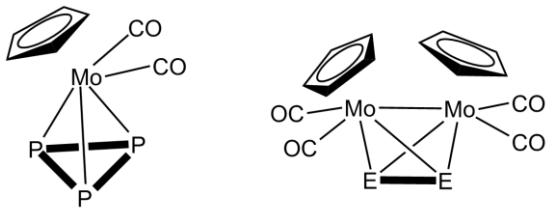

2 E = P(**3a**), As(**3b**), Sb(**3c**), Bi(**3d**)

Scheme 2. Representation of the tetrahedrane complexes [CpMo(CO)$_2$(η^3-P$_3$)] (**2**) and [{CpMo(CO)$_2$}$_2$(μ,η^2:η^2-E$_2$)] (E = P(**3a**), As(**3b**), Sb(**3c**), Bi(**3d**)).

10.2 Results and Discussion

Syntheses and Spectroscopic characterization of the products

The adducts between the pnictogenyl complexes and **1** are easily prepared by dissolving **1** and a equimolar amount of the *cyclo*-P$_3$ complex **2** or the E$_2$ complexes **3a**-**d** in 10mL of CH_2Cl_2 until a clear solution is formed. After stirring at room temperature for some time, this solution is filtered and the solvent is reduced to the minimum without precipitation of the product. This supernatant solution is kept at +4 °C and the products crystallize in a matter of hours to days. Following this approach one can obtain pure samples of equimolar adducts of **1** and the *cyclo*-P$_3$ complex **2** [(**1**)●(**2**)], the P$_2$ complex **3a** [(**1**)●(**3a**)] and the As$_2$ complex **3b** [(**1**)●(**3b**)], respectively. In case of the Sb$_2$ complex **3c** we detected two adducts with molar ratios of 1:1 [(**1**)●(**3c**)] and 2:1 [(**1**)$_2$●(**3c**)] from the same reaction. In the case of the Bi$_2$ complex **3d** we were able to determine the coexistence of the adduct [(**1**)●(**3d**)$_2$], pure **1** and pure **3d** next to each other. Moreover, the Sb$_2$ complex **3c** was isolated in 56% yield after refluxing $(Me_3Si)_2CHSbH_2$ and CpMo(CO)$_3$Me in xylene for 3 h. The Cr-As cluster **5** was characterized by chance when we intended to react [(CpCr)$_2$(μ,η^5:η^5-As$_5$)] with **1**. From this reaction conducted at room temperature we could only obtain an amorphous black powder and some dark green crystals of the adduct [(**1**)$_2$●(**5**)]. We assume that the cluster **5** was an impurity of the starting material [(CpCr)$_2$(μ,η^5:η^5-As$_5$)].

Since the described adducts are based on weak Hg···E (E = P, As, Sb, Bi) interactions we assume very weak association or dissociation in solution. In accordance with this, in the mass spectra we never observed any peaks assignable to any adduct but only the starting materials of the described products. The ^{1}H and the

^{19}F NMR spectra in CD_2Cl_2 solution are unchanged compared to the starting compounds. While the $^{31}P\{^1H\}$ NMR spectrum of [(**1**)●(**2**)] in CD_2Cl_2 solution shows a sharp singlet at –349.5 ppm which is also unchanged to the starting compound **2** we can observe an upfield shift of about 11 ppm for the singlet of the P_2 ligand **3a** in the case of the adduct [(**1**)●(**3a**)].

Structural characterization of the products in the solid state

General considerations

The solid state structures of the formed adducts exhibit short contacts below the sum of the van der Waals (vdW) radii between pnictogen atoms and the Hg atoms of 1. The vdW radius of Hg in different compounds is discussed in the literature with reported values ranging from 1.7°Å up to 2.2°Å. In the following discussion the shortest value of 1.7°A was taken as a reference.[18] Therefore, Hg-E distances that are within the sum of the vdW radii of 3.6°Å(P), 3.7 Å(As), 3.9 Å(Sb) or 4.1 Å(Bi) are highlighted by fragmented orange bonds in the following Figures 1-7.

Crystal structure of the adduct [(1)●(2)]

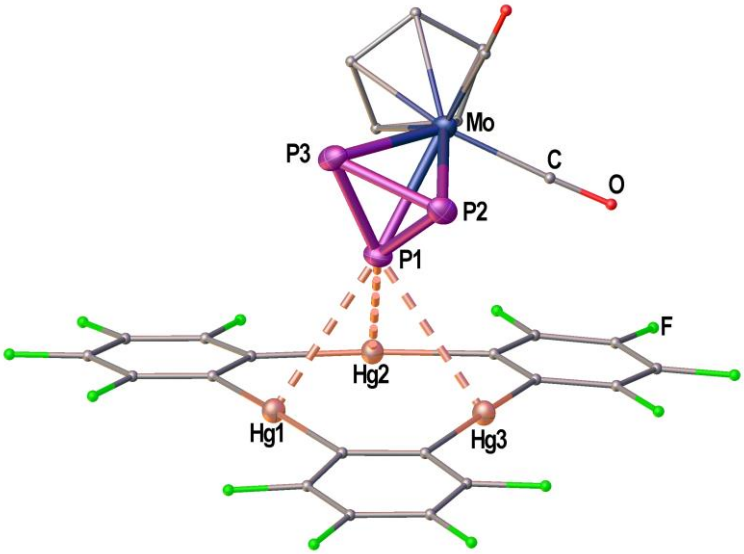

Figure 1. Solid state structure of compound the adduct [(**1**)●(**2**)]. Selected bond lengths [Å]: Hg1-P1 3.21821(9), Hg2-P1 3.19349(7), Hg3-P1 3.25262(6), P1-P2 2.140(2), P1-P3 2.145(2), P2 P3 2.147(3); interplanar angle P_3 plane – Hg_3 plane = 65.43(7)°. Ellipsoids are drawn at 50% probability. H atoms are omitted and C, F and O atoms are represented as small spheres for clarity.

Figure 1 shows the solid state structure of the adduct [(**1**)●(**2**)]. Although the symmetry of the *cyclo*-P_3 ligand of complex **2** would generally match the threefold symmetry of the planar Lewis acid **1** it shows a coordination of only one P atom

interacting with all three Hg centers of **1**. The resulting Hg-P distances (3.19349(7) – 3.25262(6) Å) lie well within the sum of the vdW radii (3.6 Å). Their lengths can very well be compared to the Hg-P distances found for **1** and [(CpMo)$_2$(μ,η^6:η^6-P_6)] (Scheme 1c), but they are a bit shorter than the closest Hg-P distance that was observed for **1** and [Cp*Fe(η^5-P_5)] (3.2878(9) Å, Scheme 1d). The angle enclosed between the P_3 plane and the Hg_3 plane measures 65.43(7)°. The P-P bonds show uniform lengths of 2.144(2) Å comparable to the free complex **2**.[19] No Cp-Hg contacts are present.

Crystal structures of the Sb_2 complex 3c, the Bi_2 complex 3d and the starting material [{CpMo(CO)$_3$}$_3$Bi] (4)

Although the synthesis of the Bi_2 complex **3d** was already reported in 1988 the solid state structure was only described of a derivative bearing one methyl group on each Cp ligand.[20,21] During our investigations we were able to determine the solid state structures of **3d** and of the starting material **4** shown in Figure 2a) and c). The synthesis and X-ray structure of the analogues Sb_2 complex **3c** was reported[22] earlier. Moreover, we could structurally characterize a new modification of **3c** by X-ray analysis (see Figure 2b).

The new modification of **3c** crystallizes in the trigonal space group *P*3$_2$21 with half a complex in the asymmetric unit. The complex is crystallographically completed by a twofold rotation axis. The determined bond lengths are in good agreement with the previously determined structure (Mo-Mo 3.114(1) Å, Sb-Sb 2.678(1) Å).

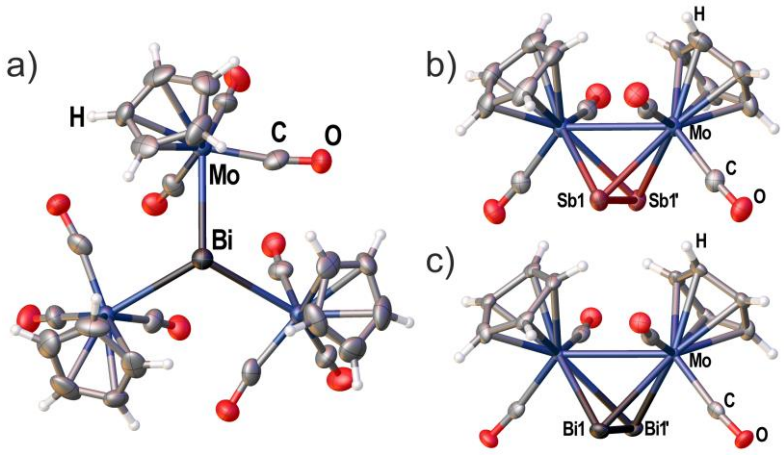

Figure 2. a) Crystal structure of [{CpMo(CO)$_3$}$_3$Bi] (**4**) with viewing direction along the threefold symmetry axis. b) Crystal structure of the Sb_2 complex **3c**. c) Crystal structure of the Bi_2 complex **3d**. Selected bond lengths [Å] and angles [°]: **4**: Mo-Bi 3.014(3), angle Mo-Bi-Mo = 113.50(5)°. **3c**: Mo1-Mo1' 3.1183(10), Sb1-Sb1' 2.6871(7). **3d**: Mo1-Mo1' 3.1378(13), Bi1-Bi1' 2.8580(7). Ellipsoids are drawn at 50% probability for **3c**,**d** and 30% probability for **4**.

The Bi_2 complex **3d** (see Figure 2b) crystallizes in the monoclinic space group *C*2/*c* with half of the complex in the asymmetric unit. The Mo-Mo bond as well as

the Bi-Bi bond is bisected by the twofold rotation axis. The Bi-Bi bond length of 2.8580(7) Å can very well be compared to 2.838(1) Å found for $[\{(\eta^5\text{-}C_5H_4Me)Mo(CO)_2\}_2(\mu,\eta^2\text{:}\eta^2\text{-}Bi_2)]$.[20,21]

Compound **4** crystallizes in the trigonal space group *P*31*c* with the central Bi atom situated on the threefold rotation axis (see Figure 2a) showing a Mo-Bi bond length of 3.014(3) Å. The bonding environment around Bi is best described as trigonal pyramidal with the three Mo-Bi-Mo angles summing up to 340.50(5)°.

Structural characterization of the adducts formed from 1 and the E_2 complexes 3a-d

The adduct [(**1**)•(**3a**)] crystallizes in the triclinic space group *P*-1 with two independent formula units [(**1**)•(**3a**)] in the asymmetric unit shown in Figure 3a) and b). Both P_2 complexes **3a** interact with all three Hg atoms of the Lewis acid **1** via one P atom which is situated above the center of **1** while the other P atom shows no Hg-P contacts. The resulting Hg-P distances lie in the range of 3.10401(15) – 3.3557(2) Å. The P-P bond lengths are not affected in comparison to free **3a** (2.079(2) Å)[23] by the coordination. The angles between the direction of the P_2 dumbbell and the Hg_3 plane measure 36.33(1)° (P1-P2) and 38.05(1)° (P3-P4), respectively.

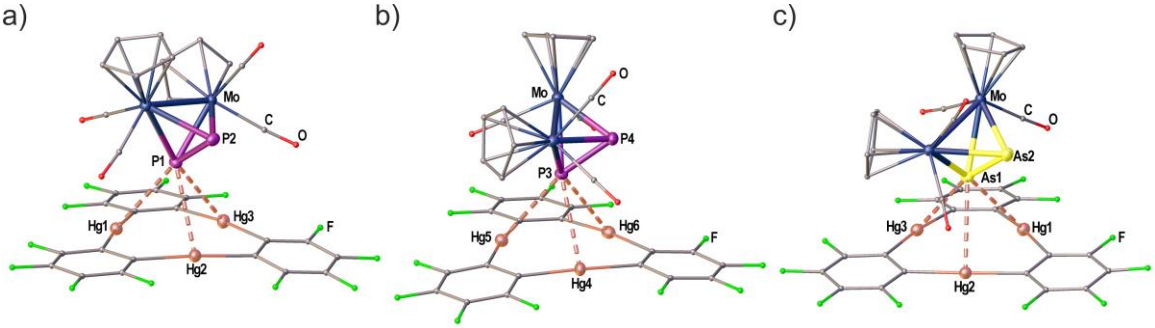

Figure 3. Formula units 1 (a) and 2 (b) found in the solid state structure of the adduct [(**1**)•(**3a**)]. c) Crystal structure of the adduct [(**1**)•(**3b**)]. Selected bond lengths [Å]: [(**1**)•(**3a**)]: Hg1-P1 3.1040(2), Hg1-P2 3.3369(2), Hg1-P3 3.1953(2), Hg4-P3 3.3557(2), Hg5-P3 3.1609(2), Hg6-P3 3.2299(2), P1-P2 2.0883(1), P3-P4 2.0948(1). [(**1**)•(**3b**)]: Hg1-As1 3.2702(2), Hg2-As1 3.3259(1), Hg3-As1 3.3788(2), As1-As2 2.3162(1). Angles of E_2 dumbbells to Hg_3 plane: P1P2-Hg1Hg2Hg3 36.33(1)°, P3P4-Hg4Hg5Hg6 38.05(1)°, As1As2-Hg1Hg2Hg3 37.00(1)°. Ellipsoids are drawn at 50% probability. H atoms are omitted and C, F and O atoms are represented as small spheres for clarity.

When looking at the As_2 complex **3b** and its interaction with **1** in the solid state shown in Figure 3c) it can be noted that the assembly in the adduct [(**1**)•(**3b**)] is very similar to the P_2 complex **3a**. This observation was very surprising since we previously observed a distinctly different assembly of *cyclo*-P_5 and *cyclo*-As_5 ligands towards **1** (see Scheme 1d) + e). The compound [(**1**)•(**3b**)] crystallizes in a different unit cell (but same space group *P*–1) than [(**1**)•(**3a**)] containing only one formula unit in the asymmetric unit. The As_2 complex **3b** is interacting with all three Hg atoms of the Lewis

acid **1** via one As atom while the second As atom does not show any Hg-As contacts. The resulting Hg-As distances lie in the range of 3.27021(13) – 3.37875(13) Å and are well within the sum of the vdW radii for Hg and As (3.7 Å). The As-As bond length is 2.31607(10) Å long which is essentially unchanged to free **3b** (2.305(3) Å).[24] The angle enclosed by the As_2 dumbbell and the Hg_3 plane (37.00(1)°) also compares very well to the analogues P_2 adduct.

When the Sb_2 complex **3c** is allowed to react with the Lewis acid **1** two sorts of crystals (orange and red) are formed from the same solution. Single crystal X-ray diffraction analysis revealed that the orange crystals consist of the equimolar adduct of **1** and **3c** [(**1**)•(**3c**)] depicted in Figure 4a. For E = Sb the assembly of the Mo_2E_2 complex is different from E = P, As. The most apparent distinction is the angle enclosed by the E_2 dumbbell and the Hg_3 plane in [(**1**)•(**3c**)] which measures only 7.03(1)°. Although Sb1 is also situated above the center of **1** the resulting Hg-Sb distances differ significantly. The shortest distance is observed for Hg1-Sb1 with 3.4336(1) Å while the distances to Hg2 and Hg3 are almost at the edge of vdW contacts (3.9 Å). The observed arrangement of **1** and **3c** shows one additional Hg-Sb contact between Sb2 and Hg3 with 3.5222(1) Å and can be described as a side-on coordination of the Sb-Sb bond to Hg3. The Sb-Sb bond length of 2.6914(1) Å is essentially unchanged compared to free **3c** (vide supra).[22] X-ray analysis of the red crystals from the same reaction consist of the adduct $[(\mathbf{1})_2\bullet(\mathbf{3c})]$ where one Sb_2 complex **3c** is surrounded by two molecules of the Lewis acid **1** depicted in Figure 5a). The Sb atom Sb1 shows only one contact to Hg1 with 3.5283(9) Å. The adduct $[(\mathbf{1})_2\bullet(\mathbf{3c})]$ crystallizes in the monoclinic space group *P*2/*n*. The twofold rotation axis bisects the Mo-Mo bond as well as the Sb-Sb bond of **3c** (see Figure 5b). The angle enclosed by both Hg_3 planes amounts 53.45(1)°. The Sb1-Sb1' bond length of 2.6863(13) Å is consistently unchanged compared to free **3c**.

When the reactivity of the Bi_2 complex **3d** towards the Lewis acid **1** was investigated we could obtain and identify black crystals of pure **3d**, colorless crystals of pure **1** and black crystals of the adduct $[(\mathbf{1})\bullet(\mathbf{3d})_2]$ next to each other from one reaction. Although several crystals were mounted we were not able to identify any adducts of **1** and **3d** in different molar ratios. The solid state structure of $[(\mathbf{1})\bullet(\mathbf{3d})_2]$ is depicted in Figure 4b). The compound crystallizes in the triclinic space group *P*–1 with two Mo_2Bi_2 complexes **3d** interacting with one molecule of the Lewis acid **1** from both sides via both Bi atoms in the asymmetric unit. The Bi-Bi dumbbells are arranged almost parallel to the Hg_3 plane with enclosed angles of 2.50(1)° and 5.72(1)°, respectively. The center of **1** is not situated below one of the Bi atoms but rather the middle of the Bi-Bi bonds. The resulting Hg-Bi distances vary significantly in the range of 3.48590(8) – 4.04806(13) Å.

The Bi-Bi bond lengths in the adduct [(**1**)●(**3d**)$_2$] are essentially identical to the free complex **3d** (vide supra).[20,21]

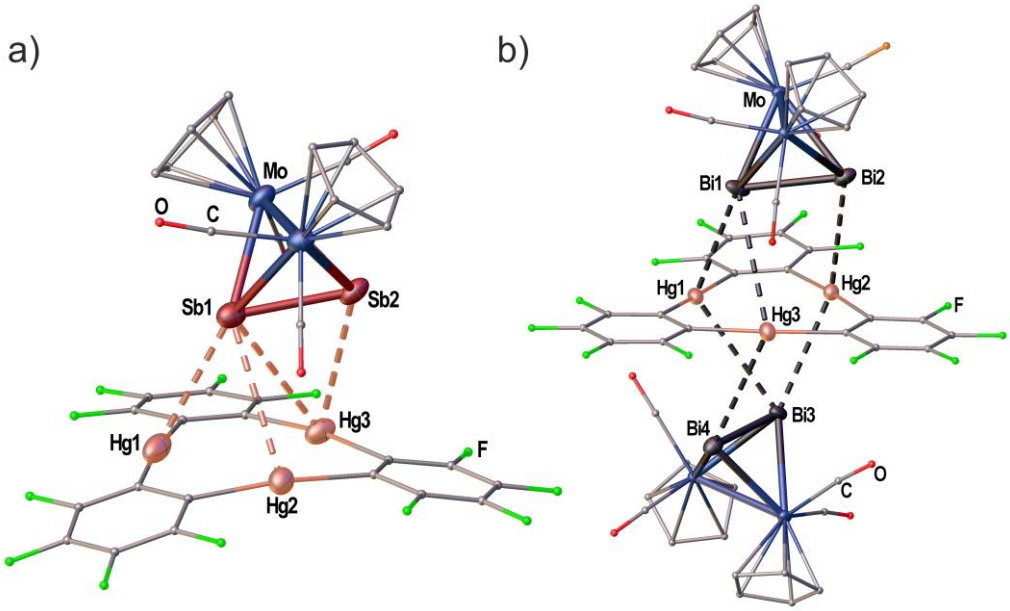

Figure 4. a) Solid state structure of the adduct [(**1**)•(**3c**)]. b) Solid state structure of the adduct [(**1**)•(**3d**)$_2$]. Selected bond lengths [Å]: [(**1**)•(**3c**)]: Hg1-Sb1 3.4336(1), Hg2-Sb1 3.8621(1), Hg3-Sb1 3.7879(2), Hg3-Sb2 3.5222(1), Sb1-Sb2 2.6914(1). [(**1**)•(**3d**)$_2$]: Hg1-Bi1 3.4859(1), Hg2-Bi2 3.6370(1), Hg3-Bi1 4.0481(2), Bi1-Bi2 2.8479(1), Hg1-Bi3 3.9046(1), Hg2-Bi3 3.5888(1), Hg3-Bi4 3.7827(1), Bi3-Bi4 2.8537(1). Ellipsoids are drawn at 50% probability. H atoms are omitted and C, F and O atoms are represented as small spheres for clarity. Angles E_2 straight to Hg_3 plane: Sb1Sb2-Hg1Hg2Hg3 7.03(1)°, Bi1Bi2-Hg1Hg2Hg3 5.72(1)°, Bi3Bi4-Hg1Hg2Hg3 2.50(1)°.

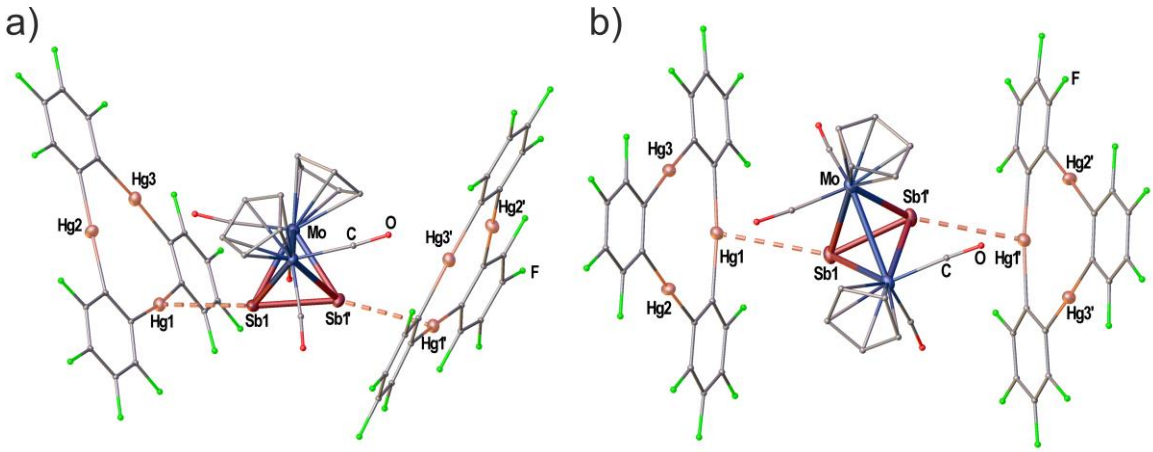

Figure 5. Solid state structure of the adduct [(**1**)$_2$•(**3c**)]. a) Viewing direction along the Mo-Mo bond. b) Viewing direction along the crystallographic *b*-axis (twofold rotation axis). Selected bond lengths [Å]: Hg1-Sb1 3.5283(9), Sb1-Sb1' 2.6863(13). Ellipsoids are drawn at 50% probability. H atoms are omitted and C, F and O atoms are represented as small spheres for clarity.

In order to better understand the assemblies of the tetrahedrane complexes **3a-d** towards the Lewis acid **1** DFT calculations were performed. Until the submission of this work we could not finish all theoretical analyses but the preliminary results are presented here. The energy gap between the LUMO of **1** and the respective HOMOs of the

E_2 complexes **3a-d** are relatively large (3.06, 3.00, 2.88, and 2.74 eV, respectively), suggesting that direct orbital interactions might not be the dominant factor for the observed arrangements in the solid state. The weak adducts may to a larger extent be based on electrostatic and dispersion forces. This is in good agreement with the previously described adducts of **1** with *cyclo*-E_5 complexes [Cp*Fe(η^5-E_5)] (E = P, As).[17] In order to probe the potential role of electrostatic forces in the observed adducts, we inspected the electrostatic potential maps of the constituent complexes shown in Figure 6.

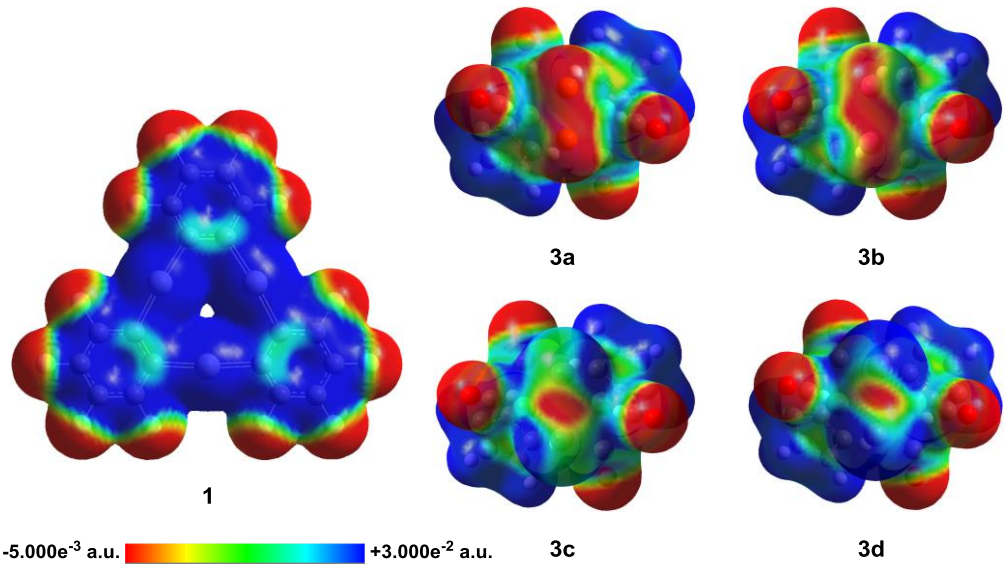

Figure 6. Electrostatic potential surfaces of compounds **1** and **3a-d** (Isovalue = 0.005). **3a-d**: viewing direction along the C_2 axis of the complexes. E_2 bonds are in front.

In both **3a** and **3b**, the electrostatic potential surface shows accumulation of negative character both across the length of the E-E bond and at the phosphorus and arsenic termini. For the electrostatic potential map of complex **3c**, negative character is preferentially accumulated at the Sb-Sb bond, with modest negative character still present at the Sb termini. Finally, in the electrostatic potential map of complex **3d**, negative character is expressed almost exclusively at the Bi-Bi bond. Taken together, these results suggest that in adducts of **1** with **3a** and **3b**, the surfaces of the pnictogen termini are complimentary with the positive surface of the mercury centers in **1**. Complex **3c** appears to be a borderline case, with both residual negative character at the Sb termini and increasing preference for negative character accumulation at the Sb-Sb bond possibly accounting for the two distinctly different modes which can be observed in the two adducts of **1** and **3c**. Finally, the lack of negative character at the Bi termini in complex **3d** accounts for the observed side-on binding mode, as the surface of the Bi-Bi bond is most complimentary with the positive character found at the mercury

surfaces in **1**. The observation that all described compounds preferentially show close contacts of the Hg centers of **1** to the pnictogen atoms of **3a-d** than to the CO ligands can be rationalized by the HSAB principle (Hard and Soft Acids and Bases). The heavier pnictogen atoms P-Bi are a better fit for the soft Hg centers of **1** than the hard oxygen atoms.

Structural characterization of the adduct $[(\mathbf{1})_2\bullet(\mathbf{5})]$ and the 'Cr_4As_5' cluster 5

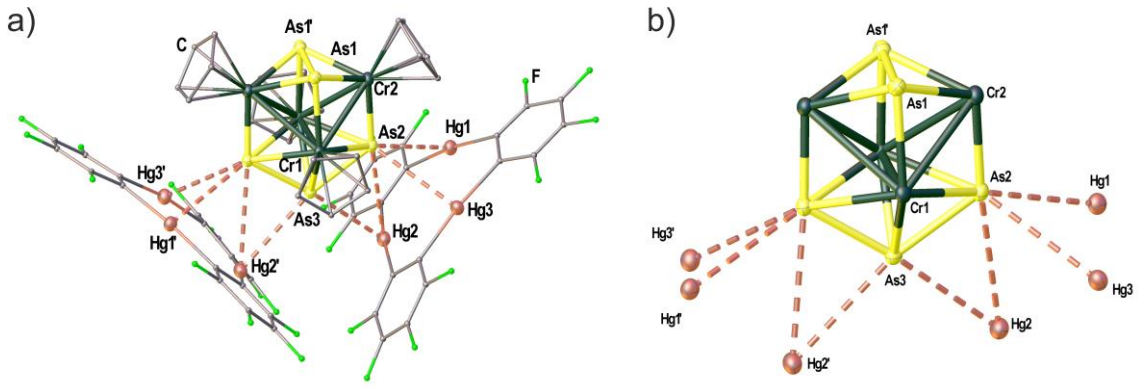

Figure 7. Solid state structure of the adduct $[(\mathbf{1})_2\bullet(\mathbf{5})]$. a) Representation of the Cr-As cluster **5** coordinated by two molecules of **1**. b) Illustration of the central cluster core of **5** omitting the four Cp ligands on Cr and only showing the contacts to the Hg atoms of **1**. Selected bond lengths [Å]: Hg1-As2 2.6863(1), Hg2-As2 3.6066(1), Hg2-As3 3.3557(1), Hg3-As2 3.3944(1), As1-As1' 2.4922(1), As2-As3 2.4456(1), Cr1-Cr1' 2.9075(1), Cr1-Cr2 2.9453(1), Cr1-Cr2' 3.0134(1), Cr1-As1 2.5067(1), Cr1-As2 2.5899(1), Cr1-As2' 2.5698(1), Cr1-As3 2.4683(1), Cr2-As1 2.4450(1), Cr2-As1' 2.4380(1), Cr2-As2 2.3604(1); Angle Hg_3 plane – Hg_3 plane 87.36(1)°; Ellipsoids are drawn at 50% probability. H atoms are omitted and C, F and O atoms are represented as small spheres for clarity.

The unprecedented Cr-As cluster **5** was identified by chance. Our intension to react the triple-decker complex $[(CpCr)_2(\mu,\eta^5\text{:}\eta^5\text{-}As_5)]$[25] with the Lewis acid **1** resulted in the formation of amorphous black powder which could not be further characterized and some dark green crystals of the adduct $[(\mathbf{1})_2\bullet(\mathbf{5})]$. The solid state structure of $[(\mathbf{1})_2\bullet(\mathbf{5})]$ is depicted in Figure 7a) showing the unprecedented 'Cr_4As_5' cluster **5** surrounded by two molecules of **1**. The adduct $[(\mathbf{1})_2\bullet(\mathbf{5})]$ crystallizes in the monoclinic space group *C*2/*c* with the twofold rotation axis running through As3 as well as the middle of the As1-As1' bond. The Hg_3 planes of the two molecules of **1** are arranged almost perpendicular with an enclosed angle of 87.36(1)°. The assembly results in eight Hg-As distances below the sum of the vdW radii (3.7 Å). The cluster core of **5** depicted in Figure 7b) consists of four Cr atoms in a butterfly structure with Cr-Cr bond lengths of 2.9075(1) – 3.0134(1) Å, one As_2 ligand and one As_3 ligand. There is a η^5-bound Cp ligand on each Cr atom. Since the Lewis acid **1** generally shows the formation of weakly interacting adducts in combination with pnictogen donors[14,17] (see above) without changing the geometry or composition of the reactants we assume that the unprecedented cluster **5** was an impurity of the used $[(CpCr)_2(\mu,\eta^5\text{:}\eta^5\text{-}As_5)]$ sample (most probably formed as a byproduct in the thermolytic

synthesis of $[(CpCr)_2(\mu,\eta^5{:}\eta^5\text{-}As_5)])$.[25] The cluster could presumably be characterized by X-ray diffraction as it crystallizes very well due to the stabilization by several Hg-As contacts in the solid state.

10.3 Conclusion

The presented results demonstrate the facile preparation of adducts starting from the planar Lewis acid **1** and polypnictogenyl complexes. While the interactions of the Hg atoms of **1** and the pnictogenyl donors are very weak resulting in dissociation in solution, several contacts below the sum of the vdW radii can be observed in the solid state. Here, the polyphosphorus complexes **2** (P_3) and **3a** (P_2) show interaction of only one P atom with all three Hg atoms of **1** in accordance with previously described results from reactions of *cyclo*-P_5 and *cyclo*-P_6 complexes with **1**. In the series of the E_2 complexes **3a**-**d** a significant influence of the pnictogenyl atom (E = P, As, Sb, Bi) is revealed. While the assembly of the As_2 complex **3b** is very similar to its P analog we observed a rearrangement for the Sb_2 as well as the Bi_2 complexes **3c** and **3d**. In case of **3c** the formation of two adducts with **1** can be observed. Herein, **3c** shows two distinctly different coordination modes towards the planar Lewis acid **1**. The Sb_2 ligand either shows a side-on arrangement towards one molecule of **1** or an end-on coordination of both Sb atoms towards two independent molecules of **1**. In contrast, the Bi_2 complex **3d** shows an almost parallel alignment of the Bi_2 dumbbell situated above the center of the planar Lewis acid **1**. Although the theoretical investigation of these adducts could not be completed during the course of this work we were able to demonstrate that the observed arrangements of the E_2 complex series can be rationalized by analysis of the electrostatic potential maps of the complexes **3a-d**. Additionally, the HSAB principle may give the explanation why the Lewis acid **1** prefers Hg-E interactions instead of possible Hg-O interactions with the CO ligands of **3a-d**. The question to which extent the obtained adducts are stabilized by dispersion forces or whether mere electrostatics are responsible for the observed interactions still has to be answered.

10.4 References

[1] B. L. Schottel, H. T. Chifotides, K. R. Dunbar, *Chem. Soc. Rev.* **2008**, *37*, 68–83.
[2] B. P. Hay, V. S. Bryantsev, *Chem. Commun.* **2008**, 2417-2428.
[3] J. F. Stoddart, *Chem. Soc. Rev.* **2009**, *38*, 1802-1820.
[4] M. A. Omary, R. M. Kassab, M. R. Haneline, O. Elbjeirami, F. P. Gabbaï, *Inorg. Chem.* **2003**, *42*, 2176-2178.
[5] P. Sartori, A. Golloch, *Chem. Ber.* **1968**, *101*, 2004-2009.
[6] M. R. Haneline, R. E. Taylor, F. P. Gabbaï, *Chem. Eur. J.* **2003**, *9*, 5188-5193.

[7] T. J. Taylor, C. N. Burress, F. P. Gabbaï, *Organometallics* **2007**, *26*, 5252-5263.
[8] M. Tsunoda, F. P. Gabbaï, *J. Am. Chem. Soc.* **2000**, *122*, 8335-8336.
[9] C. N. Burress, M. I. Bodine, O. Elbjeirami, J. H. Reibenspies, M. A. Omary, F. P. Gabbaï, *Inorg. Chem.* **2007**, *46*, 1388-1395.
[10] M. R. Haneline, M. Tsunoda, F. P. Gabbaï, *J. Am. Chem. Soc.* **2002**, *124*, 3737-3742.
[11] I. A. Tikhonova, D. A. Gribanyov, K. I. Tugashov, F. M. Dolgushin, A. S. Peregudov, D. Y. Antonov, V. I. Rosenberg, V. B. Shur, *J. Organomet. Chem.* **2010**, *695*, 1949-1952.
[12] M. R. Haneline, F. P. Gabbaï, *Angew. Chem., Int. Ed.* **2004**, *43*, 5471-5474; *Angew. Chem.* **2004**, *116*, 5587-5590.
[13] M. C. Ball, D. S. Brown, A. G. Massey, D. A. Wickens, *J. Organomet. Chem.* **1981**, *206*, 265-277.
[14] M. Fleischmann, C. Heindl, M. Seidl, G. Balázs, A. V. Virovets, E. V. Peresypkina, M. Tsunoda, F. P. Gabbaï, M. Scheer, *Angew. Chem. Int. Ed.* **2012**, *51*, 9918-9921; *Angew. Chem.* **2012**, *124*, 10056-10059.
[15] O. J. Scherer, T. Brück, *Angew. Chem. Int. Ed.* **1987**, *26*, 59-59; *Angew. Chem.* **1987**, *99*, 59-59.
[16] O. J. Scherer, C. Blath, G. Wolmershäuser, *J. Organomet. Chem.* **1990**, *387*, C21-C24.
[17] M. Fleischmann, J. S. Jones, F. P. Gabbaï, M. Scheer, *Chem. Sci.* **2015**, *6*, 132-139.
[18] a) A. J. Canty, G. B. Deacon, *Inorg. Chim. Acta* **1980**, *45*, L225-L227. b) S. S. Batsanov, *J. Chem. Soc., Dalton Trans.* **1998**, 1541-1546. c) P. Pyykko, M. Straka, *PCCP* **2000**, *2*, 2489-2493. d) K. R. Flower, V. J. Howard, S. Naguthney, R. G. Pritchard, J. E. Warren, A. T. McGown, *Inorg. Chem.* **2002**, *41*, 1907-1912. e) A. F. Holleman, E. Wiberg, N. Wiberg, *Lehrbuch der Anorganischen Chemie, Vol. 102*, Walter de Gruyter, Berlin, **2007**. f) It should be noted, that the CCDC take 1.55 Å as the vdW radius of Hg (taken from: A. Bondi, *J. Phys. Chem.*, 1964, **68**, 441), but this value is probably too small since the authors already mention the fact that it is uncertain how to estimate the vdW radius of metals in organometallic compounds.
[19] O. J. Scherer, H. Sitzmann, G. Wolmershäuser, *Acta Cryst. C* **1985**, *41*, 1761-1763.
[20] W. Clegg, N. A. Compton, R. J. Errington, N. C. Norman, *Polyhedron* **1988**, *7*, 2239-2241.
[21] W. Clegg, N. A. Compton, R. J. Errington, G. A. Fisher, N. C. Norman, T. B. Marder, *J. Chem. Soc., Dalton Trans.* **1991**, 2887-2895.
[22] J. R. Harper, A. L. Rheingold, *J. Organomet. Chem.* **1990**, *390*, C36-C38.
[23] O. J. Scherer, H. Sitzmann, G. Wolmershäuser, *J. Organomet. Chem.* **1984**, *268*, C9-C12.
[24] P. J. Sullivan, A. L. Rheingold, *Organometallics* **1982**, *1*, 1547-1549.
[25] O. J. Scherer, W. Wiedemann, G. Wolmershäuser, *J. Organomet. Chem.* **1989**, *361*, C11-C14.

10.5 Supporting Information

General considerations

Extreme precaution was used working with Hg containing compounds to not get in contacts with solid samples or solutions by wearing protective gloves, goggles and lab coats. All experiments were performed under an atmosphere of dry argon or nitrogen using standard Schlenk and drybox techniques. Solvents were freshly distilled under nitrogen from CaH_2 (CH_2Cl_2, CD_2Cl_2), Solution NMR spectra were recorded on a Bruker Avance 300 MHz NMR spectrometer (^{1}H: 300.132 MHz, ^{31}P: 121.495 MHz, ^{13}C: 75.468 MHz, ^{19}F: 282.404 MHz). The chemical shifts *δ* are presented in parts per million (ppm). The following samples were used for external reference: TMS (^{1}H, ^{13}C), $CFCl_3$ (^{19}F), H_3PO_4 85 % (^{31}P). IR spectra were recorded on a VARIAN FTS-800 FT-IR spectrometer. FD-MS spectra were measured on a Finnigan MAT 95 mass spectrometer. Elemental analyses were recorded on an Elementar Vario EL III apparatus by the microanalytical laboratory of the University of Regensburg. The solid substances were grinded together with dried KBr and pressed to pellets. The starting materials **1, 2, 3a-d, 4** were prepared according to the literature procedure, while a new synthesis for **3c** is described below.[1,2,3,4,5]

Synthetic procedures

Preparation of **3c**: 1.14 g (4.04 mmol, 1eq.) $[(Me_3Si)_2CHSbH_2]$[6] and 1.05 g (4.04 mmol, 1eq.) $[CpMo(CO)_3Me]$ were dissolved in 15 mL xylene and stirred under reflux for 3 h. After filtration and concentration the red solution was stored at -28°C to give red crystals of **3**. The crystals were isolated by filtration, the mother liquor concentrated and stored at -28°C to give two additional crops of **3**. Yield: 0.776 g (57%). For analytical data see ref. [3].

Preparation of [(**1**)●(**2**)]: 50 mg **1** (0.05 mmol, 1eq.) and 15 mg **2** (0.05 mmol, 1eq.) were dissolved together in 10 mL CH_2Cl_2 and stirred at room temperature for 1 h. After filtration and concentration of the solution the adduct [(**1**)●(**2**)] crystallizes as clear yellow blocks in the course of one day. Yield: 52 mg (80%). NMR spectra (300 MHz, CD_2Cl_2): ^{1}H: *δ*/ppm = 5.29 (s, Cp); ^{19}F{^{1}H}: *δ*/ppm = –120.6 (m, *o*-F), –155.2 (m, *p*-F); ^{31}P{^{1}H}: *δ*/ppm = –349.5 (s, P_3). IR (KBr): *ν*/cm^{-1} = 3119 (vw), 2022 (vs), 1962 (vs), 1616 (m), 1583 (m), 1472 (vs), 1418 (vs), 1356 (w), 1321 (w), 1306 (w), 1288 (m), 1251 (w), 1087 (s), 1004 (s), 814 (m), 771 (w), 732 (w). FD-MS (CH_2Cl_2): *m*/*z*(%) 312(18) [**2**], 1047.0(100) [**1**]. Elemental analysis (%) calc. for [(**1**)●(**2**)](CH_2Cl_2): C 21.67, H 0.49; found: C 21.82, H 0.53.

Preparation of [(**1**)●(**3a**)]: 105 mg **1** (0.1 mmol, 1eq.) and 50 mg **3a** (0.1 mmol, 1eq.) were dissolved together in 10 mL CH_2Cl_2 and stirred at room temperature for 1 h. After filtration and concentration of the solution the adduct [(**1**)●(**3a**)] crystallizes as clear orange blocks in the course of one day. Yield: 115 mg (75%). NMR spectra (300 MHz, CD_2Cl_2): ^{1}H: *δ*/ppm = 5.09 (s, Cp); ^{19}F{^{1}H}: *δ*/ppm = –119.9 (m, *o*-F), –155.6 (m, *p*-F); ^{31}P{^{1}H}: *δ*/ppm = –55.7 (s, P_2). IR (KBr): *ν*/cm^{-1} = 3120 (vw), 2011 (vs), 1955 (vs), 1944 (vs), 1878 (vs), 1614 (w), 1583 (w), 1471 (vs), 1418 (vs), 1356 (w), 1321 (w), 1305 (w), 1286 (m), 1248 (w), 1087 (s), 1004 (s), 812 (m), 770 (w). FD-MS (CH_2Cl_2): *m*/*z*(%) 497.1(100) [**3a**], 1047.0(37) [**1**]. Elemental analysis (%) calc. for [(**1**)●(**3a**)](CH_2Cl_2)$_{0.5}$: C 24.64, H 0.70; found: C 24.78, H 0.74.

Preparation of [(**1**)●(**3b**)]: 105 mg **1** (0.1 mmol, 1eq.) and 58 mg **3b** (0.1 mmol, 1eq.) were dissolved together in 10 mL CH_2Cl_2 and stirred at room temperature for 1 h. After filtration and concentration of the solution the adduct [(**1**)●(**3b**)] crystallizes as clear light red blocks in the course of a few days. Yield: 120 mg (74%). NMR spectra (300 MHz, CD_2Cl_2): ^{1}H: *δ*/ppm = 5.09 (s, Cp); ^{19}F{^{1}H}: *δ*/ppm = –120.4 (m, *o*-F), –155.4 (m, *p*-F). IR (KBr): *ν*/cm^{-1} = 3118 (vw),

3104 (vw), 1998 (vs), 1975 (vs), 1926 (vs), 1874 (vs), 1616 (w), 1583 (w), 1472 (vs), 1418 (vs), 1356 (w), 1321 (w), 1306 (w), 1287 (m), 1251 (w), 1088 (s), 1005 (s), 814 (m), 771 (w). FD-MS (CH_2Cl_2): *m*/*z*(%) 585.9(88) [**3b**], 1047.0(100) [**1**]. Elemental analysis (%) calc. for [(**1**)●(**3b**)]: C 23.58, H 0.62; found: C 23.59, H 0.64.

Preparation of [(**1**)●(**3c**)] and [(**1**)$_2$●(**3c**)]: 105 mg **1** (0.1 mmol) and 68 mg **3c** (0.1 mmol) were dissolved together in 10 mL CH_2Cl_2 forming a dark red solution and stirred at room temperature for 30 min. After filtration and concentration of the solution the formation of orange [(**1**)●(**3c**)] and red [(**1**)$_2$●(**3c**)] crystals is observed from the same solution. The mother liquor was decanted off and the crystals dried in vacuum. Yield: 98 mg (mixture). NMR spectra (300 MHz, CD_2Cl_2): ^{1}H: *δ*/ppm = 5.03 (s, Cp); ^{19}F{^{1}H}: *δ*/ppm = –120.7 (m, *o*-F), –155.3 (m, *p*-F). IR (KBr): *v*/cm^{-1} = 3121 (vw), 2055 (w), 2004 (w), 1967 (s), 1931 (vs), 1893 (vs), 1839 (s), 1615 (w), 1583 (w), 1471 (vs), 1418 (vs), 1357 (vw), 1321 (w), 1305 (vw), 1288 (m), 1250 (w), 1083 (s), 1005 (s), 837 (vw), 815 (m), 770 (w). FD-MS (CH_2Cl_2): *m*/*z*(%) 678.9(87) [**3c**], 1045.0(100) [**1**].

Preparation of [(**1**)●(**3d**)$_2$]: A dark red CH_2Cl_2 solution of **1** and **3d** (~0.1 mmol) was stirred for 30 min. After filtration and subsequent concentration the formation of different black and white crystals was observed. The coexistence of pure **1**, pure **3d** and the adduct [(**1**)●(**3d**)$_2$] was determined by single crystal X-ray diffraction analysis. The adduct [(**1**)●(**3d**)$_2$] could only be obtained in mixtures and was solely characterized by X-ray structure determination.

X-ray crystallography

All diffraction experiments were performed at 123 K except the one for **3c** which was performed at 173 K. The data sets were either collected on Rigaku (former: Agilent Technologies or Oxford Diffraction) Gemini R Ultra diffractometer with MoK_α or on a SuperNova diffractometer with either Cu$K\alpha$ or MoK_α or on a STOE IPDS diffractometer with MoK_α radiation. Crystallographic data together with the details of the experiments are given in the Tables 1-3. All crystal preparations were performed under mineral oil. The structure solution and refinement was done with ShelX.[7] The H atoms were calculated geometrically and a riding model was used during the refinement process. Graphical material was created with Olex2.[8]

Table 1. Crystallographic details of [**1●2**], [**1●3a**], [**1**$_2$**●3c**] and [**1●3c**].

Identification code	[**1●2**]	[**1●3a**]	[**1**$_2$**●3c**]	[**1●3c**]
formula	$C_{26}H_7Cl_2F_{12}$ $Hg_3MoO_2P_3$	$C_{66}H_{24}Cl_4F_{24}$ $Hg_6Mo_4O_8P_4$	$C_{50}H_{10}F_{24}$ $Hg_6Mo_2O_4Sb_2$	$C_{33}H_{12}Cl_2F_{12}$ $Hg_3Mo_2O_4Sb_2$
weight [g·mol^{-1}]	1440.84	3253.83	2769.50	1808.48
Temperature [K]	123(1)	123(1)	123(1)	123(1)
crystal system	triclinic	triclinic	monoclinic	triclinic
space group	*P*–1	*P*–1	*P*2/*n*	*P*–1
a [Å]	11.1294(2)	12.8301(7)	11.0707(2)	12.4435(3)
b [Å]	11.5500(2)	12.8847(6)	7.4335(2)	13.3321(3)
c [Å]	14.1425(3)	23.5633(12)	33.0847(8)	14.0134(4)
α [°]	114.075(2)	92.367(4)	90	81.649(2)
β [°]	104.952(2)	100.819(4)	95.819(2)	71.018(2)
γ [°]	91.314(2)	94.276(4)	90	63.354(2)
V [Å^3]	1586.58(6)	3809.3(3)	2708.64(11)	1964.90(9)
Z	2	2	2	2
ρ_{calc} [g·cm^{-3}]	3.016	2.837	3.396	3.057
μ [mm^{-1}]	32.529	13.011	18.488	13.877
F(000)	1296.0	2952.0	2448.0	1620.0
crystal size [mm^3]	0.30 × 0.25 × 0.04	0.17 × 0.12 × 0.06	0.08 × 0.06 × 0.03	0.12 × 0.08 × 0.04
diffractometer	SuperNova	Gemini R ultra	Gemini R ultra	Gemini R ultra
absorption correction	gaussian	analytical	gaussian	gaussian
T_{min}/T_{max}	0.016 / 0.357	0.267 / 0.582	0.359 / 0.614	0.331 / 0.621
radiation [Å]	CuK_α	MoK_α	MoK_α	MoK_α
2 *Θ* range [°]	8.31 to 134.124	5.65 to 60.372	6.796 to 59.798	5.574 to 54.206
completeness	0.988	0.998	0.974	0.999
reflns collected/unique	59642 / 5661	58978 / 19714	15226 / 6532	19426 / 8644
R_{int}/R_{sigma}	0.0628 / 0.0198	0.0356 / 0.0383	0.0287 / 0.0439	0.0321 / 0.0744
data/restraints/ parameters	5661 / 6 / 442	19714 / 12 / 1089	6532 / 0 / 397	8644 / 12 / 550
GOF on F^2	1.249	1.039	0.883	0.813
R_1/wR_2 [I ≥ 2σ(I)]	0.0264 / 0.0731	0.0247 / 0.0479	0.0216 /0.0367	0.0297 / 0.0462
R_1/wR_2 [all data]	0.0269 / 0.0743	0.0309 / 0.0505	0.0322 / 0.0377	0.0516 / 0.0482
max/min $\Delta\rho$ [e·Å^{-3}]	0.98 / –2.10	0.94 / –0.98	1.01 / –1.02	2.14 / –1.64

Table 2. Crystallographic details of [**1●3b**], [**1●3d$_2$**] and **3d**.

Identification code	[**1●3b**]	[**1●3d$_2$**]	**3d**
formula	$C_{33}H_{12}As_2Cl_2F_{12}Hg_3Mo_2O_4$	$C_{48}H_{24}Bi_4Cl_4F_{12}Hg_3Mo_4O_8$	$C_{14}H_{10}Bi_2Mo_2O_4$
weight [g·mol^{-1}]	1714.82	2919.92	852.06
Temperature [K]	123(1)	123(1)	123(1)
crystal system	triclinic	triclinic	monoclinic
space group	*P*–1	*P*–1	*C*2/*c*
a [Å]	12.7941(3)	13.5154(2)	16.5867(11)
b [Å]	13.4465(4)	14.6000(2)	7.6677(4)
c [Å]	13.5405(5)	17.6515(3)	14.3800(8)
α [°]	60.580(3)	111.087(2)	90
β [°]	71.346(3)	103.308(2)	115.265(7)
γ [°]	69.203(2)	104.4830(10)	90
V [Å^3]	1866.34(12)	2942.32(9)	1653.93(19)
Z	2	2	4
ρ_{calc} [g·cm^{-3}]	3.051	3.296	3.422
μ [mm^{-1}]	14.952	20.797	22.709
F(000)	1548.0	2584.0	1504.0
crystal size [mm^3]	0.08 × 0.04 × 0.02	0.13 × 0.08 × 0.04	0.23 × 0.19 × 0.04
diffractometer	SuperNova	Gemini R ultra	Gemini R ultra
absorption correction	gaussian	gaussian	gaussian
T_{min}/T_{max}	0.528 / 0.801	0.203 / 0.520	0.055 / 0.435
radiation [Å]	MoK_α	MoK_α	MoK_α
2 *Θ* range [°]	6.06 to 59.31	5.41 to 54.206	6.266 to 54.188
completeness	0.991	0.999	0.994
reflns collected/unique	16291 / 8975	74152 / 12972	3154 / 1812
R_{int}/R_{sigma}	0.0337 / 0.0685	0.0479 / 0.0539	0.0376 / 0.0665
data/restraints/parameters	8975 / 0 / 523	12972 / 0 / 748	1812 / 0 / 100
GOF on F^2	0.823	0.834	0.925
R_1/wR_2 [I ≥ 2σ(I)]	0.0262 / 0.0400	0.0230 / 0.0386	0.0331 / 0.0667
R_1/wR_2 [all data]	0.0425 / 0.0412	0.0359 / 0.0395	0.0438 / 0.0685
max/min Δρ [e·Å^{-3}]	1.17 / –1.27	1.49 / –1.75	1.55 / –1.52

Table 3. Crystallographic details of **3c**, **4** and [**1●5**].

Identification code	**3c**	**4**	[**1●5**]
formula	$C_{14}H_{10}Mo_2O_4Sb_2$	$C_{24}H_{15}BiMo_3O_9$	$C_{59}H_{26}As_5Cl_6Cr_4F_{24}Hg_6$
weight [g·mol^{-1}]	677.60	944.16	3189.64
Temperature [K]	173(1)	123(1)	123(1)
crystal system	trigonal	trigonal	monoclinic
space group	$P3_221$	P31c	C2/c
a [Å]	8.6935(4)	14.8747(6)	19.18520(10)
b [Å]	8.6935(4)	14.8747(6)	19.78690(10)
c [Å]	19.7356(14)	7.4995(4)	18.72880(10)
α [°]	90.00	90	90
β [°]	90.00	90	99.0540(10)
γ [°]	120.00	120	90
V [Å^3]	1291.73(17)	1437.01(14)	7021.16(7)
Z	3	2	4
ρ_{calc} [g·cm^{-3}]	2.613	2.182	3.017
μ [mm^{-1}]	4.537	7.429	33.451
F(000)	936.0	880	5756.0
crystal size [mm^3]	0.26 × 0.16 × 0.16	0.27 × 0.02 × 0.02	0.24 × 0.08 × 0.05
diffractometer	STOE IPDS	SuperNova (Mo)	Gemini R ultra
absorption correction	numerical	gaussian	gaussian
T_{min}/T_{max}	0.4495 / 0.5920	0.243 / 0.814	0.030 / 0.340
radiation [Å]	MoK_α	MoK_α	CuK_α
2 *Θ* range [°]	5.42 to 51.78	6.286 to 52.714	6.458 to 133.09
completeness	0.996	0.976	0.972
reflns collected/unique	10028 / 1686	5998 / 1680	21971 / 6190
R_{int}/R_{sigma}	0.0236 / 0.0133	0.1451 / 0.1541	0.0375 / 0.0291
data/restraints/parameters	1686 / 0 / 100	1680 / 1 / 112	6190 / 0 / 483
GOF on F^2	1.138	0.92	1.031
R_1/wR_2 [I ≥ 2σ(I)]	0.0196 / 0.0519	0.0686 / 0.1526	0.0254 / 0.0578
R_1/wR_2 [all data]	0.0207 / 0.0521	0.1111 / 0.1620	0.0284 / 0.0588
max/min Δρ [e·Å^{-3}]	1.07 / –0.48	2.32 / –1.96	1.60 / –1.71
Flack parameter	0.00(3)	0.00(2)	

DFT calculations

In order to aid in the rationalization of the observed structural trends for the adducts of **3a**-**3d** and **1**, their constituent compounds were optimized by density functional theory (DFT) methods. The large computed HOMO-LUMO gaps between **1** and **3a-d** of 3.06, 3.00, 2.88, and 2.74 eV, respectively, suggest that orbital-based interactions are not likely to be dominant within the pnictogen-mercury bonding found in these adducts. Instead, electrostatic and dispersion forces are likely to factor strongly in the stabilization of the observed structures. In order to probe the potential role of electrostatic forces in the observed adducts, we inspected the electrostatic potential maps of the constituent complexes.

Computational methods

DFT calculations (full geometry optimizations) were carried out on compounds **1** and **3a-d** starting from their crystal structure geometries observed in their respective adducts using the Gaussian09 program (B3LYP,[9] with cc-pVTZ[10] for H, C, O, and F; and aug-cc-pVTZ for P, As, Sb, and Bi;[11] Stuttgart relativistic small effective core potentials for Sb and Bi[12]). Frequency calculations were carried out on the optimized geometries, showing no imaginary frequencies.

References

[1] P. Sartori, A. Golloch, *Chem. Ber.* **1968**, *101*, 2004-2009.
[2] O. J. Scherer, H. Sitzmann, G. Wolmershäuser, *J. Organomet. Chem.* **1984**, *268*, C9-C12.
[3] J. R. Harper, A. L. Rheingold, *J. Organomet. Chem.* **1990**, *390*, C36-C38.
[4] P. J. Sullivan, A. L. Rheingold, *Organometallics* **1982**, *1*, 1547-1549.
[5] W. Clegg, N. A. Compton, R. J. Errington, G. A. Fisher, N. C. Norman, T. B. Marder, *J. Chem. Soc., Dalton Trans.* **1991**, 2887-2895.
[6] G. Balázs, H. J. Breunig, E. Lork, W. Offermann, *Organometallics* **2001**, *20*, 2666-2668.
[7] G. M. Sheldrick, *Acta Cryst. A* **2008**, *64*, 112-122.
[8] O. V. Dolomanov, L. J. Bourhis, R. J. Gildea, J. A. K. Howard, H. Puschmann, *J. Appl. Crystallogr.* **2009**, *42*, 339-341.
[9] A. D. Becke, *J. Chem. Phys.* **1993**, *98*, 5648-5652.
[10] R. A. Kendall, T.H. Dunning, R. J. Harrison, *J. Chem. Phys.* **1992**, *96*, 6796-6806.
[11] K. A. Peterson, *J. Chem. Phys.* **2003**, *119*, 11099-11112.
[12] B. Metz, H. Stoll, M. Dolg, *J. Chem. Phys.* **2000**, *113*, 2563-2569.

Preface

The following chapter includes preliminary results and by-products which will be included in future publications or provide a basis for future research efforts. Some of the obtained compound could not be fully characterized so far but all data and knowledge that was acquired about the described products and reactions will be presented.

11 Thesis Treasury

11.1 Coordination chemistry including WCAs

On the way to Cu[FAl]…

The weakly coordinating anion [FAl] (see introduction) has some advantages especially concerning the determination of crystal structures but also some drawbacks like solubility or stability compared to the [TEF] anion. Using the anion [TEF], the very flexible and interesting coordination chemistry of P_n ligand complexes towards 'naked' Cu^+ was thoroughly investigated during the last years.[1,2,3] Therefore, a soluble Cu^+ salt of the WCA [FAl] would represent a very interesting synthetic goal. During this work the synthesis of 'naked' Cu^+ featuring the WCA [FAl] was attempted several times without success. During these investigations many details could be learned from these fails.

Metathesis of CuCl and Li[FAl] in liquid SO_2

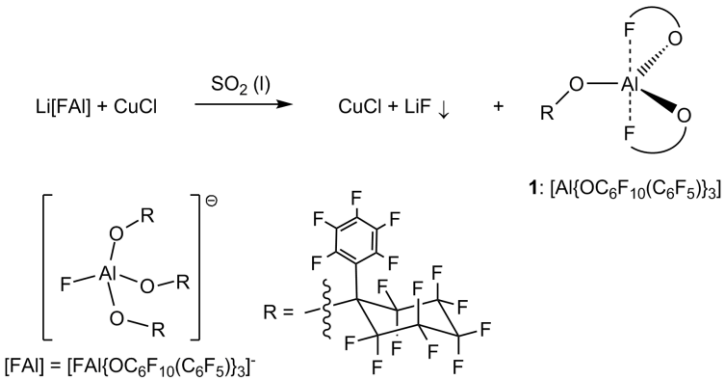

Scheme 1. Metathesis of Li[FAl] and CuCl affording the Lewis acid **1**. The coordination sphere of Al is saturated by two F atoms of two organic groups R illustrated by half circles.

Scheme 1 shows an attempt of the cation exchange of CuCl and Li[FAl]. Liquid SO_2 was chosen as solvent to ensure the solubility of Li[FAl]. The reaction does not afford the desired Cu^+[FAl] salt, but rather leads to the decomposition of the [FAl] anion and formation of the super Lewis acid [Al{$OC_6F_{10}(C_6F_5)$}$_3$] (**1**) which was previously described by *Krossing et al.* obtained from a reaction of $AlEt_3$ with three equivalents of the suitable alcohol R^F-OH.[4] During our investigation the crystal structure of a new modification of **1** could be determined shown in Figure 1. The structure can be described as a distorted trigonal bipyramidal arrangement around Al and can be compared well to the previously described modification. The equatorial positions are occupied by O atoms and the axial

positions of Al are saturated by interaction with two *ortho*-F atoms of the fluorinated phenyl groups of the organic groups R. We assume the decomposition of the anion [FAl] is taking place due to the precipitation of LiF which has very high lattice energy. Therefore, we assume that CuCl is not directly involved in this reaction. However, this still has to be ruled out and was not further investigated, since **1** is only a byproduct which was characterized during this work.

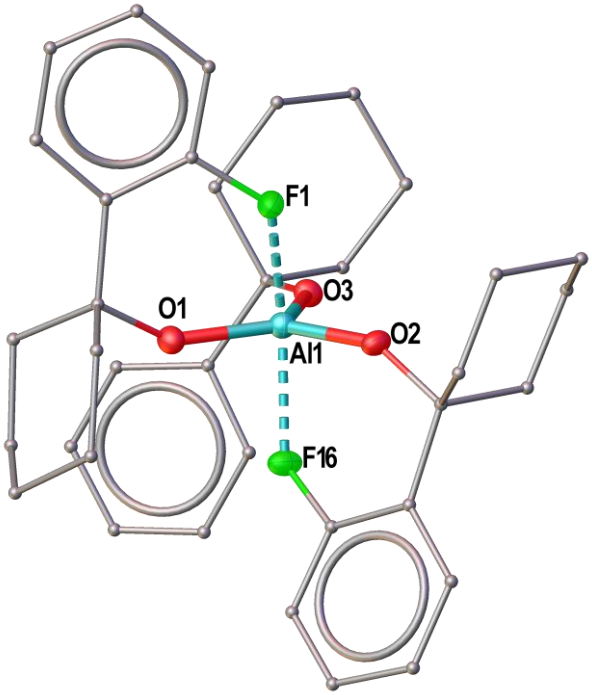

Figure 1. Crystal structure of **1**. Ellipsoids are drawn at 50% probability. All F atoms except F1 and F16 are omitted. The C atoms are represented as small spheres and the Ph rings are highlighted by central rings for clarity. Selected bond lengths [Å] and angles [°]: Al1-F1 2.01066(5), Al1-F16 2.02826(6), F1Al1F16 157.95(1).

Metathesis of TlF and Li[FAl]

During our investigations the preparation of a Tl^+ salt of the WCA [FAl] was also seemed to be a valuable step towards the isolation of Cu[FAl]. In this context, the metathesis of Li[FAl] and Tl[PF_6] was already reported by us which only leads to a mixed Li^+/Tl^+ salt of the formula [$Tl(CH_2Cl_2)_x$][$Li(FAl)_2$] (x = 2.5-3).[2] In the described compound the Li^+ cation is 'encapsulated' by two [FAl] anions which is probably the reason why Li^+ is not completely precipitated as Li[PF_6] in this reaction. This mixed Li^+/Tl^+ salt is soluble in CH_2Cl_2 and can be used as a source of *in situ* generated Tl[FAl] for coordination chemistry. Since this is not a very atom economic reaction the synthesis of pure Tl[FAl] was further pursued.

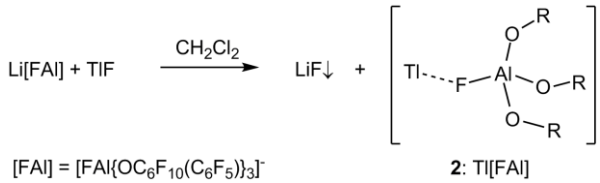

Scheme 2. Reaction of Li[FAl] and TlF.

Since $Tl[PF_6]$ does not yield Tl[FAl] in the metathesis with Li[FAl], the analogues reaction of TlF was attempted. The reasoning for this approach was that the small F^- anion should be able to reach Li^+ in its environment protected by the two [FAl] anions and LiF should be readily precipitated. Following this route we were able to obtain Tl[FAl] as colorless crystals in relatively low yield (9.9%) which were suitable for single crystal X-ray analysis. The structure of Tl[FAl] is shown in Figure 2.

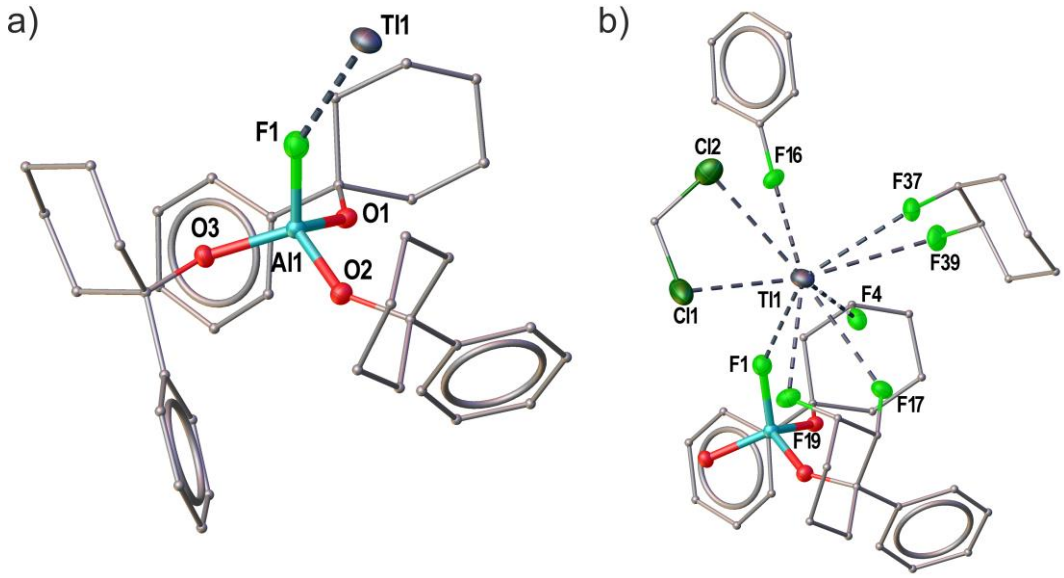

Figure 2. Section of the crystal structure of Tl[FAl] (**2**). a) Illustration of the coordination of F1 to Tl1. b) Coordination environment of Tl1 including two Tl-Cl interactions with one CH_2Cl_2 solvent molecule. In addition to F1, there are also Tl-F contacts to two other anions illustrated only by the F atoms and the connected carbon rings. Ellipsoids are drawn with 50% probability. All F atoms without Tl-F contacts are omitted. C atoms are drawn as small spheres and Ph rings are highlighted by central rings for clarity. Selected bond lengths [Å] and angles [°]: Tl1-Cl1 3.1972(13), Tl1-Cl2 3.5095(15), Tl1-F1 2.534(4), Tl1-F4 2.932(3), Tl1-F16 3.154(3), Tl1-F17 3.248(3), Tl1-F19 3.207(3), Tl1-F37 3.312(4), Tl1-F39 3.527(3), Al1F1Tl1 150.4(2).

In the crystal structure of **2** we can observe that the [FAl] anion exhibits a coordinating configuration with coordination of F1 (for an explanation please see the general introduction) with a Tl-F distance of 2.534(4) Å. This distance is very short and indicative of a very strong cation anion association. The environment of the Tl^+ cation further contains several longer Tl-F contacts to the fluorinated organic groups of the same and two other [FAl] anions. In addition one CH_2Cl_2 solvent molecule is coordinating to Tl^+ with both Cl atoms showing long Tl-Cl distances of 3.1972(13) and 3.5095(15) Å.

The obtained crystals show very low solubility in CH_2Cl_2. The $^{19}F\{^1H\}$ NMR spectrum of **2** from CD_2Cl_2 solution (256 scans needed) shows several overlapping signals which is indicative, that the anion [FAl] remains in its coordinating conformation in solution. In the ESI-MS from CH_2Cl_2 only a very small peak for free Tl^+ and no signal for heavier species can be detected.

In conclusion we can state that after several attempts Tl[FAl] can actually be prepared, but there are several drawbacks to the described method. The isolated yield was very low. Additionally, crystalline Tl[FAl] shows very low solubility and may not be a suitable Tl^+ source for coordination chemistry. In Tl[FAl] the anion [FAl] cannot be described as weakly coordinating. A promising prospect for an improved preparation of Tl[FAl] maybe the reaction of $[H(OEt_2)_2][FAl]$ (unpublished results from *Luis Dütsch*) with TlOEt.[5]

Methathesis of $[Cu(MeCN)_4][BF_4]$ and Li[FAl]

Since all previous attempts to synthesize 'naked' Cu^+ (bearing only weakly coordinating CH_2Cl_2 or *o*-DFB ligands at Cu^+) with the anion [FAl] failed, subsequently the preparation of $[Cu(MeCN)_4][FAl]$ was intended. Salts of the $[Cu(MeCN)_4]^+$ cations are stable, commercially available for small WCAs like $[BF_4]^-$ or $[PF_6]^-$ and widely used as Cu^+ sources in coordination chemistry. First experiments starting from Li[FAl] and Cu^I halides mixed in MeCN resulted in initially colorless solutions with colorless precipitate (presumably LiX). The obtained slurries turned their color to red-brown under stirring for one day (presumably Cu^0). Therefore, another strategy was followed by sonicating $[Cu(MeCN)_4][BF_4]$ with Li[FAl] in CH_2Cl_2 (see Scheme 3).

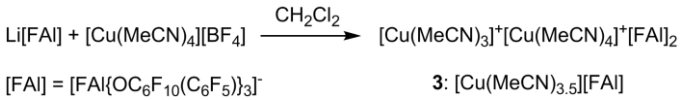

Scheme 3. Metathesis reaction affording $[Cu(MeCN)_{3.5}][FAl]$ (**3**) with alternating $[Cu(MeCN)_4]^+$ and $[Cu(MeCN)_3]^+$ complex cations.

From this reaction large colorless crystals could be obtained within one day in excellent yield (75%). Single crystal X-ray diffraction analysis reveals that **3** crystallizes in the trigonal space group *P*–3 with two close Cu^+ positions (50:50 ratio) which are both situated directly on the threefold rotational axis. The crystal structure of **3** is shown in Figure 3.

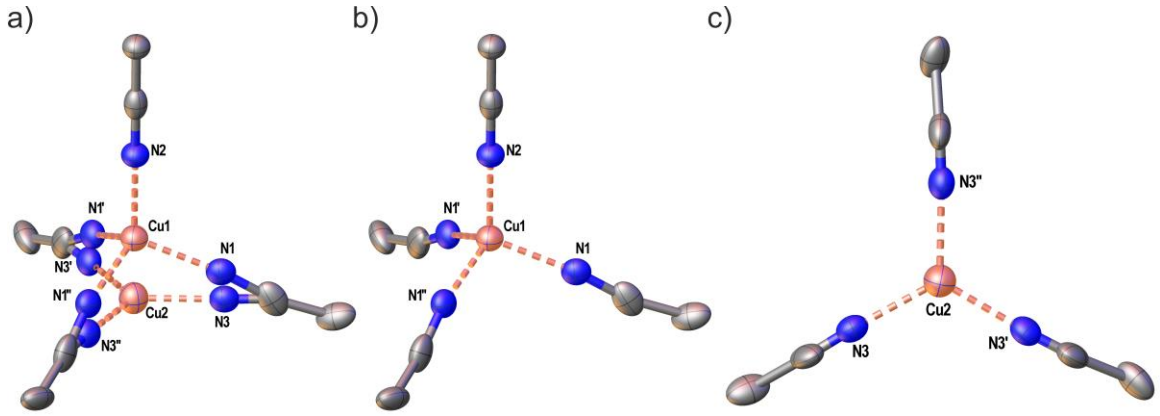

Figure 3. Cationic part in the crystal structure of $[Cu(MeCN)_{3.5}][FAl]$ (**3**). a) Superposition of the tetrahedral $[Cu(MeCN)_4]^+$ and the trigonal planar $[Cu(MeCN)_3]^+$ complex cation. b) Coordination environment of Cu1. c) Coordination environment of Cu2. Ellipsoids are drawn at 50% probability. H atoms are omitted for clarity. Selected bond lengths [Å] and angles [°]: Cu1-N1 2.009(6), Cu1-N2 2.00(11), Cu2-N3 1.935584(11), N1Cu1N1' 106.4(2), N1Cu1N2 112.4(2), N3Cu2N3' 120.00(1).

The two Cu atoms either exhibit a trigonal planar coordination by three MeCN ligands or a tetrahedral coordination by four MeCN ligands. Additionally, there is one disordered CH_2Cl_2 solvent molecule situated on the threefold axis close to Cu^+. The obtained Cu^+ salt contains the $[Cu(MeCN)_3]^+$ and $[Cu(MeCN)_4]^+$ cations in an equimolar ratio in an alternating sequence along the crystallographic *c*-axis, since otherwise the positions of the MeCN ligands would be in contradiction in the crystal structure. The composition is also confirmed by elemental analysis. The ^1H NMR spectrum of **3** from CD_2Cl_2 solution shows only one singlet at δ = 2.20 ppm for the MeCN ligands rendering them all equivalent on the NMR timescale. The $^{19}F\{^1H\}$ NMR spectrum shows a characteristic set of signals for the [FAl] anion. In the ESI-MS of a CH_2Cl_2 solution of **3**, only peaks assignable to the cations $[Cu(MeCN)_n]^+$ (n = 2, 3,4) and the anion [FAl] are observed. Elemental analysis of the crystals after 24 h storage on air is identical to the first measurement, suggesting that **3** is air-stable in crystalline form.

Reaction of $[Cu(MeCN)_{3.5}][FAl]$ (3) with $[Cp^*Fe(\eta^5\text{-}P_5)]$ (A)

We previously reported the formation of the one-dimensional coordination polymer $[Cu_2(\mathbf{A})_4]_n[TEF]_{2n}$ from the reaction of **A** with $[Cu(o\text{-}DFB)_2][TEF]$.[2] During this earlier work the analogues one-dimensional polymer $[Cu_2(\mathbf{A})_4]_n[FAl]_{2n}$ could also be structurally characterized.[6] The isolation of the soluble Cu^+ source $[Cu(MeCN)_{3.5}][FAl]$ (**3**) containing the [FAl] anion also enabled the investigation of its reactivity towards the *cyclo*-P_5 ligand complex **A** (see Scheme 4).

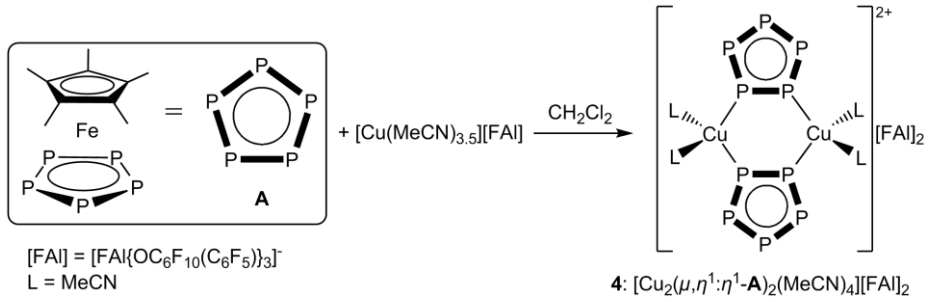

Scheme 4. Reaction of $[Cu(MeCN)_{3.5}]$ (**3**) with $[Cp^*Fe(\eta^5\text{-}P_5)]$ (**A**).

When complex **A** is reacted with **3** in a 1:1 stoichiometry in CH_2Cl_2, a clear brown solution is formed. After layering with alkanes the formation of light green crystals of compound **4** could be observed in excellent yield (75%). Reactions of **A** and **3** in 1:1 and 2:1 ratio exclusively yield the product **4** (1:1 ratio). Single crystal X-ray diffraction analysis of **4** reveals a dinuclear $[Cu_2(\mu,\eta^1\text{:}\eta^1\text{-}\mathbf{A})_2(MeCN)_4]^{2+}$ complex cation shown in Figure 4. The structure shows an almost perfectly planar central Cu_2P_4 six-membered ring which is a frequently observed structural motif in supramolecular coordination compounds including the complex **A** and Cu^I halides.[7,8,9,10,11] The [Cp*Fe] complex fragments are pointing to opposite sides of the Cu_2P_4 plane. The tetrahedral coordination environment of each Cu atom is additionally completed by two labile MeCN ligands. The Cu-P bonds lengths are uniform with 2.2781(8) and 2.2855(7) Å and all Cu-N bonds show identical lengths of 2.004(3) Å.

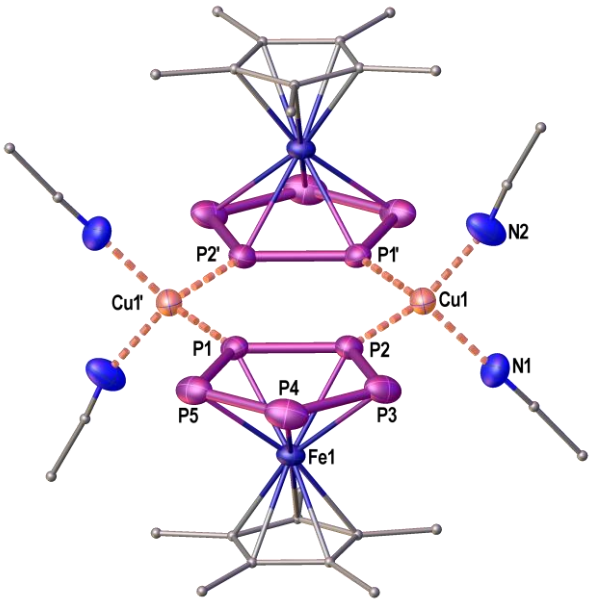

Figure 4. Crystal structure of the dinuclear complex cation in **4**. Ellipsoids are drawn at 50% probability. C atoms are drawn as small spheres and H atoms are omitted for clarity. Selected bond lengths [Å] and angles [°]: Cu1-P1' 2.2781(8), Cu1-P2 2.2855(7), Cu1-N1 2.004(3), Cu1-N2 2.004(3), P1-P2 2.1028(8), P2-P3 2.1101(10), P3-P4 2.1162(11), P4-P5 2.1245(12), P5-P1 2.1114(9), P1'Cu1P2 111.73(3), N1Cu1N2 103.2(2), N1Cu1N2(plane)-P1'Cu1'P2(plane) 81.99(7).

Compound **4** is readily soluble in CH_2Cl_2 but insoluble in alkanes. The ^{1}H NMR spectrum of **4** in CD_2Cl_2 solution shows one singlet at δ = 2.10 ppm for the MeCN ligands and one singlet at δ = 1.40 ppm for the Cp* ligand of complex **A**. The $^{31}P\{^1H\}$ NMR spectrum at room temperature exhibits only one singlet at δ = 138.9 ppm ($\omega_{1/2}$ = 21 Hz) which is shifted upfield compared to free **A** (δ = 152.2 ppm).[12] This suggests dynamic coordination in solution comparable to the previously described coordination compounds of Cu^+ towards P_n ligand complexes.[2] The $^{19}F\{^1H\}$ NMR spectrum of **4** shows a characteristic set of signals for the [FAl] anion. ESI-MS from CH_2Cl_2 solution shows signals assignable to the monocationic complexes $[Cu(MeCN)_2]^+$, $[Cu(\mathbf{A})]^+$, $[Cu(\mathbf{A})(MeCN)]^+$ and $[Cu(\mathbf{A})_2]^+$. Elemental analysis of the crystals reveals that **4** does not lose the MeCN ligands upon drying in vacuum.

In conclusion, MeCN ligands of the Cu^+ source **3** are not completely substituted by the *cyclo*-P_5 complex **A**. The heteroleptic dinuclear complex $[Cu_2(\mu,\eta^1{:}\eta^1\text{-}\mathbf{A})_2(MeCN)_4][FAl]_2$ (**4**) is obtained in good yields instead of the MeCN-free one-dimensional coordination polymer $[Cu_2(\mathbf{A})_4]_n[FAl]_{2n}$. The dinuclear complex **4** represents an interesting building block for supramolecular chemistry. Based on the presented results, similar Ag^+ and Cu^+ complexes have also been prepared by *Barbara Krämer* and *Luis Dütsch* during the preparation of this work.[5,13] Future research efforts will include attempts to interconnect these dinuclear complexes and the analogues Ag^+ complexes by addition of multidentate linker molecules and possible substitution of the labile MeCN ligands.

Reaction of $[Cp^*Fe(\mu,\eta^5{:}\eta^5\text{-}P_5)Mo(CO)_3]$ towards Au^+

Previous work of Dr. Stefan Welsch demonstrated the interesting coordination chemistry of the triple-decker complex $[Cp^*Fe(\mu,\eta^5{:}\eta^5\text{-}P_5)Mo(CO)_3]$ (**B**)[14] (see Scheme 6) towards the naked coinage metal cations Ag^+ and Cu^+ affording the complexes $[M\{Cp^*Fe(\mu_3,\eta^5{:}\eta^5{:}\eta^1\text{-}P_5)Mo(CO)_3\}_2][TEF]$ (M = Cu, Ag).[1] During this work it was attempted to extend this chemistry to Au^+. Unfortunately, the analogues complex for M = Au could not be prepared in a comfortable way so far. However, the obtained results may serve as a basis for future efforts.

Reaction of [Cp*Fe(η^5-P_5)] (A) with [$Mo(CO)_3(MeCN)_3$]

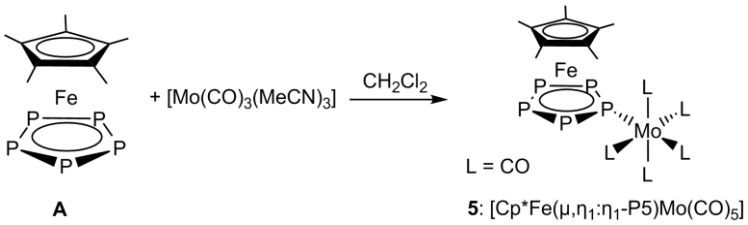

Scheme 5. Formation of 5.

During the preparation[1] of the starting material [Cp*Fe(μ,η^5:η^5-P_5)$Mo(CO)_3$] (**B**) from [Cp*Fe(η^5-P_5)] (**A**) with [$Mo(CO)_3(MeCN)_3$] a very dark red mixture of several products was obtained. The light green complex [Cp*Fe(μ,η^5:η^1-P_5)$Mo(CO)_5$] (**5**) (see Scheme 5) could be separated from this mixture by column chromatography. Medium green crystals of **5** suitable for single crystal X-ray diffraction analysis are obtained from a concentrated solution in *n*-hexane. The crystal structure is shown in Figure 5.

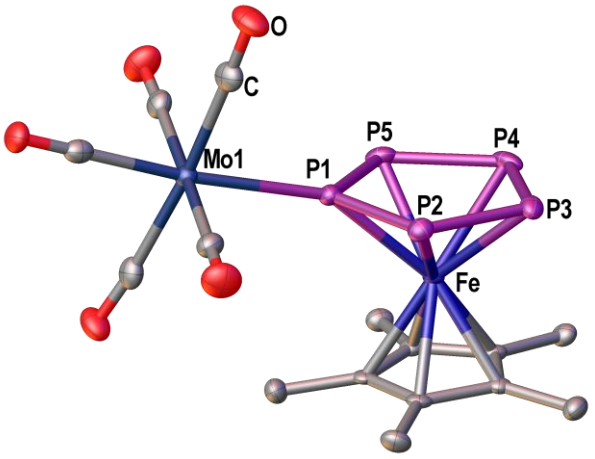

Figure 5. Crystal structure of **5**. Ellipsoids are drawn at 50% probability. H atoms are omitted for clarity. Selected bond lengths [Å]: Mo1-P1 2.54098(4), Mo-Cax 1.99216(3), Mo-Ceq(av.) 2.06, P1-P2 2.10547(4), P2-P3 2.10799(3), P3-P4 2.12234(3), P4-P5 2.11710(4), P5-P1 2.11257(4).

The crystal structure of reveals an terminal η^1-coordination of the *cyclo*-P_5 complex **A** towards the Lewis acid [$Mo(CO)_5$]. The *cyclo*-P_5 ligand is essentially planar and the Mo atom is slightly moved out of the P_5 plane away from the Fe atom. The Mo-C bond length to the CO ligand oriented trans to the P atom of **A** is significantly shorter with 1.99216(3) Å, compared to the other CO ligands with an average Mo-C bond length of 2.06 Å. This is probably caused by a stronger trans effect of CO compared to the ligand **A**.

Compound **5** is only a side-product of this work and it should probably be accessible in a simple reaction of [$Mo(CO)_5$(thf)] with **A** as the major product. Starting from **5**, the

photolytic activation may be investigated in the future to elucidate whether the initially desired triple-decker complex [Cp*Fe(μ,η^5:η^5-P_5)Mo(CO)$_3$] (**B**) can be obtained this way.

Reaction of B towards 'naked' Au$^+$

Previous work of Dr. Stefan Welsch demonstrated, that the mixed triple-decker complex [Cp*Fe(μ,η^5:η^5-P_5)Mo(CO)$_3$] (**B**) is a suitable starting material for the formation of complexes with the monovalent coinage metals Cu$^+$ and Ag$^+$ and the WCA [TEF].[1] The obtained products show a central M$^+$ cation coordinated by two ligands **B**.[1] During this work this chemistry could be expanded to the heavier congener Au$^+$.

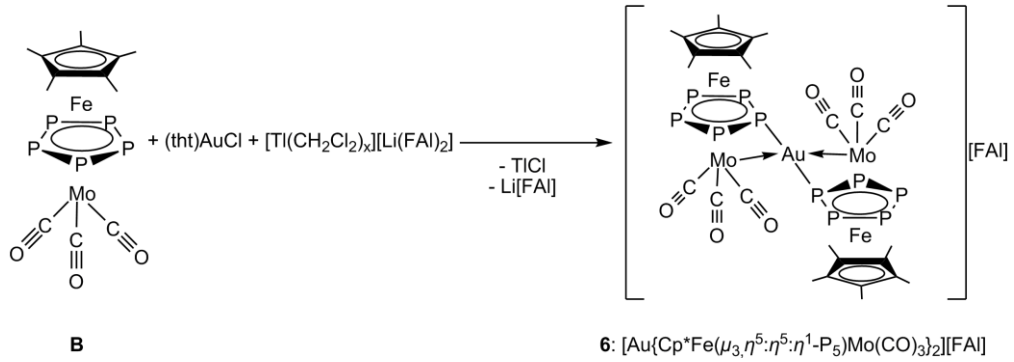

B **6**: [Au{Cp*Fe(μ_3,η^5:η^5:η^1-P_5)Mo(CO)$_3$}$_2$][FAl]

Scheme 6. Formation of the complex [Au(η^1:η^1-**B**)][FAl] (**6**).

From a one-pot reaction of (tht)AuCl, a Tl$^+$ source to precipitate Cl$^-$ and the complex **B** (see Scheme 6) some single crystals of [Au(η^1:η^1-**B**)][FAl] (**6**) suitable for X-ray diffraction analysis could be obtained. The crystal structure of **6** is shown in Figure 6. The complex cation of **6** can be regarded as isostructural to the previously described complexes of Cu$^+$ and Ag$^+$ showing a central M$^+$ cation coordinated by two ligands **B** in an η^1:η^1-coordination mode.[1] The coordination environment of the central Au atom can either be described as distorted octahedral with two axial P atoms and four C atoms of CO ligands on Mo (C1, C2, C14 and C15). The Au-C distances are rather long (> 2.7649(1) Å). Therefore, another suitable description of the coordination environment would be a distorted square planar coordination of Au by two P atoms and the two Mo atoms of the ligands **B**. The Mo-Au bond lengths measure 2.7832(1) and 2.7761(1) Å, respectively. The Au atom is slightly moved out of the Mo_2P_2 plane. The angle between the two AuMoP planes of Au with each complex **B** show a fold angle of 12.94(1)° to each other. Due to the unselective synthesis[15] compound **6** could only be structurally characterized. Future efforts will include the development of a selective synthesis of **6** including full characterization and a detailed comparison to its Cu$^+$ and Ag$^+$ analogs.

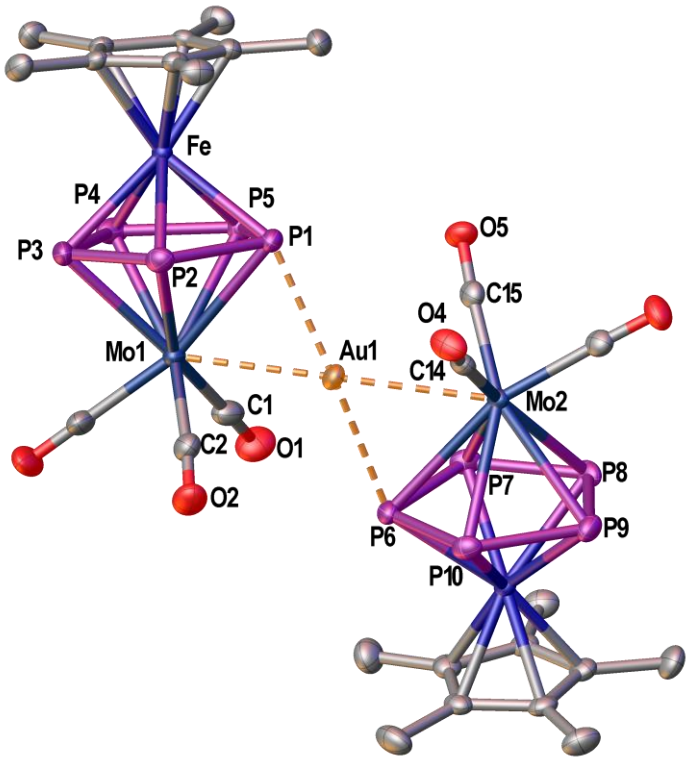

Figure 6. Complex cation of the crystal structure of **6**. Ellipsoids are drawn at 50% probability. H atoms are omitted for clarity. Selected bond lengths [Å] and angles [°]: Au1-Mo1 2.7832(1), Au1-Mo2 2.7761(1), Au1-P1 2.5181(1), Au1-P6 2.5431(1), Au1-C1 2.9459(1), Au1-C2 2.7649(1), Au1-C14 2.9102(1), Au1-C15 2.8082(1), Mo1-P1 2.7374(1), Mo2-P6 2.7598(1) Mo-P_{free}(av.) 2.64, Mo1Au1Mo2 166.57(1), P1Au1P6 170.37(1), Mo1Au1P1(plane)-Mo2Au1P6(plane) 12.94(1).

Reactivity of [{CpMo(CO)$_2$}(μ,η^2:η^2-As$_2$)] (C) towards Ag$^+$

During the last decade, extensive research has been devoted to describing the coordination chemistry of the P_2 complex [{CpMo(CO)$_2$}(μ,η^2:η^2-P_2)] towards monovalent metal cations including Cu^+, Ag^+, Au^+, Tl^+ and In^+. However, the reactivity of its heavier analog [{CpMo(CO)$_2$}(μ,η^2:η^2-As$_2$)] (**C**) towards these cations has not been investigated yet. During this work it was possible to obtain the first Ag^+ complexes of **C** with the help of the WCAs [TEF] and [FAl].

Reaction of [{CpMo(CO)$_2$}(μ,η^2:η^2-As$_2$)] (C) with Ag[TEF]

When Ag[TEF] is allowed to react with complex **C** in CH_2Cl_2 in a 1:1 molar ratio, a clear dark red solution is formed (see Scheme 7). By layering this solution with alkanes a dark red oil is obtained from which some small red crystals of **7** suitable for single crystal X-ray diffraction analysis could be isolated. The crystals slowly decompose during the measurement. Nevertheless, the cationic part of the crystal structure could be determined and the obtained model is presented in Figure 7. However, it has to be noted, that this is not a complete structure solution and the metric data should therefore

not be considered as definitive values, but the connectivity of the heavy atoms can clearly be derived from this model.

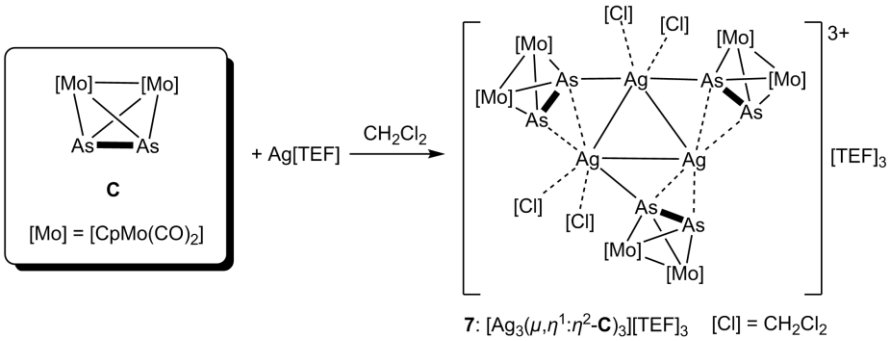

Scheme 7. Formation of the trinuclear Ag^+ complex **7**.

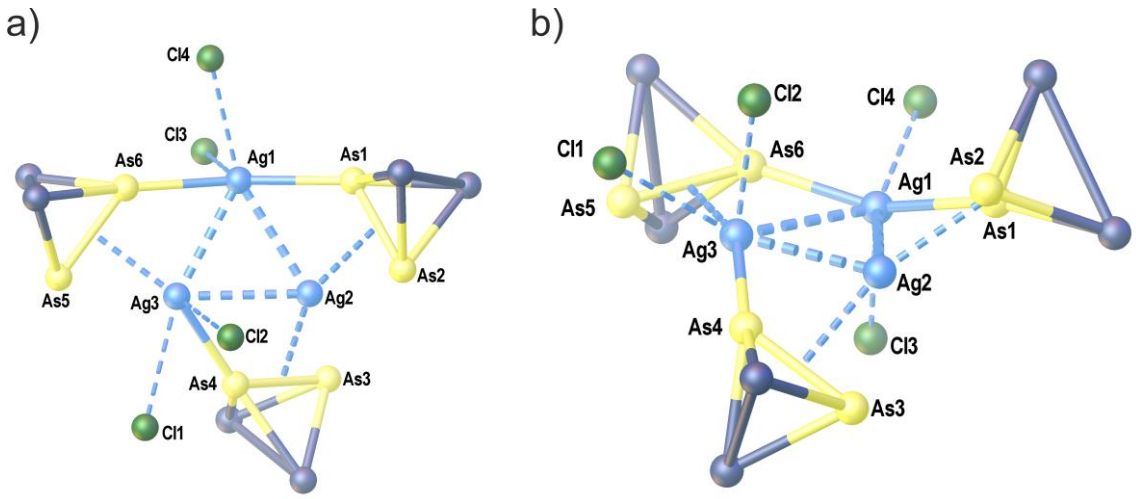

Figure 7. Illustration of the trinuclear Ag^+ complex in the model of **7**. The As_2 ligands **C** are only represented by their central distorted tetrahedral Mo_2As_2 core. Ag1 and Ag3 each shows two Ag-Cl contacts to CH_2Cl_2 solvent molecules which are only represented by the corresponding Cl atoms for clarity. Selected bond lengths [Å] and angles [°]: Ag1-Ag2 2.9303(6), Ag2-Ag3 2.9312(6), Ag3-Ag1 2.8828(6), As1-As2 2.4157(6), As3-As4 2.4106(6), As5-As6 2.4474(6), As1-Ag1 2.5465(6), As4-Ag3 2.5155(6), As6-Ag1 2.5526(6), Ag2-cent(As1-As2) 2.3949(5), Ag2-cent(As3-As4) 2.3741(5), Ag3-cent(As5-As6) 2.3418(5), Ag1-Cl3 2.8967(9), Ag1-Cl4 2.9286(10), Ag3-Cl1 3.2926(7), Ag3-Cl2 3.6815(9), Ag3Ag1Ag2 60.56(2), Ag1Ag2Ag3 58.92(2), Ag2Ag3Ag1 60.53(2), distance to Ag1Ag2Ag3(plane) [Å]: As5 0.1297(8), As6 0.2287(6), As1 0.7312(6), As4 0.7708(6), As2 1.8385(7), As3 1.8102(7).

Compound **7** crystallizes in the triclinic space group *P*–1 with three independent Ag atoms, three As_2 ligands **C**, some CH_2Cl_2 solvent molecules and three [TEF] anions in the asymmetric unit. The central structural motif of **7** consists of an almost perfect equilateral Ag_3 triangle with Ag-Ag distances of 2.8828(6) Å up to 2.9312(6) Å stabilized by three As_2 ligands **C** each showing a $\mu,\eta^2:\eta^1$-coordination mode. All Ag atoms show a different coordination environment. While Ag2 is π coordinated by two ligands **C**, Ag3 shows σ and π coordination of **C** and Ag1 shows only two σ bonds to the ligands **C**. The Ag atoms Ag1 and Ag3 show two additional contacts to Cl atoms of CH_2Cl_2 solvent molecules. The As-As bond As5-As6 is situated almost inside the

Ag1Ag2Ag3 plane, while the other two As-As bonds are rotated out of this plane with As2 lying above and As3 below the Ag_3 plane (illustrated in Figure 7 b). All As-As bonds are significantly elongated (>0.1 Å) compared to the free ligand **C** (2.305(3) Å)[16] with As5-As6 being the longest one.

Reaction of [{CpMo(CO)$_2$}(μ,η^2:η^2-As$_2$)] (C) with Ag[FAl]

When Ag[FAl] is reacted with complex **C** in CH_2Cl_2 in a 1:2 molar ratio, a clear dark red solution is formed (see Scheme 8). From this solution red crystals of **8** suitable for single crystal X-ray diffraction analysis could be isolated in 46% yield. In contrast to compound **7**, the [FAl] anions in **8** show almost no disorder. However, the whole cationic part of the crystal structure is disordered over at least three close positions rendering a final structure refinement very challenging which could not be completed during this work. The metric data should therefore not be considered as definitive values, but the connectivity of the cationic part can clearly be derived from this model which is shown in Figure 8 (major part).

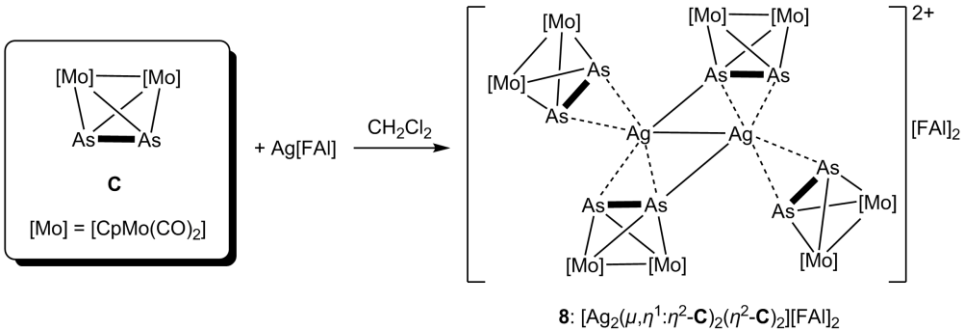

Scheme 8. Reaction of Ag[FAl] and **C** forming the dinuclear complex in **8**.

Compound **8** crystallizes in the orthorhombic space group *Pccn* with one [FAl] anion, one Ag cation two CH_2Cl_2 solvent molecules and two ligands **C** in the asymmetric unit. The central structural motif of **8** is a dicationic Ag_2 complex with an interaction of the Ag atoms (Ag1-Ag1' distance is uncertain because of disorder) stabilized by two bridging η^2:η^1-coordinating As_2 ligands **C**. Each Ag^+ cation is also η^2-coordinated by one additional ligand **C**. Figure 8 a) illustrates that the As-As bonds of the bridging ligands are almost collinear to the Ag-Ag vector. In addition, the bridging ligands are both situated above the Ag-Ag vector including an angle of 64.69(3)° towards each other. The As-As bonds in **8** are elongated compared to free **C** (2.305(3) Å)[16] although they are shorter than the As-As bonds in **7**.

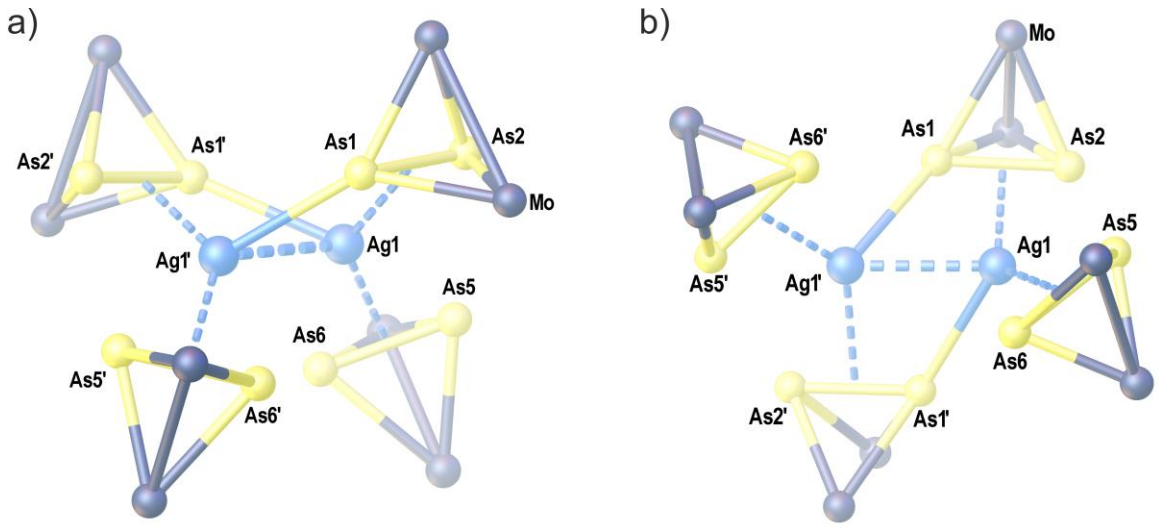

Figure 8: Illustration of the disordered dication (only major part depicted) in the model of **8**. The As_2 ligands **C** are only represented by their central distorted tetrahedral Mo_2As_2 core. The Ag1-Ag1' bond length cannot be regarded as a definitive value and may not represent the truth, since the Ag cation is disordered over at least three close positions. Selected bond lengths [Å] and angles [°]: Ag1-Ag1' 2.7341(8), As1-As2 2.3658(5), As5-As6 2.3924(8), As1-Ag1' 2.8462(9), Ag1-cent(As1-As2) 2.4419(8), Ag1-cent(As5-As6) 2.3822(6), As1As1Ag1Ag1'(plane)-As1'As2'Ag1Ag1'(plane) 64.69(3), dihedral angle cent(As5-As6)-Ag1Ag1'-cent(As5'-As6') 44.33(8).

In conclusion, it can be noted that the As_2 ligand **C** presents a valuable precursor for supramolecular coordination chemistry of monovalent cations which may be thoroughly investigated in the future. The obtained results demonstrate a preferred π coordination of **C** compared to its P_2 analog (see general introduction). In **7** and **8** the As_2 ligand **C** successfully stabilizes Ag-Ag interactions. Future investigation may also include the development of an improved synthesis of **C** to make it readily available.

11.2 Oxidation chemistry including WCAs

Reaction of [NO][TEF] with [Cp*Fe(η^5-P_5)] (A)

Previous work of *Geiger et al.* reported that single-electron oxidation of the *cyclo*-P_5 complex **A** would lead to dimerization of the obtained cation by P-P bond formation.[17] In 2013, our group finally demonstrated the accuracy of this prediction by isolating the dication $[(Cp^*Fe)_2(\mu,\eta^4{:}\eta^4\text{-}P_{10})]^{2+}$ obtained from oxidation of **A** with the organic radical of thianthrene $[C_{12}H_8S_2]^+$ (see general introduction).[18] In 2010, *Krossing et al.* reported on the reaction of P_4 and [NO][TEF] to initially form the cation $[P_4NO]^+$ by insertion of $[NO]^+$ into a P-P bond of P_4. In this context, we became interested in the investigation of the reaction of [NO][TEF] with **A** in order to answer the question whether **A** will be oxidized or $[NO]^+$ will be inserted into a P-P bond.

When [NO][TEF] is reacted with **A** in CH_2Cl_2 an immediate evolution of gas (presumably NO) and the formation of a dark red solution can be observed. From this

reaction the oxidation product $[(Cp^*Fe)_2(\mu,\eta^4{:}\eta^4\text{-}P_{10})][TEF]_2$ (**9**) can be isolated in excellent yield (87%) as dark red single crystals suitable for X-ray diffraction analysis. The crystal structure of **9** is shown in Figure 9. The ^1H NMR spectrum of **9** from CD_2Cl_2 solution shows only one singlet for the Cp* ligands. The $^{31}P\{^1H\}$ NMR spectrum shows three multiplets at δ = 198.0 ppm (4P), 125.5 ppm (4P) and –29.1 ppm (2P) which are in good agreement with the previously reported signals for $[(Cp^*Fe)_2(\mu,\eta^4{:}\eta^4\text{-}P_{10})]^{2+}$.[18] The $^{19}F\{^1H\}$ NMR spectrum shows one sharp singlet which is characteristic for the anion [TEF].

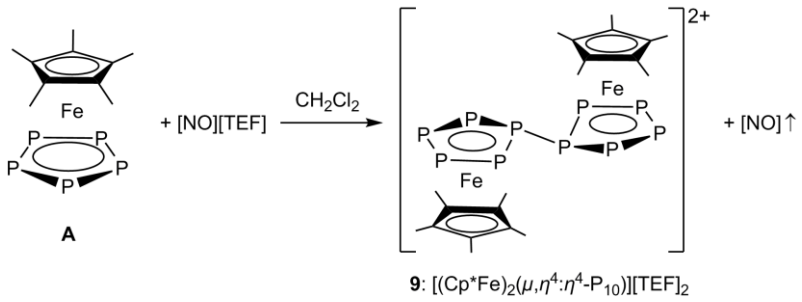

Scheme 9. Oxidation of the *cyclo*-P_5 complex **A** by [NO][TEF].

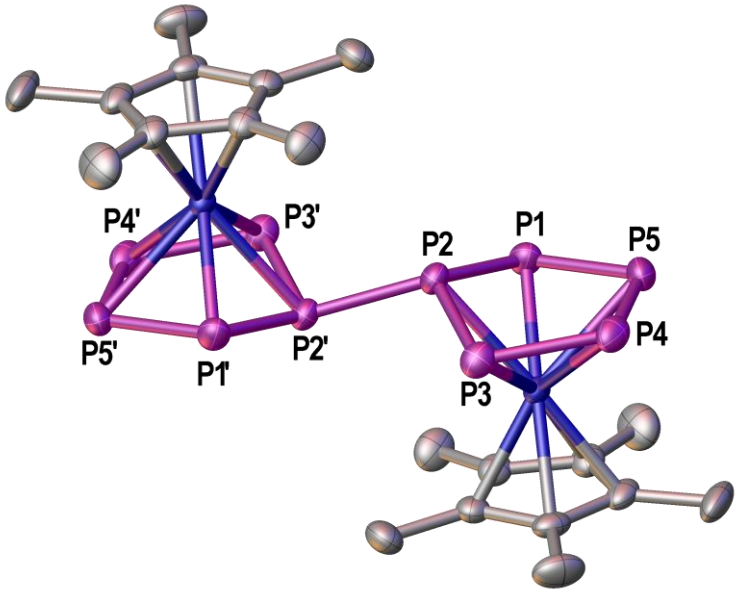

Figure 9. Crystal structure of dicationic P_{10} complex in **9**. Ellipsoids are drawn at 50% probability. H atoms are omitted for clarity. Selected bond lengths [Å] and angles [°]: P2-P2' 2.19092(3), P1-P2 2.12995(3), P2-P3 2.12540(3), P3-P4 2.12138(3), P4-P5 2.12800(3), P5-P1 2.12034(3), P1P2P3(plane)-P1P5P4P3(plane) 30.36(1).

Compound **9** crystallizes in the triclinic space group *P*–1 with one half of the dication, one anion [TEF] and one toluene solvent molecule in the asymmetric unit. The second half of the dication is generated by inversion. Figure 9 clearly shows the dication exhibiting a bicyclic P_{10} ligand coordinated to two [Cp*Fe] complex fragments. During this

reaction, the P2 atom is slightly moved out of the plane of the initially planar *cyclo*-P_5 ligand of **A** forming an envelope conformation. The newly formed P-P bond is found between P2 and P2'. The geometry of the dication can be compared well to the previously described structure containing the smaller anion $[SbF_6]^-$.[18]

Reaction of [Cp*Fe(η^5-As_5)] (D) with [Ga(*o*-DFB)$_2$][TEF]

Previous investigations showed that reactions of the *cyclo*-As_5 complex **D** with the monovalent group 13 metal cations Tl^+ and In^+ lead to the formation of the one-dimensional coordination polymers $[M(\mu,\eta^5{:}\eta^1\text{-}\mathbf{D})_3]_n[TEF]_n$ (M = Tl, In).[19] The analogues one-dimensional polymers have also been described for the *cyclo*-P_5 complex [Cp*Fe(η^5-P_5)] (**A**) and M = Tl, In, Ga (see general introduction). Several attempts to obtain an analogues product from reacting the *cyclo*-As_5 complex **D** with the Ga^+ source [Ga(*o*-DFB)$_2$][TEF] failed. In these reactions, mostly a dark precipitate is formed which could not be further characterized. From one attempt however, dark brown single crystals of $[(Cp^*Fe)_2(\mu,\eta^5{:}\eta^5\text{-}As_7)]$ (**10**) suitable for X-ray diffraction analysis could be obtained. The structure refinement of **10** is very challenging due to severe disorder of the [TEF] anions as well as one of the complex cations and could not be completed during this work. The metric data should therefore not be considered as definitive values, but the model for the ordered complex cation which allows for a general discussion is shown in Figure 10.

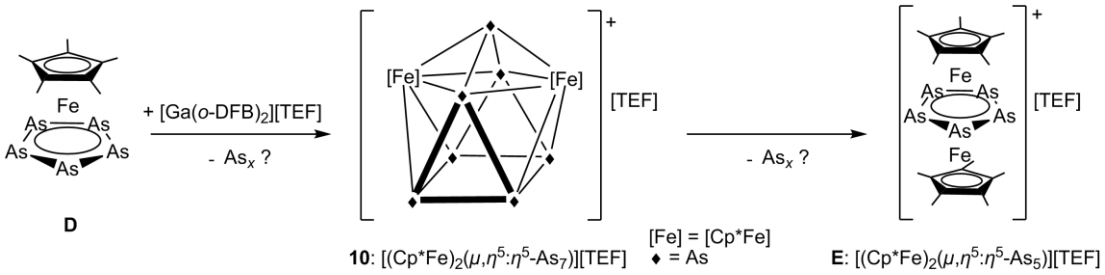

Scheme 10: Reaction of Ga^+ and the *cyclo*-As_5 complex **D** forming **10** as a possible intermediate in the formation the *cyclo*-As_5 triple-decker **E**.

Compound **10** crystallizes in the monoclinic space group $P2_1/c$ with two independent complex cations, two [TEF] anions and two toluene solvent molecules in the asymmetric unit. The central As_7 cage of one complex cations is disordered over at least three close positions while the other cation shows only rotational disorder of one Cp* ligand. The determined model of the latter is shown in Figure 10.

The bonding situation of the monocation in **10** can be described in two general ways. It may be described as a $[As_7]^-$ anion stabilized by two $[Cp^*Fe]^+$ complex fragments. The observed cluster can also be elucidated by describing the central $[Fe_2As_7]$ core by

Wade's rules.[20,21,22] According to these, the [Fe_2As_7] core has 22 ($2n$ + 4) skeletal electrons (7 × $5e^-$(As) + 2 × $8e^-$(Fe) + 2 × $5e^-$(Cp*) – $1e^-$(pos. charge) – 7 × $2e^-$(As) – 2 × $12e^-$(Fe) = $22e^-$). This results in a *nido*-type cluster which corresponds to a mono-capped square antiprism arrangement for the 9 cluster atoms. This structural motif is well-known for *Zintl* ions like $[E_9]^{4-}$ of group 14 elements.[23] This arrangement is exactly reflected in the structure of the monocation in **10** shown in Figure 10 a). The basal square consists of four As atoms and the upper half of the cluster shows a Fe_2As_2 square with alternating atoms. Finally, As6 is capping the square antiprism on top.

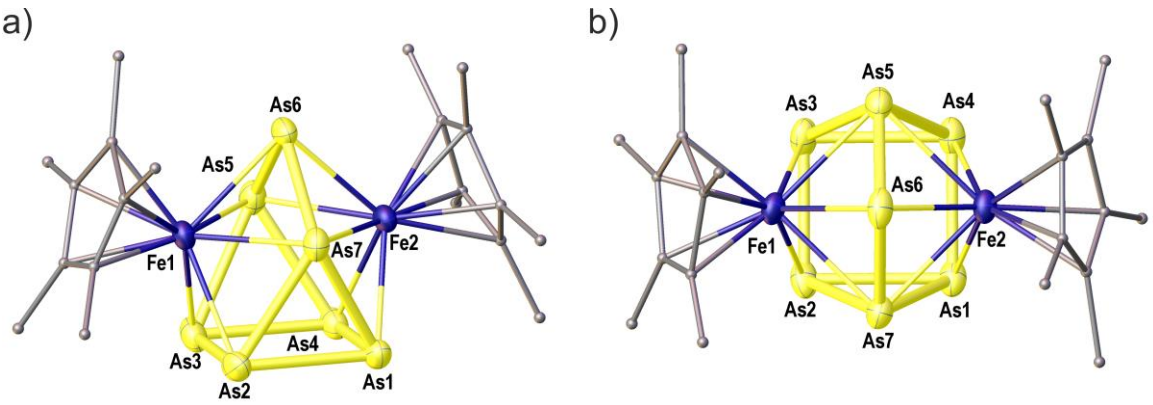

Figure 10. Representation of one of the complex cations in the final model of **10**. Ellipsoids are drawn at 50% probability. H atoms are omitted and C atoms are represented by small spheres for clarity (disordered Cp* ligand is represented only by the major part). Selected bond lengths [Å] and angles [°]: As1-As2 2.544(2), As2-As3 2.421(2), As3-As4 2.537(2), As4-As1 2.4294(19), As1-As7 2.582(2), As2-As7 2.589(2), As3-As5 2.591(2), As4-As5 2.596(2), As5-As6 2.384(2), As6-As7 2.381(2), As4As1As2 89.97(6), As1As2As3 89.87(7), As2As3As4 90.32(6), As3As4As1 89.83(7), Fe1As7Fe2 90.56(7), Fe1As5Fe2 90.96(7), As5Fe2As7 89.02(7), As7Fe1As5 89.06(7), As5As6As7 97.25(7).

In conclusion, our assumption is that **10** is formed by initial oxidation of [Cp*Fe(η^5-As_5)] (**D**). Since Ga^+ is not very stable and the starting material may have aged during storage it cannot be excluded that the observed reactivity may have been a result from decomposition products of the starting material [Ga(*o*-DFB)$_2$][TEF]. From reactions of [Cp*Fe(η^5-As_5)] (**D**) and the strong oxidant [Thia][TEF] only the formation of the cationic triple-decker complex [(Cp*Fe)$_2$(μ,η^5:η^5-As_5)] (**E**) could be detected so far. The ESI mass spectrum of **10** shows next to the molecular ion peak (*M*) also peaks assignable to (*M*–As) and (*M*–2As = **E**). Therefore, compound **10** may be an intermediate in the formation of **E** (see Scheme 10). Future efforts will include the development of a selective synthesis of 10 and other As rich complexes by oxidation of As_n ligand complexes. In this context, the preparation of a variety of oxidants featuring the WCA [TEF] will be a valuable synthetic target.

11.3 Synthesis of new E_n ligand complexes

The reactivity E_n ligand complexes is often dramatically influenced by introduction of substituents on the adjacent Cp ligands. This can often be explained by an increased solubility, better steric protection or sometimes by subtle electronic differences of the substituted Cp ligands. Therefore, the synthesis of new E_n ligand complexes and the investigation of their reactivity is an interesting topic. During this work several thermolytic reactions of suitable Cp^R substituted metal carbonyl complexes with white phosphorus (P_4) or yellow arsenic (As_4) have been investigated. Some of the obtained results are presented here.

Thermolysis of $[Cp'Mo(CO)_2]_2$ with P_4

The reaction of the mono *tert*-butyl substituted dinuclear complex $[\{Cp'Mo(CO)_2\}_2]$ with P_4 at elevated temperatures (see Scheme 11) affords the complexes **11**, **12** and **13** with 3, 2 and 6 P atoms, respectively. These P_n ligand complexes are well-known for Cp or Cp*. While the *cyclo*-P_3 complex **11** can be obtained in pure form, the complexes **12** and **13** were obtained as a mixture. The $^{31}P\{^1H\}$ NMR spectra of **11**-**13** reveal that for each complex all P atoms are chemically equivalent showing only one sharp singlet at δ = –345.9 ppm (**11**), –48.5 ppm (**12**) and –349.2 (**13**). For all complexes single crystals could be obtained which are suitable for X-ray diffraction analysis. The results are presented in Figure 11. However, analysis of the data for **12** showed signs indicative of modulation and the whole structure is disordered by reorientation of the complex. Therefore, only a model is presented for **12** and we refrain from reporting any metric data for **12**.

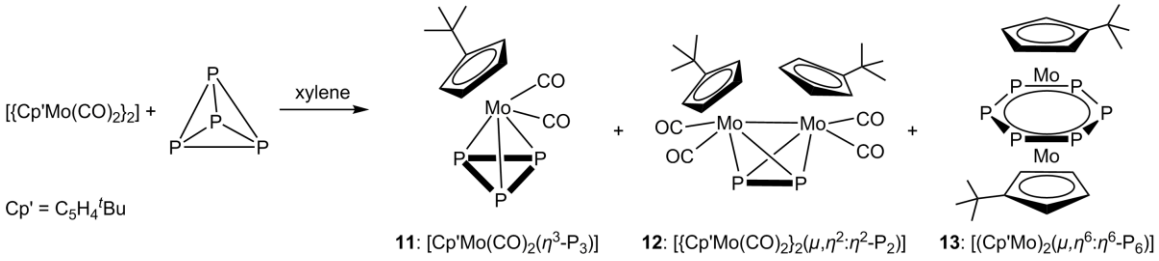

Scheme 11. Thermolytic reaction of $[\{Cp'Mo(CO)_2\}_2]$ with P_4.

Compound **11** crystallizes in the monoclinic space group $P2_1/n$ with one molecule of **11** in the asymmetric unit. The complex exhibits an almost equilateral *cyclo*-P_3 ligand. The geometry can very well be compared to the known analog containing an unsubstituted Cp ligand.[24] Compound **12** crystallizes in the triclinic space group $P\bar{1}$ with two independent molecules of the tetrahedrane complex **12** in the asymmetric unit.

Due to severe problems during the structure refinement, no metric data will be discussed. Compound **13** crystallizes in the monoclinic space group $P2_1/c$ with two independent halves of the *cyclo*-P_6 complex in the asymmetric unit. The complexes are completed by inversion. Therefore the triple-decker complexes show three planar ligands which are oriented perfectly parallel to each other. Additionally the *tert*-butyl groups on both Cp ligands are pointing to opposite sides of the Mo-Mo axis. The geometry can very well be compared to the *cyclo*-P_6 complex with unsubstituted Cp ligands.[25]

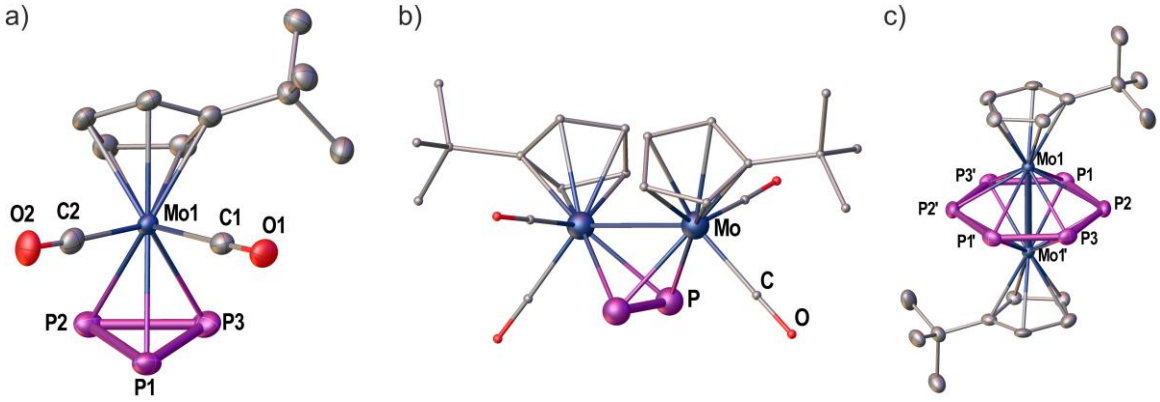

Figure 11. a) Crystal structure of **11**. b) Model of **12**. C atoms are drawn as small spheres for clarity. c) Crystal structure of **13**. Only one complex shown here. All ellipsoids are drawn at 50% probability. All H atoms are omitted for clarity. Selected bond lengths [Å] and angles [°]: **11**: P1-P2 2.1382(7), P2-P3 2.1600(7), P3-P1 2.1450(7), Mo1-P1 2.5725(5), Mo1-P2 2.5328(6), Mo1-P3 2.5193(5), P3P1P2 60.57(2), P1P2P3 59.87(2), P2P3P1 59.56(2); **12**: no metric data will be provided; **13**: P1-P2 2.1836(17), P2-P3 2.1692(17), P3-P1' 2.1744(17), Mo1-Mo1' 2.6756(4), P3'P1P2 119.76(7), P1P2P3 120.35(7), P2P3P1' 119.87(7).

Thermolysis of [{Cp''Mo(CO)$_{2/3}$}$_2$] with As$_4$

The reaction of the 1,3-di-*tert*-butyl substituted dinuclear complexes [{Cp''Mo(CO)$_{2/3}$}$_2$] with As_4 at elevated temperatures (see Scheme 12) proceeds as expected and the formation of the yellow *cyclo*-As_3 complex [Cp''Mo(CO)$_2$(η^3-As_3)] (**14**) can be observed. During the chromatographic workup the starting material [{Cp''Mo(CO)$_3$}$_2$] (**15**) with a Mo-Mo single bond could be isolated in pure form affording single crystals suitable for X-ray diffraction analysis. In addition the side product [Cp''$_3$Mo$_3$(CO)(μ-O)As_3] (**16**) could be structurally characterized. This cluster molecule still contains a terminal CO ligand and an additional bridging oxygen atom. The origin of the bridging oxygen atom in **16** remains unclear. Possible explanations would be atmospheric O_2 or residual H_2O from the silica. The determined crystal structures of **14** and **15** are shown in Figure 12 and the crystal structure of **16** is shown in Figure 13.

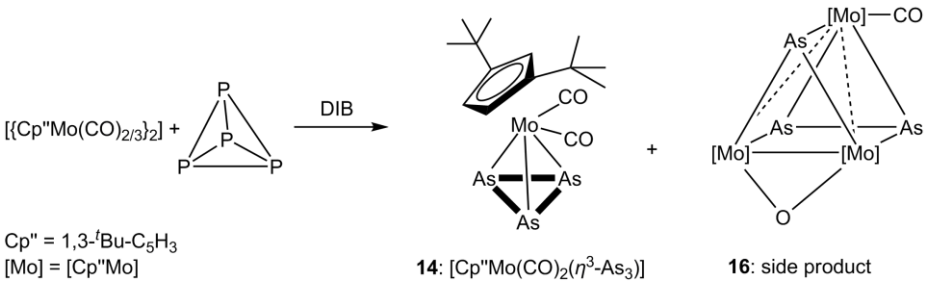

Scheme 12. Thermolytic reaction of [{Cp''Mo(CO)$_2$}$_{2/3}$] with As$_4$.

Compound **14** crystallizes in the triclinic space group *P*–1 with one molecule in the asymmetric unit. The geometry of the complex can be compared well to its Cp* analog[26] and exhibits a *cyclo*-As$_3$ ligand with rather uniform As-As bond lengths. The *tert*-butyl groups are symmetrically oriented to each side of the complex. Compound **15** crystallizes in the orthorhombic space group *Pnnm* with one quarter of the molecule in asymmetric unit. In the literature there are numerous examples for analogues complexes [{Cp^{R}Mo(CO)$_3$}$_2$], but to the best of our knowledge, the crystal structure of **15** has not been reported so far. However, there is a report for the analogues complex with 1,2-*tert*-butyl substituted Cp ligands.[27] The Cp'' ligands of **15** are oriented in a trans arrangement comparable to the Cp* analog.[28]

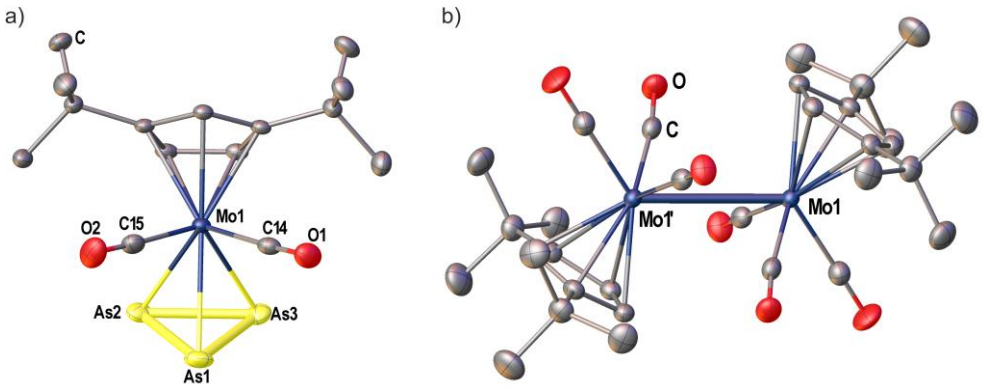

Figure 12. a) Crystal structure of the *cyclo*-As$_3$ complex **14**. b) Crystal structure of the starting material [{Cp''Mo(CO)$_3$}$_2$] (**15**). Ellipsoids are drawn at 50% probability. H atoms are omitted for clarity. Selected bond lengths [Å] and angles [°]: **14**: As1-As2 2.3657(5), As2-As3 2.3901(7), As3-As1 2.3693(6), Mo1-As1 2.7086(5), Mo1-As2 2.6489(5), Mo1-As3 2.6356(3), As3As1As2 60.63(2), As1As2As3 59.76(2), As2As3As1 59.61(2); 15: Mo1-Mo1‘ 3.28686(3).

The side-product **16** crystallizes in the triclinic space group *P*–1 with one molecule and two toluene solvent molecules in the asymmetric unit. The cluster **16** shown in Figure 13 consists of three [Cp''Mo] complex fragments forming a triangle with two long (~3.0 Å) distances and one short Mo-Mo bond (Mo2-Mo3 2.5915(6) Å). Mo1 shows one additional terminal CO ligand. The Mo triangle is capped on one side by As1 and on the other side by the As2-As3 dumbbell. The Mo2-Mo3 bond is bridged by an oxygen atom. In Figure 13 b) the cluster **16** is rotated that O1 is pointing to the front.

This view illustrates that the central Mo_3As_3 core may also be described as a distorted trigonal prism.

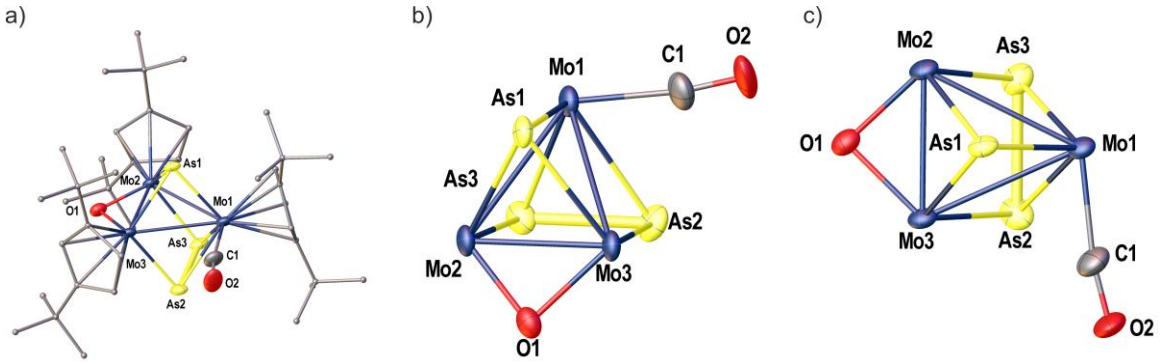

Figure 13. Crystal structure of the side product **16**. a) Representation of the cluster including all Cp'' ligands. C atoms of the Cp'' ligands are drawn as small spheres and H atoms are omitted for clarity. b) View of **16** with all Cp'' ligands omitted for clarity. O1 is shown in front. c) Viewing direction perpendicular to the Mo1Mo2Mo3 plane. All ellipsoids are drawn at 50% probability. Selected bond lengths [Å] and angles [°]: Mo1-Mo2 3.0660(8), Mo1-Mo3 3.0365(8), Mo2-Mo3 2.5915(6), Mo1-As1 2.4775(8), Mo2-As1 2.5251(9), Mo3-As1 2.5330(8), Mo1-As2 2.6353(9), Mo1-As3 2.5845(10), Mo2-As3 2.5352(8), Mo3-As2 2.5594(8), Mo2-O1 1.903(4), Mo3-O1 1.915(4), As2-As3 2.3422(10).

Thermolysis of [{Cp*Mo(CO)$_2$}$_2$] with As$_4$

The reaction of the dinuclear complexes [{Cp*Mo(CO)$_2$}$_2$] with As$_4$ at elevated temperatures (see Scheme 13) affords several products among which the triple-decker complexes [(Cp*Mo)$_2$(μ,η^5:η^5-As$_5$)] (**17**) and [(Cp*Mo)$_2$(μ,η^6:η^6-As$_6$)] (**18**) could be detected. While **18** is known in the literature,[29] for **17** only the Cp analogues *cyclo*-As$_5$ complex has been described before.[30] Unfortunately, the complex **17** could not be structurally characterized. In addition the heterocubane cluster [(Cp*Mo)$_3$(μ_3-As)(μ_3-As$_4$)] (**19**) obtained from the same reaction could be structurally characterized. The structure of **19** is shown in Figure 14.

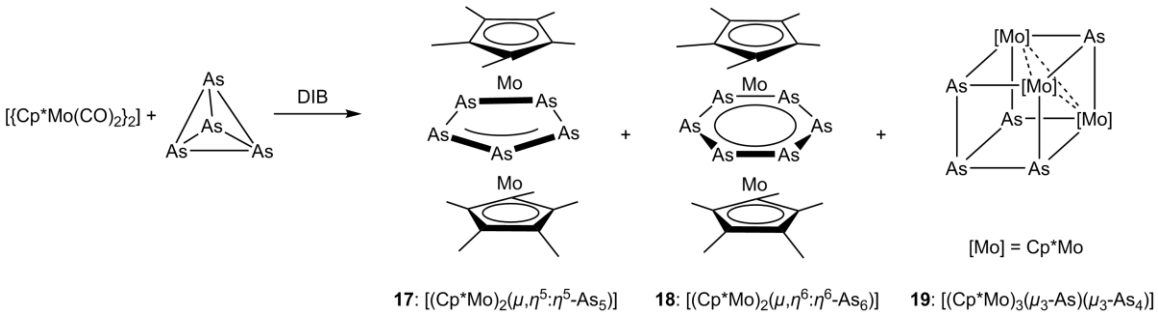

Scheme 13. Thermolytic reaction of [{Cp*Mo(CO)$_2$}$_2$] with As$_4$.

Compound **19** crystallizes in the triclinic space group *P*–1 with one cluster molecule in the asymmetric unit. The Cp* ligand on Mo2 shows a rotational disorder over two positions (67:33). Only the major part is depicted. The analogues Ni/As heterocubane [(Cp*Ni)$_3$(μ_3-As)(μ_3-As$_4$)] has been described before,[31] but to the best of our knowledge

it is unknown for Mo so far. The most striking differences between **19** and its Ni analog are the short Mo-Mo distances (~2.88 Å) compared to the Ni-Ni distances (>3.55 Å). This fact can easily be explained by the electronic structure of the complex. Ni ($10e^-$) reaches 18 valence electrons (VE) already by coordination of Cp* ($5e^-$) and the formation of three covalent Ni-As bonds ($3e^-$). Therefore, no Ni-Ni interaction is observed. For Mo ($6e^-$) coordination of Cp* ($5e^-$) and the formation of three Mo-As bonds ($3e^-$) yields a metal center with 14 valence electrons. For a stable 18 VE configuration of Mo the formation of two Mo-Mo double bonds for each Mo atom is necessary. This is in accordance with the observed Mo-Mo bond lengths of 2.8702(3) Å up to 2.8841(3) Å in **19**. The Mo-Mo single bond of [{CpMo(CO)$_3$}$_2$] measures 3.235(1) Å[32] while the triple bond of [{CpMo(CO)$_2$}$_2$] measures 2.448(1) Å for comparison.[33] Future investigations will also include the description of the bonding situation found in **19** with the help of DFT calculations.

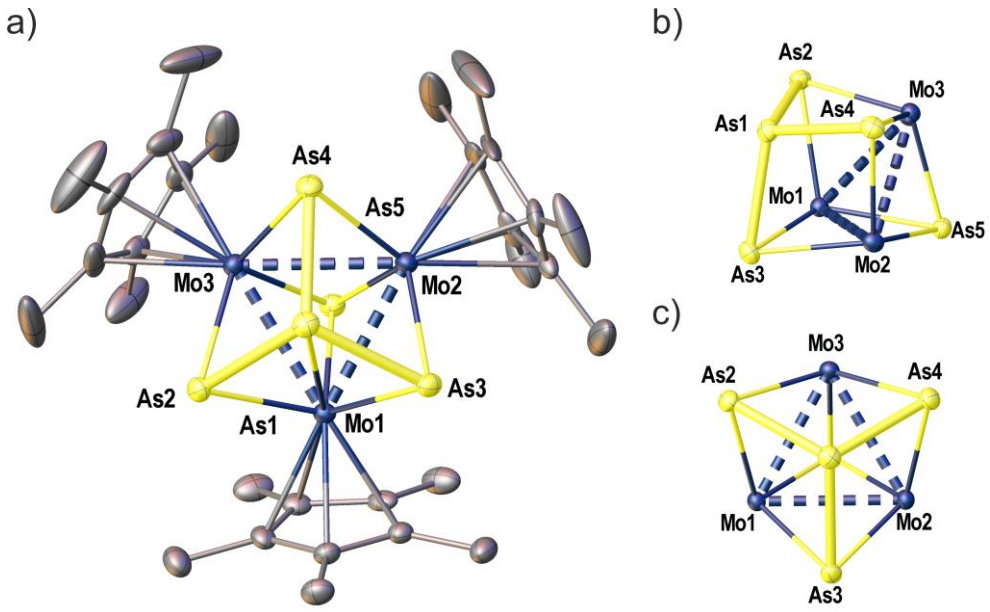

Figure 14. Crystal structure of the heterocubane **19**. a) Illustration of **19** with all Cp* ligands. b) Side view. Cp* ligands are omitted for clarity. c) Viewing direction perpendicular to the Mo1Mo2Mo3 plane. As1 is in front, As5 lies behind As1. Ellipsoids are drawn at 50% probability. H atoms are omitted for clarity. Selected bond lengths [Å] and angles [°]: Mo1-Mo2 2.8702(3), Mo2-Mo3 2.8830(4), Mo3-Mo1 2.8841(3), Mo1-As5 2.4659(5), Mo2-As5 2.4707(6), Mo3-As5 2.4657(5), Mo1-As2 2.5007(5), Mo1-As3 2.5012(5), Mo2-As3 2.5036(5), Mo2-As4 2.5008(5), Mo3-As2 2.5021(5), Mo3-As4 2.5003(5), As1-As2 2.4394(6), As1-As3 2.4353(6), As1-As4 2.4362(6), Mo3Mo1Mo2 60.13(1), Mo1Mo2Mo3 60.17(1), Mo2Mo3Mo1 59.69(1), As2As1As3 104.80(2), As3As1As4 104.75(2), As4As1As2 105.24(2), Mo1As5Mo2 71.10(2), Mo2As5Mo3 71.47(2), Mo1As5Mo3 71.58(2).

11.4 Experimental Part

Synthesis and characterization of **1**: 1g Li[FAl] (0.66 mmol) and > 600 mg CuCl (> 6 mmol) were weighed into a Schlenk vessel equipped with a Young valve and a small stirring bar. Onto these solids ~10 mL of SO_2 were condensed at –196 °C. The vessel was closed under vacuum and the reaction was slowly warmed to room temperature under constant stirring. The colorless turbid

mixture was stirred at room temperature for 2 days. The fine solid was precipitated by centrifugation and the supernatant solution was filtrated and cooled to –30 °C. Upon one day we observed 2 sorts of colorless crystals, large blocks and fine rods. Both of these contain the same compound $[Al\{OC_6F_{10}(C_6F_5)\}_3]$ (**1**). This super Lewis acid was previously described in the literature by *Krossing et al.* (determined unit cell of the fine rods) and we were able to structurally characterize a new modification (large blocks).

Synthesis of Tl[FAl] (**2**): 1.5 g Li[FAl] (1.08 mmol) and 223 mg TlF (1 mmol) were placed in a Schlenk vessel equipped with a Young valve and 50 mL of CH_2Cl_2 were added. The vessel was closed under reduced pressure. The reaction was sonicated for one day. Subsequently the fine white precipitate was removed by centrifugation. The filtered supernatant solution was layered with the fivefold amount of *n*-hexane and stored at +4 °C. After some days Tl[FAl] forms as colorless blocks on the sides of the vessel. The mother liquor is decanted off and the crystals are dried in vacuum. Yield 157 mg (9.9%). $^{19}F\{^1H\}$ NMR (CD_2Cl_2)see below. Anal. calcd. for Tl[FAl]: C, 27.27; H, 0.00. Found: C, 27.24; H, 0.32; or C, 27.27; H, 0.22. IR (KBr) $\tilde{\nu}/cm^{-1}$ = 3683 (w), 2964 (vw), 2920 (vw), 2851 (vw), 1654 (m), 1537 (s), 1482 (vs), 1322 (m), 1247 (vs), 1207 (vs), 1174 (m), 1137 (m), 1106 (s), 1034 (m), 1018 (vs), 996 (m), 952 (vs), 907 (m), 806 (w), 742 (w), 730 (m), 679 (w), 636 (m), 625 (w), 601 (vw), 531 (w).

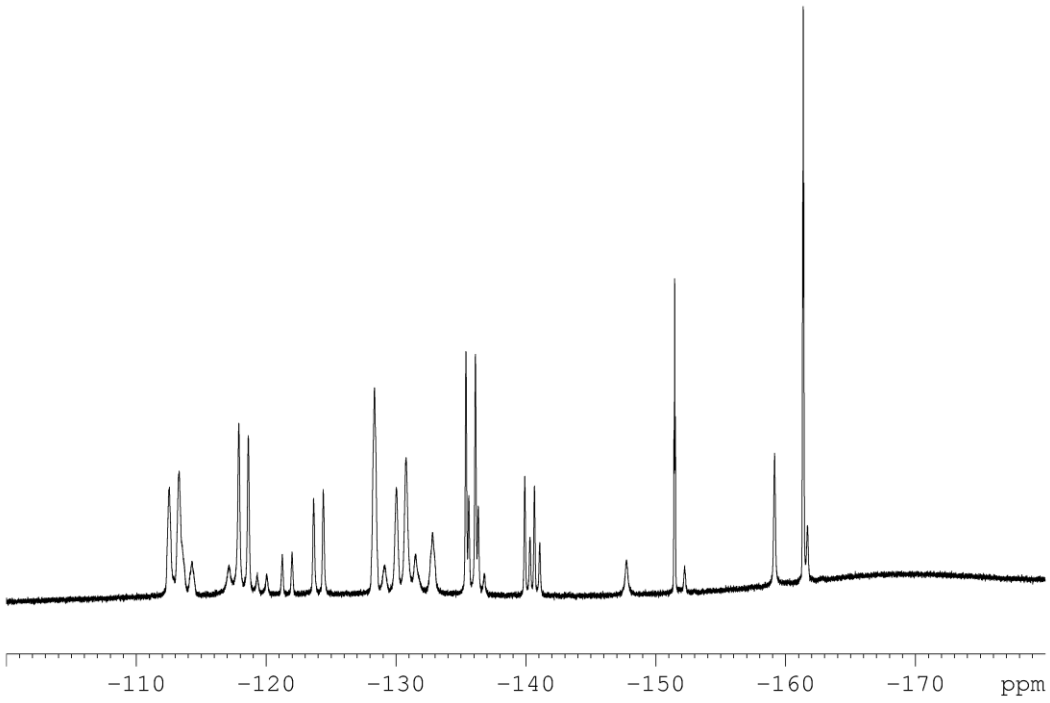

Figure 15. $^{19}F\{^1H\}$ NMR spectrum of Tl[FAl] (**2**) in CD_2Cl_2 at room temperature (number of scans 256!). Signal pattern is indicative of the coordinating conformation of the [FAl] anion. For details see reference [2].

Synthesis of $[Cu(MeCN)_{3.5}][FAl]$ (**3**): 490 mg Li[FAl] (0.35 mmol) and 223 mg $[Cu(MeCN)_4][BF4]$ (0.32 mmol) were placed in a Schlenk vessel equipped with a Young valve and 5 mL of CH_2Cl_2 were added. The vessel was closed under reduced pressure. The reaction was sonicated for one day. This affords a white to grey slurry of very fine powder in a colorless solution. Subsequently the fine white to grey precipitate was removed by centrifugation from the warm CH_2Cl_2 solution. The clear supernatant solution was filtered, layered with *n*-hexane and stored in

a fridge to afford 150 mg of clear colorless crystals. There were a lot of crystals among the grey precipitate which already formed during cooling the CH_2Cl_2 solution inside the centrifuge. Therefore, 15 mL CH_2Cl_2 were added to the precipitate and the slurry was stirred for 20 min. Subsequently, the precipitate was filtered off and the clear solution was layered with *n*-hexane to afford additional 229 mg of crystalline **3** within one day. The crystals are freed from the mother liquor, washed with *n*-hexane and dried in vacuum. Yield 379 mg (75%). ^{1}H NMR (CD_2Cl_2) δ/ppm = 2.20 (s, CH_3); $^{13}C\{^{1}H\}$ NMR (CD_2Cl_2) δ/ppm = 2.79 (s, CH_3); $^{19}F\{^{1}H\}$ NMR (CD_2Cl_2) δ/ppm = –112.6 (d, $J_{F,F}$ = 280 Hz, 2F), –117.1 (d, $J_{F,F}$ = 279 Hz, 2F), –121.5 (d, $J_{F,F}$ = 277 Hz, 2F), –127.7 (s, 2F), –130.4 (d, $J_{F,F}$ = 275 Hz, 2F), –136.8 (d, $J_{F,F}$ = 276 Hz, 2F), –140.7 (d, $J_{F,F}$ = 277 Hz, 1F), –154.2 (t, $J_{F,F}$ = 22 Hz, 1F), –164.6 (t, $J_{F,F}$ = 18 Hz, 1F), –172.1 ppm (s, AlF). Anal. calcd. for $[Cu(MeCN)_{3.5}][FAl]$: C, 32.51; H, 0.67; N, 3.09. Found: C, 32.26; H, 0.85; N, 3.05. ESI-MS (CH_2Cl_2) cations: *m/q* (%) = 144.8 (100) $[Cu(MeCN)_2]^+$, 185.8 (4) $[Cu(MeCN)_3]^+$, 226.7 (<1) $[Cu(MeCN)_4]^+$; anions: 1381.1 (100) $[FAl]^-$. IR (KBr) $\tilde{\nu}$/cm^{-1} = 3216 (vw), 3227 (vw), 3200 (vw), 3021 (vw), 2965 (vw), 2953 (w), 2410 (vw), 2361 (vw), 2323 (w), 2291 (vw), 2274 (vw), 1654 (m), 1536 (s), 1486 (vs), 1407 (w), 1376 (w), 1325 (m), 1310 (m), 1276 (m), 1246 (vs), 1205 (vs), 1187 (vs), 1156 (s), 1136 (m), 1107 (s), 1085 (w), 1034 (m), 1019 (vs), 1005 (s), 955 (vs), 911 (m), 850 (w), 811 (w), 780 (vw), 769 (s), 751 (m), 730 (s), 712 (vw), 667 (w), 647 (w), 636 (m), 624 (m), 600 (w), 586 (vw), 535 (m), 527 (m), 496 (m), 467 (m).

Synthesis of $[Cu_2(\mu,\eta^1{:}\eta^1\text{-}\mathbf{A})_2(MeCN)_4][FAl]_2$ (**4**): 100 mg $[Cu(MeCN)_{3.5}][FAl]$ (**3**) (0.063 mmol) and 25 mg $[Cp^*Fe(\eta^5\text{-}P_5)]$ (**A**) (0.072 mmol) were weighed together into a Schlenk vessel. To this 25 mL of CH_2Cl_2 were added under constant stirring affording a light brown clear solution. After 24 h stirring, the solution was filtered and layered with the fivefold amount of *n*-hexane and subsequently stored at +4 °C. After several days, compound **4** can be isolated as clear light green crystals which form at the mixing zone of the solvents. The supernatant solution is removed, the crystals are washed with *n*-hexane and dried in vacuum. Even when a larger excess of the complex **A** is used, only the product **4** with a 1:1 ratio of **A** and Cu^+ could be isolated. Yield 89 mg (75%). ^{1}H NMR (CD_2Cl_2) δ/ppm = 2.10 (s, MeCN), 1.40 (s, Cp*); $^{19}F\{^{1}H\}$ NMR (CD_2Cl_2) δ/ppm = –112.6 (d, $J_{F,F}$ = 280 Hz, 2F), –117.1 (d, $J_{F,F}$ = 279 Hz, 2F), –121.5 (d, $J_{F,F}$ = 277 Hz, 2F), –127.7 (s, 2F), –130.4 (d, $J_{F,F}$ = 275 Hz, 2F), –136.8 (d, $J_{F,F}$ = 276 Hz, 2F), –140.7 (d, $J_{F,F}$ = 277 Hz, 1F), –154.2 (t, $J_{F,F}$ = 22 Hz, 1F), –164.6 (t, $J_{F,F}$ = 18 Hz, 1F), –172.0 ppm (s, AlF); $^{31}P\{^{1}H\}$ NMR (CD_2Cl_2) δ/ppm = 138.9 (s, P5, ω½ = 21 Hz). Anal. calcd. for $[Cu_2(Cp^*FeP5)_2(MeCN)_4][FAl]_2$: C, 32.06; H, 1.13; N, 1.50. Found: C, 31.90; H, 1.21; N, 1.37. ESI-MS (CH_2Cl_2) cations: *m/q* (%) = 144.8 (93) $[Cu(MeCN)_2]^+$, 408.7 (100) $[Cu(Cp^*FeP_5)]^+$, 449.8 (95) $[Cu(Cp^*FeP_5)(MeCN)]^+$, 754.9 (50) $[Cu(Cp^*FeP_5)_2]^+$; anions: 1381.1 (100) $[FAl]^-$. IR (KBr) $\tilde{\nu}$/cm^{-1} = 2977 (vw), 2949 (w), 2921 (w), 2851 (vw), 1653 (m), 1534 (s), 1430 (vw), 1407 (vw), 1380 (w), 1324 (m), 1309 (m), 1268 (m), 1244 (s), 1204 (vs), 1187 (s), 1157 (s), 1135 (m), 1105 (s), 1033 (m), 1019 (vs), 1007 (m), 1001 (m), 956 (vs), 910 (m), 850 (w), 812 (w), 769 (m), 751 (m), 729 (s), 667 (w), 647 (w), 635 (w), 625 (w), 600 (w), 536 (w), 527 (w), 497 (vw), 468 (w).

Synthesis of $[Cp^*Fe(\mu,\eta^5{:}\eta^1\text{-}P_5)Mo(CO)_5]$ (**5**): Synthesis was modified according to the literature procedure preparation of **B**.[1] 606 mg $[Mo(CO)_3(MeCN)_3]$ (2 mmol) and $[Cp^*Fe(\eta^5\text{-}P_5)]$ (**A**) (2 mmol) were filled into a round bottom flask and 10 mL of CH_2Cl_2 were added under constant stirring. The reaction immediately turned dark red. After 1 h, ~5 g of silica were added, the solvent was removed until a freely flowing powder was obtained. This was placed on top of a chromatographic column (20 × 2 cm, packed with *n*-hexane). Elution with *n*-hexane affords a first light green fraction of $[Cp^*Fe(\mu,\eta^5{:}\eta^1\text{-}P_5)Mo(CO)_5]$ (**5**). The second olive green fraction contains $[Cp^*Fe(\mu,\eta^5{:}\eta^5\text{-}P_5)Mo(CO)_3]$ (**B**). The yields of this reaction were very low and the products could only be characterized by X-ray crystallography. It is assumed, that the starting material $[Mo(CO)_3(MeCN)_3]$ was not pure during this reaction.

Synthesis of [Au(η^1:η^1-**B**)$_2$][FAl] (**6**): During this reaction it was assumed, that the salt [Tl(CH$_2$Cl$_2$)$_x$][Li(FAl)$_2$] would actually be pure Tl[FAl]. Therefore, the used amounts are not stoichiometric. Additionally, the starting material **B** was not clean and it was used as a mixture with other complexes. Compound **6** was only characterized by single crystal X-ray diffraction so far. 80 mg [Tl(CH$_2$Cl$_2$)$_x$][Li(FAl)$_2$] (x = 2.5, 0.025 mmol), 16 mg (tht)AuCl (0.05 mmol) and 58 mg [Cp*Fe(μ,η^5:η^5-P$_5$)Mo(CO)$_3$] (**B**) (0.1 mmol) were placed into a Schlenk vessel. Under constant stirring 10 mL of CH$_2$Cl$_2$ were added affording a dark red solution (color maybe due to impurities in **B**). After 1 h of stirring, the solution was filtered and layered with *n*-hexane. After some time small crystals of compound **6** could be observed on the glass walls.

Reaction of [{CpMo(CO)$_2$}(μ,η^2:η^2-As$_2$)] (**C**) with Ag[TEF] (**7**): 58 mg of the As$_2$ complex [{CpMo(CO)$_2$}$_2$(μ,η^2:η^2-As$_2$)] (**C**) (0.10 mmol) and 116 mg Ag[TEF] (0.10 mmol) were dissolved separately in 4 mL of CH$_2$Cl$_2$ each. The Ag$^+$ solution was slowly added to the red solution of **C** under constant stirring. The dark red solution was degassed five times and the reaction stirred for 18 h. After this time, the solution was filtered, layered with the fivefold amount of *n*-hexane and subsequently stored at +4 °C. After several days a dark red oil is formed at the bottom of the flask. From this oil the formation of red rod shaped crystals of the trinuclear complex **7** can be observed after some weeks. The crystals are suitable for single crystal X-ray diffraction analysis, but they decompose on the diffractometer after some time. Several attempts to collect a complete and well-suited dataset for the structure refinement failed. However, from the obtained data it was possible to determine a model of the heavy atoms, but the refinement of three independent [TEF] anions could not be finished during this work.

Reaction of [{CpMo(CO)$_2$}(μ,η^2:η^2-As$_2$)] (**C**) with Ag[FAl] (**8**): 58 mg of the As$_2$ complex [{CpMo(CO)$_2$}$_2$(μ,η^2:η^2-As$_2$)] (**C**) (0.10 mmol) and 79 mg Ag[FAl] (0.05 mmol) were dissolved separately in 5 mL of CH$_2$Cl$_2$ each. The Ag$^+$ solution was slowly added to the red solution of **C** under constant stirring. The dark red solution was stirred for 2 h. After this time, the solution was filtered, layered with the fivefold amount of toluene and subsequently stored at +4 °C. After several days red crystals of [Ag$_2$(μ,η^1:η^2-**C**)$_2$(η^2-**C**)$_2$][FAl]$_2$ (**8**) were obtained. The crystals are washed with toluene and dried in vacuum. The crystals are suitable for single crystal X-ray diffraction analysis. However, the structure refinement of **8** is very challenging. In this compound, the [FAl] anions show almost no disorder, but the complex cations are completely disordered, most probably caused by slightly different orientation of the ligands **C** with similar energies. Therefore, a final structure refinement could not be finished during this work. However, the obtained model clearly shows the two different coordination modes of the As$_2$ ligand **C** as well as the general structural motif. Yield 48 mg (46%). ^{1}H NMR (CD$_2$Cl$_2$) δ/ppm = 5.31 (s, Cp); ^{13}C{^{1}H} NMR (CD$_2$Cl$_2$) δ/ppm = 222.40 (s, CO), 86.46 (s, Cp); ^{19}F{^{1}H} NMR (CD$_2$Cl$_2$) δ/ppm = –112.6 (d, $J_{F,F}$ = 280 Hz, 2F), –117.1 (d, $J_{F,F}$ = 279 Hz, 2F), –121.5 (d, $J_{F,F}$ = 277 Hz, 2F), –127.7 (s, 2F), –130.4 (d, $J_{F,F}$ = 275 Hz, 2F), –136.8 (d, $J_{F,F}$ = 276 Hz, 2F), –140.7 (d, $J_{F,F}$ = 277 Hz, 1F), –154.2 (t, $J_{F,F}$ = 22 Hz, 1F), –164.6 (t, $J_{F,F}$ = 18 Hz, 1F), –172.0 ppm (s, AlF). Anal. calcd. for [Ag$_2$(**C**)$_4$][FAl]$_2$·(CH$_2$Cl$_2$)·(C$_7$H$_8$)$_{0.6}$: C, 29.63; H, 0.96. Found: C, 29.55; H, 1.07. ESI-MS (CH$_2$Cl$_2$)cations: m/q (%) = 1276.5 (100) [Ag(**C**)$_2$]$^+$; anions: 1381.2 (100) [FAl]$^-$. IR (KBr) $\tilde{\nu}$/cm^{-1} = 3125 (w), 2958 (vw), 2918 (w), 2851 (vw), 2020 (m), 1981 (vs), 1929 (vs), 1652 (m), 1532 (s), 1485 (vs), 1423 (w), 1391 (vw), 1322 (m), 1307 (m), 1267 (m), 1244 (m), 1204 (vs), 1187 (s), 1154 (s), 1134 (m), 1104 (s), 1034 (m), 1019 (vs), 1005 (s), 955 (vs), 910 (m), 837 (m), 829 (m), 768 (m), 750 (w), 729 (m), 634 (w), 525 (m), 489 (w), 457 (w).

Synthesis of [(Cp*Fe)$_2$(μ,η^4:η^4-P$_{10}$)][TEF]$_2$ (**9**): 200 mg [NO][TEF] (0.2 mmol) and 69 mg [Cp*Fe(η^5-P$_5$)] (**A**) (0.2 mmol) are combined as solids. Onto this 10 mL of CH$_2$Cl$_2$ are added under constant stirring immediately forming a dark red solution. At the beginning some gas evolution (presumably NO) can be observed. The reaction mixture is degassed and stirred for 30 min at room temperature. Subsequently, the solution is filtered, carefully layered with the threefold

amount of toluene and stored at +4 °C. After several days, the formation of dark red single crystals suitable for X-ray diffraction analysis can be observed. The crystals are washed with toluene and dried in vacuum. Yield 227 mg (87%). ^{1}H NMR (CD_2Cl_2) δ/ppm = 1.59 (s, Cp*); ^{19}F{^{1}H} NMR (CD_2Cl_2) δ/ppm = –79.0 (s, [TEF]); ^{31}P{^{1}H} NMR (CD_2Cl_2) δ/ppm = 198.0 (m, 4P), 125.5 (m, 4P), –29.1 (m, 2P), see below. Anal. calcd. for $[(Cp^*Fe)_2P_{10}][TEF]_2 \cdot (C_7H_8)$: C, 26.07; H, 1.41. Found: C, 26.05; H, 1.55. IR (KBr) $\tilde{\nu}$/cm^{-1} = 2989 (vw), 2925 (vw), 1624 (vw), 1479 (w), 1429 (w), 1383 (w), 1354 (m), 1303 (vs), 1277 (vs), 1244 (vs), 1218 (vs), 1167 (m), 1019 (w), 973 (vs), 832 (w), 727 (vs), 561 (w), 537 (w), 445 (m).

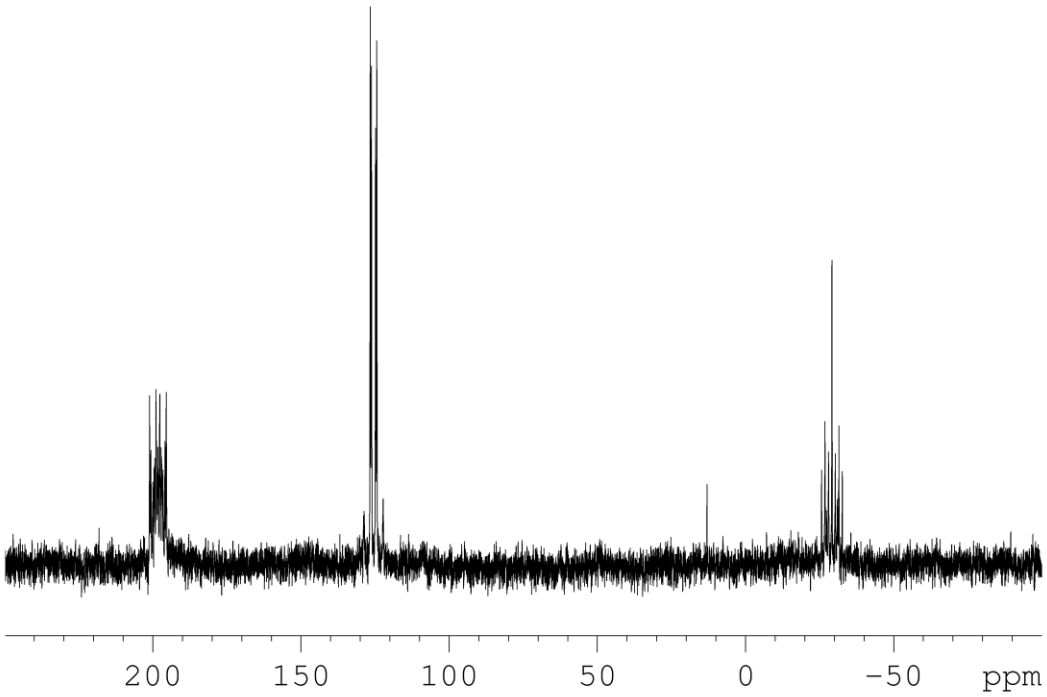

Figure 16. ^{31}P{^{1}H} NMR spectrum of **9**.

Synthesis of [(Cp*Fe)(μ,η^5:η^5-As$_7$)][TEF] (**10**): 21 mg [Ga(*o*-DFB)$_2$][TEF] (0.017 mmol) were dissolved in 3 mL of toluene and 2 mL of *o*-DFB. In another flask 28 mg [Cp*Fe(η^5-As$_5$)] (**D**) (0.05 mmol) were dissolved in 2 mL of toluene. The Ga$^+$ solution was slowly added to the solution of **D** under constant stirring. The initially dark green solution turns dark brown and some black precipitate is formed. After a short time, the solution is filtered, layered with toluene and subsequently stored at –30 °C. After a few days dark brown crystals suitable for single crystal X-ray diffraction analysis were formed from this reaction. We assume that **10** is formed by initial oxidation of [Cp*Fe(η^5-As$_5$)] (**D**). Since Ga$^+$ is not very stable and the starting material may have aged during storage we cannot completely exclude that the observed reactivity results from decomposition products of the starting material [Ga(*o*-DFB)$_2$][TEF]. From reactions of [Cp*Fe(η^5-As$_5$)] (**D**) and the strong oxidant [Thia][TEF] only the formation of the cationic triple-decker complex [(Cp*Fe)$_2$(μ,η^5:η^5-As$_5$)] (**E**) could be detected. The ESI mass spectrum of **10** also shows a large peak assignable to **E**. Therefore, compound **10** may be an intermediate in the formation of **E**. Yield 10 mg (32%). Anal. calcd. for [(Cp*Fe)$_2$As$_7$][TEF]: C, 23.08; H, 1.61. Found: C, 23.04; H, 1.77. ESI-MS (CH_2Cl_2) cations: *m/q* (%) = 906.6 (26) [*M*]$^+$, 831.7 (8) [*M*–As]$^+$, 756.7 (100) [*M*–2As]$^+$; anions: 967.0 (100) [TEF]$^-$. IR (KBr) $\tilde{\nu}$/cm^{-1} = 2981 (vw), 2919 (w), 2869 (vw), 1480 (w), 1427 (w), 1380 (w), 1352 (m), 1301 (vs), 1277 (vs), 1241 (vs), 1220 (vs), 1169 (m), 1024 (w), 974 (vs), 832 (w), 728 (vs), 561 (w), 537 (w), 445 (m).

Thermolysis of [{Cp'Mo(CO)$_2$}$_2$] and P$_4$ (**11**, **12**, **13**): 1 g [{Cp'Mo(CO)$_2$}$_2$] (1.82 mmol) and 1 g P$_4$ (8.07 mmol) were weighed together in a round bottom flask and 150 mL of xylene were added to this mixture. The reaction mixture was refluxed for 20 h under constant stirring. After cooling to room temperature, the solvent and excess P$_4$ were removed under reduced pressure to yield a brown residue. The crude product was dissolved in 20 mL of CH_2Cl_2 and mixed with ~10 g of silica and subsequently dried in vacuum until a brown freely flowing powder was obtained. This was placed on top of a chromatographic column (20 × 2 cm, packed with *n*-hexane). Elution with *n*-hexane affords a first light yellow fraction of [Cp'Mo(CO)$_2$(η^3-P$_3$)] (**11**). Yield: (340 mg, 25%). The second fraction shows an orange to red color and contains [{Cp'Mo(CO)$_2$}$_2$(μ,η^2:η^2-P$_2$)] (**12**) as well as [(Cp'Mo)$_2$(μ,η^6:η^6-P$_6$)] (**13**). Yield (combined): ~500 mg. The complexes **12** and **13** could not be separated. **11:** Yield 340 mg (25%). ^{1}H NMR (CD_2Cl_2) δ/ppm = 4.42 (m, CpH), 4.32 (br, CpH), 0.90 (s, ^{t}Bu); ^{13}C{^{1}H} NMR (CD_2Cl_2) δ/ppm = 223.81 (q, $^2J_{C,P}$ = 2.3 Hz, CO), 122.06 (s, C-^{t}Bu), 84.00 (q, $^2J_{C,P}$ = 1.7 Hz, C-H), 83.52 (br, C-H), 31.41 (s, Me), 31.16 (s, C(Me)$_3$); ^{31}P{^{1}H} NMR (CD_2Cl_2) δ/ppm = –345.9 (s, P$_3$). Anal. calcd. for [Cp'Mo(CO)$_2$P$_3$]: C, 36.09; H, 3.58. Found: C, 36.32; H, 3.56. EI-MS (CH_2Cl_2) *m/q* (%) = 367.9 (33) [*M*]$^+$, 340.0 (34) [*M*–CO]$^+$, 310.0 (100) [*M*–2CO)]$^+$. IR (KBr) $\tilde{\nu}$/cm^{-1} = 2959 (w), 2923 (vw), 2857 (vw), 1987 (vs), 1933 (vs), 1649 (w), 1458 (w), 1267 (w), 824 (m), 562 (m), 516 (m), 451 (m). **12**: ^{31}P{^{1}H} NMR (CD_2Cl_2) δ/ppm = –48.5 (s, P$_2$). **13**: ^{31}P{^{1}H} NMR (CD_2Cl_2) δ/ppm = –349.2 (s, P$_6$).

Thermolysis of [{Cp''Mo(CO)$_2$}$_2$] and As$_4$ (**14**, **15**, **16**): 1 g [{Cp''Mo(CO)$_2$}$_2$] (1.51 mmol) were placed in a round bottom flask. To this a hot solution (250 mL) of freshly prepared As$_4$ in diisopropylbenzene (DIB) was added. The reaction mixture was gently refluxed for 20 h under constant stirring. After cooling the reaction to room temperature the DIB was removed under reduced pressure. The crude product was dissolved in 20 mL of CH_2Cl_2 and mixed with ~10 g of silica and subsequently dried in vacuum until a brown freely flowing powder was obtained. This was placed on top of a chromatographic column (30 × 3 cm, packed with *n*-pentane). Elution with *n*-pentane affords a first yellow fraction of [Cp''Mo(CO)$_2$(η^3-As$_3$)] (**14**). Addition of toluene (elution with toluene/*n*-pentane ~ 1:2 to 1:1) results in the elution of a dark red band which contains the starting material [{Cp''Mo(CO)$_2$}$_2$] (Mo-Mo triple bond) and the analog [{Cp''Mo(CO)$_3$}$_2$] (**15**) with a Mo-Mo single bond. During the chromatography, the glass of the column was damaged showing a small crack, but the chromatography could still be completed. Finally elution with pure toluene afforded a dark green fraction which contains the side-product [Cp''$_3$Mo$_3$(CO)(μ-O)As$_3$] (**16**). This side-product was not pure. The origin of the bridging oxygen atom in **16** remains unclear. Possible explanations would be atmospheric O_2 or residual H_2O from the silica. The fact, that the starting material is still present after 20 h as well as the fact, that the side product 16 still contains one terminal (CO) ligand can be viewed as an indication that the reaction temperature was too low to thermally remove all CO ligands during this reaction. **15**: EI-MS (CH_2Cl_2) *m/q* (%) = 715.0 (<1) [*M*]$^+$, 658.1 (2) [*M*–2CO]$^+$, 630.1 (2) [*M*–3CO]$^+$, 600.1 (3) [*M*–4CO]$^+$, 359.1 (55) [Cp''Mo(CO)$_3$)]$^+$. **16**: EI-MS (CH_2Cl_2) *m/q* (%) = 1087.5 (20) [*M*]$^+$, 1059.6 (100) [*M*–CO]$^+$, 543.9 (1) [*M*]$^{2+}$, 529.9 (10) [*M*–CO]$^{2+}$.

Thermolysis of [{Cp*Mo(CO)$_2$}$_2$] and As$_4$ (**17**, **18**, **19**): 1.7 g [{Cp*Mo(CO)$_2$}$_2$] (2.94 mmol) were placed in a 1 L round bottom flask. To this a hot solution (~250 mL) of freshly prepared As$_4$ in DIB was added. Immediately, rigorous refluxing was started under constant stirring. After approximately 40 min another freshly prepared As$_4$ solution in DIB (~250 mL) was added to the reaction. After 24 h of intensive reflux, the heating was removed and the reaction was allowed to cool to room temperature. Subsequently, the DIB was removed under reduced pressure. The crude product was dissolved in 20 mL of CH_2Cl_2 and mixed with ~10 g of silica and subsequently dried in vacuum until a dark brown freely flowing powder was obtained. This was placed on top of a chromatographic column (30 × 3 cm, packed with *n*-hexane). The first fraction shows a dark blue to purple color. It most probably contains [(Cp*Mo)$_2$(μ,η^5:η^5-As$_5$)] (**17**) as the

major product although it was not completely pure. Yield (not pure): 840 mg (34%). Further elution with *n*-hexane affords a long red to brown fraction. This fraction contains the two products $[(Cp^*Mo)_2(\mu,\eta^6{:}\eta^6\text{-}As_6)]$ (**18**) and $[(Cp^*Mo)_3(\mu_3\text{-}As)(\mu_3\text{-}As_4)]$ (**19**) which could not be separated but could be identified by X-ray crystallography next to each other. Yield (combined): 780 mg.

X-ray crystallography

All diffraction experiments were performed at 123 K. The data sets were either collected on a Rigaku (former: Agilent Technologies or Oxford Diffraction) Gemini (R) Ultra, SuperNova or GV1000 diffractometer with CuK_α radiation. Crystallographic data together with the details of the experiments are given in the Tables 1-6. For all compounds that could not be refined completely during this work, the determined unit cells and the space groups are reported. All crystal preparations were performed under mineral oil. The cell determination, data reduction and absorption correction were performed with the help of the CrysAlis PRO software.[34] The structure solution and refinement was done with ShelX.[35] The H atoms were calculated geometrically and a riding model was used during the refinement process. Graphical material was created with Olex2.[36]

Table 1. Crystallographic details for the compound **1-3**.

Identification code	**1**	**2**	**3**
formula	$C_{36}AlF_{45}O_3$	$C_{37}H_2AlCl_2F_{46}O_3Tl$	$C_{89}H_{27}Al_2Cl_6Cu_2F_{92}N_7O_6$
weight [g·mol^{-1}]	1362.34	1670.64	3431.91
Temperature [K]	123.00(14)	123.01(14)	123.1(3)
crystal system	triclinic	triclinic	trigonal
space group	*P*–1	*P*–1	*P*–3
a [Å]	10.6203(2)	11.0920(2)	14.36351(9)
b [Å]	11.3295(3)	14.6028(2)	14.36351(9)
c [Å]	18.1366(6)	16.1231(2)	15.72381(12)
α [°]	74.166(3)	81.3970(10)	90
β [°]	73.704(2)	71.145(2)	90
γ [°]	85.079(2)	68.886(2)	120
V [Å^3]	2014.99(10)	2303.85(7)	2809.37(4)
Z	2	2	1
ρ_{calc} [g·cm^{-3}]	2.245	2.408	2.029
μ [mm^{-1}]	2.856	10.178	3.904
F(000)	1316.0	1580.0	1672.2
crystal size [mm^3]	0.486 × 0.291 × 0.145	0.613 × 0.440 × 0.210	0.269 × 0.206 × 0.183
diffractometer	Gemini Ultra	GV1000	Gemini Ultra
absorption correction	gaussian	gaussian	gaussian
T_{min}/T_{max}	0.492 / 0.704	0.047 / 0.289	0.513 / 0.602
radiation [Å]	CuK_α	CuK_α	CuK_α
2Θ range [°]	8.112 to 133.446	5.796 to 149.094	7.106 to 131.962
completeness	0.970	0.999	1.000
reflns collected/unique	16815 / 7069	35753 / 9214	54098 / 3271
R_{int}/R_{sigma}	0.0265 / 0.0298	0.0726 / 0.0486	0.0329 / 0.0105
data/restraints/parameters	7069 / 0 / 766	9214 / 0 / 812	3271 / 1 / 335
GOF on F^2	1.028	1.081	1.054
R_1/wR_2 [$I \geq 2\sigma(I)$]	0.0289 / 0.0733	0.0504 / 0.1287	0.0357 / 0.0883
R_1/wR_2 [all data]	0.0361 / 0.0759	0.0505 / 0.1288	0.0379 / 0.0896
max/min $\Delta\rho$ [e·Å^{-3}]	0.39 / –0.39	2.59 / –2.64	0.58 / –0.84

Table 2. Crystallographic details for the compound **4-6**.

Identification code	**4**	**5**	**6**
formula	$C_{102.6}H_{46.6}Al_2Cl_{2.8}Cu_2F_{92}Fe_2N_{4.6}O_6P_{10}$	$C_{15}H_{15}FeMoO_5P_5$	$C_{62}H_{30}AlAuF_{46}Fe_2Mo_2O_9P_{10}$
weight [g·mol^{-1}]	3889.34	581.91	2630.08
Temperature [K]	123.1(2)	123.00(14)	123.00(14)
crystal system	monoclinic	monoclinic	monoclinic
space group	$P2_1/n$	$P2_1/c$	$P2_1/c$
a [Å]	11.46543(5)	15.2810(3)	21.95786(9)
b [Å]	19.19929(8)	10.6446(2)	13.27421(5)
c [Å]	30.69582(13)	13.6296(3)	28.26990(11)
α [°]	90	90	90
β [°]	92.1199(4)	105.667(2)	98.2186(4)
γ [°]	90	90	90
V [Å^3]	6752.39(5)	2134.63(8)	8155.29(6)
Z	2	4	4
ρ_{calc} [g·cm^{-3}]	1.913	1.811	2.142
μ [mm^{-1}]	5.490	14.031	11.985
F(000)	3808.0	1152.0	5064.0
crystal size [mm^3]	0.350 × 0.259 × 0.125	0.185 × 0.096 × 0.030	0.202 × 0.154 × 0.033
diffractometer	Gemini Ultra	Gemini Ultra	Gemini Ultra
absorption correction	gaussian	gaussian	analytical
T_{min}/T_{max}	0.317 / 0.599	0.265 / 0.686	0.242 / 0.741
radiation [Å]	CuK_α	CuK_α	CuK_α
2*Θ* range [°]	7.378 to 132.208	10.258 to 132.038	7.008 to 134.006
completeness	0.997	0.997	0.995
reflns collected/unique	108918 / 11786	11322 / 3711	102484 / 14477
R_{int}/R_{sigma}	0.0298 / 0.0146	0.0373 / 0.0303	0.0316 / 0.0158
data/restraints/parameters	11786 / 27 / 1091	3711 / 0 / 249	14477 / 0 / 1208
GOF on F^2	1.053	1.048	1.044
R_1/wR_2 [$I \geq 2\sigma(I)$]	0.0332 / 0.0922	0.0346 / 0.0900	0.0173 / 0.0440
R_1/wR_2 [all data]	0.0348 / 0.0932	0.0392 / 0.0919	0.0196 / 0.0444
max/min $\Delta\rho$ [e·Å^{-3}]	1.01 / –0.59	0.96 / –0.66	0.96 / –0.59

Table 3. Crystallographic details for the compound **7-9**.

Identification code	**7**	**8**	**9**
formula			$C_{59}H_{38}Al_2F_{72}Fe_2O_8P_{10}$
weight [g·mol^{-1}]			2718.25
Temperature [K]			123(1)
crystal system	triclinic	orthorhombic	triclinic
space group	*P*–1	*Pccn*	*P*–1
a [Å]	19.8320(6)	18.65262(16)	12.1363(2)
b [Å]	20.0816(3)	33.7795(3)	13.0745(2)
c [Å]	20.1389(7)	25.6893(3)	15.2237(3)
α [°]	96.091(2)	90	101.090(1)
β [°]	105.294(3)	90	96.220(1)
γ [°]	94.346(2)	90	92.894(1)
V [Å^3]	7647.6(4)	16186.2(3)	2350.27(7)
Z			1
ρ_{calc} [g·cm^{-3}]			1.921
μ [mm^{-1}]			6.078
F(000)			1332.0
crystal size [mm^3]			0.296 × 0.191 × 0.144
diffractometer			Gemini R Ultra
absorption correction			analytical
T_{min}/T_{max}			0.351 / 0.603
radiation [Å]			CuK_α
2*Θ* range [°]			5.96 to 133.24
completeness			0.991
reflns collected/unique			22048 / 8263
R_{int}/R_{sigma}			0.0176 / 0.0192
data/restraints/parameters			8263 / 18 / 776
GOF on F^2			1.067
R_1/wR_2 [$I \geq 2\sigma(I)$]			0.0325 / 0.0891
R_1/wR_2 [all data]			0.0342 / 0.0900
max/min $\Delta\rho$ [e·Å^{-3}]			0.67 / –0.52

Table 4. Crystallographic details for the compound **10-12**.

Identification code	**10**	**11**	**12**
formula		$C_{11}H_{13}MoO_2P_3$	
weight [g·mol^{-1}]		366.06	
Temperature [K]		123(1)	
crystal system	monoclinic	monoclinic	triclinic
space group	$P2_1/c$	$P2_1/n$	$P\bar{1}$
a [Å]	20.3022(2)	8.5392(1)	12.9801(4)
b [Å]	20.9577(2)	15.1355(2)	13.6040(3)
c [Å]	29.9950(3)	10.9224(1)	14.0842(3)
α [°]	90	90	96.143(2)
β [°]	106.1825(12)	101.988(1)	90.267(2)
γ [°]	90	90	104.103(2)
V [Å^3]	12256.8(2)	1380.88(3)	2396.98(11)
Z		4	
ρ_{calc} [g·cm^{-3}]		1.761	
μ [mm^{-1}]		10.962	
$F(000)$		728.0	
crystal size [mm^3]		0.322 × 0.149 × 0.125	
diffractometer		Gemini R Ultra	
absorption correction		analytical	
T_{min}/T_{max}		0.183 / 0.470	
radiation [Å]		CuK_α	
2Θ range [°]		10.14 to 133.16	
completeness		1.000	
reflns collected/unique		22410 / 2435	
R_{int}/R_{sigma}		0.0890 / 0.0345	
data/restraints/parameters		2435 / 0 / 157	
GOF on F^2		1.080	
R_1/wR_2 [$I \geq 2\sigma(I)$]		0.0263 / 0.0687	
R_1/wR_2 [all data]		0.0268 / 0.0692	
max/min $\Delta\rho$ [e·Å^{-3}]		0.37 / –1.04	

Table 5. Crystallographic details for the compound **13-15**.

Identification code	**13**	**14**	**15**
formula	$C_{18}H_{26}Mo_2P_6$	$C_{15}H_{21}As_3MoO_2$	$C_{32}H_{42}Mo_2O_6$
weight [g·mol^{-1}]	620.09	554.02	714.54
Temperature [K]	123(1)	123(1)	123(1)
crystal system	monoclinic	triclinic	orthorhombic
space group	$P2_1/c$	$P\bar{1}$	$Pnnm$
a [Å]	23.0703(2)	8.4799(2)	8.3289(1)
b [Å]	793.900(1)	9.8178(3)	10.5132(1)
c [Å]	12.5936(1)	13.0795(3)	18.1959(2)
α [°]	90	69.001(2)	90
β [°]	105.822(1)	83.334(2)	90
γ [°]	90	64.467(2)	90
V [Å^3]	2219.19(3)	916.37(5)	1593.30(3)
Z	4	2	2
ρ_{calc} [g·cm^{-3}]	1.856	2.008	1.489
μ [mm^{-1}]	13.361	11.899	6.769
$F(000)$	1232.0	536.0	732.0
crystal size [mm^3]	0.102 × 0.051 × 0.030	0.346 × 0.266 × 0.132	0.134 × 0.125 × 0.069
diffractometer	SuperNova	SuperNova	SuperNova
absorption correction	analytical	analytical	analytical
T_{min}/T_{max}	0.338 / 0.710	0.093 / 0.408	0.524 / 0.684
radiation [Å]	CuK_α	CuK_α	CuK_α
2Θ range [°]	7.3 to 149.06	7.24 to 147.38	9.72 to 141.14
completeness	0.992	0.976	0.973
reflns collected/unique	74122 / 4501	19657 / 3635	5117 / 1540
R_{int}/R_{sigma}	0.0412 / 0.0126	0.0347 / 0.0151	0.0140 / 0.0102
data/restraints/parameters	4501 / 0 / 242	3635 / 0 / 197	1540 / 0 / 100
GOF on F^2	1.093	1.178	1.062
R_1/wR_2 [$I \geq 2\sigma(I)$]	0.0316 / 0.0908	0.0244 / 0.0633	0.0186 / 0.0481
R_1/wR_2 [all data]	0.0331 / 0.0960	0.0245 / 0.0634	0.0192 / 0.0484
max/min $\Delta\rho$ [e·Å^{-3}]	2.56 / –0.95	0.69 / –0.69	0.87 / –0.57

Table 6. Crystallographic details for the compound **16**, **17** and **19**.

Identification code	**16**	**17**	**19**
formula	$C_{101}H_{150}As_6Mo_6O_4$		$C_{30}H_{45}As_5Mo_3$
weight [g·mol^{-1}]	2453.38		1068.08
Temperature [K]	123(1)		123(1)
crystal system	triclinic	triclinic	triclinic
space group	*P*–1	*P*–1	*P*–1
a [Å]	10.3308(7)	9.0602(6)	8.0884(3)
b [Å]	14.4418(10)	11.7163(9)	11.2872(3)
c [Å]	17.9270(14)	12.0974(8)	18.3746(5)
α [°]	88.553(6)	107.310(6)	89.713(2)
β [°]	75.951(6)	90.832(5)	88.465(2)
γ [°]	81.736(6)	90.623(6)	78.491(3)
V [Å^3]	2567.6(3)	1225.72(15)	1643.20(9)
Z	1		2
ρ_{calc} [g·cm^{-3}]	1.587		2.159
μ [mm^{-1}]	8.350		14.967
F(000)	1238.0		1032.0
crystal size [mm^3]	0.441 × 0.074 × 0.023		0.137 × 0.034 × 0.025
diffractometer	Gemini R Ultra		SuperNova
absorption correction	analytical		analytical
T_{min}/T_{max}	0.126 / 0.827		0.368 / 0.724
radiation [Å]	CuK_α		CuK_α
2*Θ* range [°]	6.18 to 133.76		8 to 133.2
completeness	0.987		0.997
reflns collected/unique	32862 / 9020		11570 / 5794
R_{int}/R_{sigma}	0.0668 / 0.0516		0.0221 / 0.0307
data/restraints/parameters	9020 / 0 / 524		5794 / 0 / 403
GOF on F^2	1.078		1.029
R_1/wR_2 [$I \geq 2\sigma(I)$]	0.0543 / 0.1503		0.0236 / 0.0540
R_1/wR_2 [all data]	0.0575 / 0.1532		0.0287 / 0.0560
max/min $\Delta\rho$ [e·Å^{-3}]	1.38 / –1.40		0.75 / –0.68

11.5 References

[1] S. Welsch, PhD-thesis, Universität Regensburg (Regensburg), **2010**.

[2] M. Fleischmann, S. Welsch, E. V. Peresypkina, A. V. Virovets, M. Scheer, *Chem. Eur. J.* **2015**, *21*, 14332-14336.

[3] M. Fleischmann, F. Dielmann, L. J. Gregoriades, E. V. Peresypkina, A. V. Virovets, S. Huber, A. Y. Timoshkin, G. Balázs, M. Scheer, *Angew. Chem. Int. Ed.* **2015**, *54*, 13110-13115; *Angew. Chem.* **2015**, *127*, 13303-13308.

[4] A. Kraft, N. Trapp, D. Himmel, H. Böhrer, P. Schlüter, H. Scherer, I. Krossing, *Chem. Eur. J.* **2012**, *18*, 9371-9380.

[5] L. Dütsch, Master's thesis, Universität Regensburg (Regensburg), **2015**.

[6] [Cu2(**A**)4]*n*[FAl]2*n* was obtained from an indirect synthetic approach by reacting [Tl(CH2Cl2)*x*][Li(FAl)2] with CuCl and the *cyclo*-P5 complex **A**.

[7] J. Bai, A. V. Virovets, M. Scheer, *Angew. Chem. Int. Ed.* **2002**, *41*, 1737-1740; *Angew. Chem.* **2002**, *114*, 1808-1811.

[8] J. Bai, A. V. Virovets, M. Scheer, *Science* **2003**, *300*, 781-783.

[9] M. Scheer, J. Bai, B. P. Johnson, R. Merkle, A. V. Virovets, C. E. Anson, *Eur. J. Inorg. Chem.* **2005**, *2005*, 4023-4026.

[10] M. Scheer, A. Schindler, C. Gröger, A. V. Virovets, E. V. Peresypkina, *Angew. Chem. Int. Ed.* **2009**, *48*, 5046-5049; *Angew. Chem.* **2009**, *121*, 5148-5151.

[11] F. Dielmann, A. Schindler, S. Scheuermayer, J. Bai, R. Merkle, M. Zabel, A. V. Virovets, E. V. Peresypkina, G. Brunklaus , H. Eckert, M. Scheer, *Chem. Eur. J.* **2012**, *18*, 1168-1179.

[12] O. J. Scherer, T. Brück, *Angew. Chem. Int. Ed.* **1987**, *26*, 59-59; *Angew. Chem.* **1987**, *99*, 59-59.

[13] B. Krämer, Master's thesis, Universität Regensburg (Regensburg), **2014**; unpublished results.

[14] B. Rink, O. J. Scherer, G. Heckmann, G. Wolmershauser, *Chem. Ber.* **1992**, *125*, 1011-1016.

[15] For details please see experimental part.

[16] P. J. Sullivan, A. L. Rheingold, *Organometallics* **1982**, *1*, 1547-1549.

[17] R. F. Winter, W. E. Geiger, *Organometallics* **1999**, *18*, 1827-1833.
[18] M. V. Butovskiy, G. Balázs, M. Bodensteiner, E. V. Peresypkina, A. V. Virovets, J. Sutter, M. Scheer, *Angew. Chem. Int. Ed.* **2013**, *52*, 2972-2976; *Angew. Chem.* **2013**, *125*, 3045-3049.
[19] M. Fleischmann, S. Welsch, H. Krauss, M. Schmidt, M. Bodensteiner, E. V. Peresypkina, M. Sierka, C. Gröger, M. Scheer, *Chem. Eur. J.* **2014**, *20*, 3759-3768.
[20] K. Wade, *Adv. Inorg. Chem. Radiochem.* **1976**, *18*, 1-66.
[21] K. Wade, *Nucl. Chem. Lett.* **1972**, *8*, 559-562.
[22] J. D. Corbett, in *Prog. Inorg. Chem.*, John Wiley & Sons, Inc., **2007**, pp. 129-158.
[23] S. Scharfe, F. Kraus, S. Stegmaier, A. Schier, T. F. Fässler, *Angew. Chem. Int. Ed.* **2011**, *50*, 3630-3670; *Angew. Chem.* **2011**, *123*, 3712-3754.
[24] O. J. Scherer, H. Sitzmann, G. Wolmershauser, *Acta Cryst. C* **1985**, *41*, 1761-1763.
[25] M. Fleischmann, C. Heindl, M. Seidl, G. Balázs, A. V. Virovets, E. V. Peresypkina, M. Tsunoda, F. P. Gabbaï, M. Scheer, *Angew. Chem. Int. Ed.* **2012**, *51*, 9918-9921; *Angew. Chem.* **2012**, *124*, 10056-10059.
[26] I. Bernal, H. Brunner, W. Meier, H. Pfisterer, J. Wachter, M. L. Ziegler, *Angew. Chem. Int. Ed.* **1984**, *23*, 438-439; *Angew. Chem.* **1984**, *96*, 428-429.
[27] R. P. Hughes, J. R. Lomprey, A. L. Rheingold, G. P. A. Yap, *J. Organomet. Chem.* **1996**, *517*, 63-70.
[28] W. Clegg, N. A. Compton, R. J. Errington, N. C. Norman, *Acta Cryst. C* **1988**, *44*, 568-570.
[29] O. J. Scherer, H. Sitzmann, G. Wolmershäuser, *Angew. Chem. Int. Ed.* **1989**, *28*, 212-213; *Angew. Chem.* **1989**, *101*, 214-215.
[30] A. L. Rheingold, M. J. Foley, P. J. Sullivan, *J. Am. Chem. Soc.* **1982**, *104*, 4727-4729.
[31] O. J. Scherer, J. Braun, G. Wolmershäuser, *Chem. Ber.* **1990**, *123*, 471-475.
[32] R. D. Adams, D. M. Collins, F. A. Cotton, *Inorg. Chem.* **1974**, *13*, 1086-1090.
[33] R. J. Klingler, W. M. Butler, M. D. Curtis, *J. Am. Chem. Soc.* **1978**, *100*, 5034-5039.
[34] different versions, Rigaku (former: Agilent Technologies Ltd. or Oxford Diffraction Ltd.)
[35] G. M. Sheldrick, *Acta Cryst. A* **2008**, *64*, 112-122.
[36] O. V. Dolomanov, L. J. Bourhis, R. J. Gildea, J. A. K. Howard, H. Puschmann, *J. Appl. Crystallogr.* **2009**, *42*, 339-341.

12 Conclusion

12.1 Coordination chemistry of E_n ligand complexes towards monovalent cations

A major part of this thesis deals with the investigation of the coordination chemistry of E_n ligand complexes towards monovalent cations in the presence of the weakly coordinating anions (WCAs) [TEF] and [FAl]. The syntheses of new salts containing the WCA [FAl] in addition to the published Ag^+ salt represent valuable research targets. Therefore, the simple one-step synthesis of the Cu^+ source $[Cu(MeCN)_{3.5}][FAl]$ (**1**) is presented. The Tl^+ salt Tl[FAl] (**2**) could be synthesized in low yields and shows low solubility due to strong cation-anion interaction. However, the mixed Tl^+/Li^+ salt $[Tl(CH_2Cl_2)_x][Li\{FAl\}_2]$ (**3**) can be prepared easily and was described before by the author.[1] It can be used as a well-soluble Tl^+ source in CH_2Cl_2.

Scheme 1 summarizes results obtained from reactions of the *cyclo*-E_5 complexes $[Cp^*Fe(\eta^5\text{-}E_5)]$ (E = P(**A1**), As(**A2**)) with the monovalent cations Cu^+, Ag^+ and Tl^+. All presented products show a highly dynamic coordination behavior in solution. The exchange of the WCA [TEF] for the WCA [FAl] in a reaction with the *cyclo*-P_5 complex **A1** results in the formation of the one-dimensional polymer $[Cu_2(\mathbf{A1})_4]_n[FAl]_{2n}$ (**4**). The analogues polymer with [TEF] has been described before but no satisfactory X-ray structure determination could be obtained. Due to the anion exchange to [FAl] the crystal structure of **4** could finally be determined by X-ray diffraction analysis.[1] This polymer contains the unique paddle-wheel repeating unit $[Cu_2(\mathbf{A1})_3]^{2+}$. Additionally, the reactivity of the *cyclo*-E_5 complexes **A1** and **A2** towards Tl^+ including the WCA [FAl] was reported to yield isolated $[Tl(\mathbf{L})_3]^+$ (**L** = **A1**(**5**), **A2**(**6**)) complex cations which show a trigonal planar geometry in the solid state.[1,2] Here, **A1** and **A2** show a η^5 coordination towards Tl^+ via the *cyclo*-E_5 plane. These results (**4-6**) are reported in the general introduction and were published prior to the submission of this thesis together with results of Dr. Stefan Welsch and others but were excluded from the detailed discussion.[1,2] The reaction of the Cu^+ salt **1** with **A1** does not yield the one-dimensional polymer **4** as expected but leads to the formation of the dinuclear complex $[Cu_2(\mathbf{A1})_2(MeCN)_4][FAl]_2$ (**7**) instead. When **A1** is reacted with Ag[FAl] the tetranuclear complex $[Ag_4(\mathbf{A1})_8]$ (**8**) stabilized by eight ligands of **A1** is obtained selectively. In **8**, four different coordination modes of the *cyclo*-P_5 ligand **A1** (**I-IV**) can be observed in the solid state. Among these, two (**I** and **IV**) were predicted to be present in the gas phase by DFT calculations but have not been

proven experimentally, prior to this work. The structure of **8** can be rationalized by a depolymerization of the previously described one-dimensional polymer $[Ag(\mathbf{A1})_2]_n[TEF]_n$ due to the increased size of the [FAl] anion compared to [TEF].

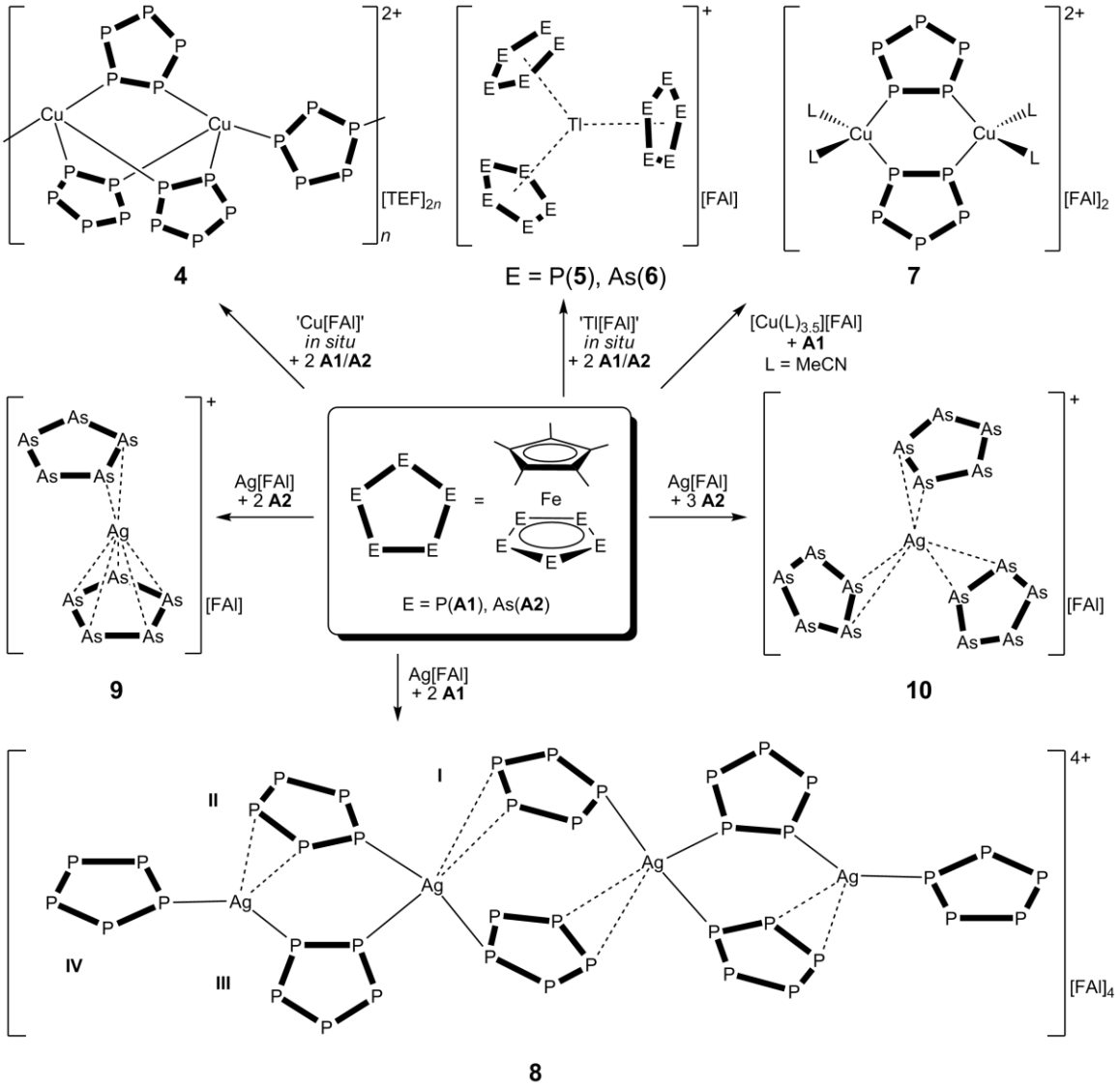

Scheme 1. Summary of the results obtained from reactions of the *cyclo*-E_5 complexes **A1** and **A2**.

Reaction of the *cyclo*-As_5 complex **A2** with Ag[FAl] in a 2:1 and a 3:1 molar ratio selectively yield the coordination compounds $[Ag(\mathbf{A2})_2][FAl]$ (**9**) and $[Ag(\mathbf{A2})_3][FAl]$ (**10**). These represent the first Ag^+ complexes of **A2**. For **9** a peculiar feature is observed in its crystal structure. The central Ag^+ cation exhibits very large oblate atomic displacement parameters when described by an anisotropic approximation of Ag. Whether this behavior is caused by static disorder of the Ag atom over several close positions or by a thermal movement of the central Ag atom inside a cavity composed of the 10 As atoms of the two π coordinating *cyclo*-As_5 ligands **A2** remains to be answered in the near future. Supporting DFT calculations are currently being performed by Prof. Dr. Marek

Sierka (Friedrich-Schiller-Universität Jena). In **10** the complex cation $[Ag(\mathbf{A2})_3]^+$ shows a trigonal planar geometry around Ag which can be compared very well to the analogues Tl^+ compound **6**. However, in **10** the **A2** ligand is π donating in a η^2 coordination mode of one As-As bond instead of the η^5 coordination mode which is present in **6**.

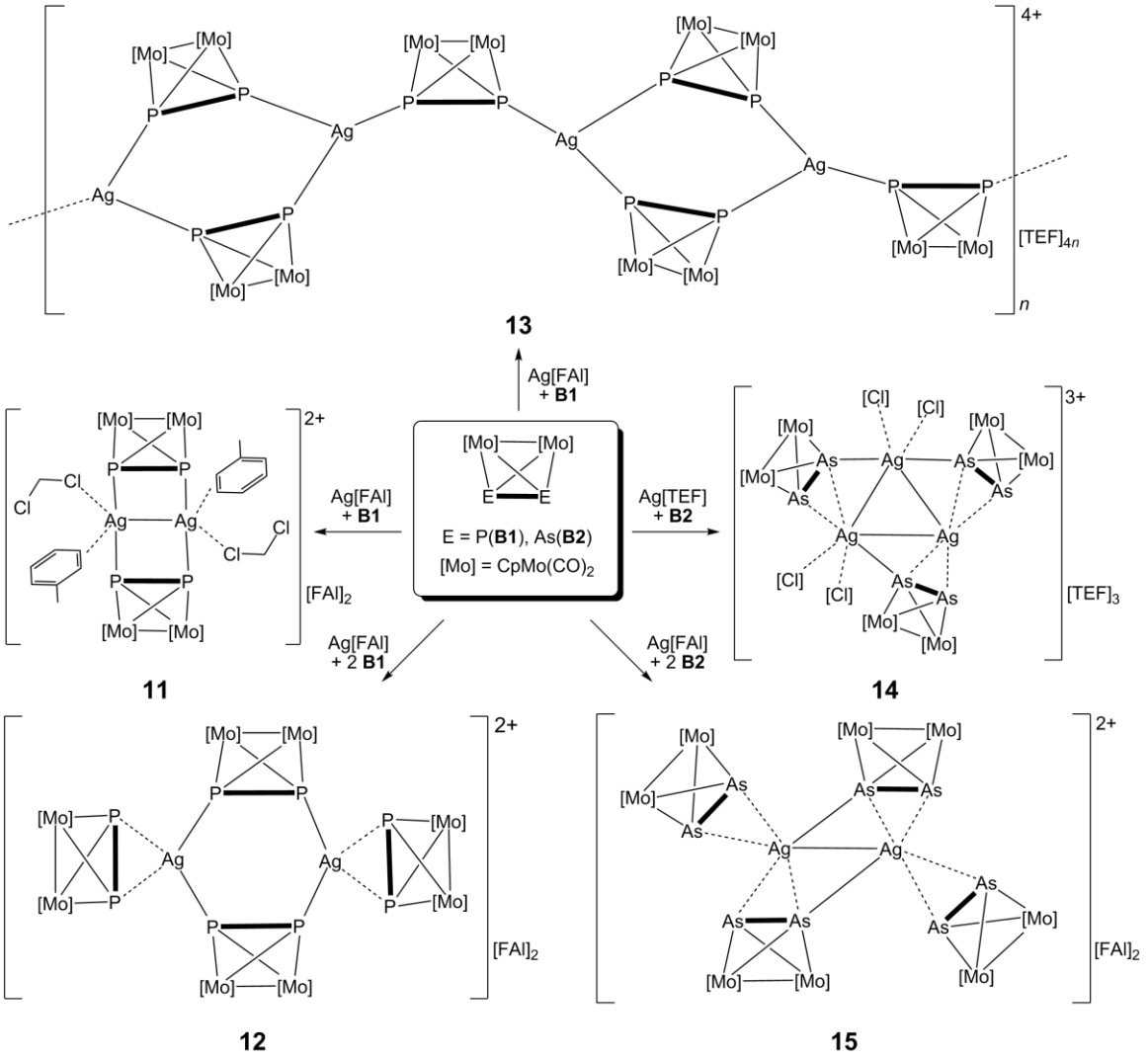

Scheme 2. Summary of the results obtained from reactions of the tetrahedrane complexes **B1** and **B2** with Ag^+.

Scheme 2 summarizes results obtained from reactions of the tetrahedrane complexes $[\{CpMo(CO)_2\}_2(\mu,\eta^2{:}\eta^2\text{-}E_2)]$ (E = P(**B1**), As(**B2**)) with Ag^+. From reactions of the P_2 ligand complex **B1** with the Ag^+ salts Ag[TEF] and Ag[FAl] three new compounds with a Ag:**B1** ratio of 1:1 (**11**), 1:2 (**12**) and 2:3 (**13**) could be obtained from separate reactions. The structure of **11** consists of a dicationic complex $[Ag_2(\mathbf{B1})_2(CH_2Cl_2)_2(C_7H_8)_2]^{2+}$ with a central $P_2Ag_2P_2$ ladder-type motif showing a Ag-Ag contact. The coordination sphere of each Ag atom in **11** is additionally saturated by one CH_2Cl_2 and one toluene solvent molecule. Therefore, **11** presents a possible starting material for supramolecular

chemistry by the introduction of organic linker molecules which should be able to substitute the coordinated solvent molecules. In contrast, **12** exhibits a dicationic complex $[Ag_2(\mathbf{B1})_4]^{2+}$ with a central six-membered Ag_2P_4 ring featuring two bridging **B1** ligands and two terminal **B1** ligands exhibiting a side-on coordination mode. This arrangement has already been reported for all coinage metals with different WCAs, except for [FAl]. Compound **13** with the general formula $[Ag_2(\mathbf{B1})_3]_n[TEF]_{2n}$ exhibits a one-dimensional polymeric structure consisting of six-membered Ag_2P_4 rings as repeating units in a zigzag chain interconnected by bridging **B1** ligands. It represents the first homoleptic coordination polymer of Ag^+ and **B1**. In addition, the coordination chemistry of the As_2 complex **B2** towards Ag^+ has been investigated for the first time. From these reactions the trinuclear complex $[Ag_3(\mathbf{B2})_3(CH_2Cl_2)_x][TEF]_3$ (**14**) showing a central triangle of three Ag atoms and the dinuclear complex $[Ag_2(\mathbf{B2})_4][FAl]_2$ (**15**) could be obtained. These preliminary investigations show that the As_2 complex **B2** is a valuable ligand for supramolecular chemistry and can stabilize multinuclear complexes exhibiting Ag-Ag contacts. Herein, **B2** shows a bridging $\eta^1{:}\eta^2$ coordination mode which has been very rarely observed for the P_2 analog **B1**.

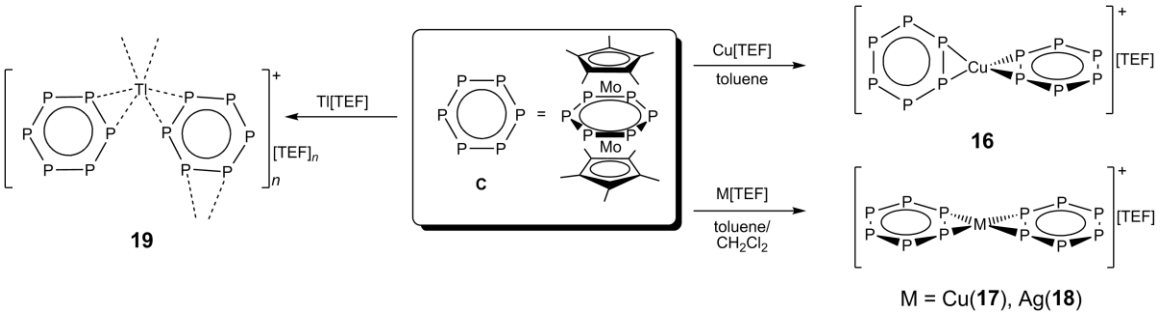

Scheme 3. Summary of the coordination compounds obtained from reactions of the *cyclo*-P_6 triple-decker complex **C** and the monovalent cations Cu^+, Ag^+ and Tl^+.

Scheme 3 summarizes coordination compounds which were obtained from reactions of the *cyclo*-P_6 triple-decker complex $[(Cp^*Mo)_2(\mu,\eta^6{:}\eta^6\text{-}P_6)]$ (**C**) with the monovalent cations Cu^+, Ag^+ and Tl^+. All presented results show a highly dynamic coordination behavior in solution. By adding donating solvents to CH_2Cl_2 in reactions with Cu^+ and Ag^+, the oxidation of **C** could successfully be prevented. From these reactions the $[M(\mathbf{C})_2][TEF]$ (M = Cu(**16**, **17**), Ag(**18**)) complexes were obtained. Compound **18** has been described before by Dr. Laurence Gregoriades obtained in a mixture with the oxidation product of **C** but it could not be isolated in pure form prior to this work. Interestingly, **16** and **17** represent two isomers with the same composition of the complex cation with either a distorted tetrahedral (**16**) or a distorted square planar (**17**) coordination environment around Cu^+. DFT calculations show that the equilibrium of

'tetrahedral' → 'square planar' geometry of the $[M(\mathbf{C})_2]^+$ complex cations is significantly shifted to the right side for M = Ag which is the reason why no tetrahedral Ag^+ complex of **C** could ever be observed in the solid state. For M = Cu however, both isomeric forms (**16** and **17**) of the complex cation are present in solution. It was demonstrated that both isomeric forms can be obtained selectively in the solid state by choosing either CH_2Cl_2/toluene (**17**) or pure toluene (**16**) as the solvent. Analysis of the crystal packing of the isostructural compounds **17** and **18** reveals a layered structure with alternating negatively charged layers of the [TEF] anions and positively charged layers of isolated $[M(\mathbf{C})_2]^+$ complex cations. Interestingly, the coordination environment of Tl^+ in **19** is distinctly different from Cu^+ and Ag^+ in **17** and **18**, however, their X-ray structures are closely related to each other. The larger Tl^+ cation shows further interconnection of the *cyclo*-P_6 ligands **C** inside the positively charged layers to form an extended 2D network which can therefore be regarded as a supramolecular analog of graphene. The preparation of **19** and preliminary results from the reaction of Cu^+ and **C** have already been reported in the Master's thesis of the author.

Additionally, the coordination chemistry of the 30 VE triple-decker complex $[Cp^*Fe(\mu,\eta^5{:}\eta^5\text{-}P_5)Mo(CO)_3]$ (**D**) towards coinage metal cations described by Dr. Stefan Welsch could be extended from Cu^+ and Ag^+ to Au^+ via structural characterization of the analogues Au^+ complex $[Au(\mathbf{D})_2][FAl]$ (**20**).

12.2 Oxidation chemistry of E_n ligand complexes

The oxidation chemistry of E_n ligand complexes has been investigated during this work. The application of WCAs in these reactions assures the stability of the obtained reactive cationic species and additionally increases the solubility of the formed ionic compounds. Scheme 4 illustrates the oxidation of the 28 VE *cyclo*-E_6 triple-decker complexes $[(Cp^RMo)_2(\mu,\eta^6{:}\eta^6\text{-}E_6)]$ (E = P, Cp^R = Cp, Cp*, $C_5(CH_2Ph)_5$; E = As, Cp^R = Cp*). It was demonstrated that single-electron oxidation leads to isolated cationic 27 VE complexes which retain their general triple-decker geometry in the solid state. Since crystals of **21a** and **21c** with the anion [TEF] were not suitable for single crystal X-ray diffraction analysis the structure of the cation could be determined from the analogs **21b** and **21d** containing the anion [FAl]. The *cyclo*-E_6 middle decks of the complexes are distorted from the initially perfect hexagonal geometry during oxidation. While **21b** shows two opposite P-P bonds to be slightly shortened, all other *cyclo*-E_6 complexes (**21d**, **21e**, **22**) show a bis-allylic distortion with an elongation of two opposite E-E bonds instead. Among these oxidized *cyclo*-E_6 complexes, **21c** and **21e** have been reported before by Dr. Laurence Gregoriades and Dr. Fabian Dielmann.

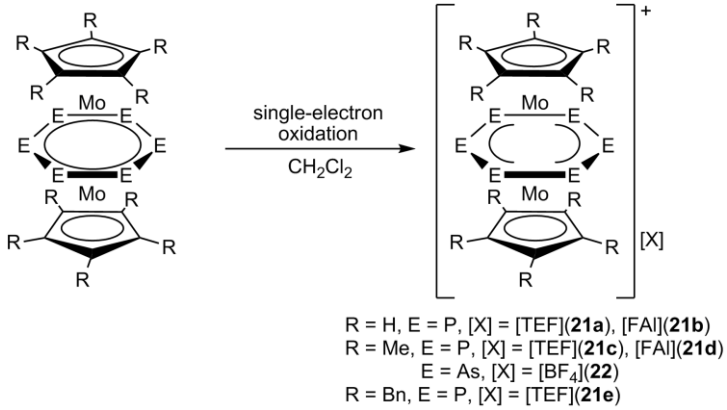

Scheme 4. Single-electron oxidation of *cyclo*-E_6 triple decker complexes $[(Cp^RMo)_2(\mu,\eta^6{:}\eta^6\text{-}E_6)]$.

Since reactions of Ag^+ with the P_2 complex **B1** result in the exclusive formation of coordination compounds instead of oxidation products it was necessary to prepare stronger oxidants with the WCAs [TEF] and [FAl]. For this reason the deep purple radical cation of thianthrene ($C_{12}H_8S_2$) $[Thia]^+$ was chosen. In the course of this work two general synthetic routes were developed which give access to the valuable starting materials [Thia][TEF] (**23a**) or [Thia][FAl] (**23b**), respectively in good yields. Among these, [Thia][TEF] is a well-soluble very strong oxidant that can now be prepared in a one-step reaction on a gram scale starting from the commercially available reagents $[NO][SbF_6]$ or $[NO][BF_4]$, thianthrene ($C_{12}H_8S_2$) and Li[TEF]. With the help of the strong oxidant $[Thia]^+$, the selective one-electron oxidation of **B1** was accomplished (see Scheme 5). The oxidized P_2 complex dimerizes via P-P bond formation yielding a dicationic complex $[\{Cp_2Mo_2(CO)_4\}_2(\mu_4,\eta^2{:}\eta^2{:}\eta^2{:}\eta^2\text{-}P_4)]^{2+}$ showing a central zigzag P_4 chain in the solid state. It was demonstrates that the cation of the well-soluble compound containing the [TEF] anion (**24a**) exhibits fast dynamic processes in CD_2Cl_2 solution rendering all P atoms equivalent on the NMR timescale but no dissociation takes place. The P_4 chain of **24a** can be obtained in a symmetric form by precipitation while during crystallization an unsymmetrical P_4 chain is formed. Interestingly, its analog (**24b**) containing the smaller WCA $[SbF_6]^-$ could be structurally characterized in its crystalline form showing a symmetric P_4 chain. The X-ray structure as well as the electrochemical and theoretical investigation of **24a** have been reported previously by Dr. Stefan Welsch but it was only obtained in trace amounts as a decomposition product prior to this work. The structure determination of **24a** was repeated by the author.

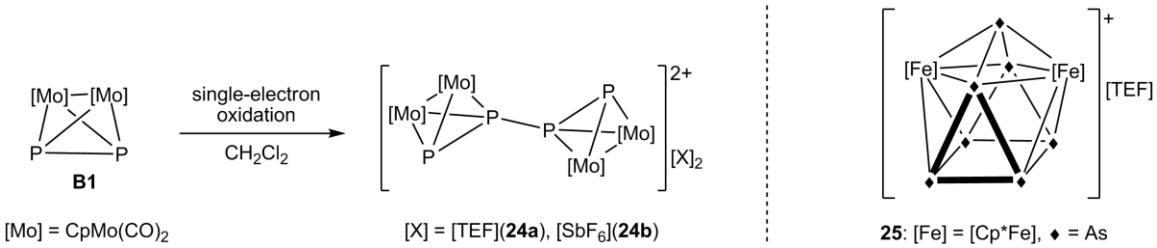

Scheme 5. (left) Oxidation and dimerization of the P_2 complex **B1**. (right) Representation of the complex cation in **25**.

Additionally, from reactions of the *cyclo*-As_5 complex [Cp*Fe(η^5-As_5)] (**A2**) with Ga^+ the formation of [(Cp*Fe)$_2$(As_7)][TEF] (**25**) was observed. The complex cation in **25** can be described as a $[As_7]^-$ anion stabilized by two $[Cp^*Fe]^+$ complex fragments. Alternatively, it can be described as a *nido*-type cluster of nine atoms (22 skeletal electrons) exhibiting a mono-capped square antiprism arrangement of the central [Fe_2As_7] cluster core. It is assumed to be the product of an initial oxidation of **A2**, but the exact reaction pathway could not be elucidated during the scope of this work.

12.3 Reactivity of E_n ligand complexes towards pre-assembled Cu^I building blocks

During this work the coordination chemistry of pre-assembled Cu^I complexes has been investigated in the course of an international cooperation with Dr. Christophe Lescop (Université de Rennes 1). The work on this topic focusses on trinuclear halide bridged Cu^I complexes which show a central $[Cu_3(\mu\text{-}X)_2(\mu\text{-dpmp})_2]^+$ (X = Cl, Br, I) core that is stabilized by the polyphosphine ligand bis(diphenylphosphinomethyl)-phenylphosphine (dpmp, Scheme 6). These cationic $[Cu_3X_2]^+$ building blocks were furthermore reacted with a variety of E_n ligand complexes shown in Scheme 6.

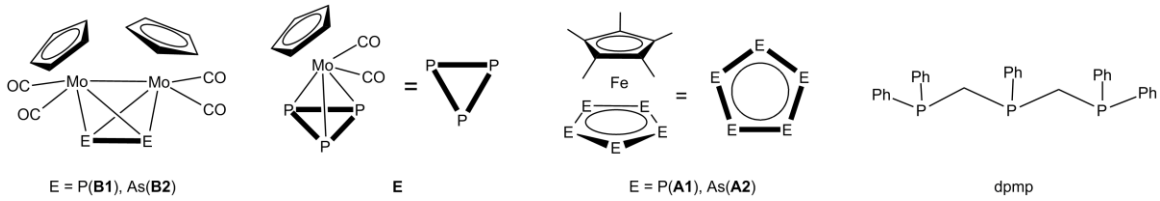

Scheme 6. Illustration of the polyphosphine ligand dpmp and the E_n ligand complexes which were reacted with the trinuclear Cu^I building blocks.

The preparation of the parent $[Cu_3X_2]^+$ building blocks is illustrated in Scheme 7. At the beginning it was demonstrated that **26a-c** with terminal MeCN ligands can easily be obtained by self-assembly in a one-step reaction of CuX, $[Cu(MeCN)_4][BF_4]$ and dpmp

from THF/MeCN solvent mixtures. The complex cations of **26a-c** have been described before in the literature with the $[ClO_4]^-$ anion. Since these complexes were shown to be unreactive towards E_n ligand complexes a new route had to be developed. By drying the complexes **26a-c** the MeCN ligands can be removed and the complexes are directly transformed to the reactive parent trinuclear complexes $[Cu_3(\mu\text{-}X)_2(\mu\text{-}dpmp)_2]^+$ (**27a-c**) with two vacant coordination sites on the terminal Cu atoms. It was shown that an alternative synthesis in CH_2Cl_2 directly yields **27a-c**. In the course of these investigations, **28b** and **28c** containing two weakly coordinating CH_2Cl_2 molecules could also be structurally characterized. The cores of the $[Cu_3(\mu\text{-}X)_2(\mu\text{-}dpmp)_2]^+$ complex cations are stable in solution when dissolved at low temperatures and show dynamic coordination behavior at elevated temperatures involving equilibria between different species. These equilibria cannot be shifted back by simply decreasing the temperature but the structural motifs of the $[Cu_3(\mu\text{-}X)_2(\mu\text{-}dpmp)_2]^+$ (X = Cl, Br, I) complex cations can be obtained selectively in the solid state upon crystallization under the applied reaction conditions.

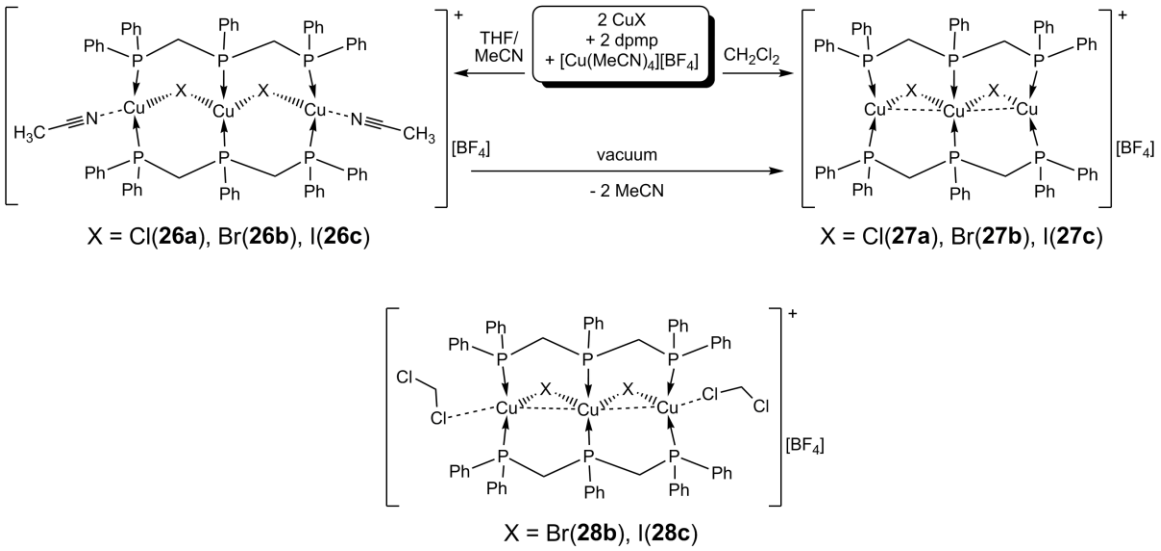

Scheme 7. Synthesis of the parent trinuclear Cu^I complexes.

The supramolecular coordination compounds which are obtained from reacting the pre-assembled $[Cu_3X_2]^+$ building blocks **27a-c** with E_n ligand complexes are summarized in Scheme 8. Reactions of **27a-c** with the E_2 complexes **B1** and **B2** lead to the isolation of the finite complexes $[Cu_3X_2(\mathbf{B1})]^+$ (X = Cl(**29a**), Br(**29b**), I(**29c**)) and $[Cu_3Cl_2(\mathbf{B2})]^+$ (**30**), respectively. The introduction of the *cyclo*-P_3 complex **E** affords the zigzag chain polymers $[Cu_3X_2(\mathbf{E})]_n[BF_4]_n$ (X = Cl(**31a**), Br(**31b**)) and the symmetrically substituted complex $[Cu_3I_2(\mathbf{E})_2]^+$ (**32**). Reactions of **27a-c** with the *cyclo*-E_5 complexes **A1** and **A2** lead either to the isostructural one-dimensional coordination polymers $[Cu_3X_2(\mathbf{A1})]_n[BF_4]_n$ (X = Cl(**33a**), Br(**33b**)) and $[Cu_3Cl_2(\mathbf{A2})]_n[BF_4]_n$ (**34**) or to the complex

$[Cu_3I_2(\mathbf{A1})_2]^+$ (**35**) containing two terminal ligands **A1**. In **33a**, **33b** and **34**, the *cyclo*-E_5 ligands **A1** and **A2** show a bridging σ-1,3-coordination of the E_5 rings. This bonding mode has been rarely observed for **A1** and it was unprecedented for **A2** prior to this work. Although all described syntheses are based on self-assembly of several components, the reactions proceed selectively and no formation of any side-product could be observed upon crystallization. The presented results demonstrate that the framework of the pre-assembled $[Cu_3(\mu\text{-}X)_2(\mu\text{-dpmp})_2]^+$ complex cations are stable towards the introduction of varying E_n ligand complexes. Interestingly, the intramolecular Cu-Cu distances inside the $[Cu_3X_2]^+$ building blocks are influenced by coordination of any ligands to the terminal Cu atoms. A comparison of analogues compounds demonstrates that a decrease of the bond length to the terminal ligand results in an elongation of the adjacent Cu-Cu distance inside the $[Cu_3X_2]^+$ building block which is also in accordance with presented DFT calculations.

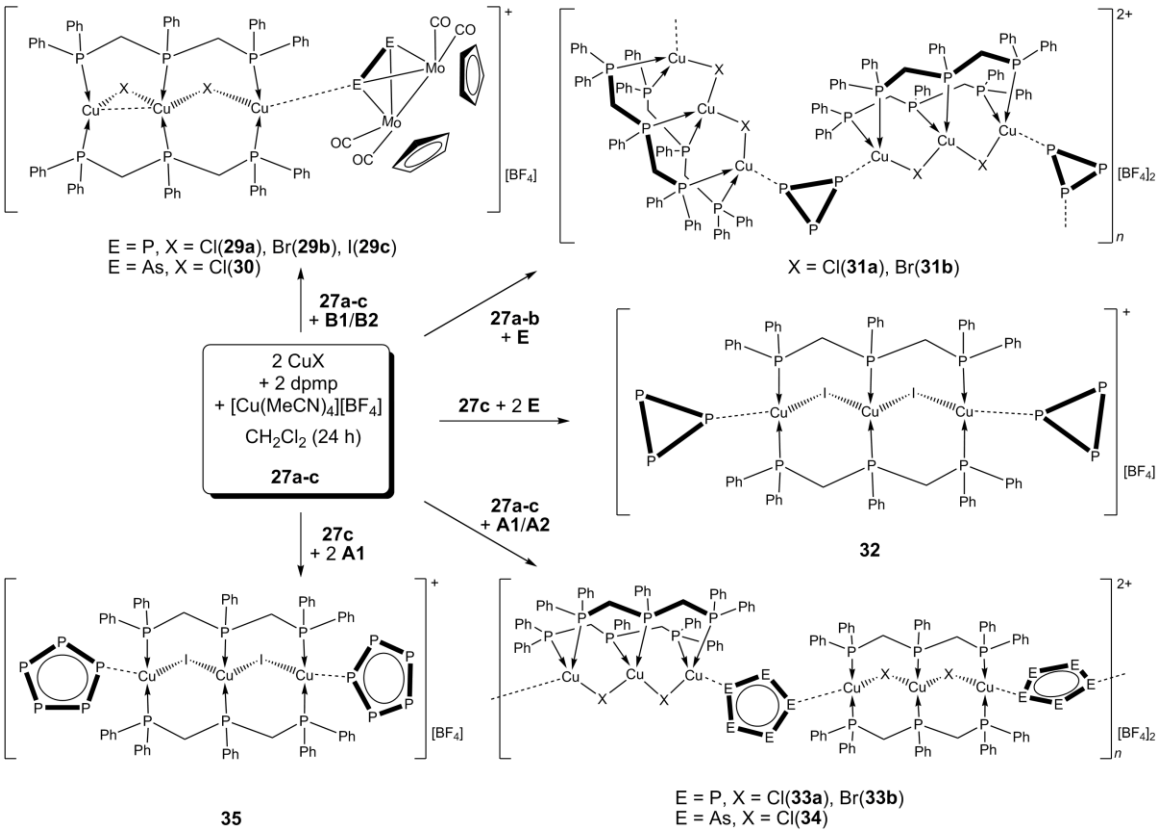

Scheme 8. Summary of the coordination compounds obtained from reactions of E_n ligand complexes and the pre-assemble $[Cu_3X_2]^+$ building blocks **27a-c**.

12.4 Reactivity of E_n ligand complexes towards the unusual Lewis acid [(*o*-$C_6F_4Hg)_3$]

It is well-known that the planar Lewis acid (perfluoro-*ortho*-phenylene)mercury (**F**) readily forms weak Lewis acid/base adducts in which the Lewis bases simultaneously interact with all three Hg centers of **F**. Additionally, it can build up alternating binary stacks with aromatic hydrocarbons and forms double-sandwich complexes with the metallocenes Cp_2Fe and Cp_2Ni. During this work the chemistry of E_n ligand complexes towards the trinuclear Lewis acid **F** has been investigated in the course of an international cooperation with the group of Prof. Dr. François Gabbaï (Texas A&M University). Preliminary results from the Master's thesis of the author have shown that **F** forms super-sandwich compounds showing weak Hg-P interactions instead of possible Hg-Cp interactions when reacted with the triple-decker complex $[(CpMo)_2(\mu,\eta^6{:}\eta^6\text{-}P_6)]$.[3] Scheme 9 summarizes the products obtained from the reactions of **F** with the *cyclo*-E_5 complexes $[Cp^*Fe(\eta^5\text{-}E_5)]$ (E = P(**A1**), As(**A2**)), the *cyclo*-P_3 complex $[CpMo(CO)_2(\eta^3\text{-}P_3)]$ (**E**) as well as the series of the tetrahedrane complexes $[\{CpMo(CO)_2\}_2(\mu,\eta^2{:}\eta^2\text{-}E_2)]$ (E = P(**B1**), As(**B2**), Sb(**B3**), Bi(**B4**)). In all cases, the reaction products show very weak interactions of the E_n ligand complexes and the Lewis acid **F** exhibiting highly dynamic behavior or dissociation in solution and no adducts can be detected in the mass spectra. The solid state structures of the obtained products show the formation of weak adducts exhibiting close contacts of the pnictogen atoms to the Hg centers of **F** below the respective sum of the van der Waals radii.

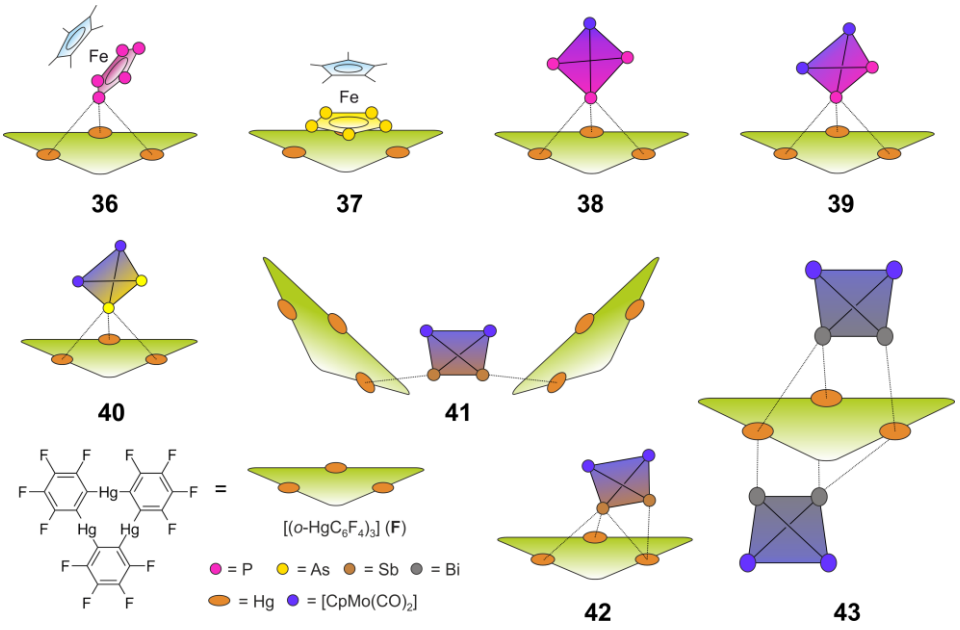

Scheme 9. Summary of the results obtained from reactions of the unusual Lewis acid **F** with E_n ligand complexes.

All P_n complexes (**A1**, **B1** and **E**) show the interaction of only one P atom with all three Hg atoms of **F** in the compounds **36**, **38** and **39**. The As_2 complex **B2** in **40** shows a very similar arrangement like its lighter congener **B1** with only one As atom situated above the center of the Lewis acid **F**. In contrast, the *cyclo*-As_5 complex **A2** is showing an almost cofacial arrangement of the As_5 plane to the Hg_3 plane in **37**. Attempts to force the *cyclo*-P_5 ligand of $[Cp^RFe(\eta^5\text{-}P_5)]$ to adopt a cofacial arrangement towards **F** by increasing the steric bulk of the Cp ligand (Cp^R = $C_5H_{5-n}{}^tBu_n$, n = 1-3) resulted in the formation of the same structural motif. This demonstrates that the observed assembly is very stable although it is only based on weak interactions of Hg and P. The Sb_2 complex **B3** yield a mixture of two products with a **B3**:**F** molar ratio of 1:1(**42**) and 1:2(**41**). The arrangement of **B3** in **42** differs from its P and As analogs and both Sb atoms of **B3** are simultaneously interacting with the Hg atoms of **F**. In **41** the Sb_2 complex **B3** is situated between two molecules of **F** showing only one close Sb-Hg contact to each one. Finally, in case of the Bi_2 complex **B4**, the adduct **43** with a molar ratio of 2:1 could be structurally characterized. Herein, the Bi_2 dumbbell of **B4** is almost parallel to the Hg_3 plane of **F**. The arrangement in all compounds **36-43** are mainly based on electrostatic interactions.

12.5 New E_n ligand complexes

During this work the unprecedented phosphorus-rich complex $[(Cp^*Mo)_2(\mu\text{-}P_{10})]$ (**44**) could be identified by structural characterization. It was obtained as a byproduct in trace amounts when the dinuclear complexes $[Cp^*Mo(CO)_{2/3}]_2$ were reacted with P_4 at elevated temperatures. The structure of **44** can be described as a dianionic *cyclo*-P_{10} ligand stabilized by two $[Cp^*Mo]^+$ complex fragments. It represents the largest known polyphosphorus cycle described so far. Additionally, the novel heterocubane complex $[(Cp^*Mo)_3As_5]$ (**45**) could be structurally characterized as one product obtained from the reaction of $[Cp^*Mo(CO)_{2/3}]_2$ with As_4 at elevated temperatures. The cluster exhibits short Mo-Mo distances which are in agreement with the presence of Mo-Mo double bonds.

12.6 References

[1] M. Fleischmann, S. Welsch, E. V. Peresypkina, A. V. Virovets, M. Scheer, *Chem. Eur. J.* **2015**, *21*, 14332-14336.

[2] M. Fleischmann, S. Welsch, H. Krauss, M. Schmidt, M. Bodensteiner, E. V. Peresypkina, M. Sierka, C. Gröger, M. Scheer, *Chem. Eur. J.* **2014**, *20*, 3759-3768.

[3] M. Fleischmann, C. Heindl, M. Seidl, G. Balázs, A. V. Virovets, E. V. Peresypkina, M. Tsunoda, F. P. Gabbaï, M. Scheer, *Angew. Chem. Int. Ed.* **2012**, *51*, 9918-9921; *Angew. Chem.* **2012**, *124*, 10056-10059.

13 Appendices

13.1 Alphabetic List of Abbreviations

Å	Angstroem, 1 Å = $1 \cdot 10^{-10}$ m
°C	degree Celsius
br(NMR)	broad
COSY	correlation spectroscopy
cov	covalent
Cp	cyclopentadienyl, C_5H_5
d(NMR)	doublet
dpmp	bis(diphenylphosphinomethyl)phenylphosphine, ($P_3C_{32}H_{29}$)
$E°_0$	reaction energy
$H°_{298}$	standard reaction enthalpy
$S°_{298}$	standard reaction entropy
$G°_{298}$	standard gibbs reaction energy
δ	chemical shift
Da	Dalton
DFT	density functional theory
e^-	electron, elemental charge
EI MS	electron impact mass spectrometry
ESI MS	electron spray ionization mass spectrometry
[FAl]	[FAl{$OC_6F_{10}(C_6F_5)$}$_3$])
Fc	Ferrocene
FD MS	field desorption ionization mass spectrometry
h	hour
HOMO	highest occupied molecular orbital
HS	Hirshfeld Surface
HSAB	Hard and Soft Acids and Bases
Hz	Hertz
IR	infrared spectroscopy
J(NMR)	coupling constant
L	ligand (specified in text)
LUMO	lowest unoccupied molecular orbital
M	molecular ion peak
m/*q*	mass to charge ratio
Me	methyl, CH_3
MHz	Megahertz, 10^6 Hz
min	minutes
mL	milliliter, 10^{-3} L
NHC	N-heterocyclic carbene
NMR	nuclear magnetic resonance
$\tilde{\nu}$	frequency/wavenumber
$\omega_{1/2}$	half width
Ph	phenyl, C_6H_5
ppm	parts per million
q(NMR)	quartett
R	organic substituent
r	radius

r.t.	room temperature
s(IR)	strong
s(NMR)	singlet
SOMO	singly occupied molecular orbital
[TEF]	$[Al\{OC(CF_3)_3\}_4]$
^{t}Bu	*tert*-butyl, C_4H_9
t(NMR)	triplet
THF	tetrahydrofurane, C_4H_8O
vdW	van der Waals
VE	valence electron
VT	Various Temperature
w(IR)	weak

13.2 Acknowledgments

Finally, I want to thank…

- Prof. Dr. Manfred Scheer for giving me the opportunity to work in his group, enabling visits to international conferences and my research stays in France and the USA, for providing excellent working conditions and the freedom to pursue my own ideas in the lab.
- Dr. Gábor Balázs for helping me with every problem that I have encountered during my research. I also thank him for all DFT calculations he has performed for me and the time he took to read my drafts even when he sometimes answered: “Ich nix verstehen” :-)
- Prof. Dr. François P. Gabbaï for giving me the opportunity to join his team in the course of a research stay in the USA. Additionally, I thank his whole group which made it a pleasant stay for me and especially James S. Jones who significantly contributed to our joint research project.
- Dr. Christophe Lescop for giving me the opportunity to join his lab in France for two research stays and the helpful advice.
- Prof. Dr. Jascha Repp and Florian Albrecht for an interesting interdisciplinary collaboration with very informative discussions for both sides.
- Dr. Alexander V. Virovets and Dr. Eugenia Peresypkina for significant contributions to the X-ray structure analyses in this thesis. I started out as a novice and learned so much from you.
- Prof. Dr. Alexey Timoshkin for DFT calculations. Surprisingly, the answer is not always 42.
- Prof. Dr. Werner Kremer and Dr. Christian Gröger for the measurement of MAS NMR spectra.
- My former lab supervisors Dr. Stefan Welsch and Dr. Michael Bodensteiner.
- All collaborators during these years.
- All staff and co-workers of the Central Analytical Services of the University of Regensburg: X-ray (Dr. Michael Bodensteiner, Sabine Stempfhuber, Katharina Beier), mass spectrometry department (Josef Kiermaier, Wolfgang Söllner), elementary analysis department (Helmut Schüller, Barbara Baumann, Wilhelmina Krutina) and the NMR Department (Dr. Ilya Shenderovich, Anette Schramm, Georgine Stühler, Fritz Kastner).
- The staff of the glass blowing, electronics and mechanics facilities of the University of Regensburg.
- My dear friends Dr. Sebastian Huber and Christian Marquardt
- All present and former members of the Scheer group for a pleasant working atmosphere and an unforgettable time: Andi, Andrea, Barbara K., Barbara T., Bianca, Boudi, Claudi, Conny, Dani, David, Eric, Eva, Fabian D., Fabian S., Felix, Gábor, Hannes, Helena, Hias, Jens, Julian, Karin, Kathl, Küken, Liese, Luigi, Luis, Matthias H., Matthias L., Mehdi, Mia, Michi, Miriam, Moni, Mo, Musch, Muschine, Oime, Olli, Patrick, Petra, Reini, Robert, Rudi, Sabine, Schotti, Sμ, Stubi, Susanne, Thomsi, Tobi, Valentin, Walter, Wast, Welschi, Wurzl.
- And especially to my family and all my friends for their enduring support.